International Series of Numerical Mathematics

Alexander Martin,
Frauke Liers,
Falk Hante, Jens Lang,
Marc E. Pfetsch,
Caren Tischendorf,
Stefan Ulbrich, Editors

174



Mathematical Modelling, Simulation and Optimization using the Example of Gas Networks

OPEN ACCESS

Birkhäuser



ISNM

International Series of Numerical Mathematics

Volume 174

Series Editors

Michael Hintermüller, Weierstrass Institute for Applied Analysis and Stochastics, Berlin, Germany

Günter Leugering, Universität Erlangen-Nürnberg, Erlangen, Germany

Associate Editors

Zhiming Chen, Chinese Academy of Sciences, Beijing, China

Ronald H. W. Hoppe, Department of Mathematics, University of Houston, Houston, TX, USA

Nobuyuki Kenmochi, Chiba University, Chiba, Japan

Victor Starovoitov, Novosibirsk State University, Novosibirsk, Russia

Honorary Editor

Karl-Heinz Hoffmann, Technical University of Munich, Garching, Germany

The International Series of Numerical Mathematics is open to all aspects of numerical mathematics with topics of particular interest including free boundary value problems for differential equations, phase transitions, problems of optimal control and optimization, other nonlinear phenomena in analysis, nonlinear partial differential equations, efficient solution methods, and approximation theory. When possible, the topic of each volume is discussed from three different angles, namely those of mathematical modelling, mathematical analysis, and numerical case studies.

Our series provides a comprehensive exploration of numerical analysis and aims to publish high quality monographs, textbooks and contributed volumes presenting the state of the art in numerical mathematics. Books published in the series are accessible to a wide range of mathematicians and experts in related fields.

All manuscripts are peer-reviewed to meet the highest standards of scientific literature. Interested authors may submit proposals by email to the series editors or to the relevant Birkhäuser editor listed under “Contacts”.

Alexander Martin · Frauke Liers · Falk Hante ·
Jens Lang · Marc E. Pfetsch · Caren Tischendorf ·
Stefan Ulbrich
Editors

Mathematical Modelling, Simulation and Optimization using the Example of Gas Networks

Birkhäuser

Editors
Alexander Martin
University of Technology Nürnberg
Nürnberg, Germany

Falk Hante
Institut für Mathematik
Humboldt-Universität zu Berlin
Berlin, Germany

Marc E. Pfetsch
Fachbereich Mathematik, AG Optimierung
Technical University of Darmstadt
Darmstadt, Germany

Stefan Ulbrich
Fachbereich Mathematik, AG Optimierung
Technical University of Darmstadt
Darmstadt, Baden-Württemberg, Germany

Frauke Liers
Department of Data Science and Department of Mathematics
Friedrich-Alexander-Universität Erlangen-Nürnberg
Erlangen, Bayern, Germany

Jens Lang
Department of Mathematics
Technical University of Darmstadt
Darmstadt, Hessen, Germany

Caren Tischendorf
Institut für Mathematik
Humboldt-Universität zu Berlin
Berlin, Germany



ISSN 0373-3149 ISSN 2296-6072 (electronic)
International Series of Numerical Mathematics
ISBN 978-3-032-34968-2 ISBN 978-3-032-34969-9 (eBook)
https://doi.org/10.1007/978-3-032-34969-9

This work was supported by Deutsche Forschungsgemeinschaft (239904186).

© The Editor(s) (if applicable) and The Author(s) 2027. This book is an open access publication.

Open Access This book is licensed under the terms of the Creative Commons Attribution-NonCommercial-NoDerivatives 4.0 International License (http://creativecommons.org/licenses/by-nc-nd/4.0/), which permits any noncommercial use, sharing, distribution and reproduction in any medium or format, as long as you give appropriate credit to the original author(s) and the source, provide a link to the Creative Commons license and indicate if you modified the licensed material. You do not have permission under this license to share adapted material derived from this book or parts of it.
The images or other third party material in this book are included in the book's Creative Commons license, unless indicated otherwise in a credit line to the material. If material is not included in the book's Creative Commons license and your intended use is not permitted by statutory regulation or exceeds the permitted use, you will need to obtain permission directly from the copyright holder.
This work is subject to copyright. All commercial rights are reserved by the author(s), whether the whole or part of the material is concerned, specifically the rights of translation, reprinting, reuse of illustrations, recitation, broadcasting, reproduction on microfilms or in any other physical way, and transmission or information storage and retrieval, electronic adaptation, computer software, or by similar or dissimilar methodology now known or hereafter developed. Regarding these commercial rights a non-exclusive license has been granted to the publisher. Unless otherwise expressly agreed by the Publisher in writing, the Publisher does not authorize use or reproduction of all or any part of this work in any manner for the purpose of training, fine-tuning, evaluating, or developing artificial intelligence models, technologies, or systems. In accordance with Article 4(3) of the EU Directive 2019/790 on copyright and related rights in the Digital Single Market, the Publisher expressly reserves all rights with respect to this work under the text and data mining exception of the directive.
The use of general descriptive names, registered names, trademarks, service marks, etc. in this publication does not imply, even in the absence of a specific statement, that such names are exempt from the relevant protective laws and regulations and therefore free for general use.
The publisher, the authors and the editors are safe to assume that the advice and information in this book are believed to be true and accurate at the date of publication. Neither the publisher nor the authors or the editors give a warranty, expressed or implied, with respect to the material contained herein or for any errors or omissions that may have been made. The publisher remains neutral with regard to jurisdictional claims in published maps and institutional affiliations.

This book is published under the imprint Birkhäuser, www.birkhauser-science.com by the registered company Springer Nature Switzerland AG
The registered company address is: Gewerbestrasse 11, 6330 Cham, Switzerland

If disposing of this product, please recycle the paper.

Preface

This book is one of the outcomes of a long-standing research process that ultimately led to the funding of the Collaborative Research Centre (CRC) Transregio TRR 154 by the German Research Foundation (DFG) from 2014 to 2026. The path leading to this point was shaped by many developments and occasionally winding stages whose origins reach far back into the past. In the following, we briefly retrace the most important milestones of this development.

We begin in the year 1998. Prof. Dr. Martin Grötschel approached Alexander Martin, Rüdiger Schultz, and Marc Steinbach with a request from a former fellow student working at Ruhrgas AG, asking whether they could prepare an expert report. The question was to what extent, beyond the ongoing digitization efforts at that time, optimization of the Ruhrgas gas network would already be possible. By way of background, Ruhrgas had commissioned PSI to digitize the entire network, among other things to enable simulations. At the same time, PSI also offered optimization capabilities, i.e., the optimal control of compressors and other active elements. Ruhrgas was apparently not entirely convinced and therefore requested an expert opinion from the Konrad Zuse Center for Information Technology Berlin, today the Zuse Institute Berlin (ZIB). This report was ultimately prepared by the three aforementioned researchers. The conclusion of the report was that simulations were certainly feasible, something that PSI, which at the time held a pioneering role in this area, was able to provide. However, automatic optimization using the methods available at that time remained a highly challenging problem requiring substantial further research. This led to the proposal of a joint research project to analyze which possibilities already existed, which approaches might become feasible in the short and medium term, and where important gaps still remained.

As a result, an initial research project entitled "Mixed Integer Optimization for Operative Gas Management," funded by the German Federal Ministry of Education and Research (BMBF), was launched in the year 2000. In this project, involving Alexander Martin, Rüdiger Schultz, Marc Steinbach, as well as PSI and Ruhrgas, the first promising results for the operation of gas networks were achieved.

By the year 2003, the three colleagues approached E.ON Ruhrgas again with these results. In the meantime, Ruhrgas had been acquired by E.ON, which explains the change in the company name. Along with the renaming came changes in management

structures and funding responsibilities. After proudly presenting their first results, the researchers were informed that the real profits in the gas sector now lay in trading rather than transportation. Whether compressors could be controlled 10% more efficiently was considered no longer relevant or only of marginal interest. The three researchers left somewhat disappointed, as they still regarded the topic as socially relevant and, if anything, even more deeply connected to fascinating mathematical research questions.

In the meantime, the professional situations of the three researchers had also changed: Rüdiger Schultz had accepted a position in Duisburg, Marc Steinbach had moved to Hannover, and Alexander Martin had gone to Darmstadt. Each of them tried, in one way or another, to keep the flame of mathematical modeling, simulation, and optimization for gas networks alive at their respective institutions and to further develop the topic through various funding programs. Among other things, Alexander Martin, together with Jens Lang and Günter Leugering (who at that time was still at TU Darmstadt), succeeded in obtaining DFG funding for a coordinated project entitled "Hybrid Dynamical Transport Systems on Networks," in which PDE and optimal control aspects were integrated more intensively.

We now move to the year 2008. Further developments had also taken place at E.ON Ruhrgas. Among other things, the regulatory authority had decided that trading and transportation operations had to be separated. E.ON Ruhrgas initially became E.ON Gastransport, whose core business focused on transport capacities in the German long-distance gas network and still does today. Later, the company was renamed Open Grid Europe (OGE), accompanied by its complete organizational unbundling from the parent company and certification as an Independent Transmission Operator (ITO)[1]. Suddenly, gas transportation once again became a central issue for the company, and the former cooperation was revived.

OGE therefore approached its former contacts at ZIB, where, however, very few experts in this area were still present. As a consequence, OGE effectively traveled across Germany to Hannover, Darmstadt, and Duisburg to reunite the former expertise. This situation turned out to be particularly fortunate for academia because OGE also provided substantial funding. Together with all partners, including ZIB and under the coordination of Thorsten Koch, OGE funded a major project entitled "Development of Mathematical Methods for the Optimization of Gas Transport Networks" from 2009 to 2013.

By then, the real world had become significantly more complicated due to the liberalization of gas markets. The development of models and methods for nomination and booking validation as well as technical capacities became central topics. Consequently, challenging research questions arose that touched virtually the entire spectrum of applied mathematics: stochastics, optimal control, partial differential equations, nonlinear optimization, combinatorial optimization, and discrete optimization. The circle of participating researchers was therefore expanded to include the expertise surrounding Werner Römisch and Marc Pfetsch, complemented theoretically by the BMWi-funded project "Technical Capacities of Gas Networks." During these years, substantial sci-

[1] Incidentally, the industrial team with whom the collaboration was established — and with whom collaboration continues to this day — has essentially remained the same over the years, apart from natural personnel fluctuations, regardless of the company's changing name.

entific progress was achieved, and, in particular, functioning prototypes for stationary cases were developed. The book *Evaluating Gas Network Capacities*, edited by Thorsten Koch, Benjamin Hiller, Marc Pfetsch, and Lars Schewe, comprehensively documents these results. Nevertheless, it should also be noted that at that time it was still not possible to enter real-time operation for a gas transmission operator, especially given the complexity of the OGE network. Despite this, mathematical curiosity and the desire for deeper insights remained entirely undiminished.

Another important impulse emerged in 2011 during a reception at the Dutch Embassy in Berlin. The senior scholars Martin Grötschel and Volker Mehrmann, together with Alexander Martin, who had by then moved to Erlangen, reflected on the developments described above. The idea arose that the topic was rich enough in mathematical challenges to justify the proposal of a Collaborative Research Centre/Transregio. It is not difficult to guess who, within this constellation of three, was entrusted with the coordination task. The idea of TRR 154 was born.

Within a small core team, later expanded by Günter Leugering, Stefan Ulbrich, and Marc Pfetsch, the central concepts for the proposal were developed and old collaborations were reactivated. This initiative benefited greatly from the DFG Priority Programme SPP 1253 "Optimization with Partial Differential Equations," running from 2006 to 2013 under the coordination of Günter Leugering, within which many important preliminary ideas had already been developed. It was thus possible to recruit outstanding principal investigators at all three locations (Berlin, Darmstadt, Erlangen), who not only excelled individually but also formed a highly effective team through their personalities and collaborative spirit.

At this point, an important remark should be made. At that time, DFG regulations permitted only three participating sites in a Transregio (Berlin, Darmstadt, Erlangen), plus at most one satellite location (Duisburg). We would therefore like to express special gratitude to Marc Steinbach (Hannover), who refrained from participating in the Transregio despite the fact that he could have contributed substantially to it.

Most readers are familiar with the procedures associated with such Collaborative Research Centre proposals: following the successful preliminary proposal in 2012, the decisive two-day review meeting took place in January 2014. We successfully defended the proposal, as usual comprising around 400 pages. The final positive decision by the DFG Senate and Grants Committee in May 2014 became possible only because many individuals, including several not explicitly mentioned here, supported the initiative until the very last moment.

From 2014 onward, two further equally demanding 400-page renewal proposals followed, together with the corresponding review meetings. Altogether, these became twelve extraordinarily successful years. This book provides a selection and partial documentation of these achievements. In total, more than 400 publications were produced, most of them appearing in leading international journals. Over the years, many new and exciting topics were incorporated, ranging from market economics involving Veronika Grimm and Gregor Zöttl to later hydrogen-related topics, ensuring that current developments in society and the energy sector were continuously reflected within the research program. These developments repeatedly gave rise to fascinating new mathematical questions and insights.

The team spirit mentioned above manifested itself time and again, whether in the leadership of teams, demonstrators, or subprojects: volunteers could always be found. It should also be highlighted that Frauke Liers took over the role of spokesperson in 2023 after Alexander Martin moved to the University of Technology Nuremberg.

Beyond all these mathematical achievements, it is worth emphasizing that all post-doctoral researchers and early-career scientists who worked within TRR 154 as principal investigators have meanwhile obtained permanent academic positions or professorships — a fact that makes us particularly proud as a team.

We are deeply grateful for the financial support provided by the DFG throughout the entire twelve-year period, without which these achievements in both research and the promotion of young scientists would not have been possible.

This book is structured into several thematic sections:

- hierarchical modeling for simulation and optimal control on gas networks,
- discrete–continuous optimization for gas networks,
- optimization under uncertainty for gas networks,
- PDE-based optimization and control for gas networks,
- practical challenges and a benchmark instance for gas–hydrogen networks.

The TRR 154 team wishes all readers an enjoyable exploration of some of the results achieved over these years. We hope that these contributions will inspire further developments — whether within mathematics itself or in transferring mathematics toward broader societal impact. Particularly the latter challenge is one that mathematicians should embrace as well, although it is not the focus of this book.

Berlin, Darmstadt, Erlangen, and Nuremberg,
May 2026

Alexander Martin
Falk Hante
Jens Lang
Frauke Liers
Marc Pfetsch
Caren Tischendorf
Stefan Ulbrich

Acknowledgements

Between 2014 and 2026, the following Principal Investigators have been or were part of the Collaborative Research Centre (CRC) Transregio 154.

Tobias Breiten
Martin Burger
Yann Disser
Pia Domschke
Herbert Egger
Caroline Geiersbach
Yiannis Giannakopoulos
Jan Giesselmann
Veronika Grimm
Martin Grötschel
Julia Grübel
Martin Gugat
Falk Hante
René Henrion
Benjamin Hiller
Michael Hintermüller
Max Klimm
Jens Lang
Günter Leugering
Frauke Liers
Nicole Marheineke
Alexander Martin
Volker Mehrmann
Marc Pfetsch
Sebastian Pokutta
Lars Schewe
Martin Schmidt
Rüdiger Schultz
Alexandra Schwartz
Martin Skutella
Michael Stingl
Caren Tischendorf
Tabea Tscherpel
Stefan Ulbrich
Andrea Walther
Winnifried Wollner
Gregor Zöttl
Enrique Zuazua

The following researchers have been members or associate members in the CRC Transregio 154.

Kevin-Martin Aigner
Denis Aßmann
Daniel Bankmann
Susanne Beckers
Daniela Bernhard
Christian Biefel
Pascal Börner
Marcello Bongarti
Jannik Breitkopf
Ingo Bremer

Yan Brodskyi
Robert Burlacu
Johanna Burtscheidt
Aidan Chaumet
Jan-Patrick Clarner
Matthias Claus
Timothée Crin-Barat
Hannes Dänschel
Marie Düker
Jonas Egerer
Antonio Esposito
Ariane Fazeny
Maria Filipkovska
Tobias Fischer
Dennis Gabriel
Adrian Göß
Jorge Andrés Gonzales Zumba
Tatiana Gonzalez-Grandon
Claudia Gotzes
Gertrud Graser
Dennis Groh
Martin Groß
Candan Güdücü
Oliver Habeck
Johannes Hahn
Christine Hayn
Holger Heitsch
Martín Hernández
Olivier Huber
Christoph Huck
Lukas Hümbs
Sven Jäger
Lennart Jansen
Li Jin
Imke Joormann
Nikolaos Kanelakis
Aswin Kannan
Attila Karsai
Thomas Kleinert
Martin Knosalla
Timo Kreimeier
Richard Krug
Martina Kuchlbauer
Christian Kuchler
Thomas Kugler
Varun Kumar
Teresa Kunkel
Katja Kutzer
Christian Lange
Fabio Leotta
Ziqian Li
Björn Liljegren-Sailer
Martin Loy
Yi Lu
Francesco Ludovici
Annette Lutz
Sandra May
Hannes Meinlschmidt
Maximilian Merkert
Arthur Miehlich
Pascal Mindt
Riccardo Morandin
Konrad Mundinger
Sabrina Nitsche
Nicola De Nitti
Daniel Nowak
Timm Oertel
Jonas Pade
Susanne Pape
Sebastian Pfaff
Lukas Pflug
Nora Philippi
Fränk Plein
Rico Raber
Alexander Rath
Kristina Rolsing
Fabian Rüffler
Henning Sauter
Maximilian Schade
Paloma Schäfer Aguilar
Jakob Schelbert
Adrian Schmidt
Johann Michael Schmitt
Moritz Schneider
Lucas Schöbel-Kröhn
Dirk Schröder
Philipp Schulze
Michael Schuster
Jonas Schweiger
Kartikey Sharma
Vsevolod Shashkov
Mathias Sirvent

Christian Sölch
Sylvain Spitz
Kai Spürkel
Jeroen Stolwijk
Elisa Strauch
Eric Laurin Strelow
Tom Streubel
Nikolai Strogies
Christian Strohm
Lea Strubberg
Michael Thiele
Johannes Thürauf
Christoph Thurner
Antonia Topalovic
Rowan Turner
Andrian Uihlein
Lisa Wagner
Yue Wang
Philipp Warode
David Weckbecker
Dieter Weninger
Jorge Weston
Ann-Katrin Wiertz
Hendrik Wilka
David Wintergerst
Lukas Wolff
Tobias Wollenberg

The management team of the CRC Transregio 154 included:

Kevin-Martin Aigner
Jens Habermann
Andreas Héran
Mathias Sirvent
Regine Stirnweiß
Christina Weber

We would especially like to thank Kevin-Martin Aigner for his outstanding support in coordinating and managing the overall book project. Our special thanks go to Christoph Eyrich for his continuous involvement in all of the CRC years, in particular, his help in preparing the three proposals, his careful typesetting work, and numerous suggestions for improving the layout of the book. We are delighted that this volume could be published as an open access book.

Ultimately, the success of TRR 154 was only achieved thanks to the dedication of everyone mentioned.

Contents

Preface v

Acknowledgements ix

Part I Hierarchical Modeling for Simulation and Control of Gas Network Dynamics

1 Introduction to Hierarchical Modeling for Simulation and Control of Gas Network Dynamics 3
Jens Lang and Caren Tischendorf

2 A Catalog of Gas Network Models: PDEs, Coupling Conditions, and Numerical Schemes 5
Tobias Breiten, Pia Domschke, Jan Giesselmann, Benjamin Hiller, Attila Karsai, Jens Lang, Volker Mehrmann, Riccardo Morandin, Caren Tischendorf, and Tabea Tscherpel

2.1 Introduction 7
2.2 The Euler Equations 7
2.2.1 The Equation of State for Real Gases and the Compressibility Factor 9
2.2.2 The Pipe Friction Coefficient 10
2.3 Model Hierarchy for Isothermal euler Equations 14
2.3.1 Semilinear Equations 15
2.3.2 Parabolic Equation 16
2.3.3 Algebraic Equations 17
2.4 Model Hierarchy for Temperature-Dependent Euler Equations 17
2.4.1 Simplified Nonlinear Equations 18
2.4.2 Stationary Model 19
2.5 Energy-Based Coupling Conditions 20
2.5.1 Network Topology 21
2.5.2 Coupling Conditions for (ISO1) 22
2.5.3 Coupling Conditions for (TA1) 25

2.6 Mixture Models . . . 26
2.6.1 Balance Laws . . . 26
2.6.2 Pressure Laws and Energy Balance . . . 27
2.6.3 Coupling Conditions for ISO1 Based Mixture Models . . . 29
2.6.4 Low Mach High Friction Limit . . . 30
2.7 Port-Hamiltonian Model Formulations . . . 32
2.7.1 The Abstract Setting . . . 32
2.7.2 Isothermal Model Hierarchy . . . 35
2.7.3 The Euler Equations (TA1) . . . 38
2.7.4 Mixture Models . . . 41
2.8 Discretization . . . 42
2.8.1 Hyperbolic Balance Laws . . . 42
2.8.2 Port-Hamiltonian Systems . . . 44
2.8.3 ISO1 Pipe Model . . . 47
2.8.4 ISO2 Pipe Model . . . 49
2.8.5 ISO3 Pipe Model . . . 50
2.9 Non-Pipe Gas Network Elements . . . 51
2.10 Network Models . . . 56
2.10.1 Coupling Conditions . . . 57
2.10.2 PDE Gas Network Models . . . 58
2.10.3 PDAE Gas Network Models . . . 60
2.10.4 DAE Gas Network Models . . . 62
2.10.5 AE Gas Network Models . . . 65
References . . . 67

3 Gas Mixtures on Networks: Modeling, Simulation and Optimization . . . 73
Pascal Börner, Jan Giesselmann, Varun M. Kumar, Marc E. Pfetsch, Michael Thiele, and Tabea Tscherpel
3.1 Introduction . . . 74
3.2 Introduction to Mixture Models . . . 76
3.3 Pressure Laws . . . 79
3.3.1 Collection of Pressure Laws . . . 80
3.3.2 Comparison of Pressure Laws . . . 83
3.4 A (Simplified) Stationary One-Velocity Model . . . 86
3.5 One- and Two-Velocity Mixtures on a Single Pipe . . . 88
3.5.1 Boundary Conditions . . . 89
3.5.2 Numerical Scheme and Computational Aspects . . . 90
3.5.3 Computation of Stationary Solutions . . . 92
3.5.4 Instationary Solutions . . . 97
3.6 Mixtures on Networks . . . 99
3.6.1 Coupling Conditions on Networks . . . 100
3.6.2 Optimization . . . 102
3.6.3 Computational Details of Stationary Flow . . . 105
3.6.4 Comparison of Pressure Laws on Networks for One-Velocity Model . . . 107
3.6.5 Validation of the Optimization Results . . . 109

3.6.6 Consistency of Coupling for One- and Two-Velocity Models 112
3.6.7 Instationary Flows on Networks 115
3.7 Open Questions 119
References 120

4 Optimal Control Under Constrained Pressure Fluctuation 123
Martin Gugat, Henning Sauter, Michael Schuster, and Caren Tischendorf
4.1 Introduction 123
4.2 Mathematical Modelling 124
4.3 The Optimal Control Problem 125
4.4 Optimal Control with DAE Constraints 127
4.5 Numerical Examples 128
4.5.1 One Compressor Connected to One Pipe 128
4.5.2 Gaslib-11 131
References 133

Part II Discrete-Continuous Optimization for Gas Networks

5 Introduction to Discrete-Continuous Optimization for Gas Networks . . . 137
Alexander Martin and Marc E. Pfetsch

6 Mixed-Integer Nonlinear Optimization in the Context of Gas Networks . 141
Robert Burlacu, Adrian Göß, Günter Leugering, Alexander Martin, Marc E. Pfetsch, Martin Schmidt, and Johannes Thürauf
6.1 Introduction 142
6.2 Brief Literature Review 142
6.3 Improvements for Solving Stationary Models 143
6.3.1 Compressor Station Modeling 144
6.3.2 Global Optimization by Exploiting Acyclicity 144
6.3.3 Global Optimization of the ODE Model 145
6.4 Improvements for Time-Dependent Models via Decomposition Methods 147
6.4.1 Graph Setting and Problem Formulation 148
6.4.2 Semi-Discretization in Time 151
6.4.3 The Fully Discrete Problem 152
6.4.4 Time-Domain Decomposition 153
6.4.5 Spatial Domain Decomposition of the Instantaneous Problem 155
6.4.6 Decomposed Instantaneous OCP in Primal Schur Form 156
6.4.7 Maximizing the Storage Capacity of Gas Networks 157
6.5 Topology Optimization 159
6.6 Lipschitz-Based Solution Approaches 160
6.6.1 The Univariate and Monotone Case 160
6.6.2 The Univariate Lipschitz Case 162
6.6.3 The Multivariate Lipschitz Case 163
6.6.4 The Multivariate and Implicit Case 164
6.6.5 Generalized Approximation of Function Domain 165

6.6.6 A-Priori Epigraph Approximations 165
6.6.7 A Step Towards the Complexity of Resulting Subproblems . 167
6.7 Outlook 168
References 168

7 Potential-Based Flows – An Overview 173
Marc E. Pfetsch, Martin Schmidt, Martin Skutella, and Johannes Thürauf
7.1 Introduction 173
7.2 Potential-Based Flows: Basic Properties 174
7.2.1 Examples 175
7.2.2 Networks and Controllable Components 176
7.2.3 Basic Properties of Potential-Based Flows 177
7.3 Complexity 180
7.4 Monotonicity of Parameter-Dependent Potential-Based Flows 182
7.5 Topology Optimization 183
7.6 Robust Approaches for Tackling Uncertainty 186
7.7 Potential-Based MINLP and Beyond 188
7.8 Conclusion and Challenges 189
References 190

8 Models for Gas Markets 195
Veronika Grimm, Julia Grübel, Johannes Hahn, Max Klimm, Lars Schewe, Martin Schmidt, and Gregor Zöttl
8.1 Introduction 196
8.2 Preliminaries 197
8.3 Multilevel Model Under Perfect Competition 198
8.3.1 Fourth Level: Gas Transport 198
8.3.2 Third Level: Nomination 199
8.3.3 Second level: Booking 202
8.3.4 First Level: Technical Capacities and Booking Fees 203
8.4 Related Models and Reformulations 204
8.5 Strategic Suppliers in the Entry-Exit Market Model 207
8.6 Further Models for Gas Markets 209
References 212

Part III Optimization under Uncertainty for Gas Networks

9 Introduction to Optimization under Uncertainty for Gas Networks 219
Frauke Liers and Stefan Ulbrich

10 From Probabilistic to Probust Constraints: Optimization Under Uncertainty 223
Daniela Bernhard, Caroline Geiersbach, Martin Gugat, Holger Heitsch, René Henrion, Jens Lang, Frauke Liers, Rüdiger Schultz, Michael Schuster, Michael Stingl, and Hendrik Wilka
10.1 Probust Constraints 224
10.2 Applications to Gas Transport 227

10.2.1 Nomination Validation Under Uncertainty 228
10.2.2 Capacity maximization under stationary and transient gas flow 230
10.2.3 Maximizing the Chance of Feasibility for Transient Gas Flow 234
10.3 Algorithmical Approaches 238
10.3.1 Numerical Methods for Solving Optimization Problems Subject to Probabilistic Constraints 239
10.3.2 Numerical Methods for Solving Optimization Problems with Probust Constraints 245
10.3.3 Numerical Methods for Solving Optimization Problems with Robust or Almost Sure Constraints 249
10.3.4 Numerical Methods for Constraint Approximation 252
10.4 Selected Theoretical Results 255
10.4.1 Existence of Chance Maximizing Controls and the Turnpike Phenomenon 255
10.4.2 Well-Posedness, Existence of Solutions and Convexity in Probabilistically Constrained Optimal Control of Linear PDEs 255
10.4.3 Optimality Conditions in PDE-Constrained Optimization Subject to Probabilistic State Constraints 256
10.5 Conclusions 259
References 260

11 Continuous Stochastic Gradient and Spherical Radial Decomposition . . 265
Daniela Bernhard, Holger Heitsch, René Henrion, Frauke Liers, Michael Stingl, Andrian Uihlein, and Viktor Zipf
11.1 Introduction 266
11.2 Basic Components 267
11.2.1 Spherical-Radial Decomposition 267
11.2.2 Continuous Stochastic Gradient Method 268
11.2.3 Combination of CSG and SRD 270
11.3 Application to Analytic Model Problems 270
11.3.1 Problem Formulations 270
11.3.2 Numerical Results 272
11.4 Extension of the CSG Convergence Theory Beyond Problems that are Globally Lipschitz 275
11.4.1 Convergence for Numerical Examples 279
11.5 Applications to Capacity Maximization 284
11.6 Conclusion and Outlook 286
References 287

12 Incremental–Decremental Optimization for the Transition to Hydrogen 289
Yann Disser, Max Klimm, Annette Lutz, and Lea Strubberg
12.1 Transition from Gas to Hydrogen Networks 289
12.1.1 Chaper Outline 290
12.1.2 Related Work 291

12.2 Double-Greedy Algorithm 292
12.3 Incremental–Decremental Minimization of Operating Costs 293
12.4 Incremental–Decremental Maximization 298
12.4.1 Further Results for Incremental–Decremental Maximization 301
References 302

Part IV PDE-based Optimization and Control for Gas Network Applications

13 Introduction to PDE-based Optimization and Control for Gas Network Applications 307
Falk M. Hante and Stefan Ulbrich

14 Optimal Control of Discontinuous Solutions of Hyperbolic Systems of Balance Laws 311
Jannik Breitkopf and Stefan Ulbrich
14.1 Introduction 311
14.1.1 Assumptions and Notation 312
14.1.2 Related Literature 313
14.2 Existence and Regularity Properties of Entropy Solutions 313
14.3 Stability and Differentiability Properties 315
14.3.1 Solution Operator in the Reference Space 315
14.3.2 Solution Operator in Physical Coordinates 317
14.4 The Adjoint Problem 319
14.4.1 Unique Existence of a Reversible Solution 320
14.4.2 Adjoint Gradient Representation 321
14.5 Conclusion 326
References 327

15 Sequential Action Control for Hybrid Dynamical Models of Gas Networks 329
Yan Brodskyi, Falk M. Hante, and Antonia Topalović
15.1 Motivation 329
15.2 SAC Principle for Hybrid Semilinear Systems 331
15.2.1 Problem Setup 332
15.2.2 The SAC Principle 333
15.3 Stabilization 335
15.3.1 Unstable Heat Equation 336
15.3.2 Numerical Results 338
15.3.3 SAC for Systems with Discrete Control Decisions 338
15.4 Gas-Network Example 341
15.4.1 Networks with Pipes, Valves, and Compressors 342
15.4.2 Abstract Problem Formulation 343
15.4.3 Numerical Example 346
15.5 Conclusion and Future Work 347
References 348

16 The Turnpike Property and the Optimal Control of Gas Networks 351
Martin Gugat and Michael Schuster
16.1 Theoretical Background on Turnpike Phenomena 351
16.2 An Example with a Neural ODE 354
16.3 An Example with a Gas Network (Gaslib11) 356
Conclusion 360
References 360

17 Domain Decomposition for Gas Network Control 363
Falk M. Hante, Martin Hernandez, Günter Leugering, Martin Schmidt, and Enrique Zuazua
17.1 Introduction 363
17.2 Space-Time Domain Decomposition Methods 365
17.2.1 Network Modeling 366
17.2.2 Space-Time Domain Decomposition 370
17.2.3 Optimal Control Problems 371
17.2.4 Doubly-Nonlinear p-Parabolic Optimal Control on Graphs and STDD 375
17.3 Mixed-Integer Control 376
17.4 Randomized Domain Decomposition 380
17.4.1 RBM for Discretized PDEs 380
17.4.2 Continuous RBM for Parabolic PDEs on Graphs 387
17.4.3 Related Work and Comments 392
17.5 A Consensus-Based Penalty Alternating Direction Method for Graph-Decompositions of Gas Networks 393
17.5.1 Modeling 393
17.5.2 Classic Penalty Alternating Direction Methods 398
17.5.3 A Consensus-Based Penalty Alternating Direction Method . 399
17.5.4 Decomposition of Gas Networks 400
17.5.5 Numerical Results 402
17.5.6 Discussion of the Results for the GasLib-134 Network 404
17.6 Conclusion 405
References 406

18 A PDE-Constrained Generalized Nash Equilibrium Approach for Modeling Gas Transport with Strategic Suppliers 413
Veronika Grimm, Michael Hintermüller, Olivier Huber, Lars Schewe, Martin Schmidt, and Gregor Zöttl
18.1 Introduction 414
18.2 A GNEP Model for Gas Transport with Strategic Suppliers 416
18.3 Well-Posedness of the Gas Flow PDE System 419
18.4 Analysis of the Jointly Convex GNEP 427
18.5 Test Cases: The Influence of Linepacking on Market Outcomes 436
18.6 Conclusion 442
A Fundamental Results 442
B Optimization Models Used for the Test Instance 444

C Discretization Scheme 446
References 448

19 p-Wasserstein Distances on Networks and 3D to 1D Convergence 451
Martin Burger, Ariane Fazeny, Gilles Mordant, and Jan-Frederik Pietschmann
19.1 Introduction 451
19.2 Dynamic Transport Distances on Metric Graphs 454
19.2.1 Metric Graphs 454
19.2.2 Continuity Equations 456
19.2.3 Action Functionals and Dynamic Distances 458
19.2.4 Gradient Flows on Metric Graphs 461
19.3 Zero-Width Limit of Gas Networks 464
19.3.1 3D Modeling of Gas Network 465
19.3.2 Main Results 465
19.3.3 Convergence on the Entire Network 466
19.3.4 Existence of an Optimal Map 468
19.3.5 Towards a Dynamical Understanding 472
19.3.6 Stability with Respect to the Gas Network Topology 473
19.4 Numerical Illustrations 475
References 476

Part V Practical Challenges and a Benchmark Instance for Gas–Hydrogen Networks

20 Introduction to Practical Challenges and a Benchmark Instance for Gas–Hydrogen Networks 481
Frauke Liers and Alexander Martin

21 Gas2Hydro – A Combined Natural Gas–Hydrogen Instance 483
Daniela Bernhard, Julian Born, Yann Disser, Caroline Geiersbach, Johannes Hahn, Anton Hoof, and Lea Strubberg
21.1 Introduction 484
21.1.1 Motivation 484
21.1.2 Prior Work 485
21.1.3 Challenges 486
21.2 Description of GasLib Instances 486
21.2.1 The `.net` File 486
21.2.2 The `.scn` File 487
21.3 The Gas2Hydro Instance 487
21.3.1 Realizing a Combined Natural Gas–Hydrogen Instance 488
21.3.2 Physical Quantities 495
21.3.3 Validation 496
21.4 Application 496
References 498

22 Mathematical Questions Arising from Practical Challenges in Gas Networks 501
Julia Grübel, Frauke Liers, Alexander Martin, Lars Schewe, and Michael Schuster
22.1 Introduction 501
22.2 Practical Challenges in Modeling and Control of Gas Networks 503
22.2.1 From Stationary Models as a Reference Point to Physically-Detailed Transient Models 503
22.2.2 From Coarse-Scale to Refined Operations: A Line Pack Example 504
22.2.3 The Impact of Perturbations and Uncertainties on Operations 505
22.2.4 Integration of Different Areas of Applied Mathematics to Obtain Validated Operations 506
22.3 Practical Challenges in Gas Markets and Real-Time Operation of Gas Networks 508
22.3.1 Long-Term Perspective: Network Topology and Technical Capacities 510
22.3.2 Mid-Term Perspective: Capacity Booking and Subsequent Nominations 510
22.3.3 Short-Term Perspective: Robust Operations Under Uncertainty 511
22.3.4 Real-Time Perspective: Adapting to System Changes 513
22.4 Practical Challenges in the Transition of Natural Gas and Hydrogen Networks 513
22.4.1 Reducing Gas Networks and Integration of Hydrogen 514
22.4.2 Organizing the Interaction between Agents Participating in Both Sectors 516
22.5 Outlook 517
References 518

Part I
Hierarchical Modeling for Simulation and Control of Gas Network Dynamics

Chapter 1
Introduction to Hierarchical Modeling for Simulation and Control of Gas Network Dynamics

Jens Lang[0000−0003−4603−6554] and
Caren Tischendorf[0000−0002−8421−7199]

Abstract The three chapters collectively develop a coherent framework for the modeling, simulation, optimization, and control of gas and hydrogen transport in pipeline networks, addressing both theoretical foundations and practical challenges arising in the transition toward low-carbon energy systems.

The first chapter, *A Catalog of Gas Network Models: PDEs, Coupling Conditions, and Numerical Schemes*, provides a structured introduction to gas flow modeling. It organizes models into hierarchies according to their physical detail and mathematical complexity, ranging from fully dynamic partial differential equation models for compressible flow to simplified algebraic formulations used in large-scale network studies. Special attention is given to the modeling of individual network components such as valves and compressors, whose behavior significantly influences system dynamics. The chapter also discusses consistent coupling conditions at network junctions to ensure mass and energy conservation. In addition, it introduces energy-based port-Hamiltonian formulations, which emphasize physical structure and facilitate model reduction and control design. A concise overview of numerical schemes for hyperbolic balance laws and port-Hamiltonian systems completes the chapter, highlighting the computational techniques required for reliable simulation of gas networks.

The second chapter, *Gas Mixtures on Networks: Modeling, Simulation and Optimization*, extends the discussion to isothermal mixtures of hydrogen and natural gas, motivated by the growing need to integrate hydrogen into existing infrastructure. It systematically analyzes different mixture model classes and studies their convergence behavior, particularly in regimes where strong interactions between constituents occur. Both stationary and time-dependent single-pipe scenarios are examined, before generalizing the analysis to network settings. Since mixture modeling strongly depends on the pressure law, the chapter compares the industry-standard GERG equation of state

Jens Lang
Department of Mathematics, TU Darmstadt, Germany, e-mail: lang@mathematik.tu-darmstadt.de

Caren Tischendorf
Institute of Mathematics, HU Berlin, Germany, e-mail: tischendorf@math.hu-berlin.de

© The Author(s) 2027

A. Martin et al. (eds.), *Mathematical Modelling, Simulation and Optimization using the Example of Gas Networks*, International Series of Numerical Mathematics 174,
https://doi.org/10.1007/978-3-032-34969-9_1

with simplified alternatives that preserve convex energy structures and significantly reduce computational effort. For network applications, consistent coupling conditions across different model classes are derived, ensuring compatibility between modeling levels. The chapter also investigates steady-state flow optimization using the algebraic Weymouth formulation and presents numerical evidence for its validity in practically relevant operating regimes. Overall, it identifies when simplified mixture models are justified and outlines key open challenges in accurately modeling hydrogen-natural gas blends.

The third chapter, *Optimal Control under Constrained Pressure Fluctuation*, focuses on the safe and efficient operation of gas and hydrogen networks under material and operational constraints. Building on differential-algebraic equation formulations of gas network models, it develops an optimal control framework that incorporates not only bounds on control inputs but also constraints on their time derivatives. These derivative constraints are particularly important for mitigating hydrogen embrittlement and reflecting the physical limitations of existing pipeline infrastructure. The resulting systems of differential-algebraic equations maintain physical consistency, energy awareness, and compatibility with hierarchical model reductions introduced earlier. Numerical examples demonstrate how derivative-constrained control strategies can effectively limit pressure fluctuations while ensuring reliable and efficient hydrogen transport. Together, the chapters provide an integrated perspective on modeling depth, computational efficiency, and operational safety in modern gas and hydrogen pipeline networks.

Acknowledgements This work was supported by the German Research Foundation (DFG) within Subprojects A01, B01, B03, C02, C03, C05, and C09 in the Sonderforschungsbereich/Transregio 154 "Mathematical Modelling, Simulation and Optimization using the Example of Gas Networks" (Project ID 239904186).

Open Access This chapter is licensed under the terms of the Creative Commons Attribution-NonCommercial-NoDerivatives 4.0 International License (http://creativecommons.org/licenses/by-nc-nd/4.0/), which permits any noncommercial use, sharing, distribution and reproduction in any medium or format, as long as you give appropriate credit to the original author(s) and the source, provide a link to the Creative Commons license and indicate if you modified the licensed material. You do not have permission under this license to share adapted material derived from this chapter or parts of it.

The images or other third party material in this chapter are included in the chapter's Creative Commons license, unless indicated otherwise in a credit line to the material. If material is not included in the chapter's Creative Commons license and your intended use is not permitted by statutory regulation or exceeds the permitted use, you will need to obtain permission directly from the copyright holder.



Chapter 2
A Catalog of Gas Network Models: PDEs, Coupling Conditions, and Numerical Schemes

Tobias Breiten[0000−0002−9815−4897],
Pia Domschke[0000−0001−6286−1613],
Jan Giesselmann[0009−0008−0217−7244],
Benjamin Hiller[0000−0003−4335−0775],
Attila Karsai[0000−0001−9905−433X],
Jens Lang[0000−0003−4603−6554],
Volker Mehrmann[0000−0001−5051−2870],
Riccardo Morandin[0000−0003−2511−041X],
Caren Tischendorf[0000−0002−8421−7199], and
Tabea Tscherpel[0000−0002−5899−1279]

Abstract This chapter aims to provide a concise and clear introduction to the topic of gas flow modeling. We present several models for gas flow, organized into hierarchies

Tobias Breiten
Institute of Mathematics, TU Berlin, Germany, e-mail: tobias.breiten@tu-berlin.de

Pia Domschke
Department of Computational Science and Philosophy, Frankfurt School of Finance & Management, Germany, e-mail: p.domschke@fs.de

Jan Giesselmann
Department of Mathematics, TU Darmstadt, Germany, e-mail: giesselmann@mathematik.tu-darmstadt.de

Benjamin Hiller
Konrad-Zuse-Institut Berlin, Germany, e-mail: hiller@zib.de

Attila Karsai
Institute of Mathematics, TU Berlin, Germany, e-mail: karsai@math.tu-berlin.de

Jens Lang
Department of Mathematics, TU Darmstadt, Germany, e-mail: lang@mathematik.tu-darmstadt.de

Volker Mehrmann
Institute of Mathematics, TU Berlin, Germany, e-mail: mehrmann@math.tu-berlin.de

Riccardo Morandin
Institute for Analysis and Numerics, Otto-von-Guericke-Universität Magdeburg, Germany, e-mail: riccardo.morandin@ovgu.de

Caren Tischendorf
Department of Mathematics, HU Berlin, Germany, e-mail: tischendorf@math.hu-berlin.de

Tabea Tscherpel
Department of Mathematics, TU Darmstadt, Germany, e-mail: tscherpel@mathematik.tu-darmstadt.de

© The Author(s) 2027

A. Martin et al. (eds.), *Mathematical Modelling, Simulation and Optimization using the Example of Gas Networks*, International Series of Numerical Mathematics 174,
https://doi.org/10.1007/978-3-032-34969-9_2

based on complexity. We discuss in detail the modeling of individual components such as valves and compressors. Network model classes based on purely algebraic relations and energy-based port-Hamiltonian models are included, along with a brief overview of basic numerical methods for hyperbolic balance laws and port-Hamiltonian systems. We do not claim completeness and refer in many places to the existing literature.

2.1 Introduction . . . 7
2.2 The Euler Equations . . . 7
2.2.1 The Equation of State for Real Gases and the Compressibility Factor . . . 9
2.2.2 The Pipe Friction Coefficient . . . 10
2.3 Model Hierarchy for Isothermal euler Equations . . . 14
2.3.1 Semilinear Equations . . . 15
2.3.2 Parabolic Equation . . . 16
2.3.3 Algebraic Equations . . . 17
2.4 Model Hierarchy for Temperature-Dependent Euler Equations . . . 17
2.4.1 Simplified Nonlinear Equations . . . 18
2.4.2 Stationary Model . . . 19
2.5 Energy-Based Coupling Conditions . . . 20
2.5.1 Network Topology . . . 21
2.5.2 Coupling Conditions for (ISO1) . . . 22
2.5.3 Coupling Conditions for (TA1) . . . 25
2.6 Mixture Models . . . 26
2.6.1 Balance Laws . . . 26
2.6.2 Pressure Laws and Energy Balance . . . 27
2.6.3 Coupling Conditions for ISO1 Based Mixture Models . . . 29
2.6.4 Low Mach High Friction Limit . . . 30
2.7 Port-Hamiltonian Model Formulations . . . 32
2.7.1 The Abstract Setting . . . 32
2.7.2 Isothermal Model Hierarchy . . . 35
2.7.3 The Euler Equations (TA1) . . . 38
2.7.4 Mixture Models . . . 41
2.8 Discretization . . . 42
2.8.1 Hyperbolic Balance Laws . . . 42
2.8.2 Port-Hamiltonian Systems . . . 44
2.8.3 ISO1 Pipe Model . . . 47
2.8.4 ISO2 Pipe Model . . . 49
2.8.5 ISO3 Pipe Model . . . 50
2.9 Non-Pipe Gas Network Elements . . . 51
2.10 Network Models . . . 56
2.10.1 Coupling Conditions . . . 57
2.10.2 PDE Gas Network Models . . . 58
2.10.3 PDAE Gas Network Models . . . 60
2.10.4 DAE Gas Network Models . . . 62
2.10.5 AE Gas Network Models . . . 65
References . . . 67

2.1 Introduction

In this survey, we present a compilation of different models, including a hierarchical model structure for the description of gas flow in networks in order to facilitate the introduction to the topic. In particular, we consider progressively simplified models, starting from a quasi-linear hyperbolic model and ending with an algebraic model.

The gas flow inside a gas duct is governed by some dynamic laws obtained by applying the conservation of mass, momentum and energy, constituting a quasi-linear hyperbolic system of PDEs. It is sufficient to consider one spatial dimension. Gas pipes are typically installed underground for safety and protection from damage. So temperature is often taken as constant, yielding the famous class of isothermal models. Further simplifications of the dynamics leads to (semi-)linear as well as purely algebraic equations. In the first three Sections, we give detailed information on these models. Physical and technical fundamentals of gas networks are described in particular in [49, Chap. 2]. In that book, further questions on the evaluation of gas network capacities can be found as well.

Gas flows through the network from regions of high pressure to regions of low pressure, with a pressure reduction occurring due to friction. We therefore pay special attention to modeling the friction coefficient in the momentum equation. Here hydraulically smooth, technically rough, and fully rough pipes are distinguished. Moody diagrams are presented to identify appropriate formulas for the friction coefficient, depending on the relative pipe roughness and the Reynolds number.

In Sect. 2.5, we discuss energy-based coupling conditions for the gas flow through junctions. Current developments in studying hydrogen–natural gas blends motivate a closer look at mixture models presented in Sect. 2.6. Models with one mixture velocity as well as individual velocities for the constituents are considered. Port-Hamiltonian model formulations are introduced and discussed in Sect. 2.7.

We also give a short overview of existing discretization methods for the numerical solution of hyperbolic balance laws and port-Hamiltonian systems in Sect. 2.8. A detailed description of individual components and network model classes including purely algebraic relations and energy-based models are presented in Sect. 2.9. Finally, we state overall network models which combine dynamic equations on pipes, coupling conditions, and various network elements as compressors, valves and resistors.

2.2 The Euler Equations

The flow of gas in a network is typically modeled by the Euler equations, which are a system of nonlinear hyperbolic partial differential equations that describe the behavior of compressible, inviscid fluids. They encode the conservation of mass and balances of momentum and energy. A constitutive equation closes the equation by relating the pressure to the density and the inner energy. Its choice depends on the specific gas under consideration. The model reads

$$\begin{aligned} \partial_t \rho + \partial_x(\rho v) &= 0, \\ \partial_t(\rho v) + \partial_x(p + \rho v^2) &= -\frac{\lambda}{2D}\rho v\,|v| - g\rho\partial_x b, \\ \partial_t\left(\rho(\frac{1}{2}v^2 + e)\right) + \partial_x\left(\rho v(\frac{1}{2}v^2 + e) + pv\right) &= -\frac{k_w}{D}\,(T - T_{\mathsf{w}})\,, \end{aligned} \tag{TA1}$$

together with an equation of state $p = R\rho T\mathsf{z}(p,T)$, cf. Sect. 2.2.1. Here ρ denotes the density, v the velocity of the gas, T the temperature and p the pressure. Furthermore, g is the gravitational acceleration, b is the height of the bottom of the gas pipe above a reference level, λ is the pipe friction coefficient, D is the pipe diameter, k_w is the thermal conductivity coefficient, $T_{\mathsf{w}} = T_{\mathsf{w}}(x)$ is the surface temperature of the pipe wall, R is the specific gas constant, and $\mathsf{z} = \mathsf{z}(p,T)$ is the compressibility factor. The variable $e = c_V T + gb$ denotes the internal energy, i.e., the sum of thermal and potential energy. Here c_V is the specific heat at constant volume. A short derivation of the equations is given in, e.g., [4], while a more extensive one focusing on thermodynamic considerations can be found in [19]. Let us briefly mention that the label TA stands for "Temperatur abhängig", the German for temperature dependent and let us comment on the physical interpretation of the equations. The first equation encodes that mass in any (fixed) subset of the pipe only changes via mass flux across its boundary and that mass flux is given by density times velocity. The second equation encodes that momentum changes due to its advection $\partial_x(\rho v^2)$, pressure gradients $\partial_x p$, friction forces exerted by the pipe walls $\rho v|v|$ and gravitational forces (if the elevation of the pipe changes). The last equation encodes balance of energy where we would like to mention that heat exchange between the gas and its surroundings is modelled via $T - T_{\mathsf{w}}$.

Depending on which model is chosen for the compressibility factor, one can resolve the equation of state according to the pressure p and insert it into the equations. The conservation or balance quantities in this system are the density ρ, the mass flux $\bar{q} = \rho v$, and the total energy $E = \rho(\frac{1}{2}v^2 + e)$.

In hyperbolic conservation and balance laws, information is transported in space-time along so-called characteristic curves, or characteristics for short, see [19] for details. There are three characteristics of the equations (TA1). Their speeds are given by the eigenvalues of the Jacobian matrix of the flux function, see [87, Table p. 347]. The eigenvalues are

$$\lambda_1 = v - c\,, \qquad \lambda_2 = v\,, \qquad \lambda_3 = v + c. \tag{2.1}$$

Here, c is the speed of sound. It is generally calculated from $c^2 = \frac{\partial p}{\partial \rho}$ (at constant entropy). In natural gas, it is about $340\,\mathrm{m\,s^{-1}}$. In the theory of hyperbolic conservation laws genuinely nonlinear and linearly degenerate characteristics are distinguished, see [19]. The first and third characteristic families of (TA1) are genuinely nonlinear, whereas the second characteristic family is linearly degenerate. In the linearly degenerate case, contact discontinuities occur. The characteristics are decisive for how or with which velocity information is transported in the gas and which boundary conditions may be set in which way, see [35] for more details.

In the following two sections, two parameters of the Euler equations will be explained in more detail: the compressibility factor z, which enters into the equation of state for

real gases, and the pipe friction coefficient λ on the right-hand side of the momentum equation.

2.2.1 The Equation of State for Real Gases and the Compressibility Factor

Recall the equation of state

$$p = R\rho T\mathsf{z}(p,T). \tag{2.2}$$

In the case of ideal gases, we have $\mathsf{z}(p,T) = 1$ and the equation simplifies to $p = R\rho T$. For real gases, the correction $\mathsf{z}(p,T)$ is not derived from first principles but instead inferred from experimental data. For low pressures and high temperatures, real gases behave approximately ideal. In Fig. 2.1, we plot the variation of the compressibility factor for a variety of pressures and temperatures. We assume the gas is mainly composed of Methane (90–95 %) and Ethane (2–6 %). For low pressures, we see that z approaches 1, i.e., the gas behaves in an approximately ideal fashion. The following model for the compressibility factor is used by the American Gas Association (AGA) (see AGA Report No. 8) and provides a good approximation for pressures up to 70 bar, see, for example, [4, 82]. It reads

$$\mathsf{z}(p,T) = 1 + 0.257\frac{p}{p_c} - 0.533\frac{pT_c}{p_cT}. \tag{2.3}$$

Here, p_c and T_c are the pseudocritical pressure and the pseudocritical temperature, respectively, which in turn depend on the mixture of the gas [4]. For isothermal equations, T is constant so that $\mathsf{z}(p,T) = \mathsf{z}(p)$. Another model to describe the compressibility factor is the formula of Papay [73], see also [82],

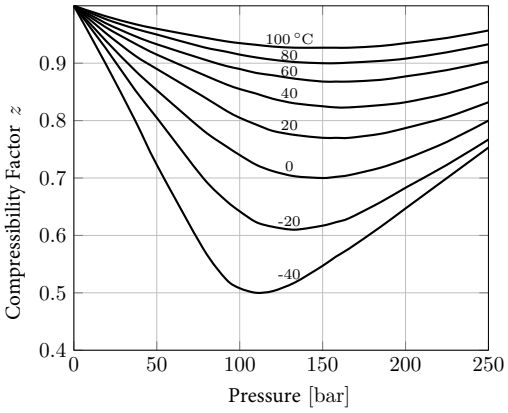


Fig. 2.1: Compressibility factor z of natural gas with standard density $\rho_0 = 0.776\,\mathrm{kg\,m^{-3}}$, according to [81].

$$z(p,T) = 1 - 3.52\frac{p}{p_c}\exp\left(-2.26\frac{T}{T_c}\right) + 0.274\left(\frac{p}{p_c}\right)^2\exp\left(-1.878\frac{T}{T_c}\right), \tag{2.4}$$

which provides good results up to a pressure of 150 bar. Thus, it has a larger range of validity than (2.3) but is harder to solve.

In [72], different equations of state are considered. Osiadacz and Chaczykowski conclude that the selection of the equation of state has only a minor influence on the result of the simulation. In contrast, the pipe friction coefficient, for which there are various calculation models, has a major influence [72].

2.2.2 The Pipe Friction Coefficient

The key parameters in the calculation of the pipe friction coefficient are the pipe roughness k and the Reynolds number Re. Pipe roughness is a measure of the small-scale irregularities or bumps on the inner surface of a pipe. These microscopic and sometimes visible surface features create friction as gas flows through the pipe, increasing resistance and causing pressure drop. Roughness is the average height of surface irregularities, measured from peak to valley on the inner pipe wall. A pipe is hydraulically smooth if the surface roughness has negligible effect on the frictional resistance, even in turbulent flow. It is technically rough if surface roughness and viscous effects significantly affect the friction and pressure loss. If the friction factor becomes independent of the Reynolds number and depends only on the relative roughness k/D of the pipe, the flow is fully rough, also known as hydraulically rough. The Reynolds number is a dimensionless quantity that predicts the flow regime, i.e., whether a fluid is laminar, transitional, or turbulent. It is calculated from

$$\mathrm{Re} = \frac{\rho v D}{\eta}. \tag{2.5}$$

The dynamic viscosity η depends on the type of fluid and is about 10^{-5} Pa s for natural gas [4].

For pipe flows, the (empirical) critical Reynolds number at which laminar flow starts to transit to an unstable flow is approximately 2300 [90]. If the pipe wall is smooth, it can be shown that the pipe friction depends only on the Reynolds number for both laminar and turbulent flow. However, if the pipe wall is fully rough (in fluid mechanical terms), the pipe friction coefficient λ depends only on the relative pipe roughness k/D. The dependence of the pipe friction coefficient on the pipe roughness and the Reynolds number is often shown in the so-called Moody diagram, see Fig. 2.2.

2.2.2.1 Laminar Flow

Below the critical Reynolds number Re_u, the flow is *laminar*, also called Hagen–Poiseuille flow. The velocity profile is parabolic for this flow, see Fig. 2.3. The pipe friction coefficient λ in this case is calculated from

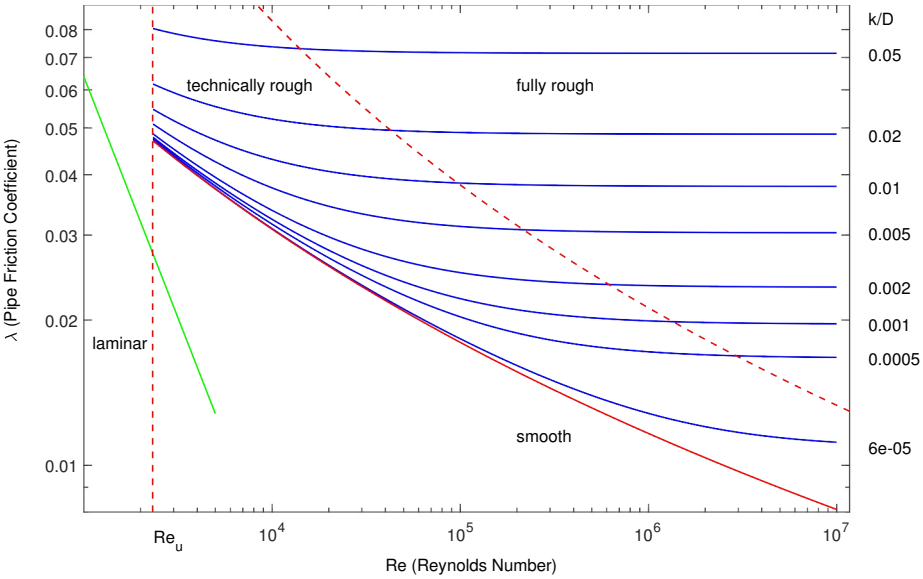


Fig. 2.2: A Moody diagram showing the friction factor as a function of Reynolds number and relative roughness for flow in circular pipes.

$$\lambda = \frac{64}{\mathrm{Re}}, \tag{2.6}$$

see [83, 90]. In the Moody diagram (Fig. 2.2), the pipe friction coefficient in the case of laminar flow is shown as a green line (curve on the far left).

2.2.2.2 Turbulent Flow

In *turbulent* flow, the velocity profile is significantly flattened because the layers flowing side by side constantly mix with each other (see Fig. 2.3). In this case, a distinction is made between hydraulically smooth, technically rough and fully rough pipes.

Hydraulically Smooth Pipe Here different models exist for the calculation of λ, e.g., the Blasius correlation

$$\lambda = (100\,\mathrm{Re})^{-\frac{1}{4}}, \tag{2.7}$$

which, however, is only suitable for Reynolds numbers smaller than 10^5. Further there is the the nonlinear model of Kármán–Prandtl[83]

$$\frac{1}{\sqrt{\lambda}} = 2\log_{10}(\mathrm{Re}\sqrt{\lambda}) - 0.8. \tag{2.8}$$

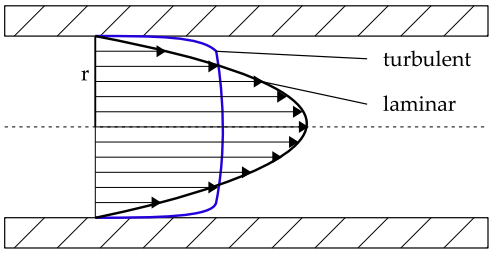


Fig. 2.3: Velocity profiles for laminar flow (parabolic, with maximum velocity at centerline) and turbulent flow (flatter profile with steeper wall gradient) in circular pipe flow.

This implicit formula is suitable for all Reynolds numbers in the turbulent range. The course of the curve is shown in a solid red line in the Moody diagram Fig. 2.2.

Technically Rough Pipe In the transition region between smooth and fully rough pipe wall, the law of Colebrook–White

$$\frac{1}{\sqrt{\lambda}} = -2\log_{10}\left(\frac{2.5226}{\mathrm{Re}\sqrt{\lambda}} + \frac{\frac{k}{D}}{3.7065}\right) \tag{2.9}$$

is generally used. The pipe friction coefficient is plotted in blue for different values of k/D in the Moody diagram (Fig. 2.2).

The formula of Chen [16] from 1979

$$\frac{1}{\sqrt{\lambda}} = -2\log_{10}\left(\frac{\frac{k}{D}}{3.7065} - \frac{5.0425}{\mathrm{Re}}\log_{10}\left[\frac{(\frac{k}{D})^{1.1098}}{2.8257} + \frac{5.8506}{\mathrm{Re}^{0.8981}}\right]\right) \tag{2.10}$$

is an explicit formula that matches the Colebrook–White formula very well, see Fig. 2.4. The values for λ from equation (2.10) are shown as light blue dotted lines.

Fully Rough Pipe For a fully rough pipe, the pipe friction coefficient depends only on the relative roughness. For this regime, the following formula is used, named after Prandtl, Kármán and Nikuradze:

$$\lambda = \left[1.14 - 2\log_{10}\left(\frac{k}{D}\right)\right]^{-2}. \tag{2.11}$$

This explicit formula is obtained by taking the limit of $\mathrm{Re} \to \infty$ in (2.9). The border between a technically and fully rough pipe is marked by a horizontal dashed line in the Moody diagram.

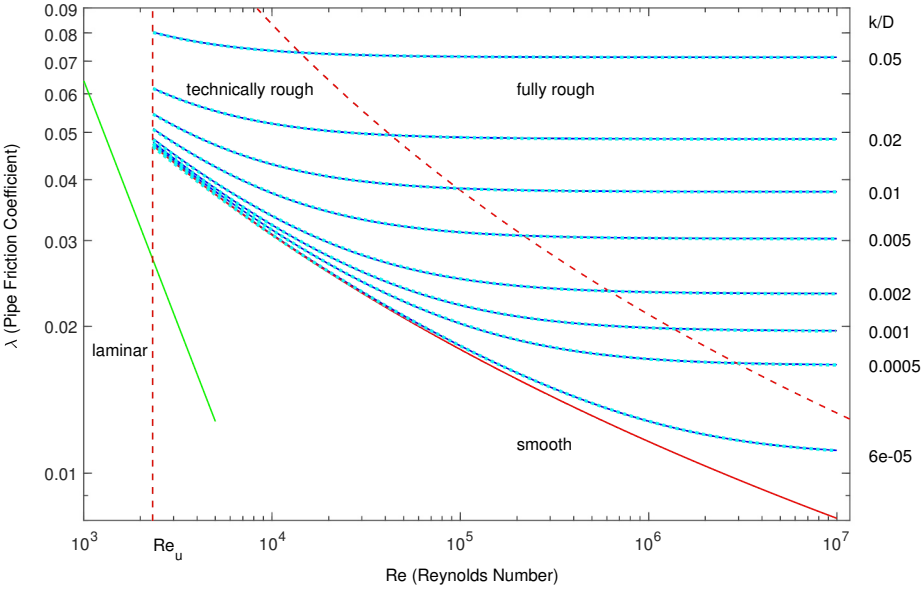


Fig. 2.4: A Moody diagram including Chen's formula

2.2.2.3 Explicit Formulas from Practice

Since implicit formulas for the calculation of the pipe friction coefficient were historically too elaborate, some simple explicit approximation formulas were established. In [83] a brief overview of approximate formulas from practice is given and partly their fields of application are described. We summarize some formulas in Table 2.1. In the Moody diagram in Fig. 2.5 the different formulas are plotted (except the formula of Spitzglass, because here $D = 1\,\mathrm{m}$ was used, so that the formula of Spitzglass is not applicable).

2.2.2.4 Summary

The gas flow model most widely accepted in practice is the Colebrook–White equation (2.9). This equation is applicable across the entire turbulent flow regime. All other formulas, particularly those from Sect. 2.2.2.3, are approximations valid only within relatively narrow ranges, see (2.5). On a double-logarithmic scale, these formulas appear only as tangents to the Colebrook–White model and only for specific parameter values. An exception is the explicit formula by Chen (2.10), which provides very accurate results throughout the entire turbulent range. Therefore, for turbulent flow, either the implicit Colebrook–White or Chen's explicit formula should be used.

Table 2.1: Empirical friction factor correlations for gas pipelines

Name	Correlation for λ	Validity/Application
Spitzglass (1912)	$\lambda = \frac{4(1+\frac{3.6}{D}+0.03\,D)}{354}$	Tubes with $D \leq 10.95$ in (27.8 cm) [83]
Weymouth (1912)	$\lambda = \frac{4}{(11.18\,D^{1/6})^2}$	Approx. $k \approx 0.005$ in fully rough regime, see Fig. 2.5.
Panhandle A	$\lambda = \frac{4}{(6.87\,\mathrm{Re}^{0.07305})^2}$	Small Reynolds numbers [83]
Panhandle B	$\lambda = \frac{4}{(16.49\,\mathrm{Re}^{0.01961})^2}$	Higher Reynolds numbers than Panhandle A; both below smooth-pipe curve in Fig. 2.5 [83]
IGT	$\lambda = \frac{4}{(4.619\,\mathrm{Re}^{0.1})^2}$	Hydraulically smooth pipes, Re $\approx 10^4$–10^7 [83]

2.3 Model Hierarchy for Isothermal euler Equations

In this section we present a model hierarchy for the isothermal case, i.e., we assume that $T = T_0$ is constant. Having a model hierarchy is important since it enables applicants to choose models that are appropriate for their use cases. In general, more complex models are more accurate and/or are applicable in a wider variety of flow regimes whereas

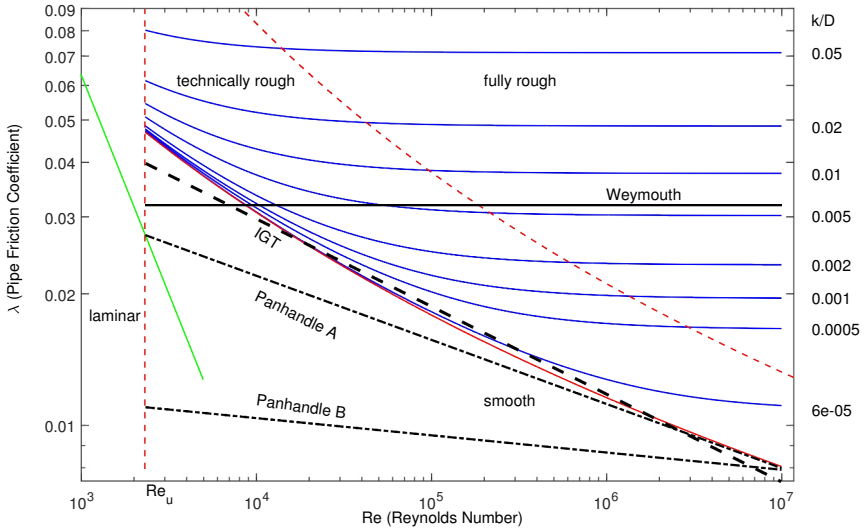


Fig. 2.5: A Moody diagram including formulas from practice

simpler models are easier to solve numerically. Thus a use case specific compromise between different targets is needed.

As discussed in [19], a constant temperature requires heat fluxes that immediately equilibrate temperature or in other words, the energy balance decouples from the rest of the equations and can only be used to determine the heat flux. Hence it is omitted from the PDE system. Since, in the isothermal case, the temperature is fixed, the compressibility factor is a function of only the pressure. The isothermal Euler equations are given by

$$\begin{aligned} \partial_t \rho + \partial_x(\rho v) &= 0, \\ \partial_t(\rho v) + \partial_x(p + \rho v^2) &= -\frac{\lambda}{2D}\rho v\,|v| - g\rho\partial_x b, \end{aligned} \tag{ISO1}$$

together with the equation of state $p = R\rho T\mathsf{z}(p)$ with $\mathsf{z}(p) = 1 + \alpha p$ as in (2.3) for fixed T. We denote this class of models by ISO as short for isothermal.

Here the eigenvalues of the Jacobian matrix of the flux function are $\lambda_1 = v - c$ and $\lambda_2 = v + c$. Thus, in the subsonic case ($|v| < c$) one always has one characteristic directed to the right and one characteristic directed to the left.

In the following, we present a sequence of increasingly simpler models going from the quasi-linear hyperbolic model (ISO1), to semilinear hyperbolic models, to a parabolic model and, finally, to an algebraic model.

2.3.1 Semilinear Equations

Throughout this section, we assume the compressibility factor $\mathsf{z}(p) = \mathsf{z}_0$ to be constant. The result is a constant speed of sound $c = \sqrt{p/\rho}$, and the term in the spatial derivative of the momentum equation can be transformed into

$$p + \rho v^2 = p\left(1 + \frac{v^2}{c^2}\right). \tag{2.12}$$

For small velocities $|v| \ll c$, Osiadacz [71] suggests to approximate the term in parentheses by 1. The method from [71] eliminates the nonlinearity on the left-hand side and results in a semilinear model that reads

$$\begin{aligned} \partial_t \rho + \partial_x(\rho v) &= 0, \\ \partial_t(\rho v) + \partial_x p &= -\frac{\lambda}{2D}\rho v\,|v| - g\rho\partial_x b. \end{aligned} \tag{ISO2}$$

In this model, the eigenvalues of the Jacobian matrix of the flux function are $\lambda_1 = -c$ and $\lambda_2 = c$, i.e., we have one negative and one positive characteristic velocity. Alternatively, one can assume that $\partial_x(\rho v^2)$ is small and continue to calculate with nonconstant z-factor. However, the resultant model is only semilinear if z is constant.

Another possibility to derive semilinear equations is to study small perturbations on a fast timescale around a constant density and velocity zero [11, Sect. 3.2.2], which

implicitly assumes $\partial_x b = 0$. To see this, we set

$$\tau = \frac{t}{\varepsilon}, \quad \rho(x,t) = \rho_0 + \varepsilon^\beta \rho_1\left(x, \frac{t}{\varepsilon}\right), \quad v(x,t) = \varepsilon^{\beta-1} w\left(x, \frac{t}{\varepsilon}\right) \tag{2.13}$$

with a small $\varepsilon > 0$ and $\varepsilon^\beta := D/\lambda$, $\beta > 0$. Then, we recover model (M1) from [11], which reads

$$\begin{aligned} \partial_\tau \rho_1 + \rho_0 \partial_x w &= 0, \\ \partial_\tau w + \frac{p'(\rho_0)}{\rho_0} \partial_x \rho_1 &= -\frac{w|w|}{2}, \end{aligned} \tag{ISO2F}$$

completed with the gas law $p(\rho) = \rho T_\mathsf{w} \mathsf{z}(\rho, T_\mathsf{w})$, where T_w is the wall temperature. We denote this model as ISO2F to stress its similarity to ISO2 and also to make it clear that it was derived based on studying fluctuations around a constant state. An advantage of (ISO2F) over (ISO2) is that it comes with an energy inequality, see Sect. 2.7.2.2. Introducing $\bar{q}_0 := \rho_0 w$ as a first-order approximation around ρ_0 to the mass flux, we may write

$$\begin{aligned} \partial_\tau \rho_1 + \partial_x \bar{q}_0 &= 0, \\ \partial_\tau \bar{q}_0 + p'(\rho_0) \partial_x \rho_1 &= -\frac{\bar{q}_0 |\bar{q}_0|}{2\rho_0}. \end{aligned} \tag{2.14}$$

This is a well-known model on the fast timescale.

2.3.2 Parabolic Equation

The next model that we present was derived from (ISO1) for the friction-dominated case in [11] using asymptotic expansions and denoted by (FD1) therein. The model is of nonlinear parabolic type and since it is isothermal, we denote it by ISO3. It reads

$$\begin{aligned} \partial_t \rho + \partial_x(\rho v) &= 0, \\ \partial_x p &= -\frac{\lambda}{2D} \rho v |v| - g\rho \partial_x b, \end{aligned} \tag{ISO3}$$

where, additionally, the gravitational force was neglected in the asymptotic consideration. The parabolic character of the pressure evolution can be made visible by equivalence transformations. With $\partial_x b = 0$ this results in

$$\partial_t p = \frac{1}{2}\sqrt{\frac{DRTz_0}{\lambda}} \partial_x \left(\frac{\partial_x p^2}{\sqrt{|\partial_x p^2|}} \right), \tag{ISO3P}$$

which is model (FD1b) from [11]. Typically, the pressure is then specified at both ends of the pipe. If one is interested in the velocity, it can be computed from $\partial_x p = -\frac{\lambda}{2D} \rho v |v|$

once the pressure is known. These types of models are also discussed in the gas literature [71]. These models and their numerical approximation were studied in [5, 85]. A rigorous derivation of (ISO3) as a low Mach and large friction limit of (ISO1) can be found in [23]. Optimal transport problems based on such PDE models can be formulated using a 3-Wasserstein distance, see [29].

2.3.3 Algebraic Equations

The model (ISO3) can be further simplified, to yield an algebraic equation, if we restrict our attention to stationary states. In the stationary case the time derivatives disappear. Neglecting gravity and using a constant compressibility factor $z = z_0$, the equations are

$$\begin{aligned} \partial_x(\rho v) &= 0, \\ \partial_x p &= -\frac{\lambda}{2D}\rho v\,|v|\,. \end{aligned} \tag{ISO4}$$

The mass flux ρv is thus constant in space and given by the boundary datum. Moreover, the second equation can be solved analytically for p with $\rho v\,|v| = \frac{c^2\rho v|\rho v|}{p}$, which yields

$$p(x) = \sqrt{p_{\text{in}}^2 - \frac{\lambda c^2 x}{D}\rho v\,|\rho v|}$$

and

$$p_{\text{out}} = \sqrt{p_{\text{in}}^2 - \frac{\lambda c^2 \ell}{D}\rho v\,|\rho v|}, \tag{ISO4-ALG}$$

respectively. Here ℓ is the length of the pipe with coordinate $x \in [0, \ell]$ and p_{in} and p_{out} are the inlet and outlet pressure, respectively. If the flow is now represented by the pressure difference in this case, the so-called Weymouth equation is obtained by solving for ρv.

Let us emphasize that while it is possible to also incorporate the effects of gravity, the analytic solution of the resulting Bernoulli differential equation is more involved. For this reason, we will not discuss this any further here.

The models presented here differ in each case by omitting individual terms or applying scaling arguments from [11]. In addition, simplified equations of state may be assumed. Fig. 2.6 gives a brief summary of the simplification steps.

2.4 Model Hierarchy for Temperature-Dependent Euler Equations

In this section we present a model hierarchy for the temperature-dependent models. We proceed as in the isothermal setting.

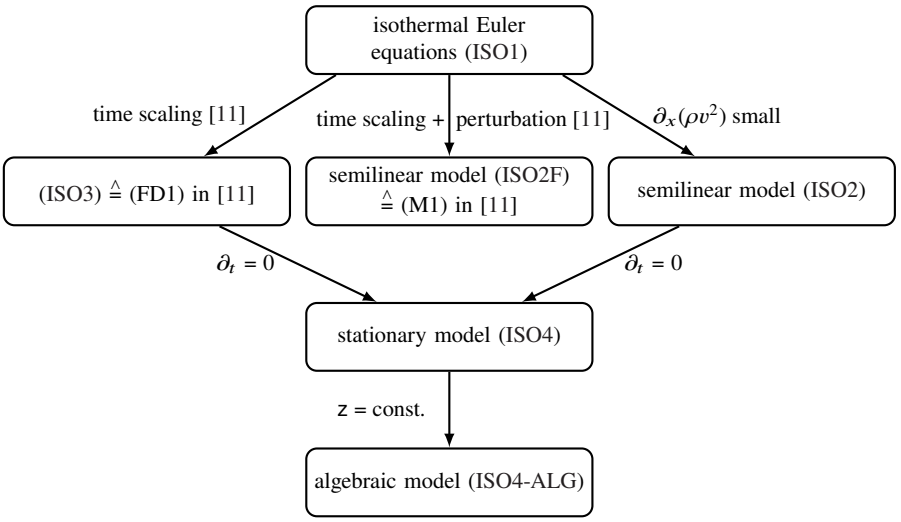


Fig. 2.6: Model hierarchy for the isothermal Euler equations

2.4.1 Simplified Nonlinear Equations

Starting from the full Euler equations (TA1), we derive a first simplified model, that should apply for flows with small velocities. To be precise, the simplifying assumption is that the temporal and spatial derivatives of ρv^2 and also ρv^3 are negligible. This results in the model

$$\begin{aligned} \partial_t \rho + \partial_x(\rho v) &= 0, \\ \partial_t(\rho v) + \partial_x p &= -\frac{\lambda}{2D}\rho v\,|v| - g\rho\partial_x b, \\ \partial_t\left(\rho e\right) + \partial_x\left(\rho v e + p v\right) &= -\frac{k_w}{D}\left(T - T_{\mathsf{w}}\right), \end{aligned} \tag{TA2}$$

together with the equation of state $p = R\rho T\mathsf{z}(p,T)$. In contrast to the isothermal case, the equation remains nonlinear when these terms are omitted. The total energy E is now given only by $E = \rho e$ (compared to $E = \rho e + \frac{1}{2}\rho v^2$ for the full equations), i.e., in the simplified model there is only inner energy, but no kinetic energy. Also, the equation of state continues to depend in a nonlinear way on p and T.

If we again follow the scaling approaches in [11] for the friction-dominated case, we obtain their model (ET3), which is of mixed hyperbolic-parabolic type. It reads as

$$\begin{aligned} \partial_t \rho + \partial_x(\rho v) &= 0, \\ \partial_x p &= -\frac{\lambda}{2D}\rho v\,|v| - g\rho\partial_x b, \\ \partial_t\left(\rho e\right) + \partial_x\left(\rho v e + p v\right) &= -\frac{k_w}{D}\left(T - T_{\mathsf{w}}\right). \end{aligned} \tag{TA3}$$

By (artificially) adding the term the term $\varepsilon\partial_t(\rho v)$ in the second equation the system can be made hyperbolic so that characteristics can be computed. In the limit case $\varepsilon \to 0$, the eigenvalues $\lambda_1 \to -\infty$, $\lambda_2 = v$ and $\lambda_3 \to \infty$ are obtained, i.e., one characteristic propagates depending on the flow direction and there is one characteristic to both left and right which has infinite propagation speed.

2.4.2 Stationary Model

As with the isothermal models, we can write down a steady state model. Neglecting gravity, the resulting equations are

$$\begin{aligned} \partial_x(\rho v) &= 0, \\ \partial_x p &= -\frac{\lambda}{2D}\rho v\,|v|\,, \\ \partial_x\left(\rho v e + p v\right) &= -\frac{k_w}{D}\left(T - T_{\mathsf{w}}\right). \end{aligned} \tag{TA4}$$

From the first equation it follows again that ρv is constant in space. However, since the more complex equation of state, with $\mathsf{z} = \mathsf{z}(p, T)$ nonlinear, applies here, the other two equations cannot directly be solved analytically. For this purpose, further simplifications may have to be assumed, such as a constant compressibility factor. If one assumes that the compressibility factor is constant, the speed of sound c is also constant and $c^2 = p/\rho$ holds. The energy equation can then be simplified using $e = c_V T$ to

$$\partial_x\left(\rho v(c_V T + c^2)\right) = -\frac{k_w}{D}\left(T - T_{\mathsf{w}}\right), \tag{2.15}$$

and since ρv is constant in space, we obtain

$$\partial_x T = -\frac{k_w}{D c_V \rho v}\left(T - T_{\mathsf{w}}\right). \tag{2.16}$$

The complete equations are thus given by

$$\begin{aligned} \partial_x(\rho v) &= 0, \\ \partial_x p &= -\frac{\lambda c^2}{2Dp}\rho v\,|\rho v|\,, \\ \partial_x T &= -\frac{k_w}{D c_V \rho v}\left(T - T_{\mathsf{w}}\right). \end{aligned} \tag{TA4b}$$

The exact solution of the energy equation is

$$T(x) = (T(x_0) - T_{\mathsf{w}})e^{-\frac{k_w}{D c_V \rho v}(x - x_0)} + T_{\mathsf{w}}, \tag{2.17}$$

and the overall system reads (with $x_0 = 0$ and $x = \ell$)

$$\begin{aligned} \rho v &= \text{const.}, \\ p_{\text{out}} &= \sqrt{p_{\text{in}}^2 - \frac{\lambda c^2 \ell}{D} \rho v \, |\rho v|}, \\ T_{\text{out}} &= (T_{\text{in}} - T_{\mathsf{w}}) e^{-\frac{k_{\mathsf{w}}}{D c_V \rho v} \ell} + T_{\mathsf{w}}. \end{aligned} \tag{TA4-ALG}$$

Similar to the situation in the isothermal case, incorporating gravity complicates the analytic solution of the resulting differential equation and will not be discussed any further here.

The previously discussed simplification steps are visualized as a model hierarchy in Fig. 2.7.

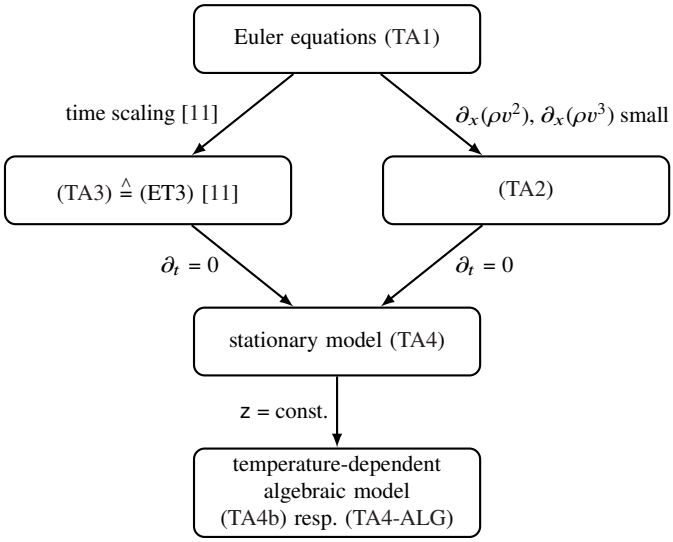


Fig. 2.7: Model hierarchy for the temperature-dependent Euler equations

2.5 Energy-Based Coupling Conditions

In this section, we discuss the specification of suitable coupling conditions between multiple pipes on a network, using the example of the isothermal Euler equations (ISO1). It also ensures that the involved energies in the network are conserved. Such energy conservation will subsequently be the starting point for a structural energy-based modeling concept by means of port-Hamiltonian systems [93], see also Sect. 2.7. Throughout this section, we mostly follow the exposition in [22, 24]. Let us also refer to the earlier

contributions [69, 79], which discuss coupling conditions that yield well-posed Riemann problems. Moreover, entropy-preserving coupling conditions for polytropic Euler equations as in (TA1) are discussed in [67, Sect. 3.1], see also [55] for the Euler system.

For the sake of simplicity, we will not specify the required function spaces and assumptions that are needed to carry out all manipulations. While the derivations should therefore be understood formally only, we refer to the previously mentioned references for more details.

2.5.1 Network Topology

The network topology can be described by a directed and weakly connected graph $G = (\mathcal{V}, \mathcal{E})$ with vertices $\mathcal{V} = \{v_1, v_2, \dots, v_V\}$ and edges $\mathcal{E} = \{e_1, e_2, \dots, e_E\}$ where $V = |\mathcal{V}|$ and $E = |\mathcal{E}|$ denote the cardinalities of the sets $\mathcal{V}$ and $\mathcal{E}$. Each edge $(v_{\text{in}}, v_{\text{out}})$ is assumed to have different incident vertices $v_{\text{in}} \neq v_{\text{out}}$. All edges incident to some vertex $v \in \mathcal{V}$ are collected in the set $\mathcal{E}(v)$.

For each edge $e = (v_{\text{in}}, v_{\text{out}})$ with the vertex v_{in} and the vertex v_{out}, see Fig. 2.9, we define

$$n^e(v) = \begin{cases} -1 & \text{if } v = v_{\text{in}}, \\ +1 & \text{if } v = v_{\text{out}}, \\ 0 & \text{if } v \in \mathcal{V} \backslash \{v_{\text{in}}, v_{\text{out}}\}. \end{cases} \tag{2.18}$$

Note that the indices "in" and "out" are properties of the directed graph and do not have anything to do with a flow direction.

For the assignment of the vertices v_{in} and v_{out} of each edge to the vertices $\mathcal{V}$, we further introduce the incidence matrices $A_{\text{in}}, A_{\text{out}} \in \mathbb{R}^{V \times E}$ with

$$(A_{\text{in}})_{ij} = \begin{cases} -1 & \text{if vertex } v_i = v_{\text{in}} \text{ of edge } e_j, \\ 0 & \text{else}, \end{cases} \tag{2.19}$$

$$(A_{\text{out}})_{ij} = \begin{cases} +1 & \text{if vertex } v_i = v_{\text{out}} \text{ of edge } e_j, \\ 0 & \text{else}. \end{cases} \tag{2.20}$$

In the following, denoting by A the cross sectional area of the pipe network, which is assumed to be spatially constant on each pipe, we denote the mass flow by

$$q = A\bar{q} = A\rho v. \tag{2.21}$$

To distinguish those quantities in the following we refer to q as mass flow and to $\bar{q}$ as mass flux.

For a given flow q defined on each edge, and for each vertex $v \in \mathcal{V}$, we further introduce

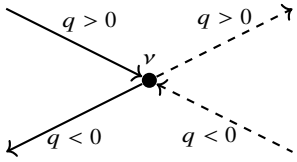


Fig. 2.8: Illustration of the in- and out-flows of a vertex v. The edges in $\mathcal{E}_{\text{in}}(v, q)$ with an inflow into v are marked solid together with the signs of the flows. Similarly, the edges in $\mathcal{E}_{\text{out}}(v, q)$ are marked dashed. Arrows represent the orientation of the edges in the graph.

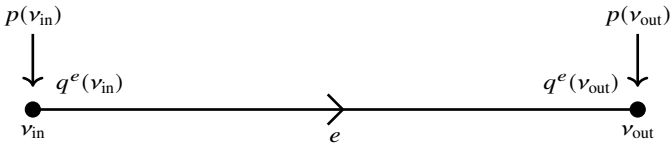


Fig. 2.9: Flows $q^e(v_{\text{in}})$ and $q^e(v_{\text{out}})$ as well as pressures $p(v_{\text{in}})$ and $p(v_{\text{out}})$ at the vertices v_{in} and v_{out} of an oriented edge e. Note that a positive flow value $q^e(v_{\text{in}})$ corresponds to a flow from v_{in} to v_{out} at vertex v_{in} whereas a negative flow value $q^e(v_{\text{in}})$ corresponds to a flow directed to v_{in} from v_{out} at vertex v_{in}.

$$\begin{aligned} \mathcal{E}_{\text{in}}(v, q) &:= \{e \in \mathcal{E}(v) \colon n^e(v) q^e(v) \geq 0\}, \\ \mathcal{E}_{\text{out}}(v, q) &:= \{e \in \mathcal{E}(v) \colon n^e(v) q^e(v) < 0\}. \end{aligned} \tag{2.22}$$

Thus, $\mathcal{E}_{\text{in}}(v, q)$ and $\mathcal{E}_{\text{out}}(v, q)$ are the sets of edges for which the gas flows into and out of vertex v, respectively, i.e., these sets depend on the flow directions and "in" and "out" are understood from a nodal perspective, see Fig. 2.8 for an illustration. Note that this notation fixes an orientation for each component and $q^e > 0$ corresponds to flow from v_{in} to v_{out} and $q^e < 0$ corresponds to flow from v_{out} to v_{in}, see Fig. 2.9.

2.5.2 Coupling Conditions for (ISO1)

We first revisit the model (ISO1) on a single pipe of length ℓ to isolate the essential momentum and pressure effects without additional geometric or topological complications. This single-pipe formulation serves as a reference problem from which the junction conditions are derived and later generalized to the full gas network. Moreover, we replace the momentum equation by an evolution equation for the flow velocity v as in [24, Appendix A]. Starting from the equations

$$\begin{aligned} \partial_t \rho + \partial_x(\rho v) &= 0 \\ \partial_t(\rho v) + \partial_x(p + \rho v^2) &= -\frac{\lambda}{2D} \rho v |v| - g \rho \partial_x b, \end{aligned}$$

using the product rule in the momentum equation in combination with the first equation we obtain

$$\begin{aligned}\partial_t v &= -\frac{1}{\rho}(v\partial_t\rho + \partial_x(p+\rho v^2) + \frac{\lambda}{2D}\rho v|v| + g\rho\partial_x b)\\ &= -\frac{1}{\rho}(-v\partial_x(\rho v) + \partial_x(p+\rho v^2) + \frac{\lambda}{2D}\rho v|v| + g\rho\partial_x b)\\ &= -\frac{1}{\rho}(\partial_x p + \rho v\partial_x v + \frac{\lambda}{2D}\rho v|v| + g\rho\partial_x b) = -\frac{1}{\rho}\partial_x p - \frac{1}{2}\partial_x v^2 - \frac{\lambda}{2D}v|v| - g\partial_x b.\end{aligned}$$

If we define the pressure potential $P(\rho) = \rho\int_1^\rho \frac{p(s)}{s^2}\,\mathrm{d}s$, it holds that

$$\partial_x P'(\rho) = \partial_x\left(\frac{p(\rho)}{\rho} + \int_1^\rho \frac{p(s)}{s^2}\,\mathrm{d}s\right) = -\frac{p(\rho)}{\rho^2}\partial_x\rho + \frac{\partial_x p(\rho)}{\rho} + \frac{p(\rho)}{\rho^2}\partial_x\rho = \frac{1}{\rho}\partial_x p(\rho).$$

Hence, we obtain an equation for the evolution of the velocity of the form

$$\partial_t v + \partial_x\left(\frac{v^2}{2} + P'(\rho) + gb\right) = -\frac{\lambda}{2D}|v|v.$$

Altogether, this leads to the following set of equations

$$\begin{aligned}\partial_t\rho + \partial_x\bar{q} &= 0,\\ \partial_t v + \partial_x h &= -\gamma|v|v,\end{aligned} \tag{2.23}$$

for the velocity v, the mass flux $\bar{q} = \rho v$ and *total specific enthalpy* $h := \frac{1}{2}v^2 + P'(\rho) + gb$ and $\gamma := \frac{\lambda}{2D}$. Moreover, we have the relation $\rho P''(\rho) = p'(\rho)$. Recall that A denotes the pipe diameter and $q = A\rho v$ is the mass flow.

For the set of equations (2.23) we may define an *energy functional*

$$\mathcal{H}(\rho, v) := \int_0^\ell A\Big(\frac{1}{2}\rho v^2 + P(\rho) + g\rho b\Big)\,\mathrm{d}x \tag{2.24}$$

and interpret (ρ, v) and (h, q) as state and co-state variables which are related via the *variational derivative*

$$\mathcal{H}' := (\delta_\rho\mathcal{H}(\rho, v), \delta_v\mathcal{H}(\rho, v)) = (Ah, q), \tag{2.25}$$

If we assume that (ρ, v) satisfies (2.23), formally we obtain

$$\begin{aligned}\frac{\mathrm{d}}{\mathrm{d}t}\mathcal{H} &= \langle\delta_\rho\mathcal{H}, \partial_t\rho\rangle + \langle\delta_v\mathcal{H}, \partial_t v\rangle = \langle Ah, -\partial_x\bar{q}\rangle + \langle q, -\partial_x h - \gamma|v|v\rangle\\ &= -\langle h, \partial_x q\rangle + \langle\partial_x q, h\rangle - qh|_0^\ell - \gamma\langle q, v|v|\rangle = -qh|_0^\ell - \mathcal{R}(\rho, v),\end{aligned} \tag{2.26}$$

where $\mathcal{R}(\rho, v) = \int_0^\ell A\gamma\rho|v|^3\,\mathrm{d}x \geq 0$ for all $\rho \geq 0$ and $\langle\cdot,\cdot\rangle$ denotes the L^2 scalar product. Therefore, we conclude that the system energy changes only due to dissipation (friction)

and energy flow across the boundary. In particular, we obtain a *dissipation inequality* of the form

$$\frac{\mathrm{d}}{\mathrm{d}t}\mathcal{H} \leq h(\ell)q(\ell) - h(0)q(0). \tag{2.27}$$

Let us now turn to gas transport problems on pipe networks. All edges of the network-describing graph $G = (\mathcal{V}, \mathcal{E})$ correspond to pipes and are identified by spatial intervals $(0, \ell_e)$ for $e \in \mathcal{E}$. Using the notation in Sect. 2.5.1, the spatial values 0 and ℓ_e of an edge belong to the vertex v_{in} and the vertex v_{out} of the edge. Similarly, as in (2.23) on each pipe $e \in \mathcal{E}$, we consider

$$\partial_t \rho^e + \partial_x \bar{q}^e = 0, \tag{2.28}$$
$$\partial_t v^e + \partial_x h^e = -\gamma^e |v^e| v^e, \tag{2.29}$$

on $(0, \ell^e)$ and for $t > 0$. Here, $\bar{q}^e$ and h^e denote mass flux and specific enthalpy for the individual pipes, i.e.,

$$\bar{q}^e = \rho^e v^e, \quad h^e = \frac{1}{2}(v^e)^2 + P'(\rho^e) + gb.$$

Let us now discuss coupling and boundary conditions, which ensure energy consistency. We generalize the exposition in [79] by allowing more flexibility in the sense that at each vertex either mass flow q^v or the enthalpy h^v can be prescribed, while the other results from the model. A thermodynamically consistent behavior at pipe junctions can be guaranteed by requiring mass conservation

$$q^v + \sum_{e \in \mathcal{E}(v)} q^e(v) n^e(v) = 0 \quad \text{for any } v \in \mathcal{V}, \qquad q^e = A^e \bar{q}^e \tag{2.30}$$

and continuity of enthalpy, i.e., for each $v \in \mathcal{V}$ there exists h^v such that

$$h^e(v) = h^v \quad \text{for any } e \in \mathcal{E}(v). \tag{2.31}$$

Together these condition also imply conservation of energy at the vertices.

While equation (2.30) is used throughout the literature, alternatives to equation (2.31) are commonly considered. A frequently considered choice is continuity of pressure

$$p^e(v) = p^v \quad \text{for any } v \in \mathcal{V}, e \in \mathcal{E}(v), \tag{2.32}$$

while continuity of momentum flux

$$\frac{(\bar{q}^e(v))^2}{\rho^e(v)} + p^e(v) = f^v \quad \text{for any } v \in \mathcal{V}, e \in \mathcal{E}(v), \tag{2.33}$$

with an external force f^v is used less frequently. It was shown in [80] that if either (2.32) or (2.33) is used at a vertex with more than one adjacent edge, and at which $\bar{q}^v$ is prescribed, then energy can be created at these vertices in certain flow regimes. It should be noted that all these coupling conditions coincide for zero velocity, and hence

their difference is rather small if the fluid velocity is very small compared to the speed of sound which is typical for flows in gas networks.

Building on (2.24), it seems reasonable to define the total energy of the network as

$$\mathcal{H}(\rho, v) := \sum_{e\in\mathcal{E}} \int_0^{\ell^e} \frac{1}{2}\rho^e (v^e)^2 + P(\rho^e) + g\rho^e b \,\mathrm{d}x. \tag{2.34}$$

Utilizing similar arguments as for a single pipe, one can easily show that

$$\frac{\mathrm{d}}{\mathrm{d}t}\mathcal{H} = \sum_{v\in\mathcal{V}} h^v q^v - \mathcal{R}(\rho, v), \tag{2.35}$$

where the energy dissipation is $\mathcal{R}(\rho, v) = \sum_{e\in\mathcal{E}} \int_0^{\ell^e} A^e \gamma^e \rho^e |v^e|^3 \mathrm{d}x \geq 0$ as long as $\rho^e \geq 0$. We conclude that the change of energy is completely determined by the energy flow across the boundary and potential dissipation due to friction within the pipes. We can thus summarize our findings as follows.

- The equations can be formulated in a specific structure with states and co-states that are related via variational derivatives of an energy functional.
- If no external energy is fed into the system, energy can at most decrease or dissipate.
- Extending the modeling from a single pipe to a network of pipes canonically leads to the total energy being the sum of the individual energies on the pipes.

2.5.3 Coupling Conditions for (TA1)

To derive coupling conditions for (TA1), we follow the discussion in [67] and in [76]. As in Sect. 2.5.2, also for the full one-dimensional Euler equations one would require conservation of mass

$$q^v + \sum_{e\in\mathcal{E}(v)} q^e(v) n^e(v) = 0 \text{ for any } v \in \mathcal{V}, \quad q^e = A^e \bar{q}^e \tag{2.36}$$

and continuity of enthalpy

$$h^e(v) = h^v \text{ for any } v \in \mathcal{V}, e \in \mathcal{E}(v), \tag{2.37}$$

where it is important to note that for the non-isobaric case the enthalpy is given by

$$h^e = \frac{(v^e)^2}{2} + \frac{p^e}{\rho^e} + e^e - T_{\mathrm{w}} s^e. \tag{2.38}$$

Here, s^e is the specific entropy and e^e is the inner energy. In case of an ideal gas the latter is given by $s^e = c_V \ln\left(\frac{p^e}{(\rho^e)^\xi}\right)$ where c_V is the heat capacity at constant volume and ξ is the adiabatic index. Since the full Euler equations have one more family of characteristics than the isothermal ones and the additional family moves with the fluid

velocity, we need one set of coupling conditions that only applies to pipes and vertices for which the gas flows into the pipe at this vertex. Here it is important to note that if q^v is positive, i.e., gas is fed into the network, then also a specific entropy s^v of that gas needs to be prescribed. Using the notation introduced in Sect. 2.5.1, we set

$$s^e(v) = \frac{\max\{q^v, 0\} s^v + \sum_{e \in \mathcal{E}_{\text{in}}(v,q)} q^e(v) s^e(v) n^e(v)}{\max\{q^v, 0\} + \sum_{e \in \mathcal{E}_{\text{in}}(v,q)} q^e(v) n^e(v)} \quad \text{for any } v \in \mathcal{V}, e \in \mathcal{E}_{\text{out}}(v, q). \tag{2.39}$$

This encodes perfect "mixing" of the entropy. This condition ensures energy conservation and entropy conservation at junctions [76, Lem. 3.19]. The fact that s^v can be prescribed if and only if $q^v > 0$ reflects the fact that there is one characteristic field in (TA1), which moves with the fluid velocity.

2.6 Mixture Models

In this section we consider extensions of the models (ISO1) and (ISO3) to binary mixtures. There are two different types: models with one mixture velocity, and others with individual velocity functions for each constituent. Furthermore, we review which pressure laws lead to thermodynamically consistent models as discussed in [9].

2.6.1 Balance Laws

In the modeling of (isothermal) fluid mixtures, two classes of models can be distinguished. In [9], one (mixture) velocity models are referred to as *Class I models* and models containing one velocity per constituent are called *Class II models*.

Before presenting the models let us note that we shall use a mass density ρ_1 of constituent 1 that is to be understood as the mass of constituent 1 per mixture volume. We proceed analogously for ρ_2. Throughout this section we will discuss binary mixtures. Mixtures with more than two constituents can be handled analogously. Here, we discuss the extension from the (ISO1) model for a single component to the case of two components.

Let us now present two versions of isothermal Class I models for inviscid, compressible and non-reacting constituents. The following version showcases conservation of mass for each constituent as well as conservation of momentum

$$\partial_t \rho_1 + \partial_x(\rho_1 v) = 0, \tag{2.40a}$$

$$\partial_t \rho_2 + \partial_x(\rho_2 v) = 0, \tag{2.40b}$$

$$\begin{aligned} \partial_t((\rho_1 + \rho_2)v) + \partial_x\left((\rho_1 + \rho_2)v^2 + p(\rho_1, \rho_2)\right) = &-\frac{\lambda}{2D}(\rho_1 + \rho_2)|v|v \\ &-g(\rho_1 + \rho_2)\partial_x b, \end{aligned} \tag{2.40c}$$

where v is the common gas velocity, $p = p(\rho_1, \rho_2)$ is a constitutive function relating the pressure to the densities, and the other parameters are as before. Specific choices of constitutive relations for the pressure are discussed in Sect. 2.6.2 below.

Let us present a reformulation of (2.40) that showcases conservation of total mass and advection of (molar) concentrations. We employ the change of variables for the total density $\rho := \rho_1 + \rho_2$, and the molar fraction of component 1 given by

$$\mu := \frac{n_1}{n_1 + n_2}. \tag{2.41}$$

Here $n_i = \rho_i / M_i$ denotes the number of moles of constituent i in a certain volume of the mixture, and M_i is the given molar mass of constituent i.

Then, we can rewrite system (2.40) as

$$\partial_t \rho + \partial_x(\rho v) = 0, \tag{2.42a}$$

$$\partial_t \mu + v \partial_x(\mu) = 0, \tag{2.42b}$$

$$\partial_t(\rho v) + \partial_x(\rho v^2 + \widehat{p}(\rho, \mu)) = -\frac{\lambda}{2D} \rho |v| v - g\, \rho \partial_x b, \tag{2.42c}$$

for some transformed pressure function $\widehat{p}(\rho, \mu)$.

In case of isothermal Class II models there is conservation of mass as well as balance of momentum for each constituent: The model in [9, Equation (101)] in the isothermal case extended by global friction forces F_i acting on component $i = 1, 2$, reads

$$\partial_t \rho_1 + \partial_x(\rho_1 v_1) = 0, \tag{2.43a}$$

$$\partial_t \rho_2 + \partial_x(\rho_2 v_2) = 0, \tag{2.43b}$$

$$\partial_t v_1 + v_1 \partial_x v_1 + \partial_x(\partial_{\rho_1} P) = -f \rho_2 (v_1 - v_2) - \gamma F_1(v_1, v_2) - g \partial_x b, \tag{2.43c}$$

$$\partial_t v_2 + v_2 \partial_x v_2 + \partial_x(\partial_{\rho_2} P) = -f \rho_1 (v_2 - v_1) - \gamma F_2(v_1, v_2) - g \partial_x b. \tag{2.43d}$$

Here $P = P(\rho_1, \rho_2)$ is a given energy and $\gamma := \frac{\lambda}{2D}$. It remains to discuss how p is connected to some pressure terms, see Sect. 2.6.2 below. In [9], the authors assume that f is a function of ρ_1, ρ_2 which is a "friction factor" for the relative friction between the two components. Friction between the constituents is modeled in such a way that it does not change the total momentum.

2.6.2 Pressure Laws and Energy Balance

In (2.42), a constitutive relation for the pressure has to be chosen, whereas in (2.43), the question arises in what sense the terms involving the energy P are related to pressure terms.

The thermodynamic pressure is defined as

$$p = -P + \sum_{i=1}^{2} \rho_i \partial_{\rho_i}(P) \tag{2.44}$$

for $P = P(\rho_1, \rho_2) = \rho\psi(\rho_1, \rho_2)$, where ψ is the Helmholtz free energy, see [9, Equation (64)]. Note that (2.44) implies

$$\partial_x p = \rho_1 \partial_x(\partial_{\rho_1} P) + \rho_2 \partial_x(\partial_{\rho_2} P). \tag{2.45}$$

For temperatures above the critical temperatures of all mixture components, the energy P has to be convex in (ρ_1, ρ_2). As a consequence, stability of the mixture is guaranteed in this regime. Note that for both natural gas and hydrogen under typical pipeline flow conditions, this condition is satisfied. Therefore, assuming convexity of P is both physically justified and crucial for stability.

2.6.2.1 Pressure Laws Based on Free Energies for One-Velocity Models

For given free Helmholtz energy ψ or given energy $P(\rho_1, \rho_2)$ by (2.44) the pressure law for Class I models is fully determined. The resulting equations (2.40) and (2.44) correspond to the isothermal case of a Class I mixture model in [9].

By choosing a suitable energy $P(\rho_1, \rho_2) = \rho\psi(\rho_1, \rho_2)$, the following pressure laws fit into this framework:

1. Pressure laws only depending on the total density

$$p = p(\rho) = p(\rho_1 + \rho_2). \tag{2.46}$$

   For such pressures, the model reduces to the model for a single component and one of the mass conservation equations may be dropped. Such pressures result from the free energy $\psi = \psi(\rho)$ as $p(\rho) = \rho^2 \partial_\rho \psi(\rho)$. This family includes the case of an ideal gas.
2. Simple mixtures are mixtures with pressure laws of the form

$$p(\rho_1, \rho_2) = p_1(\rho_1) + p_2(\rho_2). \tag{2.47}$$

   This results from an energy P of the form

$$P(\rho_1, \rho_2) = P_1(\rho_1) + P_2(\rho_2).$$

   Then, one has $p = p_1(\rho_1) + p_2(\rho_2)$ for $p_i(\rho_i) := -P_i(\rho_i) + \rho_i P_i'(\rho_i)$ and $i = 1, 2$.

2.6.2.2 Mixing at the Speed of Sound for One-Velocity Models

One popular approach for prescribing pressure laws is based on the speed of sound in a mixture of gases, see [59, 88]. We shall see that it yields a pressure law which is a special case of the one for a simple mixture in (2.47).

The following ansatz is based on the speed of sound

$$\begin{aligned} p &= c(\mu)^2\rho, \\ c(\mu)^2 &= \frac{RT}{M(\mu)} \text{ with } M(\mu) \coloneqq \mu M_1 + (1-\mu)M_2, \end{aligned} \tag{2.48}$$

for given molar mass M_i of constituent i. Furthermore, $\rho = \rho_1 + \rho_2$ is the total density, and $\mu = \mu(\rho_1, \rho_2)$ as in (2.41) is the molar fraction of component 1. The pressure law (2.48) can be rewritten as

$$p(\rho_1, \rho_2) = RT\left(\frac{\rho_1}{M_1} + \frac{\rho_2}{M_2}\right). \tag{2.49}$$

Thus, it is evident that this represents a simple fluid with convex energy

$$P(\rho_1, \rho_2) = RT\left(\frac{1}{M_1}\rho_1 \log(\rho_1) + \frac{1}{M_2}\rho_2 \log(\rho_2)\right).$$

2.6.2.3 Pressure Laws Based on Free Energies for Two-Velocity Models

For the two-velocity model (2.43), thermodynamic consistency is ensured by writing the equations in terms of the energy P. Under the assumption that the mixture is simple, i.e., the energy is of the form $P(\rho_1, \rho_2) = P_1(\rho_1) + P_2(\rho_2)$ one can define the partial pressures $p_i(\rho_i) = -P_i + \rho_i \partial_{\rho_i}(P_i)$ satisfying

$$\frac{1}{\rho_i}\partial_x p_i = \partial_x(\partial_{\rho_i} P). \tag{2.50}$$

2.6.3 Coupling Conditions for ISO1 Based Mixture Models

Coupling conditions for Class I mixture models (2.42) based on (ISO1) are very similar to those for (TA1), see Sect. 2.5.3. This is due to the fact that compared to ISO1 for both models there is one additional family of characteristics moving with the fluid velocity. Similar to the coupling conditions in the temperature-dependent case, at each vertex v a mass flow q^v or an enthalpy h^v can be prescribed. In addition, if a mass flow into the network occurs, i.e., $q^v > 0$, then also a composition c_i^v can be prescribed that specifies which fraction of the mass flowing into the network is constituent i. Obviously, the sum of the c_i^v at each vertex needs to be one. The q^v, h^v and c^v that are not prescribed are part of the solution of the networked problem.

An obvious coupling condition at each inner vertex is conservation of mass for each species, i.e.,

$$q^v c_i^v + \sum_{e \in \mathcal{E}(v)} A^e \rho_i^e(v) v^e(v) n^e(v) = 0 \qquad \text{for } i \in \{1,2\} \text{ and all } v \in \mathcal{V}, \tag{2.51}$$

with notation as in Sect. 2.5.1. Conservation of energy at vertices is guaranteed if we prescribe continuity of enthalpy, which in this setting is given by

$$\frac{1}{\rho}\sum_{i=1}^{2}\left(\rho_i \partial_{\rho_i} P\right) + \frac{1}{2}v^2, \tag{2.52}$$

where P denotes the energy and $\rho = \rho_1 + \rho_2$.

The conditions in (2.51) and (2.52) are not sufficiently many. Since currently it is not clear what the right choice of coupling conditions is, let us describe a plausible choice, which provides the correct number of conditions. It is to combine continuity of (2.52) and conservation of total mass at vertices, i.e., the equation we get from summing (2.51) over i, with perfect mixing for each species

$$\frac{\rho_i^{e'}(v)}{\rho^{e'}(v)} = \frac{\max\{q^v, 0\}c_i^v + \sum_{e\in\mathcal{E}_{\text{in}}(v,q)} A^e \rho_i^e(v) v^e(v) n^e(v)}{\max\{q^v, 0\} + \sum_{e\in\mathcal{E}_{\text{in}}(v,q)} A^e \rho^e(v) v^e(v) n^e(v)} \quad \text{for any } i \in \{1,2\} \tag{2.53}$$

for $v \in \mathcal{V}$ and $e' \in \mathcal{E}_{\text{out}}(v,q)$, see [48]. Note that if we combine (2.53) with total mass conservation, this implies the conservation of mass for each species (2.51).

One may also introduce coupling conditions for Class II mixture models (2.43). Conservation of mass for each species (2.51) seems obvious, and it appears meaningful to choose the remaining conditions such that mechanical energy is conserved (or dissipated). The way to achieve energy conservation is continuity of the enthalpies

$$\partial_{\rho_i} P + \frac{1}{2}v_i^2 \qquad \text{for } i \in \{1,2\}, \tag{2.54}$$

at the vertices. A more detailed discussion can be found in Chap. 3, "Gas Mixtures on Networks: Modeling, Simulation and Optimization".

With this choice the correct number of coupling conditions is achieved. The numerical simulations presented in Chap. 3, "Gas Mixtures on Networks: Modeling, Simulation and Optimization" suggest that on a single pipe it depends on the choice of the boundary conditions whether stationary solutions to the Class II model converge to stationary solutions to the Class I model as $f \to \infty$. On networks, we observe consistency of the coupling conditions in the sense that stationary solutions to the Class II model converge to stationary solutions to the Class I model as $f \to \infty$ if we prescribe pressures on outflow vertices and mass flows on inflow vertices. This is consistent with our observations in the single pipe case. In the case of networks, there are boundary layers so that the observed convergence is not pointwise. Rigorous results are missing to date.

2.6.4 Low Mach High Friction Limit

In resemblance to the limit taking (ISO1) to (ISO3) we formally derive some limiting models for the mixture models of Class I (2.40) and for the mixture model of Class II (2.43).

Indeed, we want to take the limit $\varepsilon \to 0$ in the following formulation for (ρ_1, ρ_2, v) of a generalization of (2.40)

$$\partial_t \rho_1 + \partial_x(\rho_1 v) = 0, \tag{2.55a}$$
$$\partial_t \rho_2 + \partial_x(\rho_2 v) = 0, \tag{2.55b}$$
$$\varepsilon \partial_t v + \varepsilon v \partial_x v + \frac{1}{\rho}\partial_x p = -\gamma |v| v - g \partial_x b. \tag{2.55c}$$

Formally, for (ρ_1, ρ_2) with $p = p(\rho_1, \rho_2)$ and $\rho = \rho_1 + \rho_2$ we obtain the following system

$$\partial_t \rho_i - \partial_x \left(\frac{\rho_i}{\sqrt{\gamma}} \frac{\rho^{-1}\partial_x p + g \partial_x b}{\sqrt{\left|\rho^{-1}\partial_x p + g \partial_x b\right|}} \right) = 0 \qquad \text{for } i = 1, 2 \tag{2.56}$$

if $\alpha = 3$ in (2.55). For linear friction, i.e., $\alpha = 2$ in (2.55), we obtain

$$\partial_t \rho_i - \frac{1}{\gamma}\partial_x \left(\rho_i (\rho^{-1}\partial_x p + g \partial_x b) \right) = 0 \qquad \text{for } i = 1, 2. \tag{2.57}$$

The latter can be rewritten as the gradient flow

$$\partial_t \overline{\rho} - \partial_x (M(\overline{\rho}) \partial_x (\nabla_{\overline{\rho}} E)) = 0 \tag{2.58}$$

for the density vector $\overline{\rho} = (\rho_1, \rho_2)^\top$ and $E = P + g\rho b$. The mobility matrix $M = M(\rho)$ is symmetric and has entries $M_{i,j} = \frac{\rho_i \rho_j}{\gamma \rho}$ and $i = 1, 2$.

Analogously, for linear friction in (2.43) meaning that $F_i(v_1, v_2) = v_i$, the limit $\varepsilon \to 0$ in

$$\begin{aligned}
\partial_t \rho_1 + \partial_x(\rho_1 v_1) &= 0, \\
\partial_t \rho_2 + \partial_x(\rho_2 v_2) &= 0, \\
\varepsilon \partial_t v_1 + \varepsilon v_1 \partial_x v_1 + \partial_x(\partial_{\rho_1} P) &= -f\rho_2(v_1 - v_2) - \gamma v_1 - g\partial_x b, \\
\varepsilon \partial_t v_2 + \varepsilon v_2 \partial_x v_2 + \partial_x(\partial_{\rho_2} P) &= -f\rho_1(v_2 - v_1) - \gamma v_2 - g\partial_x b,
\end{aligned}$$

with $\overline{\rho} = (\rho_1, \rho_2)^\top$ formally leads to the gradient flow

$$\partial_t \overline{\rho} - \partial_x \left(M(\overline{\rho}) \partial_x (\nabla_{\overline{\rho}} E) \right) = 0 \tag{2.59}$$

with symmetric mobility matrix

$$M(\overline{\rho}) = \frac{1}{\gamma(f\rho + \gamma)} \begin{pmatrix} f\rho_1^2 + \gamma\rho_1 & f\rho_1\rho_2 \\ f\rho_1\rho_2 & f\rho_2^2 + \gamma\rho_2 \end{pmatrix}. \tag{2.60}$$

2.7 Port-Hamiltonian Model Formulations

In Sect. 2.5, we have seen that solutions of (ISO1) dissipate energy and suitable coupling conditions at pipe junctions make the coupling energy conservative. These properties can very easily be seen when (ISO1) is considered in terms of density and velocity. In addition, the total energy of the network is just the sum of the energies of the individual pipes. It is well-known, see, e.g., [93, 95], that from a control theoretic perspective, properties such as dissipativity and passivity, respectively, are intimately related to the special class of *port-Hamiltonian (pH) systems*. In particular, if the modeling is done by means of an adequately chosen *storage function*, dissipativity properties and the existence of a monotonically decreasing Lyapunov function candidate are ensured automatically. In the linear case, computing possible storage functions is linked to the so-called Kalman–Yakubovich–Popov matrix inequality, see [97, 98] for more details.

In the following, we will briefly introduce port-Hamiltonian systems, recapitulate their most important structural properties and consequences thereof as well as connect them to some of the equations introduced in the beginning of this catalogue. Subsequently, we provide several port-Hamiltonian model formulations for some of the (simplified) Euler equations of the non-stationary model hierarchy presented in Sect. 2.3. We consider models for one constituent and also discuss mixture models.

Let us emphasize that we will not consider the most general class of port-Hamiltonian systems, neither on a finite nor an infinite-dimensional level. In particular, we will mostly omit detailed derivations verifying the required structural assumptions. For a more detailed discussion together with the appropriate functional analytic framework, we refer to [65, 68, 93].

2.7.1 The Abstract Setting

To present the abstract setting of port-Hamiltonian system models, on the time interval $[0, T]$ we consider a dynamic state $z\colon [0, T] \to \mathbb{R}^n$ described by a system of controlled differential equations of the form

$$\partial_t z = (J(z) - R(z))\nabla\mathcal{H}(z) + B(z)u, \quad z(0) = z_0, \tag{2.61}$$

where $J, R\colon \mathbb{R}^n \to \mathbb{R}^{n\times n}, \mathcal{H} \in C^1(\mathbb{R}^n, \mathbb{R})$ with gradient $\nabla\mathcal{H} \in C(\mathbb{R}^n, \mathbb{R}^n)$ and $B \in \mathbb{R}^{n\times m}$. Assume further that (2.61) is complemented by an output equation, e.g., modeling a measuring device, of the form

$$y = B(z)^\top \nabla\mathcal{H}(z). \tag{2.62}$$

We call the system described by (2.61) and (2.62) a *port-Hamiltonian system (pH)* if

- $J(z) = -J(z)^\top$ for all $z \in \mathbb{R}^n$,
- $R(z) = R(z)^\top \succeq 0$ for all $z \in \mathbb{R}^n$.

Here, for a matrix $A \in \mathbb{R}^{n,n}$ we write $A \succeq 0$ if $x^\top Ax \geq 0$ for all $x \in \mathbb{R}^n$. The matrices J and R are sometimes called *structure* and *dissipation matrix*, while $\mathcal{H}$ is typically referred to as a *Hamiltonian* or *storage* function, often representing energy. The *port matrix* B resembles the possibility to interact with the dynamics via a control $u\colon [0,T] \to \mathbb{R}^m$. Let us note that, in contrast to classical control theory, the role of u is often to be understood rather as a specific kind of coupling matrix which allows to distribute energy from one pH-system to another one, see also the subsequent discussion below.

Due to the particular structure of pH systems, for the Hamiltonian function $\mathcal{H}$, we immediately obtain that

$$\frac{\mathrm{d}}{\mathrm{d}t}\mathcal{H}(z(t)) = \nabla\mathcal{H}(z(t))^\top \partial_t z = -\nabla\mathcal{H}(z(t))^\top R(z(t))\nabla\mathcal{H}(z(t)) + y(t)^\top u(t) \tag{2.63}$$

where we have used skew symmetry of J and the output relation (2.62). In the sequel we may refer to $\nabla\mathcal{H}(z)$ as the co-state of the system. Equation (2.63) obviously is reminiscent of (2.26). In particular, since R is positive semi-definite, as in (2.27), we have a *dissipation inequality* of the form

$$\frac{\mathrm{d}}{\mathrm{d}t}\mathcal{H}(z(t)) \leq y^\top u, \tag{2.64}$$

where we may interpret the term $y^\top u$ as the energy introduced into the system. In the context of pH-systems, the latter inequality is often defined to be *dissipative with respect to the supply rate* $s(y,u) = y^\top u$, see [97,98]. Of course, by simple integration of (2.63) we directly arrive at the so-called *energy balance equation*

$$\mathcal{H}(z(t_1)) - \mathcal{H}(z(t_0)) = \int_{t_0}^{t_1} \Big(-\nabla\mathcal{H}(z(t))^\top R(z(t))\nabla\mathcal{H}(z(t)) + y(t)^\top u(t)\Big)\,\mathrm{d}t. \tag{2.65}$$

As a consequence of the previous relations, the Hamiltonian $\mathcal{H}$ defines a Lyapunov function and the system is automatically *passive*, cf. [92].

Another interesting property is that two pH-systems are structurally invariant under interconnected feedback relation. More specifically, for $i = 1, 2$, consider the dynamics $z^{(i)}$ given by

$$\partial_t z_i = (J_i(z_i) - R_i(z_i))\nabla\mathcal{H}_i(z_i) + B_i(z_i)u_i, \quad z_i(0) = z_{i,0}, \tag{2.66}$$

$$y_i = B_i(z_i)^\top \nabla\mathcal{H}_i(z_i). \tag{2.67}$$

Let us further assume that u_i and y_i satisfy the following linear affine coupling relations

$$u_1 = -y_2 + v_1, \quad u_2 = y_1 + v_2, \tag{2.68}$$

where v_1, v_2 are additional external inputs. Defining an *accumulated* Hamiltonian function via

$$\mathcal{H}(z_1, z_2) \coloneqq \mathcal{H}_1(z_1) + \mathcal{H}_2(z_2),$$

we can rewrite the coupled system as follows

$$\begin{pmatrix}\partial_t z_1\\ \partial_t z_2\end{pmatrix} = \left(\begin{pmatrix} J_1 & -B_1B_2^\top\\ B_2B_1^\top & J_2\end{pmatrix} - \begin{pmatrix} R_1 & 0\\ 0 & R_2\end{pmatrix}\right)\begin{pmatrix}\nabla\mathcal{H}_1\\ \nabla\mathcal{H}_2\end{pmatrix} + \begin{pmatrix} B_1 & 0\\ 0 & B_2\end{pmatrix}\begin{pmatrix} v_1\\ v_2\end{pmatrix}.$$

Finally, if we define a new output of the coupled system via

$$\begin{pmatrix}\widehat{y}_1\\ \widehat{y}_2\end{pmatrix} = \begin{pmatrix} B_1^\top & 0\\ 0 & B_2^\top\end{pmatrix}\begin{pmatrix}\nabla\mathcal{H}_1\\ \nabla\mathcal{H}_2\end{pmatrix},$$

then the overall system is in port-Hamiltonian form. We recognize that this property resembles the behavior of the energy consistent coupling discussed for (ISO1) in Sect. 2.5. Constitutive relations more general than (2.68) are possible provided that the semidefiniteness property of the dissipation operator is preserved within the coupling process, see [65].

At least on a formal level, if $z\colon [0,T] \to X$ maps to an infinite-dimensional state space X, it seems natural to replace (uncontrolled) formulations of the form (2.61) by

$$\partial_t z = (\mathcal{J}(z) - \mathcal{R}(z))\mathcal{H}'(z) + \mathcal{B}(z)u \tag{2.69}$$

where $\mathcal{J}(z) = -\mathcal{J}(z)^*, \mathcal{R}(z) = \mathcal{R}(z)^* \succeq 0$ are formally skew- and self-adjoint (nonnegative) linear operators and $\mathcal{H}'(z)$ denotes the derivative of an abstract energy functional $\mathcal{H}$. The term $\mathcal{B}(z)u$ models an external input to the system, e.g., boundary conditions. In the context of port-Hamiltonian systems the assumed control affine structure is a common assumption. Note that this model class does not generally include all boundary conditions which are necessary for the system to be well-posed. In particular, the class does not provide a formalism that reveals the required constraints. Similarly, by replacing the Euclidean inner product by duality pairings, analogue versions of (2.63), the dissipation inequality (2.64) and the energy balance equation (2.65) can be derived. In contrast to the finite-dimensional case, this typically requires a careful choice of the state space. Let us note that in some cases, instead of (2.69) it is more convenient to use the following descriptor formulation

$$\mathcal{E}(z)\partial_t z = (\mathcal{J}(z) - \mathcal{R}(z))e(z) + \mathcal{B}(z)u, \tag{2.70}$$

where in addition to $\mathcal{J}(z) = -\mathcal{J}(z)^*, \mathcal{R}(z) = \mathcal{R}(z)^* \succeq 0$ it holds that $\mathcal{H}'(z) = \mathcal{E}^*(z)e(z)$. In particular, we still obtain a dissipation inequality since

$$\begin{aligned}\frac{\mathrm{d}}{\mathrm{d}t}\mathcal{H}(z) &= \langle \mathcal{H}'(z), \partial_t z\rangle = \langle e(z), \mathcal{E}(z)\partial_t z\rangle\\ &= -\langle e(z), \mathcal{R}(z)e(z)\rangle + \langle \mathcal{B}(z)^* e(z), u\rangle \le \langle \mathcal{B}(z)^* e(z), u\rangle.\end{aligned}$$

In the context of port-Hamiltonian modeling, the term $\mathcal{B}(z)^*e(z)$ is typically referred to as the collocated output y to u, and the term $\langle y, u\rangle$ has the physical interpretation of the supplied energy. In the next chapter, we will provide examples of both formulations (2.69) and (2.70), respectively. Approaches exploiting such dissipative Hamiltonian structures have been discussed in, e.g., [23, 24, 94]. For a detailed discus-

sion on more general infinite-dimensional port-Hamiltonian descriptor systems from a bounded operator point of view, we refer to [68]. When the operators in (2.69) are unbounded, rigorous definitions for port-Hamiltonian systems so far have been limited to the case of linear dynamics related to a strongly continuous semigroup. A rather complete treatment of a specific class of first-order PDEs can be found in [47]. More recently, in [75] the authors provide a new port-Hamiltonian definition for the class of well-posed linear systems which is motivated by the theory of system vertices.

Another approach to model port-Hamiltonian systems was recently presented in [34]. For infinite-dimensions, the formulation (2.69) is then replaced by the weak formulation

$$\langle \partial_t z,\ \phi \rangle_{X',X} = j(\mathcal{H}'(z), \phi) - r(\mathcal{H}'(z), \phi) + s(\cdot, \mathcal{H}'(z), \phi), \tag{2.71}$$

where X is a Banach space, $\phi \in X$ is a test function and $j, r \colon X \times X \to \mathbb{R}$ and $s \colon [0,T] \times X \times X \to \mathbb{R}$ are linear and Lipschitz in their last argument. We assume that the state space X embeds continuously into a Hilbert space Z with inner product $\langle \cdot, \cdot \rangle$. In (2.71), j models conservative processes, r models dissipative processes, and s models source terms, such as, e.g., boundary controls. The functions j and r are assumed to satisfy $j(v,v) = 0$ and $r(v,v) \geq 0$ for all $v \in X$. Similar to the situation before, the properties of j and r then ensure that the energy balance equation

$$\mathcal{H}(z(t_1)) - \mathcal{H}(z(t_0)) = \int_{t_0}^{t_1} -r(\mathcal{H}'(z), \mathcal{H}'(z)) + s(t, \mathcal{H}'(z), \mathcal{H}'(z))\, \mathrm{d}t \tag{2.72}$$

is satisfied. In contrast to (2.69), the action of j and r on $\mathcal{H}'$ may be nonlinear. Furthermore, this modeling directly incorporates the weak form and can be advantageous in situations where the operators (2.69) exhibit singularities, see [34, Remark 2.4]. For finite-dimensional systems, one may omit the test function in (2.71) to obtain

$$\partial_t z = \widetilde{j}(\mathcal{H}'(z)) - \widetilde{r}(\mathcal{H}'(z)) + \widetilde{s}(\cdot, \mathcal{H}'(z)), \tag{2.73}$$

where $\widetilde{j}, \widetilde{r} \colon \mathbb{R}^n \to \mathbb{R}^n$ and $\widetilde{s} \colon [0,T] \times \mathbb{R}^n \to \mathbb{R}^n$ satisfy $\widetilde{j}(v)^\top v = 0$ and $\widetilde{r}(v)^\top v \geq 0$ for all $v \in \mathbb{R}^n$. Again, an energy balance equation of the form (2.72) is available.

Having the abstract framework established, in the next sections we provide port-Hamiltonian model formulations for some of the systems used in gas network modeling.

2.7.2 Isothermal Model Hierarchy

In this section we present a port-Hamiltonian formulation of the model hierarchy for isothermal Euler equations.

2.7.2.1 Isothermal Euler Equations (ISO1)

Let us recall (ISO1) which reads as

$$\partial_t \rho + \partial_x(\rho v) = 0,$$
$$\partial_t(\rho v) + \partial_x(p + \rho v^2) = -\frac{\lambda}{2D}\rho v|v| - \rho g \partial_x b.$$

In the following, we assume the pressure potential to be defined by $P(\rho) = \rho \int_1^\rho \frac{p(s)}{s^2}\,\mathrm{d}s$. As shown with the derivations from Sect. 2.5, the previous dynamics can also be expressed as

$$\partial_t \rho + \partial_x \bar{q} = 0,$$
$$\partial_t v + \partial_x h = -\gamma|v|v,$$

where $\bar{q} = \rho v$, $h = \frac{1}{2}v^2 + P'(\rho) + gb$ and $\rho P''(\rho) = p'(\rho)$.

For the sake of simplicity we assume that the cross section area is $A = 1$ throughout the remaining section. In this case the energy functional is given by

$$\mathcal{H}(\rho, v) = \int_0^\ell \frac{1}{2}\rho v^2 + P(\rho) + \rho g b \,\mathrm{d}x$$

and satisfies $\mathcal{H}' = (h, \bar{q})$. Consequently, we arrive at

$$\partial_t z = \partial_t \begin{pmatrix}\rho \\ v\end{pmatrix} = (\mathcal{J} - \mathcal{R}(z))\mathcal{H}'(z) + \mathcal{B}(z)u = \left(\begin{pmatrix}0 & -\partial_x \\ -\partial_x & 0\end{pmatrix} - \begin{pmatrix}0 & 0 \\ 0 & \gamma\frac{|v|}{\rho}\end{pmatrix}\right)\begin{pmatrix}h \\ \bar{q}\end{pmatrix} + \mathcal{B}(z)u,$$

which is a port-Hamiltonian formulation as in (2.69). As before, the term $\mathcal{B}(z)u$ corresponds to external inputs such as boundary conditions. Alternatively, we may represent the dynamics in the form (2.70) by considering

$$\begin{aligned}\mathcal{E}(z)\partial_t z = \begin{pmatrix}1 & 0 \\ 0 & \rho\end{pmatrix}\partial_t \begin{pmatrix}\rho \\ v\end{pmatrix} &= (\mathcal{J}(z) - \mathcal{R}(z))e(z) + \mathcal{B}(z)u \\ &= \left(\begin{pmatrix}0 & -\partial_x(\rho\,\cdot) \\ -\rho\partial_x & 0\end{pmatrix} - \begin{pmatrix}0 & 0 \\ 0 & \gamma\rho|v|\end{pmatrix}\right)\begin{pmatrix}h \\ v\end{pmatrix} + \mathcal{B}(z)u,\end{aligned}$$

where we indeed have

$$\mathcal{E}^*(z)e(z) = \begin{pmatrix}1 & 0 \\ 0 & \rho\end{pmatrix}\begin{pmatrix}h \\ v\end{pmatrix} = \mathcal{H}'(z)$$

For this example, it thus seems to be convenient to work with (2.69) rather than (2.70) as in the former case, the operators $\mathcal{E}$ and $\mathcal{J}$ are constant.

To represent the system in the form (2.71), we multiply (2.23) by smooth test functions ϕ and ψ and integrate over $[0, \ell]$ to arrive at

$$\begin{aligned}\int_0^\ell \phi\partial_t\rho + \psi\partial_t v \,\mathrm{d}x &= \int_0^\ell -\phi\partial_x\bar{q} - \psi\partial_x h - \psi\gamma|v|v \,\mathrm{d}x \\ &= \int_0^\ell -\phi\partial_x\bar{q} + (\partial_x\psi)h - \psi\gamma|v|v \,\mathrm{d}x + h(\cdot,0)\psi(0) - h(\cdot,\ell)\psi(\ell).\end{aligned}$$

Note that v can be expressed in terms of h and q if the subsonic condition $p'(\rho) > \frac{\bar{q}^2}{\rho^2}$ is satisfied, since then with $\rho P''(\rho) = p'(\rho)$ also $\frac{\partial}{\partial\rho} h = P''(\rho) - \frac{\bar{q}^2}{\rho^3} > 0$ holds. In this case, with $v = v(h, \bar{q})$ we can consider

$$\begin{aligned} j((h,\bar{q}),(\phi,\psi)) &:= \int_0^\ell -\phi\partial_x\bar{q} + h\partial_x\psi \,\mathrm{d}x, \\ r((h,\bar{q}),(\phi,\psi)) &:= \gamma \int_0^\ell |v|v\psi \,\mathrm{d}x, \\ s(\cdot,(h,\bar{q}),(\phi,\psi)) &:= h(\cdot,0)\psi(0) - h(\cdot,\ell)\psi(\ell) \end{aligned} \tag{2.74}$$

to arrive at a port-Hamiltonian formulation of (2.23) in the form (2.71).

2.7.2.2 Semilinear Model (ISO2F)

The model (ISO2F) admits a port-Hamiltonian structure, not with respect to the original Hamiltonian but with respect to a quadratic Hamiltonian that can viewed as an approximation of the original Hamiltonian, see the discussion from Section 2.3.1. We have

$$\partial_t \begin{pmatrix} \rho_1 \\ w \end{pmatrix} = \left(\begin{pmatrix} 0 & -\partial_x \\ -\partial_x & 0 \end{pmatrix} - \begin{pmatrix} 0 & 0 \\ 0 & \frac{|w|}{2\rho_0} \end{pmatrix} \right) \begin{pmatrix} \frac{p'(\rho_0)}{\rho_0}\rho_1 \\ \rho_0 w \end{pmatrix} + \mathcal{B}(z)u, \tag{2.75}$$

and therefore

$$\partial_t z = (\mathcal{J} - \mathcal{R}(z))\mathcal{H}'(z) + \mathcal{B}(z)u, \quad \mathcal{H}(z) = \frac{1}{2}\int_0^\ell \frac{p'(\rho_0)}{\rho_0}\rho_1^2 + \rho_0 w^2 \,\mathrm{d}x, \tag{2.76}$$

with $z = (\rho_1, w)^\top$. Here, as before, the term $\mathcal{B}(z)u$ represents an external control input such as, e.g., boundary conditions.

To represent the system in the form (2.71), first note that $\mathcal{H}'(z) = (\frac{p'(\rho_0)}{\rho_0}\rho_1, q_0)$, where $\bar{q}_0 = \rho_0 w$ is the first-order approximation around ρ_0 to the mass flux. Multiplying (ISO2F) by smooth test functions ϕ and ψ and integrating over $[0, \ell]$, analogously to the ISO1 case, we obtain

$$\begin{aligned} j\left(\left(\frac{p'(\rho_0)}{\rho_0}\rho_1, \bar{q}_0\right),(\phi,\psi)\right) &:= \int_0^\ell -\phi\partial_x\bar{q}_0 + \frac{p'(\rho_0)}{\rho_0}\rho_1\partial_x\psi \,\mathrm{d}x, \\ r\left(\left(\frac{p'(\rho_0)}{\rho_0}\rho_1, \bar{q}_0\right),(\phi,\psi)\right) &:= \frac{1}{2}\int_0^\ell |w|w\psi \,\mathrm{d}x, \\ s\left(\cdot,\left(\frac{p'(\rho_0)}{\rho_0}\rho_1, \bar{q}_0\right),(\phi,\psi)\right) &:= (\frac{p'(\rho_0)}{\rho_0}\rho_1)(\cdot,0)\psi(0) - (\frac{p'(\rho_0)}{\rho_0}\rho_1)(\cdot,\ell)\psi(\ell). \end{aligned} \tag{2.77}$$

2.7.2.3 The Friction-Dominated Model (ISO3)

Recall the friction-dominated model (ISO3), which reads as

$$\begin{aligned}\partial_t \rho + \partial_x(\rho v) &= 0,\\ \partial_x p &= -\gamma \rho v\,|v| - g\rho\partial_x b.\end{aligned}$$

We can equivalently consider

$$\begin{aligned}\mathcal{E}\partial_t z &= \begin{pmatrix}1 & 0\\ 0 & 0\end{pmatrix}\partial_t \begin{pmatrix}\rho\\ v\end{pmatrix} = (\mathcal{J} - \mathcal{R}(z))e(z) + \mathcal{B}(z)u\\ &= \left(\begin{pmatrix}0 & -\partial_x\\ -\partial_x & 0\end{pmatrix} - \begin{pmatrix}0 & 0\\ 0 & \gamma|v|\end{pmatrix}\right)\begin{pmatrix}gb + P'(\rho)\\ \rho v\end{pmatrix} + \mathcal{B}(z)u,\end{aligned}$$

such that for $\mathcal{H}(z) = \int_0^\ell \rho g b + P(\rho)\,\mathrm{d}x$ we have $\mathcal{H}'(z) = (gb + P'(\rho), 0) = \mathcal{E}^* e(z)$.

Since the formulation (2.71) does not model algebraic equations, we refrain from writing the model in weak form.

2.7.3 The Euler Equations (TA1)

To derive a port-Hamiltonian formulation of the 1D Euler equations, recall (TA1), which can be written as

$$\begin{aligned}\partial_t \rho + \partial_x(\rho v) &= 0,\\ \partial_t(\rho v) + \partial_x(p + \rho v^2) &= -\frac{\lambda}{2D}\rho v\,|v| - g\rho\partial_x b,\\ \partial_t E + \partial_x((E + p)v) &= -\frac{k_w}{D}(T - T_{\mathsf{w}}),\end{aligned} \tag{2.78}$$

together with the equation of state for real gases $p = R\rho T\mathsf{z}(\rho, T)$, for $x \in \mathcal{I} = [0, \ell]$ and $t \in \mathcal{T}$, where $\ell < \infty$ is the length of the pipe and $\mathcal{T} \subseteq \mathbb{R}$ is the time interval. As mentioned before, the variable $E = \rho(\frac{1}{2}v^2 + gb + c_V T)$ is the total energy density, where c_V is the specific heat. The first, second and third differential equation represent conservation of mass and balance of momentum and energy, respectively. The system is associated with the Hamiltonian

$$\mathcal{H}(z) = \int_0^\ell \frac{1}{2}\rho v^2 + \rho g b + c_V T\rho\,\mathrm{d}x$$

for $z = (\rho, v, T)$, which satisfies

$$\mathcal{H}'(z) = \begin{pmatrix}\frac{1}{2}v^2 + gb + c_V T\\ \rho v\\ c_V\rho\end{pmatrix} =: \begin{pmatrix}\eta\\ \bar{q}\\ c_V\rho\end{pmatrix}.$$

In the following we present port-Hamiltonian formulations (2.70), (2.69) and (2.71) of (2.78).

We can rewrite the equations with respect to the state variables $z = (\rho, v, T)$:

$$\partial_t \rho + \partial_x(\rho v) = 0, \tag{2.79a}$$

$$\rho \partial_t v + \rho \partial_x \left(\frac{1}{2} v^2 + gb \right) + p_x + \frac{\lambda}{2D} \rho v \, |v| = 0, \tag{2.79b}$$

$$c_V \rho \partial_t T + c_V \rho v T_x + p v_x - \frac{\lambda}{2D} \rho v^2 \, |v| + \frac{k_w}{D} (T - T_{\mathsf{w}}) = 0. \tag{2.79c}$$

and express this as

$$\mathcal{E}(z) \partial_t z = (\mathcal{J}(z) - \mathcal{R}(z)) e(z) + \mathcal{B}_w T_{\mathsf{w}} + \mathcal{B}(z) u, \tag{2.80}$$

where

$$\mathcal{E}(z) = \begin{pmatrix} 1 & 0 & 0 \\ 0 & \rho & 0 \\ 0 & 0 & c_V \rho \end{pmatrix}, \quad e(z) = \begin{pmatrix} \frac{1}{2} v^2 + gb + c_V T \\ v \\ 1 \end{pmatrix}, \quad \mathcal{R}(z) = \begin{pmatrix} 0 & 0 & 0 \\ 0 & 0 & 0 \\ 0 & 0 & \frac{k_w}{D} \end{pmatrix}, \quad \mathcal{B}_w = \begin{pmatrix} 0 \\ 0 \\ \frac{k_w}{D} \end{pmatrix},$$

$$\mathcal{J}(z) = \begin{pmatrix} 0 & -\partial_x(\rho \cdot) & 0 \\ -\rho \partial_x & 0 & -\partial_x(p \cdot) - \frac{\lambda}{2D} \rho v \, |v| + c_V \rho T_x \\ 0 & -p \partial_x + \frac{\lambda}{2D} \rho v \, |v| - c_V \rho T_x & 0 \end{pmatrix}$$

and $\mathcal{B}(z)u$ models external inputs such as boundary conditions. It is easy to see that indeed $\mathcal{E}(z)^* e(z) = \mathcal{H}'(z)$, and hence we have a reformulation of the form (2.70). Comparing with the port-Hamiltonian formulation for (ISO1), we see that the operator $\mathcal{J}$ contains friction terms in the off-diagonal blocks.

To obtain a formulation of the form (2.69) we start by dividing the second and third equation by ρ and $c_V \rho$, respectively, and we arrive at the system

$$\partial_t \rho + \partial_x(\rho v) = 0, \tag{2.81a}$$

$$\partial_t v + \partial_x \left(\frac{1}{2} v^2 + g \right) + \rho^{-1} p_x + \frac{\lambda}{2D} v \, |v| = 0, \tag{2.81b}$$

$$\partial_t T + v \partial_x T + \frac{1}{c_V} \rho^{-1} p \partial_x v - \frac{\lambda}{2 D c_V} v^2 \, |v| + \frac{k_w}{D c_V \rho} (T - T_{\mathsf{w}}) = 0, \tag{2.81c}$$

which in port-Hamiltonian form reads as

$$\partial_t z = (\mathcal{J}(z) - \mathcal{R}(z)) \mathcal{H}'(z) + \mathcal{B}_w(z) T_{\mathsf{w}} + \mathcal{B}(z) u \tag{2.82}$$

with

$$\mathcal{J}(z) = \begin{pmatrix} 0 & -\partial_x & 0 \\ -\partial_x & 0 & \mathcal{J}_{23}(z) \\ 0 & \mathcal{J}_{32}(z) & 0 \end{pmatrix},$$
$$\mathcal{J}_{23}(z) = -\frac{1}{\rho c_V}\partial_x(\frac{p}{\rho}\cdot) - \frac{\lambda}{2Dc_V\rho}v|v| + \frac{1}{\rho}(\partial_x T),$$
$$\mathcal{J}_{32}(z) = -\frac{p}{c_V\rho}\partial_x(\frac{1}{\rho}\cdot) + \frac{\lambda}{2Dc_V\rho}v|v| - \frac{1}{\rho}(\partial_x T),$$
$$\mathcal{R}(z) = \begin{pmatrix} 0 & 0 & 0 \\ 0 & 0 & 0 \\ 0 & 0 & \frac{k_w}{Dc_V^2\rho^2}T \end{pmatrix}, \quad \mathcal{B}_w(z) = \begin{pmatrix} 0 \\ 0 \\ \frac{k_w}{Dc_V\rho} \end{pmatrix}.$$

To represent the system in the form (2.71), we multiply (2.82) by smooth test functions ϕ, ψ and φ and integrate over $[0, \ell]$ to arrive at

$$\begin{aligned}
&\int_0^\ell \phi\partial_t\rho + \psi\partial_t v + \varphi\partial_t T \,\mathrm{d}x \\
&= \int_0^\ell -\phi\partial_x\bar{q} \\
&\quad - \psi\left(\partial_x\eta + \rho^{-1}\partial_x p + \frac{\lambda}{2D}v|v| - c_V\partial_x T\right) \\
&\quad - \varphi\left(\frac{p}{c_V\rho}\partial_x v - \frac{\lambda}{2Dc_V}v^2|v| + v\partial_x T + \frac{k_w}{Dc_V\rho}T - \frac{k_w}{Dc_V\rho}T_{\mathsf{w}}\right)\mathrm{d}x \\
&= \int_0^\ell -\phi\partial_x\bar{q} + \eta\partial_x\psi + p(\partial_x\frac{\psi}{\rho}) - \psi\frac{\lambda}{2D}v|v| + c_V\psi\partial_x T \\
&\quad - \varphi\frac{p}{c_V\rho}\partial_x v + \frac{\lambda}{2Dc_V}\varphi v^2|v| - \varphi v\partial_x T - \frac{k_w}{Dc_V\rho}\varphi T + \frac{k_w}{Dc_V\rho}\varphi T_{\mathsf{w}}\,\mathrm{d}x \\
&\quad - \left[\psi(\eta + \frac{p}{\rho})\right]_0^\ell.
\end{aligned}$$

Then, setting

$$\begin{aligned}
j((\eta, \bar{q}, c_V\rho), (\phi, \psi, \varphi)) &:= \int_0^\ell -\phi\partial_x\bar{q} + \eta(\partial_x\psi) + p(\partial_x\frac{\psi}{\rho}) - \psi\frac{\lambda}{2D}v|v| + c_V\psi\partial_x T \\
&\qquad - \varphi\frac{p}{c_V\rho}\partial_x v + \frac{\lambda}{2Dc_V}\varphi v^2|v| - \varphi v\partial_x T\,\mathrm{d}x, \\
r((\eta, \bar{q}, c_V\rho), (\phi, \psi, \varphi)) &:= \int_0^\ell \frac{k_w}{Dc_V\rho}\varphi T\,\mathrm{d}x, \\
s(\cdot, (\eta, \bar{q}, c_V\rho), (\phi, \psi, \varphi)) &:= \int_0^\ell \frac{k_w}{Dc_V\rho}\varphi T_{\mathsf{w}}\,\mathrm{d}x - \left[\psi(\eta + \frac{p}{\rho})\right]_0^\ell,
\end{aligned}$$

we arrive at a port-Hamiltonian formulation of (2.81) in the form (2.71). In the context of port-Hamiltonian modeling, taking $\eta + \frac{p}{\rho}$ as boundary conditions seems natural.

However, the formalism does not make the PDE analysis obsolete, as the system is not well-posed with only these boundary conditions. For a detailed discussion of necessary boundary conditions, we refer to [67, 76]. Here, we have used that (T, v, p) can be expressed as a function of $(\eta, \bar{q}, c_V\rho)$ as

$$\begin{pmatrix} T \\ v \\ p \end{pmatrix} = \begin{pmatrix} \frac{1}{c_V}(\eta - \frac{1}{2}c_V^2 \frac{\bar{q}^2}{(c_V\rho)^2} - gb) \\ c_V \frac{\bar{q}}{c_V\rho} \\ p(c_V^{-1}(c_V\rho), T) \end{pmatrix}.$$

2.7.4 Mixture Models

To derive port-Hamiltonian formulations for the mixture models we refer to the notation and derivations carried out in Sect. 2.6. In particular, note that an alternative formulation of the isothermal Class I model (2.40) is given by

$$\partial_t \rho_1 + \partial_x(\rho_1 v) = 0, \tag{2.83a}$$

$$\partial_t \rho_2 + \partial_x(\rho_2 v) = 0, \tag{2.83b}$$

$$\partial_t v + v\partial_x v + \frac{1}{\rho}\partial_x p = -\gamma|v|v - g\partial_x b, \tag{2.83c}$$

with $\gamma = \frac{\lambda}{2D}$. Recall that by (2.45) for the energy $P := \rho\psi$ we have the relation

$$\rho_1 \partial_x(\partial_{\rho_1} P) + \rho_2 \partial_x(\partial_{\rho_2} P) = \partial_x p.$$

For $z = (\rho_1, \rho_2, v)$, and $\rho = \rho_1 + \rho_2$ we may then define the operators

$$\mathcal{J}(z) := \begin{pmatrix} 0 & 0 & -\partial_x(\frac{\rho_1}{\rho}\cdot) \\ 0 & 0 & -\partial_x(\frac{\rho_2}{\rho}\cdot) \\ -\frac{\rho_1}{\rho}\partial_x & -\frac{\rho_2}{\rho}\partial_x & 0 \end{pmatrix}, \qquad \mathcal{R}(z) := \begin{pmatrix} 0\,0 & 0 \\ 0\,0 & 0 \\ 0\,0 & \frac{\gamma}{\rho}|v| \end{pmatrix},$$

and the Hamiltonian

$$\mathcal{H}(\rho_1, \rho_2, v) := \int \frac{\rho}{2} v^2 \,\mathrm{d}x + \int P(\rho_1, \rho_2)\,\mathrm{d}x + \int gb\rho \,\mathrm{d}x$$

to formally rewrite the dynamics as

$$\partial_t z = (\mathcal{J}(z) - \mathcal{R}(z))\mathcal{H}'(z). \tag{2.84}$$

Let us return to the isothermal Class II model (2.43)

$$
\begin{aligned}
\partial_t \rho_1 + \partial_x(\rho_1 v_1) &= 0,\\
\partial_t \rho_2 + \partial_x(\rho_2 v_2) &= 0,\\
\partial_t v_1 + v_1 \partial_x v_1 + \partial_x(\partial_{\rho_1} P) &= -f\rho_2(v_1 - v_2) - \gamma F_1(v_1, v_2) - g\partial_x b,\\
\partial_t v_2 + v_2 \partial_x v_2 + \partial_x(\partial_{\rho_2} P) &= -f\rho_1(v_2 - v_1) - \gamma F_2(v_1, v_2) - g\partial_x b.
\end{aligned}
$$

Here, we consider the Hamiltonian

$$
\mathcal{H}(\rho_1, \rho_2, v_1, v_2) = \int \frac{\rho_1}{2} v_1^2 + \frac{\rho_2}{2} v_2^2 \,\mathrm{d}x + \int P(\rho_1, \rho_2)\,\mathrm{d}x + \int g b \rho \,\mathrm{d}x,
$$

with energy function $P = \rho\psi(\rho_1, \rho_2)$. For $z = (\rho_1, \rho_2, v_1, v_2)$, we define the operators

$$
\mathcal{J} \coloneqq \begin{pmatrix} 0 & 0 & -\partial_x & 0 \\ 0 & 0 & 0 & -\partial_x \\ -\partial_x & 0 & 0 & 0 \\ 0 & -\partial_x & 0 & 0 \end{pmatrix},
$$

$$
\mathcal{R}(z) \coloneqq f(\rho_1, \rho_2) \begin{pmatrix} 0 & 0 & 0 & 0 \\ 0 & 0 & 0 & 0 \\ 0 & 0 & \frac{\rho_2}{\rho_1} & -1 \\ 0 & 0 & -1 & \frac{\rho_1}{\rho_2} \end{pmatrix} + \gamma \begin{pmatrix} 0 & 0 & 0 & 0 \\ 0 & 0 & 0 & 0 \\ 0 & 0 & \frac{\phi_1(v_1, v_2)}{\rho_1} & 0 \\ 0 & 0 & 0 & \frac{\phi_2(v_1, v_2)}{\rho_2} \end{pmatrix},
$$

assuming that $F_i(v_1, v_2) = \phi_i(v_1, v_2) v_i$ for some scalar function ϕ_i, for $i = 1, 2$. Then, we may write the above system in the port-Hamiltonian form

$$
\partial_t z = (\mathcal{J} - \mathcal{R}(z))\mathcal{H}'(z). \tag{2.85}
$$

Note that $\mathcal{R}$ is state dependent, but $\mathcal{J}$ is not.

2.8 Discretization

2.8.1 Hyperbolic Balance Laws

In the following, we present a brief summary of basic numerical methods and concepts for the treatment of hyperbolic balance laws. These have to be supplemented by appropriate handling of boundary and coupling conditions as well as further network components like compressors and valves. A review on hyperbolic balance laws on networks can be found in [10].

The Euler equations (TA1) on a single pipe can be formalized into a system of nonlinear balance equations of the form

$$
\partial_t \mathbf{u} + \partial_x \mathbf{f}(\mathbf{u}) = \mathbf{g}(x, \mathbf{u}). \tag{2.86}
$$

The standard method for solving these equations is the *finite volume method*. This method is based on the integral form of the equations above, which is often closer to the physics of the problem. This offers elegant ways to numerically approximate even non-smooth solutions containing physical phenomena such as shock waves, contact discontinuities and rarefaction waves at high precision. Among the best known classical methods are the Lax–Friedrichs and Godunov methods [56]. The latter uses the solution of local Riemann problems at cell boundaries, which is often replaced in practice by suitable approximations. For an extension of Godunov's methods to networks see [91]. In one space dimension, several finite volume methods can be reinterpreted as conservative *finite difference methods*. A rigorous convergence analysis of finite volume schemes for conservation laws on networks can be found in [31].

A common strategy is the usage of TVD or TVB methods (total variation diminishing, total variation bounded) that couple high-accuracy methods in regions with smooth solutions with lower order methods in regions with discontinuities. This is achieved by using flux and slope limiters. In between, flux and slope limiters mediate, as for example in MUSCL methods (monotonic upstream-centered scheme for conservation laws). An excellent summary can be found in the book by LeVeque [56]. Generalizations of the polynomial reconstructions of solutions across multiple cells used in these methods lead to the class of ENO and WENO methods (essentially non-oscillatory, weighted essentially non-oscillatory). An overview with further references can be found in the monograph by Shu [86].

Solving Riemann problems, especially at junctions in networks, can become very costly and also prevents a compact notation of a discretization to be used in optimization. Central methods, originating from work by Nessyahu and Tadmor [70] that use staggered grids, avoid this difficulty and are easy to implement, especially in 1D. Among this class are the attractive box methods introduced by Wendroff [96]. In time, both explicit methods, which have to satisfy a Courant–Friedrichs–Levy (CFL) condition of the form $\triangle t \leq c(\mathbf{u})\triangle x$ for stability reasons, and implicit methods are used. The special class of IMEX (implicit-explicit)-Runge–Kutta methods allows to discretize certain parts of the equations explicitly and others implicitly, in order to avoid both too severe time step restrictions and having to solve very difficult systems of equations in each time step. The IMEX methodology has, in particular, been used to construct asymptotic-preserving schemes, see, e.g., [20, 36, 89]. Among explicit methods, "strong stability preserving" (SSP) methods are very popular, cf. SSP-Runge–Kutta and SSP multi-step method [46].

In contrast to finite volume methods, *discontinuous Galerkin methods* (DG) [18] do not require reconstructions, since a higher-order polynomial is already used in each cell. However, this also requires multiple degrees of freedom to be stored and transported per cell. Classical monotone flow approximations can still be used. DG methods have excellent stability properties, they can be easily constructed for arbitrary orders, and they allow simple hp-adaptive strategies to improve local approximation properties. Space-time DG methods have also been developed. We refer to the two review articles by Cheng and Shu [17] and Ekaterinaris [26] for recent comparisons and numerous further reading.

For convergence studies towards the (physically correct) solution, satisfying the entropy admissibility criterion [19, Sec. 4.5], the so-called viscous equations are often used:

$$\partial_t \mathbf{u}^\varepsilon + \partial_x \mathbf{f}(\mathbf{u}^\varepsilon) = \mathbf{g}(x, \mathbf{u}^\varepsilon) + \varepsilon \partial_{xx} \mathbf{u}^\varepsilon. \tag{2.87}$$

These equations are themselves a starting point for further discretizations, which are derived from the treatment of parabolic differential equations, see the discussion on numerical viscosity in [56]. Adding further terms, e.g., second derivatives in time, motivates the widely used *relaxation methods* for hyperbolic balance equations. An overview of the procedure and convergence results can be found in [57].

An appropriate choice of a discretization method will always depend on the objective for numerical simulation, such as stability, high accuracy, low computation time, low memory demand, certain structure for optimization, complexity of adjoint equations, etc.

2.8.2 Port-Hamiltonian Systems

Spatial Discretization Various approaches to preserve port-Hamiltonian structure after space discretization exist [25, 34, 68], and we refer to [34] for an overview of available methods. In the following, we will briefly summarize the method presented in [34], which is based on a Galerkin approach and suitable for fully nonlinear infinite-dimensional systems. The approach can be viewed as an extension of [15] to infinite-dimensional systems.

Recall the port-Hamiltonian model (2.71) given by

$$\langle \partial_t z,\ \phi \rangle_{X',X} = j(\mathcal{H}'(z), \phi) - r(\mathcal{H}'(z), \phi) + s(\cdot, \mathcal{H}'(z), \phi). \tag{2.88}$$

In the following, our goal is to approximate $z \in X$ by $z_h \in X_h$, where $X_h \subseteq X$ is a finite-dimensional subspace. Recall that $X \hookrightarrow Z$ and let $\Pi_h \colon Z \to X_h$ denote the Z-orthogonal projection onto X_h, which satisfies $\langle \phi, z_h \rangle = \langle \phi, \Pi_h z_h \rangle = \langle \Pi_h \phi, z_h \rangle$ for all $z_h \in X_h$ and $\phi \in X$. In order to preserve the structure (2.88), we utilize a modified Galerkin approach. We seek $z_h \in X_h$ such that for all test functions $\phi_h \in X_h$, we have

$$\langle \partial_t z_h, \phi_h \rangle = j(\Pi_h \mathcal{H}'(z_h), \phi_h) - r(\Pi_h \mathcal{H}'(z_h), \phi_h) + s(\cdot, \Pi_h \mathcal{H}'(z_h), \phi_h). \tag{2.89}$$

If (2.88) is subject to the initial condition $z(0) = z_0$, then a possible choice for the initial condition for (2.89) is $z_h(0) = \Pi_h z_0$. Due to the properties of the projection Π_h, the system (2.89) is again in the form of (2.71). Further, solutions z_h of (2.89) satisfy the space-discrete energy balance

$$\begin{aligned} &\mathcal{H}(z_h(t_{i+1})) - \mathcal{H}(z_h(t_i)) \\ &\qquad = \int_{t_i}^{t_{i+1}} -r(\Pi_h \mathcal{H}'(z_h), \Pi_h \mathcal{H}'(z_h)) + s(t, \Pi_h \mathcal{H}'(z_h), \Pi_h \mathcal{H}'(z_h))\, \mathrm{d}t, \end{aligned} \tag{2.90}$$

which, up to the projection operators and the fact that it only holds on the time grid, coincides with the energy balance equation (2.72). If the projection Π_h in (2.89) is omitted, then an energy balance is not available if the operators j, r and s are nonlinear.

Equivalently, we can state the dynamics for the coefficients $w_h \in \mathbb{R}^{\dim(X_h)}$ of $z_h \in X_h$. For this, note that each $z_h \in X_h$ is uniquely determined by a coefficient vector $w_h \in \mathbb{R}^{\dim(X_h)}$. For a fixed basis of X_h, we denote the canonical interpolation operator mapping a coefficient vector to the corresponding element in X_h by $I_h \colon \mathbb{R}^{\dim(X_h)} \to X_h$. Similarly, $c_h \colon X_h \to \mathbb{R}^{\dim(X_h)}$ maps a function in X_h to its corresponding basis coefficients. We can now define the space-discrete Hamiltonian $\mathcal{H}_h \colon \mathbb{R}^{\dim(X_h)} \to \mathbb{R}$ by

$$\mathcal{H}_h(w_h) \coloneqq \mathcal{H}(I_h w_h).$$

Since the interpolation operator I_h is linear, using the projection property of Π_h for any $v_h \in \mathbb{R}^{\dim(X_h)}$, we obtain

$$\begin{aligned}
\nabla \mathcal{H}_h(w_h)^\top v_h &= \frac{\mathrm{d}}{\mathrm{d}s} \mathcal{H}_h(w_h + s v_h)|_{s=0} = \frac{\mathrm{d}}{\mathrm{d}s} \mathcal{H}(I_h(w_h) + s I_h(v_h))|_{s=0} \\
&= \langle \mathcal{H}'(I_h(w_h)), I_h(v_h) \rangle = \langle \Pi_h(\mathcal{H}'(I_h(w_h))), I_h(v_h) \rangle \\
&= (M_h c_h(\Pi_h \mathcal{H}'(I_h(w_h))))^\top v_h,
\end{aligned}$$

so that $\nabla \mathcal{H}_h(w_h) = M_h c_h(\Pi_h \mathcal{H}'(I_h(w_h)))$. Here, M_h is the mass matrix corresponding to the basis of X_h with respect to the inner product of Z. We now define $j_h, r_h \colon \mathbb{R}^{\dim(X_h)} \to \mathbb{R}^{\dim(X_h)}$ and $s_h \colon [0,T] \times \mathbb{R}^{\dim(X_h)} \to \mathbb{R}^{\dim(X_h)}$ via

$$\begin{gathered}
j_h(v_h)^\top \phi_h \coloneqq j(I_h(v_h), I_h(\phi_h)), \quad r_h(v_h)^\top \phi_h \coloneqq r(I_h(v_h), I_h(\phi_h)), \\
s_h(\cdot, v_h)^\top \phi_h \coloneqq s(\cdot, I_h(v_h), I_h(\phi_h))
\end{gathered}$$

for all $v_h, \phi_h \in \mathbb{R}^{\dim(X_h)}$. An equivalent formulation of (2.89) is then

$$M_h \partial_t w_h = j_h(M_h^{-1} \nabla \mathcal{H}_h(w_h)) - r_h(M_h^{-1} \nabla \mathcal{H}_h(w_h)) + s_h(\cdot, M_h^{-1} \nabla \mathcal{H}_h(w_h)), \tag{2.91}$$

which can easily be recast in the form of (2.73) by multiplying with M_h^{-1}. Since by construction $j_h(v_h)^\top v_h = 0$ and $r_h(v_h)^\top v_h \geq 0$ holds for all $v_h \in \mathbb{R}^{\dim(X_h)}$, solutions w_h of (2.91) satisfy the space-discrete energy balance

$$\begin{aligned}
\mathcal{H}_h(w_h(t_1)) - \mathcal{H}_h(w_h(t_0)) &= \int_{t_0}^{t_1} \nabla \mathcal{H}_h(w_h)^\top \partial_t w_h \, \mathrm{d}t \\
&= \int_{t_0}^{t_1} (M_h^{-1} \nabla \mathcal{H}_h(w_h))^\top (M_h \partial_t w_h) \, \mathrm{d}t \\
&= \int_{t_0}^{t_1} -r_h(M_h^{-1} \nabla \mathcal{H}_h(w_h))^\top M_h^{-1} \nabla \mathcal{H}_h(w_h) \\
&\qquad + s_h(\cdot, M_h^{-1} \nabla \mathcal{H}_h(w_h))^\top M_h^{-1} \nabla \mathcal{H}_h(w_h) \, \mathrm{d}t.
\end{aligned}$$

In [15], the authors consider model order reduction of finite-dimensional nonlinear port-Hamiltonian systems. With the projection matrices V and W satisfying $W^\top V = I$ and the reduced-order state approximation $z_r \in \mathbb{R}^r$, they suggest to approximate $\nabla \mathcal{H}(V z_r) \approx W \nabla \mathcal{H}(V z_r)$ to preserve the port-Hamiltonian structure of the original system in the reduced-order model with state z_r. Here, the matrix W plays the role of the projection

operator Π_h in (2.89). Furthermore, let us remark that an approach similar to (2.89) can be used for the structure (2.70), see [68].

Time Discretization In the context of time discretization, the main focus of structure-preserving methods typically is the availability of a time-discrete energy balance of the form (2.72) in prescribed time discretization points. Available structure-preserving methods include collocation schemes [12,39,52,64], operator splitting approaches [32], discrete gradient approaches [63, 84], and (Petrov–)Galerkin methods [3, 25, 34, 68], see [34] for a more detailed overview. Furthermore, the applicability of Runge–Kutta schemes for differential algebraic systems of the form (2.70) was studied in [68]. A discretization of (TA1) based on a pH formulation can be found in [41]. Here, we will shortly present the method from [34], which is a Petrov–Galerkin method suitable for fully nonlinear infinite-dimensional systems. The approach is related to the method from [68, Sect. 7.4] and mainly differs in the underlying port-Hamiltonian formulation.

Again, let us recall the port-Hamiltonian model (2.71) given by

$$\langle \partial_t z,\ \phi\rangle_{X',X} = j(\mathcal{H}'(z),\phi) - r(\mathcal{H}'(z),\phi) + s(\cdot,\mathcal{H}'(z),\phi), \tag{2.92}$$

and assume that $X \hookrightarrow Z$ with Z being a Hilbert space. In the following, for a given polynomial degree $k \in \mathbb{N}$, our goal is to approximate $z \in C([0,T],X)$ by $z_\tau \in \mathcal{P}_k^c$. Here, for given time discretization points $0 = t_0 < \cdots < t_m = T$ with maximal distance $\tau := \max_i |t_i - t_{i-1}|$ the space $\mathcal{P}_k^c$ is defined as

$$\mathcal{P}_k^c := \{p \in L^2([0,T],Z) \mid p|_{[t_{i-1},t_i]} \text{ is polynomial of degree } k\} \cap C([0,T],Z).$$

If $z_\tau \in \mathcal{P}_k^c$, then $\partial_t z_\tau \in \mathcal{P}_{k-1}$, where

$$\mathcal{P}_{k-1} := \{p \in L^2([0,T],Z) \mid p|_{[t_{i-1},t_i]} \text{ is polynomial of degree } k-1\}.$$

To obtain a time-discrete energy balance, we use a similar approach as (2.89). Let $\Pi_\tau \colon L^2([0,T],Z) \to \mathcal{P}_{k-1}$ denote the L^2-orthogonal projection onto $\mathcal{P}_{k-1}$ satisfying $\int_0^T \langle \Pi_\tau f, g\rangle \,\mathrm{d}t = \int_0^T \langle f, g\rangle \,\mathrm{d}t$ for all $f \in L^2([0,T],Z)$ and $g \in \mathcal{P}_{k-1}$. We seek $z_\tau \in \mathcal{P}_k^c$ such that $z_\tau(0) = z_0$ and

$$\langle \partial_t z_\tau, \phi_\tau\rangle = j(\Pi_\tau \mathcal{H}'(z_\tau),\phi_\tau) - r(\Pi_\tau \mathcal{H}'(z_\tau),\phi_\tau) + s(\cdot,\Pi_\tau \mathcal{H}'(z_\tau),\phi_\tau) \tag{2.93}$$

for all $\phi_\tau \in \mathcal{P}_{k-1}$. As before, due to the properties of the projection Π_τ, solutions z_τ of (2.93) satisfy the time-discrete energy balance

$$\begin{aligned}\mathcal{H}(z_\tau(t_i)) - \mathcal{H}(z_\tau(t_{i-1})) \\ = \int_{t_i}^{t_{i-1}} -r(\Pi_\tau \mathcal{H}'(z_\tau),\Pi_\tau \mathcal{H}'(z_\tau)) + s(t,\Pi_\tau \mathcal{H}'(z_\tau),\Pi_\tau \mathcal{H}'(z_\tau)) \,\mathrm{d}t\end{aligned} \tag{2.94}$$

for all $i = 1,\dots,m$, again closely resembling the energy balance equation (2.72). As in the space-discrete case, if the projection Π_τ in (2.93) is omitted, then an energy balance is not available if the operators j, r and s are nonlinear.

2.8.3 ISO1 Pipe Model

Spatial Discretization For the spatial discretization of the ISO1 pipe model we use the scheme presented in [24] based on the Galerkin equations

$$\langle \partial_t \rho_h, p_h \rangle = -\langle \partial_x \bar{q}_h, p_h \rangle, \tag{2.95}$$

$$\langle \partial_t v_h, r_h \rangle = \langle h_h, \partial_x r_h \rangle + h_{\text{in}} r_h(\nu_{\text{in}}) - h_{\text{out}} r_h(\nu_{\text{out}}) - \langle \gamma | v_h | v_h, r_h \rangle \tag{2.96}$$

with the specific enthalpies h_{in} and h_{out} prescribed at the vertex ν_{in} and vertex ν_{out} of a single pipe e represented by a bounded interval Ω. Here, the notation is

$$\bar{q}_h = \rho_h v_h, \qquad h_h = \frac{1}{2} v_h^2 + P'(\rho_h) + g \partial_x b \tag{2.97}$$

for basis functions $p_h \in \mathcal{P}_h$ and $r_h \in \mathcal{R}_h$ of the finite dimensional subspaces $\mathcal{P}_h$ and $\mathcal{R}_h$ with

$$\mathcal{P}_h \coloneqq \mathcal{P}_0(\mathcal{T}_h), \quad \mathcal{R}_h \coloneqq \mathcal{P}_1(\mathcal{T}_h) \cap H^1(\Omega).$$

By $\mathcal{P}_0(\mathcal{T}_h)$ and $\mathcal{P}_1(\mathcal{T}_h)$ we denote the spaces of piecewise constant and piecewise linear functions over the equidistant mesh $\mathcal{T}_h$ of Ω with grid length h. Furthermore, let $\Pi_h \colon L^2(\Omega) \to \mathcal{P}_0(\mathcal{T}_h)$ be the L^2-orthogonal projection. For a spatial discretization of Ω with n subintervals $\mathcal{T}_1, \ldots, \mathcal{T}_n$ with $\mathcal{T}_i = [x_{i-1}, x_i]$, we choose basis functions $p_1, \ldots, p_n$ of $\mathcal{P}_h$ and basis functions $r_1, \ldots, r_m$ of $\mathcal{R}_h$ with $m = n + 1$. With the ansatz

$$\rho_h(x,t) = \sum_{j=1}^{n} c_j^{\rho}(t) p_j(x), \qquad \bar{q}_h(x,t) = \sum_{k=1}^{m} c_k^{\bar{q}}(t) r_k(x)$$

testing (2.95) with $p_h = p_i$ reads leads to the following system

$$E_{\rho}^{\text{ma}} \partial_t c_{\rho} + \mathcal{A}_{\bar{q}}^{\text{ma}} c_{\bar{q}} = 0, \tag{2.98}$$

with $E_{\rho}^{\text{ma}} \in \mathbb{R}^{n \times n}$ and $\mathcal{A}_{\bar{q}}^{\text{ma}} \in \mathbb{R}^{n \times m}$ with entries

$$(E_{\rho}^{\text{ma}})_{ij} = \langle p_j, p_i \rangle, \qquad (\mathcal{A}_{\bar{q}}^{\text{ma}})_{ik} = \langle \partial_x r_k, p_i \rangle.$$

Consequently, the matrix E_{ρ}^{ma} is a positive definite matrix. According to (2.97) the velocity and the specific enthalpy are given by

$$v_h(x,t) = \frac{\bar{q}_h(x,t)}{\rho_h(x,t)}, \qquad h_h(x,t) = \frac{1}{2} v_h^2(x,t) + P'(\rho_h(x,t)) + g \partial_x b(x).$$

Introducing $c = (c_{\rho}, c_{\bar{q}})$, and denoting

$$\varphi_\rho(c,x) \coloneqq \sum_{j=1}^{n} c_j^\rho p_j(x), \quad \varphi_{\bar{q}}(c,x) \coloneqq \sum_{k=1}^{m} c_k^{\bar{q}} r_k(x), \quad \varphi_v(c,x) \coloneqq \frac{\varphi_{\bar{q}}(c,x)}{\varphi_\rho(c,x)},$$
$$\varphi_h(c,x) \coloneqq \frac{1}{2}\left(\varphi_v(c,x)\right)^2 + P'(\varphi_\rho(c,x)) + g\partial_x b(x)$$

testing (2.96) with test functions $r_h = r_i$ yields the system

$$E_\rho^{\mathrm{mo}}(c)\partial_t c_\rho + E_{\bar{q}}^{\mathrm{mo}}(c)\partial_t c_{\bar{q}} = f^{\mathrm{mo}}(c) - g^{\mathrm{mo}}(c) - B_h^{\mathrm{mo}} h_* \tag{2.99}$$

with $E_\rho^{\mathrm{mo}}(c) \in \mathbb{R}^{m\times n}$, $E_{\bar{q}}^{\mathrm{mo}}(c) \in \mathbb{R}^{m\times m}$, $B_h^{\mathrm{mo}} \in \mathbb{R}^{m\times|\mathcal{V}|}$, with entries given by

$$(E_\rho^{\mathrm{mo}})_{ij}(c) = \langle \partial_{c_j^\rho}\varphi_v(c,\cdot), r_i\rangle, \qquad (E_{\bar{q}}^{\mathrm{mo}})_{ik}(c) = \langle \partial_{c_k^{\bar{q}}}\varphi_v(c,\cdot), r_i\rangle,$$
$$(B_h^{\mathrm{mo}})_i = r_i(\nu_{\mathrm{in}})a_{\mathrm{in}}^\top + r_i(\nu_{\mathrm{out}})a_{\mathrm{out}}^\top.$$

Here, a_{in} and a_{out} are the columns of the incidence matrices A_{in} and A_{out} defined by (2.19) and (2.20) belonging to the pipe edge. Furthermore, $f^{\mathrm{mo}}(c) \in \mathbb{R}^m$, $g^{\mathrm{mo}}(c) \in \mathbb{R}^m$ are defined by their entries

$$(f^{\mathrm{mo}})_i(c) = \langle \varphi_h(c,\cdot), \partial_x r_i\rangle, \qquad (g^{\mathrm{mo}})_i(c) = \langle \gamma|\varphi_v(c,\cdot)|\varphi_v(c,\cdot), r_i\rangle.$$

Note that h_* in (2.99) is the vector of enthalpies at the vertices of the network.

If one chooses hat functions [77, Chap. 3] as basis function r_i (namely r_i piecewise linear with $r_i(x_j) = \delta_{ij}$ for the grid points $x_j \in \Omega$), then the matrix $E_q^{\mathrm{mo}}(c)$ is a tridiagonal, symmetric and positive definite matrix. Finally, we get with (2.98) and (2.99) the spatially discretized mass and momentum balance equations in the compact form

$$E_{\mathrm{pip}}(c)\partial_t c = f_{\mathrm{pip}}(c) - g_{\mathrm{pip}}(c) - B_{\mathrm{pip}} h_* \tag{2.100}$$

with

$$E_{\mathrm{pip}}(c) = \begin{pmatrix} E_\rho^{\mathrm{ma}} & 0 \\ E_\rho^{\mathrm{mo}}(c) & E_{\bar{q}}^{\mathrm{mo}}(c) \end{pmatrix}, \quad f_{\mathrm{pip}}(c) = \begin{pmatrix} -\mathcal{A}_{\bar{q}}^{\mathrm{ma}} c_{\bar{q}} \\ f^{\mathrm{mo}}(c) \end{pmatrix},$$
$$g_{\mathrm{pip}}(c) = \begin{pmatrix} 0 \\ g^{\mathrm{mo}}(c) \end{pmatrix}, \quad B_{\mathrm{pip}} = \begin{pmatrix} 0 \\ B_h^{\mathrm{mo}} \end{pmatrix}. \tag{2.101}$$

Let $\Pi_h\varphi_h(c,x) = \sum_{i=1}^n z_i(c)p_i(x)$ be the basis representation of the L^2-orthogonal projection $\Pi_h\varphi_h$. We define the function $z_{\mathrm{pip}} : \mathbb{R}^{n\times m} \to \mathbb{R}^{n\times m}$ by

$$z_{\mathrm{pip}}(c) \coloneqq \begin{pmatrix} z_h(c) \\ c_{\bar{q}} \end{pmatrix} \quad \text{for } z_h(c) \coloneqq \begin{pmatrix} z_1(c) \\ \vdots \\ z_n(c) \end{pmatrix} \text{ and } c = (c_\rho, c_{\bar{q}}). \tag{2.102}$$

Then, the Hamiltonian on the edge e

$$\mathsf{H}_{\mathrm{pip}}(c) \coloneqq \int_\Omega A^e \left(\varphi_\rho(c,x)\frac{1}{2}(\varphi_v(c,x))^2 + P(\varphi_\rho(c,x)) + \varphi_\rho(c,x)g\partial_x b(x)\right) \mathrm{d}x$$

satisfies

$$\nabla \mathsf{H}_{\text{pip}}(c) = A^e E_{\text{pip}}^\top(c) z_{\text{pip}}(c) \tag{2.103}$$

with the cross sectional area A^e. Furthermore, for $\mathsf{D}_{\text{pip}}(c) \coloneqq \gamma A^e \langle \varphi_\rho(c,\cdot), |\varphi_v(c,\cdot)|^3 \rangle$ one has that $\mathsf{D}_{\text{pip}}(c) = A^e z_{\text{pip}}^\top(c) g_{\text{pip}}(c)$. The functions f_{pip} and g_{pip} satisfy

$$f_{\text{pip}}(c) = J_{\text{pip}} z_{\text{pip}}(c) \qquad \text{for } J_{\text{pip}} \coloneqq \begin{pmatrix} 0 & -A_{\bar{q}}^{\text{ma}} \\ (A_{\bar{q}}^{\text{ma}})^\top & 0 \end{pmatrix}, \tag{2.104}$$

$$g_{\text{pip}}(c) = R_{\text{pip}}(c) z_{\text{pip}}(c) \quad \text{for } R_{\text{pip}}(c) \coloneqq \begin{pmatrix} 0 & 0 \\ 0 & R_{\bar{q}}^{\text{mo}}(c) \end{pmatrix} \tag{2.105}$$

with $R_{\bar{q}}^{\text{mo}}(c) \in \mathbb{R}^{m \times m}$ and $(R_{\bar{q}}^{\text{mo}})_{ij}(c) \coloneqq \langle \gamma \frac{|\varphi_v(c,\cdot)|}{\varphi_\rho(c,\cdot)} r_j, r_i \rangle$. By definition of B_{pip},

$$A^e z_{\text{pip}}^\top(c) B_{\text{pip}} = A^e (a_{\text{in}}^\top \bar{q}_{\text{in}} + a_{\text{out}}^\top \bar{q}_{\text{out}}) = a_{\text{in}}^\top q_{\text{in}} + a_{\text{out}}^\top q_{\text{out}}$$

is valid for every solution c of the pipe equation (2.100). The pipe equation (2.100) together with the mass flow contributions $q_*^e \coloneqq -a_{\text{in}}^\top q_{\text{in}} - a_{\text{out}}^\top q_{\text{out}}$ of pipe edge e to the vertices of the network, forms the system

$$\begin{aligned} E_{\text{pip}}(c)\partial_t c &= J_{\text{pip}} z_{\text{pip}}(c) - R_{\text{pip}}(c) z_{\text{pip}}(c) - B_{\text{pip}} h_*, \\ 0 &= q_*^e + A^e B_{\text{pip}}^\top z_{\text{pip}}(c) \end{aligned} \tag{2.106}$$

with a non-singular matrix E_{pip} and a skew-symmetric matrix J_{pip}. Regarding (2.103) and considering $\tilde{z}_{\text{pip}}(c) \coloneqq A^e z_{\text{pip}}(c)$, one sees that the system (2.106) forms a port-Hamiltonian system in descriptor form [64] supposed $\varphi_\rho(c,\cdot)$ is non-negative, which corresponds to non-negative discrete density values and a positive semi-definite matrix $R_{\text{pip}}(c)$. Furthermore, it can be shown that the matrix $B_{\text{pip}}^\top E_{\text{pip}}^{-1}(c) B_{\text{pip}}$ is positive definite and $B_{\text{pip}}^\top z_{\text{pip}}(c) = B_{\text{pip}}^\top c$. Finally, for every solution c of (2.106), the power balance equation on the edge e

$$\frac{\mathrm{d}}{\mathrm{d}t} \mathsf{H}_{\text{pip}}(c) + \mathsf{D}_{\text{pip}}(c) = -\langle q_*^e, h_* \rangle \tag{2.107}$$

is satisfied.

2.8.4 ISO2 Pipe Model

Full Discretization in Space and Time (Implicit Box Scheme) One can apply various discretization approaches in space and time for stable simulation and efficient optimization. One well-established method is the implicit box scheme [50, 51]. It is commonly used in optimal control applications since mass conservation is given over the control volumes and stability is ensured even for large time steps. However, it is

not well-suited to simulate highly nonlinear wave interaction phenomena like shocks. In this scenario, one should use explicit conservative numerical methods as discussed in Sect. 2.8.1 instead.

Here, using a two-point discretization in space yields

$$\begin{aligned}\frac{1}{2}\left(\rho_{\text{in}}^{n+1}+\rho_{\text{out}}^{n+1}\right) &= \frac{1}{2}\left(\rho_{\text{in}}^{n}+\rho_{\text{out}}^{n}\right)-\frac{\Delta t}{\ell}\left(\bar{q}_{\text{out}}^{n+1}-\bar{q}_{\text{in}}^{n+1}\right),\\ \frac{1}{2}\left(\bar{q}_{\text{in}}^{n+1}+\bar{q}_{\text{out}}^{n+1}\right) &= \frac{1}{2}\left(\bar{q}_{\text{in}}^{n}+\bar{q}_{\text{out}}^{n}\right)-\frac{\Delta t}{\ell}\left(p_{\text{out}}^{n+1}-p_{\text{in}}^{n+1}\right)\\ &\quad+\frac{1}{2}\Delta t\left(f(\rho_{\text{in}}^{n+1},\bar{q}_{\text{in}}^{n+1})+f(\rho_{\text{out}}^{n+1},\bar{q}_{\text{out}}^{n+1})\right),\end{aligned}$$

for the flux $\bar{q} \coloneqq \rho v$, the spatial stepsize $\Delta x = \ell$ (pipe length) and

$$f(\rho,\bar{q}) \coloneqq -\frac{\lambda}{2D}\frac{\bar{q}|\bar{q}|}{\rho}-g\rho\partial_x b.$$

The upper index n denotes the n-th time step with stepsize Δt. Recall that $\bar{q}_{\text{in}}$ and $\bar{q}_{\text{out}}$ denote the fluxes in edge direction at the vertices v_{in} and v_{out} as described in Sect. 2.5.1 and Fig. 2.9.

This nonlinear method in combination with a piecewise linearization is used to derive an efficient mixed-integer linear program for cost optimization of gas networks [21]. It is suitable for stiff as well as for non-stiff source terms. The time stepsize is only weakly limited by a lower bound $\Delta t \geq \frac{\Delta x}{2c}$ if the real gas factor $\mathsf{z}(p)$ is constant, see [50, 51].

2.8.5 ISO3 Pipe Model

For the discussion of discretization methods for (ISO3), we follow [85, Sect. 2]. For simplicity, in what follows we assume an ideal gas law $p = c^2\rho$ and that the elevation of the pipe is constant so that $\partial_x b = 0$ and the governing equations read as

$$\begin{aligned}\partial_t\rho+\partial_x(\rho v) &= 0,\\ c^2\partial_x\rho &= -\frac{\lambda}{2D}\rho v|v|.\end{aligned}\tag{2.108}$$

We now introduce $w(\rho) = \rho^2$ and observe that

$$\partial_x w = 2\rho\partial_x\rho = -\frac{\lambda}{D}\rho v|\rho v|$$

and therefore

$$\rho v = -\sqrt{\frac{D}{\lambda}}\frac{\partial_x w}{\sqrt{|\partial_x w|}}.$$

Setting $a(s) = \frac{s}{\sqrt{|s|}}$ for (2.108) we obtain

$$\partial_t a(w) - \sqrt{\frac{D}{\lambda}}\partial_x\left(a(\partial_x w)\right) = 0.$$

After testing with a smooth test function ψ, integrating over the length of the pipe and integration by parts we are left with the weak formulation

$$\int_0^\ell \psi \partial_t a(w)\,\mathrm{d}x + \sqrt{\frac{D}{\lambda}}\int_0^\ell a(\partial_x w)\partial_x\psi\,\mathrm{d}x = \sqrt{\frac{D}{\lambda}}\left[\psi a(\partial_x w)\right]_0^\ell.$$

Now, a Galerkin approach can be utilized to discretize this weak formulation in the spatial variable. For details and questions regarding existence of solutions, convergence of the scheme and stability, we refer the interested reader to [85, Sect. 2].

2.9 Non-Pipe Gas Network Elements

The next sections describe models for typical gas network elements that are not pipes. Such elements are represented by edges that we treat in a 'lumped' sense. This means that we only consider pressures $p_{\mathrm{in}} = p^e(\nu_{\mathrm{in}})$, $p_{\mathrm{out}} = p^e(\nu_{\mathrm{out}})$ at its vertices ν_{in}, ν_{out} and a spatially constant flow $q = q^e(\nu_{\mathrm{in}}) = q^e(\nu_{\mathrm{out}})$ on this edge. Note that all element variables (pressure, flow, velocity) depend on time. As in the sections before, we neglect the time argument for the purpose of better readability.

Simple Valves Various designs and models are available for valves [33, 42]. The simplest model describes a valve as a switch with two states *open* and *closed*. The isothermal model is then simply given by

$$\begin{cases} p_{\mathrm{in}} = p_{\mathrm{out}}, & \text{if the valve is open,} \\ q = 0, & \text{if the valve is closed.} \end{cases} \tag{2.109}$$

Check Valves Check valves are self-controlling valves that allow a flow only in one direction. They are used to protect the network against pressure overload and loss of outflow in the event of pipe breaks [8]. The isothermal model equations can be described by

$$q = \max\{q, 0\}, \qquad (p_{\mathrm{in}} - p_{\mathrm{out}})q = 0. \tag{2.110}$$

Resistances A resistance is a simple edge element to describe the hydraulic resistance of a device. It is also used to model the pressure loss in network components as for example filter systems. The pressure loss $p_{\mathrm{in}} - p_{\mathrm{out}}$ under isothermal conditions can be modeled by (see [30, 82])

$$p_{\mathrm{in}} - p_{\mathrm{out}} = \frac{\zeta}{2}\rho_{\mathrm{in}} v|v| = \frac{\zeta}{2}\frac{q|q|}{\rho_{\mathrm{in}} A^2}. \tag{2.111}$$

Here, ζ, v, ρ_{in} and A are the pressure loss coefficient, the velocity of the gas, the gas density at the in-terminal and the pipe cross sectional area. If the real gas factor z is assumed to be constant then we have $p_{\text{in}} = \rho_{\text{in}} c^2$ with the constant speed of sound c. Hence, with $r := \frac{c^2}{2A^2}\zeta$, we obtain

$$p_{\text{in}}(p_{\text{in}} - p_{\text{out}}) = rq|q|. \tag{2.112}$$

If the pressure loss coefficient and/or the pipe cross sectional area are not known then the pressure loss is modeled as constant, see [82]:

$$p_{\text{in}}(p_{\text{in}} - p_{\text{out}}) = \operatorname{sign}(q) c_R \tag{2.113}$$

with a pressure loss constant $c_R > 0$.

Controllers with Characteristic Curves Under isothermal conditions, controllers regulate the flow depending on the adjacent pressures and a proportional opening parameter $o \in [0, 1]$, i.e.,

$$q = f(p_{\text{in}}, p_{\text{out}}, o), \tag{2.114}$$

where f is a given function describing the characteristic curve. One example is the characteristic curve for Mokveld valves [44]:

$$q := c_1(o) \frac{241 c_2(o) p_{\text{in}}(p_o - 0.148 p_o^3)}{\sqrt{\rho T z}}, \quad p_o = \min\left\{1.5, \ \frac{1.63}{c_2(o)} \sqrt{\frac{p_{\text{in}} - p_{\text{out}}}{p_{\text{in}}}}\right\}, \tag{2.115}$$

where the coefficients $c_1(o), c_2(o) \in \mathbb{R}$ depend on the parameter o.

Preheaters High pressure in the network is reduced at the take-off stations. Gas preheating is required to prevent impermissible cooling when reducing the pressure (due to the Joule–Thomson effect [13]). In heat transfer stations the gas is heated sufficiently to ensure that its temperature exceeds the dew point of the gas after throttling [8]. The temperature difference depends on the pressure difference and can be described by [82]

$$\frac{\mathrm{d}T}{\mathrm{d}p} = \mu_{JT}(p, T) = \frac{R}{\widetilde{c}_p} \frac{T^2}{p} \frac{\partial \mathsf{z}(p, T)}{\partial T}. \tag{2.116}$$

Here, μ_{JT} is the Joule–Thomson coefficient and $\widetilde{c}_p$ is the molar heat capacity. A simple approximation using a single implicit Euler discretization step is usually sufficient for simulation and optimization [82]. This yields

$$\frac{T_{\text{out}} - T_{\text{in}}}{p_{\text{out}} - p_{\text{in}}} = \mu_{JT}(p_{\text{out}}, T_{\text{out}}) = \frac{R}{\widetilde{c}_p} \frac{T_{\text{out}}^2}{p_{\text{out}}} \frac{\partial \mathsf{z}}{\partial T}(p_{\text{out}}, T_{\text{out}}), \tag{2.117}$$

as the element equation for the preheater. There, T_{in} and T_{out} are the temperatures at the vertices v_{in} and v_{out} of the preheater. Correspondingly, T_{in} is the gas temperature before the heating and T_{out} is the gas temperature behind the heating.

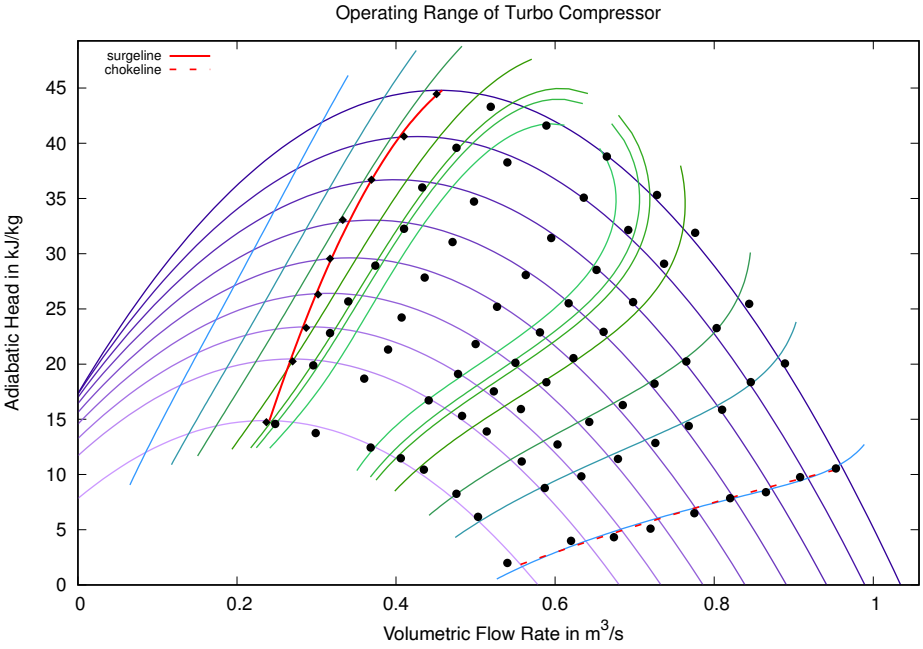


Fig. 2.10: Compressor map of a turbo compressor: Isentropic enthalpy change $h_{\text{ad}} = h_{\text{out}} - h_{\text{in}}$ vs. volumetric flow rate Q. The horizontal isolines describe the characteristic curves with constant rotational speed n. The vertical isolines represent the characteristic curves with constant efficiency η_{ad}.

Compressors Compressors are required in gas pipelines since the pressure decreases significantly after approximately 100 to 150 km and the gas speed reduces due to the friction of the gas flow on the pipe walls. The compression costs depend on the number of compressors and the compression ratio. Low compression ratios result in lower energy costs but require more compressor stations [8]. After compression, the pressure within a gas pipeline is up to 100 bar [53]. The compression is usually described by characteristic diagrams derived from measured values of the isentropic enthalpy change h_{ad}, i.e., the energy needed to compress one unit of mass of the gas, see, e.g., Fig. 2.10.

It must be ensured that compressors do not operate outside the stability limits of the map given by the chokeline and the surgeline, see the red lines in Fig. 2.10. Otherwise, the resulting stresses would exceed the machine's design limits and could lead to functional failure. The enthalpy change depends on the pressure and the temperature and can be described in the steady state without heat-exchange [14] by

$$h_{\text{ad}}(Q) = h_{\text{out}} - h_{\text{in}} = \mathsf{z}(p_{\text{in}}, T_{\text{in}}) T_{\text{in}} R \frac{\kappa}{\kappa - 1} \left(\left(\frac{p_{\text{out}}}{p_{\text{in}}} \right)^{\frac{\kappa-1}{\kappa}} - 1 \right), \tag{2.118}$$

where the isentropic exponent $\kappa > 1$ depends on pressure and temperature. However, in practice it is often considered as constant $\kappa = 1.29$ [66]. Furthermore, the volumetric flow rate is

$$Q = \frac{\mathsf{z}(p_{\text{in}}, T_{\text{in}}) T_{\text{in}} R}{p_{\text{in}}} q$$

with the temperature T_{in} at the inflow of the compressor. The temperature T_{out} at the outflow is given by [14]:

$$T_{\text{out}} = T_{\text{in}} \left(\frac{p_{\text{out}}}{p_{\text{in}}} \right)^{\frac{\kappa-1}{\kappa}}. \tag{2.119}$$

For turbo compressors, the compressor characteristic curve $h_{\text{ad}}(Q) = h_{\text{ad}}(Q, n)$ can be approximated by [43, 49]

$$h_{\text{ad}}(Q, n) = \alpha_2(n) Q^2 + \alpha_1(n) Q + \alpha_0(n) \tag{2.120}$$

with coefficients $\alpha_i(n)$ depending on the rotational speed n. Approximations of the coefficients are given by

$$\alpha_i(n) = \alpha_{i2} n^2 + \alpha_{i1} n + \alpha_{i0}.$$

The compressor map, see Fig. 2.10, is typically used for quadratic approximations for the lower, left, upper and right boundary of the compressor control curve. This gives rise to the conditions

$$\begin{aligned} h_{ad}(Q) &\geq \alpha_2^i Q^2 + \alpha_1^i Q + \alpha_0^i, \quad i \in \{\text{choke, speedMin}\}, \\ h_{ad}(Q) &\leq \alpha_2^i Q^2 + \alpha_1^i Q + \alpha_0^i, \quad i \in \{\text{surge, speedMax}\}, \end{aligned} \tag{2.121}$$

with α_j^{choke}, $\alpha_j^{\text{speedMin}}$, α_j^{surge} and $\alpha_j^{\text{speedMax}}$ describing the chokeline, minimum speed line, surgeline and maximum speed line. Besides turbo compressors also reciprocating compressors are used [74]. Reciprocating compressors are usually used only for small compressor capacities. For higher compressor capacities, one uses mainly turbo compressors with gas turbine drive [14].

Coolers The compression of the gas leads to a temperature increase due to the Joule–Thomson effect. Therefore, gas coolers are used for regulated cooling of the gas within compressor stations. The temperature decrease can be modeled as in [66], i.e.,

$$T_{\text{out}} = T_c + (T_{\text{in}} - T_c) \exp\left(-\frac{k}{q} \right). \tag{2.122}$$

Again, T_{in} and T_{out} are the temperature at the vertices v_{in} and v_{out} of the cooler, T_c is the temperature of the coolant at the inflow and k is a constant.

Compressor Groups and Compressor Stations Typical real gas networks contain compressor stations with multiple compressors. An important special case are simple compressor stations that compress gas along one pipeline in a fixed direction. Common

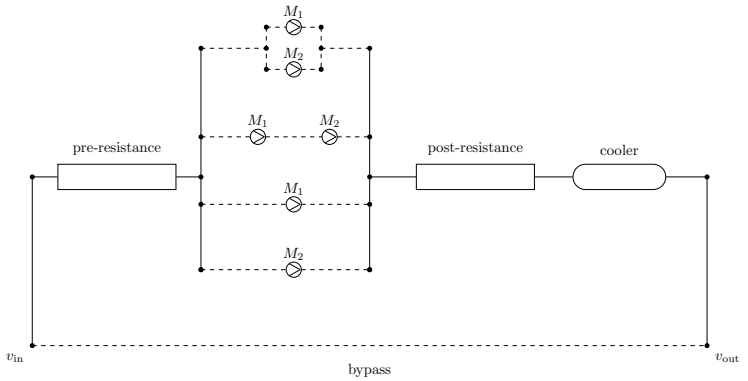


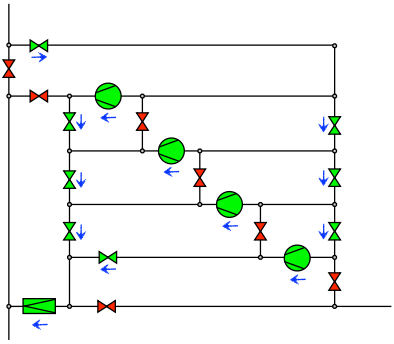
Fig. 2.11: Schematic representation of a compressor group with two compressors modelled as an edge from v_{in} to v_{out}, all theoretically possible configurations of these compressors and the bypass mode [74]. Depending on the selected configuration, gas flows through exactly one of the dotted paths, i.e., either via the bypass without pressure loss or via one compressor configuration, whereby the pressure loss in internal pipe connections is modeled by additional resistances.

simulation software such as SIMONE [58] provides macro elements describing simple compressor stations. In accordance to the terminology from [74] we denote them as *compressor groups*.

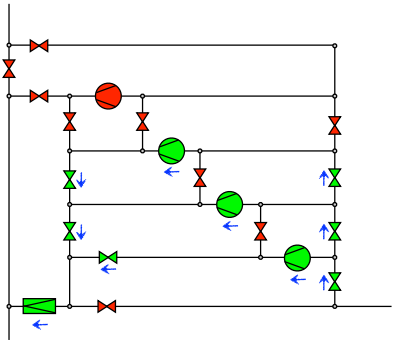
A compressor group consists of a number of compressors, one upstream and one downstream resistor modeling the cumulative pressure loss in the pipes within the compressor station, a cooler to prevent overheating and a so-called *bypass*, which controls the flow of the gas via a valve without compression, see Fig. 2.11. A compressor group allows a number of *configurations*, whereby a configuration specifies how a subset of the compressors is switched. There are series connections or parallel connections of compressors possible. Each compressor within one configuration is used at most once. Within the network, a compressor group is modeled by an edge connecting a vertex v_{in} with a vertex v_{out}. In the active case (no bypass mode), the compression direction points from v_{in} to v_{out}.

In complex gas networks, *compressor stations* connect several pipelines with each other. They are used to distribute gas between these pipelines, see Fig. 2.12. A compressor station can be operated in different *routes*. A route defines how the gas flows through the compressor station and which compressors are active. The possible routes are usually modeled on larger subnetworks that contain valves as well as pipes, compressors and compressor groups [74].

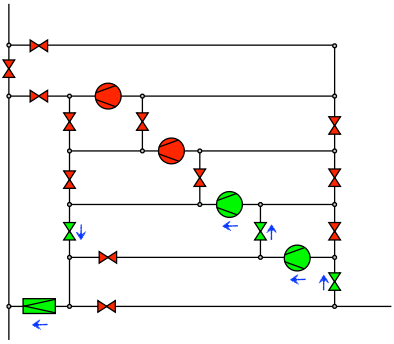
Suitable switching configurations for the valves and compressors can then be used to model the possible routes in the real network. Each route corresponds to a fixed state of each valve (open or closed) and each compressor (open, active, bypass) of the subnetwork. For an overview of additional, particularly simplified, models for compressors and compressor stations, we refer to [43].



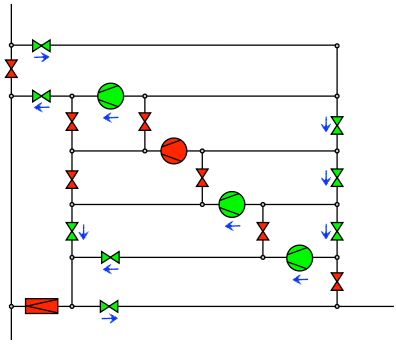
(a) 4-fold parallel compressed gas flow from north to south



(b) 3-fold parallel compressed gas flow from east to south



(c) 2-fold serial compressed gas flow from east to south



(d) 2-fold parallel compressed gas flow from north to east and 1-fold compressed gas flow from north to south

Fig. 2.12: Four routes of a real compressor station that connects one north to south pipeline with a pipeline directing to east in a T-shaped form.

2.10 Network Models

This section provides a hierarchy of gas network models with network element models on different levels of complexity described in the previous sections. It starts with a variety of coupling conditions. Those are natural extensions of the coupling conditions described in Sect. 2.5 for pipe networks, to more general networks additionally containing elements such as valves, resistances, controllers, and compressors. The descriptions here are restricted to the case of one gas component only. In case of gas mixtures, they need to be adapted to the pipe equations presented in Sect. 2.6.

Recall from Sect. 2.5.1 that the network topology is described by a directed and weakly connected graph $G = (\mathcal{V}, \mathcal{E})$ with vertices $v \in \mathcal{V}$ and edges $e \in \mathcal{E}$. The edges incident to some vertex $v \in \mathcal{V}$ are collected in the set $\mathcal{E}(v)$.

2.10.1 Coupling Conditions

This section describes the natural coupling conditions at the vertices of a gas network. They are canonical extensions of the coupling conditions for pipe networks described in Sect. 2.5 to general networks with further network elements such as valves, resistances, controllers, and compressors.

2.10.1.1 Flow Balance

Let us recall the coupling conditons for pipe networks from Sect. 2.5. Using the notation from Sect. 2.5.1 for the description of the network topology, the flow balance at each vertex $v \in \mathcal{V}$ of the network is given by

$$q^v + \sum_{e \in \mathcal{E}_{\text{pipe}}(v)} q^e(v) n^e(v) + \sum_{e \in \mathcal{E}_{\text{nopipe}}(v)} q^e n^e(v) = 0, \quad \text{for any } v \in \mathcal{V}, \tag{2.123}$$

with $\mathcal{E}_{\text{nopipe}}(v) := \mathcal{E}_{\text{comp}}(v) \cup \mathcal{E}_{\text{valv}}(v) \cup \mathcal{E}_{\text{res}}(v)$. Here q^v is the prescribed inflow/outflow at vertex v, namely $q^v = 0$ for demand vertices and $q^v \leq 0$ for supply vertices, see (2.30) in Sect. 2.5.2 and (2.36) in Sect. 2.5.3 for networks with pipes only. Note that the definition of sign factors $n^e(v)$ is given in equation (2.18). Defining the vectors

$$q_{\text{in}} := (q^e(v_{\text{in}}))_{e \in \mathcal{E}_{\text{pipe}}}, \; q := (q^e)_{e \in \mathcal{E}_{\text{nopipe}}}, \; q_* := (q^v)_{v \in \mathcal{V}},$$

condition (2.123) is equivalent to

$$q_* + A_{\text{in}}^{\text{pipe}} q_{\text{in}} + A_{\text{out}}^{\text{pipe}} q_{\text{out}} + (A_{\text{in}}^{\text{nopipe}} + A_{\text{out}}^{\text{nopipe}}) q = 0 \tag{2.124}$$

with the incidence matrices A_{in} and A_{out} defined in (2.19) and (2.20) collecting the pipe columns in $A_{\text{in}}^{\text{pipe}}$ and $A_{\text{out}}^{\text{pipe}}$ and the rest of the columns in $A_{\text{in}}^{\text{nopipe}}$ and $A_{\text{out}}^{\text{nopipe}}$. Notice that q_{in} , q_{out}, q and q_* are time dependent functions. The equations (2.123) and (2.124) are supposed to be satisfied for each point in time t.

2.10.1.2 Pressure Continuity

Pressure continuity for all vertices (cf. Sect. 2.5.2) can be written as

$$p^e(v) = p^v, \qquad v \in \mathcal{V}, \; e \in \mathcal{E}(v), \tag{2.125}$$

where p^v is the pressure value at vertex v. Defining the vectors

$$p_{\text{in}} := (p^e(v_{\text{in}}))_{e \in \mathcal{E}}, \quad p_{\text{out}} := (p^e(v_{\text{out}}))_{e \in \mathcal{E}}, \quad p_* := (p^v)_{v \in \mathcal{V}},$$

condition (2.125) is equivalent to

$$p_{\text{out}} = A_{\text{out}}^\top p_* \quad \text{and} \quad p_{\text{in}} = -A_{\text{in}}^\top p_* \tag{2.126}$$

with the incidence matrices A_{in} and A_{out} defined in (2.19) and (2.20). Notice that p_*, p_{in} and p_{out} are time dependent functions. Again equations (2.125) and (2.126) are supposed to be satisfied at each time point t.

Note that pressure continuity coupled with the flow balance equations does not guarantee energy conservation at inner vertices in certain flow regimes, see [80]. However, energy conservation is ensured when enthalpy continuity is imposed instead of pressure continuity, see [22, 79] and Sect. 2.5.2.

2.10.1.3 Enthalpy Continuity

Enthalpy continuity at all vertices (cf. (2.31) in Sect. 2.5.2) can be written as

$$h^e(v) = h^v, \qquad \text{for any } v \in \mathcal{V},\ e \in \mathcal{E}(v), \tag{2.127}$$

where h^v is the specific enthalpy at vertex v. Defining the vectors

$$h_{\text{in}} := (h^e(v_{\text{in}}))_{e\in\mathcal{E}}, \quad h_{\text{out}} := (h^e(v_{\text{out}}))_{e\in\mathcal{E}}, \quad h_* := (h^v)_{v\in\mathcal{V}},$$

condition (2.127) is equivalent to

$$h_{\text{out}} = A_{\text{out}}^\top h_* \quad \text{and} \quad h_{\text{in}} = -A_{\text{in}}^\top h_* \tag{2.128}$$

with the incidence matrices A_{in} and A_{out} defined in (2.19) and (2.20). Notice that h_*, h_{in} and h_{out} are time dependent functions. The equations (2.127) and (2.128) are to be understood as satisfied for each point in time t.

It should be noted that pressure and enthalpy continuity coincide for zero velocity. Hence, their difference can be expected to be small if the fluid velocity is very small compared to the speed of sound. Correspondingly, one should consider enthalpy continuity when models ISO1 or TA1 are used on the pipes. For the remaining models (ISO2, ISO3, ISO4, TA2, TA3, TA4) it is enough to consider pressure continuity, see Sect. 2.5.2.

2.10.2 PDE Gas Network Models

This section collects gas network models that are described by systems of PDEs. Since non-pipe elements are described by non-PDE models, we are restricted to gas networks consisting solely of pipe elements and to pipe models of type ISO1, ISO2, ISO2F, ISO3, TA1, TA2, or TA3. The following sections present the PDE systems for the pipe models ISO1, ISO2, ISO3, and TA1. They are compiled from Sections 2.3, 2.4, and 2.5. Their purpose is to illustrate the structure of the network PDEs and their boundary conditions corresponding to the chosen pipe model.

For ISO2F, TA2, and TA3 one can easily adapt the systems using the pipe equations (ISO2F), (TA2) and (TA3). For details of the isothermal and temperature-dependent pipe models see Sections 2.3 and 2.4.

2.10.2.1 ISO1 Pipe Network

The network equations are given by the isothermal Euler equations (ISO1) equipped with the enthalpy continuity equations (2.127) and the flow balance equations (2.123) ensuring energy conservation in the vertices, cf. Sect. 2.5.2:

$$\begin{aligned} \partial_t \rho^e + \partial_x \bar{q}^e = 0, \quad \partial_t v^e + \partial_x h^e = -\gamma^e |v^e| v^e, \quad & e \in \mathcal{E}, \\ h^e(\nu) = h_*^\nu, \quad & \nu \in \mathcal{V},\ e \in \mathcal{E}(\nu), \\ q^\nu + \sum_{e \in \mathcal{E}(\nu)} q^e(\nu) n^e(\nu) = 0, \quad & \nu \in \mathcal{V}, \end{aligned} \tag{2.129}$$

with the mass flux $\bar{q}^e = \rho^e v^e$, the mass flow $q^e = A^e \bar{q}^e$ and the specific enthalpy

$$h^e = \frac{1}{2}(v^e)^2 + P'(\rho^e) + g b^e$$

for each pipe e and the pressure potential $P(\rho) := \rho \int_1^\rho \frac{p(s)}{s^2}\,\mathrm{d}s$ satisfying $\rho P''(\rho) = p'(\rho)$. They are completed by an equation of state $f(p^e, \rho^e, T^e) = 0$ for each pipe, for example as described by (2.2) with T^e being fixed as the wall temperature T_w^e of the pipe.

2.10.2.2 ISO2 Pipe Network

The network equations are given by the semilinear pipe equations (ISO2) for small velocities, see Sect. 2.3.1, equipped with the pressure continuity (2.125) and the flow balance (2.123):

$$\begin{aligned} \partial_t \rho^e + \partial_x \bar{q}^e = 0, \quad \partial_t v^e + \partial_x p^e = -\gamma^e |v^e| v^e - g \rho^e \partial_x b, \quad & e \in \mathcal{E}, \\ p^e(\nu) = p_*^\nu, \quad & \nu \in \mathcal{V},\ e \in \mathcal{E}(\nu), \\ q^\nu + \sum_{e \in \mathcal{E}(\nu)} q^e(\nu) n^e(\nu) = 0, \quad & \nu \in \mathcal{V}, \end{aligned} \tag{2.130}$$

with the mass flux $\bar{q}^e = \rho^e v^e$ and the mass flow $q^e = A^e \bar{q}^e$ for each pipe e. They are completed by an equation of state $p^e = R \rho T_w^e z(p^e, T_w^e)$ for each pipe where T_w^e is the wall temperature of the pipe.

2.10.2.3 ISO3 Pipe Network

The network equations are given by the doubly nonlinear parabolic pipe equations (ISO3) for the friction-dominated case, see Sect. 2.3.1 equipped with the pressure continuity (2.125) and the flow balance (2.123):

$$\begin{aligned} \partial_t \rho^e + \partial_x \bar{q}^e = 0, \quad \partial_x p^e = -\gamma^e |v^e| v^e - g\rho^e \partial_x b, \quad & e \in \mathcal{E}, \\ p^e(v) = p_*^v, & v \in \mathcal{V},\ e \in \mathcal{E}(v), \\ q^v + \sum_{e \in \mathcal{E}(v)} q^e(v) n^e(v) = 0, & v \in \mathcal{V}, \end{aligned} \tag{2.131}$$

with the mass flux $\bar{q}^e = \rho^e v^e$ and the mass flow $q^e = A^e \bar{q}^e$ for each pipe e. They are completed by a equation of state $p^e = R\rho T_w^e \mathsf{z}(p^e, T_w^e)$ for each pipe where T_w^e is the wall temperature of the pipe.

2.10.2.4 TA1 Pipe Network

The network equations are given by the full Euler equations (TA1) equipped with the enthalpy continuity equations (2.127), the flow balance equations (2.123) and the perfect mixing condition for the entropy (2.39) ensuring energy dissipation and entropy conservation at junctions, cf. Sect. 2.5.3:

$$\begin{aligned} \partial_t \rho^e + \partial_x \bar{q}^e = 0, \quad \partial_t v^e + \partial_x h^e = -\gamma^e |v^e| v^e, \quad & e \in \mathcal{E}, \\ \partial_t E(\rho^e, v^e, T^e) + \partial_x ((E(\rho^e, v^e, T^e) + p^e) v^e) = \frac{k_w}{D^e}(T_w^e - T_w^e), \quad & e \in \mathcal{E}, \\ h^e(v) = h_*^v, & v \in \mathcal{V},\ e \in \mathcal{E}(v), \\ q^v + \sum_{e \in \mathcal{E}(v)} q^e(v) n^e(v) = 0, & v \in \mathcal{V}, \\ \frac{\max\{q^v, 0\} s^v + \sum_{e \in \mathcal{E}_{\text{in}}(v,q)} q^e(v) s^e(v) n^e(v)}{\max\{q^v, 0\} + \sum_{e \in \mathcal{E}_{\text{in}}(v,q)} q^e(v) n^e(v)} = s^e(v), & v \in \mathcal{V}, e \in \mathcal{E}_{\text{out}}(v, q), \end{aligned} \tag{2.132}$$

with the mass flux $\bar{q}^e = \rho^e v^e$, the mass flow $q^e = A^e \bar{q}^e$, the specific entropy s^e and the specific enthalpy

$$h^e = \frac{(v^e)^2}{2} + \frac{p^e}{\rho^e} + e^e - T_{\mathsf{w}} s^e$$

for each pipe e and the total energy density function $E(\rho, v, T) = \rho(\frac{1}{2}v^2 + gb + c_V T)$. They are completed by an equation of state $f(p^e, \rho^e, T^e) = 0$ for each pipe, for example as described by (2.2).

2.10.3 PDAE Gas Network Models

This section shall demonstrate that a fully dynamic modeling of the gas transport in real gas networks leads to a system of PDEs with algebraic constraints, or in other words, to a partial differential-algebraic equation system (PDAE). The full dynamic model system consists of PDE models describing pipe edges, non-differential equation models

describing non-pipe edges and algebraic models describing the coupling conditions at the vertices.

To enhance readability, here we restrict ourselves to a description of two model classes only. Other model classes can straightforwardly be derived using different pipe models from Sections 2.3 and 2.4 or other models for non-pipe elements described in Sect. 2.9. First, we consider a pipe network with compressors using the full Euler equations (TA1) for pipes. It explains how PDE pipe models are coupled to non-differential equation models for non-pipe edges using compressor edges as an example. Secondly, we formulate the PDAE system for pipe networks with compressors, check valves, and resistors using the semilinear isothermal equations (ISO2) for pipes. Stability and stable spatial discretizations of this PDAE system are presented in [45]. The numerical analysis for general PDAE systems, also considered as operator DAEs, is still an open research topic. Several approaches for linear PDAE systems are presented in [28, 54, 60, 61, 78]. For the numerical analysis of nonlinear PDAE systems in specific applications we refer to [1, 2, 6, 7, 27, 37, 62].

We introduce the notation $\mathcal{E}_{\text{pipe}}$, $\mathcal{E}_{\text{comp}}$, $\mathcal{E}_{\text{valv}}$ and $\mathcal{E}_{\text{res}}$ for the sets of pipe, compressor, valve and resistor edges, respectively. Correspondingly, the pipe, compressor, valve and resistor edges incident to some vertex $v \in \mathcal{V}$ are collected in the sets $\mathcal{E}_{\text{pipe}}(v)$, $\mathcal{E}_{\text{comp}}(v)$, $\mathcal{E}_{\text{valv}}(v)$, and $\mathcal{E}_{\text{res}}(v)$.

2.10.3.1 TA1 Pipe Network with Compressors

We consider a full dynamic model for pipe networks with compressors. It collects the full Euler equations (TA1) for pipes, the equations (2.118), (2.119) for compressors equipped with the enthalpy continuity equations (2.128), the flow balance equations (2.123) and the entropy condition (2.39) for pipes:

$$
\begin{aligned}
\partial_t \rho^e + \partial_x \bar{q}^e = 0, \quad \partial_t v^e + \partial_x h^e &= -\gamma^e |v^e| v^e, && e \in \mathcal{E}_{\text{pipe}},\\
\partial_t E(\rho^e, v^e, T^e) + \partial_x((E(\rho^e, v^e, T^e) + p^e)v^e) &= \frac{k_w}{D^e}(T_w^e - T^e), && e \in \mathcal{E}_{\text{pipe}},\\
\mathsf{z}(p_{\text{in}}^e, T_{\text{in}}^e) T_{\text{in}}^e R \frac{\kappa^e}{\kappa^e - 1} \left(\left(\frac{p_{\text{out}}^e}{p_{\text{in}}^e} \right)^{\frac{\kappa^e - 1}{\kappa^e}} - 1 \right) &= h_{\text{out}}^e - h_{\text{in}}^e, && e \in \mathcal{E}_{\text{comp}},\\
T_{\text{in}}^e \left(\frac{p_{\text{out}}^e}{p_{\text{in}}^e} \right)^{\frac{\kappa^e - 1}{\kappa^e}} &= T_{\text{out}}^e, && e \in \mathcal{E}_{\text{comp}},\\
q^v + \sum_{e \in \mathcal{E}_{\text{pipe}}(v)} q^e(v) n^e(v) + \sum_{e \in \mathcal{E}_{\text{comp}}(v)} q^e n^e(v) &= 0, && v \in \mathcal{V},\\
\frac{\max\{q^v, 0\} s^v + \sum_{e \in \mathcal{E}_{\text{in}}(v,q)} q^e(v) s^e(v) n^e(v)}{\max\{q^v, 0\} + \sum_{e \in \mathcal{E}_{\text{in}}(v,q)} q^e(v) n^e(v)} &= s^e(v), && v \in \mathcal{V}, e \in \mathcal{E}_{\text{out}}(v, q),\\
h_{\text{out}} = A_{\text{out}}^\top h_*, \quad h_{\text{in}} &= -A_{\text{in}}^\top h_*,
\end{aligned}
\tag{2.133}
$$

with the mass flux $\bar{q}^e = \rho^e v^e$, the mass flow $q^e = A^e \bar{q}^e$, the specific entropy s^e and the specific enthalpy

$$h^e = \frac{(v^e)^2}{2} + \frac{p^e}{\rho^e} + e^e - T_{\mathsf{w}} s^e$$

for each pipe e and the total energy density function $E(\rho, v, T) = \rho(\frac{1}{2}v^2 + gb + c_V T)$. They are completed by an equation of state $f(p^e, \rho^e, T^e) = 0$ for each pipe, for example as described by (2.2). The vectors h_{out} and h_{in} in $\mathbb{R}^E$ collect all enthalpy values h^e_{out} and h^e_{in} of pipes and compressors with $h^e_{\text{out}} := h^e(\nu_{\text{out}})$ and $h^e_{\text{in}} := h^e(\nu_{\text{in}})$ for pipes. Further, the vector $h_* \in \mathbb{R}^V$ consists of all h^ν_* where h^ν_* is the specific enthalpy at vertex ν.

2.10.3.2 ISO2 Pipe Network with Check Valves and Resistors

The network equations include the semilinear equations (ISO2) for pipes, the equations (2.110) for check valves, the equations (2.112) for resistors as well as the pressure continuity (2.125) and the flow balance equations (2.123):

$$\begin{aligned}
\partial_t \varphi_\rho(p^e) + \partial_x \bar{q}^e &= 0, && e \in \mathcal{E}_{\text{pipe}},\\
\partial_t \bar{q}^e + \partial_x p^e &= -\frac{\lambda^e}{2D^e}\frac{q^e\,|\bar{q}^e|}{\varphi_\rho(p^e)} - g\varphi_\rho(p^e)\partial_x b^e, && e \in \mathcal{E}_{\text{pipe}},\\
(p^e_{\text{in}} - p^e_{\text{out}})q^e &= 0, \qquad q^e = \max\{q^e, 0\}, && e \in \mathcal{E}_{\text{valv}},\\
p^e_{\text{in}}(p^e_{\text{in}} - p^e_{\text{out}}) &= r^e q^e |q^e|, && e \in \mathcal{E}_{\text{res}},\\
p^e(\nu) &= p^\nu_*, && \nu \in \mathcal{V},\ e \in \mathcal{E}(\nu),\\
-q^\nu &= \sum_{e \in \mathcal{E}_{\text{pipe}}(\nu)} q^e(\nu) n^e(\nu) + \sum_{e \in \mathcal{E}_{\text{comp}}(\nu) \cup \mathcal{E}_{\text{res}}(\nu)} q^e n^e(\nu), && \nu \in \mathcal{V},
\end{aligned} \tag{2.134}$$

with mass flux $\bar{q}^e = \rho^e v^e$, mass flow $q^e = A^e \bar{q}^e$ and density function $\varphi_\rho(p) := \frac{p}{RTz(p,T)}$ with constant temperature T and the pipe friction coefficient λ^e, see Sect. 2.2.2.3.

2.10.4 DAE Gas Network Models

Here, we present two spatially discretized network models resulting in differential-algebraic equations (DAEs). The first one is based on the energy-preserving discretization (2.106) for the model (ISO1) on each pipe which uses the port-Hamiltonian form described in Sect. 2.8.3. We show that it results in a DAE system of perturbation index 2. The second one uses a topology adapted two-point-discretization [45] resulting in a DAE of perturbation index 1 but does not guarantee energy preservation. Note that a perturbation index higher than 1 corresponds to an ill-posed problem since a DAE system

$$f(\partial_t y, y, t) = 0, \quad y(t_0) = y_0 \tag{2.135}$$

has perturbation index k [40] if and only if k is the smallest number with the property that, for all sufficiently small perturbations δ, there exists a constant $c > 0$ such that

$$\|y - y^\delta\|_\infty \leq c\left(\|y_0 - y_0^\delta\| + \sum_{i=0}^{k-1} \|\delta^{(i)}\|_\infty\right)$$

for any solution y satisfying (2.135) and any solution y^δ of the perturbed DAE system

$$f(\partial_t y^\delta, y^\delta, t) = \delta, \qquad y^\delta(t_0) = y_0^\delta. \tag{2.136}$$

2.10.4.1 ISO1 Pipe Network with Compressors in Port-Hamiltonian Form

The energy preserving discretization (2.106) for model (ISO1) described in Sect. 2.8.3 provides, for each pipe edge e, a system in port-Hamiltonian form

$$\begin{aligned} E^e(c^e)\partial_t c^e &= \tilde{J}^e \tilde{z}^e(c^e) - \tilde{R}^e(c^e)\tilde{z}^e(c^e) - B^e h_*, \\ 0 &= q_*^e + (B^e)^\top \tilde{z}^e(c^e), \end{aligned} \tag{2.137}$$

where E^e and B^e are given by (2.101), $\tilde{J}^e := \frac{1}{A^e} J^e$ by (2.104), $\tilde{R}^e := \frac{1}{A^e} R^e$ by (2.105) and $\tilde{z}^e := A^e z^e$ by (2.102).

The model for compressor edges can also be written in the form (2.137) with the compressor flux $\tilde{z}^e(c^e) := c^e := q^e$, the enthalpy change $h_{\text{in}} - h_{\text{out}} =: B^e h_*$ and

$$E^e := 0, \quad \tilde{J}^e := 0, \quad \tilde{R}^e(c^e) := \frac{h_{\text{ad}}(Q^e, n^e)}{q^e} \quad \text{with } Q^e = \frac{q^e}{\varphi_\rho(p_{\text{in}}^e)}.$$

The network DAE is then given by

$$\begin{aligned} E(c)\partial_t c &= \tilde{J}\tilde{z}(c) - \tilde{R}(c)\tilde{z}(c) - Bh_* \\ 0 &= q_* + B^\top \tilde{z}(c) \end{aligned} \tag{2.138}$$

with $c^\top := (\ldots, (c^e)^\top, \ldots)$, $(\tilde{z}(c))^\top := (\ldots, (\tilde{z}^e(c^e))^\top, \ldots)$ and

$$\begin{aligned} E(c) &:= \operatorname{diag}_{e\in\mathcal{E}}(\ldots, E^e(c^e), \ldots), & \tilde{J} &:= \operatorname{diag}_{e\in\mathcal{E}}(\ldots, \tilde{J}^e, \ldots), \\ \tilde{R}(c) &:= \operatorname{diag}_{e\in\mathcal{E}}(\ldots, \tilde{R}^e(c^e), \ldots), & B^\top &:= (\ldots, (B^e)^\top, \ldots) \quad \text{for all } e \in \mathcal{E}. \end{aligned}$$

Note that $R(c)$ is positive semidefinite only if $c_\rho \geq 0$ (which corresponds to non-negative pipe densities) and the compressors are controlled such that $\tilde{R}^e(c^e) \geq 0$ for all compressor edges. If we collect all pipe edge variables $A^e c^e$ in c_{pipe} and all compressor edge variables c^e in c_{comp}, then one can rewrite (2.138) as

$$\begin{aligned} E_{\text{pipe}}(c_{\text{pipe}})\partial_t c_{\text{pipe}} &= \varphi(c_{\text{pipe}}) - B_{\text{pipe}} h_*, \\ 0 &= \psi(c_{\text{comp}}, n_{\text{comp}}) - B_{\text{comp}} h_*, \\ 0 &= q_* + B_{\text{pipe}}^\top c_{\text{pipe}} + B_{\text{comp}}^\top c_{\text{comp}} \end{aligned} \tag{2.139}$$

with $E_{\text{pipe}}(c_{\text{pipe}}) := \operatorname{diag}_{e\in\mathcal{E}_{\text{pipe}}}(\ldots, \frac{1}{A^e}E^e(c^e), \ldots)$. Note that the in/out flow $q_{*,i}$ at vertex v_i corresponds to an unknown if and only if v_i is a boundary vertex where the enthalpy $h_{*,i}$ is fixed. We take the usual assumption from practice that the speed n_{comp} is controlled such that the second equation of (2.139) is fulfilled for a prescribed desired enthalpy change $B_{\text{comp}} h_*$ which corresponds to a prescribed pressure ratio for compressors.

For the analysis of the perturbation index of the DAE (2.139), we assume that E, φ and ψ are sufficiently smooth. Additionally, we assume that the solution components $c^e = (c_\rho^e, c_q^e)$ satisfy $c_\rho^e > 0$ for all pipe edges e and that each vertex of the network is connected to at least one pipe edge. Then, B_{pipe} has full column rank and we know from Sect. 2.8.3 that $E_{\text{pipe}}(c_{\text{pipe}})$ and $B_{\text{pipe}}^\top E_{\text{pipe}}^{-1}(c_{\text{pipe}})B_{\text{pipe}}$ are positive definite.

Then, one can verify that the DAE (2.139) has perturbation index 2 unless all vertices of the network are either supply nodes with fixed enthalpy or have a compressor edge directed to them. This becomes clear from the fact that those parts of h_* that are not prescribed by supply nodes or compressor edges are determined by a hidden constraint resulting from the first derivative of the third equation of (2.139) inserted into the first equation of (2.139).

2.10.4.2 ISO2 Pipe Networks with Valves, Resistors and Compressors

For each pipe edge e, we use the simple two-point discretization in space [38, 45]

$$\begin{aligned} \partial_t(\varphi_\rho(p_{\text{out}}^e)) + \frac{1}{A^e \ell^e}(q_{\text{out}}^e - q_{\text{in}}^e) &= 0, \\ \partial_t q_{\text{in}}^e + \frac{A^e}{\ell^e}(p_{\text{out}}^e - p_{\text{in}}^e) &= f^e(p_{\text{out}}^e, q_{\text{in}}^e), \end{aligned}$$

with φ_ρ defined in Sect. 2.10.3.2. In this formulation we take the flows $q_{\text{in}}^e = A^e \bar{q}_{\text{in}}^e$ and $q_{\text{out}}^e = A^e \bar{q}_{\text{out}}^e$ with the pipe cross sectional area A^e, the spatial stepsize ℓ^e (pipe length) and

$$f^e(p, q) := -\frac{\lambda^e}{2D^e A^e}\frac{q|q|}{\varphi_\rho(p)} - gA^e\varphi_\rho(p)\partial_x b^e$$

with the pipe diameter D^e. Recall that q_{in}^e and q_{out}^e denote the flows in edge direction at the vertices v_{in} and v_{out} as described in Sect. 2.5.1 and Fig. 2.9. For pipe networks including valves modeled by (2.110), resistors described by (2.111) and compressors expressed simply prescribing the output pressure as a given pressure p_c, we obtain the DAE system

$$
\begin{aligned}
\partial_t(\varphi_\rho(p^e_{\text{out}})) + \frac{1}{A^e \ell^e}(q^e_{\text{out}} - q^e_{\text{in}}) &= 0, && e \in \mathcal{E}_{\text{pipe}},\\
\partial_t q^e_{\text{in}} + \frac{A^e}{\ell^e}(p^e_{\text{out}} - p^e_{\text{in}}) &= f^e(p^e_{\text{out}}, q^e_{\text{in}}), && e \in \mathcal{E}_{\text{pipe}},\\
(p^e_{\text{in}} - p^e_{\text{out}})q^e = 0, \quad q^e &= \max\{q^e, 0\}, && e \in \mathcal{E}_{\text{valv}},\\
p^e_{\text{in}} - p^e_{\text{out}} &= \psi^e(p^e_{\text{in}}, q^e), && e \in \mathcal{E}_{\text{res}},\\
p^e_{\text{out}} &= p^e_c, && e \in \mathcal{E}_{\text{comp}},\\
p_{\text{in}} = -A_{\text{in}}^\top p_*, \quad p_{\text{out}} &= -A_{\text{out}}^\top p_*,\\
q + A^{\text{pipe}}_{\text{in}} q_{\text{in}} + A^{\text{pipe}}_{\text{out}} q_{\text{out}} + (A^{\text{nopipe}}_{\text{in}} + A^{\text{nopipe}}_{\text{in}})q &= 0
\end{aligned}
\tag{2.140}
$$

with

$$
\psi^e(p, q) := \frac{\zeta^e}{2(A^e)^2} \frac{q|q|}{\varphi_\rho(p)}
$$

and p_{in}, p_{out}, p_*, q_{in}, q_{out}, q and q_* defined in Sect. 2.10.1. The system (2.140) has perturbation index 1 if all of the following conditions are satisfied [45]

- No edge is directed to a supply vertex.
- All vertices that are not supply vertices have at least one pipe edge directed to them.
- If a vertex has a resistor or compressor edge directed to it then no pipe edges are directed to it.

The conditions can be fulfilled by adapting the edge directions [45] if the gas network graph satisfies the following assumptions:

- There is no pipe edge that directly connects two supply vertices.
- Each connected component of the network graph resulting from removing the valve edges contains a supply vertex.
- Non-pipe edges do not have common vertices.

Note that the adaption of the pipe edge directions is in fact an adaption of the spatial discretization since it selects at which pipe edge one evaluates the time derivatives.

2.10.5 AE Gas Network Models

We finish the section on network models with models containing only algebraic equations (AE). First, we consider the simplest case of pipe networks described by the stationary model equations (ISO4) for pipe edges. It leads to constant flows on the pipe edges and reduces, therefore, to a system of dimension $|\mathcal{E}|+|\mathcal{V}|$ with one flux value on each edge and one pressure value on each vertex. The second algebraic equation model accounts for the instationary behavior. It results from the two-point implicit box discretization given in Sect. 2.8.4 for (ISO2) pipe models. The resulting dimension is here $N_t(|\mathcal{E}|+2|\mathcal{V}|)$ with N_t the number of time steps.

2.10.5.1 ISO4 Pipe Networks

With reference to Sect. 2.3.3, the stationary pipe equations (ISO4) are given by

$$\begin{aligned}\partial_x q &= 0,\\ \partial_x(p^2) = 2p\partial_x p &= -\frac{c^2\lambda}{DA^2} q\,|q|\,,\end{aligned}$$

with the mass flow $q = A\rho v$ and the speed of sound c satisfying $c^2 = RTz_0$ for $\mathsf{z}(p) \equiv z_0$. We see that q is constant in space on each pipe e and the second equation yields

$$p_{\text{out}}^2 - p_{\text{in}}^2 = -\frac{c^2\lambda}{D} q\,|q|\,\ell, \tag{2.141}$$

where ℓ is the length of the edge e. Combining the flow balance equation (2.124) and the pressure continuity (2.126), the whole network system is then given by

$$\begin{aligned}(A_{\text{out}}^\top p_*)^2 - (A_{\text{in}}^\top p_*)^2 &= f(q),\\ q_* + (A_{\text{in}} + A_{\text{out}})q &= 0,\end{aligned} \tag{2.142}$$

with the vertex pressures $p_*^\top = (\dots, p_*^\nu, \dots)$ for all $\nu \in \mathcal{V}$ and the edge fluxes $q^\top = (\dots, q^e, \dots)$ for all $e \in \mathcal{E}$ and

$$f(q)^\top = (\dots, -\frac{(c^e)^2\lambda^e}{D^e(A^e)^2} q^e\,|q^e|\,\ell^e, \dots) \quad \text{for all } e \in \mathcal{E}.$$

Note, the squares of the vectors in (2.142) are considered as component-wise squares.

2.10.5.2 ISO2 Pipe Networks After Implicit Box Discretization

Applying the two-point implicit box discretization given in Sect. 2.8.4 to pipe networks modeled by the (ISO2) equation, we obtain the following system of algebraic equations:

$$\begin{aligned}\frac{1}{2}\left(\widehat{\varphi}_\rho(A_{\text{in}}^\top p_*^{n+1}) - \widehat{\varphi}_\rho(A_{\text{out}}^\top p_*^{n+1})\right) &= \frac{1}{2}\left(\widehat{\varphi}_\rho(A_{\text{in}}^\top p_*^{n}) - \widehat{\varphi}_\rho(A_{\text{out}}^\top p_*^{n})\right)\\ &\quad + \Delta t D_\ell\left(q_{\text{out}}^{n+1} - q_{\text{in}}^{n+1}\right),\\ \frac{1}{2}\left(q_{\text{in}}^{n+1} + q_{\text{out}}^{n+1}\right) &= \frac{1}{2}\left(q_{\text{in}}^{n} + q_{\text{out}}^{n}\right) - \Delta t D_\ell\left(A_{\text{out}}^\top p_*^{n+1} + A_{\text{in}}^\top p_*^{n+1}\right)\\ &\quad + \frac{1}{2}\Delta t\left(f(-A_{\text{in}}^\top p_*^{n+1}, q_{\text{in}}^{n+1}) + f(A_{\text{out}}^\top p_*^{n+1}, q_{\text{out}}^{n+1})\right),\\ q_*^{n+1} + A_{\text{in}} q_{\text{in}}^{n+1} + A_{\text{out}} q_{\text{out}}^{n+1} &= 0,\end{aligned} \tag{2.143}$$

with $\widehat{\varphi}_\rho(p) \coloneqq (\dots, \varphi_\rho(p^e), \dots)^\top$ using φ_ρ defined in Sect. 2.10.3.2 and

$$f(p,q) \coloneqq (\ldots, -\frac{\lambda^e}{2D^e(A^e)^2}\frac{q^e|q^e|}{\varphi_\rho(p^e)} - g\varphi_\rho(p^e)\partial_x b^e, \ldots)^\top \quad \text{for all } e \in \mathcal{E},$$

$$D_\ell \coloneqq \operatorname{diag}\{\ldots, \frac{1}{\ell^e} \ldots\} \quad \text{for all } e \in \mathcal{E}.$$

Acknowledgements This work was supported by the German Research Foundation (DFG) within Subprojects A04, B01, B03, C02, C05, and C09 in the Sonderforschungsbereich/Transregio 154 "Mathematical Modelling, Simulation and Optimization using the Example of Gas Networks" (Project ID 239904186).

References

1. G. Alì, A. Bartel, M. Günther, and C. Tischendorf. Elliptic partial differential-algebraic multiphysics models in electrical network design. *Mathematical Models and Methods in Applied Sciences*, 13(09):1261–1278, 2003. doi:10.1142/S0218202503002908.
2. R. Altmann, T. Levajković, and H. Mena. Operator differential-algebraic equations with noise arising in fluid dynamics. *Monatshefte für Mathematik*, 182(4):741–780, 2017. doi:10.1007/s00605-016-0931-z.
3. B. D. Andrews and P. E. Farrell. Enforcing conservation laws and dissipation inequalities numerically via auxiliary variables. *SIAM Journal on Scientific Computing*, 47(6):A3516–A3535, 2025. doi:10.1137/25M1756673.
4. P. Bales. Hierarchische Modellierung der Eulerschen Flussgleichungen in der Gasdynamik. Diplomarbeit, Technische Universität Darmstadt, Fachbereich Mathematik, Darmstadt, 2005.
5. A. Bamberger, M. Sorine, and J. P. Yvon. Analyse et contrôle d'un réseau de transport de gaz. In *Computing Methods in Applied Sciences and Engineering (Proc. Third Internat. Sympos., Versailles, 1977), II*, volume 91 of *Lecture Notes in Phys.*, pages 347–359. Springer, Berlin-New York, 1979. doi:10.1007/3-540-09119-X_110.
6. A. Bartel and M. Günther. PDAEs in refined electrical network modeling. *SIAM Review*, 60(1):56–91, 2018. doi:10.1137/17M1113643.
7. A. Bartel and R. Pulch. A concept for classification of partial differential algebraic equations in nanoelectronics. In L. L. Bonilla, M. Moscoso, G. Platero, and J. M. Vega, ed., *Progress in Industrial Mathematics at ECMI 2006*, pages 506–511. Springer Berlin Heidelberg, 2008. doi:10.1007/978-3-540-71992-2_79.
8. R. Boberg, M. Engshuber, and J. Garstka. *Erdgas. Bereitstellung, Anwendung, Umwandlung*. Deutscher Verlag für Grundstoffindustrie, Leipzig, 1974.
9. D. Bothe and W. Dreyer. Continuum thermodynamics of chemically reacting fluid mixtures. *Acta Mechanica*, 226(6):1757–1805, 2015. doi:10.1007/s00707-014-1275-1.
10. A. Bressan, Č. Sunčica, G. Mauro, M. Herty, and B. Piccoli. Flows on networks: recent results and perspectives. *EMS Surveys in Mathematical Sciences*, 1(1):47–111, 2014. doi:10.4171/EMSS/2.
11. J. Brouwer, I. Gasser, and M. Herty. Gas pipeline models revisited: Model hierarchies, nonisothermal models, and simulations of networks. *Multiscale Modeling & Simulation*, 9(2):601–623, 2011. doi:10.1137/100813580.
12. E. Celledoni and E. H. Høiseth. Energy-preserving and passivity-consistent numerical discretization of port-Hamiltonian systems, 2017. arXiv:1706.08621.
13. Y. Cengel and M. Boles. *Thermodynamics: An Engineering Approach*. McGraw Hill, 2015.
14. G. Cerbe. *Grundlagen der Gastechnik*. Hanser, 2008.
15. S. Chaturantabut, C. Beattie, and S. Gugercin. Structure-preserving model reduction for nonlinear port-Hamiltonian systems. *SIAM Journal on Scientific Computing*, 38(5):B837–B865, 2016. doi:10.1137/15M1055085.
16. N. H. Chen. An explicit equation for friction factor in pipe. *Industrial & Engineering Chemistry Fundamentals*, 18(3):296–297, 1979. doi:10.1021/i160071a019.

17. J. Cheng and C.-W. Shu. High order schemes for CFD: A review. *Chinese Journal of Computational Physics*, 26:636–655, 2009.
18. B. Cockburn, G. Karniadakis, and C.-W. Shu, ed. *Discontinuous Galerkin Methods: Theory, Computation and Applications*, volume 11 of *Lecture Notes in Computational Science and Engineering*. Springer, 2000. doi:10.1007/978-3-642-59721-3.
19. C. M. Dafermos. *Hyperbolic Conservation Laws in Continuum Physics*, volume 325 of *Fundamental Principles of Mathematical Sciences*. Springer-Verlag, Berlin, fourth edition, 2016. doi:10.1007/978-3-662-49451-6.
20. P. Degond and M. Tang. All speed scheme for the low Mach number limit of the isentropic Euler equations. *Communications in Computational Physics*, 10(1):1–31, 2011. doi:10.4208/cicp.210709.210610a.
21. P. Domschke, B. Geißler, O. Kolb, J. Lang, A. Martin, and A. Morsi. Combination of nonlinear and linear optimization of transient gas networks. *INFORMS Journal on Computing*, 23:605–617, 2011. doi:10.1287/ijoc.1100.0429.
22. H. Egger. A robust conservative mixed finite element method for isentropic compressible flow on pipe networks. *SIAM Journal on Scientific Computing*, 40(1):A108–A129, 2018. doi:10.1137/16M1094373.
23. H. Egger and J. Giesselmann. Stability and asymptotic analysis for instationary gas transport via relative energy estimates. *Numerische Mathematik*, 153:701–728, 2023. doi:10.1007/s00211-023-01349-9.
24. H. Egger, J. Giesselmann, T. Kunkel, and N. Philippi. An asymptotic-preserving discretization scheme for gas transport in pipe networks. *IMA Journal of Numerical Analysis*, 43(4):2137–2168, 2022. doi:10.1093/imanum/drac032.
25. H. Egger, O. Habrich, and V. Shashkov. On the energy stable approximation of Hamiltonian and gradient systems. *Computational Methods in Applied Mathematics*, 21:335–349, 2021. doi:10.1515/cmam-2020-0025.
26. J. Ekaterinaris. High-order accurate, low numerical diffusion methods for aerodynamics. *Progress in Aerospace Sciences*, 41:192–300, 2005. doi:10.1016/j.paerosci.2005.03.003.
27. E. Emmrich and V. Mehrmann. Operator differential-algebraic equations arising in fluid dynamics. *Computational Methods in Applied Mathematics*, 13(4):443–470, 2013. doi:10.1515/cmam-2013-0018.
28. M. Erbay, B. Jacob, K. Morris, T. Reis, and C. Tischendorf. Index concepts for linear differential-algebraic equations in finite and infinite dimensions. *DAE Panel*, 2, 2024. doi:10.52825/dae-p.v2i.2514.
29. A. Fazeny, M. Burger, and J.-F. Pietschmann. Optimal transport on gas networks. *European Journal of Applied Mathematics*, pages 1–33, 2025. doi:10.1017/S0956792525000051.
30. E. J. Finnemore and J. E. Franzini. *Fluid Mechanics with Engineering Applications*. McGraw-Hill, 10th edition, 2002.
31. U. S. Fjordholm, M. Musch, and N. H. Risebro. Well-posedness and convergence of a finite volume method for conservation laws on networks. *SIAM Journal on Numerical Analysis*, 60(2):606–630, 2022. doi:10.1137/21M145001X.
32. A. Frommer, M. Günther, B. Liljegren-Sailer, and N. Marheineke. Operator splitting for port-Hamiltonian systems, 2023. arXiv:2304.01766.
33. A. Fügenschuh, B. Geißler, R. Gollmer, A. Morsi, M. E. Pfetsch, J. Rövekamp, M. Schmidt, K. Spreckelsen, and M. C. Steinbach. Physical and technical fundamentals of gas networks. In T. Koch, B. Hiller, M. E. Pfetsch, and L. Schewe, ed., *Evaluating Gas Network Capacities*, MOS-SIAM Series on Optimization, chapter 2, pages 17–43. SIAM, 2015. doi:10.1137/1.9781611973693.ch2.
34. J. Giesselmann, A. Karsai, and T. Tscherpel. Energy-consistent Petrov–Galerkin time discretization of port-Hamiltonian systems. *SMAI Journal of computational mathematics*, 11:335–367, 2025. doi:10.5802/smai-jcm.127.
35. E. Godlewski and P.-A. Raviart. *Numerical Approximation of Hyperbolic Systems of Conservation Laws*, volume 118 of *Applied Mathematical Sciences*. Springer Verlag, 1996. doi:10.1007/978-1-4612-0713-9.

36. S. Gottlieb, Z. J. Grant, J. Hu, and R. Shu. High order strong stability preserving multiderivative implicit and IMEX Runge-Kutta methods with asymptotic preserving properties. *SIAM Journal on Numerical Analysis*, 60(1):423–449, 2022. doi:10.1137/21M1403175.
37. D. Groh and C. Tischendorf. Error analysis for Galerkin-BDF discretizations of DAEs with elliptic operator constraints. *Journal of Computational and Applied Mathematics*, 422:114946, 2023. doi:10.1016/j.cam.2022.114946.
38. S. Grundel, L. Jansen, N. Hornung, T. Clees, C. Tischendorf, and P. Benner. Model order reduction of differential algebraic equations arising from the simulation of gas transport networks. In S. Schöps, A. Bartel, M. Günther, E. J. W. ter Maten, and P. C. Müller, ed., *Progress in Differential-Algebraic Equations*, pages 183–205. Springer Berlin Heidelberg, 2014. doi:10.1007/978-3-662-44926-4_9.
39. E. Hairer. Energy-preserving variant of collocation methods. *Journal of Numerical Analysis, Industrial and Applied Mathematics*, 5(1-2):73–84, 2010.
40. E. Hairer and G. Wanner. *Solving Ordinary Differential Equations II*. Springer, 2010. doi:10.1007/978-3-642-05221-7.
41. S.-A. Hauschild and N. Marheineke. On a port-Hamiltonian formulation and structure-preserving numerical approximations for thermodynamic compressible fluid flow, 2024. arXiv:2404.05358.
42. F. Hennings, M. Petkovic, and T. Streubel. On the numerical treatment of interlaced target values: modeling, optimization and simulation of regulating valves in gas networks. *Optimization and Engineering*, 25(1):491–527, 2024. doi:10.1007/s11081-023-09812-0.
43. B. Hiller and T. Walther. Modelling compressor stations in gas networks. Technical report, Zuse Institute Berlin, 2017. URL: https://opus4.kobv.de/opus4-zib/frontdoor/deliver/index/docId/6744/file/ZR-17-67.pdf.
44. Honeywell. Unisim design. Operations Guide, 2010.
45. C. Huck. *Perturbation analysis and numerical discretisation of hyperbolic partial differential algebraic equations describing flow networks*. Dissertation, Humboldt-Universität zu Berlin, 2018.
46. W. Hundsdorfer and J. G. Verwer. *Numerical Solution of Time-Dependent Advection-Diffusion-Reaction Equations*, volume 33 of *Computational Mathematics*. Springer Verlag, 2003. doi:10.1007/978-3-662-09017-6.
47. B. Jacob and H. Zwart. *Linear Port-Hamiltonian Systems on Infinite-Dimensional Spaces*. Operator Theory: Advances and Applications, 223. Birkhäuser/Springer Basel AG, Basel CH, 2012. doi:10.1007/978-3-0348-0399-1.
48. S. R. Kazi, K. Sundar, S. Srinivasan, and A. Zlotnik. Modeling and optimization of steady flow of natural gas and hydrogen mixtures in pipeline networks. *International Journal of Hydrogen Energy*, 54:14–24, 2024. doi:10.1016/j.ijhydene.2023.12.054.
49. T. Koch, B. Hiller, M. E. Pfetsch, and L. Schewe, ed. *Evaluating Gas Network Capacities*. MOS-SIAM Series on Optimization. SIAM, 2015. doi:10.1137/1.9781611973693.
50. O. Kolb. *Simulation and Optimization of Gas and Water Supply Networks*. Dissertation, Technische Universität Darmstadt, 2011.
51. O. Kolb, J. Lang, and P. Bales. An implicit box scheme for subsonic compressible flow with dissipative source term. *Numerical Algorithms*, 53(2):293–307, 2010. doi:10.1007/s11075-009-9287-y.
52. P. Kotyczka and L. Lefèvre. Discrete-time port-Hamiltonian systems based on Gauss–Legendre collocation. *IFAC-PapersOnLine*, 51(3):125–130, 2018. doi:10.1016/j.ifacol.2018.06.035.
53. T. Kästner, A. Kießling, and G. Riemer. *Energie in 60 Minuten. Ein Reiseführer durch die Gaswirtschaft*. VS Verlag für Sozialwissenschaften, 2011. doi:10.1007/978-3-531-93229-3_4.
54. R. Lamour, R. März, and C. Tischendorf. *Differential-Algebraic Equations: A Projector Based Analysis*. Differential-Algebraic Equations Forum. Berlin: Springer, 2013. doi:10.1007/978-3-642-27555-5.
55. J. Lang and P. Mindt. Entropy-preserving coupling conditions for one-dimensional Euler systems at junctions. *Networks and Heterogeneous Media*, 13(1):177–190, 2018. doi:10.3934/nhm.2018008.
56. R. J. Le Veque. *Finite Volume Methods for Hyperbolic Problems*. Cambridge University Press, 2002. doi:10.1017/CBO9780511791253.

57. H. Liu. Relaxation dynamics, scaling limits and convergence of relaxation schemes. In G. Warnecke, eds., *Analysis and Numerics for Conservation Laws*, pages 453–478. Springer, 2005. doi:10.1007/3-540-27907-5_20.
58. LIWACOM Informationstechnik GmbH. SIMONE software. URL: http://www.liwacom.de.
59. T. Löfqvist, J. Delsing, and K. Sokas. Speed of sound measurements in gas-mixtures at varying composition using an ultrasonic gas flow meter with silicon based transducers. *FLOMEKO 2003 – 11th IMEKO TC9 Conference on Flow Measurement*, 01 2003.
60. W. Lucht, K. Strehmel, and C. Eichler-Liebenow. Indexes and special discretization methods for linear partial differential algebraic equations. *BIT Numerical Mathematics*, 39(3):484–512, 1999. doi:10.1023/A:1022370703243.
61. W. S. Martinson and P. I. Barton. Index and characteristic analysis of linear PDAE systems. *SIAM Journal on Scientific Computing*, 24(3):905–923, 2003. doi:10.1137/S1064827599363411.
62. M. Matthes. *Numerical Analysis of Nonlinear Partial Differential-Algebraic Equations: A Coupled and an Abstract Systems Approach*. PhD thesis, Universität zu Köln, 2012. URL: http://kups.ub.uni-koeln.de/4929/.
63. R. I. McLachlan, G. R. W. Quispel, and N. Robidoux. Geometric integration using discrete gradients. *Philosophical Transactions of the Royal Society of London. Series A: Mathematical, Physical and Engineering Sciences*, 357:1021–1045, 1999. doi:10.1098/rsta.1999.0363.
64. V. Mehrmann and R. Morandin. Structure-preserving discretization for port-Hamiltonian descriptor systems. In *2019 IEEE 58th Conference on Decision and Control (CDC)*, pages 6863–6868, Nice, France, 2019. doi:10.1109/CDC40024.2019.9030180.
65. V. Mehrmann and B. Unger. Control of port-Hamiltonian differential-algebraic systems and applications. *Acta Numerica*, pages 395–515, 2023. doi:10.1017/S0962492922000083.
66. E. S. Menon. *Gas Pipeline Hydraulics*. Taylor & Francis Group, 2005.
67. P. Mindt, J. Lang, and P. Domschke. Entropy-preserving coupling of hierarchical gas models. *SIAM Journal on Mathematical Analysis*, 51(6):4754–4775, 2019. doi:10.1137/19M1240034.
68. R. Morandin. *Modeling and Numerical Treatment of Port-Hamiltonian Descriptor Systems*. PhD thesis, Technische Universität Berlin, 2024.
69. A. Morin and G. A. Reigstad. Pipe networks: Coupling constants in a junction for the isentropic Euler equations. *Energy Procedia*, 64:140–149, 2015. doi:10.1016/j.egypro.2015.01.017.
70. H. Nessyahu and E. Tadmor. Non-oscillatory central differencing for hyperbolic conservation laws. *Journal of Computational Physics*, 87:408–463, 1990. doi:10.1016/0021-9991(90)90260-8.
71. A. J. Osiadacz. Different transient models – limitations, advantages and disadvantages. PSIG report 9606, Pipeline Simulation Interest Group, 1996.
72. A. J. Osiadacz and M. Chaczykowski. Verification of transient gas flow simulation model. PSIG report 1010, Pipeline Simulation Interest Group, 2010.
73. I. Papay. OGIL musz. tud. kozl., 1968.
74. M. E. Pfetsch, A. Fügenschuh, B. Geißler, N. Geißler, R. Gollmer, B. Hiller, J. Humpola, T. Koch, T. Lehmann, A. Martin, A. Morsi, J. Rövekamp, L. Schewe, M. Schmidt, R. Schultz, R. Schwarz, J. Schweiger, C. Stangl, M. C. Steinbach, S. Vigerske, and B. M. Willert. Validation of nominations in gas network optimization: Models, methods, and solutions. *Optimization Methods and Software*, 30(1):15–53, 2015. doi:10.1080/10556788.2014.888426.
75. F. Philipp, T. Reis, and M. Schaller. Infinite-dimensional port-Hamiltonian systems: a system node approach. *Mathematics of Control, Signals, and Systems*, 2025. doi:10.1007/s00498-025-00412-0.
76. N. Philippi. *Asymptotic Analysis and Numerical Approximation of some Partial Differential Equations on Networks*. PhD thesis, Technische Universität Darmstadt, 2023. URL: https://tuprints.ulb.tu-darmstadt.de/24732/.
77. A. Quarteroni and A. Valli. *Numerical Approximation of Partial Differential Equations*. Springer, Berlin, Germany, 1994. doi:10.1007/978-3-540-85268-1.
78. J. Rang and L. Angermann. Perturbation index of linear partial differential-algebraic equations. *Applied Numerical Mathematics*, 53(2):437–456, 2005. Tenth Seminar on Numerical Solution of Differential and Differntial-Algebraic Euqations (NUMDIFF-10). doi:10.1016/j.apnum.2004.08.017.

79. G. A. Reigstad. Existence and uniqueness of solutions to the generalized Riemann problem for isentropic flow. *SIAM Journal on Applied Mathematics*, 75:679–702, 2015. doi:10.1137/140962759.
80. G. A. Reigstad, T. Flåtten, N. E. Haugen, and T. Ytrehus. Coupling constants and the generalized Riemann problem for isothermal junction flow. *Journal of Hyperbolic Differential Equations*, 12(1):37–59, 2015. doi:10.1142/S0219891615500022.
81. D. Rist. *Dynamik realer Gase: Grundlagen, Berechnungen und Daten für Thermogasdynamik, Strömungsmechanik und Gastechnik*. Springer, 1996. doi:10.1007/978-3-642-61402-6.
82. M. Schmidt, M. C. Steinbach, and B. M. Willert. High detail stationary optimization models for gas networks. *Optimization and Engineering*, 16(1):131–164, 2015. doi:10.1007/s11081-014-9246-x.
83. D. W. Schroeder. A tutorial on pipe flow equations. PSIG report 0112, Pipeline Simulation Interest Group, 2001.
84. P. Schulze. Structure-preserving time discretization of port-Hamiltonian systems via discrete gradient pairs, 2023. arXiv:2311.00403.
85. L. Schöbel-Kröhn. *Analysis and Numerical Approximation of Nonlinear Evolution Equations on Network Structures*. PhD thesis, Technische Universität Darmstadt, München, 2020. URL: http://tubiblio.ulb.tu-darmstadt.de/121593/.
86. C.-W. Shu. Essentially non-oscillatory and weighted essentially non-oscillatory schemes for hyperbolic conservation laws. *Acta Numerica*, 29:701–762, 2020. doi:10.1017/S0962492920000057.
87. J. Smoller. *Shock Waves and Reaction-Diffusion Equations*, volume 258 of *Grundlehren der mathematischen Wissenschaften*. Springer Verlag, 1983. doi:10.1007/978-1-4612-0873-0.
88. M. Suchenek and T. Borowski. Measuring sound speed in gas mixtures using a photoacoustic generator. *International Journal of Thermophysics*, 39, 2018. doi:10.1007/s10765-017-2335-2.
89. A. Thomann, G. Puppo, and C. Klingenberg. An all speed second order well-balanced IMEX relaxation scheme for the Euler equations with gravity. *Journal of Computational Physics*, 420:109723, 25, 2020. doi:10.1016/j.jcp.2020.109723.
90. E. Truckenbrodt. *Lehrbuch der angewandten Fluidmechanik*. Springer, 1988. doi:10.1007/978-3-642-83067-9.
91. L. Vacek and V. Kučera. Godunov-like numerical fluxes for conservation laws on networks. *Journal of Scientific Computing*, 97(3), 2023. doi:10.1007/s10915-023-02386-0.
92. A. van der Schaft. *L_2-Gain and Passivity Techniques in Nonlinear Control*. Springer, 2000. doi:10.1007/978-1-4471-0507-7.
93. A. J. van der Schaft and D. Jeltsema. Port-Hamiltonian Systems Theory: An Introductory Overview. *Foundations and Trends® in Systems and Control*, 1(2-3):173–378, 2014. doi:10.1561/2600000002.
94. A. J. van der Schaft and B. M. Maschke. Hamiltonian formulation of distributed-parameter systems with boundary energy flow. *Journal of Geometry and Physics*, 42(1):166–194, 2002. doi:10.1016/S0393-0440(01)00083-3.
95. A. J. van der Schaft and B. M. Maschke. Port-Hamiltonian systems on graphs. *SIAM Journal on Control and Optimization*, 51(2):906–937, 2013. doi:10.1137/110840091.
96. B. Wendroff. On centered difference equations for hyperbolic systems. *Journal of the Society for Industrial and Applied Mathematics*, 8(3):549–555, 1960. doi:10.1137/0108040.
97. J. C. Willems. Dissipative dynamical systems part I: General theory. *Archive for Rational Mechanics and Analysis*, 45:321–351, 1972. doi:10.1007/BF00276493.
98. J. C. Willems. Dissipative dynamical systems part II: Linear systems with quadratic supply rates. *Archive for Rational Mechanics and Analysis*, 45:352–393, 1972. doi:10.1007/BF00276494.

Open Access This chapter is licensed under the terms of the Creative Commons Attribution-NonCommercial-NoDerivatives 4.0 International License (http://creativecommons.org/licenses/by-nc-nd/4.0/), which permits any noncommercial use, sharing, distribution and reproduction in any medium or format, as long as you give appropriate credit to the original author(s) and the source, provide a link to the Creative Commons license and indicate if you modified the licensed material. You do not have permission under this license to share adapted material derived from this chapter or parts of it.

The images or other third party material in this chapter are included in the chapter's Creative Commons license, unless indicated otherwise in a credit line to the material. If material is not included in the chapter's Creative Commons license and your intended use is not permitted by statutory regulation or exceeds the permitted use, you will need to obtain permission directly from the copyright holder.



Chapter 3
Gas Mixtures on Networks: Modeling, Simulation and Optimization

Pascal Börner[0009−0007−0906−8828],
Jan Giesselmann[0009−0008−0217−7244],
Varun M. Kumar[0009−0001−3256−9870],
Marc E. Pfetsch[0000−0002−0947−7193],
Michael Thiele[0009−0007−6679−8704], and
Tabea Tscherpel[0000−0002−5899−1279]

Abstract This chapter addresses mathematical models for isothermal mixtures of hydrogen and natural gas, motivated by the need for reliable simulation tools in future low-carbon energy systems. We analyze several classes of mixture models and investigate their convergence properties in the regime of strong interaction between constituents, covering stationary and instationary single-pipe settings as well as network flows. Since mixture models critically depend on the choice of pressure law, we compare the industry-standard GERG equation of state with simplified alternatives that preserve convex energies and reduce computational costs. For network applications, we discuss consistent coupling conditions across model classes, explore optimization of steady flows using the algebraic Weymouth formulation, and provide numerical evidence for its applicability in relevant operating regimes. The study reveals when simplified models are justified and outlines key open challenges for the modeling of gas mixtures.

Pascal Börner
Department of Mathematics, TU Darmstadt, Germany, e-mail: boerner@mathematik.tu-darmstadt.de

Jan Giesselmann
Department of Mathematics, TU Darmstadt, Germany, e-mail: giesselmann@mathematik.tu-darmstadt.de

Varun M. Kumar
Department of Mathematics, TU Darmstadt, Germany, e-mail: kumar@mathematik.tu-darmstadt.de

Marc E. Pfetsch
Department of Mathematics, TU Darmstadt, Germany, e-mail: pfetsch@mathematik.tu-darmstadt.de

Michael Thiele
Department of Mathematics, TU Darmstadt, Germany, e-mail: thiele@mathematik.tu-darmstadt.de

Tabea Tscherpel
Department of Mathematics, TU Darmstadt, Germany, e-mail: tscherpel@mathematik.tu-darmstadt.de

© The Author(s) 2027

A. Martin et al. (eds.), *Mathematical Modelling, Simulation and Optimization using the Example of Gas Networks*, International Series of Numerical Mathematics 174,
https://doi.org/10.1007/978-3-032-34969-9_3

3.1 Introduction

This chapter addresses the modeling, simulation, and optimization of isothermal gas mixtures, with a specific focus on mixtures of natural gas and hydrogen. A key motivation for this topic is the ongoing transition to carbon-neutral energy systems, which includes the construction of dedicated hydrogen transport infrastructure. While this transition is ongoing, blending hydrogen with natural gas offers a way to integrate renewable energy sources into existing gas transport networks [30]. The safe and efficient operation of such networks requires mathematical models that are both accurate and computationally tractable.

In practice, many studies approximate natural gas by its dominant component, methane, when analyzing hydrogen blends [24, 27]. This simplification is often justified for capturing bulk transport and pressure-flow behavior, though it neglects the influence of higher hydrocarbons and inert constituents that may matter for combustion properties or safety analyses. In this chapter we adopt this methane-hydrogen proxy, with the understanding that it is a first approximation and its validity depends on the intended application.

Although the balance equations for gas mixtures are well established (see, e.g., [3]), different choices lead to distinct classes of models. In particular, *one-velocity models* (also known as *Class I models*) for binary mixtures assume that the two constituents share a common velocity. In contrast, *two-velocity models* (also known as *Class II models*) for binary mixtures assume that each of the components has its own velocity, and that the velocities interact with each other via an *inner friction* between the constituents. Understanding these model classes and the relationship between them is crucial for reliable simulation. In particular, we focus on two key aspects. The first is the convergence of (stationary solutions of) the two-velocity model to (stationary solutions of) the one-velocity model as the inner friction goes to infinity. The second is the behavior of instationary solutions of the two-velocity model over long times for various levels of the inner friction.

In Sect. 3.2, we formally introduce the one- and two-velocity models for binary mixtures in the isothermal instationary setting; for the one-velocity model, we also introduce a simplified stationary model arising by dropping the convection term. As the models are given by *balance laws*, they require the imposition of a number of additional *constitutive relations* to be closed; in our case such a relation takes the form of a *pressure law* (also known as an *equation of state*). We introduce the notion of *thermodynamic consistency* of the models, which restricts the set of admissible pressure laws to those with an associated *energy function*. We then discuss, in an informal sense, the relationship between the two model classes.

In Sect. 3.3, we turn our attention to the investigation of pressure laws for methane-hydrogen mixtures. The *GERG-08* equation of state [21] is the industry standard for a large class of mixtures, but for methane-hydrogen mixtures it may be unnecessarily complex, resulting in high computational costs. Additionally, we were unable to find an energy function for GERG-08 and thus could not find a thermodynamically consistent formulation of the models in this case. As a result, we discuss several alternative pressure laws of varying complexity which are easier to evaluate and possess key

physical properties, in particular an associated convex energy. Computing the *relative deviation* of the pressure laws from GERG-08 as functions of the mass densities, we find an overall increase in accuracy with increasing complexity. However, outside the methane-dominated mixture regime, the deviations from GERG-08 are comparatively low for all pressure laws.

In Sect. 3.4, we further investigate the simplified stationary one-velocity model introduced in Sect. 3.2. We show that this simplified model is equivalent to a *generalized Weymouth equation*, and in particular is *algebraic*. This makes it extremely useful as an optimization constraint and as a starting point for investigating stationary solutions of the full one-velocity model.

In Sect. 3.5 we turn our attention to numerical investigations of the one- and two-velocity models applied to methane-hydrogen mixtures on a single pipe. We begin by discussing the imposition of *compatible boundary conditions* for the one- and two-velocity models in Sect. 3.5.1 before introducing the *numerical scheme* and discussing additional computational aspects in Sect. 3.5.2; these discussions are also relevant for our investigations in the network case, cf. Sect. 3.6.

In Sect. 3.5.3, we investigate the convergence of stationary solutions of the two-velocity model to those of the one-velocity model in the limit as the inner friction goes to infinity. We find that whether or not the solutions converge depends on which boundary conditions are prescribed. We proceed in Sect. 3.5.4 to investigate the impact of varying the inner friction on instationary solutions of the two-velocity model. Here we find that for short times, higher inner friction forces the two velocities to approach each other more quickly, but on longer time scales we observe two different types of behavior in the system as the friction varies.

In Sect. 3.6 we discuss the one- and two-velocity models on networks, beginning by introducing *coupling conditions* at junctions for the one- and two-velocity models in Sect. 3.6.1. In Sect. 3.6.2 we discuss optimization for a steady state model on networks based on the algebraic Weymouth equation. We show that a global optimization of mixture flows is possible for network sizes for which the single-component flows can be solved. The computational time depends on the instance, but is about two to three orders of magnitude larger compared to the single-component case.

In Sect. 3.6.3 we discuss aspects of computing stationary solutions for the one- and two-velocity models on networks, in particular the implementation of coupling conditions. Sect. 3.6.4 compares the influence of different choices of pressure laws for stationary solutions of the one-velocity model on networks. We find that while the pressure deviations are limited for the various pressure laws, the deviation in densities is considerably larger.

We then investigate the consistency between the coupling conditions of the one- and two-velocity models in Sect. 3.6.6 via numerical experiments. These are observed to be consistent in the limit as the inner friction goes to infinity. Finally, in Sect. 3.6.7 we perform a computational study investigating the convergence of the scheme for the one- and two-velocity models in the space and times grid size. We find that the convergence rates vary considerably, however, they are mostly better than expected, indicating that our experiment remains in a preasymptotic regime.

In this way, the chapter illustrates both the opportunities and the limitations of current modeling approaches for natural gas-hydrogen mixtures. To conclude, Sect. 3.7 gathers key open questions that require further investigation.

3.2 Introduction to Mixture Models

Since in the course of the chapter we address simulation and optimization for certain mixture models, we first collect the models. For the convenience of the reader, let us recall the mixture models introduced in Chap. 2, "A Catalog of Gas Network Models: PDEs, Coupling Conditions, and Numerical Schemes", Sect. 2.6, see also [3, 18]. In the following, we consider a given friction coefficient $\lambda > 0$, pipe diameter $D > 0$, gravitational constant g and elevation b of the bottom of the gas pipe above a reference level. In all subsequently discussed models, the densities ρ_1, ρ_2 denote the masses of constituents 1 and 2 in a shared reference volume, respectively. Unless otherwise specified, all quantities are given in SI units.

One-Velocity Models In isothermal one-velocity models, also called Class I models, see [3, 18], the densities, the shared velocity v and the pressure p are governed by the conservation of mass and balance of momentum

$$\partial_t \rho_1 + \partial_x(\rho_1 v) = 0, \tag{3.1a}$$

$$\partial_t \rho_2 + \partial_x(\rho_2 v) = 0, \tag{3.1b}$$

$$\partial_t(\rho v) + \partial_x(\rho v^2 + p(\rho_1, \rho_2)) = -\frac{\lambda}{2D}\rho|v|v - g\rho\partial_x b, \tag{3.1c}$$

where $\rho := \rho_1 + \rho_2 > 0$ denotes the total density. In order to close the system, a constitutive relation for the pressure $p = p(\rho_1, \rho_2)$ has to be chosen. Denoting the mass fraction of constituent 1 by

$$\tilde{\mu} := \frac{\rho_1}{\rho_1 + \rho_2} \geq 0, \tag{3.2}$$

one may consider a transformed pressure function $\tilde{p}(\rho, \tilde{\mu})$. Then, for sufficiently smooth solutions, system (3.1) can formally be rewritten as

$$\partial_t \rho + \partial_x(\rho v) = 0, \tag{3.3a}$$

$$\partial_t \tilde{\mu} + v\partial_x(\tilde{\mu}) = 0, \tag{3.3b}$$

$$\partial_t(\rho v) + \partial_x(\rho v^2 + \tilde{p}(\rho, \tilde{\mu})) = -\frac{\lambda}{2D}\rho|v|v - g\rho\partial_x b, \tag{3.3c}$$

similarly to (2.42) in Chap. 2, "A Catalog of Gas Network Models: PDEs, Coupling Conditions, and Numerical Schemes".

We also work with the following simplified auxiliary model

$$\partial_x(\rho v) = 0, \tag{3.4a}$$
$$v\partial_x(\tilde{\mu}) = 0, \tag{3.4b}$$
$$\partial_x \tilde{p}(\rho, \tilde{\mu}) = -\frac{\lambda}{2D}\rho|v|v - g\rho\partial_x b \tag{3.4c}$$

which results from neglecting the convective term $\partial_x(\rho v^2)$ in the stationary case of (3.3). This can be formalized by a rescaling as in the derivation of the ISO3-type models, see Sect. 2.6.4 of Chap. 2, "A Catalog of Gas Network Models: PDEs, Coupling Conditions, and Numerical Schemes".

This model will be used in Sect. 3.4. A key feature of this model is that for specific pressure laws, such as the ideal gas law it can be solved explicitly allowing for its use as an algebraic constraint in solving optimization problems as done in Sect. 3.6.2.

Two-Velocity Models In two-velocity models, also called Class II models, for isothermal binary mixtures, the densities $\rho_1, \rho_2 > 0$, the velocities v_1, v_2 and the pressures p_1, p_2 are related by

$$\partial_t \rho_1 + \partial_x(\rho_1 v_1) = 0, \tag{3.5a}$$
$$\partial_t \rho_2 + \partial_x(\rho_2 v_2) = 0, \tag{3.5b}$$
$$\partial_t(\rho_1 v_1) + \partial_x(\rho_1 v_1^2 + p_1) = -f\rho_1\rho_2(v_1 - v_2) - \frac{\lambda}{2D}\rho_1 F_1(v_1, v_2) - g\rho_1\partial_x b, \tag{3.5c}$$
$$\partial_t(\rho_2 v_2) + \partial_x(\rho_2 v_2^2 + p_2) = -f\rho_1\rho_2(v_2 - v_1) - \frac{\lambda}{2D}\rho_2 F_2(v_1, v_2) - g\rho_2\partial_x b. \tag{3.5d}$$

Here, $f > 0$ is an inner friction parameter, which determines the friction between the two components. The terms $F_i(v_1, v_2)$, for $i \in \{1, 2\}$, represent wall friction terms, and should satisfy

$$F_i(v_1, v_2)v_i \geq 0 \qquad \text{for } i \in \{1, 2\}$$

and for example can be chosen as

$$F_i(v_1, v_2) = |v_i|v_i \qquad \text{for } i \in \{1, 2\}. \tag{3.6}$$

For the pressures p_1, p_2, constitutive relations are required to close the system. For sufficiently smooth solutions $(\rho_1, \rho_2, v_1, v_2)$, system (3.5) can be reformulated as

$$\partial_t \rho_1 + \partial_x(\rho_1 v_1) = 0, \tag{3.7a}$$
$$\partial_t \rho_2 + \partial_x(\rho_2 v_2) = 0, \tag{3.7b}$$
$$\partial_t v_1 + v_1\partial_x v_1 + \frac{\partial_x p_1}{\rho_1} = -f\rho_2(v_1 - v_2) - \frac{\lambda}{2D}F_1(v_1, v_2) - g\partial_x b, \tag{3.7c}$$
$$\partial_t v_2 + v_2\partial_x v_2 + \frac{\partial_x p_2}{\rho_2} = -f\rho_1(v_2 - v_1) - \frac{\lambda}{2D}F_2(v_1, v_2) - g\partial_x b. \tag{3.7d}$$

Thermodynamic Consistency We shall consider pressure laws, i.e., constitutive relations for p_i in terms of ρ_1, ρ_2, which are compatible with the laws of thermodynamics,

see [3, 7]. For a given Helmholtz free energy $P = P(\rho_1, \rho_2)$, the total thermodynamic pressure is determined by the *Gibbs–Duhem relation* as

$$p(\rho_1, \rho_2) = -P(\rho_1, \rho_2) + \sum_{i=1,2} \rho_i \, \partial_{\rho_i} P(\rho_1, \rho_2), \tag{3.8}$$

see, e.g., [3, eq. (64)]. Then, we consider p_i such that one has

$$\partial_x(\partial_{\rho_i} P) = \frac{\partial_x p_i}{\rho_i} \qquad \text{for } i \in \{1, 2\}, \tag{3.9}$$

which is compatible with *Dalton's law* $p = p_1 + p_2$. Such p_i only exist as functions of (ρ_1, ρ_2) only for special choices of P. Even if they do not exist, one may insert (3.9) into (3.7) to solve the PDEs.

Choosing P and p_i such that (3.9) holds ensures the thermodynamic consistency of the two-velocity model in the sense that the energy balance

$$\begin{aligned} \partial_t \Big(\frac{\rho_1}{2} v_1^2 + \frac{\rho_2}{2} v_2^2 + P(\rho_1, \rho_2) + g\rho \partial_x b \Big) + \partial_x \Big(\sum_{i=1}^{2} \rho_i v_i (\partial_{\rho_i} P + \frac{1}{2} v_i^2) \Big) \\ = -f \rho_1 \rho_2 (v_1 - v_2)^2 - \frac{\lambda}{2D} \rho_1 v_1 F_1(v_1, v_2) - \frac{\lambda}{2D} \rho_2 v_2 F_2(v_1, v_2) \end{aligned} \tag{3.10}$$

holds for any smooth solution to (3.5). Note that the one-velocity model (3.1) with p as in (3.8) is also thermodynamically consistent with energy balance

$$\partial_t \Big(\frac{\rho}{2} v^2 + P(\rho_1, \rho_2) + g\rho \partial_x b \Big) + \partial_x \Big(\sum_i \rho_i v (\partial_{\rho_i} P(\rho_1, \rho_2) + \frac{1}{2} v^2) \Big) = -\frac{\lambda}{2D} \rho |v|^3.$$

In the regime relevant to gas networks it is reasonable to assume that $P(\rho_1, \rho_2)$ is convex. Indeed, for the relevant ranges of temperature and pressure, the mixtures are supercritical and no spontaneous phase separation occurs, see [7, Ch. 2]. In contrast, in the subcritical regime P may be non-convex in the densities, which allows for two distinct phases to coexist at the same temperature and pressure.

Relation Between One- and Two-Velocity Models A formal derivation shows that for $f \to \infty$, the two-velocity model (3.5) approaches the one-velocity model (3.1). Neglecting boundary conditions, the limit $f \to \infty$ leads to $v_1 - v_2 \to 0$ in (3.5). Inserting $v_1 = v_2 = v$ into (3.5), assuming the wall friction terms have the form indicated in (3.6), and adding the momentum equations shows that

$$\partial_t(\rho v) + \partial_x(\rho v^2 + p_1 + p_2) = -\frac{\lambda}{2D} \rho |v| v - g\rho \partial_x b.$$

This formally yields the one-velocity model (3.1) since with (3.8) and (3.9) we have

$$\partial_x p = \partial_x p_1 + \partial_x p_2. \tag{3.11}$$

Practitioners are convinced that for the relevant regimes in gas transport, the one-velocity model captures the essential physical features, since the time scales of interest are far larger than the average time between molecule collisions [11]. However, from the perspective of mathematical analysis it is less easily handled than the two-velocity model. This is because, for simple pressure laws, the two-velocity model can be viewed as two sets of one-component systems, see (ISO1) in Chap. 2, "A Catalog of Gas Network Models: PDEs, Coupling Conditions, and Numerical Schemes", coupled by the internal friction. As a result, much of the inherent structure of the one-component models carries over.

3.3 Pressure Laws

The one- and two-velocity mixture models (3.1) and (3.5) presented in the previous section still require some pressure laws to close the system. Here we collect several choices of pressure laws; for more details on mixing theory and more pressure laws see [6,7] and references therein. After introducing relevant properties of pressure laws, we collect several concrete examples in order of increasing complexity: ideal gas law [19], a law based on linearized compressibility factors [5], laws using virial expansion [8, Sec. 1.1], laws using mixed[1] virial expansion [9, Sec. 1.1], and GERG-08 [21]. Recall that throughout, we consider the isothermal case and thus treat temperature as constant.

Furthermore, we compare most of these pressure laws for a binary mixture consisting of methane and hydrogen. In this and later sections wherever numerical experiments are conducted, quantities with index 1 refer to methane, and quantities with index of 2 refer to hydrogen. For example, ρ_1 denotes the methane density and ρ_2 the hydrogen density.

Notation In the following, let c_1 and c_2 denote the speed of sound of constituent 1 and 2, respectively, which are considered as given constants. The space of polynomials of degree at most $r \in \mathbb{N}$ is denoted by $\mathcal{P}_r(X)$, where $X = \mathbb{R}^d$ for $d = 1, 2$. The molar density is given by

$$\rho_{\text{mol}}(\rho_1, \rho_2) := \frac{\rho_1}{M_1} + \frac{\rho_2}{M_2}, \tag{3.12}$$

where M_1, M_2 are molar masses of each constituent in kg/mol and T the temperature in K. For methane and hydrogen, the values of the molar mass constants are $M_1 = 16.042460$ kg/mol and $M_2 = 2.015880$ kg/mol respectively, see [21, 32, Tab. A5]. Moreover, we define the *mole fractions* by

$$x_i(\rho_1, \rho_2) = \frac{\frac{\rho_i}{M_i}}{\rho_{\text{mol}}}, \quad \text{for } i \in \{1, 2\}, \qquad \text{and set} \quad x := (x_1, x_2). \tag{3.13}$$

Properties of Pressure Laws A mixture is called

(i) *simple*, if the pressure law is of the form

[1] Here 'mixed' refers to the fact that bivariate polynomials are used rather than univariate ones.

$$p(\rho_1, \rho_2) = p_1(\rho_1) + p_2(\rho_2), \tag{3.14}$$

for some $p_i \colon \mathbb{R}_{>0} \to \mathbb{R}_{>0}$, $i \in \{1, 2\}$;

(ii) *thermodynamically consistent*, if there exists an energy $P = P(\rho_1, \rho_2)$ such that (3.8) holds, see [3].

Note that simple pressure laws are particularly easy to analyze and to implement. For thermodynamically consistent mixtures also *convexity* of P is of interest.

Thermodynamically consistent mixtures with energy of the form

$$P(\rho_1, \rho_2) = P_1(\rho_1) + P_2(\rho_2) \tag{3.15}$$

are simple. Indeed, in this case it follows from (3.8) that (3.14) holds for the partial pressures $p_i(\rho_i) = -P_i(\rho_i) + \rho_i \partial_{\rho_i} P_i(\rho_i)$ for $i \in \{1, 2\}$.

Thermodynamic consistency can be verified for general bivariate polynomial pressure laws. Indeed, for expressions of the form $P(\rho_1, \rho_2) = \rho_1^j \rho_2^k$ with $j, k \in \mathbb{R}$, $j + k > 1$, we obtain

$$\begin{aligned} p(\rho_1, \rho_2) &= -P(\rho_1, \rho_2) + \rho_1 \partial_{\rho_1} P(\rho_1, \rho_2) + \rho_2 \partial_{\rho_2} P(\rho_1, \rho_2) \\ &= -\rho_1^j \rho_2^k + \rho_1 j \rho_1^{j-1} \rho_2^k + \rho_2 k \rho_1^j \rho_2^{k-1} \\ &= (j + k - 1) \rho_1^j \rho_2^k. \end{aligned}$$

Furthermore, for monomials of order 1, e.g., $p(\rho_1) = \rho_1$, we derive the energy $P(\rho_1) = \log(\rho_1)\rho_1$. Since the monomials form a basis of the polynomials, there exists an energy for every polynomial in (ρ_1, ρ_2). Thus, for each $p \in \mathcal{P}_r$ there is a $P \in \mathcal{P}_r$ such that (3.8) holds. Since we never used that $k, j \in \mathbb{N}$, there exists also an energy for non-integer valued exponents larger than 1.

3.3.1 Collection of Pressure Laws

Let us now collect some standard pressure laws widely used in the literature.

Ideal Gas The ideal gas pressure law is based on computing the change of the speed of sound in a mixture. For a detailed derivation and physical motivation we refer to [2]. They show that

$$p_I(\rho_1, \rho_2) = RT \left(\frac{\rho_1}{M_1} + \frac{\rho_2}{M_2} \right) = c_1^2 \rho_1 + c_2^2 \rho_2, \tag{3.16}$$

where R is the universal gas constant in $\mathrm{kg\,m^2/(s^2\,K\,mol)}$, T is the temperature in K and M_1, M_2 are the molar masses in kg/mol of methane and hydrogen, and recall that c_1 and c_2 in m/s denote the constant speeds of sound.

Note that a mixture with the ideal gas law is simple and by the above consideration thermodynamically consistent with convex energy $P(\rho_1, \rho_2) = P_1(\rho_1) + P_2(\rho_2)$, where $P_i(\rho_i) = c_i^2 \rho_i \log\left(\frac{\rho_i}{\rho_{\mathrm{ref}}}\right)$ for a reference density ρ_{ref}, see Table 3.1.

Linearization of Compressibility Factors The pressure law suggested in [5] is based on linear approximations of compressibility factors. It is given by

$$p_L(\rho_1, \rho_2) = \frac{\rho_1 R_1 T + \rho_2 R_2 T}{1 - \rho_1 R_1 T a_1(T) - \rho_2 R_2 T a_2(T)}$$

where R_1, R_2 are specific gas constants and $a_1(T), a_2(T)$ are the slopes of linear approximations of the compressibility factors. This law is not defined for $\rho_1 R_1 T a_1(T) + \rho_2 R_2 T a_2(T) = 1$. The values of a_1, a_2 are such that the relevant range for pipeline operation is $\rho_1 R_1 T a_1(T) + \rho_2 R_2 T a_2(T) < 1$. This law is thermodynamically consistent with convex entropy on its domain of definition.

Virial Expansion This model uses the ansatz

$$p_V(\rho_1, \rho_2) = p_1(\rho_1) + p_2(\rho_2), \tag{3.17}$$

and hence models simple mixtures. The partial pressures are given by the so-called virial expansion, for $i \in \{1, 2\}$,

$$p_i(\rho_i) = RT\left(\frac{\rho_i}{M_i} + B_i\left(\frac{\rho_i}{M_i}\right)^2 + C_i\left(\frac{\rho_i}{M_i}\right)^3\right), \tag{3.18}$$

with constants B_i and C_i determined by experiments. A more detailed introduction can be found in [8, Introduction], and coefficients for hydrogen are presented in [8, Inorganic Compounds] and for methane in [8, C4 Organic Compounds, Second Virial Coefficients] and in [8, C4 Organic Compounds, Third Virial Coefficients]. Note that therein, the units of volumes are cm^3, and a rescaling before and after applying the pressure law is needed.

Again, by the above consideration the pressure law is thermodynamically consistent, see Table 3.1. Convexity can be tested for specific ranges of density values and specific mixtures.

Mixed Virial Expansion Virial expansions have been extended to non-simple mixtures by using bivariate polynomials of the form

$$p_M(\rho_1, \rho_2) = RT(\rho_{\mathrm{mol}} + B_{\mathrm{mix}}(x)\rho_{\mathrm{mol}}^2 + C_{\mathrm{mix}}(x)\rho_{\mathrm{mol}}^3), \tag{3.19}$$

with ρ_{mol} as in (3.12), and where B_{mix} and C_{mix} are functions of the mole fraction vector x, see (3.13). The functions B_{mix} and C_{mix} are defined by

$$\begin{aligned} B_{\mathrm{mix}}(x) &:= x_1^2 B_{11} + 2x_1 x_2 B_{12} + x_2^2 B_{22}, \\ C_{\mathrm{mix}}(x) &:= x_1^3 C_{111} + 3x_1^2 x_2 C_{112} + C_{122} x_1 x_2^2 + x_2^3 C_{222}, \end{aligned}$$

where B_{11}, B_{22} and C_{111}, C_{222} are the second and third virial coefficients of the pure substances and the remaining coefficients are again fitted to experimental data for the specific mixtures.

This model is referred to as the *mixed virial expansion*, compare [9, Introduction]. The coefficients for a methane-hydrogen mixture and a wide range of substances can be found in [9, F6S – N2 (Sulfur hexafluoride – Nitrogen)].

By the above consideration, the mixed virial expansion is thermodynamically consistent, and again convexity of P has to be checked for concrete coefficients and for the relevant range of densities, see Table 3.1.

GERG-08 The GERG-08 model [21] represents the industry standard. It is fitted to data and based on an ansatz for the free *Helmholtz energy*

$$\begin{aligned}\alpha(\delta(\rho_1,\rho_2),\tau(\rho_1,\rho_2),x(\rho_1,\rho_2)) := \alpha_0(\rho_{\mathrm{mol}}(\rho_1,\rho_2),T,x(\rho_1,\rho_2))\\ + \alpha_r(\delta(\rho_1,\rho_2),\tau(\rho_1,\rho_2),x(\rho_1,\rho_2)).\end{aligned}$$

The quantities δ, τ are given by

$$\delta(\rho_1,\rho_2) := \frac{\rho_{\mathrm{mol}}(\rho_1,\rho_2)}{\rho_r(x(\rho_1,\rho_2))}, \qquad \tau(\rho_1,\rho_2) := \frac{T_r(x(\rho_1,\rho_2))}{T}, \tag{3.20}$$

and depend on the so-called reduced density and temperature functions ρ_r, T_r given in terms of the mole fractions. These quantities are described by a fractional polynomial ansatz, whose coefficients are determined from experimental data. The energy α consists of an ideal gas part α_0 and a residual part α_r, and α_0, α_r as well as ρ_r, T_r consist of several parts, which are sums of polynomials and exponents of polynomials.

For a comparison to the other pressure laws, we note that the polynomial degree of the methane part of α_r is 24, and therefore much more complex than the models introduced before. The total pressure is defined as [21]

$$p_G(\rho_1,\rho_2) := RT\rho_{\mathrm{mol}}(\rho_1,\rho_2)\Big(1+\delta(\rho_1,\rho_2)\partial_\delta\alpha_r(\delta(\rho_1,\rho_2),\tau(\rho_1,\rho_2),x(\rho_1,\rho_2))\Big), \tag{3.21}$$

with ρ_{mol} as in (3.12). The GERG-08 model is fitted to (p,ρ,T) data sets and vapor-liquid equilibrium (VLE) data sets for the specific mixtures. We note that the volumes for reduced densities are given in dm^3 in the context of GERG-08.

It is immediate that the pressure law is not simple, but from the presentation in [21] we were not able to determine whether or not it is thermodynamically consistent in the sense of (3.8). Hence, we refrain from making any claim here, see Table 3.1. Consequently, we were unable to determine partial pressure laws for GERG-08. Therefore, we cannot use GERG-08 for simulating the two-velocity model.

Evaluating p_G requires computing derivatives of the energy α_r, for which we use automatic differentiation with the `Python` package `jax` [4]. Alternatively, one may precompute the derivative using the symbolic toolbox `sympy`, but this does not improve the computation speed, since evaluating the symbolic expression is similarly expensive as computing the derivative via automatic differentiation.

Below, we consider a binary methane-hydrogen mixture at constant temperature $T = 273.15\,\mathrm{K}$. In this case, the GERG-08 model is valid for molar fractions of constituent 2 (hydrogen) $x_2 \in [0.05, 0.91]$ only, since the measurement data used for the fit covers this range.

Least Squares Fit to GERG-08 Since the GERG-08 model (3.21) is the industry standard, we treat it as sufficiently accurate. However, it is significantly more complex than the other pressure laws. Fitting polynomial pressure laws of higher order to the data of GERG-08 allows for a compromise, in the sense that the structure is only moderately complex, and the accuracy is higher than for the ideal gas law as well as the (mixed) virial expansions. The resulting pressure laws are easier to evaluate and have structural advantages. Fitting a polynomial ensures that there exists a corresponding energy P, whereas it is unclear to us whether the GERG-08 model satisfies (3.8). Thus, it may be a compromise in situations where the evaluation of GERG-08 is too costly or an energy is needed. Since the GERG-08 model is based on $(p, (\rho_i)_i, T)$-data and we consider isothermal situations, we shall use a fit in the quantities (p, ρ_1, ρ_2). One may restrict this procedure to the range of density values needed for a specific application.

For simplicity, we use a least squares approximation in polynomial spaces, but other methods would also be possible. In our experiments, we consider simple and non-simple mixtures with polynomial pressure laws

$$p_F(\rho_1, \rho_2) = p_1(\rho_1) + p_2(\rho_2) \qquad \text{for} \quad p_i \in \mathcal{P}_k(\mathbb{R}) \quad \text{and} \quad k \in \{1, 4\}, \tag{3.22a}$$

$$p_F(\rho_1, \rho_2) \in \mathcal{P}_k(\mathbb{R}^2) \qquad \text{for} \quad k \in \{2, 4\}. \tag{3.22b}$$

As mentioned before, the resulting pressure laws are thermodynamically consistent, see Table 3.1. Convexity of the energy is not immediate to hold, but has to be tested for concrete polynomials and the specific range of densities. For the least squares fit for methane and hydrogen below we use densities $\rho_1 \in [0.1, 60]$ and $\rho_2 \in [0.1, 6]$ uniformly distributed with 1000 data points in each ρ_i-direction, for pressures not exceeding 80 bar, and the coefficients of the resulting pressure laws p_F can be found in the Git repository [10].

3.3.2 Comparison of Pressure Laws

In the following, we compare several pressure laws on the binary mixture of methane and hydrogen as functions of the densities. Since the GERG-08 pressure law (plotted in Fig. 3.1) is expected to be the most accurate, we present the absolute pressure

Table 3.1: Properties of pressure laws

Pressure law	simple	consistent	
Ideal gas [2]	✓	✓	(P convex)
Lin. compr. factors [5]	×	✓	(P convex on domain of def.)
Virial expansion [8]	✓	✓	
Mixed virial expansion [8]	×	✓	
GERG-08 [21]	×	?	
Least squares fit to GERG-08	(✓)	✓	

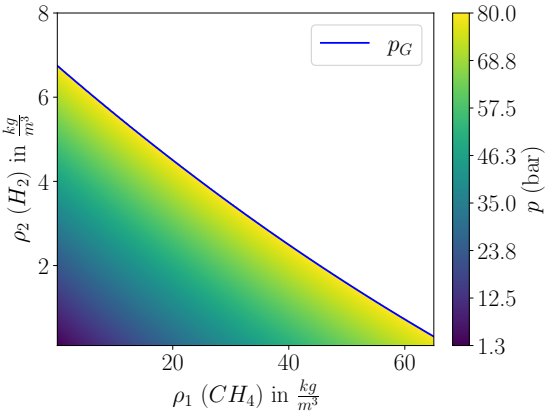


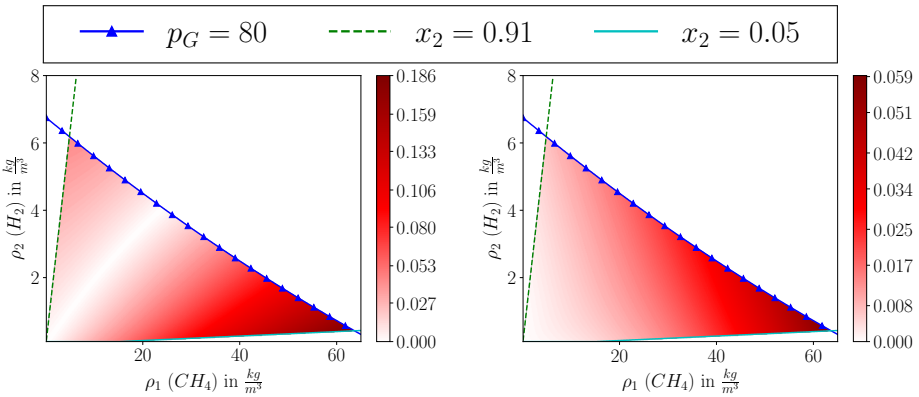
Fig. 3.1: p_G of (3.21)

deviations $p_G - p$ and relative pressure deviations $\frac{|p_G - p|}{p_G}$ between p_G and p for each of the pressure laws $p \in \{p_I, p_V, p_M, p_F\}$, see Fig. 3.2, 3.3, 3.4 and 3.5. In the following, the first constituent is methane and the second constituent is hydrogen, with molar mass constants as below (3.12). The different pressure laws are compared for pressures up to 80 bar, which is reasonable for most pipes, see [26] for common example networks. We consider densities $\rho_1 \in [0.1, 65]$ and $\rho_2 \in [0.1, 6]$ as long as they do not surpass a pressure of 80 bar and do not leave the validity range $x_2 \in [0.05, 0.91]$ of GERG-08. We use a fixed temperature of $T = 273.15$ K corresponding to $0°C$.

Figure 3.3 shows that the ideal gas model deviates by up to 14.84 bar, corresponding to a maximal relative deviation of 18.6 % (see Fig. 3.2), in regions of high methane density (see Fig. 3.1), but exhibits significantly smaller deviations at lower pressures. The virial expansion pressure law only has a difference of at most 4.74 bar, and again the deviation is largest for high methane densities. This corresponds to a maximal relative deviation of 5.9 %, see Fig. 3.2. For the mixed virial expansion, the difference increases more slowly with methane content in the high-pressure region, remaining below 4.58 bar and below 2.55 bar over most of the domain. In the high methane area a relative deviation of up to 4.9 % occurs, see Fig. 3.2. In the region of nearly pure hydrogen, the model behaves considerably worse than the virial expansion. All in all, we see a higher accuracy with increasing complexity, in the practically relevant area of high methane percentage. Let us remark that experimentally the virial expansions have a convex energy for densities $(\rho_1, \rho_2) \in [0.1, 65] \times [0.1, 6]$ and $p \leq 80$ bar.

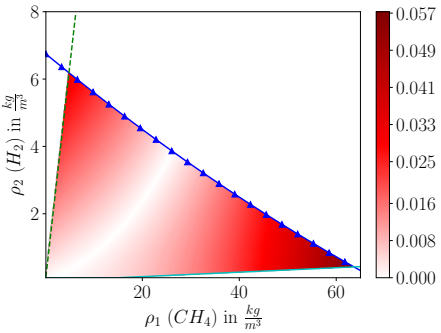
In the following, we investigate the results for a simple polynomial least squares fit and a non-simple polynomial least squares fit. We start with a simple polynomial pressure laws of the form (3.22a) with polynomials $p_i \in \mathcal{P}_k(\mathbb{R})$, for $i \in \{1, 2\}$ and $k \in \{1, 4\}$ determined by the fit. The pressure deviation between the fitted model and the GERG-08 model are presented in Fig. 3.4.

In Fig. 3.4 we can see that the fitted model with polynomial degree $k = 1$ is more accurate than the ideal gas law. The maximal deviation for the fitted model is below 3.5 bar in comparison to up to 14.84 bar. For higher polynomial degrees, the accuracy



(a) $\frac{|p_G - p_I|}{p_G}$ of (3.16)

(b) $\frac{|p_G - p_V|}{p_G}$ of (3.18)



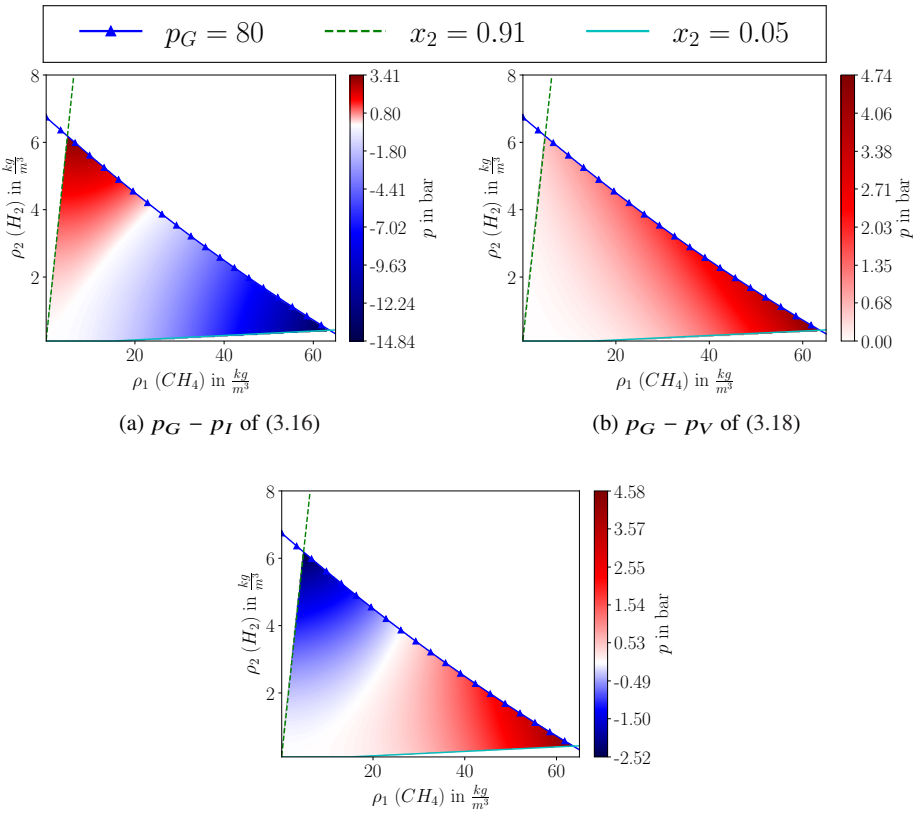
(c) $\frac{|p_G - p_M|}{p_G}$ of (3.19)

Fig. 3.2: Relative deviation in pressure over ρ_1, ρ_2.

improves up to a polynomial degree of $k = 4$, for which a maximal deviation of 0.76 bar is achieved, see Fig. 3.4. For simple laws, increasing the polynomial degree beyond $k = 4$ does not provide any further gain. Since the GERG-08 model is not simple, such a limitation is not surprising.

To further increase accuracy we consider mixed polynomials $p_F \in \mathcal{P}_k(\mathbb{R}^2)$ with total degree $k = 4$, see (3.22b). The pressure deviation with respect to the GERG-08 model is presented in Fig. 3.5. We notice that the maximal deviation decreased by two orders of magnitude for $k = 4$ compared to the fit to a simple law, see Fig. 3.4. Overall, we obtain a much smaller deviation with the non-simple approximate pressure.

Let us note that all fitted pressure laws in Fig. 3.4 and 3.5 have an energy P, which is numerically verified to be convex for densities $(\rho_1, \rho_2) \in [0.1, 65] \times [0.1, 6]$ and $p \leq 80$ bar. For even higher polynomial degrees a least square fitted polynomial might not be convex anymore and convexity would have to be imposed by other means.



(a) $p_G - p_I$ of (3.16)

(b) $p_G - p_V$ of (3.18)

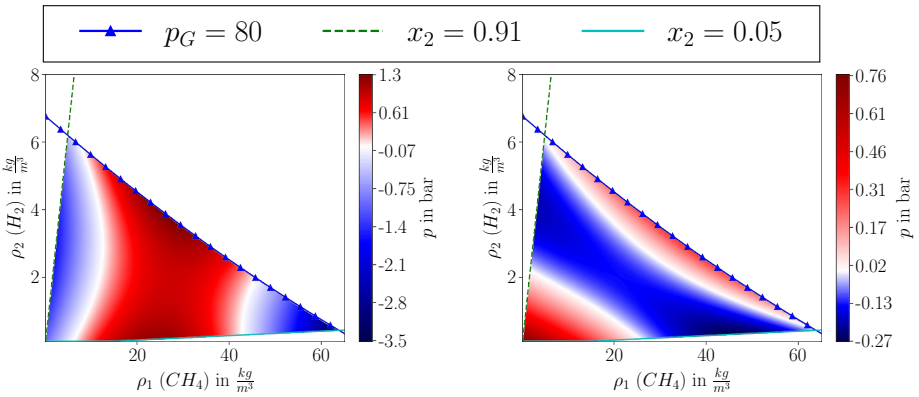
(c) $p_G - p_M$ of (3.19)

Fig. 3.3: Pressure difference over ρ_1, ρ_2.

3.4 A (Simplified) Stationary One-Velocity Model

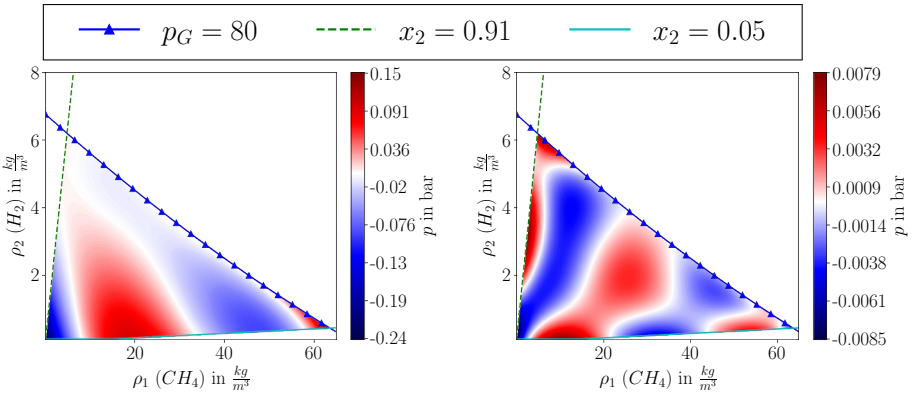
Let us now introduce a simplification of the stationary version of the one-velocity model (3.3), which can be solved analytically, and hence serves as an auxiliary problem. We consider the special case of the ideal gas law (3.16).

In the stationary case, the time derivatives vanish. Furthermore, we drop the convective term $\partial_x(\rho\, v^2)$, which is motivated by the fact that it is often small in comparison to the other model components, for details see [2] and Chap. 2, "A Catalog of Gas Network Models: PDEs, Coupling Conditions, and Numerical Schemes". We then arrive at a stationary version of the ISO3-type model for $\varepsilon = 0$ (see also (2.55) in Chap. 2, "A Catalog of Gas Network Models: PDEs, Coupling Conditions, and Numerical Schemes", Sect. 2.6.4):



(a) $p_G - p_F$ for $k = 1$ (b) $p_G - p_F$ for $k = 4$

Fig. 3.4: *Simple* polynomial least squares approximation of GERG-08 with polynomial of degree k in each direction, see (3.22a).



(a) $p_G - p_F$ for $k = 2$ (b) $p_G - p_F$ for $k = 4$

Fig. 3.5: *Non-simple* polynomial least squares approximation of GERG-08 with a mixed polynomial $p_F \in \mathcal{P}_k(\mathbb{R}^d)$ and k, see (3.22b).

$$\partial_x(\rho v) = 0, \tag{3.23a}$$

$$\partial_x(\tilde{\mu})\, v = 0, \tag{3.23b}$$

$$\partial_x p_I(\rho, \tilde{\mu}) = -\frac{\lambda}{2D}\rho|v|v. \tag{3.23c}$$

Since we use the ideal gas law (3.16), the solution of (3.23), denoted by $(\rho^s, \tilde{\mu}^s, v^s)$ can be computed explicitly: Indeed, it follows directly from (3.23a) and (3.23b) that the mass flux $q^s = A\rho^s v^s$, where A is the (constant) pipe cross section area and $\tilde{\mu}^s$ are spatially constant (on $\Omega = (0, \ell)$), provided that $v^s \neq 0$ on Ω. Thus, each of the quantities q^s, $\tilde{\mu}^s$ is uniquely determined once one boundary value is specified. For given values

q^∂ and $\tilde{\mu}^\partial$, we obtain

$$A\rho^s(x)\, v^s(x) = q^\partial \quad \text{and} \quad \tilde{\mu}^s(x) = \tilde{\mu}^\partial \qquad \text{at either } x = 0 \text{ or } x = \ell.$$

Multiplying the pressure equation (3.23c) by ρ^s and integrating in Ω yields an explicit formula for $p_I(\rho^s, \tilde{\mu}^s)$ on Ω, provided a pressure value is prescribed on one boundary vertex. For this reason, we impose the boundary condition $p_I(\rho_1^s, \rho_2^s)(0) = p_0^\partial$ for given value p_0^∂ or $p_I(\rho_1^s, \rho_2^s)(\ell) = p_\ell^\partial$ for given value p_ℓ^∂.

The simple structure of this model allows us to rephrase it as an algebraic problem where the unknowns are the pressures p^a at vertices, mass flow q^a and mass fraction $\tilde{\mu}^a$ on pipes, with constant values on each pipe. They satisfy a generalized *Weymouth equation*

$$(p_0^a)^2 - (p_\ell^a)^2 = \Lambda\, c(\tilde{\mu}^a)^2\, q^a\, |q^a|, \tag{3.24}$$

where $\Lambda := \frac{\lambda \ell}{DA^2}$. The appearance of $c(\tilde{\mu}^a)^2$ on the right hand side of (3.24) is a result of (3.16). For more details see [2].

In the following, models (3.23) and (3.24) shall be used as auxiliary models. Since the model (3.24) is given in algebraic form and can be solved explicitly, one may use it as constraints for optimization problems, see Sect. 3.6.2 below. In fact, we shall see, that in some situations, the simplification can be justified a posteriori, see Sect. 3.6.5. Furthermore, (3.24) will be used to generate initial and boundary conditions for the corresponding models with convection.

Note that there is a one-to-one relationship between the functions $(\rho^s, \tilde{\mu}^s, p_I(\rho^s))$ on Ω solving (3.23) and the quadruple $(q^a, \tilde{\mu}^a, p_0^a, p_\ell^a) \in \mathbb{R}^4$ solving (3.24). The relationship between q^a, μ^a and $\rho^s v^s$, μ^s is straight-forward thanks to (3.2) by identifying a constant function with its function value. For the pressure, we have $p_0^a = p_I(\rho_1^s, \rho_2^s)(0)$ and $p_\ell^a = p_I(\rho_1^s, \rho_2^s)(\ell)$. Similarly as before, the values of $p_I(\rho_1^s, \rho_2^s)(x)$ for $x \in \Omega$ can be obtained from one of the boundary values by integration.

3.5 One- and Two-Velocity Mixtures on a Single Pipe

In this section, we investigate and compare the behavior of the one-velocity and the two-velocity models on a single pipe using numerical simulations. Recall that in Sect. 3.2 we have argued that, as the inner friction parameter $f \to \infty$, the solutions to the two-velocity models are expected to approach the solutions to the one-velocity model, when neglecting boundary conditions. Here, we investigate this limit by numerical tests when boundary conditions are included. This requires us to impose boundary conditions which are compatible between the one- and the two-velocity model, as shall be discussed in Sect. 3.5.1. In Sect. 3.5.2 we introduce the implicit box scheme, used for the numerical discretizations, and we collect further parameters used in the following. In Sect. 3.5.3 we compute stationary solutions to the one-velocity and two-velocity models by setting up auxiliary instationary problems and computing solutions in the long time limit. The discussions on how to choose initial and boundary conditions for these auxiliary problems are also relevant for the case of networks, see Sect. 3.6. In our

experiments, it depends on the specific boundary conditions whether the solutions to the two-velocity model approach the solutions to the one-velocity model as f increases, and we use a toy example to explain this surprising behavior.

In Sect. 3.5.4 we investigate the effect of varying f on instationary solutions of the two-velocity model on a single pipe with no outflow boundary conditions. We find that, on short time scales of seconds, higher inner friction leads both velocities to approach each other more rapidly. On the time scale of minutes, however, the roles are reversed.

3.5.1 Boundary Conditions

In Sect. 3.2, we have noted that, when ignoring boundary conditions, we expect the two-velocity model to approach the one-velocity model as the inner friction $f \to \infty$, since this forces $(v_1 - v_2) \to 0$.

Meaningful comparisons of the models can only be obtained if no artificial differences are introduced via boundary conditions. Clearly, the two-velocity model has one more equation than the one-velocity model. Since the type of equations does not change, the two-velocity model needs more boundary conditions. Indeed, for subsonic flows the two-velocity model has two left-going and two right-going characteristics, whereas the one-velocity model has three characteristics: One is left-going, one is right-going and the third one moves with the fluid velocity. This means that for the two-velocity model two conditions need to be prescribed on each end of the pipe and for the one-velocity model one condition needs to be prescribed per pipe end and at pipe ends where the flow enters the computational domain an additional condition is needed.

In the following, we consider examples where the flow enters the pipe on one end and leaves it at the other. Thus, from the view of the pipe there is a well-defined inflow vertex and a well-defined outflow vertex. One has various options of how to impose boundary conditions, see Table 3.2 for two of them. Both of them are physically sound, and one has a choice here.

Note that in this section we restrict our consideration to simple pressure laws. Let us now describe how we choose boundary data in our numerical simulations so as not to introduce 'artificial' differences between the models via boundary conditions. In all of the following cases we address how the imposed data for the one-velocity model can be used to generate consistent boundary data for the two-velocity model. For simplicity, we assume that the map $(\rho_1, \rho_2) \mapsto (p, \tilde{\mu})$ is invertible in the relevant domain of pressure p

Table 3.2: Possible imposition of boundary conditions

	Model	Inflow	Outflow
Option A	one-velocity	$p, \tilde{\mu}$	q
	two-velocity	p_1, p_2	q_1, q_2
Option B	one-velocity	$q, \tilde{\mu}$	p
	two-velocity	q_1, q_2	p_1, p_2

and mixture ratio $\tilde{\mu}$. One natural, sufficient condition for this is that for any fixed mixing ratio $\tilde{\mu}$ the pressure is a strictly monotone function of the total density.

- (Option A inflow) For given values $(p^\partial, \tilde{\mu}^\partial)$ for the one-velocity model we impose

$$p(\rho_1, \rho_2) = p^\partial, \tag{3.25a}$$

$$\tilde{\mu} = \frac{\rho_1}{\rho_1 + \rho_2} = \tilde{\mu}^\partial. \tag{3.25b}$$

  Due to the invertibility of the map $(\rho_1, \rho_2) \mapsto (p, \tilde{\mu})$ we may compute $(\rho_1^\partial, \rho_2^\partial)$ from the values $(p^\partial, \tilde{\mu}^\partial)$. Provided that the pressure law is simple, the partial pressures are given as $p_i = p_i(\rho_i)$. In this case, for the two-velocity model we prescribe

$$p_i(\rho_i) = p_i^\partial := p_i(\rho_i^\partial), \tag{3.26}$$

  for $i \in \{1, 2\}$.
- (Option B inflow) Note that with $q = A(\rho_1 + \rho_2)v$ we have in the one-velocity model that

$$q_1 = A\rho_1 v = \tilde{\mu} q \qquad \text{and} \qquad q_2 = (1 - \tilde{\mu})q.$$

  Thus, for given values $(q^\partial, \tilde{\mu}^\partial)$ we impose in the one-velocity model

$$q = q^\partial \qquad \text{and} \qquad \tilde{\mu} = \tilde{\mu}^\partial, \tag{3.27}$$

  and in the two-velocity model we impose

$$q_1 = q_1^\partial := \tilde{\mu}^\partial q^\partial \qquad \text{and} \qquad q_2 = q_2^\partial := (1 - \tilde{\mu}^\partial) q^\partial. \tag{3.28}$$

- (Option A outflow) For a given value q^∂ we prescribe the total mass flux $q = q^\partial$ for the one-velocity model. We then extract $\tilde{\mu}^\partial$ from the solution to the one-velocity model and impose for the two-velocity model the same as in (3.28).
- (Option B outflow) Similarly, for a given value p^∂ we prescribe the pressure $p = p^\partial$ for the one-velocity model, and extract $\tilde{\mu}^\partial$ from the solution to the one-velocity model. From $(p^\partial, \tilde{\mu}^\partial)$ as above we compute $(\rho_1^\partial, \rho_2^\partial)$, and impose on the two-velocity model the same as in (3.26).

3.5.2 Numerical Scheme and Computational Aspects

We consider an interval $\Omega = (0, \ell)$ representing the pipe. In order to compare the one-velocity (3.1) and the two-velocity model (3.5), we restrict ourselves to the case of a spatially constant elevation b and the ideal gas pressure law (3.16).

Discretization We discretize both the one-velocity model (3.1) and the two-velocity model (3.5) with the *implicit box scheme*. This method was developed for a subsonic transient homogeneous gas flow in [20]. For a balance law of the form

$$\partial_t u + \partial_x F(u) = G(u) \tag{3.29}$$

we define $t_n := n\Delta t$, $x_i = i\Delta x$ and approximations $u_i^n \approx u(t_n, x_i)$, $F_i^n \approx F(u_i^n)$, $G_i^n \approx G(u_i^n)$.

Then the scheme reads

$$\frac{u_j^{n+1} + u_{j-1}^{n+1}}{2} = \frac{u_j^n + u_{j-1}^n}{2} - \frac{\Delta t}{\Delta x}\left(F_j^{n+1} - F_{j-1}^{n+1}\right) + \Delta t \frac{G_j^{n+1} + G_{j-1}^{n+1}}{2}. \tag{3.30}$$

For example, to write the one-velocity model (3.1) in the form (3.29), we set

$$u = \begin{bmatrix} \rho_1 \\ \rho_2 \\ \rho v \end{bmatrix}, \; F(u) = \begin{bmatrix} \rho_1 v \\ \rho_2 v \\ \rho v^2 + p(\rho_1, \rho_2) \end{bmatrix}, \; G(u) = \begin{bmatrix} 0 \\ 0 \\ -\frac{\lambda}{2D}\rho|v|v - g\rho\partial_x b \end{bmatrix}. \tag{3.31}$$

Implementation All computations in the remainder of Sect. 3.5 are done in `Python`. Since the scheme is implicit, we make use of a Newton solver at each time step. This in turn requires the Jacobian of the flux, which we compute using the automatic differentiation module `jax`, see [4]. In addition, in order to work with data from GasLib-style network structures, we make use of the `xmltodict` module, to access the network structure and pipe and vertex parameters. Plots and simulations are created using `matplotlib`, see [17], in combination with `numpy`, see [16], for algebraic manipulations.

Data and Discretization Parameters We summarize the physical parameters in Table 3.3. The first column represents given model parameters, including the pipe parameters, the constant given temperature, and fundamental physical constants. The second column displays certain derived quantities, which are needed for our computations. The pipe friction coefficient is determined using the pipe diameter and pipe roughness via the Nikuradze formula scaled by a factor of 0.65. This scaling ensures that the values match with the ones provided on https://www.pipeeng.com/ff_ng.html. The speeds of sound are determined as $c_i^2 := \frac{RT}{M_i}$ where T is the temperature, see (3.16).

Table 3.3: Physical parameters in the implementation

Given parameters		Derived quantities	
Pipe length	10^4 m	Pipe friction coefficient	$8.92094 \cdot 10^{-3}$
Pipe diameter	0.5 m	Speed of sound in CH_4 (c_1)	$3.76255 \cdot 10^2$ m/s
Pipe roughness	10^{-4} m	Speed of sound in H_2 (c_2)	$1.06141 \cdot 10^3$ m/s
Temperature	273.15 K		
Molar mass of CH_4 (M_1)	$1.60424 \cdot 10^{-2}$ kg/mol		
Molar mass of H_2 (M_2)	$2.01588 \cdot 10^{-3}$ kg/mol		
Molar gas constant (R)	8.31447 kg m^2/(s^2 K mol)		

3.5.3 Computation of Stationary Solutions

In this section, we compare the stationary solutions to the one-velocity (3.1) and two-velocity model (3.5). We present in particular our strategy to impose boundary data for both models, which relies on the options described in Sect. 3.5.1. Then, for the special case of the ideal gas law p_I (3.16) we perform a comparison.

We experimentally investigate the limit $f \to \infty$, which formally transforms the two-velocity model to the one-velocity model. We shall see that only one of the options of imposing boundary conditions in Sect. 3.5.1 yields convergence of the stationary solutions as $f \to \infty$.

For both the one- and the two-velocity models we compute the stationary solutions as long time limits of solutions to certain *auxiliary* instationary problems. Hence, we require compatible boundary conditions for the stationary model (see Sect. 3.5.1), as well as both an initial state and (possibly) time-dependent boundary data for the auxiliary instationary problem.

This discussion is relevant also to the network case, see Sect. 3.6.

Setup for the One-Velocity Model We shall use the solutions to the simplified model (3.24) to generate boundary conditions for the stationary version of the one-velocity model (3.1), since it is not straight-forward to obtain admissible boundary data otherwise. Solutions to the simplified model are computed in Sect. 3.6.2 below for a variety of different networks. More specifically, from these computations on a single pipe, we obtain the values $(q^a, \tilde{\mu}^a, p_0^a, p_\ell^a)$ solving (3.24) (and on a network we understand q^a, $\tilde{\mu}^a$ as one constant value per edge, and p^a as one value per vertex). Following the strategy in Sect. 3.5.1, for the stationary model (3.1) we prescribe

- in Option A, the pressure p_0^a, $\tilde{\mu}^a$ on the inflow and q^a on the outflow vertex, and
- in Option B, the mass flux q^a, $\tilde{\mu}^a$ at the inflow, and p_ℓ^a at the outflow vertex.

For simplicity we consider flow from left to right, i.e., $x = 0$ is the inflow vertex of the pipe and $x = \ell$ is the outflow vertex.

Next, we require initial data for the auxiliary instationary model. Our implementation for networks as described in Sections 3.6 below cannot handle changing flow directions, since this would result in a much more complicated nonlinear system of equations. For this reason it is crucial that the initial state is sufficiently close to the stationary solution to (3.1). From the given data $(q^a, \tilde{\mu}^a, p_0^a, p_\ell^a)$ we reconstruct the solution $(\rho_1^s, \rho_2^s, v^s)$ to (3.23) as described in Sect. 3.4.

Then, we determine $(\rho_1^0, \rho_2^0, v^0)$ such that

$$\begin{aligned} p(\rho_1^0, \rho_2^0)(x_i) &= p_I(\rho_1^s, \rho_2^s)(x_i), \\ \frac{\rho_1^0}{\rho_1^0 + \rho_2^0}(x_i) &= \frac{\rho_1^s}{\rho_1^s + \rho_2^s}(x_i), \\ (\rho_1^0 + \rho_2^0)\, v^0(x_i) &= (\rho_1^s + \rho_2^s)\, v^s(x_i), \end{aligned}$$

holds at each grid point x_i by using Newton's method. We emphasize that the corresponding transformation of the functions $(\rho_1^0, \rho_2^0, v^0)$ attains the algebraic values

$(q^a, \tilde{\mu}^a, p_0^a, p_\ell^a)$ at the vertices (pipe ends). When applied on networks, this property ensures that the initial data are compatible with the coupling conditions, see Sect. 3.6 below. However, in general $(\rho_1^0, \rho_2^0, v^0)$ does not represent a stationary solution to (3.1).

It remains to specify the boundary conditions for the auxiliary instationary model. Since the initial data satisfies the boundary data we want to impose for the stationary model, we may choose constant in time boundary data.

Setup for the Two-Velocity Model Recall that we aim to compare solutions to the one- and the two-velocity model. As discussed in Sect. 3.5.1, boundary conditions for the one- and two-velocity model have to be prescribed in a compatible manner. As before, for the two-velocity model we assume that the pressure law is simple. To this end, as boundary data we prescribe

- in Option A, $p_i(\rho_i^{1v})$ at the inflow and $\rho_i^{1v} v^{1v}$ at the outflow vertex, and
- in Option B, $\rho_i^{1v} v^{1v}$ at the inflow and $p_i(\rho_i^{1v})$ at the outflow vertex,

where $(\rho_1^{1v}, \rho_2^{1v}, v^{1v})$ denotes the boundary values of the previously computed one-velocity solution.

Next, we need to specify initial data for the auxiliary instationary model. For the two-velocity model, in contrast to the one-velocity model, no auxiliary problem with an explicit solution is available. This has the consequence that in the network case we do not have functions which satisfy the coupling conditions, see Sect. 3.6.1 below. Indeed, the solution to (3.5) does not allow us to reconstruct an admissible initial state for the two-velocity model, since the coupling conditions for the two-velocity model do not simply reduce to the ones for the one-velocity model for $f = \infty$. For this reason, for the two-velocity model we proceed differently than for the one-velocity model.

We choose functions $(\rho_1^0, \rho_2^0, v_1^0, v_2^0)$ that are constant in $\Omega = (0, \ell)$ with $\rho_i > 0$ as initial data. Furthermore, for the auxiliary instationary problem we need boundary conditions and data that agree with the initial data at the points $(t, x) = (0, 0)$ and $(t, x) = (0, \ell)$. For this purpose, in Option A at the inflow vertex we use the time-dependent function which interpolates the tuples $(0, p_i(\rho_i^0))$ and $(t^*, p_i(\rho_i^{1v}))$ linear-in-time for $t^* = 75$ days for each $i = 1, 2$. For larger times $t \geq t^*$ the function is extended as constant in time. Similarly, at the outflow vertex we use the linear-in time interpolation of the values $(0, \rho_i^0 v_i^0)$ and $(t^*, \rho_i^{1v} v^{1v})$, and extend it as constant for t^*. We proceed analogously in Option B.

Computational Parameters For the space step we fix $\Delta x = 200\,\text{m}$; recall that we identify the pipe with the domain $\Omega = (0, \ell)$, where $\ell = 10\,000\,\text{m}$, see Table 3.3. For the time step we take $\Delta t = 2.5$ days.

For both models, we numerically solve the respective auxiliary instationary problems using the implicit box scheme until we arrive at a stationary solution. Since the scheme is implicit, at each time step t^{n+1}, we solve for u^{n+1} using Newton's method.

More precisely, at t^{n+1}, for a given approximation u^n, we define $\Phi(\cdot, u^n)$ by moving all terms in scheme (3.30) to the left-hand side. Setting $u^{n,0} := u^n$, we compute $u^{n,k+1}$ as the solution of $J_\Phi(u^{n,k}, u^n)(u^{n,k+1} - u^{n,k}) = -\Phi(u^{n,k}, u^n)$, where J_Φ is the Jacobian of Φ. We stop the Newton iteration when $\|\Phi(u^{n,k}, u^n)\|_{\ell^2} < \texttt{tol}$, where `tol` is a fixed tolerance, and set $u^{n+1} := u^{n,k}$. At the first time step t^n such that $\|\Phi(u^n, u^n)\|_{\ell^2} < \texttt{tol}$,

we stop the time iteration and take u^n as our (approximate) stationary solution. In the two-velocity case, we additionally require that $t^n \geq t^* := 1050\,\text{days}$, where we recall that t^* is the time after which the boundary data is kept constant. In our computations, we set $\texttt{tol} := 10^{-7}$.

Results The results of the stationary solutions to the one- and two-velocity model are presented in Fig. 3.6 and 3.7 for Options A and B, respectively, see Table 3.2. Recall that both ways of imposing the boundary conditions are viable. However, only for Option B one can observe that the solution to the two-velocity model $(\rho_1^f, \rho_2^f, v_1^f, v_2^f)$ converges to (ρ_1, ρ_2, v, v), as f increases, where (ρ_1, ρ_2, v) is a stationary solution to the one-velocity model. This behavior is exhibited in Fig. 3.7 with pressure imposed on the outflow vertex. In contrast, for Option A, the values of all quantities on the outflow vertex can be observed to diverge for increasing f. This suggests that the models are compatible on a single pipe in the limit $f \to \infty$, only if the pressure is imposed at the outflow vertex.

We observe a conceptually different behavior of the two-velocity solutions in the limit $f \to \infty$ depending on the choice of boundary conditions. We aim to understand this phenomenon on a heuristic level in the following.

Explanation on a Toy Problem We consider the following toy problem to discuss the impact of boundary conditions on the $f \to \infty$ limit mentioned above. For given $\theta > 0$, we seek functions $u\colon (0,\infty) \times \Omega \to \mathbb{R}$ such that

$$\partial_t u - \partial_x u = -\theta u, \tag{3.32}$$

where $\Omega = (0, \ell)$ as above, subject to initial and boundary conditions. Note that the parameter $\theta > 0$ determines how much dissipation occurs in the time evolution. Specifically, along each characteristic the solution decays exponentially with rate θ, i.e., larger values of θ lead to faster decay along each characteristic. For well-posedness of initial boundary value problems for the advection-reaction problem at hand, it is natural to prescribe boundary data on the inflow boundary, i.e., $u(\cdot, \ell) = u^\partial$ for some given function $u^\partial\colon (0,\infty) \to \mathbb{R}$. In this case, we obtain

$$\|u(t,\cdot)\|_{L^1(\Omega)} \leq \theta^{-1} \|u^\partial\|_{L^\infty(t-\ell,t)}.$$

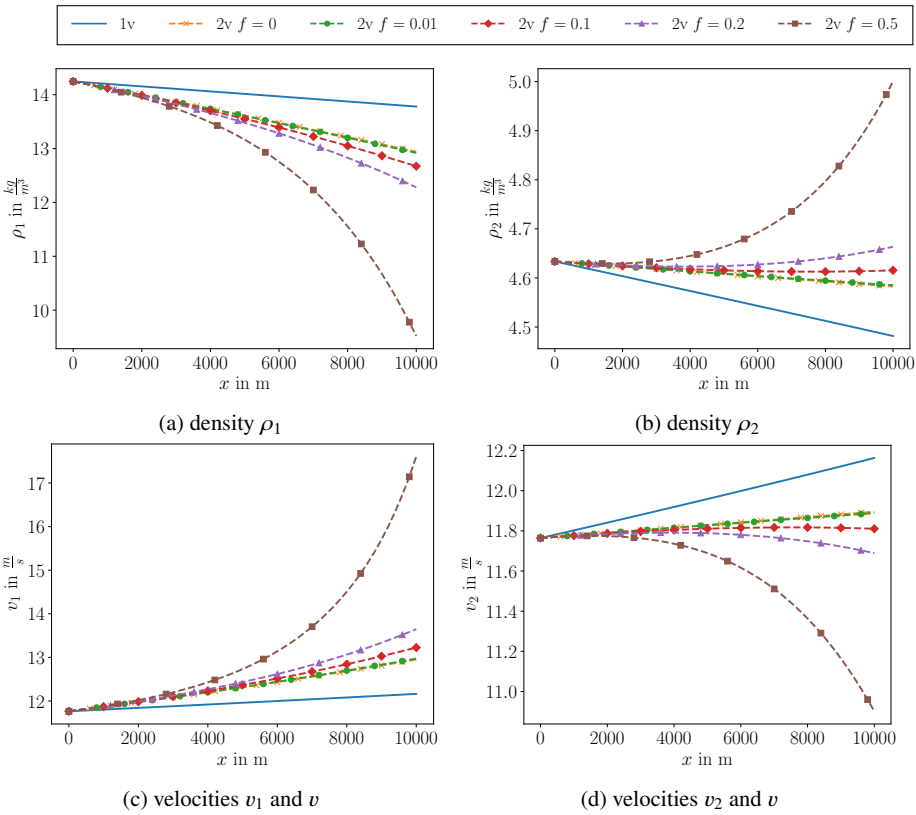
In contrast, for the stationary version of (3.32), which reads

$$-\partial_x u = -\theta u \tag{3.33}$$

integration in (y, z) yields

$$-|u(z)|^2 + |u(y)|^2 + 2\theta \|u\|^2_{L^2((y,z))} = 0.$$

Considering $y = 0$, this shows that if we prescribe $u(0) = u^\partial > 0$, then for fixed $\theta > 0$, we have that $|u(z)|^2$ grows in z, and indeed the faster, the larger θ is. In particular, by (3.33) we can show that the value $u(\ell)$ diverges as $\theta \to \infty$.



(a) density ρ_1

(b) density ρ_2

(c) velocities v_1 and v

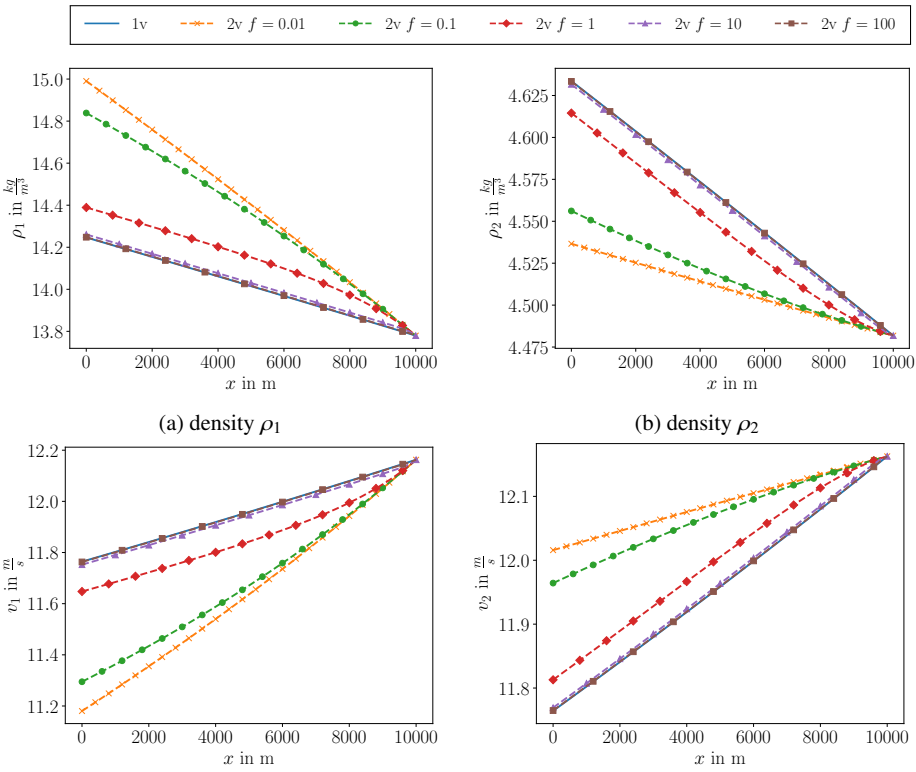
(d) velocities v_2 and v

Fig. 3.6: Stationary solution to the one-velocity model (solid line, indicated with $1v$) and two-velocity model (dashed line, indicated with $2v$) with the ideal gas law p_I for several inner friction parameters $f \in \{0.01, 0.1, 1, 10, 100\}$ in $\mathrm{m}^3/(\mathrm{kg} \times \mathrm{s})$ with compatible boundary conditions and boundary data where the pressure is imposed at the *inflow* vertex (Option A in Table 3.2).

This is not the case when considering $z = \ell$ and prescribing $u(\ell) = u^\partial > 0$. In this case the functions converge as $\theta \to \infty$.

Explanation of $f \to \infty$ ***limit*** A similar effect occurs for solutions to the two-velocity model as $f \to \infty$. To heuristically investigate this and to explain the type of phenomena observed in Fig. 3.6 and 3.7, we consider the stationary equations (3.7) together with the ideal gas law p as in (3.16) and with linear friction and flat bottom. Since for the stationary solutions $q_i = \rho_i v_i$, for $i \in \{1, 2\}$, is constant in space, it is irrelevant on which part of the boundary we prescribe the mass flux. It only matters on which part of the boundary we impose the pressure.

Applying equation (3.7a) and (3.7b) in (3.7c) and (3.7d), respectively, yields



(a) density ρ_1

(b) density ρ_2

(c) velocities v_1 and v

(d) velocities v_2 and v

Fig. 3.7: Stationary solution to the one-velocity model (solid line) and two-velocity model (dashed line) with the ideal gas law p_I for several inner friction parameters $f \in \{0.01, 0.1, 1, 10, 100\}$ in $\mathrm{m}^3/(\mathrm{kg} \times \mathrm{s})$ with compatible boundary conditions and data, where the pressure is prescribed at the *outflow* vertex (Option B in Table 3.2).

$$-v_i \partial_x v_i \left(\frac{c_i^2}{v_i^2} - 1 \right) + f \rho_j (v_i - v_j) + \tilde{\lambda} v_i = 0,$$

where $i \in \{1, 2\}$, $j \in \{1, 2\}$ with $j \neq i$ and $\tilde{\lambda} = \frac{\lambda}{2D}$. In the subsonic regime we have $|v_i| \lll c_i$ and hence $\alpha(v_i) := c_i^2/v_i^2 - 1 > 0$. Multiplying by $2/\alpha(v_i)$, yields

$$\partial_x(v_i^2) = 2f \frac{\rho_j (v_i - v_j)}{\alpha(v_i)} + 2\tilde{\lambda} \frac{v_i}{\alpha(v_i)}. \tag{3.34}$$

We assume that $v_i > 0$ for $i \in \{1, 2\}$, i.e., both components exhibit flow in positive x-direction.

Provided that independently of f we impose $v_i^\partial > v_j^\partial$ at one interval end point, then $\partial_x(v_i^2) > 0$, and it is larger, the larger $f > 0$ is. In turn, for sufficiently large f, the derivative of $(v_j)^2$ is negative.

This is the type of behavior that can be observed in Fig. 3.6c and 3.6d, where data is imposed at the inflow vertex $x = 0$ and $v_1^\partial > v_2^\partial$. Indeed, one may notice that imposing data on the inflow vertex has the effect that the faster component is accelerated and the slower one is decelerated.

In Fig. 3.7c and 3.7d, where the data is imposed at the outflow vertex $x = \ell$, we have $v_1^\partial < v_2^\partial$ for all f, and hence the roles are inverted. Indeed, the derivative of $v_2^2(\ell)$ increases in f, and the derivative of v_1^2 decreases in f. This has the effect that the velocities align at $x = \ell$, as f increases.

It should be noted that the discussion depends on the flow direction $v_i > 0, i \in \{1, 2\}$. For this reason, the imposition of boundary conditions is linked to the (expected) flow direction.

In the following, we shall focus on Option B in Table 3.2, since in this case compatibility of the two- and the one-velocity model is at least a possibility as observed above.

3.5.4 Instationary Solutions

In this section we investigate the effect of the inner friction parameter f on instationary numerical solutions to the two-velocity model (3.5) on a single pipe $\Omega := (0, \ell)$. Let us note the proof of exponential convergence for any $f > 0$ in [12]. Specifically we investigate $\|v_1 - v_2\|_{\ell^1(\Omega)}(t)$. We consider initial conditions of constant mass density for each component and velocities oriented in opposite directions, and impose $q_i^\partial = 0$ as boundary values at both ends of the interval for $i \in \{1, 2\}$. We investigate solutions for a range of values of f.

We find that on a short time scale, corresponding to the first minute, $\|v_1 - v_2\|_{\ell^1(\Omega)}(t)$ is decreasing in time for all f and is smaller for larger values of f; i.e., the inner friction causes the velocities to converge to each other and for larger inner friction the convergence is faster in time.

Over the time range corresponding to several minutes, however, we see that this monotonicity no longer holds. In particular, we find that there is a threshold value of the inner friction f^* for which the quantity $\|v_1 - v_2\|_{\ell^1(\Omega)}(t)$ experiences the quickest decay to machine precision; for f both greater and smaller than f^*, the decay is slower. We also observe a difference in behavior of the quantity $\|v_1 - v_2\|_{\ell^1(\Omega)}(t)$ depending on f^* on this time scale; for $f \leq f^*$, the norm decays with oscillations, whereas for $f > f^*$ it becomes monotonically decreasing.

Though we find evidence that on short time intervals higher inner friction forces the velocities to converge more quickly, understanding the mechanism behind the different behaviors observed for $f > f^*$ and for $f \leq f^*$ and the transition between them remains an open question. As seen in Sect. 3.5.3, the choice of boundary condition may have an influence on the behavior of the two-velocity model when varying f.

Computational Setup

Initial and Boundary Data As in Sect. 3.5.3, we consider a pipe length of $\ell := 10\,000\,\mathrm{m}$. For the initial data, we set $\rho_1^0(x) := 10\,\mathrm{kg/m^3}$, $\rho_2^0(x) := 5\,\mathrm{kg/m^3}$, and for the velocities, we set $v^* := 14\,\mathrm{m/s}$ and define

$$v_1^0(x) := \begin{cases} \frac{v^*}{100}x & \text{for } 0 \le x \le 100, \\ v^* & \text{for } 100 < x \le 9900, \\ \frac{-v^*}{100}x + 100v^* & \text{for } 9900 < x \le 10000, \end{cases} \tag{3.35}$$

$$v_2^0(x) := -v_1^0(x). \tag{3.36}$$

As boundary data, we fix $q_i^\partial(t) = 0$ for $i \in \{1, 2\}$ at both ends of the pipe.

Computational parameters For the simulation, we set $\Delta x := 50\,\mathrm{m}$, $\Delta t := 12\,\mathrm{s}$, and consider a time horizon of $T := 12\,\mathrm{h}$. Since here we do not approximate long time solutions, the time horizon is considerably shorter than before. In each time step we employ Newton's method as discussed in Sect. 3.5.3. For the stopping criterion, we compute iterates until $\|u^{n,k} - u^{n,k+1}\|_{\ell^2} < \mathtt{tol} := 10^{-7}$, at which point we take $u^{n+1} := u^{n,k+1}$. We consider inner friction values of $f \in \{0.001, 0.01, 0.1, 1, 10\}\ \mathrm{m^3/(kg \times s)}$.

Results Let N^t and N^e be the total number of temporal and spatial discretization points, respectively, so that $T = N^t \Delta t$ and $\ell = N^e \Delta x$. For a given inner friction value f let $v_i(f; t, x)$: $[0, T] \times [0, \ell] \to \mathbb{R}$ denote the velocity of constituent $i \in \{1, 2\}$. Then we set

$$D(f; t) := \frac{1}{\ell(N^e + 1)} \sum_{j=0}^{N^e} |v_1(f; t, x_j) - v_2(f; t, x_j)|, \tag{3.37}$$

which is a scaling-invariant, i.e., constant-preserving, version of $\|v_1 - v_2\|_{\ell^1(\Omega)}(t)$ for given f. We compute $D(f; t^n)$ for $0 \le n \le N^t$ and $f \in \{0.001, 0.01, 0.1, 1, 10\}$ $\mathrm{m^3/(kg \times s)}$; the results are presented in Fig. 3.8. The time axis is linear between 0 s and 12 s (i.e., for the first time step), and logarithmic beyond, in order to clearly display the results for short time scales.

We see that, for $0 \le t < \bar{t} \approx 10^{1.75}$ s, $D(f; t)$ oscillates while tending to decrease overall for all f. Additionally, for $f_1 > f_2$, one has that $D(f_1; t) \le D(f_2; t)$. On this time scale, we thus see evidence that the inner friction forces the velocities to converge to each other, and that larger inner friction causes this to occur more quickly.

For $t \ge \bar{t}$, we observe different phenomena for different values of f. For $f \in \{0.001, 0.01\}$ $\mathrm{m^3/(kg \times s)}$, we see that $D(f; t)$ remains oscillatory and decays rapidly until reaching values of the order of 10^{-19}; we do not interpret results below this level, since we expect rounding errors to have a significant impact. Additionally, for $t \ge \bar{\bar{t}} \approx 10^{2.5}$ s, we observe that $D(0.01; t) < D(0.001; t)$, supporting the idea that, for $f \le 0.01$, a larger inner friction increases the speed of convergence.

For $f \in \{0.1, 1, 10\}$ $\mathrm{m^3/(kg \times s)}$ and $10^{1.8}$ s $\approx t^* \le t \le t^{**} \approx 10^{3.2}$ s, we see that $D(f; t)$ becomes monotonically decreasing in t, with a decrease in the overall rate of change. To investigate this more closely, in Fig. 3.9 we plot the results for $f \in \{0.1, 1, 10\}$

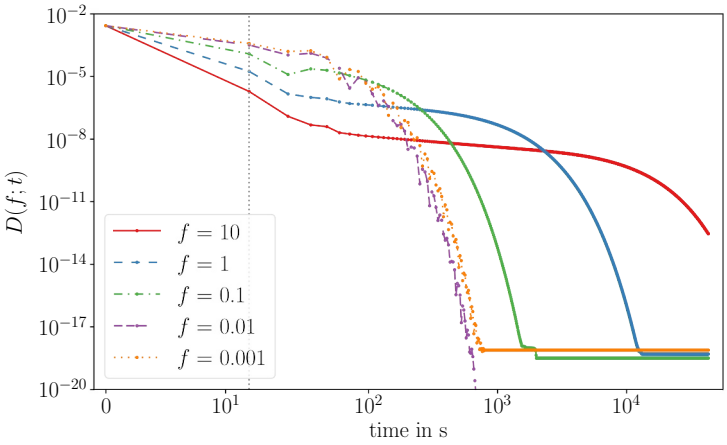


Fig. 3.8: Plot of $t \mapsto D(f;t)$ as defined in (3.37) for inner friction values $f \in \{0.001, 0.01, 0.1, 1, 10\}$ $m^3/(kg \times s)$; the time axis is linear for the first time step and logarithmic afterwards. On short time scales up to around $10^{1.6}$ s, larger inner friction forces the velocities to converge to each other more quickly. On longer time scales, $D(f;t)$ remains oscillatory for $f \in \{0.001, 0.01\}$ $m^3/(kg \times s)$ while decaying more quickly for $f = 0.01$. For $f \in \{0.1, 1, 10\}$ $m^3/(kg \times s)$, $D(f;t)$ becomes strictly decreasing and the rate of change slows down; this effect is stronger for larger f.

$m^3/(kg \times s)$, where time is scaled linearly and restricted to $t \in [0, 21600]$ s, i.e., the first 6 h.

The results demonstrate that, after the initial oscillatory period, the decay of $D(f;t)$ for these values of f becomes monotonically decreasing, with a more rapid decay in time for smaller f. This indicates that, if the velocities are near each other, higher inner friction somehow seems to impede the ability of the system to come to rest, in a manner reminiscent of overdamping. However, the precise mechanism behind this remains unclear.

Overall, we see evidence that, on short time scales, higher inner friction causes the velocities to converge to each other more rapidly. However, we also see that on the time scale of minutes to hours, while the results are in line with expectations for $f \leq 0.01$ $m^3/(kg \times s)$, they deviate considerably from expectations for $f \geq 0.1$ $m^3/(kg \times s)$. Understanding the transition in behavior of the system for $f \in [0.01, 0.1]$ $m^3/(kg \times s)$ merits further investigation, however, it is outside the scope of the current work. We thus leave this as an open question for future studies.

3.6 Mixtures on Networks

In this section we consider several mixture models on networks. Understanding the behavior of gas mixtures on networks is interesting from a mathematical perspective as

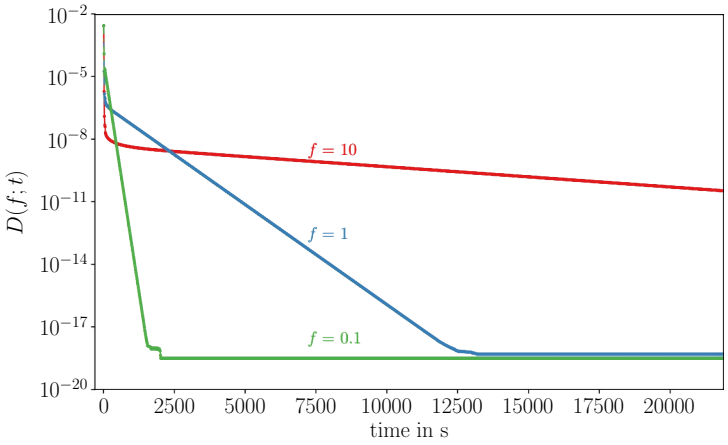


Fig. 3.9: Plot of $t \mapsto D(f;t)$ as defined in (3.37) for inner friction values $f \in \{0.1, 1, 10\}$ $m^3/(kg \times s)$ restricted to $t \in [0, 21600]$ s. After the initial oscillatory period, the decay of $D(f;t)$ for the considered values of f becomes monotonically decreasing, with smaller f inducing a faster decay.

well as from a more applied perspective like that of a gas network operator. Important questions are how the mixture is distributed across the network and if nominations with mixing involved are feasible, to name only a few.

After introducing coupling conditions on networks in Sect. 3.6.1 we address optimization in Sect. 3.6.2 and subsequently their numerical discretization in Sect. 3.6.3 and 3.6.7, for the stationary and the instationary case, respectively. Furthermore, in Sect. 3.6.4 we investigate the effect of the choice of the pressure law, and in Sect. 3.6.6 we numerically investigate the compatibility of the coupling conditions between the one- and the two-velocity model. In Sect. 3.6.5 the simplified model used for the optimization is justified.

3.6.1 Coupling Conditions on Networks

Before we discuss specific choices of coupling conditions, let us mention that there is a fundamental difference between one- and two-velocity models when it comes to the number of coupling conditions (which is related to the different number of equations in both systems). For a detailed discussion of coupling conditions, we refer to Chap. 2, "A Catalog of Gas Network Models: PDEs, Coupling Conditions, and Numerical Schemes", Sect. 2.6.3.

For neither of the two models is conservation of momentum (or equivalently force balance at the vertices) a meaningful concept to consider. This is because the pipes exert a variety of forces on the gas that are beyond the scope of network models and probably also depend on the junction geometry, which is not considered in network models.

In the model catalog we describe coupling conditions which ensure that, if mechanical energy enters or leaves the network at vertices, this is due to mass fluxes into or out of the network.

For the one-velocity model (3.1), this is ensured by imposing the conservation of mass for each mixture component, the continuity of the total enthalpy, and perfect mixing for each component; these are, respectively, (2.51), (2.52), and (2.53) in Chap. 2, "A Catalog of Gas Network Models: PDEs, Coupling Conditions, and Numerical Schemes". For the two-velocity model (3.5), energy consistency is ensured by imposing both the mass conservation and the enthalpy continuity for each component individually, as described by (2.51) and (2.54) in the same chapter. Let us mention that in the context of non-isothermal, single constituent flows perfect mixing of the temperature was considered, e.g., in [22, 25].

However, these coupling conditions rely on the existence of a pressure energy P, fulfilling the relationship (3.8), which is not clear for GERG-08 to us. Therefore, we replace enthalpy continuity by pressure continuity in the one-velocity model (3.1) and by partial pressure continuity in the two-velocity model (3.5). This may lead to an artificial increase in energy, but for small velocities we expect the change to remain moderate.

For the reader's convenience, we state the coupling conditions in the form which we use, with the notation of Chap. 2, "A Catalog of Gas Network Models: PDEs, Coupling Conditions, and Numerical Schemes", Sect. 2.6.3.

One-Velocity Coupling In addition to mass flux on the pipes, for each vertex there is a mass flux into or out of the network q_i^ν that is either prescribed or part of the solution. Then, mass conservation is expressed as

$$q_i^\nu + \sum_{e \in \mathcal{E}(\nu)} A^e \rho_i^e(\nu)\, v^e(\nu)\, n^e(\nu) = 0 \quad \text{for } i \in \{1,2\} \text{ and all } \nu \in \mathcal{V}, \tag{3.38}$$

where A^e is the cross-sectional area of a pipe e which we assume to be constant in x. Pressure continuity requires that

$$\text{for each vertex } \nu \in \mathcal{V} \text{ there exists a } p^\nu \text{ with } p(\rho_1^e, \rho_2^e) = p^\nu \text{ for all } e \in \mathcal{E}(\nu). \tag{3.39}$$

Perfect mixing is enforced by

$$\frac{\rho_i^{e'}(\nu)}{\rho^{e'}(\nu)} = \frac{\max\{q_i^\nu, 0\} + \sum_{e \in \mathcal{E}_{\text{in}}(\nu,q)} A^e \rho_i^e(\nu) v^e(\nu) n^e(\nu)}{\max\{q_1^\nu + q_2^\nu, 0\} + \sum_{e \in \mathcal{E}_{\text{in}}(\nu,q)} A^e \rho^e(\nu) v^e(\nu) n^e(\nu)} \quad \text{for any } i \in \{1,2\}, \tag{3.40}$$

for all $\nu \in \mathcal{V}$, $e' \in \mathcal{E}_{\text{out}}(\nu, q)$, for given mass flux q_i^ν. Note that which edge e adjacent to a vertex ν is in $\mathcal{E}_{\text{in}}$ or $\mathcal{E}_{\text{out}}$, respectively, depends on the flow direction q^e in the pipe. Therefore, if the flow direction remains unchanged, then the sets $\mathcal{E}_{\text{in}}$ and $\mathcal{E}_{\text{out}}$ do not change over the entire duration of the simulation. Otherwise, $\mathcal{E}_{\text{in}}$ and $\mathcal{E}_{\text{out}}$ would depend on the solution, which results in a much more complicated system to be solved. These coupling conditions are used in the following for all one-velocity type models.

In addition to the coupling conditions, we need to prescribe certain 'boundary' values q^ν, p^ν. Indeed, in terms of the number of coupling conditions at each vertex ν either

q^ν or p^ν should be prescribed. In the following we denote the set of vertices where q^ν is prescribed by Γ_q, and the set of vertices where p^ν is prescribed by Γ_p. Note that they are disjoint and $\Gamma_p \cup \Gamma_q = \mathcal{V}$. We assume that the sets Γ_p and Γ_q are both non-empty. In addition, at those vertices where mass flows into the network, we also need to prescribe $\tilde{\mu}^\nu$. We define

$$q_1^\nu := q^\nu \tilde{\mu}^\nu, \quad q_2^\nu = q^\nu(1 - \tilde{\mu}^\nu).$$

It should be noted that not every such set of boundary data p^ν and q^ν leads to a well-posed problem, since, e.g., it might lead to negative pressures.

Two-Velocity Coupling Componentwise mass conservation is given by

$$q_i^\nu + \sum_{e \in \mathcal{E}(\nu)} A^e \rho_i^e(\nu)\, v_i^e(\nu)\, n^e(\nu) = 0 \qquad \text{for } i \in \{1,2\} \text{ and all } \nu \in \mathcal{V}, \tag{3.41}$$

for given mass flux q_i^ν. This is consistent with the perfect mixing condition for the one-velocity model in the sense that perfect mixing (3.40) together with mass conservation implies partial mass conservation (3.41).

As before, provided that the mixture is simple, the partial pressures are available. Continuity of the partial pressure requires that

$$\text{for each } \nu \in \mathcal{V} \text{ there is } p_i^\nu \text{ with } p_i(\rho_i^e) = p_i^\nu \text{ for all } e \in \mathcal{E}(\nu), \text{ and } i \in \{1,2\}. \tag{3.42}$$

As in the one-velocity case we need to prescribe certain 'boundary' values q_i^ν, p_i^ν. Indeed, in terms of the number of coupling conditions at each vertex ν and each i either q_i^ν or p_i^ν should be prescribed, and we denote the respective disjoint vertex sets by $\Gamma_p[i]$ and $\Gamma_q[i]$ such that $\Gamma_p[i] \cup \Gamma_q[i] = \mathcal{V}$. Again, we assume that they are non-empty. As before, not every such set of boundary data p_i^ν and q_i^ν leads to a well-posed problem, since, e.g., it might lead to negative pressures.

3.6.2 Optimization

This section aims to give a brief overview over optimization of gas mixtures on networks for the stationary case. For simplicity we only cover the coupling of the flow to the pressures with an algebraic equation. The model used here is the algebraic one-velocity model (3.24), which relies on the ideal gas pressure law (3.16).

The network is modeled as a directed graph $G = (\mathcal{V}, \mathcal{E})$, where $\mathcal{V}$ denotes the set of vertices and $\mathcal{E}$ the set of directed edges. Vertices represent junctions of pipes, sources and sinks. Edges represent pipes or other network components, e.g., compressor stations. For the modeling of active elements we refer to [13, 14, 19]. The sets of in- and outgoing edges of a vertex $\nu \in \mathcal{V}$ are defined as

$$\delta^-(\nu) := \{e = (u, \nu) \,:\, e \in \mathcal{E}\} \quad \text{and} \quad \delta^+(\nu) := \{e = (\nu, u) \,:\, e \in \mathcal{E}\},$$

respectively. In the stationary setting it is convenient to use the mass-flow $q = \rho v$ as introduced in Sect. 3.4. Given these definitions, flow conservation at vertices can be

expressed as

$$\sum_{e\in\delta^+(v)} q_e - \sum_{e\in\delta^-(v)} q_e = b_v \qquad \text{for all } v \in \mathcal{V}. \tag{3.43}$$

Here, q_e denotes the mass flux on edge $e \in \mathcal{E}$. We assume that the given *balance vector* $b \in \mathbb{R}^{\mathcal{V}}$ satisfies $\sum_{v\in\mathcal{V}} b_v = 0$. Thus (3.43) is equivalent to (3.38).

Calculation of the Mixing Ratio In networks the gases mix at vertices and we assume *perfect mixing*, i.e., the gas leaving the vertices is perfectly homogeneous. More details can be found in Sect. 3.6.1.

Here, we show how the mixing ratio is calculated in the variables q and $\tilde{\mu}$. For each edge e, we introduce variables $\tilde{\mu}_e$ for the mass percentage of constituent 1 in the mixture. At each vertex, the mass percentage mixing ratio is calculated as the weighted average of the mixing ratios of the in-flowing pipes

$$\tilde{\mu}_v = \frac{\sum_{e\in\mathcal{E}_{\text{in}}(v,q)} \tilde{\mu}_e\,|q_e| + b_v^+\bar{\tilde{\mu}}_v}{\sum_{e\in\mathcal{E}_{\text{in}}(v,q)} |q_e| + b_v^+} \qquad \text{for all } v \in \mathcal{V}, \tag{3.44a}$$

$$\tilde{\mu}_e = \tilde{\mu}_v \qquad \text{for all } e \in \mathcal{E}_{\text{out}}(v,q),\ v \in \mathcal{V}. \tag{3.44b}$$

In (3.44a), $\bar{\tilde{\mu}}_v$ denotes the given fixed mixing ratio for all *sources* v, i.e., $\{v \in \mathcal{V} : b_v > 0\}$ and $b_v^+ = \max\{0, b_v\}$. Note that (3.44b) is equivalent to (3.40) using different variables.

Modeling of the Flow As shown in Sect. 3.4, the system (3.3) can be simplified using (3.16) and solved analytically in the stationary case. In the single gas case, the algebraic model is often called the Weymouth equation. For mixtures we obtain a generalized Weymouth equation, in which the pressure loss also depends on the gas composition and not only the mass flux. Using (3.24), the coupling of pressure differences and flow then can be expressed as

$$p_u^2 - p_v^2 = \Lambda_e\, c(\tilde{\mu}_e)^2\, q_e\,|q_e| \qquad \text{for all } e = (u,v) \in \mathcal{E}, \tag{3.45a}$$

$$c(\tilde{\mu}_e)^2 = c_1^2\,\tilde{\mu}_e + (1-\tilde{\mu}_e)\,c_2^2 \qquad \text{for all } e \in \mathcal{E}. \tag{3.45b}$$

Here c_1 and c_2 again denote the speed of sound of constituent 1 and 2, respectively, and Λ_e is a pipe dependent coefficient, for details see [19]. Equation (3.45b) is a result of the use of (3.16). For details see [2].

Note that the use of other more more complex pressure laws leads to nonlinear dependency of the pressure on the density, which complicates the explicit solution of the ODE. We therefore only consider the ideal gas pressure law here.

Objectives of the Optimization A natural objective for gas network operators is to reduce the operating cost of the network. We choose to minimize the sum of active compressor stations as objective for the optimization. However, even finding a feasible solution for a given supply and demand scenario is not easy, since it requires determining whether compressor stations are needed and which valves to open or close.

Global Optimization For stationary gas flows, we aim for a computation of a globally optimal solution, in particular, with a proof of optimality. As we will show in the computational results below, this is possible in reasonable time for networks of practical size. One benefit of such global optimization is that it allows to detect infeasibility with respect to mixing, i.e., a scenario might be feasible for a single gas, but not for a certain mixture. Even very small changes on the mixing ratio at sources can turn a scenario infeasible. In contrast, a search for local solutions cannot prove infeasibility.

The algorithm that we use for performing global optimization is *spatial branch-and-bound*, which is implemented in the framework SCIP [1]. The main idea is to recursively decompose variable domains, using dual bounds based on solving linear programming (LP) relaxations, see [28] for more information.

Complete Optimization Model To present the complete optimization model, we first note that for each edge $e \in \mathcal{E}$ there is a lower bound $\underline{q}_e$ and an upper bound $\overline{q}_e$ for the flow q_e. Similarly, there are lower and upper pressure bounds for each vertex $v \in \mathcal{V}$, $\underline{p}_v$ and $\overline{p}_v$, respectively. Furthermore, we partition the set of edges $\mathcal{E}$ into $\mathcal{E}^P \cup \mathcal{E}^C \cup \mathcal{E}^V$. The edges $\mathcal{E}^P$ represent pipes. Edges for valves are denoted by $\mathcal{E}^V$. A valve edge $e = (u, v) \in \mathcal{E}^V$ can be 'open' or 'closed', which is represented by the corresponding binary variable s_e being 1 or 0, respectively. The flow q_e through a valve edge $e \in \mathcal{E}^V$ is coupled to s_e via $\underline{q}_e s_e \le q_e \le \overline{q}_e s_e$. If $s_e = 0$, then the pressures at u and v are decoupled, while they are required to be equal if $s_e = 1$. Instead of giving a complete model for valves, we abbreviate the coupling by $C(q_e, p_u, p_v, s_e)$ and refer to the literature for details, see, e.g., [19]. The edges in $\mathcal{E}^C$ represent compressors, which allow to increase pressure. They can be turned on/off using a binary variable s_e, $e \in \mathcal{E}^C$. Similarly to valves we refer to the literature and denote the coupling constraints by $C(q_e, p_u, p_v, s_e)$. Then the model can be represented by

$$
\begin{aligned}
\min \ & \sum_{e \in \mathcal{E}^C} s_e \\
& \sum_{e \in \delta^+(v)} q_e - \sum_{e \in \delta^-(v)} q_e = b_v && \forall v \in \mathcal{V}, \\
& p_u^2 - p_v^2 = \Lambda_e \, c(\tilde{\mu}_e)^2 \, q_e \, |q_e| && \forall e = (u, v) \in \mathcal{E}^P, \\
& c(\tilde{\mu}_e)^2 = c_1^2 \, \tilde{\mu}_e \, + (1 - \tilde{\mu}_e) \, c_2^2 && \forall e \in \mathcal{E}, \\
& \tilde{\mu}_v = \frac{\sum\limits_{e \in \mathcal{E}_{\text{in}}(v,q)} \tilde{\mu}_e \, |q_e| + b_v^+ \bar{\tilde{\mu}}_v}{\sum\limits_{e \in \mathcal{E}_{\text{in}}(v,q)} |q_e| + b_v^+} && \forall v \in \mathcal{V}, \\
& \tilde{\mu}_e = \tilde{\mu}_v && \forall e \in \mathcal{E}_{\text{out}}(v, q), \ v \in \mathcal{V}, \\
& C(q_e, p_u, p_v, s_e) = 0 && \forall e = (u, v) \in \mathcal{E}^C \cup \mathcal{E}^V, \\
& \underline{q}_e \le q_e \le \overline{q}_e && \forall e \in \mathcal{E}, \\
& \underline{p}_v \le p_v \le \overline{p}_v && \forall v \in \mathcal{V}, \\
& s_e \in \{0, 1\} && \forall e \in \mathcal{E}^C \cup \mathcal{E}^V.
\end{aligned}
\tag{3.46}
$$

This full mixed-integer nonlinear problem is solved in the following.

Table 3.4: Time and branch-and-bound nodes needed to solve the mixing scenarios to global optimality

GasLib instance	time (seconds)	# nodes
GasLib40 Scn. 1	0.3	1
GasLib40 Scn. 2	0.9	25
GasLib60 Scn. 1	831.4	16634
GasLib60 Scn. 2	451.0	6991
GasLib60 Scn. 3	81.6	1342
GasLib60P Scn. 1	1.6	37
GasLib582 Scn. 1	403.7	6064
GasLib582 Scn. 2	2532.6	30895

Table 3.5: Time and branch-and-bound nodes needed to solve the scenarios to global optimality without mixing

GasLib instance	time (seconds)	# nodes
GasLib40	0.2	1
GasLib60	3.0	29
GasLib60P	0.6	1
GasLib582	43.4	4134

Computational Study In the following we present a small computational study showcasing the additional time required for solving mixing scenarios in comparison to the single gas case. This study shows that solving large, but not too complex, networks with mixtures is possible.

For this purpose, we created different mixing scenarios based on instances of the GasLib [26] and the ones used in [29]. For GasLib60, GasLib60P and GasLib582, we use different scenarios with different sources selected to supply the mixture. GasLib60P is a passive variant of GasLib60, i.e., it has no compressor stations. In comparison to the single gas case, the complexity of a scenario is not only determined by the supply and demand, but also where mixing happens. For GasLib40 we created two mixing scenarios. The molar mass of the inflowing gas at source 3 is 16.5 in the first and 16.3 in the second scenario. This small change results in the second scenario being infeasible. The computational results for this can be found in Table 3.4. In Table 3.5 one finds the time needed to solve the same scenarios but without mixing, i.e., a single gas.

The code, instances and generated data can be found at https://github.com/TRR154/GasA01 and https://github.com/TRR154/StationaryMixingData.

3.6.3 Computational Details of Stationary Flow

In this section, we provide computational details of computing stationary solutions on networks for the one-velocity model (3.1) and the two-velocity model (3.5). Similarly as

in Sect. 3.5.3, we use the auxiliary instationary model and compute the long-time limit with the implicit box scheme presented in Sect. 3.5.2. Here, the additional challenge compared to the single pipe case consists of handling coupling conditions on the network, see Sect. 3.6.1. We now need to choose boundary and coupling conditions for the stationary model, as well as both initial data and time-dependent boundary and coupling conditions for the auxiliary instationary model.

As in the single pipe case in Sect. 3.5.3, we distinguish between the one- and two-velocity models.

Setup for the One-Velocity Model *Stationary problem.* As stated in Sect. 3.6.1 for the one-velocity model (3.1) at each vertex v of the network either the pressure p^v or the mass flux q^v can be prescribed. We refer to the respective (disjoint) vertex sets as $\Gamma_p, \Gamma_q \neq \emptyset$, respectively. In addition to the coupling conditions in (3.38), (3.39), and (3.40) we need to impose a value of $\tilde{\mu}^v$ at vertices at which there is mass flux into the network (independently of whether p^v or q^v is imposed).

Next, let us discuss how to choose the boundary data. For this we use the solution to the algebraic model (3.45) subject to the coupling conditions (3.44) as a starting point. In particular, we are given one value of p^a per vertex, and one value of $\tilde{\mu}^a$, q^a per edge. On vertices $v \in \Gamma_p$ we impose $p^v = p^a(v)$, whereas for $v \in \Gamma_q$ we impose

$$q^v = -\sum_{e \in \mathcal{E}(v)} q^a|_e(v)\, n^e(v),$$

i.e., the value that ensures mass conservation (3.38) for the simplified model. The case $q^v = 0$ corresponds to no mass flux. On vertices, where we additionally need to impose $\tilde{\mu}^v$, as in Sect. 3.6.1 we use the values $\tilde{\mu}^a(v)$. In the following, consistently with Option B in Table 3.2, we choose all vertices with only one edge to be in Γ_q, if the vertex is an inflow vertex of the edge, and to be in Γ_p otherwise. Furthermore, any vertex v with more than one adjacent edge is in Γ_q if $q^v = 0$ and in Γ_p otherwise.

Auxiliary instationary problem. Next, we turn to the construction of the initial state, where we follow the procedure in Sect. 3.5.3 to construct an initial state based on the solution of the stationary model (3.23). That it is close to the stationary solution is essential, because our method cannot handle changes in the flow regime due to our implementation of the perfect mixing coupling condition (3.40). We hope that by this procedure, for each fixed edge e the sign of q^e does not change in the time iteration, and hence the sets $\mathcal{E}_{\text{in}}(v, q)$ and $\mathcal{E}_{\text{out}}(v, q)$ do not change in time.

Moreover, we notice that this initial state satisfies the coupling conditions (3.38), (3.39) and (3.40), see (3.43) and (3.44).

As boundary conditions for the auxiliary instationary model, we prescribe the constant in time 'boundary' data $t \mapsto p^v$, $t \mapsto q^v$ and $t \mapsto \tilde{\mu}^v$, on the respective vertices, which are compatible with the initial data. Similarly as in Sect. 3.5.3 this means that long time limits to the scheme satisfy the boundary conditions and data as described before.

Setup for the Two-Velocity Model *Stationary problem.* Recall that for the two-velocity model (3.5) we use the coupling conditions as in Sect. 3.6.1 and recall that no flow directions enter the conditions. As described therein, on each vertex and each $i \in \{1, 2\}$

one may impose either a value on q_i^ν or on p_i^ν. We denote the respective stets of vertices by $\Gamma_q[i] \cup \Gamma_p[i] = \mathcal{V}$. In the comparison of the one- and the two-velocity model, for the sake of consistency, we choose $\Gamma_p[1] = \Gamma_p[2] = \Gamma_p$ and $\Gamma_q[1] = \Gamma_q[2] = \Gamma_q$. Similarly as before in Sect. 3.5.3, to obtain compatible boundary and coupling data we first compute the solution $(\rho_1^{1v}, \rho_2^{1v}, v^{1v})$ to the one-velocity model. Then, based on $v_1^{2v} = v_2^{2v} = v^{1v}$ we compatibly choose the data q_i^ν at vertices $\nu \in \Gamma_q[i]$ and p_i^ν at vertices $\nu \in \Gamma_p[i]$, respectively, for the two-velocity model.

Auxiliary instationary problem. For the two-velocity model, other than for the one-velocity model, no auxiliary problem similar to (3.23) with explicit solution is available. Furthermore, the initial state constructed from solutions to the auxiliary problem for the one-velocity model does not satisfy the coupling conditions for the two-velocity model. Specifically, the conditions in the two-velocity model do not reduce to the conditions in the one-velocity model even when $v_1 = v_2$. Hence, we cannot use it as initial state for the two-velocity model.

Therefore, as initial state we choose $(\rho_1^0, \rho_2^0, v_1^0, v_2^0) \in \mathbb{R}_{>0} \times \mathbb{R}_{>0} \times \mathbb{R} \times \mathbb{R}$ as constant across the whole network. For each vertex in $\Gamma_p[i]$ we determine the value $p_i^0 := p_i(\rho_i^0)$, where we again consider only simple mixtures. Furthermore, for each $\nu \in \Gamma_q[i]$ we determine $(q_i^\nu)^0$ for each $i \in \{1, 2\}$ and each vertex $\nu \in \Gamma_q[i]$ such that the initial state satisfies the mass conservation at ν (3.41). Then, similarly as in the case of a single pipe, we consider time-dependent boundary data, which arise as linear-in-time interpolants of $(0, (q_i^\nu)^0)$ and (t^*, q_i^ν), and then are extended as constant functions for $t \geq t^*$. Those functions are imposed as 'boundary' data on all vertices in $\Gamma_q[i]$. We proceed analogously for the vertices in $\Gamma_p[i]$, where we impose a linear-in-time interpolant of $(0, (p_i^\nu)^0)$ and (t^*, p_i^ν), which is extended as constant in time. Those boundary data agree with the initial data at $t = 0$ and at all vertices, and for long times coincide with the (compatibly chosen) boundary data for the stationary problem.

3.6.4 Comparison of Pressure Laws on Networks for One-Velocity Model

In this section, we compare the influence of the choice of pressure law $p \in \{p_I, p_V, p_M, p_G, p_F\}$, collected in Sect. 3.3, in the one-velocity model (3.1) on a network referred to as *GasLib40-3 network*, see Fig. 3.10. We measure the deviations between solutions to the stationary one-velocity model (3.1) with the GERG-08 pressure law and solutions to the same model, but with other pressure laws $p \in \{p_I, p_V, p_M, p_F\}$.

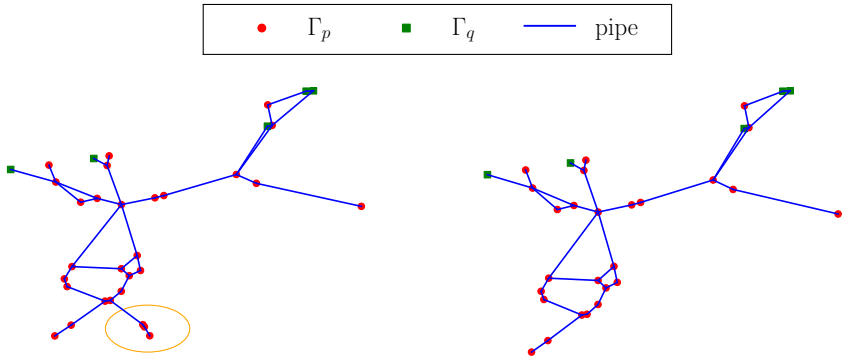
Modified Network On complex networks such as the GasLib40 network, see [26], approximating solutions to the various mixture models is challenging. One reason is that it is not obvious how to choose admissible boundary (and coupling) conditions, for which a solution exits. Indeed, characterizing the set of admissible boundary conditions is a non-trivial task and only in the recent work [31] a sufficient condition on the boundary conditions was presented. For the full problem (3.1) well-posedness is even less clear, and in situations, where no solution exists, discrete schemes might very well fail.

Only for the simplified model (3.23), we succeeded to approximate a stationary solution by computing a long-time approximate solution of the instationary model. Indeed, we have observed many scenarios, in which after small changes of the problem parameters, e.g., adding the convective term, or changing the pressure law, the numerical method fails. This is likely due to the fact that the code as implemented cannot handle changes of flow direction.

In order to demonstrate our method on a reasonably large network, we thus slightly modify GasLib40. We remove the problematic pipe and the small component (with three pipes) from the remaining network. The resulting network has 37 vertices and is referred to as *GasLib40-3*, see Fig. 3.10 and [10]. As in Sect. 3.5.3 we use the solution to (3.45) generated by the GasLib40 optimization and restrict it to the remaining vertices and edges to obtain initial and boundary conditions, see Sect. 3.6.4 and [10]. As in Sect. 3.6.1, Γ_p and Γ_q are the disjoint sets of vertices, where a value of the pressure and of the mass flux is imposed, and their choice is described in Sect. 3.6.3.

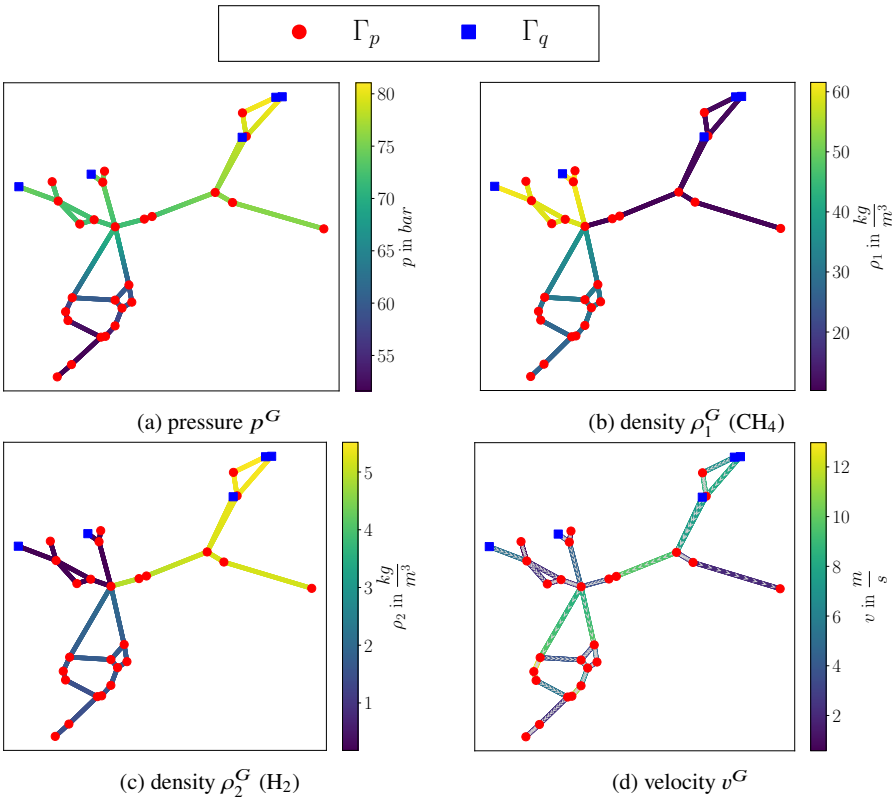
On this network, and for these initial and boundary conditions, for all pressure laws the discrete solutions to the instationary model (3.1) tend to a stationary solution, i.e., our method to compute them works. See Fig. 3.11 for the solutions for GERG-08.

Results Similarly as in Sect. 3.3.2, we use the GERG-08 pressure law as benchmark. We compare the deviations between stationary solutions $(\rho_1^G, \rho_2^G, v^G)$ as well as the associated pressure function p^G to (3.1) computed with pressure law p_G and solutions to the model with other pressure laws, denoted by superscript corresponding to the pressure laws, see Sect. 3.3. Recall that those are the ideal gas law (3.16), the virial expansion (3.18), the mixed virial expansion (3.19) and the least squares fit (3.22b) to GERG-08 with a mixed polynomial of total degree $k = 4$.



(a) GasLib-40 (b) GasLib40-3

Fig. 3.10: Graph of GasLib40 network (left) and modification GasLib40-3 (note that fur the purpose of better visualization the edges are not scaled correctly). The sets Γ_p and Γ_q denote the set of vertices, where a value of the pressure or the mass flux is imposed, respectively.



(a) pressure p^G

(b) density ρ_1^G (CH_4)

(c) density ρ_2^G (H_2)

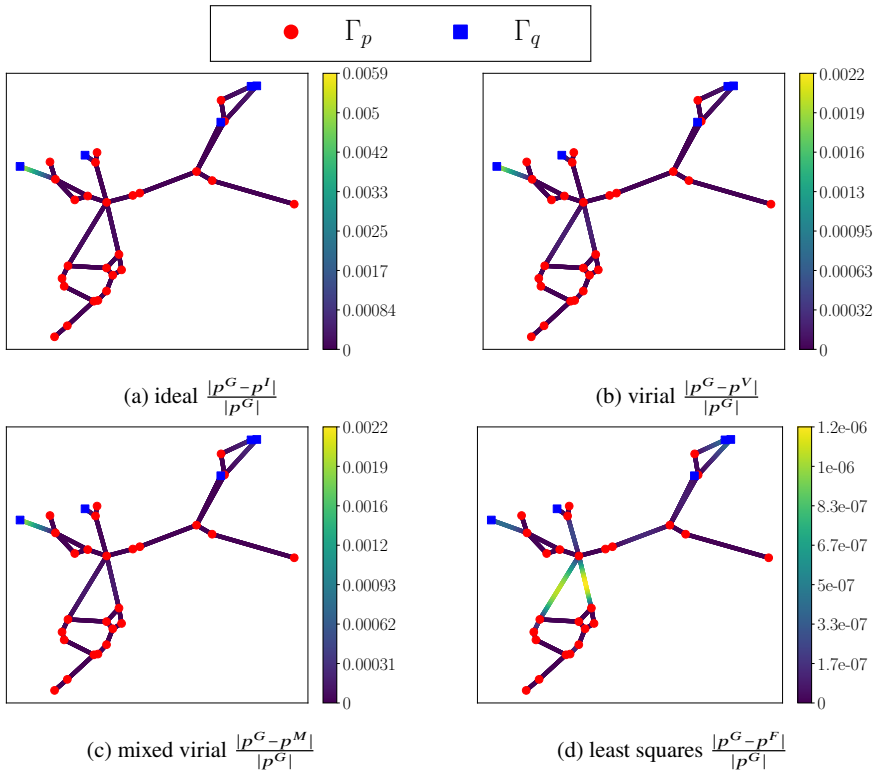
(d) velocity v^G

Fig. 3.11: Stationary solution to the one-velocity model (3.1) with pressure law GERG-08 on GasLib40-3 network, see Fig. 3.10.

Figure 3.12 shows the resulting relative pressure deviations and Fig. 3.13 shows the relative density deviations, both plotted over the network. We see that the pressure is rather robust to the choice of the pressure law, since the maximal deviation relative to GERG-08 is 0.6 % for the ideal gas law, 0.2 % for the virial expansions and mixed virial expansions and 0.0001 % for the least squares pressure law, see Fig. 3.12. However, in the relative density difference we see a maximal relative deviation up to 16 % for the ideal gas law, 8 % for the virial expansions and mixed virial expansions and 0.007 % for the least squares pressure law in Fig. 3.13.

3.6.5 Validation of the Optimization Results

For the optimization on stationary networks in Sect. 3.6.2 the simplified model (3.23) is used. However, (3.23) is an approximation of the stationary version of model (3.1). This raises the immediate question whether the solution obtained by the optimization



(a) ideal $\frac{|p^G - p^I|}{|p^G|}$ (b) virial $\frac{|p^G - p^V|}{|p^G|}$

(c) mixed virial $\frac{|p^G - p^M|}{|p^G|}$ (d) least squares $\frac{|p^G - p^F|}{|p^G|}$

Fig. 3.12: Relative *pressure* deviation between stationary solution to the one-velocity model (3.1) obtained with p_G in (3.21) and the corresponding stationary solutions obtained with p_I of (3.16), p_V of (3.18), p_M (3.19), respectively, on GasLib40-3, see Fig. 3.10.

is a solution to the stationary version of the full model (3.1). The goal of this section is to show that the difference between the solutions is negligible and thus validate the solution obtained by the optimization in Sect. 3.6.2.

Recall that the simplification leading to (3.23) arises by using the ideal gas law and by neglecting the convective term. This simplification has allowed us to derive an algebraic model. For the validation, we compare the respective solutions. We denote the solution to the stationary version of the full model (3.1) with ideal gas law for the pressure by superscript I, and the solution to the simplified model (3.23), i.e., (3.24) with superscript s.

The discrete solution to the simplified model (3.23) is obtained as described in Sect. 3.6.3. Specifically, we use the algebraic solution of the optimization problem in Sect. 3.6.2 to create an initial state for the auxiliary instationary model. The objective of the optimization problem is to maximize the network pressure. The boundary data for both problems is identical. Furthermore, the flow directions in the initial state of

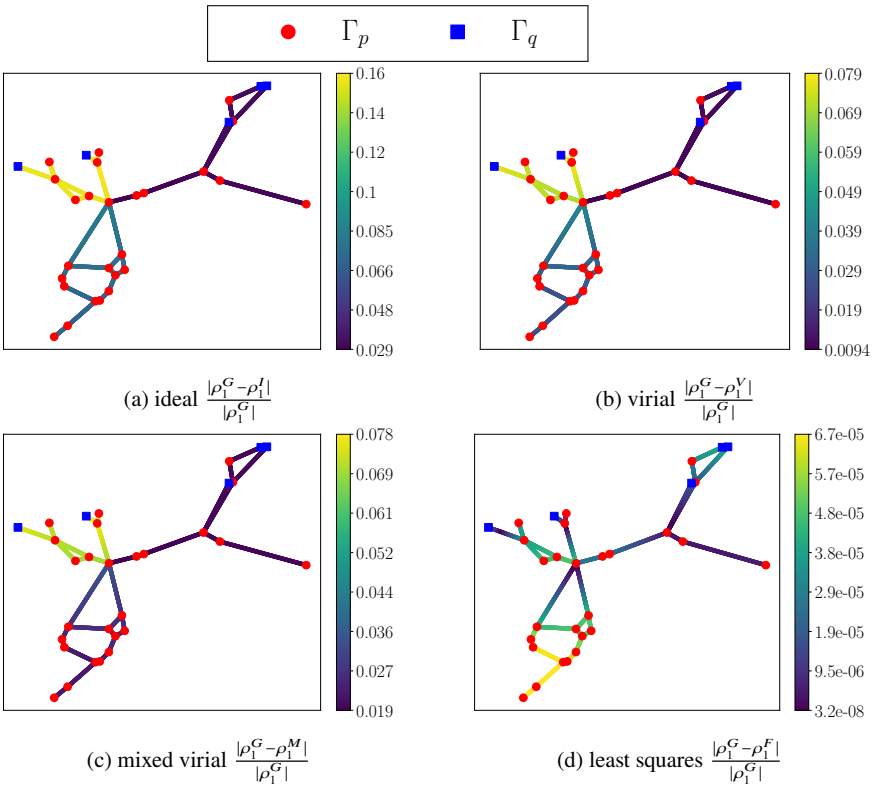


Fig. 3.13: Relative *density* deviation between stationary solution to the one-velocity model (3.1) obtained with p_G in (3.21) and the corresponding stationary solutions obtained with p_I of (3.16), p_V of (3.18), p_M (3.19), respectively, on a GasLib40-3, see Fig. 3.10.

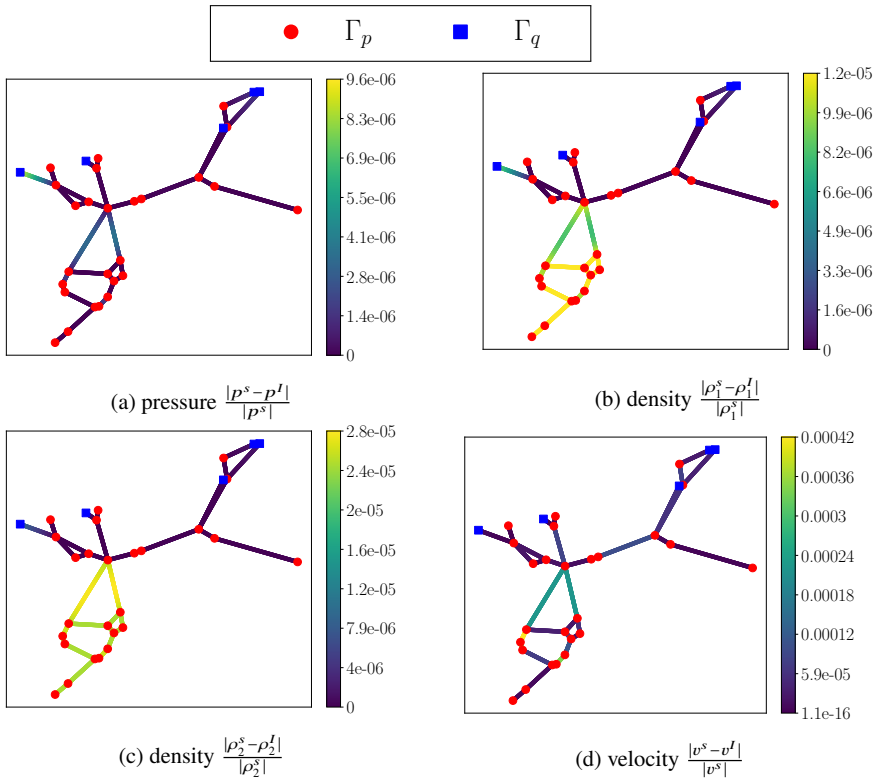
the auxiliary instationary model are set to the flow directions of the solution from the optimization problem.

The results are depicted in Fig. 3.14. They show that the relative deviation of the solutions to the different models in density as well as pressure and velocity are at most around 0.04 % on the whole network. This means that for the solution to the full model we can determine bounds on the pressure and on the flow on the whole network. Furthermore, it is straight-forward to check whether the solution to the full model also satisfies the feasibility constraints in (3.6.2).

This leads to the conclusion that—up to a small error—a solution to the optimization problem is a solution to the full model and vice versa.

Furthermore, we want to mention that choosing a different pressure law (Sect. 3.6.4) results in relative errors of up to 16 %, and thus the simplification of the model has a much smaller effect on the solutions than the choice of the pressure law. We conclude that if one is limited to the ideal gas law, one may use the algebraic model instead of the

stationary version of the full model (3.1) and hence work with explicit solutions instead of a numerical discretization.



(a) pressure $\frac{|p^s - p^I|}{|p^s|}$

(b) density $\frac{|\rho_1^s - \rho_1^I|}{|\rho_1^s|}$

(c) density $\frac{|\rho_2^s - \rho_2^I|}{|\rho_2^s|}$

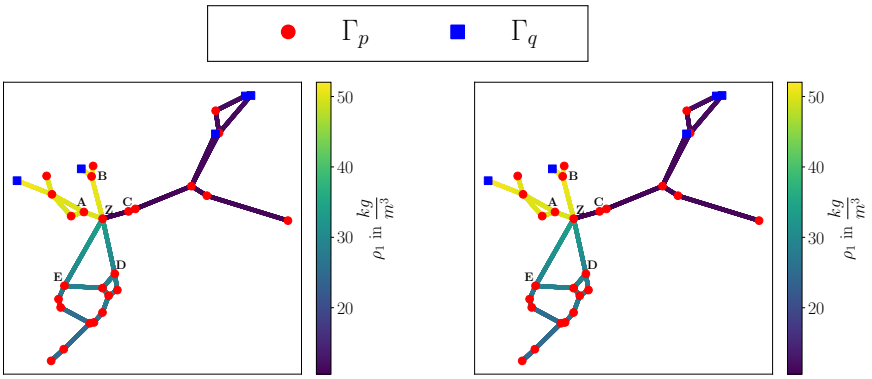
(d) velocity $\frac{|v^s - v^I|}{|v^s|}$

Fig. 3.14: Relative differences of stationary solutions to the simplified one-velocity model (3.23), i.e., (3.24) and the stationary version of one-velocity model (3.1) with the ideal gas law p^I (3.16) on GasLib40-3, see Fig. 3.10. Superscript I: Solution of the stationary version of model (3.1) with ideal gas law. Superscript s: Solution of the simplified model (3.23), i.e., (3.24).

3.6.6 Consistency of Coupling for One- and Two-Velocity Models

In this section, we experimentally investigate the compatibility of the coupling conditions of the one-velocity model and the two-velocity model, as introduced in Sect. 3.6.1 for the ideal pressure law.

Recall that on a single pipe in Sect. 3.5.3 and Sect. 3.5.4 we have seen that, for Option B of the boundary data, the solution to the two-velocity model (3.5) approaches



(a) One-velocity ρ_1^{1v} (b) Two-velocity ρ_1^{2v} with $f = 10$

Fig. 3.15: Density ρ_1 of one- and two-velocity solution with ideal gas law on Gaslib40-3 network

the one to the one-velocity model (3.1) as f increases. Here we shall see a similar behavior, even though some boundary layers may form due to the coupling conditions.

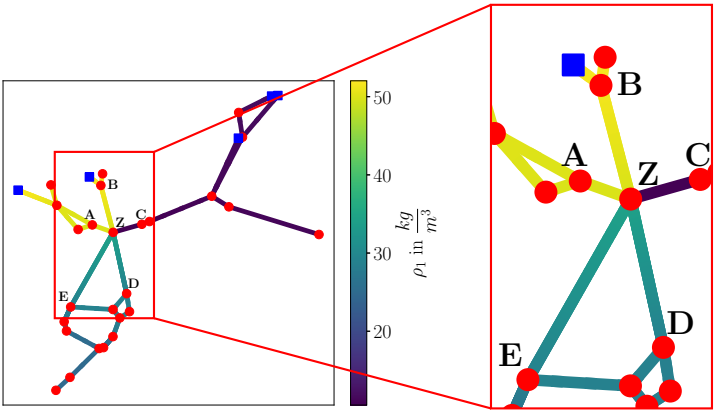
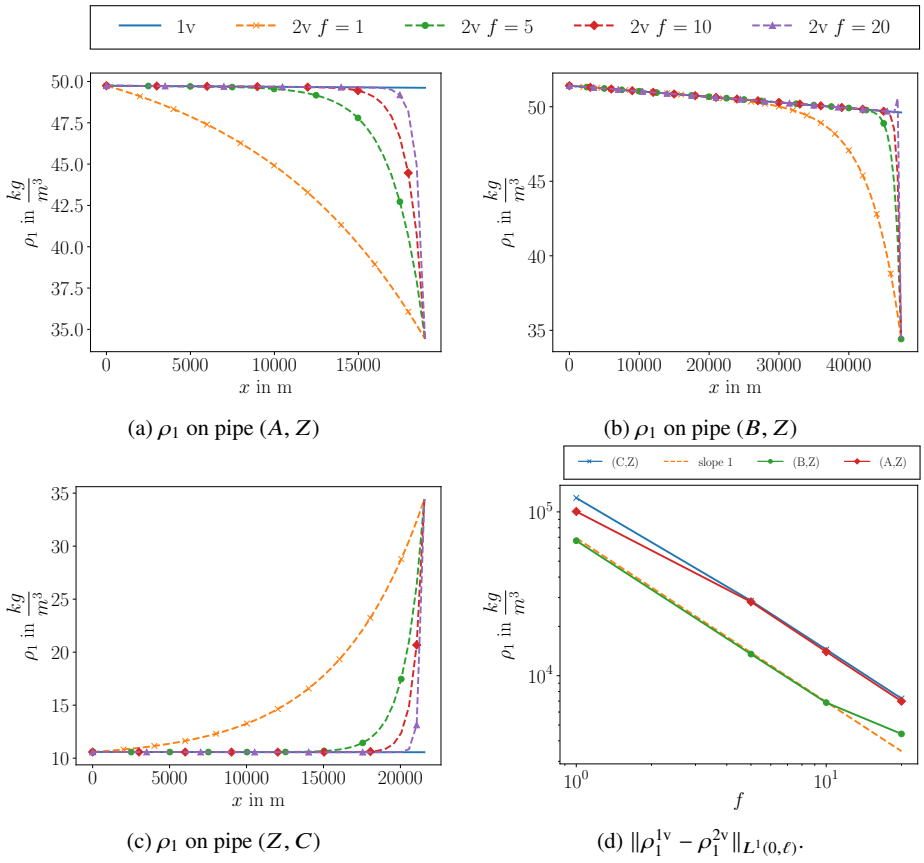


Fig. 3.16: Notation of vertices adjacent to junction in Gaslib40-3 network

Figure 3.15 shows the density ρ_1 for the one-velocity model, and the corresponding one for the two-velocity model for $f = 10$. At first glance no difference is visible. At the vertex labeled with Z mixing occurs, and we label the adjacent vertices with $A, \ldots, E$. To investigate the behavior at this vertex more in detail we plot the densities ρ_1 on the neighboring edges, see Fig. 3.17 and 3.18.

More specifically, we plot the density ρ_1 for the one-velocity model and the one for the two-velocity model for several values of f. While on all outflow edges the density functions agree well for all tested values of f, for the inflow edges some boundary layer



(a) ρ_1 on pipe (A, Z)

(b) ρ_1 on pipe (B, Z)

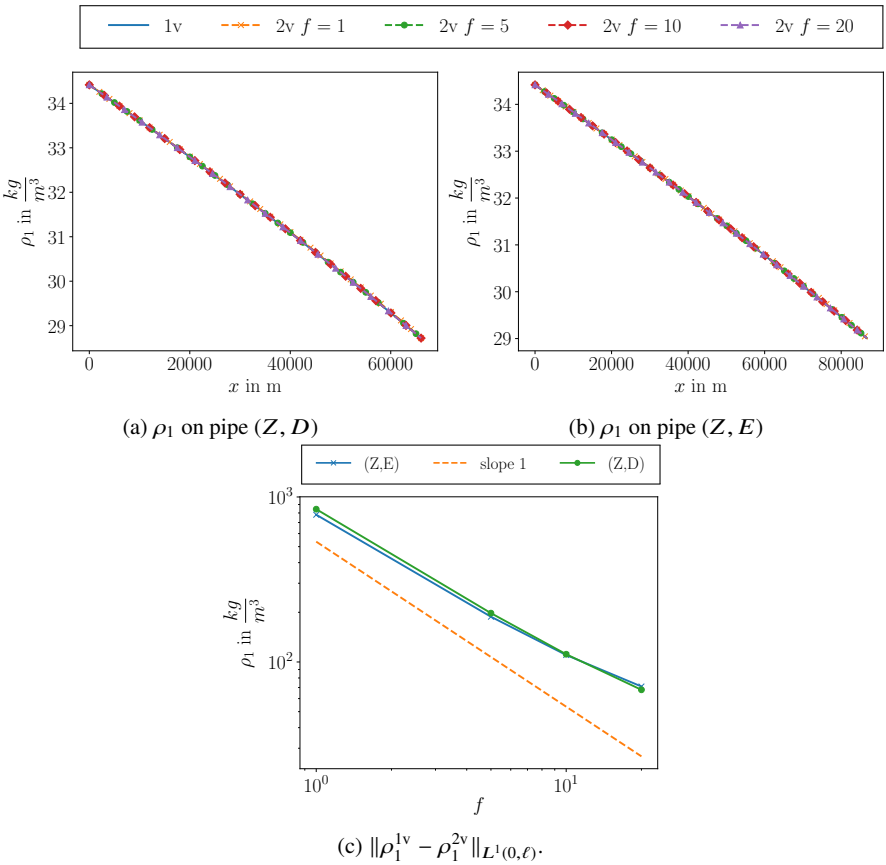
(c) ρ_1 on pipe (Z, C)

(d) $\|\rho_1^{1v} - \rho_1^{2v}\|_{L^1(0,\ell)}$.

Fig. 3.17: Density ρ_1 on the *inflow pipes* (A, Z), (B, Z), (C, Z) of vertex Z in the Gaslib40-3 network (see Fig. 3.16 for labels) for the one-velocity model and the two-velocity model for $f \in \{1, 5, 10, 20\}$ $m^3/(kg \times s)$, both with ideal gas law.

emerges as the parameter f increases. This shows that there is no convergence of the two-velocity solutions to the one-velocity solution in $L^\infty((0, \ell))$ as $f \to \infty$. However, as indicated by the convergence plots, the L^1-norms can be observed to converge nearly at first order in f^{-1}, as f increases. Note that due to the boundary layer formation, already for moderately large values of f we obtain oscillations in the solutions. To circumvent this, one would have to use a considerably finer mesh or even graded meshes for the space discretization.

Our observations indicate that even though the coupling conditions do not reduce to each other in the limit $f \to \infty$, they are consistent in a weaker sense.



(a) ρ_1 on pipe (Z, D)

(b) ρ_1 on pipe (Z, E)

(c) $\|\rho_1^{1v} - \rho_1^{2v}\|_{L^1(0,\ell)}$.

Fig. 3.18: Density ρ_1 on the *outflow pipes* $(Z, D), (Z, E)$ of vertex Z in the Gaslib40-3 network (see Fig. 3.16 for labels) for the one-velocity model and the two-velocity model for $f \in \{1, 5, 10, 20\}$ $\mathrm{m}^3/(\mathrm{kg} \times \mathrm{s})$, both with ideal gas law.

3.6.7 Instationary Flows on Networks

In this section we perform a computational study investigating the *numerical convergence* of the numerical scheme (3.30) described in Sect. 3.5.2 applied to the one- and two-velocity models (3.1) and (3.5) on the GasLib40-3 network, see Fig. 3.10. We compute instationary solutions on successively refined space-time grids, treating the solution computed on the finest available grid as a reference solution to compute a *rate of convergence* in the discretization parameters Δx and Δt. We find considerable variation in the convergence rate values which are mostly better than expected, indicating that we remain in a preasymptotic regime. We note that, due to the network structure and the consideration of instationary solutions, the experiments are computationally expensive; further refinements required to reach the asymptotic regime would be even more so.

Spatial and Temporal Discretization We wish to discretize the edges of the GasLib40-3 network, which vary in length, into quasi-uniform spatial meshes. We thus discretize each edge into a spatial mesh of fixed width, i.e., the mesh is given by an integer number of evenly-spaced grid points; the mesh widths are allowed to vary mildly for different edges. We similarly discretize the time interval into a temporal mesh of fixed time step size.

More precisely, for a given candidate space step Δx_{cand} and an edge e with length ℓ^e, we define $N^e := \operatorname{round}\left(\ell^e \cdot (\Delta x_{\mathrm{cand}})^{-1}\right)$ and $\Delta x^e := \ell^e \cdot (N^e)^{-1}$ for each $e \in \mathcal{E}$. Decomposing the edge e into N^e closed subintervals of size Δx^e, we define the *discretization* of the edge to be the set of intersection points between adjacent subintervals as well as the endpoints corresponding to $\{0, \ell^e\}$; taking the union over all edges in the network defines the set of spatial grid points Ω_Δ. Similarly, for a given candidate time step Δt_{cand} and time horizon T, we define N^t, Δt, and the set of temporal grid points $[0,T]_\Delta$.

For $\sigma \in \mathbb{N}_0 = \{0, 1, \dots\}$ we set

$$\Delta x^{(\sigma)}_{\mathrm{cand}} := 1.5^{-\sigma} \Delta x_{\mathrm{cand}}, \quad \text{and} \quad \Delta t^{(\sigma)}_{\mathrm{cand}} := 1.5^{-\sigma} \Delta t_{\mathrm{cand}} \tag{3.47}$$

corresponding to space and time grids $\Omega^{(\sigma)}_\Delta$ and $[0,T]^{(\sigma)}_\Delta$, respectively; we specify the values of Δx_{cand} and Δt_{cand} in our experiment below. We denote numerical solutions computed on the corresponding space-time grids by

$$\begin{aligned} &\rho_1^{(\sigma)}, \rho_2^{(\sigma)}, v^{(\sigma)} && \text{in the one-velocity case, and} \\ &\rho_1^{(\sigma)}, \rho_2^{(\sigma)}, v_1^{(\sigma)}, v_2^{(\sigma)} && \text{in the two-velocity case.} \end{aligned}$$

We perform numerical experiments using the ideal gas law (3.16).

Computational Setup

Initial and Boundary Data: One-Velocity Model As initial data for the one-velocity model we use stationary solutions computed as long time limits to the auxiliary instationary problem; for details, see Sect. 3.6.3. Note that at any vertex v we can evaluate the stationary solution to obtain the values p^v_{stat} kg/(m s^2), q^v_{stat} kg/s, and $\tilde{\mu}^v_{\mathrm{stat}}$ (dimensionless).

For $i \in \{1, 2\}$ and some fixed T', let

$$b_i(T'; t) := 1 + i \left(0.02 - 0.08 \frac{|t - T'|}{T}\right), \quad t \geq 0.$$

Then for the boundary data at $v \in \Gamma_p$, we prescribe

$$p^v(t) := \begin{cases} b_1(\frac{T}{4}; t) p^v_{\mathrm{stat}}, & 0 \leq t < \frac{T}{2}, \\ p^v_{\mathrm{stat}}, & \text{otherwise.} \end{cases}$$

and for $v \in \Gamma_q$ we prescribe

$$q^\nu(t) := \begin{cases} b_1(\frac{T}{4};t)q^\nu_{\text{stat}}, & 0 \le t < \frac{T}{4}, \\ 1.02q^\nu_{\text{stat}}, & \frac{T}{4} \le t < \frac{T}{2}, \\ b_1(\frac{T}{2};t)q^\nu_{\text{stat}}, & \frac{T}{2} \le t < 3\frac{T}{4}, \\ q^\nu_{\text{stat}}, & \text{otherwise}, \end{cases} \qquad \tilde{\mu}^\nu(t) := \begin{cases} b_1(\frac{T}{2};t)\tilde{\mu}^\nu_{\text{stat}}, & \frac{T}{4} \le t < 3\frac{T}{4}, \\ \tilde{\mu}^\nu_{\text{stat}}, & \text{otherwise}. \end{cases}$$

Initial and Boundary Data: Two-Velocity Model For the initial data we set $\rho_1^0(x) := 10\,\text{kg/m}^3$, $\rho_2^0(x) := 5\,\text{kg/m}^3$, and $v_1^0(x) = v_2^0(x) = 0\,\text{m/s}$. For the boundary data at $\nu \in \Gamma_p$ we define $p_i^{\text{stat}} := p_i(\rho_i^0)\,\text{kg/(m s}^2)$ for $i \in \{1,2\}$ and prescribe

$$p_i^\nu(t) := \begin{cases} b_i(\frac{T}{4};t)p_i^{\text{stat}}, & 0 \le t < \frac{T}{2}, \\ p_i^{\text{stat}} & \text{otherwise}. \end{cases}$$

For $\nu \in \Gamma_q$, we prescribe mass flux in units of kg/s as

$$q_1^\nu(t) := \begin{cases} 10\left(\frac{4t}{T}\right), & 0 \le t < \frac{T}{4}, \\ 10, & \frac{T}{4} \le t < \frac{T}{2}, \\ 10\left(\frac{-4t}{T}+3\right), & \frac{T}{2} \le t < 3\frac{T}{4}, \\ 0 & \text{otherwise}, \end{cases} \qquad q_2^\nu(t) := \begin{cases} 0, & 0 \le t < \frac{T}{4}, \\ 5\left(\frac{4t}{T}-1\right), & \frac{T}{4} \le t < \frac{T}{2}, \\ 5\left(\frac{-4t}{T}+3\right), & \frac{T}{2} \le t < 3\frac{T}{4}, \\ 0, & \text{otherwise}. \end{cases}$$

Computational Parameters In the GasLib40-3 network, the shortest pipe length is approximately 3000 m while the longest is approximately 70 000 m; we have chosen to fix $\Delta x_{\text{cand}} := 1500\,\text{m}$. We consider a time horizon of $T = 4\,\text{h}$ and take $\Delta t_{\text{cand}} := 720\,\text{s}$. Note that, since our scheme (3.30) is implicit in time, we are able to use larger time steps than would be required with an explicit scheme, which must maintain the CFL condition (see, e.g., [23, Sec. 4.4]), i.e.,

$$\frac{\Delta x_{\text{cand}}}{\Delta t_{\text{cand}}} \ge \text{wave speed} \approx 500\,\text{m s}^{-1} \text{ for } \tilde{\mu} = 0.85.$$

In our case for $\Delta x_{\text{cand}} = 1500\,\text{m}$ we would need to consider $\Delta t_{\text{cand}} \approx 3\,\text{s}$. For the refinements, we consider $\Delta x_{\text{cand}}^{(\sigma)}$ and $\Delta t_{\text{cand}}^{(\sigma)}$ as defined in (3.47) for $\sigma \in \{2,3,4,5,6,7\}$.

We fix a Newton tolerance `tol` $= 10^{-7}$, using the same stopping criterion as in Sect. 3.5.3. For the two-velocity model, we fix an inner friction of $f = 1\ \text{m}^3/(\text{kg} \times \text{s})$.

Results

One-velocity model We compute numerical solutions $\{\rho_1^{(\sigma)}, \rho_2^{(\sigma)}, v^{(\sigma)}\}$ for σ as above, taking the solutions for $\sigma = 7$ as the reference solutions. We extend these via *linear interpolation* to functions in $C([0,T] \times \Omega; \mathbb{R})$. For the linear interpolants, we use the same notation as for the corresponding numerical solution.

For $g \in C([0,T] \times \Omega; \mathbb{R})$, we may consider its restriction to the space-time grid $[0,T]_\Delta^{(7)} \times \Omega_\Delta^{(7)}$, also denoted by g; for functions on this grid we set:

$$\|g\|_\Delta := \|g\|_{\ell^1\left([0,T]_\Delta^{(7)};\ell^1\left(\Omega_\Delta^{(7)};\mathbb{R}\right)\right)}. \tag{3.48}$$

Table 3.6: Norms and log-ratios for the box scheme (3.30) applied to the one-velocity model (3.1) (3 sig. digits)

σ	2	3	4	5	6
$N(\sigma, \rho_1)$	1.92e-03	1.20e-03	6.82e-04	3.24e-04	1.78e-04
$R(\sigma, \rho_1)$	1.16	1.40	1.83	1.48	–
$N(\sigma, \rho_2)$	2.16e-03	1.35e-03	7.67e-04	3.65e-04	2.01e-04
$R(\sigma, \rho_2)$	1.16	1.39	1.83	1.47	–
$N(\sigma, v)$	1.53e-03	9.16e-04	5.07e-04	2.46e-04	1.25e-04
$R(\sigma, v)$	1.26	1.46	1.78	1.67	–

Then, for $\alpha \in \{\rho_1, \rho_2, v\}$ and $\sigma \leq 6$, we may define the *relative error*

$$N(\sigma, \alpha) := \frac{\|\alpha^{(\sigma)} - \alpha^{(7)}\|_\Delta}{\|\alpha^{(7)}\|_\Delta} \tag{3.49}$$

and for $\sigma \leq 5$ the *rate of change*

$$R(\sigma, \alpha) := \log_{1.5}\left(\frac{N(\sigma, \alpha)}{N(\sigma + 1, \alpha)}\right). \tag{3.50}$$

We record our results in Table 3.6.

Interpreting the numerical scheme (3.30) as a finite difference scheme, we may determine via Taylor expansions that the scheme is second-order consistent in space and first-order consistent in time. Since linear interpolants are second-order consistent, this should not impact the observed convergence of the scheme in our case. Fixing the ratio $\Delta t^{(\sigma)}_{\text{cand}}/\Delta x^{(\sigma)}_{\text{cand}}$ and sending $\Delta t^{(\sigma)}_{\text{cand}} \to 0$, we therefore expect that the error should decay as $O(\Delta t^{(\sigma)}_{\text{cand}})$ asymptotically for small $\Delta t^{(\sigma)}_{\text{cand}}$, i.e., that $R(\sigma, \alpha) \to 1$ for $\alpha \in \{\rho_1, \rho_2, v\}$ as σ increases.

While we see some variation in $R(\sigma, \alpha)$, we note primarily that all values are > 1, and most are close to or greater than 1.5. This indicates that we are still in a preasymptotic regime where the spatial refinement contributes to better-than-expected numerical convergence rates.

Two-Velocity Model For the two-velocity model (3.5), we proceed similarly to the one-velocity case, computing numerical solutions $\{\alpha^{(\sigma)}\}$ for $\alpha \in \{\rho_1, \rho_2, v_1, v_2\}$ and $\sigma \in \{2, 3, 4, 5, 6, 7\}$, and we construct linear interpolants which we restrict to the grid $[0, T]^{(7)}_\Delta \times \Omega^{(7)}_\Delta$. The definitions of $\|g\|_\Delta$, $N(\sigma, \alpha)$ and $R(\sigma, \alpha)$ carry over unchanged. We present the results in Table 3.7.

Following the above argument presented for the one-velocity model, we expect the error to decay as $O(\Delta t^{(\sigma)}_{\text{cand}})$ asymptotically for small $\Delta t^{(\sigma)}_{\text{cand}}$.

As in the one-velocity experiment, we observe that the majority of $R(\sigma, \alpha)$ values are greater than 1, and most of these are approximately 1.5, which again indicates that the spatial refinement plays a role in this regime. However, we also note far more variation in the trends between $R(\sigma, \alpha)$ values for α as σ increases. In particular, we note that

Table 3.7: Norms and log-ratios for the box scheme (3.30) applied to the two-velocity model (3.5) (3 sig. digits)

σ	2	3	4	5	6
$N(\sigma, \rho_1)$	7.69e-04	4.15e-04	2.12e-04	1.15e-04	6.90e-05
$R(\sigma, \rho_1)$	1.52	1.66	1.50	1.27	–
$N(\sigma, \rho_2)$	2.37e-04	1.3e-04	6.71e-05	3.52e-05	2.11e-05
$R(\sigma, \rho_2)$	1.48	1.64	1.59	1.26	–
$N(\sigma, v_1)$	1.11e-01	6.58e-02	3.66e-02	1.74e-02	1.28e-02
$R(\sigma, v_1)$	1.29	1.45	1.83	0.766	–
$N(\sigma, v_2)$	1.35e-01	8.01e-02	4.52e-02	2.18e-02	1.64e-02
$R(\sigma, v_2)$	1.29	1.41	1.79	0.701	–

for $\alpha \in \{v_1, v_2\}$, $R(4, \alpha) \approx 1.8$ while $R(5, \alpha) \approx 0.7$. This also indicates that we are in the preasymptotic regime.

3.7 Open Questions

As this chapter demonstrates, a lot is known and can be done concerning modeling, simulation and optimization of flows of gas mixtures on networks. Nevertheless, several important questions remain open:

- For our choice of boundary and coupling conditions for mixtures on networks we have observed consistency between the one- and the two-velocity model in the sense that the solutions converge in a sufficiently weak norm, as $f \to \infty$, see Sections 3.6.6. Can this be proved rigorously?
- Can other thermodynamically consistent coupling conditions be modeled by taking the 3D behavior of the flow at junctions into account?
- How can data for the coupling conditions in the two-velocity model be chosen if no solution to the one-velocity model is available?
- Can the optimization framework in Sect. 3.6.2 be extended from one-velocity to two-velocity models? Can this be used to generate compatible initial data for the simulation of the two-velocity model?
- Can local NLP-methods be used to obtain better solutions for the stationary optimization problem? See, e.g., [15] for an application of NLP methods to a reformulation of the mixing equation.
- Is the GERG-08 model introduced in Sect. 3.3 thermodynamically consistent and is the corresponding energy convex in the relevant regime?
- How can the numerical schemes for the one-velocity model be adapted to account for changing flow directions in an efficient manner?
- In the two-velocity model, what is the relationship between the inner friction parameter f and rate with which the velocities of the two constituents approach each other?

Acknowledgements We owe thanks to Prof. K. Deiters for helpful discussions. We also thank U. Gotzes and K. Spreckelsen for valuable discussions.

This work was supported by the German Research Foundation (DFG) within Subprojects A01, C05, and C09 in the Sonderforschungsbereich/Transregio 154 "Mathematical Modelling, Simulation and Optimization using the Example of Gas Networks" (Project ID 239904186).

References

1. K. Bestuzheva, M. Besançon, W.-K. Chen, A. Chmiela, T. Donkiewicz, J. van Doornmalen, L. Eifler, O. Gaul, G. Gamrath, A. Gleixner, L. Gottwald, C. Graczyk, K. Halbig, A. Hoen, C. Hojny, R. van der Hulst, T. Koch, M. Lübbecke, S. J. Maher, F. Matter, E. Mühmer, B. Müller, M. E. Pfetsch, D. Rehfeldt, S. Schlein, F. Schlösser, F. Serrano, Y. Shinano, B. Sofranac, M. Turner, S. Vigerske, F. Wegscheider, P. Wellner, D. Weninger, and J. Witzig. Enabling research through the SCIP Optimization Suite 8.0. *ACM Transactions on Mathematical Software*, 49(2), 2023. doi:10.1145/3585516.
2. P. Börner, M. E. Pfetsch, and S. Ulbrich. Mixing of gases in stationary networks: Properties and optimization, 2026. URL: https://opus4.kobv.de/opus4-trr154/629.
3. D. Bothe and W. Dreyer. Continuum thermodynamics of chemically reacting fluid mixtures. *Acta Mech.*, 226(6):1757–1805, 2015. doi:10.1007/s00707-014-1275-1.
4. J. Bradbury, R. Frostig, P. Hawkins, M. J. Johnson, C. Leary, D. Maclaurin, G. Necula, A. Paszke, J. VanderPlas, S. Wanderman-Milne, and Q. Zhang. JAX: composable transformations of Python+NumPy programs, 2018. http://github.com/jax-ml/jax (Version 0.3.13).
5. Y. Brodskyi, V. Gyrya, and A. Zlotnik. Simulation of gas mixture dynamics in a pipeline network using explicit staggered-grid discretization. *Applied Mathematical Modelling*, 137:115717, 2025. doi:10.1016/j.apm.2024.115717.
6. U. K. Deiters. ThermoC. https://thermoc.uni-koeln.de/thermoc/index.html (accessed 20/08/2025; 20:52).
7. U. K. Deiters and T. Kraska. *High-Pressure Fluid Phase Equilibria*. Elsevier, 2024. doi:10.1016/C2022-0-01727-X.
8. J. H. Dymond, K. N. Marsh, R. C. Wilhoit, and K. C. Wong. Virial coefficients of pure gases. In M. Frenkel and K. N. Marsh, ed., *Virial Coefficients of Pure Gases and Mixtures*. Springer-Verlag, Berlin Heidelberg, 2002. doi:10.1007/10693952_2.
9. M. Frenkel and K. N. Marsh. *Virial Coefficients of Pure Gases and Mixtures*. Springer-Verlag, Berlin Heidelberg, 2003. doi:10.1007/b71692.
10. J. Giesselmann, V. M. Kumar, M. Thiele, and T. Tscherpel. URL: https://github.com/TRR154/BookChapterGasMixturesOnNetworks.git.
11. U. Gotzes and K. Spreckelsen. Personal communication, 2025.
12. M. Gugat. Synchronization of velocities in pipeline flow of blended gas. *Journal of Mathematical Analysis and Applications*, 556(1, Part 1):130078, 2026. doi:10.1016/j.jmaa.2025.130078.
13. O. Habeck. *Mixed-Integer Optimization with Ordinary Differential Equations for Gas Networks*. Dissertation, TU Darmstadt, 2020. URL: https://www.dr.hut-verlag.de/9783843946537.html.
14. O. Habeck and M. E. Pfetsch. Combinatorial acyclicity models for potential-based flows. *Networks*, 79(1):83–104, 2022. doi:10.1002/net.22038.
15. F. Hante and M. Schmidt. Complementarity-based nonlinear programming techniques for optimal mixing in gas networks. *EURO Journal on Computational Optimization*, 7:299–323, 2019. doi:10.1007/s13675-019-00112-w.
16. C. R. Harris, K. J. Millman, S. J. van der Walt, R. Gommers, P. Virtanen, D. Cournapeau, E. Wieser, J. Taylor, S. Berg, N. J. Smith, R. Kern, M. Picus, S. Hoyer, M. H. van Kerkwijk, M. Brett, A. Haldane, J. F. del Río, M. Wiebe, P. Peterson, P. Gérard-Marchant, K. Sheppard, T. Reddy, W. Weckesser, H. Abbasi, C. Gohlke, and T. E. Oliphant. Array programming with NumPy. *Nature*, 585(7825):357–362, Sept. 2020. doi:10.1038/s41586-020-2649-2.

17. J. D. Hunter. Matplotlib: A 2D graphics environment. *Computing in Science & Engineering*, 9(3):90–95, 2007. doi:10.1109/MCSE.2007.55.
18. K. Hutter and K. Jöhnk. *Continuum Methods of Physical Modeling*. Springer-Verlag, Berlin, 2004. doi:10.1007/978-3-662-06402-3.
19. T. Koch, B. Hiller, M. E. Pfetsch, and L. Schewe. *Evaluating Gas Network Capacities*. SIAM, 2015. doi:10.1137/1.9781611973693.
20. O. Kolb, J. Lang, and P. Bales. An implicit box scheme for subsonic compressible flow with dissipative source term. *Numerical Algorithms*, 53(2):293–307, 2010. doi:10.1007/s11075-009-9287-y.
21. O. Kunz and W. Wagner. The GERG-2008 wide-range equation of state for natural gases and other mixtures: An expansion of GERG-2004. *Journal of Chemical & Engineering Data*, 57(11):3032–3091, 2012. doi:10.1021/je300655b.
22. J. Lang and P. Mindt. Entropy-preserving coupling conditions for one-dimensional Euler systems at junctions. *Netw. Heterog. Media*, 13(1):177–190, 2018. doi:10.3934/nhm.2018008.
23. R. J. LeVeque. *Finite volume methods for hyperbolic problems*. Cambridge Texts in Applied Mathematics. Cambridge University Press, Cambridge, 2002. doi:10.1017/CBO9780511791253.
24. D. Mahajan, K. Tan, T. Venkatesh, P. Kileti, and C. R. Clayton. Hydrogen blending in gas pipeline networks – a review. *Energies*, 15(10), 2022. doi:10.3390/en15103582.
25. N. M. Philippi. *Asymptotic analysis and numerical approximation of some partial differential equations on networks*. Dissertation, TU Darmstadt, 2023. doi:10.26083/tuprints-00024732.
26. M. Schmidt, D. Aßmann, R. Burlacu, J. Humpola, I. Joormann, N. Kanelakis, T. Koch, D. Oucherif, M. E. Pfetsch, L. Schewe, R. Schwarz, and M. Sirvent. GasLib – A Library of Gas Network Instances. *Data*, 2(4):article 40, 2017. available at gaslib.zib.de. doi:10.3390/data2040040.
27. C. Suchovsky, L. Ericksen, T. Williams, and D. Nikolic. Appliance and equipment performance with hydrogen-enriched natural gases. Technical report, Canadian Standards Association, Toronto, ON, 2021. URL: https://www.csagroup.org/article/research/appliance-and-equipment-performance-with-hydrogen-enriched-natural-gases/.
28. M. Tawarmalani and N. V. Sahinidis. Global optimization of mixed-integer nonlinear programs: A theoretical and computational study. *Mathematical Programming*, 99:563–591, 2004. doi:10.1007/s10107-003-0467-6.
29. J. Thürauf, J. Grübel, and M. Schmidt. Adjustable robust nonlinear network design without controllable elements under load scenario uncertainties. *Mathematical Programming*, 2025. doi:10.1007/s10107-025-02207-2.
30. K. Topolski, E. P. Reznicek, B. C. Erdener, C. W. S. Marchi, J. A. Ronevich, L. Fring, K. Simmons, O. J. G. Fernandez, B.-M. Hodge, and M. Chung. Hydrogen blending into natural gaspipeline infrastructure: Review of the state of technology, 2022. doi:10.2172/1893355.
31. A. Ulke, M. Schuster, and S. Göttlich. Steady state blended gas flow on networks: Existence and uniqueness of solutions. *Networks and Heterogeneous Media*, 20(3):903–937, 2025. doi:10.3934/nhm.2025039.
32. M. E. Wieser. Atomic weights of the elements 2005 (IUPAC technical report). *Pure and Applied Chemistry*, 78(11):2051–2066, 2006. doi:10.1351/pac200678112051.

Open Access This chapter is licensed under the terms of the Creative Commons Attribution-NonCommercial-NoDerivatives 4.0 International License (http://creativecommons.org/licenses/by-nc-nd/4.0/), which permits any noncommercial use, sharing, distribution and reproduction in any medium or format, as long as you give appropriate credit to the original author(s) and the source, provide a link to the Creative Commons license and indicate if you modified the licensed material. You do not have permission under this license to share adapted material derived from this chapter or parts of it.

The images or other third party material in this chapter are included in the chapter's Creative Commons license, unless indicated otherwise in a credit line to the material. If material is not included in the chapter's Creative Commons license and your intended use is not permitted by statutory regulation or exceeds the permitted use, you will need to obtain permission directly from the copyright holder.



Chapter 4
Optimal Control Under Constrained Pressure Fluctuation

Martin Gugat[0000−0002−5281−110X],
Henning Sauter[0000−0003−4603−3943],
Michael Schuster[0000−0002−4689−3663], and
Caren Tischendorf[0000−0002−8421−7199]

Abstract This chapter presents a modeling and control framework for gas and hydrogen transport in pipeline networks with a particular focus on mitigating hydrogen embrittlement, based on differential–algebraic equation (DAE) formulations of the gas network model. Therefore constraints on the controls and, crucially, on their time derivatives are incorporated to reflect material limitations of existing infrastructure. The resulting DAE systems remain physically consistent, energy-aware, and compatible with hierarchical model reductions. Numerical examples illustrate how derivative-constrained control within a DAE setting enables safe and efficient hydrogen transport.

4.1 Introduction

The transition toward carbon-neutral energy systems places increasing emphasis on hydrogen as a large-scale energy carrier. While a dedicated hydrogen pipeline infrastructure remains a long-term objective, the near-term strategy of blending hydrogen into existing natural gas networks offers a reasonable path to integrate renewable energy sources into current transport systems. This development creates new operational challenges: the networks must be controlled safely and efficiently, and the associated mathematical models must remain both accurate and computationally tractable.

A central concern in hydrogen transport is hydrogen embrittlement, a degradation mechanism in steel pipelines whereby hydrogen diffuses into the material, leading to

Martin Gugat
Department of Mathematics, FAU Erlangen-Nürnberg, Germany, e-mail: martin.gugat@fau.de

Henning Sauter
Department of Mathematics, HU Berlin, Germany, e-mail: sauter@math.hu-berlin.de

Michael Schuster
Department of Data Science, FAU Erlangen-Nürnberg, Germany, e-mail: michi.schuster@fau.de

Caren Tischendorf
Department of Mathematics, HU Berlin, Germany, e-mail: caren.tischendorf@hu-berlin.de

© The Author(s) 2027

A. Martin et al. (eds.), *Mathematical Modelling, Simulation and Optimization using the Example of Gas Networks*, International Series of Numerical Mathematics 174,
https://doi.org/10.1007/978-3-032-34969-9_4

a reduction in ductility and fracture toughness, a process that is further accelerated by cyclic loading. Experimental and theoretical studies (e.g., [9, 15–17]) show that the fatigue crack growth rate increases with the amplitude of pressure fluctuations, making the limitation of such fluctuations as crucial as the regulation of the absolute pressure. Recent modeling efforts (see [2]) further highlight the need to incorporate embrittlement effects into system-level control and optimization strategies.

In gas networks, compressor stations serve as the primary actuators. To mitigate embrittlement risks, it is therefore natural to consider optimal control problems in which the compression ratios and their rates of change are subject to bounds, and the state variables (pressures and their temporal derivatives) must satisfy constraints reflecting material safety limits. Incorporating derivative constraints requires a solution framework that guarantees sufficient regularity. The results for semi-global classical solutions of hyperbolic balance laws on networks provide the necessary setting: they ensure the existence of continuously differentiable solutions, allowing pointwise constraints on pressure derivatives to be meaningfully imposed.

Building on this analytical foundation, we define an optimal control problem for gas transport on networks that includes control bounds, rate constraints, and state constraints involving the pressure and its fluctuation amplitude. We discuss existence results derived from direct methods under suitable regularity assumptions, and we develop necessary optimality conditions within a differential–algebraic (DAE) adjoint framework. Numerical examples illustrate how appropriately constrained compressor control can effectively reduce pressure fluctuations while satisfying operational and safety requirements.

This chapter thus provides a mathematically rigorous step toward the systematic control of gas networks under embrittlement-relevant constraints, combining physical insight, analysis of hyperbolic PDEs on networks, and optimal control with state and derivative constraints.

4.2 Mathematical Modelling

Consider a connected, directed graph $\mathcal{G} = (\mathcal{V}, \mathcal{E})$, where the set of vertices $\mathcal{V}$ represents network junctions and the set of edges $\mathcal{E} \subseteq \mathcal{V} \times \mathcal{V}$ represents network pipelines and compressor stations. Every edge can either be a flow edge or a compressor edge. The set of flow edges given by $\mathcal{E}_F$ and the set of compressor edges given by $\mathcal{E}_C$ are disjoint and we have $\mathcal{E} = \mathcal{E}_F \cup \mathcal{E}_C$. For each pipeline $e \in \mathcal{E}_F$, the gas dynamics are described by the semilinear isothermal Euler equations (introduced in Sect. 2.3)

$$\begin{aligned} &\frac{\partial}{\partial t}\rho^e(t,x) + \frac{\partial}{\partial x}q^e(t,x) = 0, \\ &\frac{\partial}{\partial t}q^e(t,x) + \frac{\partial}{\partial x}p^e(t,x) = -\frac{\lambda^e}{2D^e}\frac{q^e(t,x)|q^e(t,x)|}{\rho^e(t,x)}. \end{aligned} \tag{4.1}$$

Here, ρ^e, q^e and p^e denote density, mass flux and pressure of the gas along the edge $e \in \mathcal{E}$, while λ^e and D^e denote the pipe friction coefficient and pipe diameter,

respectively. At each network junction $v \in \mathcal{V}$, as coupling conditions, we consider the conservation of mass and the continuity in pressure (see Sect. 2.5.2). The boundary data is given by prescribed gas outflow $b^v(t)$ at exit nodes (where gas leaves the network) and inlet pressures $p_0^v(t)$ at entry nodes (where gas enters the network).

Each compressor station is represented by a compressor edge $e \in \mathcal{E}_C$. While the pressure and thus also the density are increased by gas compression, mass conservation requires the flow to be constant along the compressor edges for every $t \in [0, T]$. The effect of the compressor is represented by the reachable pressure ratio. The required time-dependent compressor power $P^e(t)$ is modeled as

$$P^e(t) = A^e \, q^e(t) \left(\left(\frac{p_{\text{out}}(t)}{p_{\text{in}}(t)} \right)^{\kappa} - 1 \right), \tag{4.2}$$

where p_{in} and p_{out} denote the ingoing and outgoing pressure, A^e is the cross section, q^e denotes the flow through the compressor, and κ is the isentropic exponent. In the optimal control framework of this chapter, the pressure ratio serves as control variable, while the compressor power is to be minimized.

The existence theory for gas flow on networks with controls of bounded total variation, originating from [5], ensures L^1-regularity of optimal controls for hyperbolic balance laws. However, the pressure fluctuation constraints considered here require that control and state variables possess higher regularity, since pointwise bounds on time derivatives of pressures are imposed. To this end, we rely on the theory of semi-global classical solutions for quasilinear hyperbolic systems. The foundational work of Li Tatsien and collaborators (e.g., [10]) establishes exact boundary controllability results based on classical solutions. A comprehensive summary tailored to gas networks is provided in [4]. This theory guarantees that, on a finite time horizon $[0, T]$, the networked system admits classical C^1-solutions under suitable smallness and compatibility assumptions on the initial and boundary data. Moreover, it provides an a priori bound for the C^1-norm of the state that is linear with respect to the C^1-norm of the initial and boundary data.

4.3 The Optimal Control Problem

In this section, we consider an optimal control problem of a similar type as in [6]. Let $\mathcal{E}_C$ denote the set of compressor edges in the network. For each edge $e \in \mathcal{E}_C$, the control variable is the pressure ratio, expressed as

$$\frac{p^e_{\text{out}}(t)}{p^e_{\text{in}}(t)} = u^e(t) + u^e_{\text{ref}},$$

where u^e_{ref} denotes a reference control compatible with a static reference state of the network. We impose the *control constraint*

$$1 \le \varepsilon^e_{\min} \le u^e(t) + u^e_{\text{ref}} \le \varepsilon^e_{\max}, \tag{4.3}$$

which restricts the feasible pressure ratios. A value of $u^e(t) + u^e_{\mathrm{ref}} = 1$ corresponds to the compressor being inactive, in which case the state is unaffected by that compressor.

In order to avoid fast pressure fluctuations, we impose bounds for the first and second time-derivatives of the control function

$$\begin{aligned} \left|\frac{d}{dt}u^e(t)\right| &\le u^e_{\max,\mathrm{der}} && t \in [0,\ T], \\ \left|\frac{d^2}{dt^2}u^e(t)\right| &\le u^e_{\max,\mathrm{secder}} && \text{a. e. on } (0,\ T). \end{aligned} \tag{4.4}$$

The objective functional is defined as

$$J_0(u) = \sum_{e\in\mathcal{E}_C} \int_0^T \frac{1}{\gamma}\, A^e\, q^e(t)\, \left[\left(u^e(t) + u^e_{\mathrm{ref}}\right)^\kappa - 1\right] + |u^e(t)|^2\ dt, \tag{4.5}$$

with a penalty parameter $\gamma > 0$. The first term of J_0 models the fuel consumption of the compressor (see, e.g., [11]), while the second term penalizes high pressure ratios to account for high operational costs.

In our control problem, in addition to the C^1-compatibility conditions, *state constraints* are also imposed on all edges $e \in \mathcal{E}$. We consider box constraints for the pressure

$$p^e_{\min} \le p^e(t,\cdot) \le p^e_{\max} \tag{4.6}$$

and for the temporal derivatives of the pressure

$$p^e_{\min,\mathrm{der}} \le \frac{\partial}{\partial t} p^e(t,\cdot) \le p^e_{\max,\mathrm{der}}. \tag{4.7}$$

To avoid further model complexity, we assume that the initial state coincides with the static reference state associated with u_{ref}, and that this reference state is feasible, i.e., it satisfies all state constraints.

The optimal control problem is therefore to find controls

$$u^e \in H^2(0,T), \qquad e \in \mathcal{E}_C,$$

that are C^1-compatible with the given initial state, satisfy the control constraint (4.3), (4.4), and generate a state that satisfies the state constraints (4.6) for the pressures and (4.7) for the pressure derivatives, such that the objective function J_0 defined in (4.5) is minimized. Here, $H^2(0,T)$ is the Sobolev space $W^{2,2}(0,T)$ (cf. [1]), which is in fact a Hilbert space.

As in [6], one can show the existence of an optimal control by the direct method of the calculus of variations, provided that $\gamma > 0$ is chosen sufficiently large. In [6] and [14], an explicit H^2-regularization term is included in the objective functional. In the present formulation, the control cost contains only the L^2-term, while regularity is enforced through the derivative constraints (4.4). A related problem for boundary control in flood management is treated in [3], where no H^2-regularization term is added. However, in that case the existence of an optimal control is not established.

4.4 Optimal Control with DAE Constraints

Discretizing (4.1) in space yields the optimal control problem

$$\inf_{x\in X,\, u\in U} \quad J(x,u) := g\Big(d(x(T))\Big) + \int_{t_0}^{T} h(x,u,t)\,\mathrm{d}t \tag{4.8a}$$

$$\text{s.t.} \quad A\frac{\mathrm{d}}{\mathrm{d}t}(d(x)) + b(x,u,t) = 0, \quad d(x(t_0)) = y_0 \tag{4.8b}$$

for a given initial value $y_0 \in \mathbb{R}^k$ with $A \in \mathbb{R}^{m\times k}$, $U := C([t_0,T],\mathbb{R}^n)$,

$$X := C_d^1([t_0,T],\mathbb{R}^m) := \left\{ x \in C([t_0,T],\mathbb{R}^m) \;\middle|\; d(x(\cdot)) \in C^1([t_0,T],\mathbb{R}^k) \right\},$$

and continuous functions

$$d : \mathbb{R}^m \to \mathbb{R}^k, \qquad b : \mathbb{R}^m \times \mathbb{R}^n \times [t_0,T] \to \mathbb{R}^m,$$
$$g : \mathbb{R}^k \to \mathbb{R}, \qquad h : \mathbb{R}^m \times \mathbb{R}^n \times [t_0,T] \to \mathbb{R}.$$

Note that X is not necessarily a linear space in case of a nonlinear function d but a natural subset of $C([t_0,T],\mathbb{R}^m)$ to which solutions of (4.8b) shall belong. In our numerical examples, A is given by a finite differences matrix for the space derivative.

The next theorem provides a necessary optimization criterion for the optimal control problem (4.8). It extends the first order condition from [8] to DAE control problems with a nonlinear function $d(x)$.

Theorem 4.1 (see Chap. 4 in [12]) *Let A have full column rank. Let the nonlinear functions b, d, g and h be sufficiently smooth such that the matrix*

$$M(x,u,t) := \begin{bmatrix} A & b_x(x,u,t) & b_u(x,u,t) \\ 0 & d_x(x) & 0 \end{bmatrix}$$

and the derivatives g_y, h_x and h_u exist. If $M(x,u,t)$ has full row rank for all $(x,u,t) \in \mathbb{R}^m \times \mathbb{R}^n \times [t_0,T]$, then each solution $(x_*,u_*) \in X \times U$ of the optimization problem (4.8) *with initial value $y_0 \in \mathbb{R}^k$ yields a solution $(x_*,u_*,\lambda_*) \in X \times U \times \Lambda$ of the optimality DAE*

$$A\frac{\mathrm{d}}{\mathrm{d}t}(d(x)) + b(x,u,t) = 0 \tag{4.9a}$$

$$-d_x(x)^\top \frac{\mathrm{d}}{\mathrm{d}t}(A^\top\lambda) + b_x(x,u,t)^\top\lambda = h_x(x,u,t)^\top \tag{4.9b}$$

$$b_u(x,u,t)^\top\lambda = h_u(x,u,t)^\top \tag{4.9c}$$

$$d(x(t_0)) = y_0 \tag{4.9d}$$

$$A^\top\lambda(T) = g_y\Big(d(x(T))\Big)^\top \tag{4.9e}$$

with $\Lambda := C^1_{A^\top}([t_0,T],\mathbb{R}^m) := \{\lambda \in C([t_0,T],\mathbb{R}^m) \mid A^\top\lambda \in C^1([t_0,T],\mathbb{R}^k)\}$.

4.5 Numerical Examples

In this section, two numerical examples based on gas transport in pipeline networks are presented, where the solution of the optimal control problem (4.8) exploits the optimality DAE (4.9). In the first example we consider a compressor edge connected to a pipeline and we explicitly formulate the optimality DAE (4.9), while in the second example, we consider the GasLib-11[1], a network instance that consists of 11 nodes with 3 inflows and 3 outflows, 8 flow edges and 2 compressor stations.

4.5.1 One Compressor Connected to One Pipe

Consider a pipeline that is connected to a compressor station as shown in Fig. 4.1. In this example, we provide an explicit formulation of the optimality DAE (4.9).

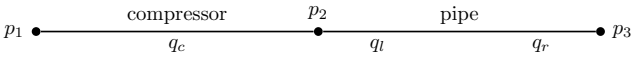


Fig. 4.1: Pressure and flow variables for a compressor coupled with one pipe

The DAE model equations of (4.8b) are given by

$$
\begin{aligned}
p_1 &= p_0 && \text{(fixed pressure at vertex 1)}\\
q_c - q_l &= 0 && \text{(flow balance at vertex 2)}\\
q_r &= b && \text{(flow balance at vertex 3)}\\
\frac{\mathrm{d}}{\mathrm{d}t}\varphi_\rho(p_3) + d_q(q_r - q_l) &= 0 && \text{(pipe mass balance)}\\
\frac{\mathrm{d}}{\mathrm{d}t}q_l + d_p(p_3 - p_2) + c_1\frac{q_l|q_l|}{\varphi_\rho(p_3)} + c_2\varphi_\rho(p_3) &= 0 && \text{(pipe momentum balance)}\\
\left(\frac{p_2}{p_1}\right)^\kappa - 1 &= u_c && \text{(compressor control)}\\
\max\{1, \frac{p_2}{p_1}\} - \frac{p_2}{p_1} &= 0 && \text{(compressor constraint)}
\end{aligned}
$$

with the parameters

$$
d_p = \frac{A}{L}, \quad d_q = \frac{c_\kappa}{L}, \quad c_1 = \frac{\lambda\, c_\kappa}{2d}, \quad c_2 = \frac{g}{c_\kappa}\sin(\alpha), \quad c_\kappa = \frac{R_s T}{A}, \quad \kappa = 0.4,
$$

and the density function

[1] Data can be found on https://gaslib.zib.de/.

Table 4.1: Network and gas parameters for the example with a pipe connected to a compressor [7]

Variable	Letter	Value	Unit
Final time	T	24	h
Pipe diameter	D	0.7	m
Pipe length	L	1	km
Pipe roughness	ε	$5 \cdot 10^{-5}$	m
Gravitational constant	g	9.8067	m/s^2
Universal gas constant	R	8.3145	J/(mol K)
Molar mass of the gas	M	0.0182	kg/mol
Gas temperature	T	283.2	K
Pseudocritical temperature	T_{crit}	202.72	K
Pseudocritical pressure	P_{crit}	46.6614	bar
Lower pressure bound	$p_{\min}$	40	bar

$$\varphi_\rho(p) = \frac{p}{z(p)} \quad \text{with real gas factor } z(p) = 1 + c_{\text{AGA}} p \quad \text{for } p \text{ in bar.}$$

The network and gas parameters are given in Table 4.1. The pipe friction coefficient is implicitly given by the pipe roughness

$$\lambda = \left(-2 \log_{10} \left(\frac{\varepsilon}{3.7065\, D} \right) \right)^{-2}. \tag{4.10}$$

The specific gas constant R_S is given by the quotient of universal gas constant R and molar mass M. The constant c_{AGA} in the compressibility factor $z(p)$ is given by

$$c_{\text{AGA}} = \left(0.257 - 0.533 \frac{T_{\text{crit}}}{T} \right) \frac{1}{p_{\text{crit}}}. \tag{4.11}$$

Note that this compressibility factor is also applied by the *American Gas Association* (see, e.g., [13]).

For the boundary data, we define the inlet pressure at the node v_1 by

$$p_0(t) = 40.1 \text{ bar},$$

and gas demand at node v_3 given by

$$b(t) = 140 - \frac{16}{\pi} \sin \left(\frac{\pi t}{12 \cdot 60 \cdot 60} \right) \frac{16}{\pi} \cos \left(\frac{\pi t}{8 \cdot 60 \cdot 60} \right) \frac{\text{kg}}{\text{s}}$$

The functions g and h in the objective function (4.8a) are chosen as $g(y) = 0$ and

$$h(x, u, t) = \omega_0 \left[q^c(t) \left(u_c^\kappa(t) - 1 \right) \right]^2 + \omega_1 \left(u_c^\kappa(t) - 1 \right)^2, \ \omega_0 = 10, \ \omega_1 = 0.01$$

where h is the weighted, regularized, squared compressor power (4.2). The DAE model equations of (4.8b) are completed by the pressure constraints

$$p_2 - \max\{p_2, p_{\min}\} = 0, \qquad \text{i.e. } p_2 \geq p_{\min},$$
$$p_3 - \max\{p_3, p_{\min}\} = 0, \qquad \text{i.e. } p_3 \geq p_{\min},$$

and the box constraints for the derivatives of the control

$$u_c' - \max\{u_c', u_{\min}'\} = 0, \qquad u_c'' - \max\{u_c'', u_{\min}''\} = 0,$$
$$u_c' - \min\{u_c', u_{\max}'\} = 0, \qquad u_c'' - \min\{u_c'', u_{\max}''\} = 0,$$

with $u_{\min}' = -1$, $u_{\max}' = 1$, $u_{\min}'' = -1$ and $u_{\max}'' = 1$ reflecting

$$u_{\min}' \leq u_c' \leq u_{\max}' \qquad \text{and} \qquad u_{\min}'' \leq u_c'' \leq u_{\max}''.$$

The problem was solved using *Python* and the results are shown in Fig. 4.2. The gas demand at node v_3 is represented by the green curve q_r. Since the inlet pressure at node v_1 is fixed at 40.1 bar, the shifted compression factor u_c increases as long as the demand increases. The factor is optimally chosen such that the lower pressure limit of 40 bar is always satisfied. Notice that the flow q_c equals the inflow q_l of the pipe and is, therefore, hidden behind the curve of q_l in Fig. 4.2.

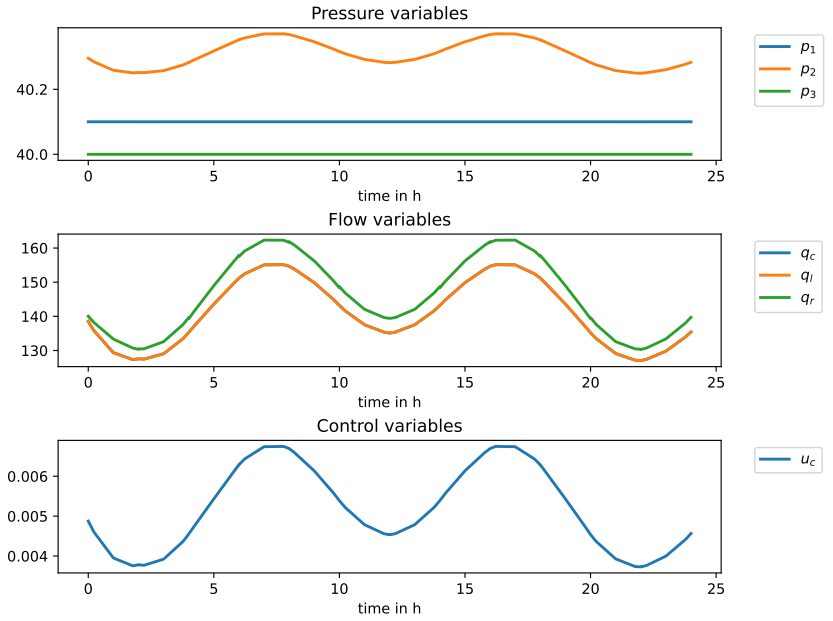


Fig. 4.2: Numerical solution with piecewise quadratic ansatz functions (with subinterval length of 1 hour) for a compressor coupled with one pipe (see Fig. 4.1) with the shifted compression factor $u_c = \frac{p_2}{p_1} - 1$ as control.

4.5.2 Gaslib-11

Consider the optimal control problem (4.8) on the gas network instance GasLib-11, which consists of 11 nodes (3 inflows, 5 inner nodes, 3 outflows), 8 edges and 2 compressor stations, as visualized in Fig. 4.3. This example demonstrates, that imposing bounds on the derivative of the control can lead to less pressure fluctuation.

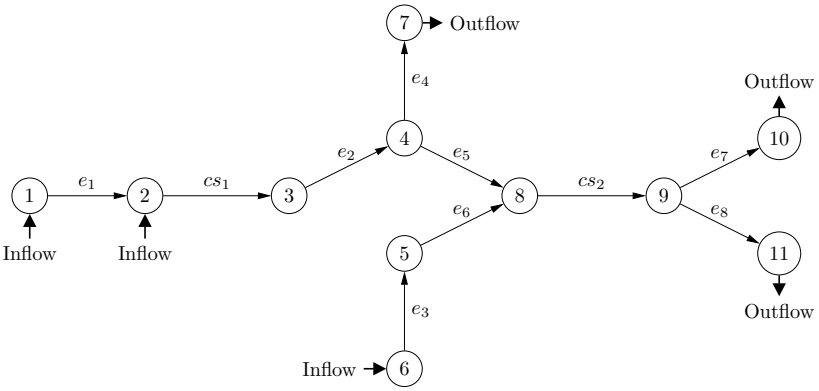


Fig. 4.3: A scheme of the GasLib-11 with closed valve

For each flow pipe $e \in \mathcal{E}_F$ we consider the isothermal Euler equation (4.1) with the compressibility factor (4.11) and pipe friction coefficient (4.10). For the readers' convenience we consider equal pipe length, diameter, roughness and angle for every flow pipe $e \in \mathcal{E}_F$. The network and gas parameters are given in Table 4.2.

For the inlet pressures we consider

$$p_1(t) = 55 \text{ bar}, \qquad p_2(t) = 52 \text{ bar}, \qquad p_6(t) = 53 \text{ bar}.$$

Table 4.2: Network and gas parameters for the GasLib-11 example

Variable	Letter	Value	Unit
Final time	T	24	h
Pipe diameter	D	0.5	m
Pipe length	L	5.5	km
Pipe roughness	ε	$5 \cdot 10^{-5}$	m
Pipe angle	α	0	
Gravitational constant	g	9.8067	m/s^2
Universal gas constant	R	8.3145	J/(mol K)
Molar mass of the gas	M	0.0182	kg/mol
Gas temperature	T	283.2	K
Pseudocritical temperature	T_{crit}	202.72	K
Pseudocritical pressure	P_{crit}	46.6614	bar
Lower pressure bound	$p_{\min}$	40	bar

The gas outflow is given by

$$b_7(t) = 30\ \sin\left(2\pi\ \frac{t}{T}\right) + 115\ \frac{\text{kg}}{\text{m}^2\text{s}},$$
$$b_{10}(t) = 50\ \sin\left(2\pi\ \left(\frac{t}{T} - \frac{3}{8}\right)\right) + 100\ \frac{\text{kg}}{\text{m}^2\text{s}},$$
$$b_{11}(t) = 40\ \sin\left(2\pi\ \left(\frac{t}{T} - \frac{1}{4}\right)\right) + 120\ \frac{\text{kg}}{\text{m}^2\text{s}}.$$

For the initial condition we compute the steady states corresponding to the boundary data at $t = 0$ and $u_1 = u_2 = 1$ with $u_{\text{ref},i} = 0$. For the objective function, we consider

$$g(y) = 0, \qquad \text{and} \qquad h(x,u,t) = \sum_{i=1}^{2} A^{c_i}\ q^{c_i}\ \left(u_{c_i}^{\kappa}(t)\right).$$

Further, we consider bounds for the control derivative, given by

$$|u_i'(t)| \le 5 \cdot 10^{-6} \qquad i \in \{1,2\}.$$

Note that the control derivative bounds are small, since the control is small compared to the time interval of 86400 seconds. The optimal compressor controls with and without bounds on the control derivative are shown in Fig. 4.4, and the corresponding optimal pressures at the outflow nodes v_7, v_{10}, and v_{11} are shown in Fig. 4.5. In the absence of bounds on the control derivative, the optimal control exhibits pronounced fluctuations and highly nonlinear behavior. In contrast, imposing bounds on the control derivative leads to significantly smoother and partly linear control profiles, as seen in Fig. 4.4. This difference in control behavior is reflected in the resulting pressure trajectories at the outflow nodes. While the overall pressure amplitudes remain comparable in both cases, the bounded control derivative yields smoother pressure profiles with reduced temporal variation, as shown in Fig. 4.5. In particular, changes in pressure occur more gradually, with reduced rates of change over time when control derivative bounds are enforced.

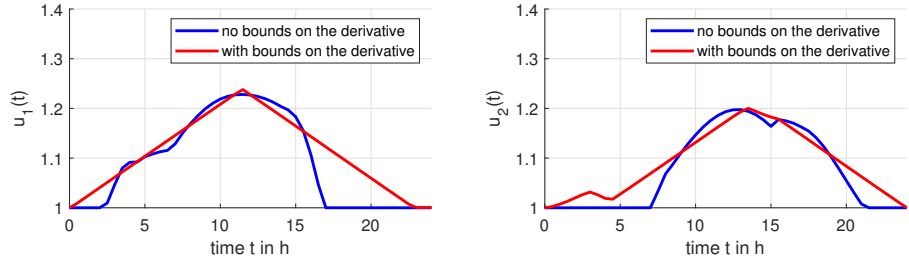


Fig. 4.4: Optimal compressor controls with bounds on the control derivative (red) and without bounds on the control derivative (blue)

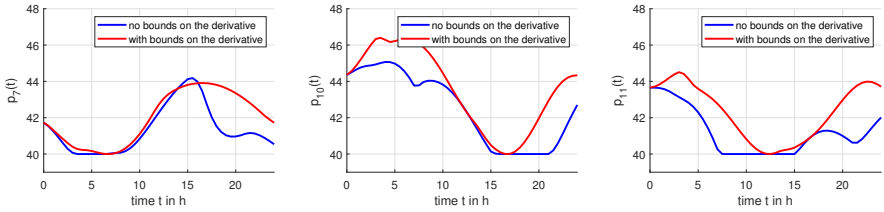


Fig. 4.5: Optimal pressures at the outflow nodes with bounds on the control derivative (red) and without bounds on the control derivative (blue)

Acknowledgements This work was supported by the German Research Foundation (DFG) within Subprojects C02, C03 and C05 in the Sonderforschungsbereich/Transregio 154 "Mathematical Modelling, Simulation and Optimization using the Example of Gas Networks" (Project ID 239904186).

References

1. R. Adams and J. Fournier. *Sobolev Spaces*. Academic Press, 2003.
2. Z. Amer, A. Avdzhieva, M. Bongarti, P. Dvurechensky, P. Farrell, U. Gotzes, F. M. Hante, A. Karsai, S. Kater, M. Liero, et al. Modeling hydrogen embrittlement for pricing degradation in gas pipelines. *language*, 2025. doi:10.20347/WIAS.PREPRINT.3201.
3. M. Gugat. Optimal boundary control in flood management. In *Control of coupled partial differential equations*, pages 69–94. Springer, 2007. doi:10.1007/978-3-7643-7721-2_4.
4. M. Gugat and M. Herty. Modeling, control, and numerics of gas networks. In *Handbook of numerical Analysis*, volume 23, pages 59–86. Elsevier, 2022. doi:10.1016/bs.hna.2021.12.002.
5. M. Gugat, M. Herty, A. Klar, G. Leugering, and V. Schleper. Well-posedness of networked hyperbolic systems of balance laws. In *Constrained optimization and optimal control for partial differential equations*, pages 123–146. Springer, 2011. doi:10.1007/978-3-0348-0133-1_7.
6. M. Gugat and J. Sokolowski. On problems of dynamic optimal nodal control for gas networks. *Pure and Applied Functional Analysis*, 5:1699–1715, 2022. URL: https://hal.science/hal-03120667.
7. T. Koch, B. Hiller, M. E. Pfetsch, and L. Schewe. *Evaluating Gas Network Capacities*. MOS-SIAM, 2015. doi:10.1137/1.9781611973693.
8. R. Lamour, R. März, and C. Tischendorf. *Differential-Algebraic Equations: A Projector Based Analysis*. Differential-Algebraic Equations Forum. Springer, 2013. doi:10.1007/978-3-642-27555-5.
9. A. Laureys, R. Depraetere, M. Cauwels, T. Depover, S. Hertelé, and K. Verbeken. Use of existing steel pipeline infrastructure for gaseous hydrogen storage and transport: A review of factors affecting hydrogen induced degradation. *Journal of Natural Gas Science and Engineering*, 101:104534, 2022. doi:10.1016/j.jngse.2022.104534.
10. T. Li, K. Wang, and Q. Gu. *Exact boundary controllability of nodal profile for quasilinear hyperbolic systems*. Springer, 2016. doi:10.1002/mma.1321.
11. A. J. Osiadacz and M. Kwestarz. Nonlinear steady-state optimization of large-scale gas transmission networks. *Energies*, 14(10):2832, 2021. doi:10.3390/en14102832.
12. H. Sauter. *Least-squares collocation for DAEs and its application in optimal control*. PhD thesis, Humboldt-Universität zu Berlin, 2025. doi:10.18452/34451.

13. M. Schmidt, M. Steinbach, and B. Willert. High detail stationary optimization models for gas networks: Validation and results. *Optim. Eng.*, 17:437–472, 2016. doi:10.1007/s11081-015-9300-3.
14. M. Schuster and M. Gugat. Max-p optimal boundary control of gas flow. In M. H. Baumann, L. Grüne, B. Jacob, and K. Worthmann, ed., *Extended Abstracts presented at the 25th International Symposium on Mathematical Theory of Networks and Systems MTNS 2022*, 2022. doi:10.15495/EPub_UBT_00006809.
15. O. Tehinse, L. Lamborn, K. Chevil, E. Gamboa, and W. Chen. Influence of load interaction and hydrogen on fatigue crack growth behavior in steel pipelines under mean load pressure fluctuations. *Fatigue & Fracture of Engineering Materials & Structures*, 44(4):1073–1084, 2021. doi:10.1111/ffe.13414.
16. X. Xing, W. Chen, and H. Zhang. Atomistic study of hydrogen embrittlement during cyclic loading: Quantitative model of hydrogen accumulation effects. *International Journal of Hydrogen Energy*, 42(7):4571–4578, 2017. doi:10.1016/j.ijhydene.2016.12.127.
17. X. Xing, M. Yu, O. Tehinse, W. Chen, and H. Zhang. The effects of pressure fluctuations on hydrogen embrittlement in pipeline steels. In *International Pipeline Conference*, volume 50251, page V001T03A025. American Society of Mechanical Engineers, 2016. doi:10.1115/IPC2016-64478.

Open Access This chapter is licensed under the terms of the Creative Commons Attribution-NonCommercial-NoDerivatives 4.0 International License (http://creativecommons.org/licenses/by-nc-nd/4.0/), which permits any noncommercial use, sharing, distribution and reproduction in any medium or format, as long as you give appropriate credit to the original author(s) and the source, provide a link to the Creative Commons license and indicate if you modified the licensed material. You do not have permission under this license to share adapted material derived from this chapter or parts of it.

The images or other third party material in this chapter are included in the chapter's Creative Commons license, unless indicated otherwise in a credit line to the material. If material is not included in the chapter's Creative Commons license and your intended use is not permitted by statutory regulation or exceeds the permitted use, you will need to obtain permission directly from the copyright holder.



Part II
Discrete-Continuous Optimization for Gas Networks

Chapter 5
Introduction to Discrete-Continuous Optimization for Gas Networks

Alexander Martin[0000−0001−7602−3653] and
Marc E. Pfetsch[0000−0002−0947−7193]

Abstract This chapter gives a short introduction into the interplay of discrete and continuous optimization in the context of gas networks and provides an introduction to the corresponding chapters of the book *Mathematical Modelling, Simulation and Optimization using the Example of Gas Networks*.

Discrete and continuous optimization are two main subfields of mathematical optimization. Discrete optimization deals with optimization problems in which discrete decision variables appear, e.g., binary or integer variables. Continuous optimization deals with problems with only continuous variables and usually some or all constraints are nonlinear.

The ties between these fields are traditionally not extremely strong. This can partly be explained by the different focus that these fields have. Very roughly, one large subarea of discrete optimization focusses on the solution to global optimality, i.e., the global optimality of a computed solution is proven. Another large subarea focusses on fast algorithms to compute solutions that provably approximate the optimal value within certain bounds. The solutions spaces are often polyhedra intersected with integer lattices. Continuous optimization usually deals with (highly) nonlinear problems. For example, a large subarea deals with nonlinear, but convex problems, while another subarea investigates the solution of problems constrainted by Partial Differential Equations (PDE). In the latter, usually only locally optimal solutions can be computed. The analysis of nonconvex solution spaces is therefore based on a local view with corresponding constraint qualifications. The properties of functions defining constraints or cones is typically quite important.

The algorithms investigated in both fields are also often of fundamentally different nature. In discrete optimization, branch-and-bound based and combinatorial algorithms

Alexander Martin
Analytics & Optimization, University of Technology Nuremberg (UTN), Germany,
e-mail: alexander.martin@utn.de

Marc E. Pfetsch
Department of Mathematics, TU Darmstadt, Germany, e-mail: pfetsch@mathematik.tu-darmstadt.de

© The Author(s) 2027

A. Martin et al. (eds.), *Mathematical Modelling, Simulation and Optimization using the Example of Gas Networks*, International Series of Numerical Mathematics 174,
https://doi.org/10.1007/978-3-032-34969-9_5

dominate. These algorithms try to exploit particular combinatorial structure in order to be theoretically or practically efficient. In continuous optimization, iterative algorithms like gradient descent or Newton's method are ubiquitous. The main focus is then on a convergence analysis, possibly including error control. Linear programming is one of the (few) topics that lie in the intersection.

Of course, the combination of both fields has been perused in the past. For instance, extending global optimization to nonlinear problems (with discrete variables) has lead to Mixed-Integer Nonlinear Programming (MINLP). Similarly, nonlinear convex relaxations like semidefinite programs have been heavily investigated.

We stress that this is a very rough classification with many blurred borders. However, it may help to assess the contributions of this book.

In the context of gas transport, many topics arise that require the combination of techniques from the two fields. For instance, the physics of gas flows is nonlinear. Discrete decisions are necessary for opening/closing valves, turning compressors on/off, and for deciding about the topology of hydrogen networks. Similarly, the handling of discrete decisions in PDE optimization is important, e.g., because of model switches. This book therefore contains many different examples where such a combination has been fruitfully exploited.

Let us give some examples.

- Chap. 6, "Mixed-Integer Nonlinear Optimization in the Context of Gas Networks" explicitly collects several MINLP techniques applied in the gas transport context. This ranges from methods to globally solve stationary gas transport problem to solving transient problems. Moreover, new techniques to derive dual bounds based on Lipschitz constants have been developed.
- Chap. 7, "Potential-Based Flows – An Overview" gives an overview on potential-based flows, a model capturing many energy networks. This also includes discrete decisions and topology optimization.
- Chap. 8, "Models for Gas Markets" treats equilibrium models, in particular for energy markets. The corresponding networks also involve valves or switches, i.e., discrete decisions. Moreover, when reformulating multi-level problems with fewer levels, optimality conditions have to be expressed. This can be done by either introducing additional binary variables or using complementarity conditions.

Further chapters that involve the interplay of continuous and discrete optimization are:

- Chap. 3, "Gas Mixtures on Networks: Modeling, Simulation and Optimization" discusses models for mixing different gas types. The core nonlinear equation expressing mixing involves the flow direction, which is commonly represented using binary variables.
- Chap. 22, "Mathematical Questions Arising from Practical Challenges in Gas Networks" covers demonstrators of the techniques of this book. This also includes discrete-continuous optimization.
- Parts of Chap. 17, "Domain Decomposition for Gas Network Control" treat mixed-integer optimal control.

In conclusion, this book contains many interesting contributions of the interaction of techniques from discrete and continuous optimization. We hope that the readers of this book enjoy them as much as we do!

Acknowledgements This work was supported by the German Research Foundation (DFG) within Subprojects A01, A05, A07, B07, B08, and B09 in the Sonderforschungsbereich/Transregio 154 "Mathematical Modelling, Simulation and Optimization using the Example of Gas Networks" (Project ID 239904186).

Open Access This chapter is licensed under the terms of the Creative Commons Attribution-NonCommercial-NoDerivatives 4.0 International License (http://creativecommons.org/licenses/by-nc-nd/4.0/), which permits any noncommercial use, sharing, distribution and reproduction in any medium or format, as long as you give appropriate credit to the original author(s) and the source, provide a link to the Creative Commons license and indicate if you modified the licensed material. You do not have permission under this license to share adapted material derived from this chapter or parts of it.

The images or other third party material in this chapter are included in the chapter's Creative Commons license, unless indicated otherwise in a credit line to the material. If material is not included in the chapter's Creative Commons license and your intended use is not permitted by statutory regulation or exceeds the permitted use, you will need to obtain permission directly from the copyright holder.



Chapter 6
Mixed-Integer Nonlinear Optimization in the Context of Gas Networks

Robert Burlacu[0000−0003−0578−6260],
Adrian Göß[0009−0002−7144−8657],
Günter Leugering[0000−0002−1086−991X],
Alexander Martin[0000−0001−7602−3653],
Marc E. Pfetsch[0000−0002−0947−7193],
Martin Schmidt[0000−0001−6208−5677], and
Johannes Thürauf[0000−0001−8516−6250]

Abstract When solving gas transport problems, mixed-integer nonlinear programs (MINLPs) arise in many forms. The nonlinearity typically arises from the physics of gas and integer decisions from using active elements, e.g., from opening/closing valves. In recent years, many solution techniques tailored towards gas transport have been developed. This chapter gives an overview of some of these methods. This ranges from stationary to instationary models and spans many different approaches.

Robert Burlacu
Analytics & Optimization, University of Technology Nuremberg (UTN), Germany,
e-mail: robburlacu@gmail.com

Adrian Göß
Analytics & Optimization, University of Technology Nuremberg (UTN), Germany,
e-mail: adrian.goess@utn.de

Günter Leugering
Department of Mathematics, Friedrich-Alexander-Universität Erlangen-Nürnberg (FAU)
and Speinshart Center for AI and SuperTech, Germany, e-mail: guenter.leugering@fau.de

Alexander Martin
Analytics & Optimization, University of Technology Nuremberg (UTN), Germany,
e-mail: alexander.martin@utn.de

Marc E. Pfetsch
Department of Mathematics, TU Darmstadt, Germany, e-mail: pfetsch@mathematik.tu-darmstadt.de

Martin Schmidt
Department of Mathematics, Trier University, Germany, e-mail: martin.schmidt@uni-trier.de

Johannes Thürauf
Discrete Optimization, University of Technology Nuremberg (UTN), Germany,
e-mail: johannes.thuerauf@utn.de

© The Author(s) 2027

A. Martin et al. (eds.), *Mathematical Modelling, Simulation and Optimization using the Example of Gas Networks*, International Series of Numerical Mathematics 174,
https://doi.org/10.1007/978-3-032-34969-9_6

6.1 Introduction

Gas transport networks, or more generally energy networks, have been one important application area of techniques for mixed-integer nonlinear programs (MINLPs). These optimization problems on networks provide challenging and interesting research topics, because they can be (very) large-scale, they are nonlinear and they incorporate integer decisions. As a consequence, both new methods – often tailored towards the particular structure – have been developed and existing approaches have been refined for this application area.

The goal of this chapter is to showcase some MINLP techniques in the context of gas transport. One common thread is that the methods need to exploit the combined structure of nonlinearity and integrality in order to achieve good solution performance. Indeed, these techniques often allow to solve instances of realistic size. The readership that we are targeting with this chapter are researchers who want to see applications of such MINLP methods.

This chapter is structured as follows. We start with a short literature review in Sect. 6.2. We then present methods for stationary gas transport (Sect. 6.3), followed by methods of transient gas transport (Sect. 6.4). In addition, we very briefly mention topology optimization (Sect. 6.5), but also refer to the discussion in Chap. 7, "Potential-Based Flows – An Overview". Sect. 6.6 gives an overview of techniques that only require (approximations of) Lipschitz constants and nonconvex relaxations. The chapter closes with an outlook in Sect. 6.7.

In total, the goal of this chapter is to give a glimpse into MINLP approaches that are connected to gas transport, but also go beyond.

6.2 Brief Literature Review

Some surveys on the application of MINLP techniques for gas transport are given by Zheng et al. [46], Shaw [43] and Ríos-Mercado and Borraz-Sánchez [36]. For a literature review until about 2015, we also refer to the chapter [38] in the book [21].

For a review on techniques especially targeted towards topology optimization, we refer to Sect. 6.5 and Chap. 7, "Potential-Based Flows – An Overview".

Recent work on MINLP include Li and Li [28], who apply a generalized Benders algorithm for an industrial natural gas production network. Borraz-Sánchez et al. [2] consider convex models based on second-order cones. A linearization of a MINLP model is studied by Mikolajková et al. [32]. The optimization of compressor stations is investigated by Mak et al. [30]. Moreover, Li et al. [29] develop an algorithm based on reformulation and enumeration. Ghilardi et al. [9] investigate an approximation based on MIPs and a decomposition applied to the Italian gas transmission network.

6.3 Improvements for Solving Stationary Models

We begin with a short recap of the models that are used for optimizing stationary gas transport. For an overview and more details, we refer to Chap. 2, "A Catalog of Gas Network Models: PDEs, Coupling Conditions, and Numerical Schemes" and [21]. Moreover, for models incorporating gas mixtures, we refer to Chap. 3, "Gas Mixtures on Networks: Modeling, Simulation and Optimization".

For a pipe in a gas network, the most accurate model for the stationary case can be derived from (ISO1) in Chap. 2, "A Catalog of Gas Network Models: PDEs, Coupling Conditions, and Numerical Schemes" by setting all time derivatives to 0:

$$\partial_x(p + \rho v^2) = -\frac{\lambda}{2D}\rho v|v| - g\rho\partial_x b, \tag{ISO1-S}$$

where x is the position along the pipe, p is the pressure, ρ the density and v the velocity of the gas. Moreover, D is the diameter, λ the friction, b the height of the pipe and g is the gravitational constant. For simplicity of exposition, we set the height to be constant in the following, i.e., $\partial_x b = 0$. Let A be the cross-sectional area of the pipe. Then using the flow rate $q = A\rho v$ (which is constant along the pipe) and speed of sound $c^2 = \frac{p}{\rho}$ we obtain

$$\begin{aligned}
\text{(ISO1-S)} \quad &\Leftrightarrow \quad \partial_x\left(p + \frac{q^2}{A^2\rho}\right) = -\frac{\lambda}{2DA^2}\frac{c^2}{p}q|q| \\
&\Leftrightarrow \quad \partial_x\left(p + \frac{c^2q^2}{A^2p}\right) = -\frac{\lambda}{2DA^2}\frac{c^2}{p}q|q| \\
&\Leftrightarrow \quad \partial_x p\left(1 - \frac{c^2q^2}{A^2p^2}\right) = -\frac{\lambda}{2DA^2}\frac{c^2}{p}q|q|,
\end{aligned} \tag{6.1}$$

where in the second to last line the derivative with respect to x is taken. If we define

$$\phi(p, q) \coloneqq -\frac{\lambda\, c^2\, q|q|\, p}{2D(A^2p^2 - c^2q^2)},$$

then (6.1) can be written as the ordinary differential equation (ODE) $p' = \partial_x p = \phi(p, q)$.

A useful algebraic approximation is given by the Weymouth equation, compare (ISO4-ALG) in Chap. 2, "A Catalog of Gas Network Models: PDEs, Coupling Conditions, and Numerical Schemes":

$$p_{in}^2 - p_{out}^2 = \frac{\lambda c^2 L}{DA^2}\,|q|q, \tag{6.2}$$

where p_{in} and p_{out} are the pressures at the beginning and end of the pipe (w.r.t. arc direction). Moreover, L is the length of the pipe.

The network is represented by a directed graph $\mathcal{G} = (\mathcal{V}, \mathcal{A})$, where we assume that there are no loops and no anti-parallel arcs. The arcs correspond to different elements in the gas network like pipes or compressors. On each arc $a \in \mathcal{A}$ there is a constant flow rate q_a. Positive values correspond to flow in the direction of the arc, while negative

values correspond to flow in the opposite direction. Each node $u \in \mathcal{V}$ of the graph has a pressure p_u. At each node, flow conservation with balance value $q_u^{\pm}$ has to hold

$$\sum_{a \in \delta^+(u)} q_a - \sum_{a \in \delta^-(u)} q_a = q_u^{\pm},$$

where $\delta^+(u) \coloneqq \{a = (u, w) \in \mathcal{A}\}$ are the arcs leaving u and $\delta^-(u) \coloneqq \{a = (w, u) \in \mathcal{A}\}$ are the arcs entering u. Node v is an *entry* if $q_u^{\pm} > 0$, an *exit* if $q_u^{\pm} < 0$ or an *inner node* if $q_u^{\pm} = 0$.

A gas network usually contains more elements, namely, control valves, valves, compressors and resistors. We do not discuss the details of the modeling of these other network elements here, but refer to Sect. 2.9 of Chap. 2, "A Catalog of Gas Network Models: PDEs, Coupling Conditions, and Numerical Schemes" and the book [21].

6.3.1 Compressor Station Modeling

Since gas flows from higher to lower pressure, compressors are sometimes needed to increase pressure and such that lower pressure bounds at customers can be satisfied. There are several types of compressors, the most commonly used are so-called turbo compressors. The modeling of these compressors is typically quite complicated, since the description of the physical behavior is generally only available through measured data. In practice, several compressors are usually installed at so-called *compressor stations* with valves deciding about the flow through the compressors, depending on the particular use case. We refer to Sect. 2.9 of Chap. 2, "A Catalog of Gas Network Models: PDEs, Coupling Conditions, and Numerical Schemes" for more details.

In order to provide an easy way of approximating the behavior of compressor stations, Hiller et al. [19] developed methods that compute suitable convex hulls of the operating ranges of the stations. Their methods result in linear inequalities that provide an outer approximation in the flow/pressure space and can easily be incorporated into MINLP models.

6.3.2 Global Optimization by Exploiting Acyclicity

Gas cannot flow in cycles, because the pressure differences cancel around a cycle, but the flow does not; see also Theorem 7.3 in Chap. 7, "Potential-Based Flows – An Overview". This fact can be exploited with the main goal to fix flow directions. If the direction of the flow along a pipe is fixed, the linear relaxation of (6.1) or (6.2) is tighter, which improves the overall approximation quality. In the following we summarize the techniques developed in [15].

The main technique is to introduce binary variables z_a^+ and z_a^- for each arc $a \in \mathcal{A}$. These are coupled to the flow q_a as follows

$$q_a \le \overline{q}_a z_a^+, \quad \underline{q}_a z_a^- \le q_a, \quad z_a^+ + z_a^- \le 1, \tag{6.3}$$

where $\underline{q}_a$ and $\overline{q}_a$ are lower and upper bounds on the flow q_a, respectively.

Let C be a cycle in the graph $\mathcal{G}$, i.e., it forms a cycle in the underlying undirected graph. Fix an arbitrary direction of C. Let C^+ and C^- be arcs in forward and backward direction, respectively. We write $C = (C^+, C^-)$. Then the following *cycle inequalities* hold:

$$\sum_{a \in C^+} z_a^+ + \sum_{a \in C^-} z_a^- \le |C| - 1, \quad \sum_{a \in C^+} z_a^- + \sum_{a \in C^-} z_a^+ \le |C| - 1,$$

which state that the flow directions along the cycle cannot be all in or against the orientation of C.

Moreover, one can add the following inequalities for every entry $s \in V$ and exit $t \in V$:

$$\sum_{a \in \delta^+(s)} z_a^+ + \sum_{a \in \delta^-(s)} z_a^- \ge 1, \quad \sum_{a \in \delta^-(t)} z_a^+ + \sum_{a \in \delta^+(t)} z_a^- \ge 1,$$

which state that at least one flow direction has to leave s and enter t. For an inner node u, one can enforce that if a flow direction enters or leaves u along an arc a then it also has to leave or enter it. For example, if $a \in \delta^-(u)$ for $a \in \mathcal{A}$ then

$$z_a^+ \le \sum_{b \in \delta^+(v)} z_b^+ + \sum_{b \in \delta^-(v) \setminus \{a\}} z_b^-,$$

holds.

Besides a theoretical investigation of flow directions, [15] also contains computational experiments that show the superiority of exploiting acyclicity. For instance, when using the Weymouth equation (6.2), for the GasLib-582 instance [39], among the 4227 scenarios the best method (which enumerates and adds all cycle inequalities) could solve 2015 to optimality and 2179 are detected to be infeasible. Note that these instances were originally constructed to be at the boundary of in/feasibility, which explains the large number of infeasible instances. This leaves only 33 instances that cannot be solved within one hour. Without flow direction variables, 1830 cannot be solved. If we only use binary flow direction variables this number drops to 1229. If the ODE model (6.1) is used (see Sect. 6.3.3), only 349 instances cannot be solved with the best version (again using all cycles).

6.3.3 Global Optimization of the ODE Model

For an accurate handling of gas flow, i.e., when using the ODE model (6.1), the article [16] developed a global optimization approach, which we briefly describe in the following.

One main observation is that in the MINLP formulation, the pressure function only needs to be evaluated at nodes and not along pipes of a stationary network. Moreover,

$p(x)$ is shown to be non-increasing and concave along a pipe. This makes it possible to compute tight bounds for the pressure at the end or start of a pipe, given the pressure at the other end and the flow rate q.

To this end, we assume that we have discretized the range $[0, L]$ of the pipe using $N + 1$ equidistant discretization points $0 = x_N < \ldots < x_1 < x_0 = L$. Let $h \coloneqq \frac{L}{N}$ be the step size. Then the *explicit midpoint rule* computes pressures $p_0^\ell, \ldots, p_N^\ell$ as follows

$$p_0^\ell = p^0, \quad p_{i+1}^\ell = p_i^\ell - h\,\phi(p_i^\ell - \frac{h}{2}\phi(p_i^\ell, q), q), \quad \forall i = 0, \ldots, N-1,$$

where p^0 is a given pressure at L. Moreover, the *implicit trapezoidal rule* is

$$p_0^u = p^0, \quad p_{i+1}^u = p_i^u - \frac{h}{2}\left[\phi(p_i^u, q) + \phi(p_{i+1}^u, q)\right], \quad \forall i = 0, \ldots, N-1.$$

Then it is proved in [16] that under certain weak conditions, the explicit midpoint rule provides a lower bound on the pressure at 0 and the trapezoidal rule an upper bound. Note that the direction is reversed for simplicity of notation. Moreover, one can show that these bounds are convex, which allows to derive gradient inequalities to generate a dynamically adjusted linear programming relaxation, see Fig. 6.1 for an illustration. This is then combined with an algorithm that automatically refines the stepsize h on certain pipes and performs spatial branching in order to obtain a tighter linear relaxation. The practical applicability of this overall approach is then demonstrated through computational results on GasLib instances [39], see also Sect. 6.3.2.

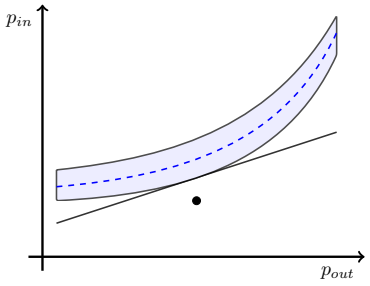


Fig. 6.1: Illustration of the approximation of the solution function of the ODE $p' = \phi(p, q)$ (dashed). The shaded area is the approximation given by the numerical discretization schemes. The black point is a candidate solution, which can be cut off using a gradient cut at the lower bound.

6.4 Improvements for Time-Dependent Models via Decomposition Methods

Large-scale mixed-integer nonlinear programming problems (MINLP) are far beyond one-shot applications of standard software. The key features are the interaction of discrete (integer) and continuous variables and the complexity of the domains, i.e., the underlying graphs. Consequently, two types of decompositions are in order: first, a decomposition into discrete and continuous variables (e.g., Benders decomposition) and, second, space–time domain decomposition methods (STDDM) of the time–graph structure. Discrete methods aim to compute global minima for physically less accurate and often time-independent models, while continuous PDE-based methods focus on physically faithful PDE models but notoriously lack guarantees of global optimality, since they typically rely on gradient-based methods for nonconvex problems. On the one hand, short time horizons make it possible to employ time expansions of discrete (integer-based) models and methods, while on the other hand, small subnetworks improve the accessibility of continuous optimization methods.

A first way to reduce the complexity of the optimal control problem consists of an Euler time discretization of the PDE and the implementation of a rolling-horizon scheme, which results in a so-called instantaneous control problem on the network. In this way, the original time-dependent problem turns into a sequence of static optimal control problems which, in turn, can be treated as MINLPs on large networks or, preferably, on subnetworks. In [13] this reduction method was pursued, enabling a decomposition into integer-based and continuous problems.

Time-domain decompositions, has been considered [22, 23, 26], while spatial domain decomposition on metric graphs has been extensively studied in [25]. Here, we restrict ourselves to the model (ISO2) from Chap. 2, “A Catalog of Gas Network Models: PDEs, Coupling Conditions, and Numerical Schemes”, even though similar results have meanwhile also been achieved for (ISO3), see [27]. It should be noted that, after an (implicit) Euler time discretization, for (ISO2)/(ISO3) can be reduced to an extended version of (ISO4), which, in turn, is the classical model for MINLP applications. IS Here we concentrate on optimal control problems for systems of semilinear hyperbolic balance laws derived from (ISO2) pipe network model. We formulate a generic optimal control problem for semilinear hyperbolic balance laws on a metric graph, using Riemann invariants and *nonlinear* flux control at the leaves *and* nonlinear actuation at interior junctions. We present (i) the continuous-time optimal control problem (OCP) in Riemann variables, (ii) a semi-discretization with respect to the time via an implicit (backward) Euler discretization, while keeping the space variables continuous and provide an analysis of the resulting elliptic-in-time operator equation, (iii) a fully discrete upwind version and the associated KKT/adjoint system and reduced gradient, (iv) a junction/node solver derived from pressure continuity and mass conservation in Riemann variables (and its controlled generalization), (v) the instantaneous/rolling-horizon control problem obtained by neglecting the time sum, and (vi) a spatial domain decomposition of the instantaneous problem on a single time level together with interface variables and Schur-complement structure.

6.4.1 Graph Setting and Problem Formulation

Let $\mathcal{G} = (\mathcal{V}, \mathcal{A})$ be a directed metric graph. Each edge $e \in \mathcal{E}$ is a pipe of length L_e with coordinate $x \in (0, L_e)$. On each edge we consider a 2×2 strictly hyperbolic, semilinear balance law for gas dynamics. Let conservative/physical variables be $U_e = (p_e, q_e)^\top$ (pressure, mass flux), and define the Riemann invariants

$$R_e = \begin{pmatrix} r_e^+ \\ r_e^- \end{pmatrix}, \qquad (p, q) = \Psi(R), \quad R = \Phi(U),$$

where Φ maps the physical variables into the Riemann invariants and Ψ denotes the inverse of Φ. In particular, $r^\pm = q \pm Z_e p$ with constant impedance $Z_e > 0$. In the case of linear gas transport (the nonlinearity is provided by the friction term), the characteristic speeds are $\lambda_e^+(R_e) = a_e = \lambda_e^-(R_e)$. We define the diagonal operator

$$\Lambda_e(R_e) \coloneqq \operatorname{diag}(\lambda_e^+(R_e), -\lambda_e^-(R_e)), \qquad \lambda_e^\pm > 0.$$

We now introduce the dynamics. For each $e \in \mathcal{E}$,

$$\partial_t r_e^+ + \lambda_e^+(R_e)\, \partial_x r_e^+ = S_e^+(R_e), \qquad \partial_t r_e^- - \lambda_e^-(R_e)\, \partial_x r_e^- = S_e^-(R_e). \tag{PDE}$$

Here $S_e^\pm$ collect sources (e.g., friction). For isothermal gas with nonlinear friction $f(q) = \kappa_e |q| q$, one has $S_e^+ = S_e^- = -\frac{1}{2}\kappa_e |q_e| q_e$ with $q_e = \frac{1}{2}(r_e^+ + r_e^-)$. The system dynamics is complemented by nodal and initial conditions. Let $\delta(v)$ denote edges incident to node $v \in V$. With the outward normal $n_{e,v} = +1$ if $x = 0$ is at v and -1 if $x = L_e$ is at v, define

$$r_{e,v}^{\text{in}} = \begin{cases} r_e^-(0,t), & \text{if } n_{e,v} = +1, \\ r_e^+(L_e,t), & \text{if } n_{e,v} = -1, \end{cases} \qquad r_{e,v}^{\text{out}} = \begin{cases} r_e^+(0,t), & \text{if } n_{e,v} = +1, \\ r_e^-(L_e,t), & \text{if } n_{e,v} = -1. \end{cases}$$

For *uncontrolled* junctions, interior-node physics (pressure continuity and mass-flux conservation) yield

$$\mathbf{r}_v^{\text{out}}(t) \;=\; S_v(\mathbf{r}_v^{\text{in}}(t)) + b_v(t), \tag{NODE}$$

where $\mathbf{r}_v^{\text{in/out}}$ stack $r_{e,v}^{\text{in/out}}$ over $e \in \delta(v)$. The operator S_v can be seen as a global *scattering* operator which maps incoming information along the characteristics to outgoing signals. Let $\mathcal{V}_c \subseteq \mathcal{V} \setminus \mathcal{V}_\ell$ be the set of *junction-controlled* interior nodes. For $v \in \mathcal{V}_c$ we impose a general nonlinear node law

$$\mathcal{N}_v(\mathbf{r}_v^{\text{in}}(t), \mathbf{r}_v^{\text{out}}(t), u_v(t)) = 0, \quad v \in \mathcal{V}_c, \tag{NODE-CTRL}$$

with $\mathcal{N}_v \colon \mathbb{R}^{d_v} \times \mathbb{R}^{d_v} \times \mathbb{R} \to \mathbb{R}^{d_v}$, $d_v = |\delta(v)|$, of class C^1 and locally Lipschitz. Typical special cases are:

(i) *Controlled scattering:* $\mathbf{r}_v^{\text{out}} = S_v(\mathbf{r}_v^{\text{in}}, u_v) + b_v(t, u_v)$;
(ii) *Additive actuation:* $\mathbf{r}_v^{\text{out}} = S_v \mathbf{r}_v^{\text{in}} + b_v(t) + G_v(u_v)$.

Let $\mathcal{V}_\ell \subset \mathcal{V}$ denote the simple nodes ($\deg(v) = 1$). We control the incoming characteristic at each leaf via a *nonlinear actuator law*:

$$r^{\text{in}}_{e(v),v}(t) = h_v(u_v(t)), \qquad v \in \mathcal{V}_\ell, \tag{CTRL-BC$_{\text{NL}}$}$$

with possibly nonlinear control-to-state input maps $h_v(\cdot)$, while the outgoing characteristic at a leaf follows from the PDE.

Example: Two-Port Gas Compressor in Riemann Invariants (On/Off Control) Consider a junction v with exactly two incident edges: upstream e_1 and downstream e_2, with impedances $Z_1, Z_2 > 0$. Let $s_i \in \{-1, +1\}$ encode the edge orientation at v: $s_i = +1$ if $n_{e_i,v} = +1$ (edge starts at v) and $s_i = -1$ if $n_{e_i,v} = -1$ (edge ends at v). For each side $i \in \{1, 2\}$, define the node pressure/flux from the local incoming/outgoing characteristics by

$$q_i \;=\; \frac{r^{\text{in}}_{i,v} + r^{\text{out}}_{i,v}}{2}, \qquad p_i \;=\; \frac{s_i}{2Z_i}\,(r^{\text{out}}_{i,v} - r^{\text{in}}_{i,v}).$$

The compressor enforces *mass conservation* and a *pressure ratio* $\alpha(u_v) \geq 1$:

$$q_2 - q_1 = 0, \qquad p_2 - \alpha(u_v)\, p_1 = 0. \tag{6.4}$$

These two equations for the two unknown outgoing traces $(r^{\text{out}}_{1,v},\, r^{\text{out}}_{2,v})$ (given $(r^{\text{in}}_{1,v}, r^{\text{in}}_{2,v})$ and control u_v) define the junction law $\mathcal{N}_v(\mathbf{r}^{\text{in}}, \mathbf{r}^{\text{out}}, u_v) = 0$ with components (6.4). Equivalently, one obtains the explicit scattering form

$$\begin{bmatrix} r^{\text{out}}_{1,v} \\ r^{\text{out}}_{2,v} \end{bmatrix} \;=\; \underbrace{\frac{1}{Z_1 s_2 - Z_2 \alpha(u_v) s_1} \begin{bmatrix} -(Z_1 s_2 + Z_2 \alpha(u_v) s_1) & 2Z_1 s_2 \\ -2Z_2 \alpha(u_v) s_1 & (Z_1 s_2 + Z_2 \alpha(u_v) s_1) \end{bmatrix}}_{S^{\text{comp}}_v(\alpha(u_v))} \begin{bmatrix} r^{\text{in}}_{1,v} \\ r^{\text{in}}_{2,v} \end{bmatrix}. \tag{COMP-S}$$

We model the *switch* by combining a discrete or a smooth control:

(i) *Binary (MINLP) switch:* $u_v \in \{0, 1\}$ and $\alpha(u_v) = 1 + u_v(\alpha_{\max} - 1)$.
(ii) *Smooth switch (continuous OCP):* $\alpha(u_v) = 1 + (\alpha_{\max} - 1)\,\sigma(u_v)$ with a C^1 sigmoid, e.g., $\sigma(u) = \frac{1}{2}(1 + \tanh(k(u - u_0)))$.

In both cases $\alpha(0) = 1$ (*off*, continuity at v, according to (6.4)); $\alpha(1) = \alpha_{\max} > 1$ (*on*, pressure boost). Writing (6.4) as $\mathcal{N}_v(\mathbf{r}^{\text{in}}, \mathbf{r}^{\text{out}}, u_v) = 0$ with

$$\mathcal{N}_v^{(1)} = q_2 - q_1, \qquad \mathcal{N}_v^{(2)} = p_2 - \alpha(u_v)\, p_1,$$

the junction multiplier is $\eta_v = (\eta_v^{(1)}, \eta_v^{(2)})^\top$. Then the junction optimality condition gives

$$\beta_v\, u_v(t) + (\partial_u \mathcal{N}_v)^\top \eta_v(t) = \beta_v\, u_v(t) - \alpha'(u_v(t))\, p_1(t)\, \eta_v^{(2)}(t) = 0.$$

The adjoint traces follow using $\partial_{\mathbf{r}^{\text{in}}} \mathcal{N}_v$ and $\partial_{\mathbf{r}^{\text{out}}} \mathcal{N}_v$ implied by the formulas for q_i, p_i above. If both edges start at v (i.e., $s_1 = s_2 = +1$), then with $D \coloneqq Z_1 - Z_2 \alpha(u_v)$,

$$\begin{bmatrix} r^{\text{out}}_{1,v} \\ r^{\text{out}}_{2,v} \end{bmatrix} = \frac{1}{D} \begin{bmatrix} -(Z_1 + Z_2\alpha) & 2Z_1 \\ -2Z_2\alpha & Z_1 + Z_2\alpha \end{bmatrix} \begin{bmatrix} r^{\text{in}}_{1,v} \\ r^{\text{in}}_{2,v} \end{bmatrix}, \qquad \alpha = \alpha(u_v).$$

Remark 6.1 (Degenerate match) The denominator $Z_1 s_2 - Z_2 \alpha s_1$ in (COMP-S) must be nonzero. The singular case ($Z_1 s_2 = Z_2 \alpha s_1$) corresponds to a perfectly matched impedance/boost that collapses (6.4) into a dependent pair. In practice one avoids this by (i) excluding that operating point, or (ii) adding a small loss term (head curve) to (6.4).

As for the optimal control problem, let $(p, q) = \Psi(R)$ and choose tracking weights ω_p, $\omega_q \geq 0$, actuation weights $\beta_v > 0$, and references $(\bar{p}, \bar{q})$. We keep a quadratic control penalty with a time horizon $T > 0$:

$$J(u) \coloneqq \int_0^T \left[\sum_{e \in \mathcal{E}} \int_0^{L_e} \frac{\omega_p}{2} (p_e - \bar{p}_e)^2 + \frac{\omega_q}{2} (q_e - \bar{q}_e)^2 \, dx + \sum_{v \in \mathcal{V}_\ell \cup \mathcal{V}_c} \frac{\beta_v}{2} u_v(t)^2 \right] dt. \quad \text{(COST)}$$

The continuous-in-space-and-time optimal control problem is

$$\begin{aligned} \min_{u \in \mathcal{U}} \quad & J(u) \\ \text{s.t.} \quad & \text{(PDE) on each } e \in \mathcal{E}, \\ & \text{(NODE) on each } v \in \mathcal{V} \setminus (\mathcal{V}_\ell \cup \mathcal{V}_c), \\ & \text{(NODE-CTRL) on each } v \in \mathcal{V}_c, \\ & \text{(CTRL-BC}_{\text{NL}}\text{) on each } v \in \mathcal{V}_\ell, \\ & R_e(\cdot, 0) = R_{e,0}(\cdot). \end{aligned} \qquad (\text{OCP}_{\text{cts}})$$

Remark 6.2 (Leaf and junction stationarity, continuous time) If $\mu_v(t)$ denotes the adjoint multiplier of $r^{\text{in}}_{e(v),v} - h_v(u_v) = 0$ at a leaf, then

$$\beta_v \, u_v(t) \; - \; (h_v'(u_v(t)))^\top \mu_v(t) = 0 \quad \text{a.e. in } (0, T).$$

If $\eta_v(t) \in \mathbb{R}^{d_v}$ denotes the multiplier for the node law $\mathcal{N}_v = 0$ at a controlled junction, then

$$\beta_v \, u_v(t) + (\partial_u \mathcal{N}_v)^\top \eta_v(t) = 0, \qquad v \in \mathcal{V}_c.$$

Adjoint trace coupling at nodes is given by

$$\mathfrak{B}^{\text{in}}_v = (\partial_{\mathbf{r}^{\text{in}}} \mathcal{N}_v)^\top \eta_v, \quad \mathfrak{B}^{\text{out}}_v = -(\partial_{\mathbf{r}^{\text{out}}} \mathcal{N}_v)^\top \eta_v \quad (v \in \mathcal{V}_c),$$

and $\mathfrak{B}^{\text{in}}_v = (\partial_{\mathbf{r}^{\text{in}}} S_v)^\top \mathfrak{B}^{\text{out}}_v$ if $v \notin \mathcal{V}_c \cup \mathcal{V}_\ell$.

6.4.2 Semi-Discretization in Time

We now discretize in time by backward Euler while keeping x continuous on each edge. Let $t^n = n\tau$, $n = 1, \dots, N$, with $N\tau = T$. Denote $R_e^n(x) \approx R_e(x, t^n)$. For each edge e we write, for $x \in (0, L_e)$,

$$\frac{r_e^{+,n} - r_e^{+,n-1}}{\tau} + \lambda_e^+(R_e^n)\,\partial_x r_e^{+,n} = S_e^+(R_e^n), \tag{6.5a}$$

$$\frac{r_e^{-,n} - r_e^{-,n-1}}{\tau} - \lambda_e^-(R_e^n)\,\partial_x r_e^{-,n} = S_e^-(R_e^n). \tag{6.5b}$$

Nodal relations at time t^n are imposed as

$$\begin{aligned} &\mathbf{r}_v^{\mathrm{out},n} = S_v(\mathbf{r}_v^{\mathrm{in},n}) + b_v^n, && v \in \mathcal{V} \setminus (\mathcal{V}_\ell \cup \mathcal{V}_c),\\ &\mathcal{N}_v(\mathbf{r}_v^{\mathrm{in},n}, \mathbf{r}_v^{\mathrm{out},n}, u_v^n) = 0, && v \in \mathcal{V}_c,\\ &r_{e(v),v}^{\mathrm{in},n} = h_v(u_v^n), && v \in \mathcal{V}_\ell. \end{aligned} \tag{6.6}$$

With the usual bulk adjoint recursion, the boundary/junction contributions yield

$$\nabla_{u_v^n} J_\tau = \begin{cases} \tau\,\beta_v\,u_v^n - \tau\,(h_v'(u_v^n))^\top \mu_v^n, & \text{if } v \in \mathcal{V}_\ell,\\ \tau\,\beta_v\,u_v^n + \tau\,(\partial_u \mathcal{N}_v)^\top \eta_v^n, & \text{if } v \in \mathcal{V}_c. \end{cases}$$

(Single-Step) Optimal Control Problem on the Semi-Discrete Level When discretizing with respect to time, the time integral in (COST) is converted to a sum over the time indices t^n. Clearly, this necessitates an evolution of the PDE over these discrete time instances. We instead resort to a scheme that has come to be known as *instantaneous control* or *rolling horizon control* in the context of moving horizon predictive control regimes. To this end, we collapse the time-sum in (COST) to a single time cap t^n. At each time step t^n, we may, therefore, isolate the implicit backward-Euler subproblem subject to a static optimal control problem on the graph. Given the previous state R^{n-1} and the time step $\tau > 0$, we define:

$$\begin{aligned} \min_{R^n, u^n} \quad & \tau \sum_{e \in \mathcal{E}} \int_0^{L_e} \frac{\omega_p}{2}\,(p_e^n - \bar{p}_e^n)^2 + \frac{\omega_q}{2}\,(q_e^n - \bar{q}_e^n)^2\,dx + \tau \sum_{v \in \mathcal{V}_\ell \cup \mathcal{V}_c} \frac{\beta_v}{2}\,(u_v^n)^2 \\ \text{s.t.} \quad & \frac{R^n - R^{n-1}}{\tau} + A(R^n) = S(R^n) && \text{on each edge } e \in \mathcal{E},\\ & \mathbf{r}_v^{\mathrm{out},n} = S_v(\mathbf{r}_v^{\mathrm{in},n}) + b_v^n, && v \in \mathcal{V} \setminus (\mathcal{V}_\ell \cup \mathcal{V}_c),\\ & \mathcal{N}_v(\mathbf{r}_v^{\mathrm{in},n}, \mathbf{r}_v^{\mathrm{out},n}, u_v^n) = 0, && v \in \mathcal{V}_c,\\ & r_{e(v),v}^{\mathrm{in},n} = h_v(u_v^n), && v \in \mathcal{V}_\ell. \end{aligned} \tag{IC$_n^{\mathrm{semi}}$}$$

Here $A(\cdot)$ is the edgewise transport operator, and $\mathcal{N}_v(\cdot)$ denotes the nonlinear junction law at a controlled node $v \in \mathcal{V}_c$ (for example, a compressor or valve model). Problem

($\mathrm{IC}_n^{\mathrm{semi}}$) represents the instantaneous, time-slab–local optimal control problem obtained after implicit Euler time discretization, while keeping the spatial structure of the graph continuous.

Remark 6.3 The instantaneous problem ($\mathrm{IC}_n^{\mathrm{semi}}$) is the semi-discrete analogue of the continuous-time problem ($\mathrm{OCP}_{\mathrm{cts}}$) and directly parallels the fully discrete formulation (IC_n). Its advantage is that the forward operator $(R^n - R^{n-1})/\tau + A(R^n) - S(R^n) = 0$ can be solved by standard PDE tools, while the optimization acts only at the discrete time level. This problem is a spatially distributed MINLP if integer controls are present, in particular when a compressor is considered.

6.4.3 The Fully Discrete Problem

Consider one edge e with grid $x_i = i\Delta x_e$, $i = 0, \dots, M_e$. Denote $r_{e,i}^{\pm,n} \approx r_e^{\pm}(x_i, t^n)$. We use the upwind scheme. For $i = 1, \dots, M_e$ and $i = 0, \dots, M_e - 1$, respectively,

$$\frac{r_{e,i}^{+,n} - r_{e,i}^{+,n-1}}{\tau} + \lambda_e^{+}(R_{e,i}^n)\,\frac{r_{e,i}^{+,n} - r_{e,i-1}^{+,n}}{\Delta x_e} = S_e^{+}(R_{e,i}^n), \tag{6.7a}$$

$$\frac{r_{e,i}^{-,n} - r_{e,i}^{-,n-1}}{\tau} - \lambda_e^{-}(R_{e,i}^n)\,\frac{r_{e,i+1}^{-,n} - r_{e,i}^{-,n}}{\Delta x_e} = S_e^{-}(R_{e,i}^n), \tag{6.7b}$$

with inflow traces from the node solver or controls. The nodal conditions are as follows.

$$\begin{aligned} &\mathbf{r}_v^{\mathrm{out},n} = S_v(\mathbf{r}_v^{\mathrm{in},n}) + b_v^n, && v \in \mathcal{V} \setminus (\mathcal{V}_\ell \cup \mathcal{V}_c),\\ &\mathcal{N}_v(\mathbf{r}_v^{\mathrm{in},n}, \mathbf{r}_v^{\mathrm{out},n}, u_v^n) = 0, && v \in \mathcal{V}_c,\\ &r_{e(v),v}^{\mathrm{in},n} = h_v(u_v^n), && v \in \mathcal{V}_\ell. \end{aligned} \tag{BE-NODE/BC}$$

Stacking yields the nonlinear residual $F(R^n, u^n; R^{n-1}) = 0$. With cell weights $w_{e,i} \approx \Delta x_e$ and (p, q) reconstructed from (r^+, r^-),

$$L^n(R^n, u^n) \coloneqq \sum_e \sum_i w_{e,i}\left[\frac{\omega_q}{2}(q_{e,i}^n - \bar{q}_{e,i}^n)^2 + \frac{\omega_p}{2}(p_{e,i}^n - \bar{p}_{e,i}^n)^2\right] + \sum_{v \in \mathcal{V}_\ell \cup \mathcal{V}_c} \frac{\beta_v}{2}(u_v^n)^2.$$

$$\begin{aligned} \min_{\{u^n\}} \quad & J_\tau = \sum_{n=1}^{N} \tau\, L^n(R^n, u^n) \\ \text{s.t.} \quad & F(R^n, u^n; R^{n-1}) = 0, \quad n = 1, \dots, N, \quad R^0 \text{ given.} \end{aligned} \tag{$\mathrm{OCP}_{\mathrm{BE}}$}$$

Let $J_R^n \coloneqq \partial_R F(R^n, u^n; R^{n-1})$ and $J_{R,+}^n \coloneqq \partial_{R^n} F(R^{n+1}, u^{n+1}; R^n)$. The discrete adjoint is

$$(J_R^n)^\top \Lambda^n = -\tau\, \partial_R L^n(R^n, u^n) \;+\; (J_{R,+}^n)^\top \Lambda^{n+1}, \qquad \Lambda^{N+1} = 0. \tag{6.8}$$

Reduced control gradients:

$$\nabla_{u_v^n} J_\tau = \begin{cases} \tau\,\beta_v\,u_v^n - \tau\,(h_v'(u_v^n))^\top \mu_v^n, & \text{if } v \in \mathcal{V}_\ell, \\ \tau\,\beta_v\,u_v^n + \tau\,(\partial_u \mathcal{N}_v)^\top \eta_v^n, & \text{if } v \in \mathcal{V}_c. \end{cases}$$

Dropping the time sum yields, at step n, the fully discrete instantaneous optimal control problem reads:

$$\min_{u^n, R^n} \quad \tau\, L^n(R^n, u^n) \quad \text{s.t.} \quad F(R^n, u^n; R^{n-1}) = 0. \tag{IC$_n$}$$

Adjoint for the single step:

$$(J_R^n)^\top \Lambda^n = -\tau\,\partial_R L^n(R^n, u^n), \qquad \nabla_{u_v^n}(\tau L^n) = \begin{cases} \tau\,\beta_v\,u_v^n - \tau\,(h_v'(u_v^n))^\top \mu_v^n, & \text{if } v \in \mathcal{V}_\ell, \\ \tau\,\beta_v\,u_v^n + \tau\,(\partial_u \mathcal{N}_v)^\top \eta_v^n, & \text{if } v \in \mathcal{V}_c. \end{cases}$$

Remark 6.4 Problem IC$_n$ is now a finite-dimensional optimization problem containing control variables that may be integer-valued or continuous. Thus, at this fully discretized level, problem IC$_n$ is a standard MINLP.

6.4.4 Time-Domain Decomposition

As discussed in the introduction, it is often advantageous—especially for large simulation horizons or parallel-in-time implementations—to decompose the optimal control problem (OCP$_{\text{cts}}$) in the *time domain*. In our particular context, the instantaneous control strategy has proved useful. However, for large time horizons, as in gas networks, one may need a large number of time iterations. Therefore, the idea is to reduce time horizons on the continuous level to small time slabs. This is the subject of time-domain decomposition (TDD). Once achieved, we have an outer iteration with respect to TDD; within such an iteration, we may adopt an instantaneous optimization scheme (IC$_n^{\text{semi}}$). In the following, we sketch such a time-domain decomposition in the framework of Riemann invariants, and show how the characteristic structure provides natural *transmission conditions in time* analogous to the spatial scheme. For a more detailed treatment, we refer to the chapter on domain decomposition.

Remark 6.5 We notice that the TDDM described below does not depend on the nonlinear nodal controls as far as the time interface iterations are concerned. Therefore, for sake of simplicity, we do not explicitly consider non-linear nodal controls here.

Recall that $T > 0$ is the control horizon and let $0 = T_0 < T_1 < \cdots < T_J = T$ be a partition of the time axis into subintervals $I_m := (T_{m-1}, T_m)$. We aim to decompose the overall optimal control problem in time so that each subinterval I_j becomes a *temporal subproblem* with local state and adjoint variables, coupled by transmission (matching) conditions at the *time interfaces* $t = T_m$.

Given the interface (characteristic/Robin) data from iteration k, $\phi_{m,m-1}^k$ and $\phi_{m,m+1}^k$, the *local* problem on the time slab I_m consists of the coupled forward–adjoint optimality system in *Riemann variables*, with controls restricted to I_m and with *mixed temporal*

conditions imposed at $t = T_{m-1}$ and $t = T_m$. We define the forward Riemann invariants $R_{m,e}(t,x) = (r^+_{m,e}(t,x),\ r^-_{m,e}(t,x))^\top$ and the adjoint Riemann invariants on each edge e: $P_{m,e}(t,x) = (\pi^+_{m,e}(t,x),\ \pi^-_{m,e}(t,x))^\top$. The leaf (flux) controls on the slabs are: $u_m(t) = \{u_{m,v}(t)\}_{v\in\mathcal{V}_\ell}$.

For each edge $e \in \mathcal{E}$ and $t \in (T_{m-1}, T_m)$, $x \in (0, L_e)$, the forward state evolves according to

$$\partial_t r^+_{m,e} + \lambda^+_e(R_{m,e})\,\partial_x r^+_{m,e} = S^+_e(R_{m,e}),\ \partial_t r^-_{m,e} - \lambda^-_e(R_{m,e})\,\partial_x r^-_{m,e} = S^-_e(R_{m,e}), \quad (6.9)$$

with spatial *interior-node* coupling (pressure continuity + mass conservation) written in the scattering form at each $v \in \mathcal{V} \setminus \mathcal{V}_\ell$:

$$\mathbf{r}^{\text{out}}_{m,v}(t) = S_v\,\mathbf{r}^{\text{in}}_{m,v}(t) + b_v\,s_v(t). \quad (6.10)$$

At leaf nodes $v \in \mathcal{V}_\ell$, the controlled incoming characteristic is imposed:

$$r^{\text{in}}_{m,e(v),v}(t) = u_{m,v}(t). \quad (6.11)$$

Correspondingly, for the adjoint state, let $\ell(R,u)$ denote the running cost density (edge-wise space integral of tracking terms) and recall $(p,q) = \Psi(R)$. The adjoint (backward in time) is, for each edge e,

$$\begin{aligned} -\partial_t \pi^+_{m,e} - \partial_x(\lambda^+_e(R_{m,e})\,\pi^+_{m,e}) &= [\partial_{r^+}\ell](R_m,u_m)\ +\ C^+_e(R_m,P_m),\\ -\partial_t \pi^-_{m,e} + \partial_x(\lambda^-_e(R_{m,e})\,\pi^-_{m,e}) &= [\partial_{r^-}\ell](R_m,u_m)\ +\ C^-_e(R_m,P_m), \end{aligned} \quad (6.12)$$

where $C^\pm$ collects semilinear terms from differentiating the sources and the node couplings.[1] At interior nodes v the adjoint satisfies the *transpose* scattering condition,

$$\mathbf{ß}^{\text{in}}_{m,v}(t) = S_v^\top\,\mathbf{ß}^{\text{out}}_{m,v}(t), \quad (6.13)$$

and at controlled leaves one gets the usual boundary multipliers yielding the control gradient (see below). Let y_m and p_m denote the chosen primitive forward/adjoint quantities at the time interfaces, reconstructed linearly from the forward/adjoint Riemann variables by

$$y_m = C_y R_m, \quad p_m = C_p P_m \quad \text{(acting pointwise on the edge traces at } t = T_{m-1}, T_m).$$

Given impedance parameter $\beta > 0$, the *Robin/characteristic* conditions to be enforced at iteration $k+1$ are

$$\begin{aligned} (C_y R_m - \beta\, C_p P_m)(T_{m-1}) &= \phi^k_{m,m-1},\\ (C_y R_m + \beta\, C_p P_m)(T_m) &= \phi^k_{m,m+1}. \end{aligned} \quad (6.14)$$

These two algebraic constraints *close* the coupled forward–adjoint two-point (in time) boundary-value problem on I_m. This is essentially the method explored in [22, 23].

[1] Concretely, $C^\pm$ contains $(\partial_R S)^\top P$ contributions and transpose scattering blocks at interior nodes.

6.4.5 Spatial Domain Decomposition of the Instantaneous Problem

We elaborate the single-time-level decomposition of (IC_n) *using the explicit scattering matrix* S_γ at each interface node γ, and we clarify the connection with the "rotated variables" (characteristic) scheme in the spirit of Lions' optimized Schwarz alternating domain decomposition. To this end, let Γ be the set of interface nodes shared by at least two subdomains. Fix $\gamma \in \Gamma$ and enumerate the incident edges across *all* neighboring subdomains as

$$\mathcal{E}_\gamma = \{e_1, \dots, e_{d_\gamma}\}, \qquad d_\gamma := \deg(\gamma).$$

For each incident edge e_j let $Z_{e_j} > 0$ be its impedance. Stack the *incoming* and *outgoing* Riemann traces at time t^n as

$$r_\gamma^{\mathrm{in},n} := \begin{bmatrix} r_{e_1,\gamma}^{\mathrm{in},n} \\ \vdots \\ r_{e_{d_\gamma},\gamma}^{\mathrm{in},n} \end{bmatrix} \in \mathbb{R}^{d_\gamma}, \qquad r_\gamma^{\mathrm{out},n} := \begin{bmatrix} r_{e_1,\gamma}^{\mathrm{out},n} \\ \vdots \\ r_{e_{d_\gamma},\gamma}^{\mathrm{out},n} \end{bmatrix} \in \mathbb{R}^{d_\gamma}.$$

Let $z_\gamma := (Z_{e_1}, \dots, Z_{e_{d_\gamma}})^\top$ and $\Sigma_{Z,\gamma} := \sum_{j=1}^{d_\gamma} Z_{e_j}$. The *node scattering law* (pressure continuity + mass conservation) reads

$$r_\gamma^{\mathrm{out},n} = S_\gamma\, r_\gamma^{\mathrm{in},n} + b_\gamma\, s_\gamma^n, \quad S_\gamma = I - \frac{2}{\Sigma_{Z,\gamma}} \operatorname{diag}(z_\gamma)\, \mathbb{1}\mathbb{1}^\top, \quad b_\gamma = \frac{2}{\Sigma_{Z,\gamma}} z_\gamma, \tag{6.15}$$

where $\mathbb{1} = (1, \dots, 1)^\top$. Let $\mathcal{G} = \bigcup_{k=1}^K \mathcal{G}_k$ be an edge-disjoint partition. For a fixed γ, denote by $\mathcal{E}_{k,\gamma} \subset \mathcal{E}_\gamma$ the set of edges of subdomain $\mathcal{G}_k$ meeting at γ, and define the *selection matrix* $\Pi_{k,\gamma} \in \{0,1\}^{|\mathcal{E}_{k,\gamma}| \times d_\gamma}$ that extracts the components belonging to $\mathcal{E}_{k,\gamma}$. We use the *subdomain incoming* vector $\Xi_{k,\gamma}^n := \Pi_{k,\gamma}\, r_\gamma^{\mathrm{in},n}$ as the interface primal unknown for $\mathcal{G}_k$, and we denote by

$$\mathsf{N}_{k,\gamma} : \Xi_{k,\gamma}^n \longmapsto \mathcal{T}_{k,\gamma}(\mathcal{S}_k(\{\Xi_{\ell,\gamma}^n\}_\ell, u_k^n; R_k^{n-1}))$$

the (generally nonlinear) *Dirichlet-to-Neumann* map returning the *outgoing* characteristics belonging to $\mathcal{G}_k$ at γ once the subdomain forward problem has been solved.

The physical requirement is that the outgoing traces produced by each subdomain *match* the outgoing traces dictated by the scattering of the *global* incoming vector $r_\gamma^{\mathrm{in},n}$. Using (6.15), this yields the *Schur* residual

$$\mathcal{R}_\gamma(\{\Xi_{k,\gamma}^n\}) := \begin{bmatrix} \Pi_{1,\gamma} \\ \vdots \\ \Pi_{m_\gamma,\gamma} \end{bmatrix} \left(S_\gamma\, r_\gamma^{\mathrm{in},n} + b_\gamma\, s_\gamma^n \right) - \begin{bmatrix} \mathsf{N}_{1,\gamma}(\Xi_{1,\gamma}^n) \\ \vdots \\ \mathsf{N}_{m_\gamma,\gamma}(\Xi_{m_\gamma,\gamma}^n) \end{bmatrix} = 0, \tag{6.16}$$

$$r_\gamma^{\mathrm{in},n} \equiv \sum_{k:\gamma\in\mathcal{V}_k} \Pi_{k,\gamma}^\top\, \Xi_{k,\gamma}^n. \tag{6.17}$$

Here m_γ is the number of subdomains touching γ. Equation (6.17) *uses* S_γ *explicitly*: the nonlinearity and heterogeneity (friction, varying $\lambda^\pm$) are confined to the subdomain

DtN maps $\mathsf{N}_{k,\gamma}$, while the cross-subdomain algebraic coupling is an explicit sparse linear map built from S_γ, $\Pi_{k,\gamma}$, b_γ.

Remark 6.6 (Two-subdomain interface ($m_\gamma = 2$)) If exactly two subdomains meet at γ, write $r_\gamma^{\text{in}} = \Pi_{1,\gamma}^\top \Xi_{1,\gamma} + \Pi_{2,\gamma}^\top \Xi_{2,\gamma}$. The residual (6.17) becomes

$$\begin{cases} \mathsf{N}_{1,\gamma}(\Xi_{1,\gamma}) = \Pi_{1,\gamma}\, S_\gamma(\Pi_{1,\gamma}^\top \Xi_{1,\gamma} + \Pi_{2,\gamma}^\top \Xi_{2,\gamma}) + \Pi_{1,\gamma} b_\gamma\, s_\gamma, \\ \mathsf{N}_{2,\gamma}(\Xi_{2,\gamma}) = \Pi_{2,\gamma}\, S_\gamma(\Pi_{1,\gamma}^\top \Xi_{1,\gamma} + \Pi_{2,\gamma}^\top \Xi_{2,\gamma}) + \Pi_{2,\gamma} b_\gamma\, s_\gamma, \end{cases}$$

which is a compact fixed-point system in the incoming traces $(\Xi_{1,\gamma}, \Xi_{2,\gamma})$.

6.4.6 Decomposed Instantaneous OCP in Primal Schur Form

Restrict the running cost to each subdomain, $L_k^n(R_k^n, u_k^n)$. Eliminating interior states by the subdomain solvers $R_k^n = \mathcal{S}_k(\{\Xi_{\ell,\gamma}^n\}_\ell, u_k^n; R_k^{n-1})$ gives the interface-augmented problem

$$\begin{aligned} \min_{\{u_k^n\},\{\Xi_{k,\gamma}^n\}} \quad & \tau \sum_{k=1}^{K} L_k^n\Big(\mathcal{S}_k(\{\Xi_{\ell,\gamma}^n\}_\ell, u_k^n; R_k^{n-1}),\, u_k^n\Big) \\ \text{s.t.} \quad & \mathcal{R}_\gamma(\{\Xi_{k,\gamma}^n\}) = 0, \qquad \forall \gamma \in \Gamma, \end{aligned} \tag{6.18}$$

with $\mathcal{R}_\gamma$ given by (6.17). This formulation exposes (i) parallel subdomain solves for a given interface iterate and (ii) a small, explicit interface coupling driven by S_γ.

Because the forward interface operator is explicit in S_γ, the *adjoint* interface coupling uses $S_\gamma^\top$ (together with the transposes of the subdomain DtN derivatives). At γ the instantaneous adjoint residual reads

$$\bigoplus_{k:\gamma\in\mathcal{V}_k} \Lambda_{k,\gamma}^{\text{out}} \;-\; \begin{bmatrix} \Pi_{1,\gamma} \\ \vdots \\ \Pi_{m_\gamma,\gamma} \end{bmatrix} S_\gamma^\top \left(\sum_{k:\gamma\in\mathcal{V}_k} \Pi_{k,\gamma}^\top \Lambda_{k,\gamma}^{\text{in}} \right) \;=\; 0,$$

which is again a sparse, explicit interface map. As before, control gradients at leaves are unaffected by interior-interface multipliers unless a control acts directly at an interface node.

As for the controls, let $\mathcal{V}_c$ be the set of controlled junctions (with nonlinear node laws $\mathcal{N}_v = 0$) and $\mathcal{V}_\ell$ the leaves. When the domain is decomposed *only at free interior nodes*, define

$$\Gamma_{\text{free}} \;\coloneqq\; \{\gamma \in \mathcal{V} :\ \deg(\gamma) \geq 2\} \setminus (\mathcal{V}_c \cup \mathcal{V}_\ell).$$

All interface nodes are thus *uncontrolled*, and the explicit scattering (6.15) remains valid at every interface. Accordingly, in Sect. 6.4.5 replace Γ by Γ_{free} and keep the Schur residual (6.17) *as is*. Nonlinear node controls $\mathcal{N}_v$ then appear *only inside* subdomain solvers $\mathcal{S}_k(\cdot)$ and their DtN maps $\mathsf{N}_{k,\gamma}$, i.e., they affect the *local* forward residuals/Jacobians but not the *interface* algebra.

Remark 6.7 With the space-time domain decomposition method outlined above we are now able to decompose the overall continuous (in space and time) optimal control problem on the entire graph ($\mathrm{OCP}_{\mathrm{cts}}$) into possibly small space-time containers, where each such container includes the dynamics of a sub-graph over a small time horizon (time slab). In fact, we can go down to a single edge at the cost of many outer iterations. We can also even reduce the time interval to a single time cap using the rolling horizon principle. Thus, we may—in adaptive way—reduce the MINLP-problems to a size that allows the application of the corresponding MINLP-routines which, in turn, are not available on the time continuous PDE-level. This process can be made truly adaptive, once a posteriori error estimates (which we do not display here) are implemented in order to decide on the size of the containers; see, e.g., [13, 17, 22–24, 26].

6.4.7 Maximizing the Storage Capacity of Gas Networks

In this section, we summarize the approach in [5] for the global optimization of transient gas transport networks with a focus on maximizing their storage capacity. This problem is of particular importance in the context of Power-to-Gas, where renewable energy is converted into gas, which is temporarily stored in the network. Due to the dynamic nature of storing additional gas over a limited period of time, a transient model of gas physics is required, which substantially increases both the mathematical and computational complexity.

The approach follows a first-discretize-then-optimize methodology. Starting from the isothermal Euler equations, combined with algebraic models for valves and compressors, we introduce a new discretization of the resulting nonlinear and parabolic PDE system. The scheme employs a finite-volume formulation on staggered grids for spatial discretization together with an implicit Euler method for time discretization. In [5], well-posedness of the fully discretized model is proven and it is shown that each time step can be formulated as a convex minimization problem, which ensures existence and uniqueness of solutions. This provides a rigorous foundation for the subsequent optimization.

The Time-Expanded Graph A key observation is that the discretization produces a system in which all quantities change only at discrete time points. This allows for a natural representation via a time-expanded graph: the gas network $\mathcal{G} = (\mathcal{V}, \mathcal{A})$ is copied for each discrete time step $n \in [N] := \{1, \ldots, N\}$, and for every vertex $v \in \mathcal{V}$, a temporal arc (v_n, v_{n+1}) connects the copy at time step n to the one at time step $n+1$; see Fig. 6.2. The flow $q_{(v_n, v_{n+1})}$ along these temporal arcs encodes the amount of gas stored in the control volume surrounding each vertex.

This viewpoint reveals a crucial structural property: within each time layer, the constraints have precisely the structure of a stationary gas transport model, as discussed in Sect. 6.3. The only coupling between consecutive time steps is provided by the temporal arcs. Since methods for the global optimization of stationary gas networks are already well-established [6, 8], we can leverage these techniques and extend them to the transient setting via the time-expanded graph.

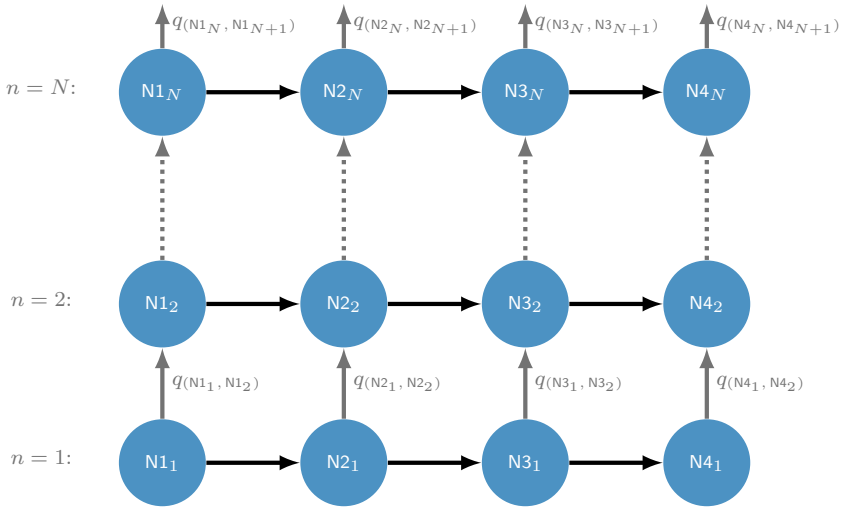


Fig. 6.2: Time-expanded graph of a gas network with four vertices and three pipes. Each copy of a vertex is connected to the next by a temporal arc (gray), representing the gas stored in the corresponding control volume.

Concretely, mass conservation at each vertex v and time step n now reads

$$q_{(v_n,v_{n+1})} + \sum_{a\in\delta^+(v)} q_{a,n} - \sum_{a\in\delta^-(v)} q_{a,n} = q_{(v_{n-1},v_n)} + d_{v,n},$$

where $d_{v,n}$ is the supply or demand at v. The pressure loss per time step takes the same form as the stationary Weymouth equation (6.2), and the temporal arc flows are linked to the pressures by $q_{(v_n,v_{n+1})} = (\alpha_v/c^2)\, p_{v,n}$, where α_v depends on the geometry of the control volume. Valves and compressors are modeled as in Sect. 6.3 via binary variables $s_{a,n} \in \{0,1\}$ and big-M constraints for each time step n, with additional switching constraints ensuring that each active element remains in its new state for a minimum number of time steps after any change of status.

The MINLP Formulation Let a base nomination d be given for all boundary vertices and time steps, and suppose that a feasible stationary solution for the initial time step is available. Within prescribed time windows, an amount of gas $q^{\text{add}}_{v,n} \geq 0$ can be injected at selected entries $\mathcal{V}_s$ additionally and must be withdrawn at selected exits $\mathcal{V}_t$, subject to the balance condition $\sum_{v\in\mathcal{V}_s,n} q^{\text{add}}_{v,n} = \sum_{v\in\mathcal{V}_t,n} q^{\text{add}}_{v,n}$, i.e., the sum of additional injected gas equals the withdrawn one. The objective constitutes of storing the maximal amount of gas over time. To favor solutions with minimal compressor usage, we include a small energy penalty with parameters $\gamma_1, \gamma_2 > 0$. The complete storage capacity maximization problem reads:

$$\max \quad \sum_{\substack{v\in\mathcal{V}_s,\\ n\in[N]}} q^{\text{add}}_{v,n} \; - \sum_{\substack{a\in\mathcal{A}_{\text{comp}},\\ n\in[N]}} \gamma_1\,\Delta p_{a,n} + \gamma_2\,|\Delta p_{a,n} - \Delta p_{a,n-1}|$$

$$\text{s.t.} \quad \text{mass conservation, pipe model, valve, compressor, switching,}$$

$$\underline{p}_{v,n} \le p_{v,n} \le \overline{p}_{v,n}, \quad \underline{q}_{a,n} \le q_{a,n} \le \overline{q}_{a,n}, \quad s_{a,n} \in \{0,1\},$$

$$\underline{q}^{\text{add}}_{v,n} \le q^{\text{add}}_{v,n} \le \overline{q}^{\text{add}}_{v,n} \qquad \text{for all } v \in \mathcal{V}_s \cup \mathcal{V}_t,\ n \in [N],$$

where $\Delta p_{a,n} \coloneqq p_{v_2(a),n} - p_{v_1(a),n}$. The only source of nonconvexity is the pressure loss equation, whose nonlinear terms are univariate and therefore particularly amenable to piecewise linear relaxation. Building on this, [5] extends the MIP relaxation-based approach of [6] to the transient setting, iteratively refining mixed-integer linear relaxations until a globally optimal or near-optimal solution is certified. Case studies on the GasLib-11 network demonstrate that the method delivers solutions within almost 5 % of global optimality in under three hours, significantly outperforming general-purpose MINLP solvers such as Baron and Scip, which achieve gaps of 89 % and 109 %, respectively, within a four-hour time limit.

6.5 Topology Optimization

A particularly important application of MINLPs is topology optimization, which is highly relevant in practice for the design of utility or energy networks. The use of MINLPs in this context is rather natural. On the one hand, utility networks involve the transport of fluids governed by nonlinear physical laws. On the other hand, MINLPs provide a modeling framework capable of accurately representing such physical constraints. Moreover, many design and operational decisions, such as building a new pipe or operating a compressor in gas networks, contain discrete decisions. Consequently, topology optimization problems are often formulated as MINLPs.

Overall, a wide variety of explicit MINLP formulations have been developed for different tasks in topology optimization with applications in gas [2, 29, 42], electricity [20], or water networks [3, 4]. For instance, existing models address tasks such as designing a network from scratch [29, 45], reinforcing existing networks [1], or determining specific network configurations, such as in the diameter selection problem for a given network topology [37, 44]. Using state-of-art MINLP techniques and solvers, it is currently possible to solve topology design problems for real-world based small- to medium-sized gas networks (up to about 40 nodes and arcs) and to obtain feasible solutions for larger instances, such as the GasLib-582 network with hundreds of nodes and pipes; see [29]. Providing a comprehensive overview on topology optimization is beyond the scope of this chapter. Instead, we refer to Chap. 7, “Potential-Based Flows – An Overview”, which includes an in-depth overview of topology optimization for potential-based flows. The potential-based flow framework serves as a general modeling approach that encompasses gas, water, and power networks under the lossless DC power flow model and typically results in challenging MINLPs.

6.6 Lipschitz-Based Solution Approaches

In this section we consider the abstract problem

$$\min_{x,y} \quad c(x) \tag{6.20}$$

$$\text{s.t.} \quad f(x) \sim y, \tag{6.21}$$

$$x \in X,\ y \in Y, \tag{6.22}$$

where $\sim \in \{\leq, =\}$. The sets X and Y collect classic constraints on the variables x and y, e.g., integrality or linear constraints. In contrast, function f together with the operator $\sim$ and the right-hand side y represent the challenging part of the problem, which requires special treatment. The problem is to be solved to approximate global optimality, implying that a solution is a global one and satisfies constraint (6.21) up to a predefined accuracy $\varepsilon > 0$ and a certain norm.

In terms of gas network optimization problems, f can, for instance, be a solution operator to the differential equation that maps boundary conditions to a solution. Alternatively, recent work in the area of machine learning (ML) advertises the use of neural networks (NNs) to mimic physical interrelations [35]. This promotes the idea to train an NN, say f, and incorporate it as a constraint in the optimization problem, posing constraints like (6.21).

In both cases, f is highly nonlinear and often not known in closed form. This advises against a direct use of f but to consider the respective constraint as some special type of black-box constraint. Often, there exist ways to compute Lipschitz constants for solution operators of differential equations. In addition, the articles [7,34] demonstrate a convenient way to compute Lipschitz constants for certain types of NNs. This motivates to treat f as a black-box Lipschitz function and to develop methods to tackle the resulting optimization problems. For instance, a respective handling for the case of an NN has already been applied in the field of bilevel optimization, where the NN is trained to predict the solutions of the lower level [33].

In the following, the particular form of f, the constraint (6.21), and the "manageable" sets X and Y differ between each method described and will be clarified case-by-case.

6.6.1 The Univariate and Monotone Case

By relying on (sub/super-)gradients, [14] provides a first step in the direction of handling black-box constraints as described above. The authors assume that the underlying MINLP is presented as an mixed-integer linear problem subject to nonlinear equality constraints on the continuous part of the variables. Specifically, any involved nonlinear function f is assumed to be univariate, monotonic, and strictly convex or concave, posing a constraint of the form $f(x) = y$.

The proposed algorithm to tackle this type of problem iteratively solves a *master problem*, which constitutes a relaxation of the original problem, and a *subproblem*, whose outcome provides a refinement of the former. The initial master problem is

obtained by mainly resorting to the mixed-integer linear part, i.e., by relaxing the nonlinear constraints. After solving the master problem in iteration k, the respective solution (x^k, y^k) is checked to fulfill a prescribed accuracy of the constraint violation $|f(x^k) - y^k|$. If the required accuracy is exceeded, the solution is directed to the subproblem.

Here, for every nonlinear constraint function f, the closest point in iteration k on the graph $\mathrm{gr}(f)$ of f with respect to the current solution (x^k, y^k) is computed. Specifically, the corresponding subproblem is given by

$$\min_{x,y} \left\{ \|(x, y) - (x^k, y^k)\|_2^2 \,:\, f(x) = y,\, x \in X,\, y \in Y \right\}.$$

This procedure is illustrated in Fig. 6.3, where the closest point on $\mathrm{gr}(f)$ is $(\tilde{x}^k, \tilde{y}^k)$. Together with using (sub/super-)gradients, this allows to construct a piecewise linear relaxation of $\mathrm{gr}(f)$ by a combination of the incremental method [31] and linear outer approximations. In Fig. 6.3, the resulting relaxation after such a refinement is highlighted in darker color than before.

After the refinement step, the relaxation to be used in the next master problem is refined and the current solution is cut off. In particular, the master problem uses unions of polyhedra to describe the relaxation of the graph of the nonlinear function. The method is shown to be correct and to terminate after a finite number of iterations for a prescribed $\varepsilon > 0$.

The described method is applied to gas network optimization instances. In particular, it is used to solve the stationary model as described in Sect. 6.3 for the GasLib-135 instance from [39]. For the nominations, over a thousand different days, i.e., scenarios, are considered, from which $\approx 58\,\%$ are solved to global optimality and the remaining ones are proven to be infeasible.

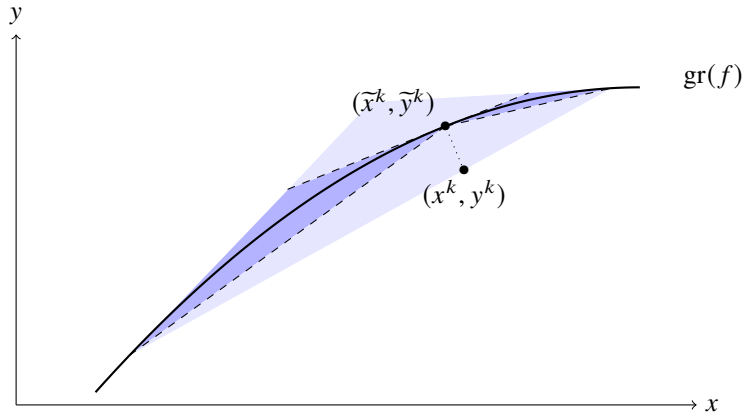


Fig. 6.3: Original approximation of $\mathrm{gr}(f)$ and refinement based on subgradients; adjusted from [14].

6.6.2 The Univariate Lipschitz Case

The work described above paved the way for the succeeding article [40]. The key differences between [14] and [40] are as follows. First, [40] does not rely on monotonicity or convexity/concavity assumptions regarding the constraint function f. Second, the method leverages Lipschitz constants instead to compute a polyhedral outer approximation of the function's graph. Since under practical circumstances, a global Lipschitz constant may be unknown or function evaluations may be inexact, the authors also consider these cases and analyze the respective implications for their approach.

The approach proposed in [40] also follows the idea of splitting the original problem into a mixed-integer linear master problem and several subproblems. In each iteration k, the approach considers a given solution (x^k, y^k) to the master problem and an existing union of polyhedra yielding a relaxation Ω^k of the graph of a constraint function f, where the relaxation may be initialized by considering the bounds of the function domain and estimations of its minimum/maximum. The master problem in the kth iteration can generally be posed as

$$\begin{aligned} \min \quad & c(x) \\ \text{s.t.} \quad & (x, y) \in \Omega^k, \\ & x \in X,\ y \in Y. \end{aligned}$$

Assuming exactness of the involved Lipschitz constant and the evaluation of f, the nearest point $(\tilde{x}^k, \tilde{y}^k) \in \operatorname{gr}(f)$ is again computed in a subproblem. Exploiting the global Lipschitz constant at the newly computed feasible point then allows to tighten the relaxation Ω^{k+1} of $\operatorname{gr}(f)$ for the next master problem; see Fig. 6.4. As before, the relaxation is given as a union of polyhedra.

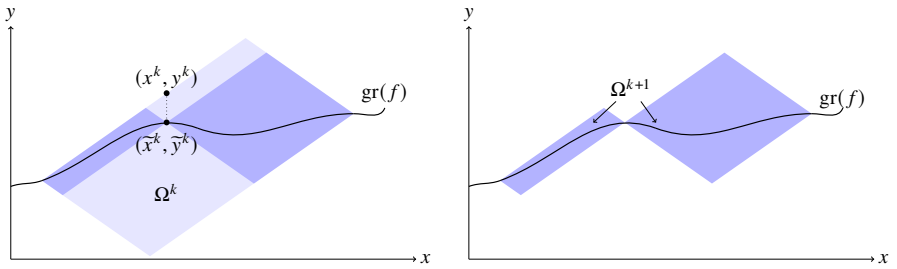


Fig. 6.4: Original linearization Ω^k with refinement based on nearest point and resulting non-overlapping master problem with exact computations; adjusted from [40].

The situation differs, however, when considering inexactness of the respective function evaluations, where the inaccuracy is bounded by $\varepsilon^f > 0$. The overall scheme leads to less tight relaxations as shown in Fig. 6.5. This alters the termination analysis, but eventually again allows to prove its finiteness.

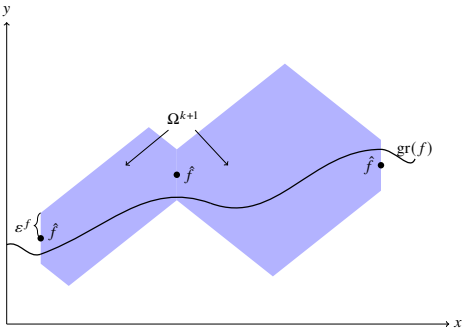


Fig. 6.5: Overlapping master problems based on approximate computations; adjusted from [40].

For the case of unknown global Lipschitz constants, the authors resort to local ones. Since the range of potential local Lipschitz constants is typically unknown, the proposed approach may construct an approximation of the graph that is not a relaxation anymore. For handling such situations, the authors introduce the concept of *potential infeasibility* of the original problem. For the technical details, we refer the interested reader to the paper.

As above, the method is applied to stationary gas network problems (see Sect. 6.3) and tested for the GasLib-135 instance from [39] for the network topology. An interesting insight is that a larger ε^f hinders the detection of infeasibility and leads to larger master problems according to an increase in the number of necessary refinements.

6.6.3 The Multivariate Lipschitz Case

As a natural next step, the techniques presented in [12] generalize the techniques introduced above and extend it to multivariate constraint functions. Based on box partitions of the function's domain, the authors leverage the Lipschitz property to derive a successively tightened outer approximations of the function's graph. In computational experiments the importance of a tight Lipschitz constant with respect to the computational efficacy are highlighted.

After retrieving a solution to the current master problem, the relaxation is tightened for constraints that exceed a certain tolerance with respect to the solution. Thereby, a refinement of the master problem is conducted based, again, on solutions of appropriately chosen subproblems. Correctness of the resulting algorithmic scheme is shown and an upper bound on the maximal number of iterations is derived. This bound is of the order $O(L|X|/\varepsilon)$, where L is the Lipschitz constant, $|X|$ is a proxy for the "size" of the function's domain, and $\varepsilon > 0$ is the desired accuracy. As applications, the article [12] features computational results for bilevel optimization and gas network optimization problems.

6.6.4 The Multivariate and Implicit Case

The same group of authors as in [40] also presents an outer approximation approach for a similar setting in [41], featuring multivariate constraint functions. Opposed to before, they assume implicitly given equality constraints in the form $f(x_1, x_2) = 0$ that cannot be solved for x_2 analytically. Instead of refining an outer approximation of the graph of f as before, the method iteratively excludes infeasible regions and, by doing so, achieves a good approximation of feasible points in the end. The method again requires knowledge of exact global Lipschitz constants.

First, a master problem is solved, which is again initialized by relaxing the nonlinear constraints. In every subsequent iteration, as long as the solution to the current master problem does not fulfill a certain accuracy with respect to the nonlinear constraints, a tightening step is performed. Specifically, this step adds a constraint to the master problem that bounds the distance of the variable to the current solution in terms of the infinity norm from below. This bound constitutes the absolute value of the function evaluation at the current solution divided by the Lipschitz constant. Intuitively, the incorporated constraint is equivalent to an exclusion of multidimensional boxes from the feasible region, which constitutes an inherently nonconvex operation. In order to circumvent solving such a nonconvex problem, the infinity norm term is remodeled by means of integer programming techniques, leading to a MIP master problem after all. Fig. 6.6 visualizes the domain of the current constraint function, where its zero set $\mathcal{D}$ is the bold curved line. The two boxes B_1 and B_2 centered at (x_1^1, x_2^1) and (x_1^2, x_2^2) are excluded from the feasible set of the next master problem to be solved.

Besides presenting the reformulation explicitly, the authors show the correctness of their approach and give a bound on the iteration complexity. This bound is similar to the one above in [12], and involves the size of the function's domain, the Lipschitz constant and the accuracy.

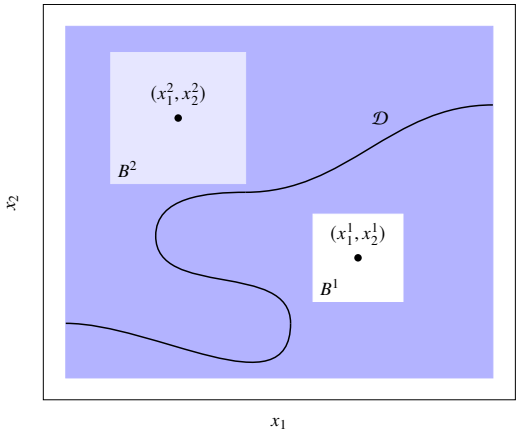


Fig. 6.6: Illustration of the feasible set of the master problem in [41] after two iterations

In terms of computations, the authors consider the small gas network instances GasLib-4, GasLib-4-Tree, GasLib-11, and GasLib-24 from [39] and tackle the stationary gas network control problem laid out in Sect. 6.3. It is highlighted that knowing global Lipschitz constants only in contrast to the algebraic expression is, as expected, increasing the cost of the solving process in terms of run time.

6.6.5 Generalized Approximation of Function Domain

The article [11] generalizes the previous approach in the sense that general fields and arbitrary monotonic norms are considered. As a result, the former reformulation technique is not applicable anymore in general. Hence, the resulting method only considers an iterative incorporation of the nonconvex constraints, which are coined as norm-induced cuts, into the original problem relaxation. Refer to Fig. 6.7 (left) for an illustrated example of the set $\mathcal{D} = \{(x_1, x_2) : f(x_1, x_2) \leq 0\}$ and the optimal solution (x_1^*, x_2^*) of the problem. In Fig. 6.7 (right) two norm-induced cuts with respect to the Euclidean norm are depicted in the same fashion as above. Here, only positivity of f at a given point is penalized. Note that instead of boxes, cuts featuring this type of norm include balls; compare above. Due to the consideration of a general norm the analysis with regard to convergence and computational complexity depends on the assumption of oracles to solve the refined master problems.

Since the character of the posed problems depends on the particular norm involved, the work also highlights respective pitfalls and discusses suitable solution strategies. This includes the mentioned reformulation technique for the infinity norm and analogously the 1-norm. By example it is also highlighted that a local oracle may lead to convergence to a feasible yet non-optimal point. This is complemented by a run-time comparison of the quality of global Lipschitz constants and their availability for a vector function and/or its components. As a key result, it depends on the quality of the Lipschitz constants whether one wants to use the Lipschitz constant for the entire vector or the component functions. If minimal Lipschitz constants are available for either, then a component-wise contemplation is favorable.

6.6.6 A-Priori Epigraph Approximations

All methods summarized in this section so far are adaptive ones, since a master problem is refined in every iteration. That is, an approximation of the original feasible set is tightened in every step of the method until a certain accuracy is reached. In contrast, [10] introduces a scheme to first compute an approximation of the feasible set, which is tight enough, and then advocates to solve this problem once.

The main part of this work thus is an approximation framework for the Lipschitz function, which can be multivariate. Inspired by the non-convex quadratic constraints, resulting from norm-induced cuts with respect to the Euclidean norm, it considers so-called *paraboloids*, i.e., polynomials of degree two with univariate quadratic terms

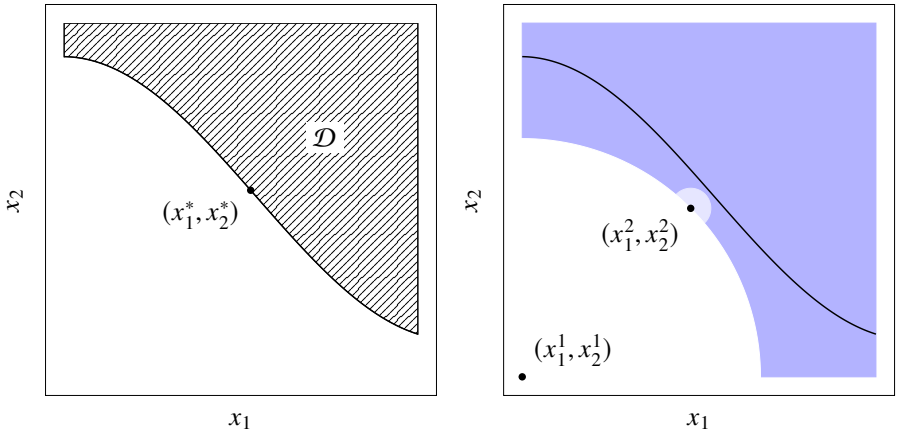


Fig. 6.7: Example of feasible region (hatched) with optimal solution and two norm-induced cuts with Euclidean norm; adjusted from [11].

only, as the approximating functions. For a fixed number of paraboloids, a MIP problem is proposed that includes the paraboloids' coefficients as its variables. The constraints of this MIP ensure the approximation property and are defined on grid points of the function domain. The width of such a grid depends on the global Lipschitz constant of the constraint function. In order to determine a low number of approximating paraboloids and, thus, a low number of constraints when applied to the original problem, a binary search is conducted, solving several such MIP problems.

For the sake of clarity, consider an inequality constraint $f(x_1, x_2) \leq y$ and an accuracy $\varepsilon > 0$. The procedure described above returns paraboloids

$$p^k(x_1, x_2) = a_1 x_1^2 + a_2 x_2^2 + b_1 x_1 + b_2 x_2 + c,$$

for $k = 1, \ldots, K$ such that

$$f(x_1, x_2) - \varepsilon \leq \max_k p^k(x_1, x_2) \leq f(x_1, x_2).$$

This allows to replace the original constraint by $p^k(x_1, x_2) \leq y$ for all k to retrieve a true relaxation of the original problem. Alternatively, one can incorporate these constraints to potentially strengthen the continuous relaxation of the problem.

In computational experiments on a set of MINLP problems, the relaxation and the strengthened formulations are solved with modern-day solvers. It is demonstrated that for coarse accuracies, the relaxations may be solved significantly faster, which advertises its usage for computing starting points. Further, a solution of the strengthened formulations appears to be beneficial when tackling problems with trigonometric functions, e.g., sin or cos, in the constraints, since their solution times decrease significantly on average.

Note that an incorporation of the parabolic constraints does not require big-M methods to determine a currently active parabolic one. Instead, the constraints can be con-

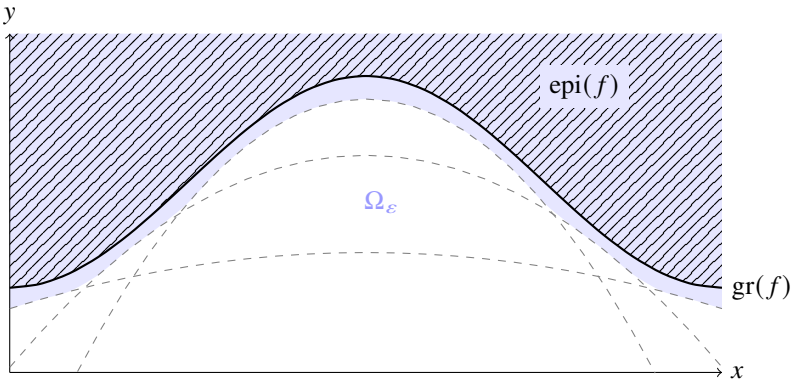


Fig. 6.8: Epigraph approximation of sin on $[-\pi/2, 3\pi/2]$ from below by 3 paraboloids; inspired by [10].

sidered simultaneously as-is. This is due to the fact that the paraboloids represent an *epigraph* or *one-sided approximation* of f. Such a property is based on the MIP problem forcing paraboloids to represent a one-sided approximation. That is, the set of all paraboloids is an approximation of the constraint function's epi-/hypograph. In Fig. 6.8 the approximation of the epigraph of f, short epi(f), is visualized. The feasible set epi(f) is given in hatched, the paraboloids in dashed lines and the corresponding approximation Ω_ε with respect to accuracy $\varepsilon > 0$ in color.

6.6.7 A Step Towards the Complexity of Resulting Subproblems

All methods laid out in the current section require the solution of certain manipulated problems. Whereas the question about computational complexity in case of MIP problems is well-investigated, especially the last two approaches introduce problems which are inherently non-convex and not in the MIP realm. In abstract terms, they require to solve an integer problem on a polyhedral domain (typically bounds) from which other convex sets are excluded. The article [18] tries to give an answer on the resulting computational complexity.

The key ingredient is an assumption on the excluded convex sets to have a *boundary hyperplane cover*. That is, one is faced with a set of hyperplanes covering the intersections of the boundaries of the excluded convex sets. Then, [18] shows that solving such a problem can be conducted in oracle polynomial time, keeping the dimension fixed. A similar result is known, for instance, for MIP as well. In other terms, this implies a certain equivalence of the hardness between solving mixed-integer linear and solving the posed integer programs.

In summary, there exist several practical and theoretical contributions that analyze the incorporation of Lipschitz constraints into (mixed-)integer problems. Combined

with the advances to simulate physical dynamics by means of Lipschitz functions, e.g., certain NNs, this provides the ground work to couple the areas of ML and optimization, especially in the context of gas network control. In the future, such coupling could enable to tackle large-scale problems, where approaches from a single area either struggle to even compute solutions or simply produce inaccurate results.

6.7 Outlook

When looking back at the topics covered in this chapter, one can identify the following challenges for the future. The performance of the methods for stationary gas transport (Sect. 6.3) is quite satisfactory from a practical viewpoint. Large-scale, but maybe not the largest available, instances can be solved to global optimality, even with very accurate ODE models. However, the compressor models are often idealistic, which opens potential for future research. In contrast, transient, i.e., time-dependent, problems are generally *much* harder to solve. This motivates the decomposition and discretization methods of Sect. 6.4. In this context, any significant progress on solving transient problems to global optimality would be an important achievement.

Topology optimization problems are somewhat between the previous two settings. One can solve small-sized instances and improvements in the future might enable the solution of practically more interesting sizes. Moreover, the techniques of Sect. 6.6 provide a bridge to general MINLP techniques and show how the usage of Lipschitz constants and nonconvex relaxations can help to approach hard problems.

Overall, while this chapter demonstrates the research ground already covered, there are plenty of opportunities for future research.

Acknowledgements This work was supported by the German Research Foundation (DFG) within Subprojects A01, A05, and B08 in the Sonderforschungsbereich/Transregio 154 "Mathematical Modelling, Simulation and Optimization using the Example of Gas Networks" (Project ID 239904186).

References

1. F. Babonneau, Y. Nesterov, and J.-P. Vial. Design and operations of gas transmission networks. *Operations Research*, 60(1):34–47, 2012. doi:10.1287/opre.1110.1001.
2. C. Borraz-Sánchez, R. Bent, S. Backhaus, H. Hijazi, and P. Van Hentenryck. Convex relaxations for gas expansion planning. *INFORMS Journal on Computing*, 28(4):645–656, 2016. doi:10.1287/ijoc.2016.0697.
3. C. Bragalli, C. D'Ambrosio, J. Lee, A. Lodi, and P. Toth. On the optimal design of water distribution networks: a practical MINLP approach. *Optimization and Engineering*, 13(2):219–246, June 2012. doi:10.1007/s11081-011-9141-7.
4. C. Bragalli, C. D'Ambrosio, J. Lee, A. Lodi, and P. Toth. An MINLP solution method for a water network problem. In Y. Azar and T. Erlebach, ed., *Algorithms – ESA 2006*, volume 4168 of *Lecture Notes in Computer Science*, pages 696–707. Springer Berlin Heidelberg, 2006. doi:10.1007/11841036_62.

5. R. Burlacu, H. Egger, A. M. Martin Groß, M. E. Pfetsch, L. Schewe, M. Sirvent, and M. Skutella. Maximizing the storage capacity of gas networks: a global MINLP approach. *Optimization and Engineering*, 20:543–573, 2019. doi:10.1007/s11081-018-9414-5.
6. R. Burlacu, B. Geißler, and L. Schewe. Solving mixed-integer nonlinear programmes using adaptively refined mixed-integer linear programmes. *Optimization Methods and Software*, 35(1):37–64, 2020. doi:10.1080/10556788.2018.1556661.
7. M. Fazlyab, M. Morari, and G. J. Pappas. Safety verification and robustness analysis of neural networks via quadratic constraints and semidefinite programming. *IEEE Transactions on Automatic Control*, 67(1):1–15, 2022. doi:10.1109/tac.2020.3046193.
8. B. Geißler, A. Martin, A. Morsi, and L. Schewe. Using piecewise linear functions for solving minlps. In J. Lee and S. Leyffer, ed., *Mixed Integer Nonlinear Programming*, pages 287–314, New York, NY, 2012. Springer New York.
9. L. M. P. Ghilardi, F. Casella, D. Barbati, R. Palazzo, and E. Martelli. A detailed MILP model and an ad hoc decomposition algorithm for the operational optimization of gas transport networks. *Computers & Chemical Engineering*, 195:109006, 2025. doi:10.1016/j.compchemeng.2025.109006.
10. A. Göß, R. Burlacu, and A. Martin. Parabolic approximation & relaxation for MINLP, 2025. arXiv:2407.06143.
11. A. Göß, A. Martin, S. Pokutta, and K. Sharma. Norm-induced cuts: Outer approximation for Lipschitzian constraint functions. *Journal of Global Optimization*, 94:35–63, 2026. doi:10.1007/s10898-025-01563-9.
12. J. Grübel, R. Krug, M. Schmidt, and W. Wollner. A successive linear relaxation method for MINLPs with multivariate Lipschitz continuous nonlinearities. *Journal of Optimization Theory and Applications*, 198(3):1077–1117, 2023. doi:10.1007/s10957-023-02254-9.
13. M. Gugat, G. Leugering, A. Martin, M. Schmidt, M. Sirvent, and D. Wintergerst. MIP-based instantaneous control of mixed-integer PDE-constrained gas transport problems. *Computational Optimization and Applications*, 70(1):267–294, 2018. doi:10.1007/s10589-017-9970-1.
14. M. Gugat, G. Leugering, A. Martin, M. Schmidt, M. Sirvent, and D. Wintergerst. Towards simulation based mixed-integer optimization with differential equations. *Networks*, 72(1):60–83, 2018. doi:10.1002/net.21812.
15. O. Habeck and M. E. Pfetsch. Combinatorial acyclicity models for potential-based flows. *Networks*, 79(1):83–104, 2021. doi:10.1002/net.22038.
16. O. Habeck, M. E. Pfetsch, and S. Ulbrich. Global optimization of mixed-integer ODE constrained network problems using the example of stationary gas transport. *SIAM Journal of Optimization*, 29(4):2949–2985, 2019. doi:10.1137/17M1152668.
17. F. M. Hante, R. Krug, and M. Schmidt. Time-domain decomposition for mixed-integer optimal control problems. *Applied Mathematics & Optimization*, 87(3):Article 36, 2023. doi:10.1007/s00245-022-09949-x.
18. R. Hildebrand and A. Göß. Complexity of integer programming in reverse convex sets via boundary hyperplane cover, 2024. arXiv:2409.05308.
19. B. Hiller, R. Saitenmacher, and T. Walther. Improved models for operation modes of complex compressor stations. *Mathematical Methods of Operations Research*, 94:171–195, 2021. doi:10.1007/s00186-021-00745-x.
20. A. Kaya, A. J. Conejo, and S. Rebennack. Fifty years of power systems optimization. *European Journal of Operational Research*, 329(1):1–23, 2026. doi:10.1016/j.ejor.2025.05.022.
21. T. Koch, B. Hiller, M. E. Pfetsch, and L. Schewe. *Evaluating gas network capacities*. MOS-SIAM Series on Optimization. SIAM, 2015. doi:10.1137/1.9781611973693.
22. R. Krug, G. Leugering, A. Martin, M. Schmidt, and D. Weninger. Time-domain decomposition for optimal control problems governed by semilinear hyperbolic systems. *SIAM Journal on Control and Optimization*, 59(6):4339–4372, 2021. doi:10.1137/20M138329X.
23. R. Krug, G. Leugering, A. Martin, M. Schmidt, and D. Weninger. Time-domain decomposition for optimal control problems governed by semilinear hyperbolic systems with mixed two-point boundary conditions. *Control and Cybernetics*, 50(4):427–455, 2021. doi:10.2478/candc-2021-0026.

24. R. Krug, G. Leugering, A. Martin, M. Schmidt, and D. Weninger. A consensus-based alternating direction method for mixed-integer and pde-constrained gas transport problems. *INFORMS Journal on Computing*, 36(2):397–416, 2024. doi:10.1287/ijoc.2022.0319.
25. J. E. Lagnese and G. Leugering. *Domain Decomposition Methods in Optimal Control of Partial Differential Equations*, volume 148 of *International Series of Numerical Mathematics*. Birkhäuser Verlag, 2004.
26. G. Leugering. Space-time-domain decomposition for optimal control problems governed by linear hyperbolic systems. *Journal of Optimization, Differential Equations and Their Applications*, 29(2):24–47, 2021. doi:10.15421/142107.
27. G. Leugering. Nonoverlapping domain decomposition for instantaneous optimal control of friction dominated flow in a gas-network. In G. Floridia and E. Zuazua, ed., *Analysis and Numerics of Design, Control and Inverse Problems*, pages 176–196, Singapore, 2025. Springer. doi:10.1007/978-981-96-6182-4_9.
28. D. Li and X. Li. Global optimization of an industrial natural gas production network. *IFAC-PapersOnLine*, 48(8):337–342, 2015. 9th IFAC Symposium on Advanced Control of Chemical Processes ADCHEM 2015. doi:10.1016/j.ifacol.2015.08.204.
29. Y. Li, S. S. Dey, and N. V. Sahinidis. A reformulation-enumeration MINLP algorithm for gas network design. *Journal of Global Optimization*, 90(4):931–963, 2024. doi:10.1007/s10898-024-01424-x.
30. T. W. K. Mak, P. V. Hentenryck, A. Zlotnik, and R. Bent. Dynamic compressor optimization in natural gas pipeline systems. *INFORMS Journal on Computing*, 31(1):40–65, 2019. doi:10.1287/ijoc.2018.0821.
31. H. M. Markowitz and A. S. Manne. On the solution of discrete programming problems. *Econometrica*, 25:84–110, 1957. doi:10.2307/1907744.
32. M. Mikolajková, H. Saxén, and F. Pettersson. Linearization of an MINLP model and its application to gas distribution optimization. *Energy*, 146:156–168, 2018. Process Integration for Energy Saving and Pollution Reduction – PRES 2016. doi:10.1016/j.energy.2017.05.185.
33. I. Molan and M. Schmidt. Using neural networks to solve linear bilevel problems with unknown lower level. *Optimization Letters*, 17(5):1083–1103, 2023. doi:10.1007/s11590-022-01958-7.
34. P. Pauli, A. Koch, J. Berberich, P. Kohler, and F. Allgöwer. Training robust neural networks using Lipschitz bounds. *IEEE Control Systems Letters*, 6:121–126, 2022. doi:10.1109/lcsys.2021.3050444.
35. M. Raissi, P. Perdikaris, and G. E. Karniadakis. Physics-informed neural networks: a deep learning framework for solving forward and inverse problems involving nonlinear partial differential equations. *Journal of Computational Physics*, 378:686–707, 2019. doi:10.1016/j.jcp.2018.10.045.
36. R. Z. Ríos-Mercado and C. Borraz-Sánchez. Optimization problems in natural gas transportation systems: A state-of-the-art review. *Applied Energy*, 147:536–555, 2015. doi:10.1016/j.apenergy.2015.03.017.
37. M. Robinius, L. Schewe, M. Schmidt, D. Stolten, J. Thürauf, and L. Welder. Robust optimal discrete arc sizing for tree-shaped potential networks. *Computational Optimization and Applications*, 73(3):791–819, 2019. doi:10.1007/s10589-019-00085-x.
38. L. Schewe, T. Koch, A. Martin, and M. E. Pfetsch. Mathematical optimization for evaluating gas network capacities. In T. Koch, B. Hiller, M. E. Pfetsch, and L. Schewe, ed., *Evaluating Gas Network Capacities*, MOS-SIAM Series on Optimization, chapter 5, pages 87–102. SIAM, 2015. doi:10.1137/1.9781611973693.ch5.
39. M. Schmidt, D. Aßmann, R. Burlacu, J. Humpola, I. Joormann, N. Kanelakis, T. Koch, D. Oucherif, M. E. Pfetsch, L. Schewe, R. Schwarz, and M. Sirvent. GasLib – A Library of Gas Network Instances. *Data*, 2(4):Article 40, 2017. doi:10.3390/data2040040.
40. M. Schmidt, M. Sirvent, and W. Wollner. A decomposition method for MINLPs with Lipschitz continuous nonlinearities. *Mathematical Programming*, 178(1-2):449–483, 2019. doi:10.1007/s10107-018-1309-x.
41. M. Schmidt, M. Sirvent, and W. Wollner. The cost of not knowing enough: mixed-integer optimization with implicit Lipschitz nonlinearities. *Optimization Letters*, 16(5):1355–1372, 2022. doi:10.1007/s11590-021-01827-9.

42. J. Schweiger and F. Liers. A decomposition approach for optimal gas network extension with a finite set of demand scenarios. *Optimization and Engineering*, 19(2):297–326, 2018. doi: 10.1007/s11081-017-9371-4.
43. D. Shaw. Pipeline system optimization: A tutorial. Technical Report PSIG 9405, Pipeline Simulation Interest Group, 1994.
44. N. Shiono and H. Suzuki. Optimal pipe-sizing problem of tree-shaped gas distribution networks. *European Journal of Operational Research*, 252(2):550–560, 2016. doi:10.1016/j.ejor.2016.01.008.
45. J. Thürauf, J. Grübel, and M. Schmidt. Adjustable robust nonlinear network design without controllable elements under load scenario uncertainties. *Mathematical Programming*, 2025. doi:10.1007/s10107-025-02207-2.
46. Q. Zheng, S. Rebennack, N. Iliadis, and P. Pardalos. Optimization models in the natural gas industry. In *Handbook of Power Systems I*, pages 121–148. Springer, 2010. doi:10.1007/978-3-642-02493-1_6.

Open Access This chapter is licensed under the terms of the Creative Commons Attribution-NonCommercial-NoDerivatives 4.0 International License (http://creativecommons.org/licenses/by-nc-nd/4.0/), which permits any noncommercial use, sharing, distribution and reproduction in any medium or format, as long as you give appropriate credit to the original author(s) and the source, provide a link to the Creative Commons license and indicate if you modified the licensed material. You do not have permission under this license to share adapted material derived from this chapter or parts of it.

The images or other third party material in this chapter are included in the chapter's Creative Commons license, unless indicated otherwise in a credit line to the material. If material is not included in the chapter's Creative Commons license and your intended use is not permitted by statutory regulation or exceeds the permitted use, you will need to obtain permission directly from the copyright holder.





Chapter 7
Potential-Based Flows – An Overview

Marc E. Pfetsch[0000−0002−0947−7193],
Martin Schmidt[0000−0001−6208−5677],
Martin Skutella[0000−0002−9814−1703], and
Johannes Thürauf[0000−0001−8516−6250]

Abstract Potential-based flows provide an algebraic way to model static physical flows in networks, for example, in gas, water, and lossless DC power networks. The flow on an arc in the network depends on the difference of the potentials at its end-nodes, possibly in a nonlinear way. Potential-based flows have several nice properties like uniqueness and acyclicity. The goal of this chapter is to provide an overview of the current knowledge on these models with a focus on optimization problems on such networks. We cover basic properties, computational complexity, monotonicity, uncertain parameters, and the corresponding behavior of the network as well as topology optimization.

7.1 Introduction

A potential-based flow consists of a flow x_a on the arcs a in a network and potentials π_v on the nodes v. For an arc $a = (u, v)$, they are coupled through the equation $\pi_u - \pi_v = \beta_a \psi_a(x_a)$, where ψ_a is a continuous, strictly increasing function with $\psi_a(0) = 0$ and $\beta_a > 0$ is a given parameter. This covers applications like gas and water flow, as well as lossless DC power flow (see Sect. 7.2.1). The flow has to satisfy flow conservation constraints in the network and guarantee a given load.

This setting shares common features with classical flows, but a potential-based flow satisfies additional properties like uniqueness and acyclicity (see Sect. 7.2.3). Classical

Marc E. Pfetsch
Department of Mathematics, TU Darmstadt, Germany, e-mail: pfetsch@mathematik.tu-darmstadt.de

Martin Schmidt
Department of Mathematics, Trier University, Germany, e-mail: martin.schmidt@uni-trier.de

Martin Skutella
Institute of Mathematics, TU Berlin, Germany, e-mail: martin.skutella@tu-berlin.de

Johannes Thürauf
Discrete Optimization, University of Technology Nuremberg (UTN), Germany,
e-mail: johannes.thuerauf@utn.de

© The Author(s) 2027

A. Martin et al. (eds.), *Mathematical Modelling, Simulation and Optimization using the Example of Gas Networks*, International Series of Numerical Mathematics 174,
https://doi.org/10.1007/978-3-032-34969-9_7

flows have been investigated in the literature for over 60 years, see, e.g., Ford and Fulkerson [21], and are very well understood, see, e.g., Ahuja et al. [3].

Potential-based flows provide an interesting model because of their ability to model relatively realistic problems and because the coupling of the flows and potential differences can be nonlinear. This setting provides structure that can be exploited, which makes it possible to handle corresponding optimization problems. Moreover, they provide a way to unify methods that would have otherwise been repeatedly developed for particular applications like water or gas network optimization. Indeed, many techniques have already been rediscovered in the different application areas.

One of the first publications on potential-based flows is by Birkhoff and Diaz [7] from the 1960ies, already highlighting existence and uniqueness properties. Thus, the model is around for quite some time, but it had been not used very frequently. One exception is the book by Rockafellar [63] from 1998, which is devoted to the investigation of potential-based flows. In recent years, there has been an increased interest in potential-based flows, probably because of the reasons mentioned above.

The goal of this chapter is to provide an overview of the current state-of-the-art in this area. In particular, we want to highlight the mathematical techniques that are used when dealing with optimization problems using potential-based flows. Thus, this chapter can be used as a reference for results and as a possible motivation for future investigations of such models.

Note that although we try to be comprehensive, this is not an easy task, since there are many works for particular applications like water and gas network optimization problems that are quite close to potential-based flows, but still expressed for the particular problem. At some places, we will mention such works, but try to focus on articles that explicitly deal with potential-based flows. We further note that AC power flow problems cannot be modeled by the presented potential-based flows.

Finally, we mention that potential-based flows often form an approximation of more detailed models, e.g., for gas networks they arise from a simplification of the stationary Euler equations. The accuracy depends on the domain of application and should be kept in mind when analyzing results.

The remainder of this chapter is structured as follows. In Sect. 7.2, we introduce the required notation, present some examples, and discuss basic properties of potential-based flows such as uniqueness or acyclicity. Sect. 7.3 then collects some basic complexity results for potential-based flows, while their monotonicity properties are discussed in Sect. 7.4. The more specific topics of topology optimization and robust optimization to tackle uncertainties are summarized in Sect. 7.5 and 7.6, respectively. The area of potential-based mixed-integer nonlinear problems is touched upon in Sect. 7.7 before the chapter is closed with a summary in Sect. 7.8.

7.2 Potential-Based Flows: Basic Properties

Potential-based flows form a basic algebraic way to model static, i.e., time-independent, physical flows through a network. Such a network consists of a directed graph $G = (V, A)$ with a finite node set V and an arc (multi-)set $A \subseteq V \times V$. We assume that there are no

self-loops, but parallel arcs are allowed. The *flow* for arc $a \in A$ in the graph is denoted by x_a. The flow can be negative, if it is in the opposite direction of the arc. Moreover, there are *potentials* π_v on each node v.[1] For an arc $a = (u, v)$, the flow x_a and the potentials π_u, π_v on the end nodes are coupled through the *potential equation*

$$\pi_u - \pi_v = \beta_a \psi_a(x_a), \tag{7.1}$$

where $\beta_a > 0$ is an arc-specific *resistance* constant and $\psi_a : \mathbb{R} \to \mathbb{R}$ is a *potential function*. We denote by (G, β) the corresponding potential network. We omit the potential functions ψ_a in the potential network notation because we will assume that the potential functions are the same function ψ for all arcs. This assumption is fulfilled in most applications, since they express the basic physical behavior of the medium to be transported. Nevertheless, most of the results presented in this survey also apply to potential networks in which different arcs may have different potential functions.

In the literature, several assumptions are made about the potential functions ψ. The most common are quite natural: ψ is continuous, strictly increasing, and $\psi(0) = 0$. In particular, ψ^{-1} exists under these assumptions. Throughout this chapter, we will use these properties.

Note that, given the potentials at the incident nodes, we can compute the flow on an arc $a = (u, v)$ by

$$x_a = \psi^{-1}((\pi_u - \pi_v)/\beta_a).$$

Moreover, sometimes one assumes that ψ is *odd*, i.e., $\psi(x) = -\psi(-x)$. Further properties of ψ that are used sometimes is that it is *positively homogeneous* of order $r > 0$, i.e.,

$$\psi(\lambda x) = \lambda^r \psi(x), \quad \lambda > 0.$$

Homogeneity is motivated by physical laws, and its order r depends on the specific application. Moreover, it implies that ψ is of the form

$$\psi(x) = \alpha \operatorname{sgn}(x)|x|^r, \tag{7.2}$$

for some constant $\alpha = \psi(1) > 0$ and order $r > 0$. Note that here ψ is odd.

Remark 7.1 Alternative, equivalent models have also been investigated. For instance, one can introduce anti-parallel arcs and make the flow anti-symmetric; see Vuffray et al. [75]. Undirected models can be used as well; see Klimm et al. [44].

7.2.1 Examples

Potential-based flows arise in many areas; see, e.g., Hendrickson and Janson [36]. We give some examples here.

[1] Note that the name "potential" is motivated by physical applications. The term is also used with a different meaning for the dual variables of the classical flow problem.

- *Lossless DC Power*: Here, the potentials are the voltages and the flow is electric current. The potential function is $\psi(x) = x$. The resistances $\beta_a = 1/B_a$ are the reciprocal of the susceptance B_a of the line $a \in A$; see, e.g., [43].
- *Gas*: In stationary models of gas transport through pipe networks, the potentials correspond to the square of the pressures at the corresponding nodes. For horizontal pipes, the potential function is $\psi(x) = \operatorname{sgn}(x)\, x^2 = x\,|x|$ and β_a depends on technical parameters of the pipe like its diameter, length, or roughness of its inner wall. For more details on modeling stationary gas flow in pipeline networks we refer the reader to the Chap. 2, "A Catalog of Gas Network Models: PDEs, Coupling Conditions, and Numerical Schemes" in this book as well as Chap. [22] of the book by Koch et al. [46] and the references therein. See also the discussion in Groß et al. [29] for the handling of non-horizontal settings.
- *Water*: In water networks, potentials correspond to hydraulic heads. The head-loss model uses $\psi(x) = \operatorname{sgn}(x)|x|^{1.852}$ or $\psi(x) = \operatorname{sgn}(x)|x|^2$ in fully filled pipes [1, 13, 52, 56]. The resistances β_a again depend on the properties of the pipes.

7.2.2 Networks and Controllable Components

So far, we introduced the model for potential-based flows for a single arc. We now extend this to entire networks that may also include controllable elements such as switches.

The amount of flow that should be inserted or extracted from the network is specified by a balanced vector $b \in B(V) \coloneqq \{b \in \mathbb{R}^V : \sum_{v \in V} b_v = 0\}$. Thus, if flow moves through the network, then *flow conservation* has to hold, i.e.,

$$\sum_{a \in \delta^{\text{out}}(v)} x_a - \sum_{a \in \delta^{\text{in}}(v)} x_a = b_v, \quad v \in V,$$

where $\delta^{\text{out}}(v) \coloneqq \{(v, w) \in A\}$ are the outgoing arcs and $\delta^{\text{in}}(v) \coloneqq \{(u, v) \in A\}$ are the incoming arcs of $v \in V$. Note that $b_v > 0$ refers to injections (entries), $b_v < 0$ to withdrawals (exits), and $b_v = 0$ to inner nodes with flow conservation.

Often, there are lower and upper bounds on the flows and potentials. For arc $a \in A$, the lower and upper flow bounds are $\underline{x}_a$ and $\overline{x}_a \in \mathbb{R}$, respectively, where $\underline{x}_a \le \overline{x}_a$ holds. For node $v \in V$, the lower and upper potential bounds are $\underline{\pi}_v, \overline{\pi}_v \in \mathbb{R}$ with $\underline{\pi}_v \le \overline{\pi}_v$.

Further network components allow to control the flows through the network. To this end, the arc set A is partitioned into arcs $A_L = A_L(G)$ representing so-called *lines* used for transport and arcs $A_S = A_S(G)$ representing *switches*, which allow to block flow. We call a potential network *passive* if $A_S = \emptyset$ holds. Otherwise, we call it *active*.

For a *line-arc* $a = (u, v) \in A_L$, the *flow* x_a and potentials π_u and π_v satisfy (7.1). For every *switch-arc* $a = (u, v) \in A_S$, we have a control variable $z_a \in \{0, 1\}$, specifying the state of the switch. If $z_a = 1$, then $\pi_u = \pi_v$ has to hold and the flow x_a is not restricted by the incident potentials. Otherwise, if $z_a = 0$, the flow on the arc has to be 0, i.e., $x_a = 0$, and the potentials are decoupled from x_a. In these cases, the switch is said to be "on" and "off", respectively.

A *potential-based flow* (x, π, z) in a potential network $(G, \beta) = ((V, A), \beta)$ consists of a flow $x \in \mathbb{R}^A$, potentials $\pi \in \mathbb{R}^V$, and control variables $z \in \{0, 1\}^{A_S}$. We call (x, π, z) *feasible* for a given balance vector $b \in B(V)$, if it satisfies the constraints

$$\sum_{a \in \delta^{\text{out}}(v)} x_a - \sum_{a \in \delta^{\text{in}}(v)} x_a = b_v, \qquad v \in V, \tag{7.3a}$$

$$\pi_u - \pi_v = \beta_a \psi(x_a), \qquad a = (u, v) \in A_L, \tag{7.3b}$$

$$-\underline{x}_a z_a \leq x_a \leq \overline{x}_a z_a, \qquad a \in A_S, \tag{7.3c}$$

$$(\underline{\pi}_u - \overline{\pi}_v)(1 - z_a) \leq \pi_u - \pi_v \leq (\overline{\pi}_u - \underline{\pi}_v)(1 - z_a), \qquad a = (u, v) \in A_S, \tag{7.3d}$$

$$x_a \in [\underline{x}_a, \overline{x}_a], \qquad a \in A_L, \tag{7.3e}$$

$$\pi_v \in [\underline{\pi}_v, \overline{\pi}_v], \qquad v \in V, \tag{7.3f}$$

$$z_a \in \{0, 1\}, \qquad a \in A_S. \tag{7.3g}$$

Note that the system implies that if $z_a = 1$ for a switch arc $a \in A_S$, then $\pi_u = \pi_v$ and the flow is not restricted by (7.3c). Similarly, if $z_a = 0$, then $x_a = 0$ and the potentials are not restricted by (7.3d).

Remark 7.2 Note that the flow and potential bounds often arise from safety or legal considerations in order to guarantee the reliable operation of the network. These bounds can often be used to further strengthen other bounds (given some balance vector b).

Remark 7.3 While this work focuses on *static* potential-based flows, we remark that generalizations to transient, i.e., time-dependent models, have been studied in the literature as well. In the classical network flow literature, time-dependent flows are referred to as *dynamic* flows or *flows over time*, and have been extensively studied in the literature; see Skutella [68, 69] for recent surveys. In the context of potential-based flows, Groß, Pfetsch, and Skutella [30] study the computational complexity of a simplistic model of transient potential-based flows consisting of a sequence of k stationary potential-based (gas) flows. They present efficiently solvable cases and NP-hardness results, establishing complexity gaps between stationary and transient potential-based flows as well as between transient potential-based s-t-flows and transient potential-based b-flows. Burlacu et al. [14] study the transient optimization of gas networks, focusing on maximizing the storage capacity of the network. Their model is obtained by discretizing a coupled system of nonlinear parabolic partial differential equations. The resulting nonlinear discretized system contains a potential-based flow in each time-step and is proved to be well-posed.

Remark 7.4 We note that other components like compressors or control valves in gas networks are important in respective applications as well. These are usually not covered in a potential-based flow context, because they might require specific physical modeling.

7.2.3 Basic Properties of Potential-Based Flows

One very important result concerns uniqueness—a result that has been rediscovered and reproved several times in the past; see Remark 7.5 below.

Theorem 7.1 (Theorem 7.1 in [46]) *Let (G, β) be passive and weakly connected potential network with a balanced load vector $b \in B(V)$. Let the potential function ψ be continuous, strictly increasing, and satisfy $\psi(0) = 0$. Suppose that there are no flow and potential bounds. Then, there is a unique flow $x \in \mathbb{R}^A$ satisfying Constraints* (7.3a) *and* (7.3b)*. Moreover, there exist potentials $\pi \in \mathbb{R}^V$ such that the set of feasible points is given by*

$$\{(x,\ \pi + \eta \mathbb{1}) \,:\, \eta \in \mathbb{R}\},$$

where $\mathbb{1} = (1, \dots, 1)^\top \in \mathbb{R}^V$ is a vector of ones.

Proof idea. Consider the optimization problem

$$\begin{aligned} \min_x \quad & \sum_{a \in A} \beta_a \int_0^{x_a} \psi(\xi)\, \mathrm{d}\xi \\ \text{s.t.} \quad & \sum_{a \in \delta^{\mathrm{out}}(v)} x_a - \sum_{a \in \delta^{\mathrm{in}}(v)} x_a = b_v, \quad v \in V. \end{aligned} \tag{7.4}$$

Because of the assumptions on ψ (monotonicity), the objective is strictly convex. Thus, this problem has a unique flow solution. Using π_v as dual variables for the flow conservation constraints and formulating the KKT conditions yields (7.1). Since (7.1) only depends on the differences of potentials, there is still one degree of freedom regarding the potentials. □

Corollary 7.1 *Let the requirements of Theorem 7.1 hold and additionally assume that the potential level π_s of one single node $s \in V$ is fixed. Then, there is a unique feasible potential-based flow (x, π) that satisfies b.*

Remark 7.5 Uniqueness as in Theorem 7.1 has already been discussed by Birkhoff and Diaz [7]. The argument illustrated in the proof was used by Maugis [57] for $\psi(x) = x\,|x|$. Collins et al. [17] used this argument in the general setting. Finally, Ríos-Mercado et al. [61] provide a different proof.

Remark 7.6 For homogeneous potential functions and without flow and potential bounds, one can formulate the dual problem of (7.4) for which strong duality holds; see Maugis [57] for $\psi(x) = x\,|x|$. Rockafellar [63] contains a general discussion; see also [29].

Exploiting the uniqueness result of Theorem 7.1, the feasibility of potential-based flows can be characterized by validating flow bounds and potential differences. This characterization was first established by Gotzes et al. [27] for the case of gas networks and was then extended to general potential-based flows by Labbé et al. [50, Theorem 7].

Theorem 7.2 *Let (G, β) be a passive and weakly connected potential network with a potential function ψ that is continuous, strictly increasing, and that satisfies $\psi(0) = 0$. Further, let $b \in B(V)$ be a balanced load vector and let (x, π) be flows and potentials satisfying* (7.3a)*,* (7.3b)*, and* (7.3e)*. Then, there exist potentials $\tilde{\pi}$ satisfying the potential bounds* (7.3f)*, i.e., the point $(x, \tilde{\pi})$ is a feasible potential-based flow for b, if and only if the following inequalities are satisfied*

$$\pi_u - \pi_v \le \overline{\pi}_u - \underline{\pi}_v, \quad (u, v) \in V^2. \tag{7.5}$$

This characterization allows to check if there exists a feasible potential-based flow for a given load b by first computing flows and potentials according to Theorem 7.1 and then validating (7.5) without explicitly shifting the potentials to satisfy the corresponding potential bounds (7.3f).

Another fundamental property is acyclicity, which has been observed many times in particular applications, e.g., Kirchhoff's Circuit Law, and is explicitly formulated in Habeck and Pfetsch [33] for potential-based flows. For a flow $x \in \mathbb{R}^A$, define

$$\begin{aligned} A(x) \coloneqq &\{(u,v) \in V \times V \,:\, a = (u,v) \in A \text{ with } x_a > 0\} \\ &\cup \{(v,u) \in V \times V \,:\, a = (u,v) \in A \text{ with } x_a < 0\}, \end{aligned}$$

i.e., the set of arcs with positive flow and reverse arcs that have a negative flow in the original.

Theorem 7.3 *Let (x, π) be a potential-based flow in a passive potential network (G, β). Then $A(x)$ is acyclic in the directed sense.*

Proof. Assume there exists a directed cycle C in $A(x)$. Sum along forward ($C \cap A$) and backward ($C \setminus A$) arcs and use (7.1) to obtain

$$\begin{aligned} &\sum_{a \in C \cap A} \beta_a \, \psi(x_a) - \sum_{(u,v) \in C \setminus A} \beta_{(v,u)} \, \psi(x_{(v,u)}) \\ = &\sum_{(u,v) \in C \cap A} \pi_u - \pi_v + \sum_{(u,v) \in C \setminus A} \pi_u - \pi_v = 0, \end{aligned}$$

because the potentials cancel out along the cycle. Since $\beta_a > 0$, ψ is strictly increasing, and $\psi(0) = 0$, it holds that $\beta_a \, \psi(x_a) > 0$ for all $a \in C \cap A$ and $\beta_{(v,u)} \, \psi(x_{(v,u)}) < 0$ for all $(u,v) \in C \setminus A$. Thus, the left hand side is positive—a contradiction. □

One interesting property is that passive potential networks with homogeneous potential functions and a single entry and a single exit behave like a graph with a single arc.

Theorem 7.4 (Theorem 3.6 in [29]) *Let (G, β) be a passive weakly connected potential network without flow and potential bounds and homogeneous potential functions of order $r > 0$. Let $b \in B(V)$ with only two nonzero entries with values $b_s = L$ and $b_t = -L$ for $s, t \in V$. Consider the graph $\tilde{G} = (\{\tilde{s}, \tilde{t}\}, \{(\tilde{s}, \tilde{t})\})$ with two distinct nodes $\tilde{s}$, $\tilde{t}$ and one arc $(\tilde{s}, \tilde{t})$ as well as $\tilde{b}$ with $\tilde{b}_{\tilde{s}} = L$, $\tilde{b}_{\tilde{t}} = -L$. Then, there exists a constant $\tilde{\beta}$ such that there exists a potential-based flow (x, π) in (G, β) for b if and only if there exists a potential-based flow $(\tilde{x}, \tilde{\pi})$ in $(\tilde{G}, \tilde{\beta})$ with for $\tilde{b}$ and $\pi_s = \tilde{\pi}_{\tilde{s}}$ and $\pi_t = \tilde{\pi}_{\tilde{t}}$.*

Note that if G is series-parallel, then [29] describes rules how $\tilde{\beta}$ can be iteratively computed based on the β-values of G.

Klimm et al. [45] study possible generalizations of Theorem 7.4 to passive weakly connected potential networks with more than two terminals, i.e., entries and exits. For the special case of electrical networks with linear potential function $\psi(x) = x$, the so-called Kron [48] reduction (see also Dorfler and Bullo [19]) yields a smaller equivalent network that only contains the terminal nodes and edges connecting them. Here, two

networks with the same set of terminals are *equivalent* if for any b-vector the potentials at the terminals are always the same, where the potential at one node is fixed. Thus, these networks cannot be distinguished by measuring the potentials at terminals.

For more than two terminals, however, the existence of the Kron reduction strongly relies on the linearity of the mapping between loads and potentials in such networks. Nevertheless, for general homogeneous potential functions ψ, there exist sufficient conditions under which passive potential networks can be reduced to equivalent networks defined on the set of terminals:

Theorem 7.5 (Theorem 3 in [45]) *Let (G, β) be a potential network, $T \subseteq V$ be the set of terminals and $v \in V$ be chosen arbitrarily. We define*

$$N_T(v) := \{t \in T \,:\, \exists\, v\text{-}t\text{-path which does not contain any terminal except } t\}$$

and assume that all potential functions $\psi(x)$ are $\operatorname{sgn}(x)|x|^r$ for some degree $r > 0$. Moreover, suppose that $|N_T(v)| \leq 2$ for every inner node $v \in V \setminus T$. Then, (G, β) is equivalent to a potential network (G', β'), where $G' = (T, E')$ with $E' \subseteq T \times T$.

However, Theorem 5 in [45] shows that for every $m \in \mathbb{N}$, there exists a potential network with potential functions of order $r = 2$ and three terminals such that no network with at most m arcs is equivalent to it. Notably, the proof of this result uses insights from semi-algebraic geometry.

7.3 Complexity

In this section, we briefly collect some central results about computational complexity in the context of potential networks.

We start with s-t-flows for some $s, t \in V$. Here, the balanced load vector b satisfies $b_v = 0$ for all $v \in V \setminus \{s, t\}$ and a feasible potential-based s-t-flow satisfies (7.3); in particular, switches are allowed in the model. The following problem was introduced in [29]:

---

s-t-FlowFeasibility
Input: A potential network (G, β)
Problem: Is there a feasible potential-based s-t-flow (x, π, z) for (G, β)?

On top of that, when maximizing the flow from s to t, feasible s-t-flows do not have to satisfy Constraints (7.3a) for s and t:

---

s-t-MaxFlow
Input: A potential network (G, β)
Problem: Find a feasible potential-based s-t-flow (x, π, z) for (G, β) of maximal value $\operatorname{val}(x)$.

Here, the value of the flow is defined as usual via

$$\operatorname{val}(x) = \sum_{a \in \delta^{\text{out}}(s)} x_a - \sum_{a \in \delta^{\text{in}}(s)} x_a.$$

These two problems are natural analogues of classical flow problems. Let us note that one could also consider an analogue of the min-cost-flow problem. This, however, seems less natural since the flow is unique on passive potential networks with fixed balance vector b, i.e., unless switches are present.

Let us start by reviewing what is known for these two problems in the literature. First of all, both problems are polynomial-time solvable for linear potential functions ψ on passive potential networks because both problems are linear problems. Other variants with linear ψ are mainly discussed in the literature on DC power flow problems. In Lehmann et al. [53], the following is shown.

Theorem 7.6 (Corollary 1 in [53]) *The DC s-t-FlowFeasibility problem is strongly NP-hard for planar graphs of maximum degree 3 with switches.*

They also showed that the extension of the s-t-MaxFlow problem with at least two sources and sinks cannot be approximated in polynomial time better than $2^{(\log n)^{1-\varepsilon}}$ for an $\varepsilon > 0$ unless problems in NP can be solved in quasi-polynomial deterministic time. For arbitrarily many sources and sinks, the DC flow feasibility problem is weakly NP-hard even on cactus graphs of maximum degree 3.

For gas flow networks, Szabó [72] showed that the so-called active gas nomination validation problem, which is the same as the s-t-FlowFeasibility problem for gas networks, is weakly NP-hard even for series-parallel networks. For arbitrary networks, Humpola [38] showed that a problem similar to the s-t-FlowFeasibility problem is strongly NP-hard. The problem is called the topology optimization problem there.

While there are numerous complexity results for the special cases of DC power flow networks as well as for natural gas networks, the literature on complexity results for general potential-based flows is scarce. One important problem in the more general literature is the problem of computing the *maximum potential-difference nomination* (MPD). Here, the nodes are split into entry nodes V_+, exit nodes V_-, and the remaining inner nodes V_0, i.e., $V = V_+ \cup V_- \cup V_0$ holds. Then, feasibility is defined by satisfying the constraints

$$\sum_{a \in \delta^{\text{out}}(v)} x_a - \sum_{a \in \delta^{\text{in}}(v)} x_a = \tilde{b}_v, \qquad v \in V, \tag{7.6a}$$

$$\pi_u - \pi_v = \beta_a \psi(x_a), \qquad a = (u, v) \in A_L, \tag{7.6b}$$

$$0 \le b_v \le \bar{b}_v \qquad v \in V, \tag{7.6c}$$

where $\tilde{b}_v = b_v$ for entry nodes $v \in V_+$, $\tilde{b}_v = -b_v$ for exit nodes $v \in V_-$, and $\tilde{b}_v = 0$ for inner nodes $v \in V_0$. Hence, this is a variant of the feasibility problem above in which we are choosing the loads within some bounds but otherwise only have a passive network.

Then, for two given nodes v_1 and v_2, the optimization variant of the MPD problem is to solve

$$\max\{\pi_{v_1} - \pi_{v_2} \,:\, (b, x, \pi) \text{ satisfy (7.6)}\}.$$

It is shown in [73] that this problem is NP-hard for quadratic potential functions and general networks even if all flow directions are known in advance. Note that this problem is easy for linear potential flows, because it can again be modeled as a linear optimization problem. Moreover, the problem is easy for trees [50] and for a single cycle [51]. One open complexity question is the hardness of the nonlinear case on cactus graphs.

The optimization variant of the MPD problem has been applied in various applications such as in robust network design [62, 74], see also Sect. 7.6, or for solving multilevel markets models [10, 64].

7.4 Monotonicity of Parameter-Dependent Potential-Based Flows

Different to many settings for classical flows, potential-based flows do not behave monotonously with respect to changes in certain parameters of the network. The goal of this section is to provide some intuition when this is the case. We start by first highlighting cases in which monotonicity does not hold.

Example 7.1 (Nonmonotonicity of potentials w.r.t. flow balances) One could think that increasing the flow demand would require increasing the maximal potential difference. However, this is not true in general, not even for trees.

The following notation for two balanced load vectors $b^1, b^2 \in B(V)$ will be useful:

$$b^1 \preceq b^2 \iff \begin{cases} b^1_v \le b^2_v & \text{for all } v \in V \text{ with } b^1_v \ge 0, \\ b^2_v \le b^1_v & \text{for all } v \in V \text{ with } b^1_v \le 0. \end{cases}$$

We also define the maximal potential difference $\Delta(\pi) \coloneqq \max_{u,v \in V} |\pi_u - \pi_v|$ for $\pi \in \mathbb{R}^V$. Then for a potential-based flow network (G, β) with balanced load vectors $b^1 \preceq b^2$, the maximal potential difference is not monotone in the following sense: Let (x^1, π^1) and (x^2, π^2) be potential-based flows for b^1 and b^2, respectively. Then $\Delta(\pi^1) \le \Delta(\pi^2)$ does not hold in general.

This can be shown by the following simple example; see Fig. 7.1. Consider a path graph $G = (V, A)$ with four nodes, i.e., $V = \{1, 2, 3, 4\}$, $A = \{(1, 2), (2, 3), (3, 4)\}$. All β-values are equal to 1 and $\psi(x) = \operatorname{sgn}(x)\,|x|^r$, $r > 0$. Let $b^1 = (1, 0, 0, -1)^\top$ and $b^2 = (1, -1, 1, -1)^\top$. Then $b^1 \preceq b^2$ and $x^1 = (1, 1, 1)^\top$, $\pi^1 = (3, 2, 1, 0)^\top$ is a solution for b^1, because the flow is 1 for all arcs (and thus b^1 is satisfied), so the right-hand side of (7.1) is 1, while the left-hand side is 1 as well. Similarly, $x^2 = (1, 0, 1)^\top$, $\pi^2 = (2, 1, 1, 0)^\top$ is feasible for b^2. That the flow balance b^2 is satisfied is easy to see. Moreover, by the same argument as before, (7.1) is satisfied on the first and last arc. On the middle arc, we have $0 = 1 - 1 = \pi_2 - \pi_3 = \beta\, 0\, |0|$. Thus, $\Delta(\pi^1) = 3 \not\le \Delta(\pi^2) = 2$.

Example 7.1 shows that the opposite case is also not monotone: Increasing the maximal potential difference does not necessarily increase the flow balance.

Remark 7.7 Note that because of Theorem 7.4, monotonicity holds if there is a single entry and single exit.

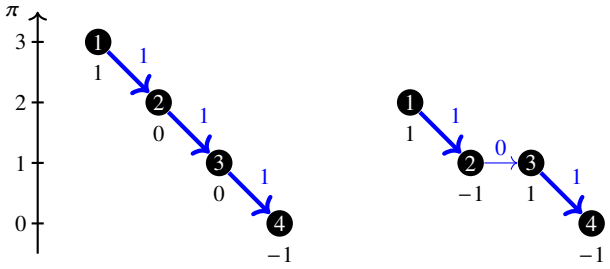


Fig. 7.1: Flows (indicated above the arcs) and potentials (indicated by height) for Example 7.1. *Left*: balance vector $b^1 = (1, 0, 0, -1)^\top$; *Right*: $b^2 = (1, -1, 1, -1)^\top$.

Example 7.2 (Nonmonotonicity of potentials w.r.t. switches/topology extension) Consider the same example as in Example 7.1 with balanced load vector $b^2 = (1, -1, 1, -1)^\top$, but first without the middle arc. Then $\pi = (1, 0, 1, 0)^\top$ and $x = (1, 0, 1)^\top$ are feasible. Therefore, the maximal difference in potentials $\Delta(\pi)$ is 1. If we re-add the middle edge and keep the same balanced load vector, the solution is given in Example 7.1 with a maximal difference in potentials of 2. The addition of the middle arc corresponds to a valve that is opened or an arc that is built in addition. Thus, the maximal difference does not necessarily decrease if we add arcs. By considering two parallel arcs, one of which can be added, it is easy to see that the opposite is not true in general as well.

To provide a positive example of monotonicity, define the so-called *power-loss*, see, e.g., Calvert and Keady [15],

$$\sum_{v \in V} b_v \pi_v = \sum_{a=(u,v) \in A} (\pi_u - \pi_v) x_a$$

for some potential-based flow (x, π) with respect to the balanced load vector $b \in B(V)$. In the s-t-case, the power-loss simply reads $b_s(\pi_s - \pi_t)$.

Theorem 7.7 (Theorem 5.1 in [29]) *Consider a potential-based flow network (G, β) with homogeneous potential function and without potential and flow bounds. Then, for a given balanced load vector $b \in B(V)$, the power-loss of a feasible potential-based flow is minimized if all switches are on.*

7.5 Topology Optimization

Topology optimization, or network design, is a well-established and active research field in mathematical optimization and operations research. It is one of the main applications for potential-based flows. This connection is primarily driven by the modeling capabilities of potential-based flows that can accurately represent a wide range of energy or utility networks. Further, the class of topology optimization problems is of high

practical relevance and, in particular, building resilient networks has gained increased interest in the recent years.

In topology optimization, one can generally distinguish between two types of optimization problems. The first ones consider a given and fixed network topology, for which the optimization task consists of selecting specific properties, e.g., diameters of pipes, without altering the network topology. If these properties are modeled by continuous variables, the resulting models are generally continuous nonlinear optimization problems. In contrast to these problems, the second type of topology optimization problems does not assume a predetermined network topology. Instead, the optimization also determines which network elements should be constructed and where they should be located. These problems are often referred to as a green-field approach or design-from-scratch problems and typically lead to mixed-integer nonlinear optimization problems.

The general goal of topology optimization is to find a network G and resistances β of smallest cost such that given b-vectors can be transported. Based on the model in [8], we can derive the following particular model for passive potential-based networks in which we choose arcs to be built:

$$\min \quad \sum_{a \in A} c_a z_a \tag{7.7a}$$

$$\text{s.t.} \quad \beta_a \psi_a(x_a) = z_a (\pi_u - \pi_v), \qquad a = (u,v) \in A, \tag{7.7b}$$

$$\sum_{a \in \delta^{\text{out}}(v)} x_a - \sum_{a \in \delta^{\text{in}}(v)} x_a = b_v, \quad v \in V, \tag{7.7c}$$

$$x_a \in [\underline{x}_a, \overline{x}_a], \qquad a \in A, \tag{7.7d}$$

$$\pi_v \in [\underline{\pi}_v, \overline{\pi}_v], \qquad v \in V, \tag{7.7e}$$

$$z \in \{0,1\}^A. \tag{7.7f}$$

Here, $z_a \in \{0,1\}$ decides whether the arc $a \in A$ is built and $c_a > 0$ is its cost. In the model, it is assumed that every arc can be decided on (green field), but it is easy to integrate existing arcs as well. We note that a large variety of different modeling approaches for topology optimization exist. Even for tree-shaped networks, topology optimization is NP-hard; see [78].

The literature on topology optimization with general potential-based flows is scarce—in particular when compared to the vast literature on topology optimization for specific instantiations of potential-based flows such as gas or water networks.

One of the first publications considering topology optimization with general potential-based flows is [60], in which for a given network, resistances are selected from a discrete set. In this work, convex relaxations for the nonconvex mixed-integer nonlinear network design problem are developed and combined with a linearizations-based LP/NLP branch-and-bound framework to solve a topology optimization problem. The authors of [39] also exploit convex relaxations together with a branch-and-bound approach to solve nonlinear and nonconvex network optimization problems arising in gas transmission networks.

Another area that has attracted increasing attention in the recent years is the optimization of resilient networks with general potential-based flows. The latter networks are protected from uncertainties such as arc failures or load fluctuations. The authors

of [58] develop a tailored branch-and-cut approach for building networks that can withstand specific arc failures. Moreover, the works [62, 74] develop methods to compute robust passive potential-based networks with load uncertainties by exploiting the characterization (7.10) presented below in Sect. 7.6.

In contrast to network optimization with capacitated linear flows, the field of developing valid inequalities for potential-based topology optimization is still in its infancy. To the best of our knowledge, the recent work [8] is the first to propose cuts based on potentials.

Theorem 7.8 (Theorem 5 in [8]) *Let (G, β) be a passive potential network with potential functions that are positively homogeneous of order $r > 0$ and let $\mu_a := 1/\sqrt[r]{\beta_a}$ be the conductance of arc $a \in A$. Let $T = T^+ \cup T^-$ be the terminal set, i.e., the set of all entries T^+ and exits T^-. If (x, π, z) is feasible for* (7.7b) *and* (7.7c) *with global potential bounds $0 \le \pi_v \le \bar{\pi}$ for all $v \in V$, then*

$$\frac{1}{k\sqrt[r]{k}} \sum_{i=1}^{k} \sum_{a \in \delta(S_i)} \mu_a z_a \ge \frac{b(Z)}{\sqrt[r]{\bar{\pi}}} \tag{7.8}$$

for all subsets $Z \subseteq T$ and all k disjoint $(T^+ \cap Z, T^- \setminus Z)$-cuts $S_1 \subseteq \ldots \subseteq S_k \subseteq V$, i.e., $(T^+ \cap Z) \subseteq S_i$, $(T^- \setminus Z) \cap S_i = \emptyset$ for all $i = 1, \ldots, k$ and $\delta(S_i) \cap \delta(S_j) = \emptyset$ for all $i \neq j$, where $\delta(S_i) := \delta^{in}(S_i) \cup \delta^{out}(S_i)$.

Note that (7.8) is a linear inequality in the design variables z. Furthermore, [8] shows that these inequalities can be separated in polynomial time using submodular function minimization.

Remark 7.8 A large branch of research on topology optimization with nonlinear flows focuses on the application of gas or water networks. Many of these works solve the nonconvex topology optimization problem by exploiting (convex) relaxations of the original problem such as in [9, 54]. Specific algorithms for topology optimization with a given network design such as with continuous design decisions [18], e.g., continuous diameter selections, or discrete ones [67] are developed. Moreover, there exist works on valid inequalities [40], pruning conditions [41], or decompositions [66] in the context of gas network optimization. Furthermore, the design of robust gas pipeline networks, with interval uncertainties in the sinks only, is solved by applying a mixed-integer second-order cone formulation; see [71]. For stochastic gas network design such as the location of compressors under load uncertainties, we refer to [32].

For water networks, tailored mixed-integer nonlinear optimization methods for choosing optimal diameters are developed in [11, 12]. Furthermore, two decomposition methods are presented in the recent work [55]. For the literature on lossless DC power flow networks, we refer to [20] and the recent survey [42].

Many of these approaches, in particular for gas and water networks, can most likely be extended to general potential-based flows (7.3) as demonstrated for the relaxation of [9] in [74].

7.6 Robust Approaches for Tackling Uncertainty

The field of potential-based flows under uncertainty is mainly driven by specific applications over the last years, e.g., topology optimization [58, 62, 74], operation of utility networks [4], or the analyses of specific energy markets [50]. Different types of uncertainty have been addressed, which can be classified into load uncertainties of injections and withdrawals as well as uncertainties in technical parameters, e.g., estimations of the roughness of gas pipelines. The resulting uncertain optimization problems are mainly tackled by using robust, stochastic, or so-called probust approaches. The latter is a combination of robust and stochastic optimization. We now briefly summarize corresponding approaches that address uncertainties in potential-based optimization problems.

The overall goal of robust optimization consists of computing a robust solution that is feasible for all possible realizations within an a priori defined uncertainty set. For a general introduction to robust optimization, we refer to, e.g., [5, 25, 77].

Robust optimization methods for potential-based flow problems have attracted growing attention in the recent years. In particular, the corresponding research focuses on adjustable robust approaches. In these optimization problems, the variables partition into "here-and-now" decisions that have to be decided before the uncertainty realizes and into so-called "wait-and-see" decisions that can be adjusted after the realization of the uncertainty. A prominent example for this problem class is adjustable robust network design with uncertain loads; see [74]. The optimization task consists of building a network at minimum cost so that all, possibly infinitely many, load scenarios of the uncertainty set, can be transported through the network. This can be formulated as

$$\min_{z} \left\{ \sum_{a \in A} c_a z_a \,:\, z \in \{0,1\}^A \text{ and } \forall b \in U \; \exists\, (x, \pi) \text{ satisfying (7.7b)–(7.7e)} \right\}. \quad (7.9)$$

The non-empty and compact uncertainty set U includes all load uncertainties such as forecasts of future energy demand. The variables z represent the here-and-now decisions of building an arc, which has to be decided prior to the realization of the uncertain load b. After the worst-case realization of the uncertain load, the wait-and-see variables x, π guarantee a feasible transport of the realized load through the network.

Note that considering the potential-based variables x and π as here-and-now decisions directly leads to the infeasibility of (7.9) in many cases. This is a consequence of the uniqueness results of Theorem 7.1, because for fixed x and π changing the load b directly renders the potential-based flow infeasible.

The wait-and-see decisions in (7.9) are restricted by nonlinear and nonconvex constraints leading to a nonlinear adjustable robust optimization problem. General methods for this problem class are scarce [77] and, in particular, there are no general methods of robust optimization directly applicable to solve Problem (7.9). For different use cases, specific methods to solve Problem (7.9) have been developed over the recent years, e.g., starting with tree-shaped networks and further developments to more general networks.

The majority of the works focus on passive networks with load uncertainties because integer wait-and-see decisions are an additional challenge beyond the nonconvex nature of the problem. We now highlight one of the main algorithmic developments

of this research branch that has emerged out of multiple different publications on this topic [4, 50, 51, 59, 62, 73, 74]. To this end, we follow the most general form of these results given in the recent publication [74]. The key idea consists of deciding robust feasibility of a network by solving polynomially many optimization problems instead of individually checking the feasibility for all, possible infinitely many, realizations of the uncertainty $b \in U$.

Theorem 7.9 (Theorem 1 in [74]) *Let $z \in \{0,1\}^A$ be fixed and the corresponding potential network (G, β) be passive and weakly connected. Further, the potential function ψ is continuous, strictly increasing, and satisfies $\psi(0) = 0$, and a load uncertainty set $U := \{b \in \mathbb{R}^V : \sum_{v \in V} b_v = 0\} \cap Z$, with Z being nonempty and compact, is given. Then, the potential network (G, β) is robust feasible, i.e.,*

$$\forall b \in U \; \exists (x, \pi) \text{ satisfying } (7.7b)\text{–}(7.7e),$$

if and only if

$$\overline{\pi}_u - \underline{\pi}_v \geq \max_{b,x,\pi} \{\pi_u - \pi_v : (7.7b)\text{–}(7.7c),\ b \in U\}, \quad (u,v) \in V^2, \tag{7.10a}$$

$$\overline{x}_a \geq \max_{b,x,\pi} \{x_a : (7.7b)\text{–}(7.7c),\ b \in U\}, \quad a \in A, \tag{7.10b}$$

$$\underline{x}_a \leq \min_{b,x,\pi} \{x_a : (7.7b)\text{–}(7.7c),\ b \in U\}, \quad a \in A. \tag{7.10c}$$

The key intuition of this characterization of robust feasibility is the following. For two given nodes u, v, the right-hand sides of Constraint (7.10a) represent the most stressful load scenarios w.r.t. the potential differences by optimizing over the uncertainty set U. If and only if the maximum potential differences stays within the corresponding potential bounds for every pair of nodes, we can shift the potentials to stay within the potential bounds, i.e., we can satisfy Constraints (7.3f). Analogously, Constraints (7.10b) and (7.10c) check if the most stressful load scenarios for the maximum and minimum arc flow stay within the flow bounds. Thus, by solving at most $|V|^2 + 2|V|$ optimization problems, we can check whether a network design is robust feasible regarding, possibly infinitely many, uncertainties in U. We note that for proving the corresponding results, the uniqueness result of Theorem 7.1 and the intuition of the characterization of feasible potential-based flows of Theorem 7.2 play a crucial rule.

Note that for capacitated linear flows without potentials, the characterization of Theorem 7.9 does not hold because flows along cycles will be infinity, which directly renders Constraint (7.10b) infeasible. This is also one reason why this characterization has only been proven in its general form for passive networks, in which no cyclic flow can occur; see Theorem 7.3.

Large parts of this characterization of robust feasibility have been developed in the context of the economic application of deciding the feasibility of a so-called booking within the European entry-exit market; see [50,51,73,74]. From a mathematical point of view, this application is equivalent to deciding the robust feasibility of a given here-and-now decision and a specific interval uncertainty set for the loads. For more details on this economic application we refer to [28], which introduces the underlying mathematical model of the European entry-exit gas market; see also the Chap. 8, "Models for Gas

Markets" in this book. Moreover, there are first approaches for deciding the feasibility of bookings in active networks under the restrictions that no active element lies on a cycle; see [59].

We further note that robust potential-based flows in which uncertain loads only occur in the sinks of the network are considered in [76]. For this special case, the authors also provide a characterization of robustness using finitely many worst-case load scenarios.

A different notion of robustness is studied in [44], in which a network is defined to be robust if for every feasible load $b \in B(V)$ also $b' \in B(V)$ with $|b'_v| \leq |b_v|$ is feasible. If the resistances β can be changed, this allows for a characterization of such networks via graph minors, i.e., via resorting to purely combinatorial properties of the underlying graph.

In addition to load uncertainties, first research on other types of uncertainty has started. For instance, the authors of [58] propose a generic approach to compute systems that are robust/resilient against a failure of at most a given number of components and apply it to topology optimization of gas networks. Moreover, in [4] uncertainties in the resistance constant β are considered, which can represent measurement errors of the involved physical parameters.

Remark 7.9 To the best of our knowledge, there are no approaches for stochastic potential-based flows given in their general form (7.3). However, there are multiple approaches driven by specific applications such as gas networks, which we very briefly summarize in the following. The authors of [27] study the probability of feasible loads for networks with uncertain exit loads and a single entry. To this end, they develop and apply a spheric-radial decomposition of Gaussian random vectors in combination with Quasi Monte-Carlo sampling. In [31], again the probability of the loads is estimated, this time for tree-shaped gas networks with compressors. In addition, also a stochastic version of the economic application of deciding the feasibility of a booking is studied in [37]. For more details, see also the Chap. 10, "From Probabilistic to Probust Constraints: Optimization under Uncertainty" in this book.

Remark 7.10 In the recent years, the combination of stochastic and robust optimization via so-called probust constraints has gained increased attention. These probust constraints are probabilistic constraints including a robustified infinite inequality system; see [2] for a detailed introduction as well as the Chap. 10, "From Probabilistic to Probust Constraints: Optimization under Uncertainty". Again results for probust constraints focus on specific applications such as gas networks [2, 26, 35] or water networks [6].

7.7 Potential-Based MINLP and Beyond

One line of research focuses on replacing potential-based networks by smaller, equivalent potential-based networks to simplify solving potential-based MINLPs in line with the results of [29]; see Theorem 7.4. In the recent work [45] the authors show that it is generally not possible to replace a potential-based network by a smaller network depending on the number of sinks. Furthermore, they characterize specific potential-based

networks that can be reduced either to a complete graph or to a path. We note that there exists network reduction techniques for lossless DC power flows [16, 19, 34, 47, 48]. However, it is not obvious if and how these results can be extended to general potential-based flows.

Research on decomposition methods for general potential-based flows is still in its early stages; see, e.g., [70], which introduces a network partitioning algorithm for general potential-based networks. However, for specific fluids such as natural gas, tailored decomposition methods have been developed, in, e.g., [23,24,49]. For related decomposition techniques on the PDE-level, we refer to the Chap. 17, "Domain Decomposition for Gas Network Control".

For general active potential-based networks, structural properties, in particular about the control of active elements, remain relatively underexplored in the literature. Notably, first specific characteristics related to the control of active elements in such networks are examined in [29]; see also the Chap. 6, "Mixed-Integer Nonlinear Optimization in the Context of Gas Networks" in this book.

Finally, we note that the structural properties of uniqueness and positive homogeneity, see Lemmas 7.1 and Remark 7.6, have been successfully exploited in bilevel optimization; see [59,65]. More precisely, for bilevel problems with a lower level that is a passive potential-based flow problem, it can be shown that specific constraints of (7.3) can be equivalently moved from the lower- to the upper-level problem. The latter then allows to derive a single-level reformulation of the original bilevel problem that has a nonconvex lower level.

7.8 Conclusion and Challenges

The goal of this chapter was to highlight basic properties of potential-based flows and to highlight recent developments in this area. We believe that this model makes it possible to develop generic techniques that would otherwise be reinvented for the different applications.

The field also offers the opportunity for future developments. For instance, there are most likely properties that have been studied for certain applications but that are not yet generalized to the setting of potential-based flows. Moreover, one can try to generalize certain network components like compressors and control valves and incorporate them into the potential-based flow framework. The development of new valid inequalities and cuts for potential-based networks also is a largely open field, offering multiple opportunities for future research. Finally, open questions that we mentioned in this survey are the theoretical hardness of the MPD problem on trees with active elements, the development of robust optimization models and techniques for active potential networks, the treatment of the area of bilevel network design, or, finally, the study of further decomposition techniques for hard (MI)NLPs on potential networks.

Acknowledgements This work was supported by the German Research Foundation (DFG) within Subprojects A04, A007, and B08 in the Sonderforschungsbereich/Transregio 154 "Mathematical Modelling, Simulation and Optimization using the Example of Gas Networks" (Project ID 239904186).

References

1. J. Abreu, E. Cabrera, J. Izquierdo, and J. García-Serra. Flow modeling in pressurized systems revisited. *Journal of Hydraulic Engineering*, 125(11):1154–1169, 1999. doi:10.1061/(ASCE)0733-9429(1999)125:11(1154).
2. D. Adelhütte, D. Aßmann, T. Gonzàlez Grandòn, M. Gugat, H. Heitsch, R. Henrion, F. Liers, S. Nitsche, R. Schultz, M. Stingl, and D. Wintergerst. Joint model of probabilistic-robust (probust) constraints applied to gas network optimization. *Vietnam Journal of Mathematics*, 49(4):1097–1130, 2021. doi:10.1007/s10013-020-00434-y.
3. R. K. Ahuja, T. L. Magnanti, and J. B. Orlin. *Network flows: theory, algorithms, and applications*. Prentice-Hall, Inc., USA, 1993.
4. D. Aßmann, F. Liers, and M. Stingl. Decomposable robust two-stage optimization: an application to gas network operations under uncertainty. *Networks*, 74(1):40–61, 2019. doi:10.1002/net.21871.
5. A. Ben-Tal, L. E. Ghaoui, and A. Nemirovski. *Robust Optimization*. Princeton University Press, 2009. URL: https://press.princeton.edu/books/hardcover/9780691143682/robust-optimization.
6. H. Berthold, H. Heitsch, R. Henrion, and J. Schwientek. On the algorithmic solution of optimization problems subject to probabilistic/robust (probust) constraints. *Mathematical Methods of Operations Research*, 96(1):1–37, 2022. doi:10.1007/s00186-021-00764-8.
7. G. Birkhoff and J. B. Diaz. Non-linear network problems. *Quarterly of Applied Mathematics*, 13:431–443, 1956. doi:10.1090/qam/77398.
8. P. Börner, M. Klimm, A. Lutz, M. E. Pfetsch, M. Skutella, and L. Strubberg. Valid cuts for the design of potential-based flow networks. In N. Megow and A. Basu, ed., *Integer Programming and Combinatorial Optimization*, pages 142–156, Cham, 2025. Springer Nature Switzerland.
9. C. Borraz-Sánchez, R. Bent, S. Backhaus, H. Hijazi, and P. Van Hentenryck. Convex relaxations for gas expansion planning. *INFORMS Journal on Computing*, 28(4):645–656, 2016. doi:10.1287/ijoc.2016.0697.
10. T. Böttger, V. Grimm, T. Kleinert, and M. Schmidt. The cost of decoupling trade and transport in the European entry-exit gas market with linear physics modeling. *European Journal of Operational Research*, 297(3):1095–1111, 2022. doi:10.1016/j.ejor.2021.06.034.
11. C. Bragalli, C. D'Ambrosio, J. Lee, A. Lodi, and P. Toth. On the optimal design of water distribution networks: a practical MINLP approach. *Optimization and Engineering*, 13(2):219–246, 2012. doi:10.1007/s11081-011-9141-7.
12. C. Bragalli, C. D'Ambrosio, J. Lee, A. Lodi, and P. Toth. An MINLP solution method for a water network problem. In Y. Azar and T. Erlebach, ed., *Algorithms – ESA 2006*, volume 4168 of *Lecture Notes in Computer Science*, pages 696–707. Springer Berlin Heidelberg, 2006. doi:10.1007/11841036_62.
13. J. Burgschweiger, B. Gnädig, and M. C. Steinbach. Optimization models for operative planning in drinking water networks. *Optimization and Engineering*, 10(1):43–73, 2009. doi:10.1007/s11081-008-9040-8.
14. R. Burlacu, H. Egger, M. Groß, A. Martin, M. E. Pfetsch, L. Schewe, M. Sirvent, and M. Skutella. Maximizing the storage capacity of gas networks: a global MINLP approach. *Optimization and Engineering*, 20(2):543–573, 2019. doi:10.1007/s11081-018-9414-5.
15. B. Calvert and G. Keady. Braess's paradox and power-law nonlinearities in networks. *The Journal of the Australian Mathematical Society Series B Applied Mathematics*, 35:1–22, 1993.
16. S. Chaudhuri, K. V. Subrahmanyam, F. Wagner, and C. D. Zaroliagis. Computing mimicking networks. *Algorithmica*, 26(1):31–49, 2000. doi:10.1007/s004539910003.
17. M. Collins, L. Cooper, R. Helgason, J. Kennington, and L. LeBlanc. Solving the pipe network analysis problem using optimization techniques. *Management Science*, 24(7):747–760, 1978. doi:10.1287/mnsc.24.7.747.
18. D. de Wolf and Y. Smeers. Optimal dimensioning of pipe networks with application to gas transmission networks. *Operations Research*, 44(4):596–608, 1996. doi:10.1287/opre.44.4.596.
19. F. Dorfler and F. Bullo. Kron reduction of graphs with applications to electrical networks. *IEEE Transactions on Circuits and Systems I: Regular Papers*, 60(1):150–163, 2013. doi:10.1109/TCSI.2012.2215780.

20. H. Farias de Barros, M.-C. Alvarez-Herault, B. Raison, and Q. T. Tran. Optimal AC/DC distribution systems expansion planning from DSO's perspective considering topological constraints. *IEEE Transactions on Power Delivery*, 38(5):3417–3428, 2023. doi:10.1109/TPWRD.2023.3277089.
21. J. Ford, L.R. and D. R. Fulkerson. A suggested computation for maximal multi-commodity network flows. *Management Science*, 5:97–101, 1958.
22. A. Fügenschuh, B. Geißler, R. Gollmer, A. Morsi, M. E. Pfetsch, J. Rövekamp, M. Schmidt, K. Spreckelsen, and M. C. Steinbach. Physical and technical fundamentals of gas networks. In Koch et al. [46], chapter 2, pages 17–44. doi:10.1137/1.9781611973693.ch2.
23. B. Geißler, A. Morsi, L. Schewe, and M. Schmidt. Solving power-constrained gas transportation problems using an MIP-based alternating direction method. *Computers & Chemical Engineering*, 82:303–317, 2015. doi:10.1016/j.compchemeng.2015.07.005.
24. B. Geißler, A. Morsi, L. Schewe, and M. Schmidt. Solving highly detailed gas transport MINLPs: Block separability and penalty alternating direction methods. *INFORMS Journal on Computing*, 30(2):309–323, 2018. doi:10.1287/ijoc.2017.0780.
25. M. Goerigk and M. Hartisch. *An Introduction to Robust Combinatorial Optimization – Concepts, Models and Algorithms for Decision Making Under Uncertainty*, volume 361 of *International Series in Operations Research & Management Science*. Springer, Cham, 2024. doi:10.1007/978-3-031-61261-9.
26. T. González Grandón, H. Heitsch, and R. Henrion. A joint model of probabilistic/robust constraints for gas transport management in stationary networks. *Computational Management Science*, 14(3):443–460, 2017. doi:10.1007/s10287-017-0284-7.
27. C. Gotzes, H. Heitsch, R. Henrion, and R. Schultz. On the quantification of nomination feasibility in stationary gas networks with random load. *Mathematical Methods of Operations Research*, 84(2):427–457, 2016. doi:10.1007/s00186-016-0564-y.
28. V. Grimm, L. Schewe, M. Schmidt, and G. Zöttl. A multilevel model of the European entry-exit gas market. *Mathematical Methods of Operations Research*, 89(2):223–255, 2019. doi:10.1007/s00186-018-0647-z.
29. M. Gross, M. E. Pfetsch, L. Schewe, M. Schmidt, and M. Skutella. Algorithmic results for potential-based flows: Easy and hard cases. *Networks*, 73(3):306–324, 2019. doi:10.1002/net.21865.
30. M. Groß, M. E. Pfetsch, and M. Skutella. On the complexity of instationary gas flows. *Operations Reearch Letters*, 46(3):286–290, 2018. doi:10.1016/J.ORL.2018.01.007.
31. M. Gugat and M. Schuster. Stationary gas networks with compressor control and random loads: optimization with probabilistic constraints. *Mathematical Problems in Engineering*, pages Art. ID 7984079, 17, 2018. doi:10.1155/2018/7984079.
32. M. Gugat, M. Schuster, and J. Sokolowski. The location problem for compressor stations in pipeline networks. *Mathematics and Mechanics of Complex Systems*, 12:507–546, 2024. doi:10.2140/memocs.2024.12.507.
33. O. Habeck and M. E. Pfetsch. Combinatorial acyclicity models for potential-based flows. *Networks*, 79(1):83–104, 2021. doi:10.1002/net.22038.
34. T. Hagerup, J. Katajainen, N. Nishimura, and P. Ragde. Characterizing multiterminal flow networks and computing flows in networks of small treewidth. *Journal of Computer and System Sciences*, 57(3):366–375, 1998. doi:10.1006/jcss.1998.1592.
35. H. Heitsch, R. Henrion, and C. Tischendorf. Probabilistic maximization of time-dependent capacities in a gas network. *Optimization and Engineering*, 26(1):365–400, 2025. doi:10.1007/s11081-024-09908-1.
36. C. T. Hendrickson and B. N. Janson. A common network flow formulation for several civil engineering problems. *Civil Engineering Systems*, 1(4):195–203, 1984. doi:10.1080/02630258408970343.
37. B. Hiller, C. Hayn, H. Heitsch, R. Henrion, H. Leövey, A. Möller, and W. Römisch. Methods for verifying booked capacities. In *Evaluating gas network capacities*, volume 21 of *MOS-SIAM Series on Optimization*, pages 291–315. SIAM, Philadelphia, PA, 2015. doi:10.1137/1.9781611973693.ch14.
38. J. Humpola. *Gas network optimization by MINLP*. Dissertation, Technische Universität Berlin, 2014. doi:10.14279/depositonce-4255.

39. J. Humpola and A. Fügenschuh. Convex reformulations for solving a nonlinear network design problem. *Computational Optimization and Applications*, 62(3):717–759, 2015. doi:10.1007/s10589-015-9756-2.
40. J. Humpola, A. Fügenschuh, and T. Koch. Valid inequalities for the topology optimization problem in gas network design. *OR Spectrum*, 38(3):597–631, 2016. doi:10.1007/s00291-015-0390-2.
41. J. Humpola and F. Serrano. Sufficient pruning conditions for MINLP in gas network design. *EURO Journal on Computational Optimization*, 5(1-2):239–261, 2017. doi:10.1007/s13675-016-0077-8.
42. A. Kaya, A. J. Conejo, and S. Rebennack. Fifty years of power systems optimization. *European Journal of Operational Research*, 2025. doi:10.1016/j.ejor.2025.05.022.
43. D. Kirschen and G. Strbac. *Transmission Networks and Electricity Markets*, chapter 6, pages 141–204. John Wiley & Sons, Ltd, 2004. doi:10.1002/0470020598.ch6.
44. M. Klimm, M. E. Pfetsch, R. Raber, and M. Skutella. On the robustness of potential-based flow networks. *Mathematical Programming*, 197(1):337–374, 2023. doi:10.1007/s10107-021-01760-w.
45. M. Klimm, M. E. Pfetsch, R. Raber, and M. Skutella. Reduction of potential-based flow networks. *Mathematics of Operations Research*, 48(4):2287–2303, 2023. doi:10.1287/moor.2022.1338.
46. T. Koch, B. Hiller, M. E. Pfetsch, and L. Schewe, ed. *Evaluating Gas Network Capacities*. MOS-SIAM Series on Optimization. SIAM, Philadelphia, PA, USA, 2015. doi:10.1137/1.9781611973693.
47. R. Krauthgamer and I. Rika. *Mimicking Networks and Succinct Representations of Terminal Cuts*, pages 1789–1799. SIAM, 2013. doi:10.1137/1.9781611973105.128.
48. G. Kron. *Tensor Analysis of Networks*. John Wiley and Sons, Inc., London, 1949.
49. R. Krug, G. Leugering, A. Martin, M. Schmidt, and D. Weninger. A consensus-based alternating direction method for mixed-integer and PDE-constrained gas transport problems. *INFORMS Journal on Computing*, 2023. doi:10.1287/ijoc.2022.0319.
50. M. Labbé, F. Plein, and M. Schmidt. Bookings in the European gas market: characterisation of feasibility and computational complexity results. *Optimization and Engineering*, 21(1):305–334, 2020. doi:10.1007/s11081-019-09447-0.
51. M. Labbé, F. Plein, M. Schmidt, and J. Thürauf. Deciding feasibility of a booking in the European gas market on a cycle is in P for the case of passive networks. *Networks*, 78(2):128–152, 2021. doi:10.1002/net.22003.
52. B. E. Larock, R. W. Jeppson, and G. Z. Watters. *Hydraulics of Pipeline Systems*. CRC press, 2010.
53. K. Lehmann, A. Grastien, and P. V. Hentenryck. The complexity of DC-switching problems, 2014. arXiv:1411.4369.
54. Y. Li, S. S. Dey, and N. V. Sahinidis. A reformulation-enumeration MINLP algorithm for gas network design. *Journal of Global Optimization*, 2024. doi:10.1007/s10898-024-01424-x.
55. Y. Li, S. S. Dey, N. V. Sahinidis, N. Susarla, M. A. Zamarripa, and M. G. Drouven. Optimizing the design and operation of water networks: Two decomposition approaches. *Computers & Chemical Engineering*, 192:108897, 2025. doi:10.1016/j.compchemeng.2024.108897.
56. A. Martin, K. Klamroth, J. Lang, G. Leugering, A. Morsi, M. Oberlack, M. Ostrowski, and R. Rosen, ed. *Mathematical Optimization of Water Networks*. Birkhäuser Basel, 2012. doi:10.1007/978-3-0348-0436-3.
57. J. J. Maugis. Etude de réseaux de transport et de distribution de fluide. *RAIRO. Recherche opérationnelle*, 11(2):243–248, 1977.
58. M. E. Pfetsch and A. Schmitt. A generic optimization framework for resilient systems. *Optimization Methods & Software*, 38(2):356–385, 2023. doi:10.1080/10556788.2022.2142581.
59. F. Plein, J. Thürauf, M. Labbé, and M. Schmidt. A bilevel optimization approach to decide the feasibility of bookings in the European gas market. *Mathematical Methods of Operations Research*, 95(3):409–449, 2022. doi:10.1007/s00186-021-00752-y.
60. A. U. Raghunathan. Global optimization of nonlinear network design. *SIAM Journal on Optimization*, 23(1):268–295, 2013. doi:10.1137/110827387.
61. R. Z. Ríos-Mercado, S. Wu, L. R. Scott, and E. A. Boyd. A reduction technique for natural gas transmission network optimization problems. *Annals of Operations Research*, 117(1):217–234, 2002. doi:10.1023/A:1021529709006.

62. M. Robinius, L. Schewe, M. Schmidt, D. Stolten, J. Thürauf, and L. Welder. Robust optimal discrete arc sizing for tree-shaped potential networks. *Computational Optimization and Applications*, 73(3):791–819, 2019. doi:10.1007/s10589-019-00085-x.
63. R. T. Rockafellar. *Network Flows and Monotropic Optimization*. Athena Scientific, Belmont, Mass., USA, 2nd edition, 1998.
64. L. Schewe, M. Schmidt, and J. Thürauf. Global optimization for the multilevel European gas market system with nonlinear flow models on trees. *Journal of Global Optimization. An International Journal Dealing with Theoretical and Computational Aspects of Seeking Global Optima and Their Applications in Science, Management and Engineering*, 82(3):627–653, 2022. doi:10.1007/s10898-021-01099-8.
65. M. Schmidt and J. Thürauf. An exact method for nonlinear network flow interdiction problems. *SIAM Journal on Optimization*, 34(4):3623–3652, 2024. doi:10.1137/22M152983X.
66. J. Schweiger and F. Liers. A decomposition approach for optimal gas network extension with a finite set of demand scenarios. *Optimization and Engineering*, 19(2):297–326, 2018. doi:10.1007/s11081-017-9371-4.
67. N. Shiono and H. Suzuki. Optimal pipe-sizing problem of tree-shaped gas distribution networks. *European Journal of Operational Research*, 252(2):550–560, 2016. doi:10.1016/j.ejor.2016.01.008.
68. M. Skutella. An introduction to network flows over time. In W. Cook, L. Lovász, and J. Vygen, ed., *Research Trends in Combinatorial Optimization*, pages 451–482. Springer, 2009. doi:10.1007/978-3-540-76796-1_21.
69. M. Skutella. An introduction to transshipments over time. In F. Fischer and R. Johnson, ed., *Surveys in Combinatorics 2024*, pages 239–270. Cambridge University Press, 2024. doi:10.1017/9781009490559.009.
70. S. Srinivasan and K. Sundar. Hierarchical network partitioning for solution of potential-driven, steady-state nonlinear network flow equations. *IEEE Control Systems Letters*, 2025. doi:10.1109/lcsys.2025.3533383.
71. K. Sundar, S. Misra, A. Zlotnik, and R. Bent. Robust gas pipeline network expansion planning to support power system reliability. In *2021 American Control Conference (ACC)*, pages 620–627, 2021. doi:10.23919/ACC50511.2021.9483249.
72. J. Szabó. The set of solutions to nomination validation in passive gas transportation networks with a generalized flow formula. ZIB-Report 11-44, Zuse Intitute Berlin, 2012.
73. J. Thürauf. Deciding the feasibility of a booking in the European gas market is coNP-hard. *Annals of Operations Research*, 318(1):591–618, 2022. doi:10.1007/s10479-022-04732-1.
74. J. Thürauf, J. Grübel, and M. Schmidt. Adjustable robust nonlinear network design without controllable elements under load scenario uncertainties. *Mathematical Programming*, 2025. doi:10.1007/s10107-025-02207-2.
75. M. Vuffray, S. Misra, and M. Chertkov. Monotonicity of dissipative flow networks renders robust maximum profit problem tractable: General analysis and application to natural gas flows. In *54th IEEE Conference on Decision and Control (CDC)*, pages 4571–4578, 2015. doi:10.1109/CDC.2015.7402933.
76. M. Vuffray, S. Misra, and M. Chertkov. Monotonicity of dissipative flow networks renders robust maximum profit problem tractable: General analysis and application to natural gas flows. In *2015 54th IEEE Conference on Decision and Control (CDC)*, pages 4571–4578, 2015. doi:10.1109/CDC.2015.7402933.
77. İ. Yanıkoğlu, B. L. Gorissen, and D. den Hertog. A survey of adjustable robust optimization. *European Journal of Operational Research*, 277(3):799–813, 2019. doi:10.1016/j.ejor.2018.08.031.
78. D. Yates, A. Templeman, and T. Boffey. The computational complexity of the problem of determining least capital cost designs for water supply networks. *Engineering Optimization*, 7:2:143–155, 1984. doi:10.1080/03052158408960635.

Open Access This chapter is licensed under the terms of the Creative Commons Attribution-NonCommercial-NoDerivatives 4.0 International License (http://creativecommons.org/licenses/by-nc-nd/4.0/), which permits any noncommercial use, sharing, distribution and reproduction in any medium or format, as long as you give appropriate credit to the original author(s) and the source, provide a link to the Creative Commons license and indicate if you modified the licensed material. You do not have permission under this license to share adapted material derived from this chapter or parts of it.

The images or other third party material in this chapter are included in the chapter's Creative Commons license, unless indicated otherwise in a credit line to the material. If material is not included in the chapter's Creative Commons license and your intended use is not permitted by statutory regulation or exceeds the permitted use, you will need to obtain permission directly from the copyright holder.



Chapter 8
Models for Gas Markets

Veronika Grimm[0000−0002−9025−9731],
Julia Grübel[0009−0001−0808−9463],
Johannes Hahn[0009−0005−3016−2996],
Max Klimm[0000−0002−9061−2267],
Lars Schewe[0000−0002−3778−262X],
Martin Schmidt[0000−0001−6208−5677], and
Gregor Zöttl[0000−0002−2729−1173]

Abstract This chapter reviews models for gas markets that serve as a mathematical abstraction of the entry-exit system employed in the European gas market. A particular focus is on a four-level model where, in the first level, the transmission system operator sets technical capacities and (lower bounds on) booking prices for network nodes. In the second level, producers and consumers book capacities at their respective entry and exit points covering multiple time periods. In the third level, producers and consumers nominate production and consumption for the individual periods, and in the fourth level, the transmission system operator realizes the gas flow in all time periods based on the nominated gas demands of producers and consumers. Further modeling variants are discussed.

Veronika Grimm
Energy Systems & Market Design, University of Technology Nuremberg (UTN), Germany,
e-mail: veronika.grimm@utn.de

Julia Grübel
Analytics & Optimization, University of Technology Nuremberg (UTN), Germany,
e-mail: julia.gruebel@utn.de

Johannes Hahn
Analytics & Optimization, University of Technology Nuremberg (UTN), Germany,
e-mail: johannes.hahn@utn.de

Max Klimm
Department of Mathematics, TU Berlin, Germany, e-mail: klimm@tu-berlin.de

Lars Schewe
School of Mathematics, The University of Edinburgh, UK, e-mail: lars.schewe@ed.ac.uk

Martin Schmidt
Department of Mathematics, Trier University, Germany, e-mail: martin.schmidt@uni-trier.de

Gregor Zöttl
Industrial Organization and Energy Markets, Friedrich-Alexander-Universität Erlangen-Nürnberg,
Germany, e-mail: gregor.zoettl@fau.de

© The Author(s) 2027

A. Martin et al. (eds.), *Mathematical Modelling, Simulation and Optimization using the Example of Gas Networks*, International Series of Numerical Mathematics 174,
https://doi.org/10.1007/978-3-032-34969-9_8

8.1 Introduction

The current gas market design in the European Union is the result of the liberalization process that began in the 1990s. The first Gas Directive [16], passed in 1998, stipulated the principle of non-discriminatory access to the gas network. It was followed in 2003 by the second Gas Directive [15] mandating the implementation of rules allowing buyers to purchase gas from the supplier of their choice. These rules, however, did not fully prevent discriminatory behavior as transmission system operators (TSOs) still had incentives to prevent network access to third-party suppliers. The third Gas Directive [16] of 2009 was introduced to mitigate this issue by requiring the unbundling of network operation and network usage. It further introduced the entry-exit system as a target market design for the gas market in the European Union.

The entry-exit system largely abstracts from the physical properties of the gas network. Instead, it allows producers and consumers to book capacity rights independently at entry points V_+ and exit points V_- of the network. A booking is a right, sold to the producers and consumers at a price, that allows them to withdraw or inject gas up to a volume defined in the booking. The transmission system operators (TSOs) have to make sure that the bookings made for the entry and exit points can be realized with the network. To this end, they can impose technical capacities for the total bookings that can be made for an entry or exit node. When the total capacity bookings for a node do not exceed the capacity, the principle of non-discriminatory access requires that all bookings will be accepted. If, on the other hand, the total bookings for a node exceed its capacity, in practice, an auction mechanism is used to allocate the bookings. After the bookings have been fixed, gas is traded on a day-to-day basis. To model this, we introduce a set T of scenarios, each corresponding to a day in the booking period. In every scenario $t \in T$, all producers and consumers can submit a nomination for the amount of gas that they would like to inject into or withdraw from the network. The nomination itself is free of charge and only constrained by the long-term bookings made beforehand. In each scenario, after all nominations have been submitted, it is the task of the TSO to ensure that there is a feasible gas transport in the network that satisfies the given nominations.

Structure of this Chapter

After setting up the mathematical terminology in Sect. 8.2, we present a basic four-level model proposed by Grimm et al. [24] in Sect. 8.3. In Sect. 8.4, we discuss the related models and reformulations. While the basic model in Sect. 8.3 assumes that producers and consumers are non-strategic and act as price-takers, we discuss possible models for strategic players in Sect. 8.5. Additional models are mentioned in Sect. 8.6.

8.2 Preliminaries

The gas network is modeled as a directed and weakly connected graph $G = (V, A)$ where V is the set of nodes and $A \subseteq V^2$ is the set of arcs. For a node $v \in V$, we denote by $\delta^-(v) = \{a \in A : a = (w, v) \text{ with } w \in V\}$ the set of ingoing arcs and by $\delta^+(v) = \{a \in A : a = (v, w) \text{ with } w \in V\}$ the set of outgoing arcs. Arcs may represent both inactive network pipes and active elements such as compressor stations and control valves. A flow of gas is allowed both in the direction and against the direction of the arc, where we will use the convention that the former corresponds to a positive gas flow and the latter corresponds to a negative gas flow. We assume that there is a set $V_+ \subset V$ of entry nodes where gas is fed into the network and a set $V_- \subset V$ of exit nodes where gas is withdrawn from the network. We assume that V_- and V_+ are disjoint. The gas is fed into the network and withdrawn from it by individual and selfishly acting players. More formally, for each node $u \in V_+$ there is a set P_u of *producers* interested in injecting gas into the network and for each node $u \in V_-$ there is a set P_u of *consumers* interested in withdrawing gas from the network. We denote by $P_+ = \bigcup_{u \in V_+} P_u$ the set of producers, by $P_- = \bigcup_{u \in V_-} P_u$ the set of consumers, and by $P = P_+ \cup P_-$ their union. We call the union of producers and consumers the *players* of the four-level model.

We consider a finite set T of scenarios, modeling days or other trading periods. For each scenario $t \in T$ and each consumer $i \in P_-$, there is an *inverse market demand function* $P_{i,t} : \mathbb{R}_{\geq 0} \to \mathbb{R}_{\geq 0}$ that determines the price consumer i is willing to pay as a function of the quantity offered to the consumer. Intuitively, this means that consumer i, after having received a total volume of s units of gas, has a utility of $P_{i,t}(s)$ for the next gas particle. As all gas at a node is sold at the same price point, this means that for consumer i to accept a total volume of s units of gas, the price cannot be larger than $P_{i,t}(s)$. It is assumed that the inverse demand functions are continuous and strictly decreasing. When, in scenario t, a consumer receives a quantity $q_{i,t}$ of gas, their consumer surplus equals

$$\text{consumer surplus:} \quad \int_0^{q_{i,t}} P_{i,t}(s)\,\mathrm{d}s. \tag{8.1}$$

For each producer $i \in P_+$, there are variable production costs $c_i^{\text{var}} \geq 0$ so that when they produce a quantity $q_{i,t}$ in scenario t, their costs equal

$$\text{production costs:} \quad c_i^{\text{var}} q_{i,t}. \tag{8.2}$$

Vectors of quantities are denoted in boldface, e.g., we write $\mathbf{q} = (q_{i,t})_{i \in P, t \in T}$ for the vector of in- and outflows into and out of the network for all scenarios. Equations and inequalities for vectors are to be understood entry-wise, e.g., $\mathbf{0} \leq \mathbf{q}$ means that $0 \leq q_{i,t}$ for all $i \in P$ and $t \in T$. Here and throughout the chapter, we use $\mathbf{0}$ to denote the all-zero vector of appropriate dimension.

8.3 Multilevel Model Under Perfect Competition

We consider a market design featuring a TSO and gas traders operating under perfect competition, where all players $i \in P$ act as price-takers. The TSO uses an entry-exit system where, in the first level, technical capacities and booking prices are determined for the nodes. In the second level, players compete for the booking capacities based on the technical capacities and the prices set by the TSO in the first level. In the third level, players nominate actual gas in- and outflows for the network where their nominations are constrained by their respective bookings made in the second level. In the fourth level, the TSO faces the task of determining actual gas flows for all scenarios that satisfy the players' nominations from the third level.

We find it useful to describe the model in detail in reverse order, starting with level four and then working our way upwards in the four-level hierarchy.

8.3.1 Fourth Level: Gas Transport

In the fourth and lowest level of the four-level model, the gas transport is determined by the TSO. The main inputs for this problem are the actual inflow and outflow nominations $q^{\mathrm{nom}}_{i,t}$ that have been fixed by all players i and all scenarios t in the third level. A nomination $q^{\mathrm{nom}}_{i,t}$ of a consumer i, $i \in P_u$, $u \in V_-$ is the total volume of gas that they withdraw from the network at node u in scenario t. Similarly, a nomination $q^{\mathrm{nom}}_{i,t}$ of a producer i, $i \in P_u$, $u \in V_+$, is the total volume of gas that they feed into the network at node u in scenario t. We define $\mathbf{q}^{\mathrm{nom}}_t = (q^{\mathrm{nom}}_{i,t})_{i \in P}$ for the nomination vector of scenario t, and $\mathbf{q}^{\mathrm{nom}} = (q^{\mathrm{nom}}_{i,t})_{i \in P, t \in T}$ for the vector of all nominations. We further write $q^{\mathrm{nom}}_{u,t} = \sum_{i \in P_u} q^{\mathrm{nom}}_{i,t}$ as the total balance of node u in scenario t. Constraints on the third level ensure that all vectors $\mathbf{q}^{\mathrm{nom}}_t$ are balanced, i.e., $\sum_{i \in P_+} q^{\mathrm{nom}}_{i,t} = \sum_{i \in P_-} q^{\mathrm{nom}}_{i,t}$ for all $t \in T$. At the fourth level, the TSO seeks a feasible gas flow for each scenario t that satisfies the corresponding nomination vector $\mathbf{q}^{\mathrm{nom}}_t$, adheres to physical constraints, and minimizes a cost functional. As discussed in detail in Chap. 2, "A Catalog of Gas Network Models: PDEs, Coupling Conditions, and Numerical Schemes", there is an entire hierarchy of possible mathematical models for gas flows of different complexities. To give a specific example, we proceed to describe the optimization problem of the TSO that arises when using (ISO4).

In this model, in every scenario t, the flow $q_{a,t} \in \mathbb{R}$ along each pipe $a = (u, v)$ is determined by the squared pressures $p^2_{u,t}$ and $p^2_{v,t}$ at its endpoints, and is governed by the equation

$$p^2_{u,t} - p^2_{v,t} = \gamma_a \, q_{a,t} \, |q_{a,t}|,$$

where γ_a is a parameter that depends on the physical properties of the pipe, such as diameter, roughness, and length. Safe operation of the network requires that the pressure $p_{u,t}$ of each node u in all scenarios t is in a given interval, i.e., there are $\widehat{p}_u, \check{p}_u \in \mathbb{R}$ with $\widehat{p}_u < \check{p}_u$ such that $p_{u,t} \in [\widehat{p}_u, \check{p}_u]$ for all $t \in T$.

A basic model for network operation costs is to assume that there is a subset of arcs $A^{\mathrm{c}} \subset A$ that can be switched on or off. When switched off, they cannot be used by the flow, and when switched on, they can be used, but the TSO incurs costs of $c_a \in \mathbb{R}_{\geq 0}$. Under these assumptions, the problem of the TSO is to find a feasible flow for each scenario t that satisfies the given nominations and minimizes the costs, i.e., the TSO solves

$$\begin{aligned}
\min \quad & \sum_{t \in T} \sum_{a \in A^{\mathrm{c}}} c_a \, x_{a,t} && && \text{(8.3a)}\\
\text{s.t.} \quad & x_{a,t}(p_{u,t}^2 - p_{v,t}^2) = \gamma_a q_{a,t} \, |q_{a,t}| && \text{for all } a = (u,v) \in A,\, t \in T, && \text{(8.3b)}\\
& \omega_u q_{u,t}^{\mathrm{nom}} = \sum_{a \in \delta^-(u)} q_{a,t} - \sum_{a \in \delta^+(u)} q_{a,t} && \text{for all } u \in V,\, t \in T, && \text{(8.3c)}\\
& x_{a,t} \in \{0,1\} && \text{for all } a \in A^{\mathrm{c}},\, t \in T, && \text{(8.3d)}\\
& q_{a,t} \in \mathbb{R} && \text{for all } a \in A,\, t \in T, && \text{(8.3e)}\\
& p_{u,t} \in [\widehat{p}_u, \check{p}_u] && \text{for all } u \in V,\, t \in T, && \text{(8.3f)}
\end{aligned}$$

where $\omega_u = -1$ for $u \in V_+$, $\omega_u = 1$ for $u \in V_-$, and $\omega_u = 0$ for all other nodes. For future reference, we denote the optimal value of this optimization problem as a function of the nomination vector $\mathbf{q}^{\mathrm{nom}}$ as $\varphi^4(\mathbf{q}^{\mathrm{nom}})$, and the set of feasible gas flows by $\mathcal{F}(\mathbf{q}^{\mathrm{nom}})$. The TSO's decisions in the first level have to ensure that the optimization problem (8.3) always has a solution. The optimization problem (8.3) is a mixed-integer nonlinear optimization problem. Although solving (8.3) is challenging, a broad range of methods for mixed-integer nonlinear optimization is available; see Chap. 6, "Mixed-Integer Nonlinear Optimization in the Context of Gas Networks".

Summarizing this section, for every set of balanced nomination vectors $\mathbf{q}_t^{\mathrm{nom}}$, the TSO finds a cost-minimal gas flow satisfying $\mathbf{q}_t^{\mathrm{nom}}$, resulting in total costs of $\varphi^4(\mathbf{q}^{\mathrm{nom}})$. The next section discusses how these nomination vectors $\mathbf{q}_t^{\mathrm{nom}}$ are obtained.

8.3.2 Third Level: Nomination

In the third level of the four-level model, the nominations $q_{i,t}^{\mathrm{nom}}$ of each player i and scenario t, which were assumed as given in the previous section, are determined. Based on the decisions of the players in this level, a market price π_t^{nom} emerges for each scenario t. We assume that when computing the values $q_{i,t}^{\mathrm{nom}}$, each player i acts as a price-taker, i.e., they neglect the fact that the market price π_t^{nom} for gas in scenario t actually depends on the amount of gas that they nominate. The players are constrained in their nominations by the bookings they made in the second level. Specifically, the booked capacity q_i^{book} determined by player i in the second level is an input to this level.

Each producer $i \in P_+$ maximizes their profit depending on the market prices, i.e., each producer $i \in P_+$ solves for every scenario $t \in T$ the optimization problem

$$\max\{q_{i,t}^{\mathrm{nom}}(\pi_t^{\mathrm{nom}} - c_i^{\mathrm{var}}) : \; q_{i,t}^{\mathrm{nom}} \in [0, q_i^{\mathrm{book}}]\}. \tag{8.4}$$

For future reference, we denote the objective function of that optimization problem by $f_{i,t}(q^{\text{nom}}_{i,t}) = q^{\text{nom}}_{i,t}(\pi^{\text{nom}}_t - c^{\text{var}}_i)$ and its optimal value as a function of q^{book}_i by $\varphi^3_{i,t}(q^{\text{book}}_i) = \max\{f_{i,t}(q^{\text{nom}}_{i,t}) : q^{\text{nom}}_{i,t} \in [0, q^{\text{book}}_i]\}$.

Similarly, each consumer $i \in P_-$ maximizes their benefit depending on the market prices, i.e., each consumer $i \in P_-$ solves for every scenario $t \in T$ the optimization problem

$$\max\left\{\int_0^{q^{\text{nom}}_{i,t}} P_{i,t}(s)\,\mathrm{d}s - \pi^{\text{nom}}_t q^{\text{nom}}_{i,t} : q^{\text{nom}}_{i,t} \in [0, q^{\text{book}}_i]\right\}. \tag{8.5}$$

Again, for future reference, we denote the objective function of that optimization problem by $f_{i,t}(q^{\text{nom}}_{i,t}) = \int_0^{q^{\text{nom}}_{i,t}} P_{i,t}(s)\,\mathrm{d}s - \pi^{\text{nom}}_t q^{\text{nom}}_{i,t}$ and its optimal value as a function of q^{book}_i by $\varphi^3_{i,t}(q^{\text{book}}_i) = \max\{f_{i,t}(q^{\text{nom}}_{i,t}) : q^{\text{nom}}_{i,t} \in [0, q^{\text{book}}_i]\}$.

For given market prices π^{nom}_t, the consumers' optimization problems (8.5) are concave as we assume that the inverse market demand functions $P_{i,t}$ are continuous and strictly decreasing. Thus, for fixed market prices, these concave optimization problems can be solved efficiently to arbitrary precision by standard convex optimization methods. Similarly, for given market prices, the producers' optimization problems are linear programs that can be solved exactly in polynomial time as well.

In addition, we have the market-clearing conditions

$$\sum_{i \in P_+} q^{\text{nom}}_{i,t} = \sum_{i \in P_-} q^{\text{nom}}_{i,t} \quad \text{for all } t \in T. \tag{8.6}$$

A market equilibrium is reached when the individual players' optimization problems (8.4) and (8.5) are solved and, in addition, the market-clearing conditions (8.6) are satisfied. It can be shown that the market equilibrium can be obtained from solving the following welfare maximization problem:

$$\max \quad \sum_{t \in T}\left(\sum_{u \in V_-}\sum_{i \in P_u}\int_0^{q^{\text{nom}}_{i,t}} P_{i,t}(s)\,\mathrm{d}s - \sum_{u \in V_+}\sum_{i \in P_u} c^{\text{var}}_i q^{\text{nom}}_{i,t}\right) \tag{8.7a}$$

$$\text{s.t.} \quad q^{\text{nom}}_{i,t} \geq 0 \qquad \text{for all } i \in P, t \in T, \tag{8.7b}$$

$$q^{\text{nom}}_{i,t} \leq q^{\text{book}}_i \qquad \text{for all } i \in P, t \in T, \tag{8.7c}$$

$$0 = \sum_{u \in V_-}\sum_{i \in P_u} q^{\text{nom}}_{i,t} - \sum_{u \in V_+}\sum_{i \in P_u} q^{\text{nom}}_{i,t} \qquad \text{for all } t \in T. \tag{8.7d}$$

Theorem 8.1 (Grimm et al. [24, Theorem 3]) *Let* $(\mathbf{q}^{\text{nom}}, \boldsymbol{\beta}^-, \boldsymbol{\beta}^+, \boldsymbol{\alpha})$ *be an optimal primal-dual pair of solutions of the welfare maximization problem* (8.7)*, where* $\boldsymbol{\beta}^-$ *corresponds to the constraints* (8.7b)*,* $\boldsymbol{\beta}^+$ *corresponds to the constraints* (8.7c)*, and* $\boldsymbol{\alpha}$ *corresponds to the constraints* (8.7d)*. Then,* $\mathbf{q}^{\text{nom}}$ *and* $\boldsymbol{\pi}^{\text{nom}} = \boldsymbol{\alpha}$ *are a market equilibrium, i.e., they solve* (8.4) *for all* $i \in P_+$*,* $t \in T$*, they solve* (8.5) *for all* $i \in P_-$*,* $t \in T$*, and satisfy* (8.6)*.*

Proof. In our proof, we here follow the general treatment of market equilibria via Lagrangian duality as in Harks and Schwarz [28]. Let us denote by

$$Q = \{\mathbf{q}^{\text{nom}} \in \mathbb{R}^{P\cdot T}_{\geq 0} : q^{\text{nom}}_{i,t} \leq q^{\text{book}}_i \text{ for all } i \in P, t \in T\}$$

the set of all vectors obeying the booking constraints. Then, we may write (8.7) compactly as

$$\begin{aligned} \max \quad & \sum_{t\in T, i\in P} f_{i,t}(q^{\text{nom}}_{i,t}) \\ \text{s.t.} \quad & 0 = \sum_{u\in V_-}\sum_{i\in P_u} q^{\text{nom}}_{i,t} - \sum_{u\in V_+}\sum_{i\in P_u} q^{\text{nom}}_{i,t} \quad \text{for all } t \in T, \\ & \mathbf{q}^{\text{nom}} \in Q. \end{aligned}$$

The Lagrangian for this problem becomes

$$L(\mathbf{q}^{\text{nom}}, \boldsymbol{\lambda}) = \sum_{t\in T, i\in P} f_{i,t}(q^{\text{nom}}_{i,t}) + \sum_{t\in T} \lambda_t \left(\sum_{u\in V_-}\sum_{i\in P_u} q^{\text{nom}}_{i,t} - \sum_{u\in V_+}\sum_{i\in P_u} q^{\text{nom}}_{i,t} \right).$$

The Lagrangian dual is then the function $\mu : \mathbb{R}^T \to \mathbb{R}$ defined as

$$\mu(\boldsymbol{\lambda}) = \sup\{L(\mathbf{q}^{\text{nom}}, \boldsymbol{\lambda}) : \mathbf{q}^{\text{nom}} \in Q\},$$

and the dual problem is $\inf\{\mu(\boldsymbol{\lambda}) : \boldsymbol{\lambda} \in \mathbb{R}^T\}$. This primal-dual pair of optimization problems is said to have zero duality gap if there are $\bar{\boldsymbol{\lambda}} \in \mathbb{R}^T$ and $\bar{\mathbf{q}}^{\text{nom}} \in Q$ such that $L(\bar{\mathbf{q}}^{\text{nom}}, \bar{\boldsymbol{\lambda}}) = \mu(\bar{\boldsymbol{\lambda}})$. Since (8.7) is a concave maximization problem over a nonempty convex feasible set defined by affine and box constraints, strong duality follows from standard convex duality results. We then obtain

$$\bar{\mathbf{q}}^{\text{nom}} \in \arg\max\{L(\mathbf{q}^{\text{nom}}, \bar{\boldsymbol{\lambda}}) : \mathbf{q}^{\text{nom}} \in Q\}.$$

This is equivalent to

$$\bar{\mathbf{q}}^{\text{nom}}_i \in \arg\max\left\{ \sum_{t\in T} \int_0^{q^{\text{nom}}_{i,t}} P_{i,t}(s)\,\mathrm{d}s - \bar{\lambda}_t q^{\text{nom}}_{i,t} : \mathbf{q}^{\text{nom}}_i \in [0, q^{\text{book}}_i]^T \right\} \quad \text{for all } i \in P_-,$$

$$\bar{\mathbf{q}}^{\text{nom}}_i \in \arg\max\left\{ \sum_{t\in T} q^{\text{nom}}_{i,t}(\bar{\lambda}_t - c^{\text{var}}_i) : \mathbf{q}^{\text{nom}}_i \in [0, q^{\text{book}}_i]^T \right\} \quad \text{for all } i \in P_+,$$

and, thus, implies the result. □

It can be further shown that the solution is unique under mild conditions.

Theorem 8.2 (Grimm et al. [24, Theorem 4]) *If the variable costs c^{var}_i, $i \in P_+$, are pairwise distinct and all inverse demand functions are continuous and strictly decreasing, then the optimal primal solution $\mathbf{q}^{\text{nom}}$ to the welfare maximization problem* (8.7) *is unique.*

Proof. Under the conditions of the theorem, the objective function of the optimization problem (8.7) is clearly strictly concave in the consumers' nominations $q^{\text{nom}}_{i,t}$, $i \in P_-$, and hence, their values are unique. Given the uniqueness of the consumed quantities,

a simple exchange argument establishes that only producers with the smallest costs produce at their booking capacity. □

Summarizing this section, we have seen that every vector $\mathbf{q}^{\text{book}}$ of booked capacities leads (under reasonable assumptions) to a unique vector $\mathbf{q}^{\text{nom}}$ of nominated quantities in a market equilibrium. The next section discusses how the players choose the booked capacities $\mathbf{q}^{\text{book}}$.

8.3.3 Second level: Booking

In this level of the four-level model, each player $i \in P$ determines their booking capacity q_i^{book}. The main inputs for this problem are the technical capacity q_u^{tec} and a lower bound on the booking fees $\widehat{\pi}_u^{\text{book}}$ that the TSO determines for all $u \in V_+ \cup V_-$ in the first level of the model.

The objective of each player i is to choose their booking capacity q_i^{book} such that the anticipated benefit that they can generate over all scenarios in the third level minus the price that has to be paid to the TSO for making the booking is maximized. The booking capacities q_i^{book} of all players $i \in P_u$ for some $u \in V_+ \cup V_-$ are constrained by the technical capacity imposed by the TSO in the first level, i.e., we require that $\sum_{i \in P_u} q_i^{\text{book}} \leq q_u^{\text{tec}}$ for all $u \in V_+ \cup V_-$. We assume that there is perfect competition among these players for the technical capacity, resulting in a market price π_u^{book}. Thus, the booking price for node $u \in V_+ \cup V_-$ has two components. The first is the booking fee $\widehat{\pi}_u^{\text{book}}$ set by the TSO in the first level, and the second π_u^{book} arises as a market price from the perfect competition.

Specifically, every player i solves the problem

$$\max\left\{\sum_{t \in T} \varphi_{i,t}^3(q_i^{\text{book}}) - (\widehat{\pi}_u^{\text{book}} + \pi_u^{\text{book}})q_i^{\text{book}} : q_i^{\text{book}} \geq 0\right\}. \tag{8.8}$$

We further assume the market-clearing conditions

$$\sum_{i \in P_u} q_i^{\text{book}} \leq q_u^{\text{tec}} \quad \text{for all } u \in V_+ \cup V_-. \tag{8.9}$$

To avoid multiple solutions, which are often difficult to interpret, for each fixed node $u \in V_+ \cup V_-$, we select the equilibrium induced by the following optimization problem:

$$\max \quad \sum_{i \in P_u} \left(\sum_{t \in T} \varphi_{i,t}^3(q_i^{\text{book}}) - \widehat{\pi}_u^{\text{book}} q_i^{\text{book}} \right) \tag{8.10a}$$

$$\text{s.t.} \quad q_i^{\text{book}} \geq 0 \quad \text{for all } i \in P_u, \tag{8.10b}$$

$$\sum_{i \in P_u} q_i^{\text{book}} \leq q_u^{\text{tec}}. \tag{8.10c}$$

We denote by $\varphi_i^2(q_u^{\text{tec}}, \widehat{\pi}_u^{\text{book}})$ the optimal value function of the optimization problem (8.8). With similar arguments as in the proof of Theorem 8.1, one can show that a primal-dual pair of the optimization problem (8.10) corresponds to a market equilibrium; we omit here the proof and refer instead to [24].

Theorem 8.3 (Grimm et al. [24, Theorem 1]) *Let* $((q_i^{\text{book}})_{i\in P_u}, \boldsymbol{\beta}, \alpha_u)$ *be an optimal primal-dual pair of solutions of* (8.10)*, where* $\boldsymbol{\beta}$ *corresponds to the constraints* (8.10b) *and* α_u *corresponds to the constraint* (8.10c)*. Then,* $(q_i^{\text{book}})_{i\in P_u}$ *and* $\pi_u^{\text{book}} = \alpha_u$ *form a market equilibrium, i.e., they solve* (8.8) *for all* $i \in P_u$ *and satisfy* (8.9)*.*

Again, under additional assumptions, one can show that the solution is unique.

Theorem 8.4 (Grimm et al. [24, Theorem 2]) *If the variable costs* c_i^{var}*,* $i \in P_+$*, are pairwise distinct and the inverse demand functions are continuous and strictly decreasing, then the optimal solution is unique.*

Summarizing this section, we have seen that for every vector $\mathbf{q}^{\text{tec}}$ of technical capacities and every vector $\widehat{\boldsymbol{\pi}}^{\text{book}}$ of lower bounds on the booking fees, there is (under reasonable assumptions) a unique market equilibrium at each node $u \in V_+ \cup V_-$, determining the booked capacities $\mathbf{q}^{\text{book}}$ and corresponding booking prices $\boldsymbol{\pi}^{\text{book}}$. In the next section, we explain how the TSO chooses the technical capacities $\mathbf{q}^{\text{tec}}$ and the lower bounds on the booking fees $\widehat{\boldsymbol{\pi}}^{\text{book}}$.

8.3.4 First Level: Technical Capacities and Booking Fees

In the first level, the TSO determines the maximum technical capacities at the network nodes, i.e., the maximum quantity of gas that can be fed in or withdrawn there. Formally, the TSO sets the technical capacities q_u^{tec} for all $u \in V_+ \cup V_-$ and lower bounds on the booking fees $\widehat{\pi}_u^{\text{book}} \geq 0$ for all $u \in V_+ \cup V_-$. For ease of notation, we define $q_u^{\text{tec}} = 0$ and $\widehat{\pi}_u^{\text{book}} = 0$ for all $u \in V \setminus (V_+ \cup V_-)$. We then write $\mathbf{q}^{\text{tec}} = (q_u^{\text{tec}})_{u\in V}$ for the vector of technical capacities and $\widehat{\boldsymbol{\pi}}^{\text{book}} = (\widehat{\pi}_u^{\text{book}})_{u\in V}$ for the vector of lower bounds on the booking fees.

The values $\widehat{\pi}_u^{\text{book}}$ are lower bounds on the fees that the TSO can require to ensure that the costs for the gas transport are covered. We further assume that there is a constant $C \in \mathbb{R} > 0$ which corresponds to exogenously given costs that the TSO needs to be reimbursed for from revenues.

Furthermore, the TSO has to set the technical capacities $\mathbf{q}^{\text{tec}}$ such that all bookings that are feasible for these technical capacities always result in nominations that can be feasibly routed in the gas network. Formally, let

$$\mathcal{N}(\mathbf{q}^{\text{tec}}) = \left\{ \mathbf{q} \in \mathbb{R}^V : \mathbf{0} \leq \mathbf{q} \leq \mathbf{q}^{\text{tec}} \text{ and } \sum_{u\in V_+} q_u = \sum_{u\in V_-} q_u \right\} \tag{8.11}$$

be the set of all balanced vectors that obey the technical capacities. By the constraints enforced in the second level, we have $\sum_{i\in P_u} q_i^{\text{book}} \leq q_u^{\text{tec}}$ for all $u \in V_+ \cup V_-$.

Let $\bar{q}^{\text{nom}}_{u,t} = \sum_{i \in P_u} q^{\text{nom}}_{i,t}$ be the aggregated in- and outflow into node u in time t, and $\bar{\mathbf{q}}^{\text{nom}}_t = (\bar{q}^{\text{nom}}_{u,t})_{u \in V}$ the corresponding vector. Furthermore, by the constraints enforced in the third level, we have for each $t \in T$ that $\sum_{i \in P_+} q^{\text{nom}}_{i,t} = \sum_{i \in P_-} q^{\text{nom}}_{i,t}$ and that $0 \le q^{\text{nom}}_{i,t} \le q^{\text{book}}_i$. Together, these constraints imply that for each $t \in T$, only nodal nomination vectors $\bar{\mathbf{q}}^{\text{nom}}_t \in \mathcal{N}(\mathbf{q}^{\text{tec}})$ can occur, and the TSO has to ensure that a feasible gas flow for these nominations in the fourth level of the model can be found, i.e., the TSO has to ensure that $\mathcal{F}(\mathbf{q}) \neq \emptyset$ for all $\mathbf{q} \in \mathcal{N}(\mathbf{q}^{\text{tec}})$.

We assume that the TSO is interested in maximizing the nomination-based social welfare defined as the sum of the consumer and producer surplus minus the TSO's costs for transportation, which depends on the nomination vector $\mathbf{q}^{\text{nom}}$, is denoted by $\varphi^4(\mathbf{q}^{\text{nom}})$, and was defined in Sect. 8.3.1.

The optimization problem in the first level is

$$\max \quad \sum_{t \in T} \left(\sum_{u \in V_-} \sum_{i \in P_u} \int_0^{q^{\text{nom}}_{i,t}} P_{i,t}(s)\,\mathrm{d}s - \sum_{u \in V_+} \sum_{i \in P_u} c^{\text{var}}_i q^{\text{nom}}_{i,t} \right) - \varphi^4(\mathbf{q}^{\text{nom}}) - C \tag{8.12a}$$

$$\text{s.t.} \quad \varphi^4(\mathbf{q}^{\text{nom}}) + C = \sum_{u \in V_+ \cup V_-} \sum_{i \in P_u} \widehat{\pi}^{\text{book}}_u q^{\text{book}}_i, \tag{8.12b}$$

$$\mathcal{F}(\mathbf{q}) \neq \emptyset \qquad \text{for all } \mathbf{q} \in \mathcal{N}(\mathbf{q}^{\text{tec}}), \tag{8.12c}$$

$$\mathbf{0} \le \mathbf{q}^{\text{tec}}, \tag{8.12d}$$

$$\mathbf{0} \le \widehat{\boldsymbol{\pi}}^{\text{book}}, \tag{8.12e}$$

$$q^{\text{book}}_i \in \arg\max\{\varphi^2_i(q^{\text{tec}}_u, \widehat{\pi}^{\text{book}}_u)\} \qquad \text{for all } u \in V_+ \cup V_-, i \in P_u, \tag{8.12f}$$

$$q^{\text{nom}}_{i,t} \in \arg\max\{\varphi^3_{i,t}(q^{\text{book}}_i)\} \qquad \text{for all } u \in V_+ \cup V_-, i \in P_u, t \in T. \tag{8.12g}$$

The objective function (8.12a) is the total value of all players and the TSO. The constraint (8.12b) makes sure that the TSO sets the minimal booking prices $\widehat{\boldsymbol{\pi}}^{\text{book}}$ high enough so that the total costs of the TSO given by $\varphi^4(\mathbf{q}^{\text{nom}}) + C$ are covered. Note that the total revenue of the TSO from the minimal booking fees depends on the booking vector $\mathbf{q}^{\text{book}}$ and the total costs of transporting gas depends on the nomination vector $\mathbf{q}^{\text{nom}}$. The constraint (8.12c) ensures that the technical capacities are set in such a way that every resulting booking and, in turn, every nomination vector can be realized by a feasible gas flow in the network. In robust optimization terminology, this constraint could be called an *adjustable robust constraint*, emphasizing that there are infinitely many possible nomination vectors obeying the technical capacities for which a feasible flow needs to be found, but the TSO can adjust their gas flow to render the nomination vector feasible. Constraints (8.12f) and (8.12g) make sure that bookings and nominations are selected so that the equilibrium conditions of the players in the lower levels are satisfied.

8.4 Related Models and Reformulations

Grimm et al. [24] show that the model presented in Sect. 8.3 can be reformulated as a bilevel optimization problem. In general, bilevel problems are known to be NP-

hard [35]. For the problem at hand, Schewe et al. [52] analyze the structural properties of the set of feasible bookings. Their findings indicate that, even for simple linear gas transport models, the set of feasible bookings can be nonconvex. Nevertheless, for passive networks and for many gas transport model variants, verifying the feasibility of bookings is in P [38, 39]. Exceptions arise in two cases: Capacitated linear flows on cyclic networks and nonlinear potential-based flows with capacity or potential bounds on general cyclic networks. From a complexity-theoretic perspective, the current state of knowledge regarding the latter two cases is that the respective problems are coNP-hard [38,56]. In addition, it is known that the problem of computing technical capacities is NP-complete on trees and NP-hard in general [51]. Hence, to render the four-level entry-exit gas market model computationally tractable and thus to enable quantitative analysis, several simplifying assumptions are necessary. In the following, we provide an overview of the main contributions that apply the entry-exit model computationally, emphasizing the changes required to obtain computational tractability.

Böttger et al. [10] derive a single-level reformulation of the entry-exit market model for general networks in order to assess potential welfare effects resulting from the decoupling of trade and transport in the European entry-exit gas market. To render the single-level reformulation computationally tractable, gas physics are represented by potential-based *linear* flow equations, i.e., $|q_a|$ in equation (8.3b) is replaced by an a priori determined mean flow. This linear representation of gas flows is crucial for deriving a mixed-integer linear reformulation of the challenging, infinitely many adjustable-robust constraints (8.12c) based on the characterization for feasible bookings stated in Labbé et al. [38]. Böttger et al. [10] do not consider active elements and the objective function (8.3b) of the fourth level capturing the transportation costs is alternatively modeled by

$$\sum_{t\in T}\sum_{a=(u,v)\in A} c_t^{\text{trans}}\,|p_{u,t}^2 - p_{v,t}^2| \tag{8.13}$$

with $c_t^{\text{trans}} > 0$. The numerical results reveal that the decoupling of trade and transport can be quite costly. In addition, the decoupling costs are highly dependent on the specific network structure, implying that trade and transport are not decoupled in the long-run. Moreover, booking price regimes must be chosen carefully since some regimes might substantially reduce overall welfare and can be highly discriminatory against individual market participants. Finally, relaxing the robustness requirement of the entry-exit system, i.e., only considering economically relevant nominations instead of all nominations in (8.11), can already yield significant welfare improvements in practice.

Heitsch et al. [29] build on the reformulation of the entry-exit market model by Böttger et al. [10] and incorporate, as an extension, a joint chance constraint at the nomination level to account for uncertain loads. To achieve computational tractability, the robustness requirement of the entry-exit model is relaxed so that only the actually realized nominations need to be transportable through the network. Since the joint chance constraint is not available in closed form, but only function and gradient evaluations thereof, a problem-tailored cutting-plane algorithm is developed to compute approximate bilevel-feasible solutions for the resulting variant of the entry-exit market

model. The computational study investigates the welfare losses that arise from imposing specific safety levels for covering uncertain loads. The results show that, up to a load coverage level of 90 %, welfare losses increase only moderately. In contrast, significantly higher welfare losses are observed for stricter safety requirements. Overall, the findings suggest that a load coverage level of 90 % constitutes a reasonable compromise between the TSO's objective of ensuring a fail-safe network and the welfare losses induced by the imposed safety level.

Schewe et al. [53] present an alternative single-level reformulation of the entry-exit market model. In contrast to the one by Böttger et al. [10], this reformulation applies only to tree networks but, in turn, takes into account the nonlinear model (ISO4) to represent gas flows. Here, too, no active elements are considered, and the transportation costs on the fourth level are modeled as in (8.13). Exploiting the tree structure of the network allows for a finite convex mixed-integer formulation of the infinitely many nonlinear adjustable constraints (8.12c), yielding a computationally tractable mixed-integer nonlinear optimization problem as a single-level reformulation. Besides this reformulation, problem-tailored cutting planes are derived to speed up the solution process. The applicability of their approach is demonstrated by solving a real-world network, namely the Greek gas network, to global optimality; see the instance GasLib-134 of GasLib [54].

Gugat et al. [27] introduce a gas flow model on the fourth level that is governed by partial differential equations (PDEs) and thus includes time dependency on the lowest level. Further, they present an aggregated bilevel problem for the resulting four-level entry-exit model and outline a clear pathway towards deriving a computationally tractable single-level optimal control problem from this bilevel formulation. A particular challenge when considering the optimal control of the PDE system on the fourth level is on how to couple the objective functional, i.e., an integral in continuous time, to the aggregated market values in discrete time. Gugat et al. [27] show a consistent way to overcome this challenge that further ensures the existence of a solution to the resulting optimal control problem. The robust constraint (8.12c) on the technical capacities is not implemented in its strictest form, but replaced by a probabilistic constraint ensuring that the probability of delivering the nominated gas is greater than or equal to an a priori defined safety level. In contrast to Grimm et al. [24], the aggregation of the second and third level is argued based on the use of potential functions. The numerical results indicate the presence of a turnpike structure for the optimal states and controls, see Chap. 16, "The Turnpike Property and the Optimal Control of Gas Networks".

In contrast to the aforementioned contributions, Plein et al. [49] explicitly consider stationary networks with active elements, albeit modeled only linearly. In addition, to maintain computational tractability, the authors verify the feasibility of bookings rather than optimizing them. While passive networks can be addressed by single-level approaches [38], the presence of active elements requires a bilevel formulation. On the upper level, an adversarial player seeks to identify the balanced load flow within the given booking that is most difficult to transport. Meanwhile, the TSO controls the active elements on the lower level in order to route this worst-case load flow through the network. Assuming that no active element is part of a cycle, the lower-level problem becomes linear. This allows for several single-level reformulations including the classical Karush–Kuhn–Tucker (KKT) reformulation as well as three further problem-specific

optimal-value-function reformulations. The performance of these reformulations is evaluated using the GasLib-40 and GasLib-134 instances [54]. The computational experiments indicate that the KKT-based reformulation already provides an effective method for deciding the feasibility of bookings. The more problem-specific approaches can, in some cases, outperform the KKT reformulation, particularly when parallel computing resources are available. However, their performance depends heavily on the network under consideration, especially on the number of active elements and nodes.

8.5 Strategic Suppliers in the Entry-Exit Market Model

The models considered above rely on the assumption of perfectly competitive behavior of gas sellers when making booking decisions in the second level and when making nomination decisions in the third level. More specifically, in the model described in Sect. 8.3, all players i maximize their profits taking prices π_u^{book} and π_t^{nom} in problems (8.4), (8.5), and (8.8) respectively as given. This allows us to aggregate players' decisions to single-objective problems as stated in (8.7) and (8.10). However, strategically acting gas sellers could anticipate the impact of their output decisions on prices for bookings and nominations in a resulting market equilibrium. This is particularly important in European gas markets, where market power and strategic behavior of gas sellers play an important role due to the dependence on a limited number of gas-exporting countries [12, 58].

In general, modeling different strategically acting gas sellers at the second and third levels leads to highly intractable problems. Thus, simplifying assumptions are necessary again to gain insight into the impact of strategic behavior on players' booking and nomination decisions.

Grimm et al. [22] consider a single gas seller acting as a monopolist for booking and nomination decisions. To capture the strategic behavior of the monopolistic firm, the sequence of decisions on the market levels must be adjusted. The TSO still makes decisions at the first and fourth level. On a second level, the monopolistic seller now decides both on the bookings and the nominations at all entry nodes. In addition, the seller sets prices for all exit nodes. The competitive gas buyers then observe these prices on a third level and react to them by choosing their own bookings and nominations. Similar to [10, 53], sufficient conditions are derived that allow for a single-level reformulation of the resulting four-level model. However, in contrast to [10, 53], the robust constraints (8.12c) are not imposed in their strictest form. More precisely, only the economically relevant nominations are considered in the set defined in (8.11) instead of all possible nominations. In line with [10, 53], active elements are not considered and transportation costs are modeled as in (8.13). The numerical results indicate that the scarcer the network capacities, the stronger the impact of different pricing regimes on overall welfare, supplier profits, and consumer surplus. Interestingly, the possibility of price discrimination, particularly perfect discrimination, tends to increase both profit and consumer surplus, as it seems to allow for a more accurate representation of network congestion, i.e., more favorable technical capacities can be chosen at the upper level.

The case of several strategic sellers turns out to be more involved. A separate consideration of booking and nominating in two separate levels is required to fully capture the strategic complexity of the situation. Grimm et al. [23] take the TSO's decisions on the first and the last level as exogenously fixed. This allows them to formulate the resulting booking and nomination problem with strategic sellers as a multi-leader-multi-follower situation. They analyze a class of two-level multi-leader-multi-follower games (MLFGs) in which several asymmetric firms first compete on an upper level by making booking or capacity-expansion decisions and subsequently engage on a lower level in capacity-constrained Cournot competition. This structure captures the strategic interdependence that arises in liberalized electricity and gas markets, where firms act sequentially across different market stages. While single-level Nash equilibrium problems are well understood, the computation of equilibria in MLFGs remains challenging because of the hierarchical decision-making and the potential nonconvexities in firms' profit functions. They develop an exact algorithm capable of computing the complete set of pure-strategy Nash equilibria for this class of games, while previous approaches focus typically on stationary points or local equilibria [41, 42, 47, 48]. They prove that the equilibrium set is finite and provide examples in which no pure-strategy equilibrium exists.

These results extend and unify several strands of literature in the field of classical peak-load pricing and strategic capacity choice models. In contrast to earlier works that focused on simplified multi-leader settings or on approximate equilibrium concepts (e.g., [6, 7, 18, 25, 34, 36, 43, 44]), Grimm et al. [23] characterize the full equilibrium set for a tractable but still economically relevant MLFG class. Their framework accommodates multiple asymmetric and strategically behaving firms inducing concave kinks in profit functions, and thus allows for a much richer representation of competitive behavior.

The setup outlined above implicitly assumes a perfect reaction of consumers to nomination prices π_t^{nom} in each period t. In practice, however, the retail prices that customers face do not necessarily reflect the short-run spot market prices that result from nominations. More precisely, in the context of the above-described four-level model, the nomination level (where firms nominate quantities and spot market prices are formed) could itself be further disentangled into several levels. Retailers purchase energy at wholesale markets at prices π_t^{nom}, but offer contracts to customers that either perfectly reflect these wholesale prices (real-time pricing) or fix them over longer time horizons (fixed-price tariffs).

In the following, we extend the discussion by considering situations where retail companies strategically decide on tariffs offered to final customers while purchasing energy at wholesale prices that fluctuate over time. In this context, Oggioni et al. [46] and Wiertz et al. [57] analyze strategic retail pricing and competition in liberalized energy markets, with a particular focus on the implications of introducing dynamic tariff schemes. Both contributions share the underlying idea that retailers act as strategic leaders purchasing at fluctuating wholesale markets and offering differentiated contracts to customers, who respond to these price signals on the lower level.

More specifically, Oggioni et al. [46] introduce a two-level multi-leader–multi-follower framework to study dynamic retail pricing where retailers strategically decide on tariff structures while anticipating consumers' demand responses. They investigate

the equilibrium implications of real-time pricing compared to fixed-price contracts, combining analytical characterization with a computational algorithm capable of identifying all resulting equilibria. Building on this foundation, Wiertz et al. [57] present a broader and more general framework that captures the strategic interaction of multiple, potentially asymmetric retailers offering contracts characterized by both price and non-price attributes. Their model accommodates uncertainty, price-responsive consumption, and heterogeneous customer preferences, thereby reflecting realistic competition in electricity, gas, and potentially hydrogen retail markets. They analytically characterize the resulting equilibria for both fixed-price and real-time pricing schemes and develop an algorithm capable of computing all such equilibria. In the symmetric case, analytical comparison reveals that while retailer profits remain unchanged across tariff regimes, consumer surplus and total welfare are strictly higher under real-time pricing, particularly in the presence of strong wholesale price fluctuations.

Methodologically, Wiertz et al. [57] advance the literature on multi-leader-multi-follower games (see [5,30]) and connect to classical models of differentiated competition (see [11,32,50]), extending them to a multi-period and price-elastic demand setting. The paper also unifies insights from previous single-retailer studies [3, 4, 33] and empirical analyses of consumer responsiveness [2, 17, 55], offering a tractable yet comprehensive framework for analyzing strategic retail markets under dynamic pricing.

Beyond equilibrium-based models, markets can also be analyzed through auction mechanisms. Giannakopoulos and Hahn [20] revisit the classical mechanism design framework of Myerson [45], generalizing it beyond the single-item case to allocation problems that admit arbitrary convex feasibility constraints. As shown by Klimm et al. [37], certain gas network problems can be represented using convex-quadratic constraints, which fit naturally into this extended mechanism framework. In practice, for energy markets, the equilibrium is effectively established through an auction-based clearing process. In the context of the four-level market model, the theory and the mechanism presented in [20] can be naturally embedded as a mechanism-design variant within the hierarchical market structure: as a booking auction in the second level or as a nomination auction in the third level. The mechanism then replaces the competitive equilibrium assumption by a truthful, direct-revelation mechanism that determines efficient allocations under private information. In contrast to the assumption of price-taking behavior, participants in the auction setting explicitly recognize their strategic impact on prices, which the mechanism internalizes through its incentive-compatible design.

8.6 Further Models for Gas Markets

The existence results for market equilibria in the second and third level of the model presented in Sect. 8.3 hinge on the fact that the corresponding welfare problems are concave, all constraints are linear, and hence strong duality holds. Grimm et al. [21] consider a model where consumers and producers nominate their production and consumption (as in the third level), while a TSO *simultaneously* makes the gas transport decision (as in the fourth level). The incorporation of the decision of the TSO together with the decisions of consumers and producers renders this problem nonconvex,

so that standard arguments for strong duality do not apply. Thus, the authors investigate whether a relation between (i) the market equilibrium problem, (ii) the nonlinear complementary problem (NCP), which results from the players' Karush–Kuhn–Tucker (KKT) conditions together with the market-clearing conditions, and (iii) the welfare optimization problem can be maintained despite a TSO that accounts for nonconvex gas flows. They show that, under mild assumptions, a market equilibrium is also a solution to the corresponding NCP, i.e., the KKT conditions of the TSO are necessary optimality conditions. However, already simple examples show that the TSO's KKT conditions are not sufficient, implying that equilibria cannot be determined by the NCP. Moreover, the welfare optima might also not correspond to market equilibria, and equilibria might not exist at all.

Grübel et al. [26] consider this phenomenon further based on a general result by Harks and Schwarz [28], which establishes that the existence of a market equilibrium is equivalent to the welfare optimization problem having zero duality gap. Building on this result, the authors develop an algorithm that decides for a market equilibrium problem with one nonconvex player whether a market equilibrium exists, and in case of existence, computes such an equilibrium. They further apply their algorithm to various instances of gas networks, exhibiting that despite the theoretical threat of the non-existence of a market equilibrium, market equilibria do exist in most real-world instances.

Another modeling approach for European gas markets, which was widely applied during the phase of liberalization and implementation of the entry-exit system, abstracts from entry-exit market rules and a detailed representation of gas physics. Instead, only transport capacity limits between the different agents are considered, derived from the underlying network structure. The main focus of these contributions is to quantitatively assess the impact of strategically acting producers or traders on the gas market. Typically, an optimization problem is formulated for each agent type. The optimal solutions are then characterized by suitable optimality conditions that, when fulfilled together with appropriate market-clearing conditions, yield a market equilibrium. The problems to be solved are thus complementarity problems, possibly mixed, nonlinear, or linear, depending on the specific application.

Gabriel et al. [19] formulate a mixed nonlinear complementarity problem (NCP) for the North American natural gas market, in which the assumption of simultaneous decisions actually reflects the prevailing market design. Almost all considered players (producers, storage reservoir operators, and peak gas operators) are modeled as price-takers, except for the marketers, who are Nash–Cournot players as long as they compete against each other. Different consumer groups are described by different inverse demand functions, and the pipeline operators allocate scarce pipeline capacity based on charging flow premiums for the pipeline's usage. As optimality conditions for the player's optimization problems, the KKT optimality conditions are used, yielding jointly with the market-clearing conditions the NCP. Gabriel et al. [19] further investigate conditions under which an equilibrium, i.e., a solution to this NCP, exists and is unique.

Zwart and Mulder [59] propose the NATural GAS model (NATGAS) for the European wholesale gas market. The model focuses on the long-term development of the European gas market and especially on the strategic behavior of the different gas producers with regard to exploring new production sites while facing gas resource constraints over time as well as increasing investment costs in dependency on the region's

depletion rate. All other players (consumers, TSOs, storage operators, arbitrage traders, and LNG importers) are modeled as classic price-takers.

The equilibrium model for the European natural gas market developed by Egging et al. [13] includes the following players: Producers, traders, LNG liquefiers, LNG regasifiers, storage operators, pipeline operators, and marketers. Consumers and LNG tankers are implicitly modeled by aggregate inverse demand and cost functions. All players are price-takers except for the internationally operating traders. Each trader is directly linked to a single producer but operates independently of this producer. A conjectured variation approach is chosen to depict different levels of market power between Cournot and perfect competition for the traders' sales to the marketers and storage operators. Each player's optimization problem is convex such that the necessary and sufficient KKT conditions form, together with the market-clearing conditions, a mixed complementarity problem. The distinctive feature of this model is the explicit representation of market power of gas exporters in a global market framework including global LNG trade.

GASTALE (Gas mArket System for Trade Analysis in a Liberalising Europe) follows a successive approach, in which Cournot producers decide upstream on their gas productions and traders downstream on their gas trade; see Boots et al. [8, 9]. The downstream trading can be monopolistic, oligopolistic, or perfectly competitive, depending on the considered application. Transmission constraints and consumer behavior are reflected by adequately chosen transport tariffs and demand elasticities. The KKT conditions are used to assess the equilibrium on the trading level. The upstream producers account for these equilibrium reactions when determining their optimal production levels, which can also be characterized by respective first-order conditions. In total, a mixed nonlinear complementarity problem arises. Two model modifications are further taken into account: (i) within-country arbitrage and (ii) a rule in line with the Gas Directive that a producer's market share is not allowed to exceed 75 % in a country. Egging and Gabriel [14] present an extension of GASTALE including season-dependent demand as well as transmission system and storage operators as additional price-taking players. The producers' model differs slightly from the one in [8, 9], neglecting downstream traders and assuming producers produce only in one country. Lise and Hobbs [40] further incorporate the investment decisions of the price-taking agents in the latter approach and thereby analyze the impact of the producers' market power on investments in pipeline and LNG infrastructure as well as storage facilities.

Holz et al. [31] provide a successive approach called GASMOD for the European gas market. The gas exporters to Europe as well as the domestic producers decide on the upstream market while the European wholesale trade takes place downstream. The setting is similar to the one in GASTALE [8, 9] with the two additions that domestic production and infrastructure transport limitations are explicitly modeled. Further, demand in the end-markets is assumed to be nonlinear instead of linear.

The GaMMES (Gas Market Modeling with Energy Substitution) model presented by Abada et al. [1] forms a generalized Nash–Cournot problem for the northwestern European natural gas market. The producers and independent traders decide as Cournot players on investment and operations, while the storage and pipeline operators act as price-takers. As in GASTALE [8, 9] and GASMOD [31], both the European upstream and downstream market are represented. However, there are two key distinguishing

features. First, Abada et al. [1] capture potential fuel substitutions, such as from gas to oil, in the demand representation of the consumers. This aspect is particularly important when assessing market power, since substitution possibilities might mitigate its extent. Second, long-term contracts are modeled endogenously. More precisely, producers can sell either directly to the end-users at the wholesale market (downstream) or to the independent traders in the form of long-term contracts (upstream), who then sell the contracted quantities to the end-users at the wholesale market. Although this upstream activity is not modeled as oligopolistic, it remains challenging because including the long-term contracts causes the producers' feasibility sets to depend on the traders' decisions and vice versa. This challenge is addressed by selecting the equilibrium solution with the same duals for the shared constraints in the mixed complementarity problem constituted by the KKT conditions of all players.

All of the aforementioned complementarity-based modeling approaches abstract from considering the inherent nonlinearity of gas physics in order to capture the strategic behavior of the suppliers active in the market. Chap. 18, "A PDE-Constrained Generalized Nash Equilibrium Approach for Modeling Gas Transport with Strategic Suppliers" studies a market model where entry-exit market rules are still abstracted from in the sense that both the technical capacities and the booking decisions are assumed to be exogenously fixed. The strategic suppliers then directly take into account the resulting shared network, leading to a formulation that can be expressed as a generalized Nash equilibrium problem. In contrast to almost all setups presented in this chapter, the network representation is not modeled in discrete time. Instead, strategic suppliers there face shared network constraints described by partial differential equations.

Acknowledgements This work was supported by the German Research Foundation (DFG) within Subprojects A05, B07, B08, and B09 in the Sonderforschungsbereich/Transregio 154 "Mathematical Modelling, Simulation and Optimization using the Example of Gas Networks" (Project ID 239904186).

References

1. I. Abada, S. Gabriel, V. Briat, and O. Massol. A generalized Nash–Cournot model for the northwestern European natural gas markets with a fuel substitution demand function: The GaMMES model. *Networks and Spatial Economics*, 13:1–42, 2013. doi:10.1007/s11067-012-9171-5.
2. V. V. Agrawal and Ş. Yücel. Design of electricity demand-response programs. *Management Science*, 68(10):7441–7456, 2022. doi:10.1287/mnsc.2021.4278.
3. R. Aïd, D. Possamaï, and N. Touzi. Optimal electricity demand response contracting with responsiveness incentives. *Mathematics of Operations Research*, 47(3):2112–2137, 2022. doi:10.1287/moor.2021.1201.
4. C. Alasseur, I. Ekeland, R. Élie, N. Hernández Santibáñez, and D. Possamaï. An adverse selection approach to power pricing. *SIAM Journal on Control and Optimization*, 58(2):686–713, 2020. doi:10.1137/19M1260578.
5. D. Aussel, S. Lepaul, and L. von Niederhäusern. A multi-leader-follower game for energy demand-side management. *Optimization*, 72(2):351–381, 2023. doi:10.1080/02331934.2021.1954179.
6. D. Aussel, M. Červinka, and M. Marechal. Deregulated electricity markets with thermal losses and production bounds: models and optimality conditions. *RAIRO – Operations Research*, 50(1):19–38, 2016. doi:10.1051/ro/2015009.

7. M. Boiteux. Peak-load pricing. *The Journal of Business*, 33(2):157–179, 1960.
8. M. G. Boots, F. A. M. Rijkers, and B. F. Hobbs. GASTALE: An oligopolistic model of production and trade in the European gas market. Technical report, ECN, Petten, NL, 2003.
9. M. G. Boots, F. A. M. Rijkers, and B. F. Hobbs. Trading in the downstream European gas market: A successive oligopoly approach. *The Energy Journal*, 25(3):73–102, 2004.
10. T. Böttger, V. Grimm, T. Kleinert, and M. Schmidt. The cost of decoupling trade and transport in the European entry-exit gas market with linear physics modeling. *European Journal of Operational Research*, 297(3):1095–1111, 2022. doi:10.1016/j.ejor.2021.06.034.
11. Y. Chen and M. H. Riordan. Price and variety in the spokes model. *The Economic Journal*, 117(522):897–921, 2007. doi:10.1111/j.1468-0297.2007.02063.x.
12. C. K. Chyong, D. M. Reiner, and D. Aggarwal. Market power and long-term gas contracts: The case of Gazprom in central and eastern European gas markets. *The Energy Journal*, 44(1):55–74, 2023. doi:10.5547/01956574.44.1.cchy.
13. R. Egging, S. A. Gabriel, F. Holz, and J. Zhuang. A complementarity model for the European natural gas market. *Energy Policy*, 36(7):2385–2414, 2008. doi:10.1016/j.enpol.2008.01.044.
14. R. G. Egging and S. A. Gabriel. Examining market power in the European natural gas market. *Energy Policy*, 34(17):2762–2778, 2006. doi:10.1016/j.enpol.2005.04.018.
15. European Parliament and Council of the European Union. Directive 2003/55/EC of the European Parliament and of the Council of 26 June 2003 concerning common rules for the internal market in natural gas and repealing Directive 98/30/EC, 2003.
16. European Parliament and Council of the European Union. Directive 2009/73/EC of the European Parliament and of the Council of 13 July 2009 concerning common rules for the internal market in natural gas and repealing Directive 2003/55/EC, 2009.
17. N. Fabra, D. Rapson, M. Reguant, and J. Wang. Estimating the elasticity to real-time pricing: Evidence from the Spanish electricity market. *AEA Papers and Proceedings*, 111:425–429, 2021. doi:10.1257/pandp.20211007.
18. S. A. Gabriel, A. J. Conejo, J. D. Fuller, B. F. Hobbs, and C. Ruiz. *Complementarity Modeling in Energy Markets*, volume 180. Springer, New York, 2012. doi:10.1007/978-1-4419-6123-5.
19. S. A. Gabriel, S. Kiet, and J. Zhuang. A mixed complementarity-based equilibrium model of natural gas markets. *Operations Research*, 53(5):799–818, 2005. doi:10.1287/opre.1040.0199.
20. Y. Giannakopoulos and J. Hahn. Discrete single-parameter optimal auction design. In G. Schäfer and C. Ventre, ed., *Algorithmic Game Theory*, pages 165–183, Cham, 2024. Springer Nature Switzerland. doi:10.1007/978-3-031-71033-9_10.
21. V. Grimm, J. Grübel, L. Schewe, M. Schmidt, and G. Zöttl. Nonconvex equilibrium models for gas market analysis: Failure of standard techniques and alternative modeling approaches. *European Journal of Operational Research*, 273(3):1097–1108, 2019. doi:10.1016/j.ejor.2018.09.016.
22. V. Grimm, J. Grübel, M. Schmidt, A. Schwartz, A.-K. Wiertz, and G. Zöttl. On a tractable single-level reformulation of a multilevel model of the European entry-exit gas market with market power. *Journal of Global Optimization*, 91:953–985, 2025. doi:10.1007/s10898-025-01475-8.
23. V. Grimm, D. Nowak, L. Schewe, M. Schmidt, A. Schwartz, and G. Zöttl. A tractable multi-leader multi-follower peak-load-pricing model with strategic interaction. *Mathematical Programming*, 195(1):605–647, 2022. doi:10.1007/s10107-021-01708-0.
24. V. Grimm, L. Schewe, M. Schmidt, and G. Zöttl. A multilevel model of the European entry-exit gas market. *Mathematical Methods of Operations Research*, 89(2):223–255, 2019. doi:10.1007/S00186-018-0647-Z.
25. V. Grimm and G. Zöttl. Investment incentives and electricity spot market competition. *Journal of Economics and Management Strategy*, 22(4):832–851, 2013. doi:10.1111/jems.12029.
26. J. Grübel, O. Huber, L. Hümbs, M. Klimm, M. Schmidt, and A. Schwartz. Nonconvex equilibrium models for energy markets: Exploiting price information to determine the existence of an equilibrium. *Optimization Methods and Software*, 38(1):153–183, 2023. doi:10.1080/10556788.2022.2117358.
27. M. Gugat, M. Schuster, and S. Steffensen. A dynamic multilevel model of the European gas market. *Communications in Optimization Theory*, 2023(11):1–26, 2023.
28. T. Harks and J. Schwarz. A unified framework for pricing in nonconvex resource allocation games. *SIAM Journal on Optimization*, 33(2):1223–1249, 2023. doi:10.1137/21M1400924.

29. H. Heitsch, R. Henrion, T. Kleinert, and M. Schmidt. On convex lower-level black-box constraints in bilevel optimization with an application to gas market models with chance constraints. *Journal of Global Optimization*, 84:651–685, 2022. doi:10.1007/s10898-022-01161-z.
30. M. Herty, S. Steffensen, and A. Thünen. Solving quadratic multi-leader-follower games by smoothing the follower's best response. *Optimization Methods and Software*, 37(2):772–799, 2022. doi:10.1080/10556788.2020.1828412.
31. F. Holz, C. von Hirschhausen, and C. Kemfert. A strategic model of European gas supply (GASMOD). *Energy Economics*, 30(3):766–788, 2008. doi:10.1016/j.eneco.2007.01.018.
32. H. Hotelling. Stability in competition. *The Economic Journal*, 39(153):41–57, 1929. doi:10.2307/2224214.
33. S. Hu, X. Hu, and Q. Ye. Optimal rebate strategies under dynamic pricing. *Operations Research*, 65(6):1546–1561, 2017. doi:10.1287/opre.2017.1642.
34. X. Hu and D. Ralph. Using EPECs to model bilevel games in restructured electricity markets with locational prices. *Operations Research*, 55(5):809–827, 2007. doi:10.1287/opre.1070.0431.
35. R. G. Jeroslow. The polynomial hierarchy and a simple model for competitive analysis. *Mathematical Programming*, 32:146–164, 1985. doi:10.1007/BF01586088.
36. P. Joskow and J. Tirole. Reliability and competitive electricity markets. *The RAND Journal of Economics*, 38(1):60–84, 2007. doi:10.1111/j.1756-2171.2007.tb00044.x.
37. M. Klimm, M. E. Pfetsch, R. Raber, and M. Skutella. Packing under convex quadratic constraints. *Mathematical Programming*, 192(1):361–386, 2022. doi:10.1007/s10107-021-01675-6.
38. M. Labbé, F. Plein, and M. Schmidt. Bookings in the European gas market: Characterisation of feasibility and computational complexity results. *Optimization and Engineering*, 21:305–334, 2020. doi:10.1007/s11081-019-09447-0.
39. M. Labbé, F. Plein, M. Schmidt, and J. Thürauf. Deciding feasibility of a booking in the European gas market on a cycle is in P for the case of passive networks. *Networks*, 78(2):128–152, 2021. doi:10.1002/net.22003.
40. W. Lise and B. F. Hobbs. Future evolution of the liberalised European gas market: Simulation results with a dynamic model. *Energy*, 33(7):989–1004, 2008. doi:10.1016/j.energy.2008.02.012.
41. B. S. Mordukhovich. Equilibrium problems with equilibrium constraints via multiobjective optimization. *Optimization Methods and Software*, 19(5):479–492, 2004. doi:10.1080/10556780420002189 66.
42. B. S. Mordukhovich. Optimization and equilibrium problems with equilibrium constraints. *Omega*, 33(5):379–384, 2005. doi:10.1016/j.omega.2004.07.001.
43. S. Mousavian, A. J. Conejo, and R. Sioshansi. Equilibria in investment and spot electricity markets: a conjectural-variations approach. *European Journal of Operational Research*, 281(1):129–140, 2020. doi:10.1016/j.ejor.2019.07.054.
44. F. H. Murphy and Y. Smeers. Generation capacity expansion in imperfectly competitive restructured electricity markets. *Operations Research*, 53(4):646–661, 2005. doi:10.1287/opre.1050.0211.
45. R. B. Myerson. Optimal auction design. *Mathematics of Operations Research*, 6(1):58–73, 1981. doi:10.1287/moor.6.1.58.
46. G. Oggioni, A. Schwartz, A.-K. Wiertz, and G. Zöttl. Dynamic pricing and strategic retailers in the energy sector: A multi-leader-follower approach. *European Journal of Operational Research*, 312(1):255–272, 2024. doi:10.1016/j.ejor.2023.05.036.
47. J.-S. Pang. Partially B-regular optimization and equilibrium problems. *Mathematics of Operations Research*, 32(3):687–699, 2007. doi:10.1287/moor.1070.0262.
48. J.-S. Pang and M. Fukushima. Quasi-variational inequalities, generalized Nash equilibria, and multi-leader-follower games. *Computational Management Science*, 2(1):21–56, 2005. doi:10.1007/s10287-004-0010-0.
49. F. Plein, J. Thürauf, M. Labbé, and M. Schmidt. A bilevel optimization approach to decide the feasibility of bookings in the European gas market. *Mathematical Methods of Operations Research*, 95:409–449, 2022. doi:10.1007/s00186-021-00752-y.
50. C. Reggiani. Non-localised spatial competition: The "spokes model". In S. Colombo, eds., *Spatial Economics Volume I: Theory*, pages 129–167. Springer International Publishing, 2020. doi:10.1007/978-3-030-40098-9_6.

51. L. Schewe, M. Schmidt, and J. Thürauf. Computing technical capacities in the European entry-exit gas market is NP-hard. *Annals of Operations Research*, 295:337–362, 2020. doi:10.1007/s10479-020-03725-2.
52. L. Schewe, M. Schmidt, and J. Thürauf. Structural properties of feasible bookings in the European entry-exit gas market system. *4OR*, 18:197–218, 2020. doi:10.1007/s10288-019-00411-3.
53. L. Schewe, M. Schmidt, and J. Thürauf. Global optimization for the multilevel European gas market system with nonlinear flow models on trees. *Journal of Global Optimization*, 82:627–653, 2022. doi:10.1007/s10898-021-01099-8.
54. M. Schmidt, D. Aßmann, R. Burlacu, J. Humpola, I. Joormann, N. Kanelakis, T. Koch, D. Oucherif, M. E. Pfetsch, L. Schewe, R. Schwarz, and M. Sirvent. GasLib—A library of gas network instances. *Data*, 2(4), 2017. doi:10.3390/data2040040.
55. C. E. Simeone, I. Lange, and B. Gilbert. Pass-through in residential retail electricity competition: Evidence from Pennsylvania. *Utilities Policy*, 80:101479, 2023. doi:10.1016/j.jup.2022.101479.
56. J. Thürauf. Deciding the feasibility of a booking in the European gas market is coNP-hard. *Annals of Operations Research*, 318:591–618, 2022. doi:10.1007/s10479-022-04732-1.
57. A.-K. Wiertz, A. Walther, and G. Zöttl. Strategic retailers in the energy sector. Preprint available under https://opus4.kobv.de/opus4-trr154/561, 2024.
58. G. T. Zwart. European natural gas markets: Resource constraints and market power. *The Energy Journal*, 30:151–165, 2009.
59. G. T. Zwart and M. Mulder. NATGAS: A model of the European natural gas market. CPB Memorandum 144, CPB Netherlands Bureau for Economic Policy Analysis, 2006. URL: https://ideas.repec.org/p/cpb/memodm/144.html.

Open Access This chapter is licensed under the terms of the Creative Commons Attribution-NonCommercial-NoDerivatives 4.0 International License (http://creativecommons.org/licenses/by-nc-nd/4.0/), which permits any noncommercial use, sharing, distribution and reproduction in any medium or format, as long as you give appropriate credit to the original author(s) and the source, provide a link to the Creative Commons license and indicate if you modified the licensed material. You do not have permission under this license to share adapted material derived from this chapter or parts of it.

The images or other third party material in this chapter are included in the chapter's Creative Commons license, unless indicated otherwise in a credit line to the material. If material is not included in the chapter's Creative Commons license and your intended use is not permitted by statutory regulation or exceeds the permitted use, you will need to obtain permission directly from the copyright holder.



Part III
Optimization under Uncertainty for Gas Networks



Chapter 9
Introduction to Optimization under Uncertainty for Gas Networks

Frauke Liers[0000−0002−1671−0344] and
Stefan Ulbrich[0000−0003−4036−2607]

Abstract This chapter briefly introduces methods and approaches to protect optimization problems against uncertainties as they appear in the subsequent chapters of the book *Mathematical Modelling, Simulation and Optimization using the Example of Gas Networks*. Next to classical approaches in stochastic and robust optimization, it also touches methodologies at the interface between robustness and stochasticity.

In practical applications across diverse domains, optimization problems are frequently subject to uncertainty. The latter may be caused, for example, by errors in parameter value measurements, by the fact that input data may fluctuate or be only partly known. Ignoring such uncertainties however may either lead to solutions of bad quality or even to solutions that are infeasible, already in slightly perturbed settings. Instead of assuming perfect information, optimization under uncertainty thus takes these perturbations into account both in the modelling steps and in the development of solution approaches. Naturally, we can only summarize some main research directions here.

Specifically, robust optimization (RO) and stochastic programming (SP) have emerged as established paradigms. Robust Optimization predefines a so-called uncertainty set containing 'typical' uncertainties against which protection is sought. A robust feasible solution has to be valid regardless of how the uncertainty manifests itself within this set. A robust feasible solution is also robust optimal if it yields the best possible guaranteed objective function value. In contrast, stochastic optimization models uncertainty in a probabilistic sense, using probability distributions, often taking expectations into account and managing associated risks. They may optimize expected cost or contain chance constraints that need to be satisfied by at least a given probability.

Robust optimization does not assume any knowledge about underlying probability distributions which needs to be available in stochastic optimization. However, being

Frauke Liers
Department of Data Science and Department of Mathematics,
Friedrich-Alexander Universität Erlangen-Nürnberg, Germany, e-mail: frauke.liers@fau.de

Stefan Ulbrich
Department of Mathematics, TU Darmstadt, Germany, e-mail: ulbrich@mathematik.tu-darmstadt.de

© The Author(s) 2027

A. Martin et al. (eds.), *Mathematical Modelling, Simulation and Optimization using the Example of Gas Networks*, International Series of Numerical Mathematics 174,
https://doi.org/10.1007/978-3-032-34969-9_9

able to operate with less information may come at the price that robust solutions may involve larger costs than stochastic optimization results. Both robust as well as stochastic approaches can be computationally demanding. Thus, depending on the application and the considered setting, robust or stochastic approaches are advantageous. Recently, methodologies at the interface of both robustness and stochasticity have been developed as well. In the area of distributional robustness, it is assumed that underlying probability distributions may be uncertain themselves. Optimized solutions need to be robust against probability distributions contained in an ambiguity set. Distributional robustness has the advantage that it often comes with smaller robustness price, when compared to a purely robust solution. It however is more robust than a purely stochastic solution. A combination of both approaches are so-called probust constraints, where a robust constraint needs to be satisfied with at least some predefined probability.

In all these areas, important research questions are currently intensively studied. They for example consist in obtaining further structural insights in the underlying models as well as in the development of practically efficient solution algorithms together with convergence theories.

These challenges are particularly pronounced if nonconvex functions or partial differential equations are present, as many approaches rely on convexity assumptions or have been developed in finite-dimensional optimization. The subsequent articles give some examples for approaches in optimization under uncertainty that have shown to be very successful for gas network optimization. These systems are prone to uncertainty but also contain nonconvex constraints and/or partial differential equations. Both, very general approaches, which are tailored for gas networks, as well as problem-specific methodologies are presented.

The next chapters cover the following topics specified for gas networks.

- Chap. 10, "From Probabilistic to Probust Constraints: Optimization under Uncertainty" covers different aspects in optimization under uncertainty and gives an overview of topics such as stochastic and robust optimization as well as probust and distributional robustness.
- Chap. 11, "Continuous Stochastic Gradient and Spherical Radial Decomposition" introduces a novel approach for chance-constrained optimization that integrates stochastic gradient algorithms with a decomposition approach based on spherical radial decomposition. The approach is shown to be successful for capacity maximization in gas networks.
- Chap. 12, "Incremental-Decremental Optimization for the Transition to Hydrogen" presents a new algorithm to determine an optimized order to transform or renew some infrastructure. The algorithm is made concrete for the transition from natural gas to hydrogen networks.

Acknowledgements This work was supported by the German Research Foundation (DFG) within Subprojects A07, A09, B01, B02, B04, B06, B10, C03 in the Sonderforschungsbereich/Transregio 154 "Mathematical Modelling, Simulation and Optimization using the Example of Gas Networks" (Project ID 239904186).

Open Access This chapter is licensed under the terms of the Creative Commons Attribution-NonCommercial-NoDerivatives 4.0 International License (http://creativecommons.org/licenses/by-nc-nd/4.0/), which permits any noncommercial use, sharing, distribution and reproduction in any medium or format, as long as you give appropriate credit to the original author(s) and the source, provide a link to the Creative Commons license and indicate if you modified the licensed material. You do not have permission under this license to share adapted material derived from this chapter or parts of it.

The images or other third party material in this chapter are included in the chapter's Creative Commons license, unless indicated otherwise in a credit line to the material. If material is not included in the chapter's Creative Commons license and your intended use is not permitted by statutory regulation or exceeds the permitted use, you will need to obtain permission directly from the copyright holder.



Chapter 10
From Probabilistic to Probust Constraints: Optimization Under Uncertainty

Daniela Bernhard[0009−0001−7839−202X],
Caroline Geiersbach[0000−0002−6518−7756],
Martin Gugat[0000−0002−5281−110X],
Holger Heitsch[0000−0002−2692−4602],
René Henrion[0000−0001−5572−7213],
Jens Lang[0000−0003−4603−6554],
Frauke Liers[0000−0002−1671−0344],
Rüdiger Schultz,
Michael Schuster[0000−0002−4689−3663],
Michael Stingl[0000−0002−3626−0723], and
Hendrik Wilka[0009−0000−9929−7374]

Daniela Bernhard
Department of Data Science and Department of Mathematics, FAU Erlangen-Nürnberg, Germany, e-mail: daniela.db.bernhard@fau.de

Caroline Geiersbach
Department of Mathematics, University of Klagenfurt, Austria, e-mail: caroline.geiersbach@aau.at

Martin Gugat
Department of Mathematics, FAU Erlangen-Nürnberg, Germany, e-mail: martin.gugat@fau.de

Holger Heitsch
Weierstrass Institute for Applied Analysis and Stochastics, Berlin, Germany, e-mail: heitsch@wias-berlin.de

René Henrion
Weierstrass Institute for Applied Analysis and Stochastics, Berlin, Germany, e-mail: henrion@wias-berlin.de

Jens Lang
Department of Mathematics, TU Darmstadt, Germany, e-mail: lang@mathematik.tu-darmstadt.de

Frauke Liers
Department of Data Science and Department of Mathematics, FAU Erlangen-Nürnberg, Germany, e-mail: frauke.liers@fau.de

Rüdiger Schultz
Department of Mathematics, Universität Duisburg-Essen, Germany, e-mail: ruediger.schultz@uni-due.de

Michael Schuster
Department of Data Science, FAU Erlangen-Nürnberg, Germany, e-mail: michi.schuster@fau.de

Michael Stingl
Department of Mathematics, FAU Erlangen-Nürnberg, Germany, e-mail: michael.stingl@fau.de

Hendrik Wilka
Department of Mathematics, TU Darmstadt, Germany, e-mail: wilka@mathematik.tu-darmstadt.de

© The Author(s) 2027

A. Martin et al. (eds.), *Mathematical Modelling, Simulation and Optimization using the Example of Gas Networks*, International Series of Numerical Mathematics 174,
https://doi.org/10.1007/978-3-032-34969-9_10

Abstract Uncertainty plays a central role in many real-world optimization problems, particularly in energy systems, where tasks may depend on random variables such as loads, temperatures, or renewable energy generation. Two classical modeling paradigms address such uncertainty: probabilistic (chance) constraints, which assume a known probability distribution, and robust constraints, which protect against all realizations within some pre-defined uncertainty set. Recently, also models and approaches at the interface of both robustness and stochasticity have been introduced successfully. This chapter introduces and explores different approaches in optimization under uncertainty, combining probabilistic as well as robust elements in constraints. We will give an overview both for finite-dimensional as well as for infinite-dimensional optimization problems under uncertainty. Probust constraints require that a decision remains feasible with high probability, uniformly over a family of uncertain parameters. This model is especially relevant in applications where some components of uncertainty are stochastic (such as gas transport with random loads) and others are only assumed to be bounded (such as uncertain pipe parameters). Distributionally robust constraints require that chance constraints shall be satisfied regardless how probability distributions manifest themselves within given sets of probability distributions. Beyond introducing modeling approaches, we highlight key challenges of probust constraints in terms of algorithmic tractability and analytical properties. Motivated by various applications of optimization problems under uncertainty in the gas context, the chapter provides an overview of existing approaches together with motivating example approaches for handling various constraint types, and theoretical insights into structure and solution properties. We show that probust constraints offer a versatile pathway for risk-averse decision-making with complex, hybrid uncertainty.

10.1 Probust Constraints

The constraints of an optimization problem are often affected by uncertain parameters. This is a typical situation, in particular, in energy management, where the constraints might reflect load coverage, pressure bounds in gas pipes, state of charge or temperature of batteries etc., while uncertainty enters the model, for instance, as random load, ambient temperature, solar or wind energy, or precipitation. Corresponding optimization problems have the typical form

$$\min\{f(x) \mid g(x, z) \leq 0\}, \tag{10.1}$$

where x is a decision vector, z is an uncertain parameter, f is some objective function, and g denotes a function imposing a constraint on the decision while being affected by uncertainty. There exist two basic approaches for reformulating (10.1) in a way that does not depend on the concrete value of the uncertain parameter but rather yields decisions that are risk-averse with regard to all possible outcomes: the first one is the use of *probabilistic constraints* (also called 'chance constraints'). It is based on the assumption that historical data is available to estimate the probability distribution of the uncertain parameter which allows one to consider it as a random vector ξ. Then, (10.1)

may be given in the probabilistic form

$$\min\{f(x) \mid \mathbb{P}(g(x,\xi) \le 0) \ge \mathrm{p}\}. \tag{10.2}$$

Accordingly, a decision x is defined to be feasible if the original random inequality system in (10.1) is satisfied with a probability p, a level usually chosen close to, but not identical to one. Evidently, the larger p, the smaller the set of feasible decisions x in (10.2), and hence the higher the costs for an optimal solution. For a classical reference on probabilistic constraints, we refer to the monograph [52].

The second prominent approach is *robust optimization*, where the uncertain parameter is not endowed with historical data or stochastic information. All one might know is some uncertainty set $\mathcal{U}$ to which it belongs. Then, robustness of decisions cannot be understood in a probabilistic sense but rather in a worst-case sense, which means that feasibility will be enforced for all possible outcomes of the random parameter. The resulting optimization problem then reads

$$\min\{f(x) \mid g(x,u) \le 0 \quad \forall u \in \mathcal{U}\}. \tag{10.3}$$

We observe that both optimization problems (10.2) and (10.3) are conventional deterministic problems, because unlike the uncertain problem (10.1), they do not depend on the concrete outcome of the uncertain parameter. More precisely, their constraints can be written in the form $\varphi(x) \ge \mathrm{p}$ and $w(x) \le 0$ with the probability function φ and the worst-case function w, respectively, defined as

$$\varphi(x) := \mathbb{P}(g(x,\xi) \le 0); \quad w(x) := \sup\{g(x,u) \mid u \in \mathcal{U}\}. \tag{10.4}$$

The main difference with conventional optimization problems consists in not having at hand, in general, analytic expressions for φ and w. This fact complicates, in particular for the case of probabilistic constraints, the theoretical analysis and the numerical solution.

A main issue in robust optimization is the proper choice of an uncertainty set $\mathcal{U}$. Simple-shaped sets like polyhedra or ellipsoids are preferred for computational tractability [3]. When $\mathcal{U}$ is chosen such that $\mathbb{P}(\xi \in \mathcal{U}) = \mathrm{p}$, the feasible set of decisions in (10.3) is contained in that of (10.2). Therefore, an optimal solution to (10.3) is a feasible solution to (10.2), so that a conservative approximation of a probabilistically constrained optimization problem is obtained that is easier to deal with.

The degree of conservatism, however, may be significant; one might end up at potentially small or even empty feasible sets. This leads to solutions with much higher costs than under a probabilistic constraint. The mentioned trade-off suggests to apply probabilistic constraints in the presence of statistical information at least in moderate dimension. It is worth mentioning that the two models (10.2) and (10.3) meet in the consideration of optimization problems subject to so-called almost sure constraints:

$$\min\{f(x) \mid g(x,\xi) \le 0 \quad \mathbb{P}\text{-almost surely}\}. \tag{10.5}$$

Clearly (10.5) is equivalent with (10.2) for the special case of $\mathrm{p} = 1$. On the other hand, if g is lower semicontinuous in ξ, then (10.5) is equivalent with (10.3) where $\mathcal{U}$ is chosen as the support of ξ, see [19, Lemma 9].

In many applications, the two mentioned approaches are dealt with separately. More than often, however, one is faced with uncertainty of both mentioned types. This motivates naturally the consideration of uncertain inequalities in (10.1) in which the uncertain parameter has a stochastic and a non-stochastic component, i.e., $z = (\xi, u)$. A prototypical example arises in optimal gas transport in the presence of uncertain loads. For the latter, historical data are often available and can be exploited in order to model (multivariate) distributions [38, Chap. 13]. On the other hand, it is hard to access data on uncertain roughness coefficients in pipes underground. Therefore, it appears to be natural to merge the originally separate models (10.2) and (10.3). One possibility to do so is to formulate a probabilistic constraint (w.r.t. ξ) involving a robustified (w.r.t. u) infinite inequality system:

$$\mathbb{P}(g(x, \xi, u) \leq 0 \quad \forall u \in \mathcal{U}) \geq \mathrm{p}. \tag{10.6}$$

This model was introduced independently in [58] and [23], where the latter publication was devoted to optimal gas transport. The term *probust* constraints for (10.6) was coined in [1] as an acronym for the term '*pro*babilistic/ro*bust*' constraints introduced in [23]. In more complex settings, the uncertainty set could depend itself on decisions and/or on the random parameter, yielding the general probust model

$$\mathbb{P}(g(x, \xi, u) \leq 0 \quad \forall u \in \mathcal{U}(x, \xi)) \geq \mathrm{p}. \tag{10.7}$$

It is noteworthy that there exists an alternative way of combining the probabilistic and robust parts in (10.6) by interchanging their arrangements:

$$\mathbb{P}(g(x, \xi, u) \leq 0) \geq \mathrm{p} \quad \forall u \in \mathcal{U}. \tag{10.8}$$

In this way, one ends up not at a probabilistic constraint involving infinitely many random inequalities as in (10.6), but rather at an infinite system of probabilistic constraints. This setting is relevant in first-order stochastic dominance constraints [12] or in optimization under (continuous) path chance constraints [16]. A closely related model, also leading to an infinite system of probabilistic constraints are distributionally robust constraints [64] (see Sect. 10.3.2.2).

So far, we have interpreted the uncertain parameter u from the perspective of robust optimization, where decisions have to be found for all possible outcomes—or equivalently, for the worst-case outcome—of this parameter within the uncertainty set $\mathcal{U}$. There is, however, another perspective leading to the same mathematical model that interprets u as a continuously varying quantity like time or space rather than an uncertain parameter. Then, the 'uncertainty set' $\mathcal{U}$ can play the role of a time interval or of some spatial domain. The function $g(x, \xi, u)$ might represent a certain physical quantity, like temperature, depending on some control x, on some random parameter ξ and on space and/or time u. Then, the meaning of (10.6) is as follows: the control x has to guarantee that the random state g stays below some critical value (here: zero) *uniformly* over the time interval or space domain $\mathcal{U}$ with a probability of at least p. This interpretation opens a significant perspective on optimal risk-averse PDE or ODE control using probust constraints, including many potential applications to optimal robust gas transport under uncertainty.

With an abstract look at (10.6), one might define an aggregated constraint function $\tilde{g}(x,\xi) := \sup\{g(x,\xi,u) \mid u \in \mathcal{U}\}$ and verify that this constraint can be rewritten as a conventional probabilistic constraint (10.2) with g replaced by $\tilde{g}$. While this abstract perspective is helpful in certain situations, it tends to ignore information, for instance about differentiability of the original constraint function g. For instance, the quality of $\tilde{g}$ is heavily influenced by the nature of the uncertainty set $\mathcal{U}$ (singleton, finite set, continuous set etc.). This defines the main challenge in dealing with probust constraints, be it algorithmically, be it for understanding their structure, deriving optimality conditions and so on.

The chapter is organized as follows: In the first section, we collect several examples in the optimization of gas transport in the stationary as well as transient case that carry probust constraints as their main feature. The second section presents main algorithmic approaches for dealing with probabilistic, probust, robust, and almost sure constraints. Finally, the last section is devoted to selected theoretical results in the context of optimization problems with probust constraints.

10.2 Applications to Gas Transport

Before stating important applications like the nomination validation or the maximization of booking capacities in gas transport networks, we want to start this section by recalling the physics of stationary gas flow in an entry-exit based gas transport network.

The most important network parameters are the physical quantities gas pressure and gas flow. Both are interacting by Kirchhoff's first and second laws. By describing the gas network as a directed and connected graph, given by a set of nodes (vertices) and arcs (edges) (V,E), the Kirchhoff laws can be formulated in terms of the node-arc incidence matrix A. If $p \in \mathbb{R}^{|V|}$ and $q \in \mathbb{R}^{|E|}$ denote the pressures at nodes in V and the flows along the arcs in E, respectively, in a passive network we have that:

$$Aq = b, \qquad A^\top p^2 = -\Phi|q|q, \qquad p \in [p^{\min}, p^{\max}], \tag{10.9}$$

where $b \in \mathbb{R}^{|V|}$ is a fixed load vector of supply and demand values associated with the entry and exit nodes, respectively, Φ is a diagonal matrix with coefficients of pipe roughness as entries, and $p^{\min}$, $p^{\max}$ are technical lower and upper pressure limits. This problem is called Nomination Validation. Note that vector operations are understood component-wise here. Figure 10.1 highlights the network parameters and their relations in a steady state gas network.

The quantity of interest concerns the gas demand at the exit nodes and the gas supply at the entry nodes of the network. By convention, the demand corresponds to the positive entries of b, gas supply at entry nodes receives negative signs. For a given load b, the network operator attempts to control the network parameters such that the above conditions can be satisfied. More precisely, we say that the load b is *technically feasible*, if some setting (p,q) satisfying conditions (10.9) exists. This implies that b must be *balanced*, that means, the sum of all entries must be zero.

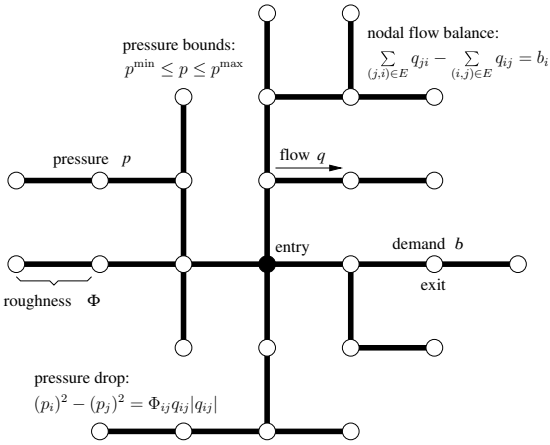


Fig. 10.1: Illustration of network parameters and feasibility conditions for stationary gas flow

10.2.1 Nomination Validation Under Uncertainty

One of the basic tasks in gas network operation is the nomination validation problem, which is here considered under uncertainty in the demands and pressure loss coefficients. We study robust as well as (robust) chance-constrained approaches here. Robust approaches are demanded in particular when protecting against physical parameters that are uncertain and cannot easily be measured, e.g., the roughness of a pipe, whereas demands can be handled robustly or stochastically depending on the concrete amount of data. Concretely, we focus on the algebraic model for gas transport including active elements like compressors or control valves that can be used to change the pressures in the network. In the following, one aims at a cost-optimal control of these active elements that leads to feasible transports respecting the uncertainties. We note that feasibility is characterized by (10.9) for the flow and pressure variables extended to active elements. Concretely, active elements are modeled with additional arcs in the network and we consider a linear model for the active elements, this means the pressure difference for active elements is given by the value of the corresponding control variable. Therefore, the right-hand side in the second equation in (10.9) for rows that correspond to active elements are given by the control variables. In our model, the control has to be decided before the realizations of the uncertain parameters are known, but the flows and pressures adjust themselves as second-stage variables to the uncertainties. The problem can be formulated as a single-stage problem due to the uniqueness of the physical states: once a control of the active elements and a realization of the uncertain parameters is fixed and the pressure at, e.g., the root node is fixed, there is a unique physical state. Concretely, there exists a function $\pi(x, y; d, \Phi)$ depending on the control variables, the demands and the pressure loss coefficients that models the squared pressure at the nodes. For a concrete description of this function we refer for example to [40].

In the robust setting, the task consists in solving a mixed-integer nonlinear robust optimization problem and the pressure bounds have to be fulfilled for every possible realization of the uncertain parameters.

The robust gas transport problem can be written as a mixed-integer nonlinear robust optimization problem as follows. The variables x, y denote discrete-continuous controls with control costs $f(\cdot)$, and with d and Φ being uncertain demand and pressure loss coefficients:

$$\begin{aligned} \min_{x,y} \quad & f(x,y) \\ \text{s.t.} \quad & (p^{\min})^2 - \pi(x,y;d,\Phi) \le 0 \quad \forall (d,\Phi) \in \mathcal{U} \\ & \pi(x,y;d,\Phi) - (p^{\max})^2 \le 0 \quad \forall (d,\Phi) \in \mathcal{U} \\ & x \in X,\ y \in Y \cap \mathbb{Z}^{n_y}. \end{aligned} \tag{RO_{gas}}$$

Our approach to this robust optimization problem is to interpret it as a nonsmooth optimization problem with the optimal value function of an adversary as a constraint function. In detail, constraints of the form $g_i(x,y;d,\Phi) \le 0$, $i \in \{1,\dots,n\}$, need to be fulfilled for every possible realization of d and Φ. They hence need to be fulfilled in particular for the case where the uncertain parameters are chosen such that they maximize the constraints' violation. We call this maximization problem the adversarial problem. For more details we refer to [40]. Using the optimal value function of the adversarial problem, the uncertain constraints can be equivalently replaced by a single, nonsmooth constraint:

$$G(x,y) = \max_{(d,\Phi)\in\mathcal{U}} \sum_{i=1}^{n} \max\{0, g_i(x,y;d,\Phi)\} \le 0.$$

This reformulation then results in a nonsmooth mixed-integer nonlinear optimization problem (MINLP) of the form

$$\begin{aligned} \min_{x,y} \quad & f(x,y) \\ \text{s.t.} \quad & G(x,y) \le 0, \\ & x \in X,\ y \in Y \cap \mathbb{Z}^{n_y}. \end{aligned} \tag{P}$$

This problem is difficult to treat computationally. An effective solution approach uses approximate robust formulations by a linearization in the uncertainty [14]. In [40], a solution approach to this problem is developed under very general assumptions. In particular, one allows for non-concavities of g in the uncertain parameters. This has the consequence that the adversarial problem may not be solvable to global optimality in a reasonable time anymore. This is overcome by allowing for inexact solutions and hence inexact evaluations of the adversarial optimal value function. For details, see Sect. 10.3.3.1.

Alternatively, the uncertainties in the demands can be treated stochastically if the distribution is known. We focus here on uncertain demands and assume that the pressure loss coefficients are fixed. Furthermore, we restrict to continuous control variables x. Then, the pressure bound constraints can be formulated as chance constraints and the chance-constrained nomination validation problem in the form of (10.2) is given by

$$\begin{aligned} \min_{x} \quad & f(x) \\ \text{s.t.} \quad & \mathbb{P}((p^{\min})^2 - \pi(x; d, \Phi) \leq 0,\ \pi(x; d, \Phi) - (p^{\max})^2 \leq 0) \geq p, \\ & x \in X \end{aligned} \tag{NV-CC}$$

for some given probability level p. This formulation is a classical joint chance-constrained problem that is in general non-linear, non-convex and contains a measure integral for continuous distributions. We will shortly discuss a stochastic gradient algorithm for this problem class in Sect. 10.3.1.3.

Nevertheless, there are often also additional uncertainties with respect to the distributions. Distributionally robust optimization combines stochastic uncertainties with robustly protecting against a whole set of distributions collected in a so-called ambiguity set. We call the resulting collection of infinitely many chance constraints a robust chance constraint. So, instead of assuming a fixed distribution for the uncertain demands in the nomination validation problem, we protect robustly against all distributions in a predefined ambiguity set $\mathcal{U}$. We discuss this setting further in Sect. 10.3.2.2. We conclude this section by pointing out that there is further literature on robust protection against uncertainties in gas networks. When we focus only on robust protection against demand uncertainties (and do not fix the pressure at any node), the computational complexity of robust nomination validation, also called checking the feasibility of a booking, has been analyzed in detail. Complexity results and solution algorithms have been examined for different problem variants and for various network structures. For further details, we refer to [42], [43], and [57].

10.2.2 Capacity maximization under stationary and transient gas flow

The optimization problem of maximizing bookable capacities under uncertainty is a highly relevant optimization challenge for network operators. We present an approach of rigorous examination of the underlying optimization problem with nonlinear probabilistic constraints that focuses on the free capacities on the exit side in a classical entry-exit model. A couple of publications appeared recently on the topic of maximizing network capacities in a probust, that means probabilistic and robust, setting. In [1] the authors deal with an optimization model for the capacity maximization that focuses on both the entry and exit side. The focus in [34] is on the evaluation of free network capacities on the exit side, which allows to reduce the mixed probabilistic and robust optimization model to a pure probabilistic one, moreover, a deeper theoretical justification by an analysis of the problem structure is presented. Whereas the contents of the two mentioned papers are based on the stationary gas flow model according to the algebraic model (ISO4-ALG), in [35] the approach of maximizing network capacities is extended to a transient gas flow model.

10.2.2.1 Stationary Gas Flow

First, we are going to take a closer look at the situation of stationary gas flow and, therefore, here we want to follow the optimization model that is presented in [34]. A special situation, which allows to formulate explicit feasibility conditions on the gas demand in terms of inequalities, is given for tree structured gas networks with single entry. Let $V = \{0, 1, \ldots, N\}$ be the set of all nodes, assign the index 0 to the single entry node that is assumed also to be the *root* of the tree, and let $b = (b_1, \ldots, b_N)$ be the demand at the exits. For $k, \ell \in V$, denote $k \succeq \ell$ if, in G, the unique directed path from the root to k, denoted $\Pi(k)$, passes through ℓ. Define for any $k \in V$ the functionals

$$h_k(b) := \begin{cases} 0, & \text{if } k = 0, \\ \sum\limits_{e \in \Pi(k)} \Phi_e\left(\sum\limits_{n \succeq \tau(e)} b_n \right)^2, & \text{otherwise,} \end{cases} \tag{10.10}$$

with $\tau(e)$ denoting the head of arc e. According to [24], some demand ξ is (technically) feasible, if and only if ξ satisfies the inequality:

$$\max_{k=0,\ldots,N} \left((p_k^{\min})^2 + h_k(b) \right) - \min_{\ell=0,\ldots,N} \left((p_\ell^{\max})^2 + h_\ell(b) \right) \leq 0. \tag{10.11}$$

Because the demand reflects the behavior of gas consumers, the demand is in fact a random quantity with some probability distribution. For that reason, technical feasibility is expressed in terms of probabilities. The gas demand is realized by *nominations* of the gas customers matching *booking capacities* that are offered by the network operator to each customer. However, the network operator is responsible for a reliable network operation for any possible nomination within the offered booking limit. For that reason, the evaluation of booking capacities turns out to be a challenging task.

For our formulation of the capacities problem, we want to assume that there are already existing customers with demand profiles whose probability distribution can be estimated by historical data records. The scope of our approach is to find out whether the network reliability allows for additional customers, and if so, how much capacity can be offered without losses with respect to the reliability of the network operation.

As opposed to existing gas consumers, the consumption behavior of new customers is barely predictable. For that reason, it is appropriate to suggest a probabilistic approach for existing customers and a robust approach for new customers in order to model uncertainties of the overall gas demand. This leads to a *probust* formulation of constraints as introduced in (10.7). Let ξ denote the random vector corresponding to nominations of former gas consumers and let y denote the nominations of new customers according to the new booking capacity vector u. Then, the overall gas demand is $\xi + y$, and hence, by (10.11) the probability for a valid network operation reads

$$\mathbb{P}\Big(\max_{k=0,\ldots,N} \left((p_k^{\min})^2 + h_k(\xi + y) \right) - \min_{\ell=0,\ldots,N} \left((p_\ell^{\max})^2 + h_\ell(\xi + y) \right) \leq 0 \quad \forall y \in [0, u] \Big). \tag{10.12}$$

Note that the control u is just the shape of the uncertainty set here, which is subject to optimization now. As shown in [34] the robust part in (10.12) can be eliminated

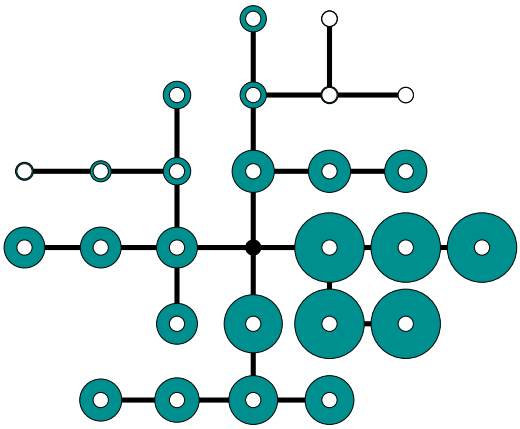


Fig. 10.2: Allocated free network capacities in the case of stationary gas flow for an example tree network with single entry node. A larger size of the colored surrounding of a node indicates a higher quantity of available free capacity at this node.

by a transformation of the random constraint. Due to (10.10), the 'for all' condition is resolved explicitly when passing to the random inequality system

$$g_{k,\ell}(u,\xi) := (p_k^{\min})^2 + \sum_{e\in\Pi(k)\setminus\Pi(\ell)} \Phi_e\left(\sum_{n\succeq\tau(e)} (\xi_n + u_n)\right)^2 - (p_\ell^{\max})^2 - \sum_{e\in\Pi(\ell)\setminus\Pi(k)} \Phi_e\left(\sum_{n\succeq\tau(e)} \xi_n\right)^2 \leq 0 \quad (10.13)$$

for all $k,\ell = 0,\ldots,N$. The problem of maximizing booking capacities becomes a classic optimization problem with probabilistic (chance) constraints according to (10.2) now. It can be formulated as

$$\min\left\{\langle c,u\rangle \;\middle|\; \mathbb{P}\left(g_{k,\ell}(u,\xi)\leq 0 \quad k,\ell = 0,\ldots,N\right) \geq \mathrm{p}\right\} \quad (10.14)$$

with c denoting some cost vector allowing for preferences of the network operator and with $g_{k,\ell}(\cdot,\cdot)$ defined in (10.13). Problem (10.14) is a probabilistic program that can be solved by techniques provided in Sect. 10.3.1.1.

Figure 10.2 shows the computed free capacities as the solution of problem (10.14) for an example gas network that has originally been presented in [34]. The network is just a tree with a single entry and 26 exit nodes. The stochastic part of the exit nominations ξ is represented here by a (truncated) Gaussian normal distribution that is obtained via historical data.

10.2.2.2 Transient Gas Flow

Now we are going to discuss a more general approach of maximizing capacities in a gas network by incorporating time dependencies and, in particular, a transient gas flow model. While this approach is applicable to general networks with tree structure (see [35]), we restrict our considerations here, for simplicity, to single pipes. Dynamic gas flow in a single pipe is modeled by the isothermal Euler equations (ISO2) see Chap. 2, "A Catalog of Gas Network Models: PDEs, Coupling Conditions, and Numerical Schemes". Pressure and flow along the pipe are now functions with space and time as arguments solving

$$\begin{aligned} \partial_t p(x,t) + \alpha\, \partial_x q(x,t) &= 0 \\ \partial_t q(x,t) + \beta\, \partial_x p(x,t) + \gamma\, \frac{q(x,t)|q(x,t)|}{p(x,t)} &= 0 \end{aligned} \qquad (x,t) \in [L,R] \times [0,T]. \quad (10.15)$$

The quantities α, β, and γ are fixed pipe parameters depending on speed of sound, cross section, diameter, friction and length of the pipe. Recall that the algebraic conditions (10.9) applied for a single pipe are obtained from the solution of (10.15) when considering a stationary flow, i.e., where $\partial_x q = \partial_t q \equiv 0$.

In general, the Euler equations above are solved by discretization techniques. As a result, one obtains flow and pressure profiles $q_{\text{entry}}(t)$, $q_{\text{exit}}(t)$, $p_{\text{entry}}(t)$ and $p_{\text{exit}}(t)$ at the entry and exit of the pipe. The exit demand, for both existing and new customers, enters the model as boundary condition in (10.15). Then, technical feasibility means that the obtained pressure profiles match the given pressure bounds, in particular, there are constraints of the form

$$p_{\text{entry}}(t) \in [p_{\text{entry}}^{\min}, p_{\text{entry}}^{\max}]; \quad p_{\text{exit}}(t) \in [p_{\text{exit}}^{\min}, p_{\text{exit}}^{\max}] \qquad \forall t \in [0,T].$$

Finally, the optimization problem of maximizing booking capacities is formulated as a probabilistic program similar to (10.14), but with two additional challenges: first, the optimal control u is time dependent now, and second, instead of evaluating explicit inequality constraints, the Euler equations must be solved in order to prove technical feasiblity for some control u. Clearly, this increases the numerical effort significantly when solving the capacity problem.

The authors in [35] compare two approaches, a *transient* and a *quasi-static* one, to solve the Euler equations numerically. In the transient consideration (10.15) is solved by replacing the x-derivatives by difference quotients (space approximation) and the t-derivatives by an implicit Euler scheme (time approximation). Much less numerical effort is required by the alternative approach of quasi-static consideration that is completely based on the algebraic model (ISO4-ALG) only (see Chap. 2, "A Catalog of Gas Network Models: PDEs, Coupling Conditions, and Numerical Schemes"). After discretizing the time horizon, the network is assumed to be a stationary state at each time step such that the stationary solution (10.9) provided in the previous section is applied for each time step. It turns out that this might be a good assumption as long as changes of the boundary conditions develop smoothly in time. The capacity problem

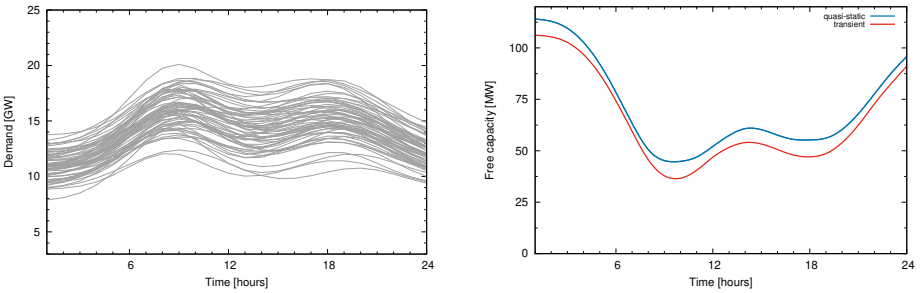


Fig. 10.3: Stochastic demand profiles (left) and the allocated free network capacities in the case of transient and quasi-static gas flow in a single pipe. The picture shows that the computed two alternative solutions are very close.

is well suited in this respect, because the critical quantity is the demand that usually provides reasonably smooth profiles.

We conclude this section by some results from the numerical study in [35]. Both approaches, the quasi-static and transient consideration, applied for allocating free network capacities in a single pipe and in a small tree network configuration, have been compared. The numerical tests reveal that the quasi-static implementation is an excellent alternative to the fully transient implementation in both examples. Figure 10.3 shows stochastic demand profiles for one day and the solutions of the (transient) capacity problem for the single pipe example.

10.2.3 Maximizing the Chance of Feasibility for Transient Gas Flow

In a gas transportation network, an essential goal of the Transmission System Operator (TSO) is to satisfy the demand of the customers according to their nominations. This process is governed by the rules of the European Union for the gas markets. A dynamic multilevel model of the European gas market is studied for example in [30]. The customer demand is influenced by numerous factors that cause uncertainty (for example the weather), hence it makes sense to model it as a random variable.

In the operation of the pipeline system, there is a desired operational range for the gas pressure. The pressure decreases along the pipes in the direction of the gas flow. Hence, there is a need for compressor control action to increase the pressure in order to avoid that it falls below an acceptable value. On the other hand, there is also an upper bound for the pressure that is feasible in the pipe which limits the admissible pressure increase by the control action. The pressure at the exit points to the customers should be greater than a lower bound $p_{\min}$. The compressors should be operated in such a way that the probability that these bounds are satisfied at all times is sufficiently high. This is a probust constraint of the type (10.7), where the decision parameter is the control, which should be chosen in such a way that the control cost is acceptable.

This leads to problem of optimal control, where the probability that the pressure bound is satisfied is a part of the objective function. The objective function also contains a control cost. In [29], this problem is stated for the case of a single pipe. It is shown that an optimal control does exist. In this section we present an example with a small network.

10.2.3.1 Chance Maximizing Controls

In the optimal control problem, the gas pipeline flow is modeled by the isothermal Euler equations (ISO1). Thus, the gas network is represented as a networked quasi-linear system where the flow on the edges is coupled by algebraic node conditions that require the conservation of mass (Kirchhoff condition) and the continuity of the pressure at the nodes, see [2, 28].

Let a time horizon $T > 0$ be given. Let $N \in \{1, 2, 3, \ldots\}$ denote the number of compressors and $u \in X(T) = \left[H^2(0, T)\right]^N$ denote the compressor controls. A sufficiently regular initial state is supposed to be given such that the pressure bounds are strictly satisfied. Moreover, a reference control $u_{ref} \in X(T)$ is given that is C^1-compatible with the initial state and generates a continuously differentiable state.

For $u \in X(T)$ and a penalty parameter $\gamma > 0$, define the objective function

$$J(u) = \gamma \|u - u_{ref}\|^2_{X(T)} - \ln\left(\mathbb{P}\left(\min_{t\in[0,T], e\in E} \min_{x\in[0,L^e]} p^{e,\omega}(t, x) \geq p^{\min}\right)\right), \qquad (10.16)$$

where $p^{e,\omega}$ denotes the pressure in pipe e that is generated with the (boundary or compressor) control u and uncertain customer demand, where the superscript ω denotes the random variable.

10.2.3.2 A Numerical Example

In this section, we present a numerical example for *chance maximizing controls*, similar as it was done in [29] for a single pipe. We consider a network junction as shown in Fig. 10.4a) with a single inflow node v_0, one inner node v_1, two exit nodes v_2, v_3 and three pipes e_1, e_2, e_3, where e_i ends in node v_i $(i = 1, 2, 3)$. Let the ISO1-model for real gas be given on every pipe. The corresponding data is given in Fig. 10.4b), and we assume that the data is equal on every pipe. The coupling conditions (see, e.g., [2, 28]) at the network junction are given by mass conservation

$$q_{e_1}(t, L) = q_{e_2}(t, 0) + q_{e_3}(t, 0) \qquad \forall t \in [0, T], \qquad (10.17)$$

and pressure continuity

$$p_{e_1}(t, L) = p_{e_2}(t, 0), \quad p_{e_1}(t, L) = p_{e_3}(t, 0), \qquad \forall t \in [0, T], \qquad (10.18)$$

where q_{e_i} in $\frac{kg}{m^2 s}$ and p_{e_i} in bar are flow and pressure at edge e_i.

In our numerical approach, the uncertain boundary data are modeled by random Fourier series (see, e.g., [37, 46]), where as in the *Karhunen–Loève Theorem*, the coefficients in the series are random variables. For a function f in $L^2(0, T)$ and for $m = 0, 1, \ldots$, we define the orthonormal basis functions

$$\psi_m(t) = \frac{\sqrt{2}}{\sqrt{T}} \sin\left(\left(\frac{\pi}{2} + mx\right)\frac{t}{T}\right),$$

and the Fourier coefficients

$$a_m^0(f) = \int_0^T f(t)\, \psi_m(t)\, dt.$$

For a sequence of identically distributed random variables $(\xi_m)_{m\geq 0}$, the random Fourier series is given by

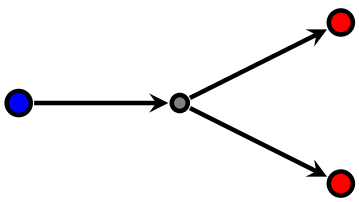
$$f^\omega(t) = \sum_{m=0}^{\infty} \xi_m(\omega) a_m^0 \psi_m(t).$$

Then, due to an extension of the *Paley–Zygmund Theorem*, for $f \in X(T)$, the random Fourier series f^ω converges almost surely in L^2. Thus, the randomized Fourier series has the same regularity properties as the original function. In our example, we use the boundary functions

$$f_{v_2}(t) = 15\left(1 - \cos\left(\frac{t}{T}2\pi\right)\right) + 80 \quad \text{and} \quad f_{v_3}(t) = 15\left(1 - \sin\left(\frac{t}{T}4\pi\right)\right) + 75, \quad (10.19)$$

and as a multiplier we apply Gaussian distributed random variables with mean value $\mu = 1$ and variance $\sigma^2 = 0.1$. The corresponding randomized boundary functions for $T = 12$ hours are shown in Fig. 10.5.

We consider the chance maximizing optimal control problem (10.16), and the corresponding chance maximizing optimal control problem with $X(T) = L^2(0, T)$, where the pressures are given by the solution of ISO1 on the graph in Fig. 10.4a) with the coupling conditions (10.17), (10.18) and the randomized boundary functions (10.19). The control $u(t)$ acts at the source node by increasing the inlet pressure, thereby defining the boundary control condition



Variable	Letter	Value	Unit
inlet pressure	p_0	55	bar
lower pressure bound	$p_{\min}$	43	bar
pipe friction coefficient	λ^F	0.1	
pipe diameter	D	0.5	m
pipe length	L	10	km
sound speed in the gas	c	360	m/s

Fig. 10.4: Scheme of the network junction (left) with one source, one inner node and two sinks, and parameters of the isothermal Euler equations (ISO1) for the chance maximizing control problem (right).

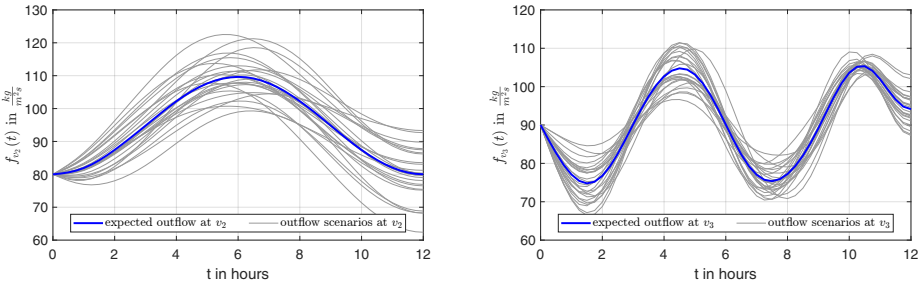


Fig. 10.5: Outflows f_{v_2} (left) and f_{v_3} (right) with 25 random scenarios for the expected scenarios stated in (10.19).

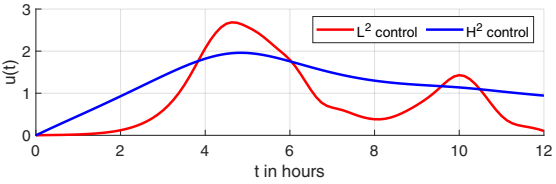


Fig. 10.6: Optimal controls of (10.16) for $X(T) = L^2(0,T)$ and $X(T) = H^2(0,T)$.

$$p_{e_1}(t,0) = p_0 + u(t).$$

Note that the control is a scalar function in this example. As initial condition we consider the corresponding steady state with boundary data p_0, $f_{v_2}(0)$ and $f_{v_3}(0)$. With $u_{ref} = 0$, for the H^2-norm in (10.16) we consider different weights for the derivatives, i.e., we consider

$$J_{H^2}(u) = \gamma_1 \| u \|^2_{L^2(0,T)} + \gamma_2 \| u' \|^2_{L^2(0,T)} + \gamma_3 \| u'' \|^2_{L^2(0,T)} - \ln\left(\mathbb{P}\left(\min_{t\in[0,T],e\in E}\ \min_{x\in[0,\,L^e]} p^{e,\omega}(t,x) \geq p^{\min}\right)\right),$$

with $\gamma_1 = 10^{-5}$, $\gamma_2 = 10^3$ and $\gamma_3 = 10^{10}$, because otherwise, the influence of the gradients vanish due to the long time period of 43.200 seconds. Note that γ_1 is also the weight of the L^2-norm. The optimal controls for $X(T) = L^2(0,T)$ and for $X(T) = H^2(0,T)$ are shown in Fig. 10.6 and the corresponding pressures at node v_2 and v_3 for 25 scenarios are shown in Fig. 10.7.

As it was expected, the optimal control w.r.t. the H^2-norm is less oscillatory than the optimal control w.r.t. the L^2-norm. The resulting optimal probabilities are given by

$$\mathbb{P}_{L^2}\left(\min_{t\in[0,T],e\in E}\ \min_{x\in[0,\,L^e]} p^{e,\omega}(t,x) \geq p^{\min}\right) = 79.5\%$$

$$\mathbb{P}_{H^2}\left(\min_{t\in[0,T],e\in E}\ \min_{x\in[0,\,L^e]} p^{e,\omega}(t,x) \geq p^{\min}\right) = 63.5\%.$$

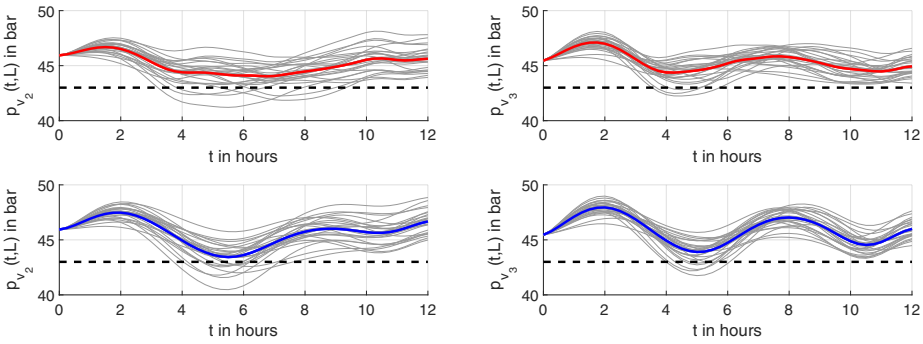


Fig. 10.7: Optimal pressures of (10.16) at nodes v_2 (left) and v_3 (right) for $X(T) = L^2(0,T)$ (above) and $X(T) = H^2(0,T)$ (below) for 25 random scenarios.

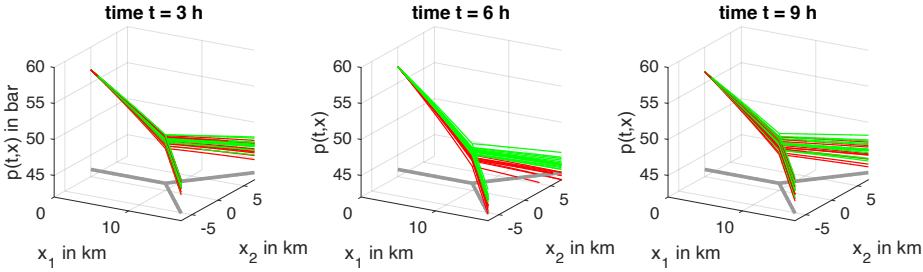


Fig. 10.8: 25 scenarios for the pressure profiles on the network at $t = 3$h, $t = 6$h and $t = 9$h. Pressure profiles, that are above the lower bound for all times, are shown in green, other profiles are shown in red.

Due to the additional derivatives in the optimal control problem with the H^2-norm, the probability is weighted less in relation to the L^2 optimization, leading to a smaller probability. The pressure profiles for the H^2 optimization at different time points are shown in Fig. 10.8. One can see, that at $t = 3$ h and at $t = 9$ h, all scenarios are feasible, while at $t = 6$ h, some scenarios are below the bound of 43 bar. This matches the results of Fig. 10.7.

10.3 Algorithmical Approaches

In this section, we want to review some algorithmical approaches related with probabilistic, robust, and probust constraints.

10.3.1 Numerical Methods for Solving Optimization Problems Subject to Probabilistic Constraints

It is evident that, before dealing with a probust constraint (10.6), one has to be able to handle numerically conventional probabilistic constraints induced by finitely many (smooth) random inequalities, which can be understood as probust constraints with finite uncertainty set $\mathcal{U}$. Numerical approaches for probabilistic constraints can roughly be classified into methods that relax the constraints, resulting in formulations with nicer properties (e.g., convexity, differentiability) and methods that approximate the original probabilistic constraints. One method falling into the first class relies on the Conditional Value-at-Risk, but other relaxations are possible (e.g., [9, 39, 47]). Facilitating solution methods through relaxation of the probabilistic constraint comes at the cost of possibly significant conservatism of the resulting solutions. The second class of approaches approximate the original probabilistic constraints. This approximation could be discrete (as in sample average approximation [50]) or smooth (as in, e.g., [22, 51]). A special case of the latter methodology is kernel density estimation (e.g., [8, 56]). Typically, the aforementioned approaches are applicable to general probability distributions and just require the possibility to sample them without exploiting special structure of concrete distributions. In contrast, certain classes of distributions admit specially tailored methods such as the spherical-radial decomposition of elliptically distributed (e.g., Gaussian) random vectors (e.g., [59]). In the following, we present some methods in a bit more detail.

10.3.1.1 Spherical-Radial Decomposition

In this section, we revisit the *spherical-radial decomposition* (SRD) as a methodology for addressing chance constraints. We assume that the decision variable x in the probabilistic constraint (10.2) belongs to some Banach space. The SRD has a somewhat greater level of complexity when compared to alternative methods cited above, which are moreover applicable to any distribution accessible through sampling. Although the SRD is confined to a specific class of multivariate distributions, namely elliptically symmetric (including Gaussian) distributions, it exploits their intrinsic properties to provide three significant benefits: First, it facilitates the analysis of the original problem (e.g., Lipschitz continuity or differentiability of the probabilistic constraint) without requiring approximations at the outset [31, 59, 60]. This aspect has been utilized in [19, 61] to derive optimality conditions for a continuous PDE optimal control problem with uniform random state constraints (see Sect. 10.4.3). Second, the SRD exhibits a potentially strongly reduced variance in probability estimation compared to crude Monte-Carlo or methods based on Monte-Carlo samples. Third, the SRD provides explicit (sub-)gradient expressions for the probability function in both the original and numerically approximated formulations. This is crucial for addressing probabilistic constraints through non-linear optimization methods.

Though SRD applies to the broad class of elliptically symmetric distributions (see [17]), we will present it here for simplicity for the special case of a d-dimensional

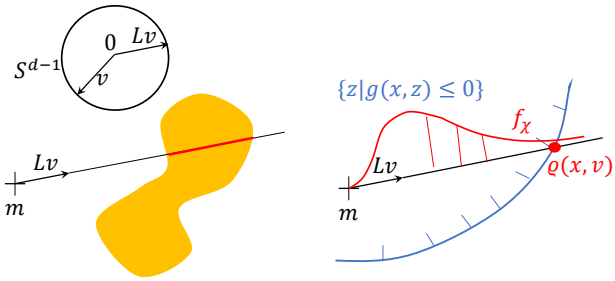


Fig. 10.9: Spherical-radial decomposition of a Gaussian random vector for determining the probability of a general set (left) and of a set described as a (decision-dependent) inequality (right).

Gaussian random vector $\xi \sim \mathcal{N}(m, \Sigma)$. Then, the probability of a measurable set $M \subseteq \mathbb{R}^d$ can be represented as a spherical integral

$$\mathbb{P}(\xi \in M) = \int_{v \in \mathbb{S}^{d-1}} \mu_\chi \left(\{ r \geq 0 \mid m + rLv \in M \} \right) d\mu_U(v).$$

Here, μ_χ is the one-dimensional Chi-distribution with d degrees of freedom, $d\mu_U$ is the uniform distribution on the sphere $\mathbb{S}^{d-1}$, and L is a Cholesky factor of the covariance matrix $\Sigma = LL^T$. In illustrative terms, the probability of M is obtained by scanning one-dimensional probabilities along rays (see Fig. 10.9 (left)). Since we are interested in probabilistic constraints such as (10.2), we set $M := \{z \in \mathbb{R}^d \mid g(x, z) \leq 0\}$ for some fixed decision x and obtain

$$\mathbb{P}(g(x, \xi) \leq 0) = \int_{v \in \mathbb{S}^{d-1}} \mu_\chi \left(\{ r \geq 0 \mid g(x, m + rLv) \leq 0 \} \right) d\mu_U(v). \tag{10.20}$$

Much more can be said under the additional assumptions for all decisions x:

$$g(x, \cdot) \text{ is convex}, \exists \bar{z} : g(x, \bar{z}) < 0, \text{ and } \mathbb{P}(g(x, \xi) \leq 0) \geq 0.5. \tag{10.21}$$

The last two conditions are mild: indeed, the existence of a Slater point can be taken for granted under proper modeling of the problem. Moreover, in probabilistic constraints (10.2), one is usually interested in probabilities close to one, hence iterations of an algorithm will likely produce decisions x realizing probabilities larger than 0.5. It is shown in [59, Prop. 3.11] that these last two conditions imply the relation $g(x, m) < 0$, i.e., the mean of the distribution is an interior point of the set M. This situation is illustrated in the right part of Fig. 10.9. It entails that

$$\{ r \geq 0 \mid g(x, m + rLv) \leq 0 \} = [0, \rho(x, v)] \quad \forall v \in \mathbb{S}^{d-1},$$

where $\rho(x, v)$ is possibly infinite in case that the entire ray emanating from m in direction Lv is contained in M. Plugging this into (10.20), we arrive at the more explicit expression

$$\mathbb{P}(g(x,\xi) \le 0) = \int_{v\in\mathbb{S}^{d-1}} \underbrace{F_\chi(\rho(x,v))}_{e(x,v)}\, d\mu_U(v) \qquad (F_\chi(\infty) := 1), \tag{10.22}$$

where F_χ denotes the distribution function of the Chi-distribution with d degrees of freedom and we exploit the relations $F_\chi(0) = 0, \lim_{t\to\infty} F_\chi(t) = 1$. By definition, F_χ is the integral over the density f_χ illustrated in Fig. 10.9 (right). As shown in [36], the ratio of variances between the SRD and Monte-Carlo estimates tends to zero for large, small and symmetric sets. This makes SRD particularly interesting for rare events. The potentially arbitrary improvement in variance reduction compensates the typically larger computational effort for determining the radius function ρ (although the effort is negligible when g is linear or quadratic in its second variable).

Most important for dealing with chance constraints within the framework of nonlinear optimization is first-order information about the probability function φ in (10.4), which is computed via (10.22). Assumptions (10.21) imply that φ is continuous. Unfortunately, even when adding continuous differentiability of g to assumptions (10.21), there is no guarantee that φ itself is more than just continuous, see [31, Example 1], where φ even fails to be Lipschitz continuous. This issue is closely related with the boundedness of set $M := \{z \mid g(x,z) \le 0\}$. If M fails to be bounded as in Fig. 10.9 (right), then the transition from finite to infinite values of the radial function ρ may cause problems in deriving nice properties of φ. When imposing the boundedness of M, however, and assuming that g as a function of both variables is locally Lipschitz continuous, then one may derive the Lipschitz continuity of φ and even estimate from above its Clarke subdifferential [10] as

$$\partial^C \varphi(x) \subseteq \int_{v\in\mathbb{S}^{d-1}} \partial_x^C e(x,v) d\mu_U(v), \tag{10.23}$$

where e is defined in (10.22) and the integral has to be understood in the sense of Aumann, see [31, Theorem 5]. The boundedness of M can be dispensed with when assuming a certain growth condition that is satisfied in common applications. More precise statements can be made if g is not just locally Lipschitzian but, say, a maximum of finitely many continuously differentiable functions g_i, thus representing a smooth random inequality system. Then, the upper estimate of the Clarke subdifferential in (10.23) can be made fully explicit in terms of the input data (gradients of the g_i), see [31, Corollary 3]. If, in addition, the so-called 'Rank-2 Constraint Qualification' is satisfied, then the probability function turns out to be differentiable [60, Corollary 4.4]. This constraint qualification addresses couples of active gradients, so if g is continuously differentiable itself, it is automatically satisfied. In the latter case, one ends up with the following gradient formula (where f_χ is the density of the Chi-distribution):

$$\nabla\varphi(x) = \int_{v\in\mathbb{S}^{d-1}} \frac{f_\chi(\rho(x,v))}{\langle \nabla_z g(x, m+\rho(x,v)Lv), Lv\rangle} \nabla_x g(x, m+\rho(x,v)Lv) d\mu_U(v). \tag{10.24}$$

While the mentioned (sub-)gradient formulae are tied with the original probability function φ and could be exploited for theoretical considerations, such as optimality conditions (see Sect. 10.4.3 or [61]), a numerical solution method would rather replace the spherical integrals in (10.22) and (10.24), respectively, by finite sums:

$$\varphi(x) \approx \sum_{i=1}^{K} F_\chi(\rho(x, v^i));$$
$$\nabla\varphi(x) \approx \sum_{i=1}^{K} \frac{f_\chi(\rho(x, v^i))}{\langle \nabla_z g(x, m + \rho(x, v^i)Lv), Lv^i\rangle} \nabla_x g(x, m + \rho(x, v^i)Lv^i).$$

Here, $\{v^1, \ldots, v^K\}$ refers to a sample of the uniform distribution on the sphere, which can be obtained, for instance, by normalizing to unit length a (Monte-Carlo or Quasi Monte-Carlo) sample of a d-dimensional standard Gaussian distribution $\mathcal{N}(0, I)$.

10.3.1.2 Kernel Density Estimation

In this section, we introduce the concept of kernel density estimation (KDE) (see, e.g., [13]) and demonstrate how it can be applied to evaluate and approximate probust constraints of the form (10.6) (see, e.g., [8, 56]). KDE is a non-parametric technique for estimating the probability density function (PDF) of a random variable based on a finite sample set, without assuming any specific parametric form for the underlying distribution. This flexibility makes KDE particularly valuable in optimization under uncertainty, where the true distribution of the random vector ξ may be unknown or only available through empirical data. By constructing a smooth approximation of the underlying density, KDE facilitates the estimation of complex probabilistic events—such as those represented by probust constraints—enabling us to evaluate the probability in (10.6) using data-driven methods. One of the key advantages of KDE is that it does not impose strict assumptions on the distribution of ξ. This allows it to capture a wide variety of distributions commonly encountered in real-world applications, while maintaining continuity and smoothness properties that are beneficial for numerical optimization.

Before addressing the probust constraints (10.6), we apply KDE to evaluate pure probabilistic constraints of the form

$$\mathbb{P}(g(x, \xi) \leq 0) \geq \mathrm{p}, \tag{10.25}$$

for a probability level $\mathrm{p} \in (0, 1)$, as they appear in (10.2). We assume that ξ is a d-dimensional, absolutely continuous random vector with PDF ρ_ξ. For a decision variable x that belongs to a Banach space $\mathcal{V}$, and a constraint $g\colon \mathcal{V} \times \mathbb{R}^d \to \mathbb{R}^m$, we assume that $g(x, \xi)$ is also an absolutely continuous random vector with PDF ρ_g. The probability in (10.25) can then be evaluated by integrating the PDF of ξ over the feasible set, i.e.,

$$\mathbb{P}\left(g(x, \xi) \leq 0\right) = \int_{M(x)} \rho_\xi(z)\, dz, \tag{10.26}$$

where the feasible set $M(x)$ is given by

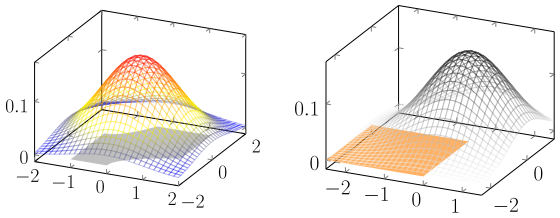


Fig. 10.10: Well-known probability distribution with unknown feasible set (left) as in (10.26) and unknown probability distribution with well-known feasible set (right) as in (10.27).

$$M(x) := \{\omega \in \Omega \mid g(x, \xi(\omega)) \leq 0\}.$$

While the SRD discussed in Sect. 10.3.1.1 is based on scanning the feasible set $M(x)$, KDE is applied to obtain an approximation of the PDF ρ_g. Thus, instead of evaluating (10.26), we have

$$\mathbb{P}\left(g(x, \xi) \leq 0\right) = \int_{(-\infty, 0]} \rho_g(z)\, dz. \tag{10.27}$$

A visualization of both approaches is given in Fig. 10.10.

Consider now an independent and identically distributed sample

$$\mathcal{S}_\xi = \{y_1, \cdots, y_{N_{\text{kde}}}\} \subseteq \mathbb{R}^d,$$

of length $N_{\text{kde}} \in \mathbb{N}$ of the random vector ξ. Defining $Y_i(x) := g(x, y_i)$ for $x \in \mathcal{V}$, the sample

$$\mathcal{S}_g = \{Y_1(x), \cdots, Y_{N_{\text{kde}}}\} \subseteq \mathbb{R}^m$$

is an independent and identically distributed sample of the random vector $g(x, \cdot)$. For a multivariate kernel function $K\colon \mathbb{R}^m \to \mathbb{R}_{\geq 0}$ and a bandwidth matrix $H \in \mathbb{R}^{m \times m}$, the KDE is given by

$$\rho_{g, N_{\text{kde}}}(z) = \frac{1}{N_{\text{kde}} \sqrt{\det H}} \sum_{i=1}^{N_{\text{kde}}} K\left(H^{-\frac{1}{2}}(z - Y_i(x))\right). \tag{10.28}$$

Note, that $\rho_{g, N_{\text{kde}}}$ is an approximation of ρ_g. In [25, 54], different kernel functions are investigated, and in [32], the authors discuss a suitable choice for the bandwidth matrix H. Under slight assumptions on the kernel function and the bandwidth matrix (see, e.g, [25, Chap. 6, Theorem 1]), the KDE (10.28) converges in L^1 as the number of samples goes to infinity, i.e.,

$$\|\rho_{g, N_{\text{kde}}} - \rho_g\|_{L^1(\mathbb{R}^m)} \xrightarrow{N_{\text{kde}} \to \infty} 0 \qquad \mathbb{P} - \text{almost surely}.$$

Due to *Scheffé's lemma* (see, e.g., [25, Chap. 1, Theorem 1]), also the approximated probability converges, i.e.,

$$|\mathbb{P}_{N_{\text{kde}}}(g(x,\xi) \le 0) - \mathbb{P}(g(x,\xi) \le 0)| \xrightarrow{N_{\text{kde}}\to\infty} 0 \qquad \mathbb{P}-\text{almost surely.}$$

In [54, 56], the authors apply a Gaussian product kernel and a diagonal bandwidth matrix to approximate the probabilistic constraints for steady state gas flow in pipeline networks, which can be generalized for probabilistic constraints of the form (10.27). Consider a multivariate Gaussian product kernel

$$K(z) = \frac{1}{(2\pi)^{\frac{m}{2}}} \prod_{j=1}^{m} \exp\Big(-\frac{1}{2}z_j^2\Big),$$

and a diagonal bandwidth matrix

$$H_{j,j} = h^2 \Sigma_{j,j} \qquad \text{with} \qquad h = \left(\frac{4}{(m+2)N_{\text{kde}}}\right)^{\frac{1}{m+4}},$$

where Σ is the covariance matrix of the sample $\mathcal{S}_g$. Then, the KDE (10.28) is given by

$$\rho_{g,N_{\text{kde}}} = \frac{1}{N_{\text{kde}} \prod_{j=1}^{m} \sqrt{H_{j,j}}} \sum_{i=1}^{N_{\text{kde}}} \prod_{j=1}^{m} \frac{1}{\sqrt{2\pi}} \exp\left(-\frac{1}{2}\Big(\frac{z_j - Y_{i,j}(x)}{\sqrt{H_{j,j}}}\Big)^2\right).$$

For the corresponding probability (10.27), we can apply *Fubini's theorem*, which yields

$$\mathbb{P}_{N_{\text{kde}}}(g(x,\xi) \le 0) = \frac{1}{N_{\text{kde}} \prod_{j=1}^{m} \sqrt{H_{j,j}}} \sum_{i=1}^{N_{\text{kde}}} \prod_{j=1}^{m} \int_{-\infty}^{0} \frac{1}{\sqrt{2\pi}} \exp\left(-\frac{1}{2}\Big(\frac{z_j - Y_{i,j}(x)}{\sqrt{H_{j,j}}}\Big)^2\right) dz_j.$$

Integration by substitution shows

$$\mathbb{P}_{N_{\text{kde}}}(g(x,\xi) \le 0) = \frac{1}{N_{\text{kde}}} \sum_{i=1}^{N_{\text{kde}}} \prod_{j=1}^{m} \int_{-\infty}^{-\frac{Y_{i,j}(x)}{\sqrt{2H_{j,j}}}} \frac{1}{\sqrt{\pi}} \exp(-\tau^2)\, d\tau,$$

and applying the *Gauss error function* implies

$$\mathbb{P}_{N_{\text{kde}}}(g(x,\xi) \le 0) = \frac{1}{N_{\text{kde}} 2^m} \sum_{i=1}^{N_{\text{kde}}} \prod_{j=1}^{m} \left(1 + \operatorname{erf}\Big(-\frac{Y_{i,j}(x)}{\sqrt{2H_{j,j}}}\Big)\right). \tag{10.29}$$

Thus, considering g continuously differentiable in x, the probability (10.27) can be approximately evaluated by the continuously differentiable algebraic formula (10.29). The convergence of probabilistic constrained optimization problems, where the probability is approximated by a KDE approach, is analyzed in [55].

For probust constraints (10.6), we can utilize the fact that

$$\mathbb{P}(g(x,\xi,u) \le 0 \quad \forall u \in \mathcal{U}) = \mathbb{P}\Big(\sup_{u\in\mathcal{U}} g(x,\xi,u) \le 0\Big).$$

By defining $Y_i(x) = \sup_{u\in\mathcal{U}} g(x, y_i, u)$ for $i = 1, \dots, N_{\text{kde}}$, the whole approach can analogously be applied to probust constraints. Due to the maximum, the resulting

approximated probability (10.29) is not differentiable anymore, but for the optimization, the kink in the maximum can be replaced by a smooth function, implying a continuously differentiable approximation of the probust constraint based on a sample of the random vector ξ.

10.3.1.3 Continuous Stochastic Gradient Method

When dealing with chance-constrained problems with continuous distributions, one crucial question is how the distribution can be evaluated or approximated. Whereas typical methods focus on special distributions as Gaussians or approximate them with discrete distributions, the Continuous Stochastic Gradient method (CSG) directly deals with general continuous distributions and improves the approximation quality over the iterations by cleverly combining past information about sample points. For a detailed introduction of the CSG method we refer to [26]. The general idea of CSG consists of drawing only one random sample in each iteration and evaluating the respective function values and gradients. The approximation of the whole integral and its gradients is then computed as a weighted linear combination of the already sampled values. In Chap. 11, "Continuous Stochastic Gradient and Spherical Radial Decomposition" in this book a combination of spherical-radial decomposition and the CSG method for chance-constrained problems is discussed and the CSG method is explained in more detail there. Whereas the combined method is restricted to distributions, where the spherical-radial decomposition is applicable, the pure CSG method can be used for every continuous distribution. As a drawback, an additional approximation is necessary to guarantee the existence of gradients. Therefore, we combine the penalty approximation from the combined approach with an additional smoothing of the indicator functions to obtain continuously differentiable expressions. The resulting approximation problem can be directly solved with the CSG method. For a concrete description of the approximation problem and the concrete smoothing functions we refer to [5]. Applying this approach to GasLib 24, 40, and 134 yields nearly feasible solutions within a few minutes which implies that the approximation problem works well and does not preclude finding good solutions to the chance-constrained nomination validation problems (NV-CC). For concrete results, we refer again to [5].

10.3.2 Numerical Methods for Solving Optimization Problems with Probust Constraints

10.3.2.1 Adaptive Index Selection for Probust Constraints

When solving an optimization problem including probust constraints (10.6), one could replace the uncertainty set $\mathcal{U}$ by some finite grid $\mathcal{U}^* = \{u^1, \ldots, u^K\}$. In this way, one would return to the case of conventional probabilistic constraints with the possible need to refine the grid whenever numerical accuracy requires one to do so. A straightforward uniform geometric grid approximation of $\mathcal{U}$, however, may turn out not to be efficient,

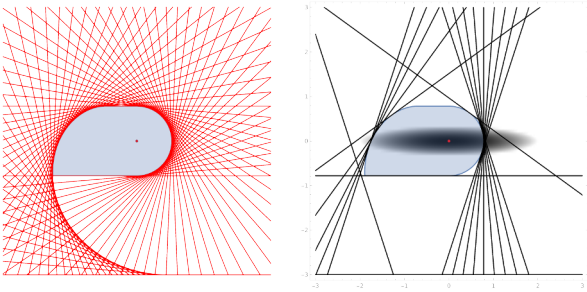


Fig. 10.11: Illustration of geometric (left) vs. probability-informed (right) approximation of some convex set which is defined as an infinite intersection of half spaces (details see text.)

in general. In the following, we sketch a probability-informed approximation of $\mathcal{U}$ as presented in [7] that is potentially more efficient. The main idea is illustrated in Fig. 10.11. The figure shows some convex set represented as the intersection of an infinite number (indexed by some interval $[0,T]$) of closed half spaces. The left figure shows a finite selection of these half spaces indexed by a fine uniform subgrid of $[0,T]$. As one can see, the geometric approximation of the set is close to perfect. However, if one is interested in an approximation of the probability of a set of infinitely many inequality constraints—and such is the case with the probust constraint (10.6)—then one can do better: The right part of Fig. 10.11 shows in addition some confidence ellipsoid (shaded) in order to symbolize some given, say Gaussian, distribution determining the probability of the mentioned set. Then it turns out that the intersection of a much smaller finite selection of half spaces is sufficient to approximate the desired probability as precisely as would do the large number in the left figure. Indeed, the geometric approximation of this small set of half spaces is quite poor, but the deficiency becomes visible only in regions with low probability, whereas close to the probability mass the approximation is much finer.

The justification of the observation above is as follows: in the context of the probust constraint (10.6) (with a fixed decision x), one always has the trivial inequality

$$\mathbb{P}(g(x,\xi,u)\le 0 \quad \forall u\in\mathcal{U}) \le \mathbb{P}(g(x,\xi,u)\le 0 \quad \forall u\in\mathcal{U}^*) \quad \forall \mathcal{U}^*\subseteq\mathcal{U}.$$

In particular, no matter what (potentially finite) subset $\mathcal{U}^*\subseteq\mathcal{U}$ we select, we always get an upper estimate for the true probability. Therefore, in order to make the approximation as efficient as possible, an additional element should be joined to $\mathcal{U}^*$ in a way that it minimizes the probability of the new intersection (which still is larger than the true one). This suggests the following conceptual two-phase algorithm for solving the probust optimization problem

$$\min\{f(x) \mid \mathbb{P}(g(x,\xi,t)\le 0 \quad \forall t\in[0,T]) \ge \mathrm{p}\}$$

with one-dimensional uncertainty set $\mathcal{U} := [0,T]$ (e.g., time interval):

Algorithm 1 Conceptual two-level algorithm for probust optimization problems

(i) Choose an initial point $x^0 \in X$. Set $I_0 := \emptyset$ and $k := 0$.

(ii) (**lower level problem**) Solve the following optimization problem with conventional probabilistic constraints in t:

$$\min_t \left\{ \mathbb{P}\left(g(x^k, \xi, \tilde{t}) \leq 0 \ \forall \tilde{t} \in I_k \cup \{t\} \right) \,\middle|\, t \in T \right\}$$

and denote by t_k^* one of its solutions.

(iii) (**upper level problem**) Set $I_{k+1} := I_k \cup \{t_k^*\}$ and solve (with x^k as a starting point) the following optimization problem with conventional probabilistic constraints in x:

$$\min_x \{ f(x) \mid \mathbb{P}(g(x, \xi, t) \leq 0 \ \forall t \in I_{k+1}) \geq \mathrm{p}, \ x \in X \}$$

and denote by x^{k+1} one of its solutions.

(iv) Set $k := k + 1$ and verify a suitable stopping criterion. If satisfied, then STOP, otherwise go to ii.

On the upper level of this algorithm, the optimization problem is solved on a fixed finite grid for the inequality system. On the lower level, the decision is fixed and the grid enhanced by one more index in the described way of minimizing the arising probability. The efficient implementation of this conceptual algorithm requires some additional heuristics in order to avoid that the lower level problem becomes too time consuming (for details, see [7]).

10.3.2.2 Distributionally Robust Chance Constraints with Bundle Methods

As an alternative to probust constraints, combining robust and stochastic perspectives can also be done by distributionally robust chance constraints. First, the focus lies on discrete distributions over a fixed and finite set of realizations, but an outlook to continuous distributions is also given. In general, we consider robust joint chance-constrained problems of the form

$$\begin{aligned} &\min_x f(x) \\ &\text{s.t. } \mathbb{P}_\mu(g(x,\xi) \leq 0) \geq \mathrm{p} \qquad \forall \mu \in \mathcal{U} \\ &\quad x \in X, \end{aligned} \tag{DRO}$$

where $g = (g_1, \ldots, g_{|\mathcal{J}|})^T$ is a vector-valued function modeling a joint chance constraint with $|\mathcal{J}|$ conditions for some finite set $\mathcal{J}$. Then, the joint condition in the chance constraint can be equivalently expressed by $\tilde{g}(x,\xi) := \max_{j \in \mathcal{J}} \{g_j(x,\xi)\}$ and together with the discrete nature of the distributions over a finite set $\Delta = \{\xi_1, \ldots, \xi_{|\Delta|}\}$ the robust chance constraint equivalently reads

$$\min_{\zeta \in \mathcal{U}} \sum_{i=1}^{|\Delta|} \zeta_i \chi_{]-\infty,0]}(\tilde{g}(x, \xi_i)) \geq \mathrm{p},$$

where ζ are the respective weights of each scenario in Δ and χ is the indicator function. This problem should be solved with the classical unconstrained bundle method introduced by Noll [48] that is extended to an inexact version for robust problems in [40], which is the subject of Sect. 10.3.3.1. To apply this unconstrained bundle method, one performs again a smoothing and penalty approximation as for nominal chance constraints in Sect. 10.3.1.3. Concretely, the respective approximation problem reads

$$\min_x \; f(x) + \lambda_{cc} \max_{\zeta \in \mathcal{U}} \left\{ \max \left\{ 0, p - \sum_{i=1}^{|\Delta|} \zeta_i s(\tilde{g}(x, \xi_i), \beta) \right\} \right\} + \lambda_{con} p_X(x), \tag{10.30}$$

where λ_{cc} and λ_{con} are positive penalty parameters, p_X is an exact penalty term for the constraint set X, and s is a smoothing function with respect to the parameter β. For a concrete version of the smoothing function to ensure convergence to the indicator function, we refer to [4] and the references therein. We note that sufficiently large choices of the penalty parameters can be easily determined for the gas setting by some preliminary computations. We refer to [4] for a more detailed explanation. If the input functions are continuously differentiable in x and the ambiguity set $\mathcal{U}$ is compact, the objective function of the approximation problem is locally Lipschitz continuous, and therefore, Clarke subgradients exist and the bundle method is applicable. Nevertheless, it sometimes produces slightly infeasible solutions to the original robust chance-constrained problem and the solutions are mostly suboptimal. Therefore, the method described in [4] combines solving the approximation problem via a bundle method with a scenario-based postprocessing. Here, one uses the bundle solution to determine which scenarios to include in the scenario-based formulation. In this formulation, the chance constraint is replaced by the constraints

$$\tilde{g}(x, \xi_i) \leq 0 \quad \forall i \in S$$

for a subset of scenarios $S \subseteq \Delta$. The numerical results for nomination validation problems in [4] demonstrate that this combined approach produces always feasible solutions and globally optimal solutions in about 90 % of the tests. Furthermore, depending on the concrete choice of the ambiguity set and the number of scenarios in Δ the combined bundle method often outperforms solving the direct robust reformulation with big-M constraints, initially introduced in [53], with standard optimization software and can even produce feasible solutions if the direct reformulation cannot be built due to memory limitations.

Nevertheless, the scenario-based bundle method is restricted to discrete distributions, since the bundle method cannot deal directly with measure integrals in the indicator function, and the scenario-based postprocessing is only meaningful for finite scenario sets. An extension of the ideas presented in this section to continuous distributions is given in [6], where finite mixtures of arbitrary reference distributions build the ambiguity set. Besides applying the bundle method, the CSG method discussed for nominal chance constraints in Sect. 10.3.1.3 is also able to handle this problem class.

10.3.3 Numerical Methods for Solving Optimization Problems with Robust or Almost Sure Constraints

10.3.3.1 Algorithms for Robust Nonlinear Optimization

In [41] an outer approximation approach for mixed-integer nonlinear robust optimization problems, which can be formulated in the form of (P), is developed. In the literature, there already exist outer approximation methods for nonsmooth MINLPs [11,62]. They, however, require exact evaluations of function values and subgradients of the objective and constraint functions. In [41] the outer approximation approach is extended to the case of only inexact evaluations of the constraint function as they result from the novel bundle algorithm that we will detail further below. In detail, a framework is established that specifies which type of inexactness in function value and subgradients we can allow such that the outer approximation approach still converges finitely.

In an outer approximation approach, as originally proposed by [15,18], one generates a mixed-integer linear master problem that is a relaxation of the original problem. To this master problem, one adds cutting planes in every iteration that are generated via function values and subgradients. It is hence iteratively refined and in the end, it yields a solution of the original problem. To generate new constraints for the master problem, one solves a continuous, nonlinear subproblem in every iteration. The framework for inexactness imposes requirements that solutions to the subproblems and the subgradients have to fulfill.

It has been shown in [41] that the adaptive bundle method [40] can be used to solve these nonlinear subproblems and is also able to generate subgradients that fulfill the required properties. We summarize its main algorithmic ingredients next. Nonlinear robust optimization problems with continuous decision variables cover the case of the continuous subproblems of the outer approximation approach from [41]. Moreover, the setting is extended to non-concavities in the uncertain parameters *and* non-convexities in the decision variables. Such a nonlinear robust optimization problem can be written in the following form of a minimax problem:

$$\min_{x\in X} \max_{u\in\mathcal{U}} v(x,u) =: \min_{x\in X} f(x), \tag{Minimax}$$

where X is a continuous set and v is a function depending on the variables x and the uncertainties u. Again, we allow for inexact solutions to the adversarial problem, which is the inner maximization problem. In [40], the problem of minimizing the nonsmooth and non-convex optimal value function f via an adaptive bundle method is solved. Problem (Minimax) is a nonsmooth optimization problem, for which bundle methods are a method of choice. They are an efficient tool for such problems and require access to function values and subgradients. Usually, one uses subgradients out of the Clarke subdifferential, $\partial^C f(\cdot)$, which is for the optimal value function f defined as

$$\partial^C f(x) = \operatorname{conv}\left\{\partial_x^C v(x;u_x^*) \mid v(x,u_x^*) = \max_{u\in\mathcal{U}} v(x,u)\right\}.$$

There are also inexact bundle methods in the literature, as, e.g., [33, 49], which are applicable for the case of non-convex functions. Even though Noll's bundle method can handle inexactness and non-convexities, it is not applicable to our setting. In detail, we assume to have access only to an approximate worst case for a given x, i.e., to an uncertain parameter $\tilde{u}_x \in \mathcal{U}$ such that, for a desired tolerance ϵ,

$$v(x, \tilde{u}_x) \geq \max_{u \in \mathcal{U}} v(x, u) - \epsilon.$$

Having such an inexact worst case at hand, we further assume that we can compute a corresponding inexact subgradient $\tilde{g}_x$ in the following sense:

$$\tilde{g}_x \in \partial_x^C v(x; \tilde{u}_x) \subseteq \tilde{\partial}^C f(x) := \operatorname{conv}\left\{\partial_x^C v(x; \widehat{u}_x) \mid \widehat{u}_x \in \mathcal{U}, v(x, \widehat{u}_x) \geq \max_{u \in \mathcal{U}} v(x, u) - \epsilon\right\}.$$

Existing bundle methods require a bounded distance of inexact subgradients to the exact Clarke subdifferential. The distance of the approximate subdifferential $\tilde{\partial}^C f(\cdot)$ to the exact one, however, cannot be bounded in general. This made an extension of existing bundle methods necessary. In [40] this difficulty is overcome by adaptively refining the approximations of function values in the course of a bundle method and Noll's bundle method has been extended in [40] to render it applicable to nonlinear robust optimization. Convergence of the resulting adaptive bundle method has been proven in [40]. In detail, it converges to a stationary point in the sense that 0 lies in the approximate subdifferential at the solution. The resulting adaptive bundle method is applicable to nonlinear robust optimization problems of the form (Minimax) under very mild assumptions. First, the function $v(\cdot, \cdot)$ needs to be lower C^1, which is the class of functions that can locally be written as the maximum of C^1-functions. Second, at every point x and for every required precision ϵ, an approximate worst case and a corresponding approximate function value and subgradient need to be accessible.

The robust gas transport with uncertainties in the demand and in pressure loss coefficients from Sect. 10.2.1 fits into the considered setting. In order to apply the adaptive bundle method [40] integrated in the outer approximation scheme [41], one needs access to an approximate global solution to the adversarial problem. This adversarial problem, however, includes non-convexities in the constraints. The adversarial problem maximizes the violation of pressure bounds such that the pressure loss constraint and further constraints such as flow conservation are fulfilled. We approximately solve this problem by piecewise linear relaxation [21]: The non-convex pressure loss constraint is relaxed to piecewise linear constraints, which can be modeled via a mixed-integer linear formulation. The resulting mixed-integer linear program (MIP) can then be solved to global optimality by state-of the art methods. It has been proven for the adversarial problem that a bound on the error in the pressure loss constraint leads to a guaranteed error bound in the optimal value. We hence can guarantee a distance of the approximate optimal value to the global optimal value of this non-convex problem. Further, a formula for a corresponding subgradient is derived in [40]. These results made it possible to apply the adaptive bundle method to the robust gas transport problem with uncertainties in the demands and pressure loss coefficients. In detail, the problem is solved in [40] on

the GasLib-instances of sizes 11, 24, 40 and 134, each within less than a few minutes, when the pressure at a chosen node is fixed beforehand.

By the outer approximation method from [41] the inclusion of binary decisions is possible that allows an extension of the considered setting to the control of valves and the option of a bypass-mode for the compressors. In order to fulfill the outer approximation method's requirements, one, however, has to restrict to the case of compressors that are not on cycles. This leads to a convex problem. A reformulation of the problem enables the derivation of subgradients also with respect to the binary decisions on valves and hence to solve the resulting problem.

10.3.3.2 Almost Sure Constraints

As observed in the introduction, almost sure constraints (10.5) are closely related with robust constraints (10.3), when the uncertainty set $\mathcal{U}$ is chosen as the support of ξ and with probabilistic constraints (10.2) when choosing $p = 1$. However, applying methods tailored to robust or probabilistic constraints in this setting may be difficult: on the one hand, the support of the distribution may not be known explicitly or may be complicated so that the uncertainty set $\mathcal{U}$ is impossible or hard to deal with by means of robust optimization. On the other hand, coping with probabilistic constraints on the maximum level $p = 1$ may lead to numerical degeneracies. Therefore, we present here a further approach to handling almost sure constraints and illustrate it for the example (10.34) in Sect. 10.4.3. The random state constraint $y(x, \omega) \leq \alpha$ for all $x \in D$ imposed there, which should hold almost surely, is penalized in the objective in the form of an additional term corresponding to a Moreau–Yosida-type regularization. The regularized problem is

$$\min_{u \in L^2(D)} \quad F(u) + \gamma \mathbb{E}[\|\max(0, y - \alpha)\|^2_{L^2(D)}]$$

subject to the PDE constraints in (10.34). It is possible to show that the solutions u^γ to the regularized problem are consistent with the solution of the original problem (10.34) as γ is taken to infinity; see [20]. This process is illustrated in the left part of Fig. 10.12 for a one-dimensional instance of the control problem. The expectation in the expression above is evaluated by means of a sample average approximation based on a sample of the random vector ξ. Therefore, not only the penalty parameter but also the sample size has to be increased. It is important to note that more knowledge about the support (e.g., convexity) may lead to potentially more efficient sampling. In our example, we have considered ξ obeying a Gaussian distribution truncated to some ellipsoid. With a concrete formula of the ellipsoid known and owing to the linearity of the state y in the random parameter, it is possible here to solve the almost sure problem as a robust optimization problem numerically precisely. The resulting solution is illustrated in the right part of Fig. 10.12 (red curve). Comparing this with the Moreau–Yosida model based on direct sampling of the distribution (yellow curve) corresponding to the largest value of γ (see lowest curve in the left part of the figure), we observe a considerable gap with the exact solution. At the same time, we know from the

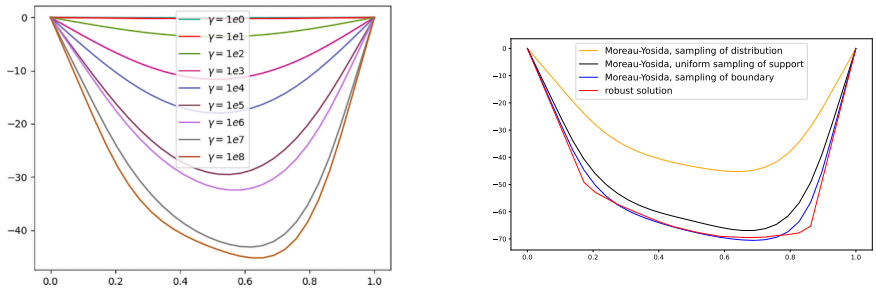


Fig. 10.12: Illustration of the Moreau–Yosida approximation for dealing with almost sure constraints (details see text).

mentioned theoretical results that with the penalty parameter and sampling size tending to infinity convergence must take place, while the computational effort and numerical stability might prevent us from reaching a reasonable vicinity of the solution. Still, hoping for some improvement in efficiency, we might be interested in implementing the Moreau–Yosida approach because it yields differentiable approximations of the non-differentiable robust problem [20, p. 24]. As a consequence of the fact that linear functions attain their maximum at boundary points of the support, it is evident that the original sampling of the distribution is rather inefficient in that it generates a lot of interior points without much information on the constraints. A more promising approach would rely on a uniform sampling of the support (thus avoiding concentration in its interior) or even better of its boundary. The progress in efficiency is illustrated in the right part of Fig. 10.12, where all three approaches of Moreau–Yosida approximation are based on a common penalty parameter and a common sample size.

10.3.4 Numerical Methods for Constraint Approximation

The main challenge in probabilistic or probust constraint approximation for PDE-based gas network modelling is that any evaluation of the function $g(x, \xi, u)$ for a specific $\xi \in \mathcal{U}$ in one of the problem formulations (10.4)–(10.6) requests a possibly expensive numerical solution calling for a stationary or even dynamic flow model with uncertain data on networks. As an illustrative example, let us consider the practically important task of transferring a stationary state $Y_A = (p_A, q_A)$ described by a certain pressure p_A and mass flow rate q_A into another stationary state $Y_B(\xi)$ which is considered to be uncertain due to in advance unknown mass flow rates $q_B(\xi)$ at the exits, i.e., the gas demand of the consumers. We denote this transfer process by $Y_A \rightarrow Y_B(\xi)$. Then we would like to solve the following probust optimal control problem:

$$u_c \in \mathcal{U}_{ad} = \operatorname{argmin} C(u_c)$$
$$\text{subject to } Y_A \rightarrow Y_B(\xi), \quad \xi \in \mathcal{U},$$
$$\mathbb{P}\left(p(x,t,\xi;u_c) \in \Pi \quad \forall (x,t) \in \Omega \times [0,T]\right) \geq \alpha.$$

Here, the objective function C models the cost of all compressors, which can operate in the range of the admissible set $\mathcal{U}_{ad}$ restricting the controls u_c. In addition, the pressure must lie inside certain intervals defined through the set Π. The robust condition $p(x,t,\xi;u_c) \in \Pi$ for all $(x,t) \in \Omega \times [0,T]$ can be reformulated as

$$\min_{x,t} p(x,t,\xi;u_c) \geq p^{\min} \quad \text{and} \quad \max_{x,t} p(x,t,\xi;u_c) \leq p^{\max}.$$

For given $u_c \in \mathcal{U}_{ad}$ and $\xi \in \mathcal{U}$, a numerical PDE solver uses discrete space-time points (x_i, t_j) with (i,j) varying in a finite index set $\mathbb{I}$ to compute approximations $Y_h(x_i,t_j,\xi;u_c)$ of the state vector $Y(x_i,t_j,\xi;u_c)$ with (possibly adaptive) resolution $h = (\triangle x, \triangle t)$ over the whole gas network. Hence, the corresponding discrete robust conditions are then defined by

$$\min_{(i,j)\in\mathbb{I}} p_h(x_i,t_j,\xi;u_c) \geq p^{\min} \quad \text{and} \quad \max_{(i,j)\in\mathbb{I}} p_h(x_i,t_j,\xi;u_c) \leq p^{\max},$$

where p_h is the approximation of the pressure p at the discrete space-time points. The inherent pressure loss in gas networks due to friction usually allows to monitor the pressure in a small number of discrete spatial points to guarantee the pressure bounds in the probust sense. However, large dimensions of the stochastic space $\mathcal{U}$ request hundreds or even thousands of PDE solutions for certain $\xi^{(k)} \in \mathcal{U}$ to approximate the probability density function of the minimum and maximum of the approximate pressures. In what follows, we will discuss such approximations in a more general context.

A key point to efficiently approximate the probability density function of a general quantity of interest $\psi(Y)$ depending on the network solution vector (for example, the minimum and maximum pressure above) is to use a *reduced order model* based on a few, but well selected samples to compute the overall gas network solution. Such a model can be efficiently derived by an adaptive stochastic collocation method based on a set of deterministic sample points $\{\xi^{(q)}\}_{q=1,\ldots,Q}$, chosen to compute independent, finite dimensional space-time approximations $\psi(Y_h(\xi^{(q)})) \approx \psi(Y(\xi^{(q)}))$. These approximations are used to construct a single-level interpolant

$$\Psi_{Q,h}(\xi) = \mathcal{I}_Q[\psi(Y_h)](\xi) = \sum_{q=1}^{Q} \psi_q \phi_q(\xi)$$

for the function $\psi(Y)$ in the polynomial space $\mathcal{P}_Q$ with global basis functions ϕ_q. The interpolation conditions $\mathcal{I}[\psi(Y_h)](\xi^{(q)}) = \psi(Y_h(\xi^{(q)}))$ for $q = 1,\ldots,Q$ determine the coefficients ψ_q. The quality of the interpolation process depends on the accuracy of the space-time approximations $Y_h(\xi^{(q)})$, the regularity of the solution with respect to the stochastic parameters ξ, and on the number of collocation points Q, which grows rapidly with increasing stochastic dimension N. The interpolant $\Psi_{Q,h}(\xi)$, also called *response surface approximation*, can be used to directly calculate moments such as

expectation and variance. Since its evaluation is extremely cheap, it also forms the basis for approximating its probability density function by a spherical-radial decomposition or kernel density estimator described in Sect. 10.3, and determining the practically relevant probability that $\Psi_{Q,h}(\xi)$ lies in a certain interval over the whole time horizon.

The whole approach can be extended to an error-controlled multilevel stochastic collocation method [44, 45]. Using a telescopic sum of single-level interpolants, we construct a K-level interpolant for the functional $\psi(Y)$ through

$$\Psi_K(\xi) = \sum_{k=0}^{K} \left(\Psi_{Q_{K-k},h_k}(\xi) - \Psi_{Q_{K-k},h_{k-1}}(\xi)\right),$$

where h_k refers to different resolutions in space and time, ranging from coarse ($k = 0$) to fine ($k = K$). We have applied this approach to check the validity that gas is delivered in a pressure range stipulated in a contract between gas company and consumer [44].

In some cases, piecewise smooth quantity of interests $\psi(\xi)$ with kinks have to be approximated. Then hp-adaptive sparse grid collocation algorithms that combine low-order basis functions with local support in parts of the domain with less regularity and variable-order basis functions elsewhere have shown to work very efficiently and robust [63]. Spatial refinement in the stochastic space is realized by means of hierarchical multivariate knot trees which allows the construction of localised hierarchical basis functions with varying order. Hierarchical surplus is used as an error indicator to automatically detect the non-smooth region and adaptively refine the collocation points there. The local polynomial degrees can be optionally selected by a greedy approach or a kink detection procedure. An example is given in Fig. 10.13.

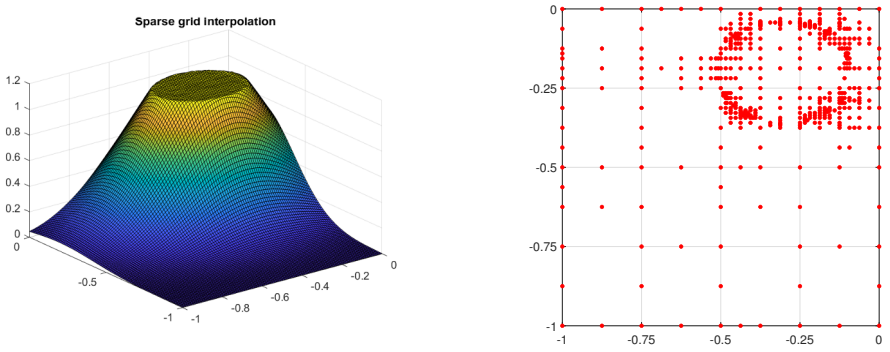


Fig. 10.13: Adaptive hp-sparse grid approximation (left) and corresponding collocation points (right) for $\psi(\xi) = \min(1, 1.3\exp(-6(\xi_1 + 0.3)^2 - 10(\xi_2 + 0.2)^2))$ with $\xi \in [-1, 0] \times [-1, 0]$.

10.4 Selected Theoretical Results

10.4.1 Existence of Chance Maximizing Controls and the Turnpike Phenomenon

For the chance maximizing controls, due to the H^2 control regularization term in the objective functional J that is defined in (10.16), similarly as in [29] using the direct method of the calculus of variations, we can prove the following theorem about the existence of an optimal control:

Theorem 10.1 *Assume that $J(u_{ref})$ is finite. Then there exists an optimal control that solves the problem*

$$\min_{u \in U} J(u).$$

In general, due to the nonlinearity of the system, a uniqueness result for the optimal controls does not hold.

It is important to note that the optimal control problem is posed in a framework that leads to semi-global classical solutions, in particular to solutions without shocks.

In the dynamic optimal control problem that is stated in the above theorem, and also in general, the time horizon T is an essential parameter. In the context of the gas pipeline flow, the state changes with the speed of sound, so that the time that the pressure waves need to travel through the system is often longer than T. In this situation of large time horizons, often the optimal controls show a turnpike structure, where in the interior of the time interval after a dynamic initial phase the optimal state is close to a steady state which is the solution of the corresponding static optimal control problem.

For the situation where the trajectories depend on random variables, under certain assumptions a turnpike property can be shown for the expected states. In [27], a proof is presented for dynamic optimal control problems where the objective functional contains a tracking term. In [27], the time-discrete case of the system is considered with a probust constraint of the form (10.7).

10.4.2 Well-Posedness, Existence of Solutions and Convexity in Probabilistically Constrained Optimal Control of Linear PDEs

For a bounded, sufficiently regular domain $\mathcal{D} \subseteq \mathbb{R}^d$, we consider an optimal control problem under uncertainty, i.e.,

$$\min_{u \in U_{\text{ad}}} \mathcal{J}(u) \quad \text{subject to} \quad \varphi(u) \geq \mathrm{p}, \tag{10.31}$$

where $U_{\text{ad}} \subseteq L^2(\mathcal{D})$ is a convex closed set of admissible controls and φ is a probability function defined by

$$\varphi(u) := \mathbb{P}\left(\omega \in \Omega : \underline{y}(x) \leq y^u(x, \omega) \leq \bar{y}(x) \quad \text{for a. a. } x \in \mathcal{D}\right).$$

Here, $y^u(x, \omega)$ refers to the random state depending on the control u as being the solution of an elliptic PDE

$$A(u)y(\omega) + B\xi(\omega) + Cu = f, \tag{10.32}$$

where the random variable ξ takes values in a Hilbert space $\mathscr{H}$ and, for $u \in U_{\text{ad}}$, $A(u) : Y \to H^{-1}(\mathcal{D})$ with Y a subspace of $H^1(\mathcal{D})$ is a linear invertible elliptic operator that is differentiable with respect to u. Moreover, $B : \mathscr{H} \mapsto H^{-1}(\mathcal{D})$ and $C : U_{\text{ad}} \to L^2(\mathcal{D})$ are bounded linear operators, and $f \in L^2(\mathcal{D})$. Finally, $\underline{y}, \bar{y} \in L^2(\mathcal{D})$ are given lower and upper bounds, respectively.

The probust character of the probabilistic constraint in (10.31) is reflected by the fact that the two-sided constraint has to hold almost everywhere. A first natural question that arises is whether the probability function φ is well-defined in the sense that the event, whose probability is taken, is measurable. A second question relates to the convexity of the set $U_{\text{pr}} := \{u \in L^2(\mathcal{D}) \mid \varphi(u) \geq \text{p}\}$. This, in combination with natural convexity assumptions on $\mathcal{J}$ and U_{ad} would turn (10.31) into a convex optimization problem. In order to address these questions, we assume that the random variable ξ is defined as a linear combination of finitely many functions $\xi_0, e_k \in L^2(\mathcal{D})$ $(k = 0, \ldots, K)$:

$$\xi(\omega) := \xi_0 + \sum_{k=1}^{K} \zeta_k(\omega) e_k, \tag{10.33}$$

where $\zeta = (\zeta_1, \ldots, \zeta_K)$ is a K-dimensional random vector on the probability space $(\Omega, \mathcal{A}, \mathbb{P})$. Then, we have the following:

Theorem 10.2 ([36], Theorem 2.1) *The probability function φ is well-defined and weakly sequentially upper semicontinuous. As a consequence, the feasible set U_{pr} is weakly sequentially closed for arbitrary* $\text{p} \in [0, 1]$. *If the random vector ζ has a log-concave density (e.g., Gaussian and many others, see [52, Sect. 4.4]), then U_{pr} is also convex for arbitrary* $\text{p} \in [0, 1]$.

On the basis of this theorem, one may easily formulate results on the existence of solutions along well-known lines:

Corollary 10.1 ([36], Theorem 2.2) *Assume that $\mathcal{J}$ is coercive, convex, and lower semicontinuous, and that $U_{\text{ad}} \cap U_{\text{pr}} \neq \emptyset$. Then,* (10.31) *admits a solution. The same holds if we replace the coercivity of $\mathcal{J}$ by the additional boundedness of U_{ad}. If, in either of the two settings, $\mathcal{J}$ is strictly convex and ζ has a log-concave density, then* (10.31) *has a unique solution.*

10.4.3 Optimality Conditions in PDE-Constrained Optimization Subject to Probabilistic State Constraints

In some models for the optimal control of gas transportation, it is natural to impose constraints on the state of the system; this provides, for instance, controls that do not result in unreasonably high pressures in the network. If the state is described by a PDE,

constraints must be applied uniformly along the pipeline. A natural extension of this model is to allow for uncertainty in the inputs or parameters of the PDE. The state constraint is still required to be satisfied uniformly on the physical domain, but possibly only with high probability.

A representative example studied in [19] is the following optimal control problem with random linear elliptic PDE and uniform probabilistic constraints:

$$\begin{aligned} &\min_{u\in L^2(D)} F(u) \\ \text{s.t.}\quad &-\Delta y(x,\omega) = u(x) + f(x,\xi(\omega)), \quad x\in D \quad \mathbb{P}\text{-a.s.}, \\ &\qquad y(x,\omega) = 0, \qquad\qquad\qquad x\in \partial D \quad \mathbb{P}\text{-a.s.}, \\ &\qquad \mathbb{P}(y(x,\omega)\le \alpha \quad \forall x\in D) \ge \mathrm{p}. \end{aligned} \tag{10.34}$$

Here, D is a bounded domain in $\mathbb{R}^d$ for $d = 1, 2, 3$ and p is assumed to be close to, or equal to, one (the latter being the robust or almost sure case). The control u is distributed on the domain and the state y is random on account of the random term f on the right-hand side. The random vector is supposed to follow an m- dimensional centered Gaussian distribution $\xi \sim \mathcal{N}(0,\Sigma)$. Mild conditions ensure that each realization of the state belongs to $C(\bar{D})$; in particular, it is continuous on D up until the boundary.

To solve (10.34), it is common to apply approximation or regularization instead of relying on optimality conditions. On the other hand, optimality conditions are fundamental to understanding the consistency of these schemes and the resulting theory can contribute optimality certificates or even more efficient methods. Additionally, in considering the problem as is, nonsmoothness inherent to the model can be taken into account.

If the noise on the right-hand side is introduced in a structured way with

$$f(x,z) := f_0(x) + \sum_{i=1}^{m} z_i \phi_i(x) \tag{10.35}$$

for some given $f_0, \phi_i \in L^2(D)$, then it is possible to exploit some hidden convexity for the case $p < 1$ to derive necessary and sufficient optimality conditions of the form

$$DF(u^*) \in \lambda^* \partial^C \varphi(u^*), \quad \lambda^* \ge 0, \quad \varphi(u^*) \ge \mathrm{p}, \quad \lambda^*(\varphi(u^*) - \mathrm{p}) = 0, \tag{10.36}$$

where φ is the probability function

$$\varphi(u) := \mathbb{P}(\omega \mid g(u,\xi(\omega)) \le 0)$$

defined on $L^2(D)$ with $g(u,z) := \sup_{x\in D} [S(u,z)](x) - \alpha$, and $S\colon L^2(D)\times\mathbb{R}^m \to C(\bar{D})$ is the parametrized control-to-state operator. Moreover, an explicit formula for the Clarke subdifferential of the probability function $\partial^C \varphi$ can be derived using the spheric-radial decomposition of a (Gaussian) random vector ξ.

The formula uses the following decomposition, which is available thanks to the linearity of the parametrized control-to-state operator:

$$S(u,z) = \bar{y}_{(u)} + \sum_{i=1}^{m} z_i y^{(i)} \quad (u \in L^2(D), z \in \mathbb{R}^m).$$

Here, the 'mean state' $\bar{y}_{(u)}$ and $y^{(i)}$ are solutions to

$$-\Delta y(x) = h(x) \quad x \in D; \quad y(x) = 0, \quad x \in \partial D \tag{10.37}$$

with $h = u + f_0$ and $h = \phi_i$, $(i = 1, \ldots, m)$, respectively. Given $h \in L^2(D)$, we denote $\mathbf{u}_x(h) := y^h(x)$, where y^h is the solution of (10.37). Now, under assumptions in [19,20] that are verifiable for (10.34), it is possible to show equality in (10.23) with the following explicit formula for the Clarke subdifferential:

$$\partial^C \varphi(\bar{u}) = - \int_{\{v \in \mathbb{S}^{m-1} | \rho(v) < \infty\}} \operatorname{clco} \left\{ \frac{f_\chi(\rho(v))}{\varkappa(v,x)} \cdot \mathbf{u}_x \mid x \in M^*(v) \right\} \mathrm{d}\mu_\zeta(v), \tag{10.38}$$

where 'clco' refers to the closed convex hull, μ_ζ is the uniform distribution on the unit sphere $\mathbb{S}^{m-1}$, f_χ is the density of the one-dimensional Chi-distribution μ_χ with m degrees of freedom, and

$$\begin{aligned}
\varkappa(v,x) &:= \sum_{i=1}^{m} (\Sigma^{1/2} v)_i y^{(i)}(x), \\
\rho(v) &:= \max\{r \geq 0 \mid \bar{y}_{(\bar{u})}(x) + r\varkappa(v,x) \leq \alpha \ \forall x \in \bar{D}\}, \\
M^*(v) &:= \{x \in \bar{D} \mid \varkappa(v,x) > 0, \ \bar{y}_{(\bar{u})}(x) + \rho(v)\varkappa(v,x) = \alpha\}.
\end{aligned}$$

Figure 10.14 illustrates the application of the optimality conditions (10.36). The first diagram on the left shows two solutions to a specific instance of problem (10.34) with similar optimal value and obtained with different algorithmic approaches. In order to identify the correct solution, we apply the optimality condition. According to (10.36), at an optimal solution the derivative of the objective should be equal to an appropriate multiple (the Lagrange multiplier) of a Clarke subgradient of the probability function. In this example, it turns out that the probability function is continuously differentiable at the respective solutions, hence Clarke's subdifferential reduces to the classical derivatives. The middle and right diagrams of the figure plot the respective derivatives DF of the objective and successive multiples of the derivatives $D\varphi$ of the probability functions at the two solutions. As can be seen, only solution 1 satisfies the optimality conditions. The existence of the Lagrange multplier λ^* in (10.36) relies on the availability of a strictly feasible point $\widehat{u}$, i.e., one in which $\varphi(\widehat{u}) > \mathrm{p}$. This leaves the case of almost sure and robust constraints unclarified. It is not possible to consider optimality conditions in the limit when driving p towards one as demonstrated by [19, Example 3.1]. To arrive at optimality conditions for the almost sure case, one must rely on functional-analytic approaches originally developed for two-stage stochastic programming. The resulting theory allows for more generality in the way randomness is introduced than (10.35); the resulting optimality conditions are however less useful in the sense that they contain singular Lagrange multipliers, which may not be tractable in practical computation.

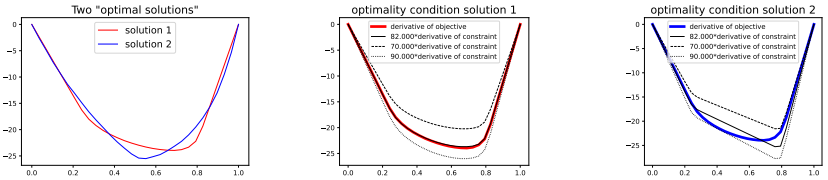


Fig. 10.14: Illustration of the optimality conditions (10.36).

As already mentioned in the introduction, in some cases, the almost sure constraint is equivalent to a robust constraint of the type "$g(u, z) \leq 0$" for all z belonging to the support of the random vector. Then, it is possible to make a connection to semi-infinite programming and obtain optimality conditions of the form

$$-DF(u^*) \in \lambda^* \partial \widehat{g}(u^*), \quad \lambda^* \geq 0, \quad \widehat{g}(u^*) \leq 0, \quad \lambda^* \widehat{g}(u^*) = 0.$$

Here, $\widehat{g}(u) := \max_{(x,z)\in D\times\Xi}[\widehat{\mathcal{S}}(u)](x, z) - \alpha$ with $\widehat{\mathcal{S}}$ being the control-to-state mapping from $L^2(D)$ to $C(\bar{D} \times \Xi)$. The (convex) subdifferential of g has the form

$$\partial g(u^*) = \left\{ \int_{\bar{D}\times\Xi} \partial g_{x,z}(u^*) \mathrm{d}\mu(x, z) \,\middle|\, \mu \text{ is a probability measure supported on } M(u^*) \right\},$$

and

$$M(u) := \left\{ (x, z) \in \bar{D} \times \Xi \mid [\widehat{\mathcal{S}}(u)](x, z) = \max_{(x',z')\in\bar{D}\times\Xi} [\widehat{\mathcal{S}}(u)](x', z') \right\}.$$

As is the case in the setting of probabilistic constraints, this formula can be made explicit for the problem (10.34), which makes it amenable to numerical simulation.

10.5 Conclusions

We have discussed how probust constraints can be used in optimization problems that model rational decision under uncertainty. The probust constraints contain a parameter

$$\mathrm{p} \in (0,\ 1)$$

which is a prescribed probability level for the satisfaction of an inequality constraint that is subject to uncertainty. Similarly as in semi-infinite optimization, where the inequality constraints depend on a parameter in a compact set, in our setting we consider a family of constraints that depend on a random variable. Since also the probability distribution may be uncertain, the distributional robustness of such constraints is discussed as well.

Applications to the optimal operation of gas networks are presented. The problem of nomination validation under uncertainty, where the aim is to find feasible transport

plans to satisfy the customer demands is discussed. Next, static capacity maximization is considered. For the dynamic case, chance maximizing controls are studied.

Finally, we have presented numerical algorithms, where the gradients of the probability with respect to the decision variables play an important role. The use of kernel density estimation in connection with the stochastic gradient method is described. The application of bundle methods for the numerical solution of distributionally robust chance constraints is discussed. Then numerical methods for solving optimization problems with robust or almost-sure constraints are considered and numerical examples are presented.

Also related theoretical results about the well-posedness, existence of solutions and convexity in probabilistically constrained optimal control of linear PDEs, the necessary optimality conditions and the turnpike property are discussed.

Our overview illustrates that for optimization under uncertainty with constraints that are of probust type, a number of numerical methods is available that allows to solve this class of problems which is useful for many applications. We have also presented theoretical results that indicate the mathematical challenges in this interesting area that spans from mixed-integer problems to PDE-constrained optimal control.

Acknowledgements This work was supported by the German Research Foundation (DFG) within Subprojects B01, B02, B04, B06, B10, C03 in the Sonderforschungsbereich/Transregio 154 "Mathematical Modelling, Simulation and Optimization using the Example of Gas Networks" (Project ID 239904186).

References

1. D. Adelhütte, D. Aßmann, T. Grandón Gonzáles, M. Gugat, H. Heitsch, R. Henrion, F. Liers, S. Nitsche, R. Schultz, M. Stingl, and D. Wintergerst. Joint model of probabilistic-robust (probust) constraints applied to gas network optimization. *Vietnam J. Math.*, 49:1097–1130, 2020. doi:10.1007/s10013-020-00434-y.
2. M. K. Banda, M. Herty, and A. Klar. Coupling conditions for gas networks governed by the isothermal Euler equations. *Netw. Heterog. Media*, 1(2):295–314, 2006. doi:10.3934/nhm.2006.1.295.
3. C. Bandi and D. Bertsimas. Tractable stochastic analysis in high dimensions via robust optimization. *Math. Program.*, 134:23–70, 2012. doi:10.1007/s10107-012-0567-2.
4. D. Bernhard, F. Liers, and M. Stingl. Robust chance-constrained optimization with discrete distributions. *Journal of Global Optimization*, 2026. doi:10.1007/s10898-026-01608-7.
5. D. Bernhard, F. Liers, M. Stingl, and A. Uihlein. A gradient-based method for joint chance-constrained optimization with continuous distributions. *Optimization Methods and Software*, 41(1):38–81, 2026. doi:10.1080/10556788.2025.2581585.
6. D. Bernhard, M. Stingl, and F. Liers. Algorithms for robust chance-constrained optimization with mixture ambiguity. *Optimization and Engineering*, 2026. doi:10.1007/s11081-026-10093-6.
7. H. Berthold, H. Heitsch, R. Henrion, and J. Schwientek. On the algorithmic solution of optimization problems subject to probabilistic/robust (probust) constraints. *Math. Methods Oper. Res.*, 96:1–37, 2021. doi:10.1007/s00186-021-00764-8.
8. J.-B. Caillau, M. Cerf, A. Sassi, E. Trélat, and H. Zidani. Solving chance constrained optimal control problems in aerospace via kernel density estimation. *Optim. Control Appl. Methods*, 39(5):1833–1858, 2018. doi:10.1002/oca.2445.

9. G. Calafiore and M. Campi. The scenario approach to robust control design. *IEEE Trans. Automat. Control*, 51:742–753, 2006. doi:10.1109/TAC.2006.875041.
10. F. Clarke. *Optimization and Nonsmooth Analysis*. Wiley New York, 1983. doi:10.1137/1.9781611971309.
11. A. Delfino and W. de Oliveira. Outer-approximation algorithms for nonsmooth convex MINLP problems. *Optimization*, 67(6):797–819, 2018. doi:10.1080/02331934.2018.1434173.
12. D. Dentcheva and A. Ruszczyński. Robust stochastic dominance and its application to risk-averse optimization. *Math. Program.*, 123:85–100, 2009. doi:10.1007/s10107-009-0321-6.
13. L. Devroye and L. Györfi. *Nonparametric Density Estimation: the L_1 View*. Wiley Series in Probability and Mathematical Statistics. Wiley, 1985.
14. M. Diehl, H. G. Bock, and E. Kostina. An approximation technique for robust nonlinear optimization. *Math. Program.*, 107(1):213–230, 2006. doi:10.1007/s10107-005-0685-1.
15. M. A. Duran and I. E. Grossmann. An outer-approximation algorithm for a class of mixed-integer nonlinear programs. *Math. Program.*, 36(3):307–339, 1986. doi:10.1007/BF02592064.
16. P. Elango, A. P. Vinod, K. Kitamura, B. Açikmeşe, S. Di Cairano, and A. Weiss. Successive convexification for passively-safe spacecraft rendezvous on near rectilinear halo orbit, 2025. arXiv:2505.17251.
17. K.-T. Fang, S. Kotz, and K. W. Ng. *Symmetric Multivariate and Related Distributions*. Chapman and Hall/CRC, London, 1990. doi:10.1201/9781351077040.
18. R. Fletcher and S. Leyffer. Solving mixed integer nonlinear programs by outer approximation. *Math. Program.*, 66(3, Ser. A):327–349, 1994. doi:10.1007/BF01581153.
19. C. Geiersbach and R. Henrion. Optimality conditions in control problems with random state constraints in probabilistic or almost sure form. *Math. Oper. Res.*, 2024. doi:10.1287/moor.2023.0177.
20. C. Geiersbach, R. Henrion, and P. Pérez-Aros. Numerical solution of an optimal control problem with probabilistic and almost sure state constraints. *J. Optim. Theory Appl.*, 204(7), 2025. doi:10.1007/s10957-024-02578-0.
21. B. Geißler, A. Martin, A. Morsi, and L. Schewe. Using piecewise linear functions for solving MINLPs. In *Mixed Integer Nonlinear Programming*, volume 154 of *The IMA Volumes in Mathematics and its Applications*, pages 287–314. Springer, New York, 2012. doi:10.1007/978-1-4614-1927-3_10.
22. A. Geletu, A. Hoffmann, M. Klöppel, and P. Li. An inner-outer approximation approach to chance constrained optimization. *SIAM J. Optim.*, 27(3):1834–1857, 2017. doi:10.1137/15M1049750.
23. T. González Grandón, H. Heitsch, and R. Henrion. A joint model of probabilistic/robust constraints for gas transport management in stationary networks. *Comput. Manag. Sci.*, 14:443–460, 2017. doi:10.1007/s10287-017-0284-7.
24. C. Gotzes, H. Heitsch, R. Henrion, and R. Schultz. On the quantification of nomination feasibility in stationary gas networks with random load. *Math. Methods Oper. Res.*, 84:427–457, 2016. doi:0.1007/s00186-016-0564-y.
25. A. Gramacki. *Nonparametric kernel density estimation and its computational aspects*, volume 37 of *Studies in Big Data*. Springer, Cham, 2018. doi:10.1007/978-3-319-71688-6.
26. M. Grieshammer, L. Pflug, M. Stingl, and A. Uihlein. The continuous stochastic gradient method: part I–convergence theory. *Comput. Optim. Appl.*, 87(3):935–976, 2023. doi:10.1007/s10589-023-00542-8.
27. M. Gugat, R. Henrion, and H. Heitsch. A turnpike property for optimal control problems with dynamic probabilistic constraints. *J. Convex Anal.*, 30(3):1025–1052, 2021. URL: https://www.heldermann.de/JCA/JCA30/JCA303/jca30047.htm.
28. M. Gugat and M. Herty. Modeling, control, and numerics of gas networks. In *Handbook of Numerical Analysis*, volume 23, pages 59–86. Elsevier, 2022. doi:10.1016/bs.hna.2021.12.002.
29. M. Gugat and M. Schuster. Max-p optimal boundary control of gas flow. In M. H. Baumann, L. Grüne, B. Jacob, and K. Worthmann, ed., *Extended Abstracts presented at the 25th Int. Symposium on Math. Theory of Networks and Systems MTNS 2022*, 2022. doi:10.15495/EPub_UBT_00006809.
30. M. Gugat, M. Schuster, and S. Steffensen. A dynamic multilevel model of the European gas market. *Commun. Optim. Theory*, 11:1–26, 2023. doi:10.23952/cot.2023.11.

31. A. Hantoute, R. Henrion, and P. Pérez-Aros. Subdifferential characterization of probability functions under Gaussian distribution. *Math. Program.*, 174:167–194, 2019. doi:10.1007/s10107-018-1237-9.
32. W. Härdle, A. Werwatz, M. Müller, and S. Sperlich. *Nonparametric and Semiparametric Models*. Series in Statistics. Springer, 2004. doi:10.1007/978-3-642-17146-8.
33. W. Hare, C. Sagastizábal, and M. Solodov. A proximal bundle method for nonsmooth nonconvex functions with inexact information. *Comput. Optim. Appl.*, 63(1):1–28, 2016. doi:10.1007/s10589-015-9762-4.
34. H. Heitsch. On probabilistic capacity maximization in a stationary gas network. *Optimization*, 69:575–604, 2020. doi:10.1080/02331934.2019.1625353.
35. H. Heitsch, R. Henrion, and C. Tischendorf. Probabilistic maximization of time-dependent capacities in a gas network. *Optim. Eng.*, 26(1):365–400, 2025. doi:10.1007/s11081-024-09908-1.
36. R. Henrion, G. Stadler, and F. Wechsung. Optimal control under uncertainty with joint chance state constraints: almost-everywhere bounds, variance reduction, and application to (bi-)linear elliptic PDEs. *to appear in: SIAM/ASA J. Uncertain. Quantif.*, 2024. Preprint available at https://arxiv.org/abs/2412.05125.
37. J.-P. Kahane. *Some Random Series of Functions*, volume 5. Cambridge University Press, 1985.
38. T. Koch, B. Hiller, M. E. Pfetsch, and L. Schewe, ed. *Evaluating Gas Network Capacities*. MOS-SIAM Series on Optimization. Society for Industrial and Applied Mathematics, 2015. doi:10.1137/1.9781611973693.
39. D. P. Kouri, M. Staudigl, and T. M. Surowiec. A relaxation-based probabilistic approach for PDE-constrained optimization under uncertainty with pointwise state constraints. *Comput. Optim. Appl.*, 85:441–478, 2023. doi:10.1007/s10589-023-00461-8.
40. M. Kuchlbauer, F. Liers, and M. Stingl. Adaptive bundle methods for nonlinear robust optimization. *Informs J. Comput.*, 34(4), 2022. doi:10.1287/ijoc.2021.1122.
41. M. Kuchlbauer, F. Liers, and M. Stingl. Outer approximation for mixed-integer nonlinear robust optimization. *J. Optim. Theory Appl.*, 195:1056–1086, 2022. doi:10.1007/s10957-022-02114-y.
42. M. Labbé, F. Plein, and M. Schmidt. Bookings in the european gas market: characterisation of feasibility and computational complexity results. *Optimization and Engineering*, 21(1):305–334, 2019. doi:10.1007/s11081-019-09447-0.
43. M. Labbé, F. Plein, M. Schmidt, and J. Thürauf. Deciding feasibility of a booking in the european gas market on a cycle is in p for the case of passive networks. *Networks*, 78(2):128–152, 2021. doi:10.1002/net.22003.
44. J. Lang, P. Domschke, and E. Strauch. Adaptive single- and multilevel stochastic collocation methods for uncertain gas transport in large-scale networks. In *Mesh Generation and Adaptation–Cutting-Edge Techniques*, volume 30 of *SEMA SIMAI Springer Series*, pages 113–135. Springer, Cham, 2022. doi:10.1007/978-3-030-92540-6_6.
45. J. Lang, R. Scheichl, and D. Silvester. A fully adaptive multilevel stochastic collocation strategy for solving elliptic PDEs with random data. *J. Comput. Phys.*, 419:109692, 2020. doi:10.1016/j.jcp.2020.109692.
46. M. B. Marcus and G. Pisier. *Random Fourier Series with Applications to Harmonic Analysis.(AM-101)*. Annals of Mathematics Studies. Princeton University Press, 1981. doi:10.1515/9781400881536.
47. A. Nemirovski and A. Shapiro. Convex approximations of chance constrained programs. *SIAM J. Optim.*, 17(4):969–996, 2006. doi:10.1137/050622328.
48. D. Noll. Cutting plane oracles to minimize non-smooth non-convex functions. *Set-Valued Var. Anal.*, 18:531–568, 2010. doi:10.1007/s11228-010-0159-3.
49. D. Noll. Bundle method for non-convex minimization with inexact subgradients and function values. In *Computational and Analytical Mathematics*, volume 50 of *Springer Proceedings in Mathemathcs & Statistics*, pages 555–592. Springer, New York, 2013. doi:10.1007/978-1-4614-7621-4_26.
50. B. K. Pagnoncelli, S. Ahmed, and A. Shapiro. Sample average approximation method for chance constrained programming: Theory and applications. *J. Optim. Theory Appl.*, 142:399–416, 2009. doi:10.1007/s10957-009-9523-6.

51. A. Peña Ordieres, J. R. Luedtke, and A. Wächter. Solving chance-constrained problems via a smooth sample-based nonlinear approximation. *SIAM J. Optim.*, 30(3):2221–2250, 2020. doi:10.1137/19M1261985.
52. A. Prékopa. *Stochastic Programming*. Mathematics and Its Applications. Dordrecht: Kluwer Academic Publishers, 1995. doi:10.1007/978-94-017-3087-7.
53. A. Ruszczyński. Probabilistic programming with discrete distributions and precedence constrained knapsack polyhedra. *Math. Program.*, 93:195–215, 2002. doi:10.1007/s10107-002-0337-7.
54. M. Schuster. *Nodal Control and Probabilistic Constrained Optimization using the Example of Gas Networks*. Dissertation, FAU Erlangen-Nürnberg, Germany, 2021. URL: https://opus4.kobv.de/opus4-trr154/frontdoor/index/index/docId/410.
55. M. Schuster. On the convergence of optimization problems with kernel density estimated probabilistic constraints. *Appl. Set-Valued Anal. Optim.*, 7:209–221, 2025. doi:10.23952/asvao.7.2025.2.05.
56. M. Schuster, E. Strauch, M. Gugat, and J. Lang. Probabilistic constrained optimization on flow networks. *Optim. Eng.*, 23:1–50, 2022. doi:10.1007/s11081-021-09619-x.
57. J. Thürauf. Deciding the feasibility of a booking in the european gas market is conp-hard. *Annals of Operations Research*, 318(1):591–618, 2022. doi:10.1007/s10479-022-04732-1.
58. W. van Ackooij, A. Frangioni, and W. de Oliveira. Inexact stabilized Benders' decomposition approaches with application to chance-constrained problems with finite support. *Comput. Optim. Appl.*, 65(3):637–669, 2016. doi:10.1007/s10589-016-9851-z.
59. W. van Ackooij and R. Henrion. Gradient formulae for nonlinear probabilistic constraints with Gaussian and Gaussian-like distributions. *SIAM J. Optim.*, 24(4):1864–1889, 2014. doi:10.1007/s10107-018-1237-9.
60. W. van Ackooij and R. Henrion. (Sub-)gradient formulae for probability functions of random inequality systems under Gaussian distribution. *SIAM/ASA J. Uncertain. Quantif.*, 5(1):63–87, 2017. doi:10.1137/16M1061308.
61. W. van Ackooij, R. Henrion, and H. Zidani. Pontryagin's principle for some probabilistic control problems. *Appl. Math. Optim.*, 90,5, 2024. doi:10.1007/s00245-024-10151-4.
62. Z. Wei, M. Montaz Ali, L. Xu, B. Zeng, and J.-C. Yao. On solving nonsmooth mixed-integer nonlinear programming problems by outer approximation and generalized Benders decomposition. *J. Optim. Theory Appl.*, 181(3):840–863, 2019. doi:10.1007/s10957-019-01499-7.
63. H. Wilka and J. Lang. Adaptive hp-polynomial based sparse grid collocation algorithms for piecewise smooth functions with kinks. *J. Comput. Phys.*, 537:114065, 2025. doi:10.1016/j.jcp.2025.114065.
64. S. Zymler, D. Kuhn, and B. Rustem. Distributionally robust joint chance constraints with second-order moment information. *Math. Program.*, 137:167–198, 2011. doi:10.1007/s10107-011-0494-7.

Open Access This chapter is licensed under the terms of the Creative Commons Attribution-NonCommercial-NoDerivatives 4.0 International License (http://creativecommons.org/licenses/by-nc-nd/4.0/), which permits any noncommercial use, sharing, distribution and reproduction in any medium or format, as long as you give appropriate credit to the original author(s) and the source, provide a link to the Creative Commons license and indicate if you modified the licensed material. You do not have permission under this license to share adapted material derived from this chapter or parts of it.

The images or other third party material in this chapter are included in the chapter's Creative Commons license, unless indicated otherwise in a credit line to the material. If material is not included in the chapter's Creative Commons license and your intended use is not permitted by statutory regulation or exceeds the permitted use, you will need to obtain permission directly from the copyright holder.



Chapter 11
Continuous Stochastic Gradient and Spherical Radial Decomposition

Daniela Bernhard[0009−0001−7839−202X],
Holger Heitsch[0000−0002−2692−4602],
René Henrion[0000−0001−5572−7213],
Frauke Liers[0000−0002−1671−0344],
Michael Stingl[0000−0002−3626−0723],
Andrian Uihlein[0000−0002−0650−3747], and
Viktor Zipf

Abstract In this chapter, a new method is presented for solving chance-constrained optimization problems. The method combines the well-established Spherical-Radial Decomposition approach with the Continuous Stochastic Gradient method. While the Continuous Stochastic Gradient method has been successfully applied to chance-constrained problems in the past, only the combination with the Spherical-Radial Decomposition allows to avoid smoothing of the integrand. In this chapter, we prove this fact for a relevant class of chance-constrained problems and apply the resulting method to the capacity maximization problem for gas networks.

Daniela Bernhard
Department of Data Science & Department of Mathematics, Germany,
Friedrich-Alexander-Universität Erlangen-Nürnberg, e-mail: daniela.db.bernhard@fau.de

Holger Heitsch
Weierstrass Institute for Applied Analysis and Stochastics, Berlin, Germany,
e-mail: holger.heitsch@wias-berlin.de

René Henrion
Weierstrass Institute for Applied Analysis and Stochastics, Berlin, Germany,
e-mail: rene.henrion@wias-berlin.de

Frauke Liers
Department of Data Science & Department of Mathematics,
Friedrich-Alexander-Universität Erlangen-Nürnberg, Germany, e-mail: frauke.liers@fau.de

Michael Stingl
Department of Mathematics, Friedrich-Alexander-Universität Erlangen-Nürnberg, Germany,
e-mail: michael.stingl@fau.de

Andrian Uihlein
Department of Mathematics, Friedrich-Alexander-Universität Erlangen-Nürnberg, Germany,
e-mail: andrian.uihlein@fau.de

Viktor Zipf
Department of Mathematics, Friedrich-Alexander-Universität Erlangen-Nürnberg, Germany,
e-mail: viktor.v.zipf@fau.de

© The Author(s) 2027

A. Martin et al. (eds.), *Mathematical Modelling, Simulation and Optimization using the Example of Gas Networks*, International Series of Numerical Mathematics 174,
https://doi.org/10.1007/978-3-032-34969-9_11

11.1 Introduction

We consider optimization problems with a *probabilistic constraint* or *chance constraint* of the following form:

$$\begin{aligned} \min_{x} \quad & g_0(x), \\ \text{s.t.} \quad & \varphi(x) := \mathbb{P}_\zeta(g(x,\zeta) \leq 0) \geq p. \end{aligned} \tag{P}$$

Here, the decision x belongs to some finite- or infinite-dimensional space, g_0 is an objective function to be minimized, g is a random constraint function, ζ is a random vector defined on some probability space $(\Omega, \mathcal{A}, \mathbb{P})$ and $p \in (0, 1]$ is a probability level. The interpretation of the chance constraint is as follows: the decision x is defined to be feasible, whenever the random inequality $g(x, \zeta) \leq 0$ is satisfied with probability at least p. Formally, a chance constraint is a deterministic inequality constraint of the form $\varphi(x) \geq p$, where φ denotes the probability function assigning to each x the probability of satisfying the random inequality. The challenge posed by chance constraints relies on the fact that usually no explicit formula for φ is given. This is even more prevalent for gradients $\nabla\varphi$, if they exist at all. For a comprehensive classical introduction to chance constraints, we refer to the monograph [20] and to the more recent presentation in [26]. Algorithms and applications in the context of gas networks involving chance constraints can be found in Chap. 10, "From Probabilistic to Probust Constraints: Optimization under Uncertainty" of this book.

The concept of chance constraints to model stochastic uncertainties in the data was first introduced by [8]. As already mentioned, φ is often not given explicitly in the case of continuous distributions. Therefore, much research focuses on approximating the chance constraint with easier functions. One possibility is to replace the continuous distribution by a finite sample. Here, scenario approximations (e.g., [7, 16]) or sample approximation techniques (e.g., [1,15,18]) are often the methods of choice. The approximations result in classical mixed-integer nonlinear programming problems (MINLPs) that can be solved by available approaches from this field. Nevertheless, good discrete approximations of the original distribution often need too many samples to solve the resulting MINLPs efficiently in practice. So, there also exist various different approximations of the function φ dealing directly with the continuous distributions. Common methods are for example the Bernstein approximation [17], conditional Value-at-Risk approximations [23] or robust approximations (e.g., [2, 3, 28]).

Concentrating on special kinds of distributions, there also exist results to directly deal with the chance-constrained function φ. For example, in the case of elliptically symmetric (e.g., Gaussian) random vectors (see Sect. 11.2.1 and Sect. 10.3.1.1 in Chap. 10, "From Probabilistic to Probust Constraints: Optimization under Uncertainty"), a successful workhorse for the numerical solution of optimization problems (P) is the so-called *Spherical-Radial Decomposition* (SRD), which provides strong regularity guarantees for φ.

Nevertheless, evaluating the probability function with respect to a multivariate Gaussian distribution is still necessary. So far, quasi Monte-Carlo methods are often used

for this task. In this work, we propose a different approach, combining the *Continuous Stochastic Gradient* (CSG) method [19] with SRD.

To avoid a numerically expensive (quasi) Monte-Carlo integration for the probability function in each iteration, CSG follows ideas from traditional stochastic sample-based optimization like the *Stochastic Gradient* (SG) method [22] or similar related approaches [6]. Thus, in each iteration, rather than being fully evaluated, the probability function is sampled for a small number of realizations of the random variable (mini-batch). In contrast to most other stochastic sample-based optimization schemes, these gradient samples are not discarded after the iteration but instead stored to accumulate information during the optimization process. By adaptively recombining old and new gradient information, CSG constructs a gradient approximation with vanishing approximation error [11, 19], resulting in an overall reduction in the required number of gradient evaluations.

To apply the CSG method to the chance-constrained problem, we penalize constraint violations in the objective function. We note that the article [4] already uses the CSG method to solve chance-constrained problems. However, convergence results for CSG are restricted to probability functions with strong regularity assumptions [11]. To be precise, in [11], φ is assumed to be of the form

$$\varphi(x) = \mathbb{E}_\zeta [\phi(x, \zeta)],$$

with globally Lipschitz $\nabla_x \phi$. Thus, an additional smoothing approximation to obtain the necessary regularity of the underlying functions is carried out in [4]. By combining SRD and CSG, we circumvent this smoothing operation in a nontrivial fashion. Nonetheless, the SRD reformulation of (P) is still not sufficiently regular to apply known convergence results of CSG. Therefore, we present an extension of CSG convergence theory that covers our numerical examples and more general classes of objectives.

The efficiency of the proposed method is numerically demonstrated for small analytical problems as well as for the capacity maximization problem in gas networks.

11.2 Basic Components

11.2.1 Spherical-Radial Decomposition

The concept of *Spherical-Radial Decomposition* (SRD) relates to random vectors having an elliptically-symmetric distribution (e.g., Gaussian, Student, Laplace, etc.). Such distributions can be decomposed into a uniform distribution over the unit sphere and some one-dimensional radial distribution (e.g., Chi-distribution for the Gaussian case). For a basic monograph on this topic, we refer to [9]. Exploiting this property for elliptically-symmetric distributions leads to several benefits like variance reduction in the estimation of probabilities or representation formulae for gradients or subdifferentials of probability functions. SRD has been successfully applied to the numerical solution of many problems of operations research and optimal control involving prob-

abilistic or chance constraints (e.g., [10, 12, 13]). For an introduction to SRD, we refer to Sect. 10.3.1.1 of Chap. 10, "From Probabilistic to Probust Constraints: Optimization under Uncertainty".

11.2.2 Continuous Stochastic Gradient Method

The *Continuous Stochastic Gradient* (CSG) method [19] is an optimization scheme designed for problems containing expected values. Consider a set of admissible designs $x \in \mathcal{X} \subseteq \mathbb{R}^{d_x}$, a set of uncertain parameters $\zeta \in \mathcal{Z}^{\mathrm{ad}} \subseteq \mathbb{R}^{d_\zeta}$ as well as a Borel probability measure μ on $\mathcal{Z}^{\mathrm{ad}}$ with $\zeta \sim \mu$. Then, we consider CSG's application to the problem

$$\begin{aligned} \min_{x \in \mathcal{X}} \quad & g_0(x), \\ \text{s.t.} \quad & \varphi(x) := \mathbb{E}_\zeta\left[\phi(x,\zeta)\right] = \int_{\mathcal{Z}^{\mathrm{ad}}} \phi(x,\zeta)\mu(\mathrm{d}\zeta) \geq p. \end{aligned} \tag{11.1}$$

Note that this includes problem (P) from the introduction, by reformulating the probability $\mathbb{P}$ as the expected value of an appropriate indicator function. In such cases, gradient-based methods require the calculation of

$$\nabla\varphi(x) = \mathbb{E}_\zeta\left[\nabla_x \phi(x,\zeta)\right]$$

in each iteration, which may be numerically intractable. Thus, following the concepts of the *Stochastic Gradient* (SG) method in [22], the current true gradient $\nabla\varphi(x_n)$ is replaced by a stochastic direction $\widehat{G}_n$, which is obtained by sampling $\nabla_x\phi(x_n,\cdot)$ at a small number N_B (batch size) of independent and identically distributed random samples $\{\zeta_n^{(i)}\}_{i=1,\ldots,N_B}$. In SG, this direction is constructed by simply setting

$$\widehat{G}_n^{\mathrm{SG}} := \frac{1}{N_B}\sum_{i=1}^{N_B} \nabla_x \phi\left(x_n, \zeta_n^{(i)}\right),$$

which yields an *unbiased* gradient estimator, i.e.,

$$\mathbb{E}_{\{\zeta_n^{(i)}\}}[\widehat{G}_n^{\mathrm{SG}}] = \nabla\varphi(x_n).$$

Unfortunately, this approach has two major drawbacks we want to avoid in this contribution:

(i) If evaluating $\nabla_x\phi(x,\cdot)$ is time consuming, e.g., because it requires the simulation of a highly complex system, discarding gradient samples from previous iterations is wasting precious information.
(ii) The constraint appearing in (11.1) will later on be handled by a penalty approach. However, the resulting penalty term

$$P_\lambda(x) = \frac{\lambda}{2}\max\{0, p - \varphi(x)\}^2 \tag{11.2}$$

depends on φ in a nonlinear fashion. Thus, by the chain rule, we cannot construct an unbiased estimator to $\nabla P_\lambda(x_n)$, as this would require knowledge of $\varphi(x_n)$. Therefore, the resulting optimization problem is out of scope for SG.

To deal with both of these drawbacks simultaneously, CSG stores old gradient information. Then, in each iteration, old and new gradient samples are used to build a *biased* gradient approximation

$$\widehat{G}_n^{\mathrm{CSG}} := \sum_{i,k} \alpha_{k,i} \nabla_x \phi\left(x_k, \zeta_k^{(i)}\right), \quad i = 1, \dots, N_B,\ k = 1, \dots, n.$$

The parameters $\alpha_{k,i} \geq 0$ are called *integration weights* and correspond to an efficient on-the-fly integration of the nearest neighbor surrogate model

$$\nabla_x \phi(x, \zeta) \approx \nabla_x \phi(x_k, \zeta_k^{(i)}), \quad (k, i) \in \operatorname*{arg\,min}_{(u,v)} \|(x, \zeta) - (x_u, \zeta_u^{(v)})\|.$$

Several numerical schemes for the calculation of integration weights have been proposed in [11]. Therein, a key result for CSG convergence theory, the *approximation property* ([11, Lemma 4.6]), was shown as well. It states that, assuming some regularity of ϕ and $\nabla_x \phi$, we have

$$\|\widehat{G}_n^{\mathrm{CSG}} - \nabla\varphi(x_n)\| + |\widehat{J}_n^{\mathrm{CSG}} - \varphi(x_n)| \xrightarrow{a.s.} 0 \quad (n \to \infty),$$

where $\widehat{J}_n^{\mathrm{CSG}}$ corresponds to the stochastic CSG approximation of $\varphi(x_n)$, i.e.,

$$\widehat{J}_n^{\mathrm{CSG}} = \sum_{i,k} \alpha_{k,i}\, \phi\left(x_k, \zeta_k^{(i)}\right).$$

This result now implies the following properties of CSG:

(i) As the gradient (and function value) approximation error vanishes over the course of iterations, the method asymptotically behaves like an exact full gradient scheme.
(ii) Using the function value approximations $\widehat{J}_n^{\mathrm{CSG}}$, the CSG method is capable of handling the penalty term P_λ, see (11.2), allowing us to solve the chance-constrained optimization problem (P).

Nonetheless, there are some drawbacks we need to address before combining CSG with SRD. First off, the integration weight calculation requires additional effort, but can be seen as fixed costs for the optimization, added on top of the gradient and function evaluations. Especially in settings where evaluating $\nabla_x \phi(x, \cdot)$ is numerically expensive, the amount of time spent calculating integration weights is negligible in contrast to the time gained by performing fewer evaluations overall. However, if evaluations come basically for free, it is likely that CSG will be outperformed by other approaches.

Moreover, one of the prerequisites for the approximation property is global Lipschitz continuity of ϕ and $\nabla_x \phi$ in all arguments. As we will see, this assumption is violated when reformulating φ via SRD. Thus, we will extend the approximation property to cases with less regularity in Sect. 11.4.

11.2.3 Combination of CSG and SRD

Since a general chance constraint is typically not continuous, the authors in [4] smoothen the indicator function with a continuously differentiable one, which is a common technique in chance-constrained optimization (see, e.g., [14, 21, 24, 25]). Reformulating the chance constraint via SRD, this challenge no longer occurs, as the probability function is continuous in this case. Therefore, we get rid of the necessity to smooth the expressions. Similarly to [4], we penalize a violation of the chance constraint in the objective function, since the CSG method is only able to handle constraints directly by projecting onto the feasible set, which is typically impossible for the chance constraint. We apply a quadratic penalty term to keep the differentiability properties of the probability function φ. Concretely, the approximation to the chance-constrained problem reads for a fixed penalty parameter $\lambda > 0$

$$\min_x \; g_0(x) + \frac{1}{2}\lambda \max\{0, p - \varphi(x)\}^2.$$

We note that we only consider finite values for λ instead of $\lambda \to \infty$ in our numerical tests since appropriately chosen values already produce nearly feasible solutions. With the extended convergence analysis for the CSG method in Sect. 11.4 this approximation problem can be directly solved with the CSG method for a large number of applications.

11.3 Application to Analytic Model Problems

After presenting the general framework for combining the CSG method with SRD, we discuss its performance on small analytic examples with two different chance constraints. The first one contains a norm constraint that defines a ball, and the second one is a joint chance constraint whose inner constraints define a box. Before presenting the numerical results in Sect. 11.3.2, we briefly introduce the two problem classes.

11.3.1 Problem Formulations

Our first analytic example contains a single chance constraint and is formally given by

$$\begin{aligned} &\min_x \; \sum_{i=1}^{m} x_i \\ &s.t. \;\; \varphi_{\text{ball}}(x) := \mathbb{P}_\zeta(\|\zeta - x\|^2 \leq R^2) \geq p, \end{aligned}$$

where $R > 0$ is a given radius, $p \in (0, 1)$ is the desired probability level, $\|\cdot\|$ denotes the Euclidean norm and ζ follows a standard multivariate Gaussian distribution in $\mathbb{R}^m$. Owing to SRD, we know that $\varphi_{\text{ball}}(x) \geq p$ is equivalent to

$$\|x\| \leq \sqrt{q_{p,m}},$$

where $q_{p,m}$ is the solution of the equation $F_{\chi^2}^{m,q}(R^2) = p$ in q. We note that the existence of $q_{p,m}$ is guaranteed only for sufficiently large $R > 0$ and sufficiently small $p \in (0, 1)$, which is the case in our following numerical examples. Here, $F_{\chi^2}^{m,q}$ denotes the distribution function of the non-central χ^2-distribution with m degrees of freedom and non-centrality parameter q^2. Evidently, the unique globally optimal solution to the chance-constrained problem is given by the analytic formula

$$x^* = -\left(\sqrt{\frac{q_{p,m}}{m}}, \ldots, \sqrt{\frac{q_{p,m}}{m}}\right)^T$$

due to the symmetry of the objective function.

The second example extends the first setting to a joint chance constraint, where multiple conditions have to hold simultaneously with probability p. Concretely, the conditions in the chance constraint are given by a box. Considering again a linear objective function, we obtain the optimization problem

$$\begin{aligned} &\min_x \sum_{i=1}^m x_i \\ &s.t.\ \ \varphi_{\text{box}}(x) := \mathbb{P}_\zeta(-R \le \zeta_i - x_i \le R \text{ for all } i = 1, \ldots, m) \ge p, \end{aligned}$$

where $R > 0$ is the given size of the box, $p \in (0, 1)$ is again the desired probability level, and ζ follows a standard multivariate Gaussian distribution. Compared to the first setting, a globally optimal solution can no longer be computed analytically. Since the components of ζ are independent, the chance constraint is equivalent to

$$p \le \varphi_{\text{box}}(x) = \prod_{i=1}^m [\Phi(x_i + R) - \Phi(x_i - R)],$$

where Φ is the distribution function of the one-dimensional standard Gaussian distribution. Since the objective function is again symmetric, finding a globally optimal solution can be reduced to computing a scalar t with

$$\Phi(t + R) - \Phi(t - R) = \sqrt[m]{p}.$$

Although there is no analytical solution to this equation, high-quality solutions can be computed numerically. Therefore, it is possible to compare the results of our method to this solution.

Coming back to the example with a ball constraint, choosing appropriate combinations of the radius R and the probability level p, the gradient of the respective penalized objective function is globally Lipschitz continuous, which implies that the convergence theory for the CSG method holds. Nevertheless, there also exist parameter combinations, where this property is violated. For the box constraints global Lipschitz continuity is always violated.

11.3.2 Numerical Results

Although the convergence criteria for the CSG method are only fulfilled in special settings with the ball constraint, we numerically test our combination of SRD and CSG on both problem formulations. Concretely, we choose instances with dimension $m = 3$ for both chance constraints. The radius of the ball and the size of the box are chosen as $R = 5$ and the penalty parameter for our formulation is given by $\lambda = 10^4$. As mentioned above, choosing $p \in (0, 1)$ large enough guarantees Lipschitz continuity of $\nabla\varphi_{\text{ball}}$. Loosely speaking, in this case, the SRD rays are viewed from a point within the ball and the length of these rays depends smoothly on the direction. In our numerical experiments, we found $p = 0.8$ to be sufficiently large. Note that similar regularity cannot be expected for $\nabla\varphi_{\text{box}}$, due to edges and corners (see also Sect. 11.4).

To obtain examples, where SRD rays are constructed from points outside the ball or box, we use the probability levels $p = 0.4$ (ball) and $p = 0.1$ (box). In these cases, the Lipschitz condition is violated. We note that we choose these values to obtain different settings, where the convergence criteria for the CSG method are sometimes satisfied and sometimes not, to compare the method's performance for these cases, but the concrete values do not matter for these small analytical examples. We stop the CSG method after 4000 iterations and evaluate the feasibility for the original chance constraint with a quasi Monte-Carlo (QMC) approximation with 50000 sample points. To overcome the issue of randomness we perform 500 random runs of the CSG method with the zero-vector as starting point. Furthermore, we choose the decreasing step size $\tau_n = 0.2/n^{0.7}$. We note that these parameters have been chosen with some preliminary computational experiments, but do not represent optimal choices.

The algorithm is implemented in Matlab R2024b and all computations are executed on a machine with an Intel Xeon E3-1240 v6 CPU (3.7 gigahertz base frequency), 2 cores and 32 gigabyte RAM.

We start by numerically evaluating the convergence of the CSG method for the four tested problems. To this end, we study the original and penalized objective functions over the iterations. We note that there is no significant difference between the penalized and the original version, and therefore, we only show the medians and some quantile values of the original one in Fig. 11.1.

On the left-hand side we see the development over all iterations, whereas on the right-hand side the y-axis is shrunk to have a better view on the quantiles. We observe that the CSG method converges for all four instances within the allowed number of iterations. Studying the quantiles we observe larger quantiles for boxes with $p = 0.1$ than for the other instances. Considering the maximal deviation, given by the fraction of the maximal difference between the objective function values over all runs and the median of the objective function values, we obtain for the final iteration deviations between 0.02 and 0.04 for all four instances and there is no significant difference between boxes and balls. Therefore, the larger quantiles result from the larger objective function values for $p = 0.1$ and the CSG method behaves similarly in all four tests.

To analyze the feasibility of the returned solutions with respect to the original problem, we study the QMC approximation of the chance constraint as well as the returned violation by the CSG method for the quality of the penalty approximation.

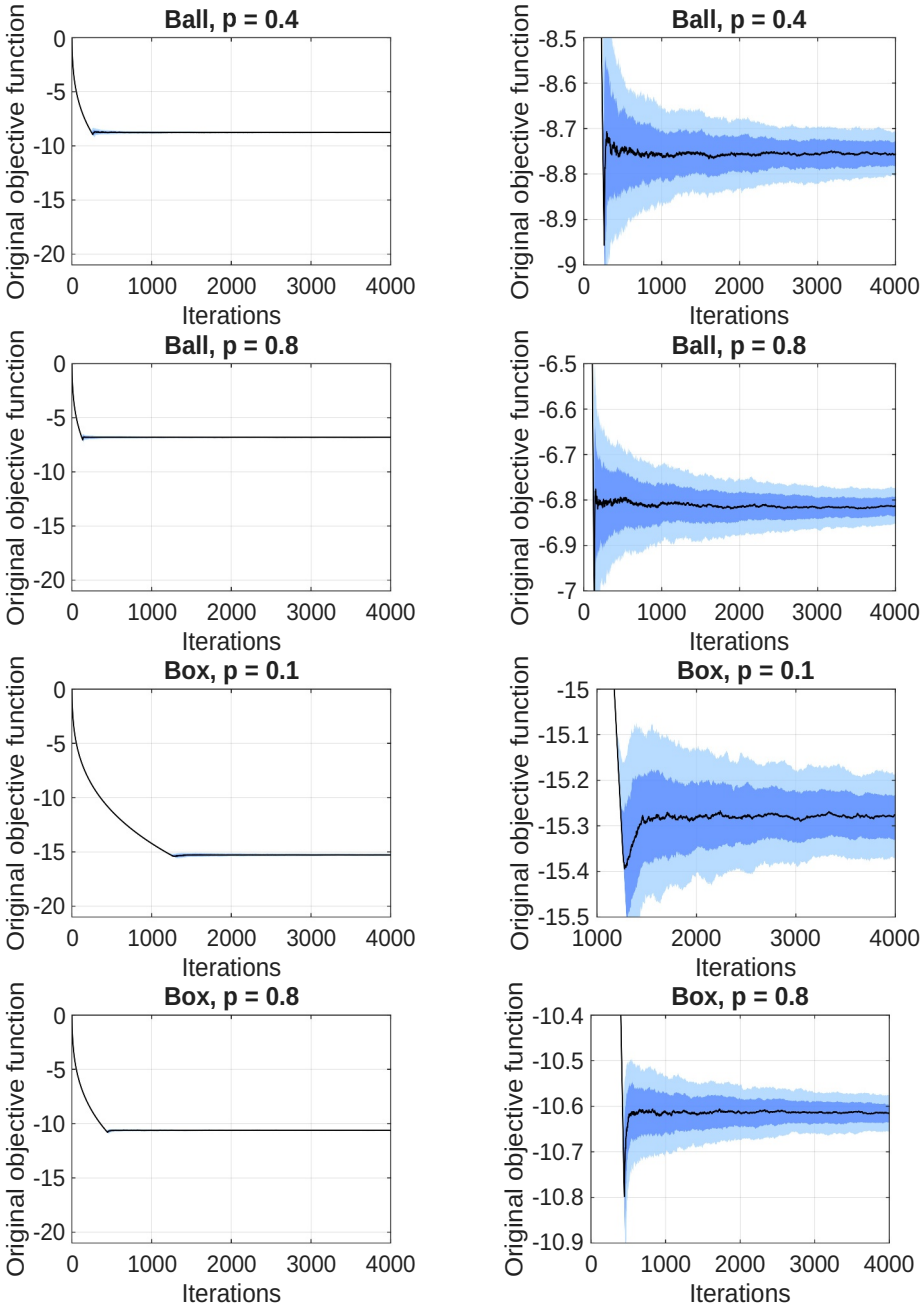


Fig. 11.1: Objective function values over iterations for the median (black line), shaded areas for quantiles $P_{0.25,0.75}$ (dark) and $P_{0.1,0.9}$ (light)

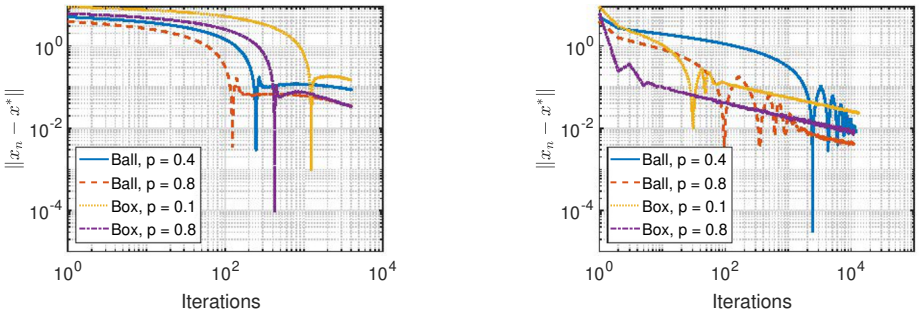


Fig. 11.2: Median distance of the CSG iterates (left) and the SCGD iterates (right) to the optimal solution x^* in every iteration

Since the maximal returned violation is 0.004 for all instances, we conclude that the penalty parameter is chosen large enough. With respect to the QMC approximations we see that the median probability always meets exactly the desired probability level and the minimal and maximal values deviate up to 2 % in each direction from the desired level p. Furthermore, we do not notice a significant difference between the tested examples.

Since we have access to the globally optimal solution for the ball problems and to a high-quality approximation for the boxes, we furthermore compare our solutions to the exact ones in the left part of Fig. 11.2.

We see that the CSG method reaches for all four instances an accuracy of about 10^{-1} to 10^{-2}. Nevertheless, the CSG method seems to be more accurate for $p = 0.8$ than for the smaller probability levels. Furthermore, we notice in all four cases one sudden improvement before the difference to the optimal solution becomes larger again. At this point, the CSG iteration is closest to the analytical solution over all iterations. We note that we start for all four instances with a feasible point and the CSG method reduces the objective function values until the penalty term for the chance constraint becomes active. Since we deal with an inexact penalty term, the solution returned by the CSG method is always slightly infeasible and the peak occurs exactly where the CSG iterations cross the analytical solutions, but due to the inexact penalty term, the CSG method reduces the objective function even more before reaching the optimum of the penalty problem. Therefore, the distance to the analytical solution becomes larger again after the peak. Nevertheless, we conclude that our combined approach produces high-quality solutions for all four instances although the theoretical convergence criteria of the CSG method are sometimes violated. For this reason, the next section deals with an extension of the convergence theory to these cases.

Before stating these theoretical results, we briefly compare the CSG method with another stochastic gradient method from the literature, namely the Stochastic compositional gradient descent algorithm (SCGD) introduced by Wang et al. [27]. Although this method is not as flexible as the CSG method, it is designed to handle two nested expectations, and is therefore applicable to our penalty formulation of the chance-constrained problem. SCGD needs the same number of evaluations per iteration than the CSG

method, but instead of reusing information from the last iterations SCGD decomposes the approximation of the two nested functions by separately calculating efficient step sizes. Therefore, the additional effort for calculating the integration weights in CSG no longer occurs, but SCGD typically needs much more iterations to converge. To compare the two approaches, we allow a running time of 70 seconds for SCGD since all performed runs of the CSG method need between 60 and 70 seconds. The respective distance with respect to the exact solution over the iterations is shown in the right part of Fig. 11.2. We note that the maximal difference to the optimal solution for the vectors created with SCGD is typically one decimal better than for CSG. But if we compare the results for both methods with the same number of iterations, namely 4000, CSG outperforms SCGD in the minimal, maximal and median values.

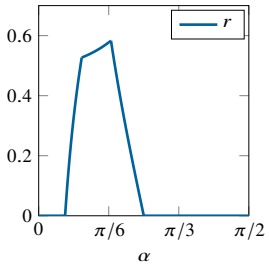
In general, we conclude that for these small analytic examples, both methods work quite well, but SCGD needs way more iterations to approximate the optimal solution well. Therefore, CSG should be preferred if the function or gradient evaluations are time-consuming or complicated to avoid a huge number of iterations, and for easy evaluation as in this example, SCGD is an alternative to the CSG approach. Nevertheless, we will not focus on SCGD in the following, but concentrate on an extension of the convergence theory for CSG.

11.4 Extension of the CSG Convergence Theory Beyond Problems that are Globally Lipschitz

As stated in Sect. 11.2.2, convergence results for CSG require the inner gradient function $\nabla_x \phi$ to be Lipschitz in both arguments. However, the numerical results presented above indicate that this assumption can be weakened to cover a more general setting. In fact, both academic examples violate this assumption, as can be seen in Fig. 11.3 and Fig. 11.4.



Fig. 11.3: Illustration of the setup in the academic example using φ_{box}. Utilizing the SRD reformulation, the probability of a region with center $\bar{x} \in \mathcal{X}$ (blue dot) is obtained by integrating the (weighted) intersection length r (red) over all possible directions $v \in \mathbb{S}^1$. The value of r might change non-smoothly when varying the direction v (left) or moving $\bar{x}$ (right).



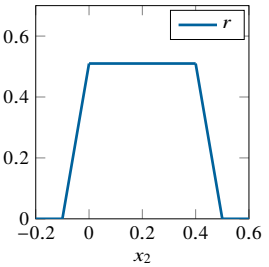


Fig. 11.4: Left: Intersection length r (see Fig. 11.3) for fixed midpoint $\bar{x}$ and different directions, parametrized by the angle α. Right: Value of r for fixed direction v and varying $\bar{x} = (1, x_2)$, see Fig. 11.3. In both cases, we observe that kinks in the graph of r correspond to cases in which the considered ray $\{\lambda v : \lambda \geq 0\}$ passes through one of the four corners of the square.

In this section, we will extend the convergence theory of CSG to cover more general classes of problems and show that, due to the SRD reformulation of φ, the examples presented above fall within this category. An important observation is that for fixed $x \in \mathbb{R}^{d_x}$, discontinuities of $\nabla_x \phi$ appear precisely in directions $\zeta \in \mathbb{R}^{d_\zeta}$ for which the ray $\{\lambda\zeta : \lambda \geq 0\}$ is tangent to the boundary of the box or passes through a corner. In other words, the discontinuity set of $\nabla_x \phi$ is directly correlated to geometric properties of the set $\mathcal{Z}^{\mathrm{ad}}$. With this in mind, we construct our general set of assumptions.

Assumption 11.1 (Regularity of $\mathcal{X}$, $\mathcal{Z}^{\mathrm{ad}}$ and μ) The set $\mathcal{X} \subseteq \mathbb{R}^{d_x}$ is compact and convex. The set $\mathcal{Z}^{\mathrm{ad}} \subseteq \mathbb{R}^{d_\zeta}$ is bounded with $\mathrm{supp}(\mu) \subseteq \mathcal{Z}^{\mathrm{ad}}$.

Assumption 11.2 (Regularity of φ and ϕ)

(i) The function $\nabla\varphi : \mathcal{X} \to \mathbb{R}$ is Lipschitz continuous.

(ii) For all $\varepsilon > 0$ and for all $x \in \mathcal{X}$ exists a closed subset $\mathcal{M}(\varepsilon, x) \subseteq \mathcal{Z}^{\mathrm{ad}}$ and a $\delta(\varepsilon, x) > 0$ such that

$$\mu(\mathcal{M}(\varepsilon, x)) < \varepsilon \quad \text{and} \quad \phi(\cdot, \zeta) \in C^1(\mathcal{B}_{\delta(\varepsilon,x)}(x)) \quad \text{for every } \zeta \in (\mathcal{M}(\varepsilon, x))^{\mathrm{c}}.$$

In particular, the set

$$\mathcal{V}(x) := \left\{\zeta \in \mathcal{Z}^{\mathrm{ad}} : \phi(\cdot, \zeta) \text{ is not continuously differentiable in } x\right\}$$

has zero measure for all $x \in \mathcal{X}$.

(iii) The gradient $\nabla_x \phi$ is uniformly piecewise Lipschitz continuous, i.e., there exists $N \in \mathbb{N}$ such that for each $\varepsilon > 0$ and all $x \in \mathcal{X}$ there exists a partition of $\mathcal{M}(\varepsilon, x)^{\mathrm{c}}$ consisting of open sets $\left\{O_j(\varepsilon, x)\right\}_{j=1,\ldots,N}$ with the property that $\nabla_x \phi$ is uniformly Lipschitz continuous on the sets $\mathcal{B}_{\delta(\varepsilon,x)}(x) \times O_j(\varepsilon, x)$.
Hence, there exists a constant $L \in \mathbb{R}_{>0}$, independent of $\varepsilon > 0$ and $x \in \mathcal{X}$, such that

$$\|\nabla_x \phi(x_1, \zeta_1) - \nabla_x \phi(x_2, \zeta_2)\| \leq L \left(\|x_1 - x_2\|_{\mathcal{X}} + \|\zeta_1 - \zeta_2\|_{\mathcal{Z}^{\mathrm{ad}}}\right)$$

for all $(x_1, \zeta_1), (x_2, \zeta_2) \in \mathcal{B}_{\delta(\varepsilon,x)}(x) \times O_j(\varepsilon, x)$, $j = 1, \ldots, N$.

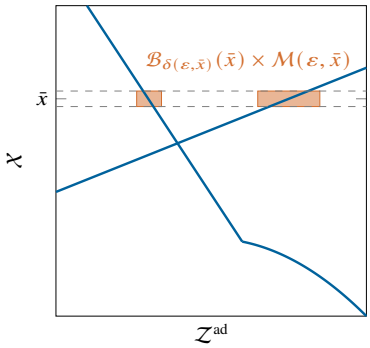


Fig. 11.5: Product space $\mathcal{X} \times \mathcal{Z}^{\mathrm{ad}}$ with possible discontinuity set (blue). Given $\bar{x} \in \mathcal{X}$ and $\varepsilon > 0$, we can construct a set $\mathcal{B}_{\delta(\varepsilon,\bar{x})}(\bar{x}) \times \mathcal{M}(\varepsilon, \bar{x})$ (red) that locally contains these discontinuities.

Assumption 11.2 allows us to decompose the product space $\mathcal{X} \times \mathcal{Z}^{\mathrm{ad}}$ into smaller regions on which $\nabla_x \phi$ is well-behaved. An illustration is provided in Fig. 11.5. The key idea to show that the approximation property [11, Lemma 4.6] remains valid under these milder assumptions is to "cut out" small regions around the discontinuities of $\nabla_x \phi$. By Assumption 11.2, these regions can be chosen small enough such that their contribution to the value of $\nabla\varphi$ is arbitrary small. On the remaining regions, we can proceed as in the proof of [11, Lemma 4.6].

To simplify notation in the upcoming convergence result, we only consider a batch size of $N_B = 1$ and define the nearest neighbor index of $\zeta \in \mathcal{Z}^{\mathrm{ad}}$ in iteration n as

$$k^n(\zeta) := \min\left\{ i \in \{1, \dots, n\} \,:\, i \in \operatorname*{arg\,min}_{k=1,\dots,n} \|(x_n, \zeta) - (x_k, \zeta_k)\| \right\}.$$

Thus, $k^n(\zeta)$ denotes the index of the sample point with minimal distance to (x_n, ζ). If the minimum is attained at multiple indices, $k^n(\zeta)$ is chosen as the smallest one. With $k^n(\zeta)$, the CSG gradient approximation can be expressed as

$$\widehat{G}_n = \sum_{k=1}^{n} \alpha_k \nabla_x \phi(x_k, \zeta_k) = \int_{\mathcal{Z}^{\mathrm{ad}}} \nabla_x \phi(x_{k^n(\zeta)}, \zeta_{k^n(\zeta)}) \mu(\mathrm{d}\zeta).$$

Proposition 11.1 *(Approximation Result for $\nabla\varphi$) Under Assumptions 11.1 and 11.2, the approximation error for $\nabla\varphi$ almost surely vanishes in the course of iterations, i.e., $\|\nabla\varphi(x_n) - \widehat{G}_n\| \xrightarrow{a.s.} 0$ for $n \to \infty$.*

Proof. Let $\varepsilon, \tilde{\varepsilon} > 0$ and $0 < \tilde{\varepsilon} \leq \frac{\varepsilon}{6C}$, with $C > 0$ to be defined later. Utilizing the compactness of $\mathcal{X}$, we find a finite cover $(\mathcal{B}_{\delta_i^{\tilde{\varepsilon}}}(\bar{x}_i))_{i=1,\dots,K}$ of $\mathcal{X}$ consisting of $K \in \mathbb{N}$ balls with radius $\delta_i^{\tilde{\varepsilon}} := \delta(\tilde{\varepsilon}, \bar{x}_i)$ centered at points $\bar{x}_i \in \mathcal{X}$. In addition, we choose compact subsets $K_j(\tilde{\varepsilon}, \bar{x}_i) \subseteq O_j(\tilde{\varepsilon}, \bar{x}_i)$ and a radius $r(\tilde{\varepsilon}) > 0$ such that

$$\sum_{j=1}^{N} \mu\left(O_j\left(\tilde{\varepsilon}, \bar{x}_i\right) \setminus K_j\left(\tilde{\varepsilon}, \bar{x}_i\right)\right) < \tilde{\varepsilon} \quad \text{and} \quad K_j\left(\tilde{\varepsilon}, \bar{x}_i\right) + \mathcal{B}_{r(\tilde{\varepsilon})}(0) \subseteq O_j\left(\tilde{\varepsilon}, \bar{x}_i\right)$$

for $i = 1, \ldots, K$ and $j = 1, \ldots, N$. Now, by applying [11, Lemma 4.5], we find $N(\varepsilon) \in \mathbb{N}$ such that for all $n \geq N(\varepsilon)$ and all $\zeta \in \mathcal{Z}^{\mathrm{ad}}$ we have

$$Z_n(\zeta) := \|x_n - x_{k^n(\zeta)}\|_{\mathcal{X}} + \|\zeta - \zeta_{k^n(\zeta)}\|_{\mathcal{X}} < \min\left\{r(\tilde{\varepsilon}), \frac{\lambda(\tilde{\varepsilon})}{2}, \frac{\varepsilon}{3L}\right\},$$

with probability 1. Here, $\lambda(\tilde{\varepsilon}) > 0$ denotes the corresponding Lebesgue number of the finite cover. In particular, for each $n \geq N(\varepsilon)$ this implies the existence of an index $i_n \in \{1, \ldots, K\}$ with the property $x_n, x_{k^n(\zeta)} \in \mathcal{B}_{\delta^{\tilde{\varepsilon}}_{i_n}}(\bar{x}_{i_n})$ and $\zeta_{k^n(\zeta)} \in O_j\left(\tilde{\varepsilon}, \bar{x}_i\right)$ for all $\zeta \in K_j\left(\tilde{\varepsilon}, \bar{x}_i\right)$. Now, we decompose $\mathcal{Z}^{\mathrm{ad}}$ as illustrated in Fig. 11.5. We obtain for all $n \geq N(\varepsilon)$

$$\begin{aligned}
\left\|\nabla\varphi(x_n) - \widehat{G}_n\right\| &\leq \left\| \int_{\mathcal{Z}^{\mathrm{ad}}} \nabla_x \phi(x_n, \zeta) \mu(\mathrm{d}\zeta) - \int_{\mathcal{M}\left(\tilde{\varepsilon}, \bar{x}_{i_n}\right)^{\mathrm{c}}} \nabla_x \phi(x_n, \zeta) \mu(\mathrm{d}\zeta) \right\| \\
&\quad + \left\| \int_{\mathcal{M}\left(\tilde{\varepsilon}, \bar{x}_{i_n}\right)^{\mathrm{c}}} \nabla_x \phi(x_n, \zeta) \mu(\mathrm{d}\zeta) - \int_{\mathcal{Z}^{\mathrm{ad}}} \nabla_x \phi(x_{k^n(\zeta)}, \zeta_{k^n(\zeta)}) \mu(\mathrm{d}\zeta) \right\| \\
&\leq 2C(\bar{x}_{i_n}) \mu\left(\mathcal{M}\left(\tilde{\varepsilon}, \bar{x}_{i_n}\right)\right) \\
&\quad + \sum_{j=1}^{N} \int_{O_j\left(\tilde{\varepsilon}, \bar{x}_{i_n}\right)} \left\|\nabla_x \phi(x_n, \zeta) - \nabla_x \phi(x_{k^n(\zeta)}, \zeta_{k^n(\zeta)})\right\| \mu(\mathrm{d}\zeta) \\
&\leq 2C(\bar{x}_{i_n}) \tilde{\varepsilon} + 2C(\bar{x}_{i_n}) \sum_{j=1}^{N} \mu\left(O_j\left(\tilde{\varepsilon}, \bar{x}_{i_n}\right) \setminus K_j\left(\tilde{\varepsilon}, \bar{x}_{i_n}\right)\right) \\
&\quad + \sum_{j=1}^{N} \int_{K_j\left(\tilde{\varepsilon}, \bar{x}_{i_n}\right)} \left\|\nabla_x \phi(x_n, \zeta) - \nabla_x \phi(x_{k^n(\zeta)}, \zeta_{k^n(\zeta)})\right\| \mu(\mathrm{d}\zeta) \\
&\leq 4C(\bar{x}_{i_n}) \tilde{\varepsilon} + \sum_{j=1}^{N} \int_{K_j\left(\tilde{\varepsilon}, \bar{x}_{i_n}\right)} L Z_n(\zeta) \mu(\mathrm{d}\zeta).
\end{aligned}$$

Note that, by the assumed regularity of $\nabla\varphi$ and compactness of $\mathcal{X}$, the constants $C(\bar{x}_{i_n})$ with

$$\left\| \int_{\mathcal{M}(\tilde{\varepsilon}, \bar{x}_{i_n})} \nabla_x \phi(x_n, \zeta)\, \mu(\mathrm{d}\zeta) \right\| \leq 2C(\bar{x}_{i_n}) \mu\left(\mathcal{M}\left(\tilde{\varepsilon}, \bar{x}_{i_n}\right)\right)$$

can be chosen independent of x_n and $\bar{x}_{i_n}$. Thus, setting $\tilde{\varepsilon} \leq \dfrac{\varepsilon}{6C}$ yields

$$\left\|\nabla\varphi(x_n) - \widehat{G}_n\right\| < \varepsilon,$$

finishing the proof. □

11.4.1 Convergence for Numerical Examples

By Proposition 11.1, we know that the CSG method converges for our numerical examples, as long as the regularity assumptions (Assumption 11.2) are satisfied. To show that this is indeed the case, we note that both settings can be captured by the following general framework:

Assumption 11.3 Given $x \in \mathbb{R}^{d_x}$, we denote

$$\mathcal{Z}_x^{\mathrm{ad}} := \left\{\zeta \in \mathbb{R}^{d_\zeta} \,:\, g(x,\zeta) \leq 0\right\}.$$

We assume that there exists a set $\mathcal{Z}^{\mathrm{ad}} \subset \mathbb{R}^{d_\zeta}$ with the following properties:

(i) $\mathcal{Z}^{\mathrm{ad}}$ is compact and convex.
(ii) There exists $\tilde{g} \in C^1(\mathbb{R}^{d_\zeta}; \mathbb{R}^m)$ such that $\mathcal{Z}^{\mathrm{ad}} = \left\{\zeta \in \mathbb{R}^{d_\zeta} \,:\, \tilde{g}(\zeta) \leq 0\right\}$. Moreover, linear independence constraint qualification LICQ is satisfied for all $\zeta \in \mathcal{Z}^{\mathrm{ad}}$.
(iii) There exist functions $R \in C^{1,1}(\mathbb{R}^{d_x}; \mathrm{SO}(d_\zeta))$ and $T \in C^{1,1}(\mathbb{R}^{d_x}; \mathbb{R}^{d_\zeta})$ such that

$$\mathcal{Z}_x^{\mathrm{ad}} = R(x)\mathcal{Z}^{\mathrm{ad}} + T(x) \quad \text{for all } x \in \mathbb{R}^{d_x},$$

i.e., $\mathcal{Z}_x^{\mathrm{ad}}$ is obtained by rotations and translations of $\mathcal{Z}^{\mathrm{ad}}$. Here, $\mathrm{SO}(d_\zeta)$ denotes the special orthogonal group.
(iv) There exists a vector $\bar{\zeta} \in \mathcal{Z}^{\mathrm{ad}}$ satisfying the Slater condition $\tilde{g}(\bar{\zeta}) < 0$.

Note that, by construction, both examples from Sect. 11.3 satisfy these assumptions. The remainder of this section is dedicated to prove that Assumption 11.1 and Assumption 11.3 imply Assumption 11.2, i.e., that the generalized convergence result (Proposition 11.1) is applicable for our numerical examples.

First off, we show that these assumptions imply the Lipschitz continuity of $\nabla\varphi$ on the set $\mathcal{X}$. Since this latter set is compact by Assumption 11.1, it is sufficient to verify the local Lipschitz continuity of the globally defined probability function $\nabla\varphi$ in (P). The following lemma provides a verifiable condition on the density of the random vecor ζ which is in particular satisfied for the Gaussian distribution.

Lemma 11.1 *Let $A \subseteq \mathbb{R}^d$ be a compact set. Let $T : \mathbb{R}^n \to \mathbb{R}^d$ and $R : \mathbb{R}^n \to \mathbb{R}^{d\times d}$ be mappings with locally Lipschitz continuous derivatives such that $R(x)$ is a regular $d \times d-$ matrix for all $x \in \mathbb{R}^n$. Finally, let ξ be a $d-$ dimensional random vector having a density f_ξ with locally Lipschitz continuous derivative (e.g., multivariate Gaussian distribution). Then, the probability function*

$$\varphi(x) := \mathbb{P}(\xi \in T(x) + R(x)A) \quad (x \in \mathbb{R}^n)$$

is continuously differentiable and its derivative is locally Lipschitz.

Proof. By assumption, we have that, thanks to regularity of $R(x)$,

$$\varphi(x) = \int_{T(x)+R(x)A} f_\xi(z)dz = \int_A \underbrace{f_\xi(T(x) + R(x)y)\det R(x)}_{h(x,y)}\, dy \quad (x \in \mathbb{R}^n).$$

Fix an arbitrary $\bar{x} \in \mathbb{R}^n$. Our assumptions ensure that h is continuously differentiable. In particular, thanks to the compactness of A, there exists a constant M such that for all x close to $\bar{x}$, for all $y \in A$ and all $j = 1, \ldots, n$, the estimate $\left|\frac{\partial h}{\partial x_j}(x, y)\right| \leq M$ holds true. Next, fix an arbitrary $j \in \{1, \ldots, n\}$ and denote by e_j the corresponding standard unit vector in $\mathbb{R}^n$. For an arbitrary sequence $t_k \to 0$, we obtain that

$$\frac{\varphi(\bar{x} + t_k e_j) - \varphi(\bar{x})}{t_k} = \int_A \frac{h(\bar{x} + t_k e_j, y) - h(\bar{x}, y)}{t_k} dy.$$

By the Mean Value Theorem, for each $y \in A$, there exists some $\tau_k(y)$ with $|\tau_k(y)| \leq |t_k|$ such that

$$\frac{h(\bar{x} + t_k e_j, y) - h(\bar{x}, y)}{t_k} = \frac{\partial h}{\partial x_j}(\bar{x} + \tau_k(y) e_j, y) \to \frac{\partial h}{\partial x_j}(\bar{x}, y).$$

Moreover, $|\frac{\partial h}{\partial x_j}(\bar{x} + \tau_k(y) e_j, y)| \leq M$ for all k sufficiently large and all $y \in A$. Now, since A has finite Lebesgue measure as a compact set, the Bounded Convergence Theorem yields that

$$\frac{\varphi(\bar{x} + t_k e_j) - \varphi(\bar{x})}{t_k} \to \int_A \frac{\partial h}{\partial x_j}(\bar{x}, y) dy = \frac{\partial \varphi}{\partial x_j}(\bar{x})$$

because $t_k \to 0$ was arbitrary. Since $\bar{x} \in \mathbb{R}^n$ and $j \in \{1, \ldots, n\}$ were arbitrary, we have that all partial derivatives of φ exist and are given by

$$\frac{\partial \varphi}{\partial x_j}(x) = \int_A \frac{\partial h}{\partial x_j}(x, y) dy \quad (j = 1, \ldots, n;\ x \in \mathbb{R}^n).$$

Now, let again $\bar{x} \in \mathbb{R}^n$ and $j \in \{1, \ldots, n\}$ be arbitrary and consider an arbitrary converging sequence $x^{(k)} \to \bar{x}$. Then, repeating the argument of the Bounded Convergence Theorem already employed above, we check that

$$\frac{\partial h}{\partial x_j}(x^{(k)}, y) \to \frac{\partial h}{\partial x_j}(\bar{x}, y); \quad \left|\frac{\partial h}{\partial x_j}(x^{(k)}, y)\right| \leq M \ \forall k \geq k_0,$$

whence

$$\frac{\partial \varphi}{\partial x_j}(x^{(k)}) \to \int_A \frac{\partial h}{\partial x_j}(\bar{x}, y) dy = \frac{\partial \varphi}{\partial x_j}(\bar{x}).$$

Therefore, φ is continuously differentiable. It remains to show that the partial derivatives are locally Lipschitz. To this aim, let once more $\bar{x} \in \mathbb{R}^n$ and $j \in \{1, \ldots, n\}$ be arbitrary. Observe that our assumptions imply that $\frac{\partial h}{\partial x_j}$ is locally Lipschitz. As a consequence of A being compact, there exists an open neighborhood $\mathcal{U}(\bar{x})$ of $\bar{x}$ and a modulus $L > 0$ such that

$$\left|\frac{\partial h}{\partial x_j}(x^a, y) - \frac{\partial h}{\partial x_j}(x^b, y)\right| \leq L \|x^a - x^b\| \quad \forall x^a, x^b \in \mathcal{U}(\bar{x})\ \forall y \in A.$$

This then entails, with c denoting the Lebesgue measure of A, that

$$\left|\frac{\partial\varphi}{\partial x_j}(x^a) - \frac{\partial\varphi}{\partial x_j}(x^b)\right| \leq Lc\|x^a - x^b\| \quad \forall x^a, x^b \in \mathcal{U}(\bar{x}).$$

Hence, the derivative of φ is locally Lipschitz. □

For the other properties listed in Assumption 11.2 we have to distinguish two cases: tangent directions and directions passing through an edge of $\mathcal{Z}^{\mathrm{ad}}$. We begin with the latter.

Edges Let $\mathcal{P}_{\mathbb{S}^{d_\zeta-1}}(\zeta) := \frac{\zeta}{\|\zeta\|}$ for $\zeta \in \mathbb{R}^{d_\zeta} \setminus \{0\}$ denote the projection of $\zeta \in \mathbb{R}^{d_\zeta}$ on the unit sphere $\mathbb{S}^{d_\zeta-1}$. Moreover, for $\mathcal{I} \subseteq \{1,\dots,m\}$, we define $\mathcal{I}^{\mathrm{c}} := \{1,\dots,m\} \setminus \mathcal{I}$ and

$$\mathcal{E}(\mathcal{I}) := \{\zeta \in \mathcal{Z}^{\mathrm{ad}} \,:\, \tilde{g}_{\mathcal{I}^{\mathrm{c}}}(\zeta) < 0,\ \tilde{g}_{\mathcal{I}}(\zeta) = 0\}.$$

By Assumption 11.3, it holds

$$\partial\mathcal{Z}^{\mathrm{ad}} = \bigcup_{|\mathcal{I}|\geq 1} \mathcal{E}(\mathcal{I}).$$

Furthermore, the edges of the set $\mathcal{Z}^{\mathrm{ad}}$ correspond to points of $\mathcal{Z}^{\mathrm{ad}}$ at which at least two inequalities are active, i.e., they are given by

$$\bigcup_{|\mathcal{I}|\geq 2} \mathcal{E}(\mathcal{I}).$$

We show that the corresponding set of directions $v \in \mathbb{S}^{d_\zeta-1}$ passing through an edge is of Hausdorff measure zero, as our regularity assumptions imply that $\mathcal{Z}^{\mathrm{ad}}$ has a finite amount of edges and each individual edge is of low dimension.

Lemma 11.2 *Under Assumption 11.3, it holds that* $\mathcal{H}^{d_\zeta-1}_{\mathbb{S}^{d_\zeta-1}}\left(\mathcal{P}_{\mathbb{S}^{d_\zeta-1}}\left(\bigcup_{|\mathcal{I}|\geq 2}\mathcal{E}(\mathcal{I})\right)\right) = 0$.

Proof. Let $k := |\mathcal{I}|$. Utilizing LICQ and the preimage theorem, we conclude that $\mathcal{E}(\mathcal{I})$ is a $(d_\zeta - k)$-dimensional submanifold. Hence, for every $p \in \mathcal{E}(\mathcal{I})$ there exists a C^1-diffeomorphism Φ_p on an open neighborhood V_p of p such that

$$\Phi_p\left(\mathcal{E}(\mathcal{I}) \cap V_p\right) = \Phi_p\left(V_p\right) \cap \left(\mathbb{R}^{d_\zeta-k} \times \{0\}^k\right).$$

Then, $\psi_p :\equiv \Phi_p^{-1}(\cdot, 0)$ defines a C^1-mapping on the open set

$$U_p := \left\{\zeta \in \mathbb{R}^{d_\zeta-1} \mid (\zeta, 0) \in \Phi_p\left(V_p\right)\right\} \subseteq \mathbb{R}^{d_\zeta-1}.$$

Now, let $W_p := \left\{\zeta \in U_p \mid \zeta_{d_\zeta-j} = 0 \text{ for all } j < k\right\}$ and note that $\psi_p(W_p) = \mathcal{E}(\mathcal{I}) \cap V_p$ as well as $\lambda_{d_\zeta-1}(W_p) = 0$. We consider φ_p to be a local parametrization of the sphere $\mathbb{S}^{d_\zeta-1}$ such that $\mathcal{P}_{\mathbb{S}^{d_\zeta-1}}\left(\mathcal{E}(\mathcal{I}) \cap V_p\right) \subseteq \mathrm{im}(\varphi_p)$. Since

$$\varphi_p^{-1} \circ \mathcal{P}_{\mathbb{S}^{d_\zeta-1}} \circ \psi_p \in C^1\left(U_p; \mathbb{R}^{d_\zeta-1}\right),$$

we deduce

$$\lambda_{d_\zeta-1}\left(\varphi_p^{-1}\left(\mathcal{P}_{\mathbb{S}^{d_\zeta-1}}\left(\mathcal{E}(\mathcal{I}) \cap V_p\right)\right)\right) = \lambda_{d_\zeta-1}\left(\left(\varphi_p^{-1} \circ \mathcal{P}_{\mathbb{S}^{d_\zeta-1}} \circ \psi_p\right)(W_p)\right) = 0$$

and the claim follows from the compactness of $\mathcal{Z}^{\mathrm{ad}}$. □

Tangent Directions By the assumed convexity of $\mathcal{Z}^{\mathrm{ad}}$, if $0 \in \operatorname{int}(\mathcal{Z}^{\mathrm{ad}})$, there can be no directions $v \in \mathbb{S}^{d_\zeta-1}$ that are tangent to $\mathcal{Z}^{\mathrm{ad}}$ and therefore nothing has to be shown in this case. Thus, we always assume $0 \notin \operatorname{int}(\mathcal{Z}^{\mathrm{ad}})$ in the following, without mentioning it explicitly every time.

Definition 11.1 (Tangential Points) We say $\zeta \in \mathcal{Z}^{\mathrm{ad}}$ is a tangential point of the set $\mathcal{Z}^{\mathrm{ad}}$, if there exists an outer normal vector $n_\zeta \in \mathbb{R}^{d_\zeta} \setminus \{0\}$ and a corresponding half space $\mathcal{H}_\zeta := \left\{x \in \mathbb{R}^{d_\zeta} \mid \langle n_\zeta, x\rangle \le \langle n_\zeta, \zeta\rangle\right\}$ such that $\mathcal{Z}^{\mathrm{ad}} \subseteq \mathcal{H}_\zeta$ and $0 \in \left(\operatorname{int}\left(\mathcal{H}_\zeta\right)\right)^{\mathrm{c}}$. We denote the set of tangential points of $\mathcal{Z}^{\mathrm{ad}}$ by $\mathcal{T}$.

Definition 11.2 (Tangential Directions) Let $\mathcal{T}_0 := \left\{\zeta \in \mathcal{T} \mid \langle n_\zeta, \zeta\rangle = 0\right\} \setminus \{0\}$. We define the set of tangential directions of $\mathcal{Z}^{\mathrm{ad}}$ as $\mathcal{V} := \mathcal{P}_{\mathbb{S}^{d_\zeta-1}}(\mathcal{T}_0)$.

In the following, we denote the closed and convex conical hull of the set $\mathcal{Z}^{\mathrm{ad}}$ as

$$\mathcal{K}^* := \operatorname{cone}(\mathcal{Z}^{\mathrm{ad}}) = \left\{\lambda\zeta \mid \zeta \in \mathcal{Z}^{\mathrm{ad}}, \lambda \ge 0\right\}.$$

Note that if $0 \in \partial\mathcal{Z}^{\mathrm{ad}}$, $\mathcal{K}^*$ is identical to the usual tangential cone of $\mathcal{Z}^{\mathrm{ad}}$ at 0.

Lemma 11.3 *Under Assumption 11.3, it holds that* $\mathcal{V} = \partial_{\mathbb{S}^{d_\zeta-1}}\left(\mathbb{S}^{d_\zeta-1} \cap \mathcal{K}^*\right) = \mathbb{S}^{d_\zeta-1} \cap \partial\mathcal{K}^*$.

Proof. Let $v \in \mathcal{V}$. Then, there exists $\lambda > 0$ such that $v \in \lambda^{-1}\mathcal{T}_0 \subseteq \lambda^{-1}\partial\mathcal{Z}^{\mathrm{ad}} \subseteq \mathcal{K}^*$. Hence, we find an outer normal vector $n_{\lambda v} \in \mathbb{R}^{d_\zeta} \setminus \{0\}$ such that $\langle n_{\lambda v}, v\rangle = 0$ and $\mathcal{Z}^{\mathrm{ad}} \subseteq \mathcal{H}_{\lambda v}$. This implies $\mathcal{K}^* \subseteq \mathcal{H}_{\lambda v}$ and for every $\delta > 0$, there exists $\alpha_\delta > 0$ such that

$$\mathcal{P}_{\mathbb{S}^{d_\zeta-1}}(\lambda v + \alpha_\delta n_{\lambda v}) \in \mathbb{S}^{d_\zeta-1} \cap (\mathcal{K}^*)^{\mathrm{c}} \cap \mathcal{B}_\delta(v).$$

Thus, $v \notin \operatorname{int}_{\mathbb{S}^{d_\zeta-1}}\left(\mathbb{S}^{d_\zeta-1} \cap \mathcal{K}^*\right)$, which implies $v \in \partial_{\mathbb{S}^{d_\zeta-1}}\left(\mathbb{S}^{d_\zeta-1} \cap \mathcal{K}^*\right)$.

Now, let $v \in \partial_{\mathbb{S}^{d_\zeta-1}}\left(\mathbb{S}^{d_\zeta-1} \cap \mathcal{K}^*\right)$. Then, $v \in \partial\mathcal{K}^* \subseteq \mathcal{K}^*$ and we find $\mu > 0$ such that $\mu v \in \mathcal{Z}^{\mathrm{ad}}$. The convexity of $\mathcal{K}^*$ implies the existence of $n_{\mu v} \in \mathbb{R}^{d_\zeta} \setminus \{0\}$ such that $\langle n_{\mu v}, k - \mu v\rangle \le 0$ for all $k \in \mathcal{K}^*$. Choosing $\lambda > 1$, we obtain

$$0 \ge \langle n_{\mu v}, \lambda\mu v - \mu v\rangle = (\lambda - 1)\langle n_{\mu v}, \mu v\rangle \ge 0.$$

Hence, $\langle n_{\mu v}, \mu v\rangle = 0$ and the claim follows. □

Next, we show that $\mathcal{V}$ is of Hausdorff measure zero and has open neighborhoods of arbitrary small Hausdorff measure. For $\varepsilon > 0$, let $(\mathcal{V})_\varepsilon := \left\{v \in \mathbb{S}^{d_\zeta-1} \mid \operatorname{dist}(v, \mathcal{V}) \le \varepsilon\right\}$.

Lemma 11.4 *Under Assumption 11.3, it holds that* $\mathcal{H}^{d_\zeta-1}_{\mathbb{S}^{d_\zeta-1}}(\mathcal{V}) = 0$. *Furthermore, for every* $\delta > 0$ *there exists* $\varepsilon_\delta > 0$ *such that* $\mathcal{H}^{d_\zeta-1}_{\mathbb{S}^{d_\zeta-1}}\left((\mathcal{V})_{\varepsilon_\delta}\right) < \delta$.

Proof. First, assume that $0 \notin \mathcal{Z}^{\mathrm{ad}}$. From the convexity of $\mathcal{Z}^{\mathrm{ad}}$, it follows that $\mathcal{K}^*$ is a convex and pointed cone. Thus, the set $\mathbb{S}^{d_\zeta-1} \cap \mathcal{K}^*$ is spherically convex and we can choose $w \in \mathrm{int}_{\mathbb{S}^{d_\zeta-1}}\left(\mathbb{S}^{d_\zeta-1} \cap \mathcal{K}^*\right)$ such that

$$\mathbb{S}^{d_\zeta-1} \cap \mathcal{K}^* \subseteq S^+_w := \left\{v \in \mathbb{S}^{d_\zeta-1} \mid \langle w, v\rangle > 0\right\}.$$

Now, let $\mathbb{R}^{d_\zeta}_w := \left\{\zeta \in \mathbb{R}^{d_\zeta} \mid \langle w, \zeta\rangle = 0\right\}$ and denote the corresponding gnomonic projection as $g_w : S^+_w \to \mathbb{R}^{d_\zeta}_w, v \mapsto \langle w, v\rangle^{-1} v - w$. The function g_w is a bijection with inverse $g_w^{-1} :\equiv \mathcal{P}_{\mathbb{S}^{d_\zeta-1}}(\cdot + w)$ and it maps closed and spherically convex subsets in S^+_w to convex sets in $\mathbb{R}^{d_\zeta}_w$, see [5]. In the following, we proceed in a similar way to Lemma 11.3. By choosing a parametrization φ of the sphere $\mathbb{S}^{d_\zeta-1}$ with the property $\mathbb{S}^{d_\zeta-1} \cap \mathcal{K}^* \subseteq \mathrm{im}(\varphi)$, rotating the hyperplane $\mathbb{R}^{d_\zeta}_w$ by a linear mapping $R \in \mathrm{SO}(d_\zeta)$ such that $R(\mathbb{R}^{d_\zeta}_w) \subseteq \mathbb{R}^{d_\zeta-1} \times \{0\}$, then applying the canonical embedding E from $\mathbb{R}^{d_\zeta-1}$ to $\mathbb{R}^{d_\zeta}$ and denoting $\phi :\equiv E^{-1} \circ R \circ g_w$, we obtain

$$\lambda_{d_\zeta-1}\left(\varphi^{-1}(\mathcal{V})\right) \leq \lambda_{d_\zeta-1}\left(\left(\varphi^{-1} \circ \phi^{-1}\right)\left(\partial\left(\phi\left(\mathbb{S}^{d_\zeta-1} \cap \mathcal{K}^*\right)\right)\right)\right) = 0.$$

Here, we utilized that the set $\partial\left(\phi\left(\mathbb{S}^{d_\zeta-1} \cap \mathcal{K}^*\right)\right)$ has zero measure as the boundary of the convex set $\phi\left(\mathbb{S}^{d_\zeta-1} \cap \mathcal{K}^*\right) \subseteq \mathbb{R}^{d_\zeta-1}$.

If $0 \in \partial\mathcal{Z}^{\mathrm{ad}}$, $\mathcal{K}^*$ is either a convex pointed cone, or a half-space, due to the convexity of $\mathcal{Z}^{\mathrm{ad}}$. In the first case, we can proceed as above, while in the second case, $\mathcal{H}^{d_\zeta-1}_{\mathbb{S}^{d_\zeta-1}}(\mathcal{V}) = 0$ follows directly from $\mathcal{H}^{d_\zeta-1}_{\mathbb{S}^{d_\zeta-1}}\left(\mathbb{S}^{d_\zeta-2}\right) = 0$.

We now prove the second assertion. Since $\mathcal{V}$ is compact, we have $\mathcal{V} = \bigcap_{i=1}^{\infty}(\mathcal{V})_{\varepsilon_i}$ for any monotonically decreasing null sequence $\{\varepsilon_i\}_{i\in\mathbb{N}}$ and this implies

$$0 = \mathcal{H}^{d_\zeta-1}_{\mathbb{S}^{d_\zeta-1}}(\mathcal{V}) = \mathcal{H}^{d_\zeta-1}_{\mathbb{S}^{d_\zeta-1}}\left(\bigcap_{i=1}^{\infty}(\mathcal{V})_{\varepsilon_i}\right) = \lim_{i\to\infty}\mathcal{H}^{d_\zeta-1}_{\mathbb{S}^{d_\zeta-1}}\left((\mathcal{V})_{\varepsilon_i}\right).$$

□

To show that part 2 of Assumption 11.2 is indeed satisfied, we need to make sure that the set $\mathcal{V}$ does not change too rapidly for varying designs $x \in \mathcal{X}$.

Lemma 11.5 *For all* $\varepsilon > 0$ *and all* $x \in \mathbb{R}^{d_\zeta}$, *there exists* $\delta(\varepsilon, x) > 0$ *and a set* $\mathcal{M}(\varepsilon, x) \supseteq \mathcal{V}(x)$ *such that* $\mathcal{H}^{d_\zeta-1}_{\mathbb{S}^{d_\zeta-1}}(\mathcal{M}(\varepsilon, x)) < \varepsilon$ *and*

$$\mathcal{V}(y) \subseteq \mathcal{M}(\varepsilon, x) \quad \textit{for all } y \in \mathcal{B}_{\delta(\varepsilon,x)}(x).$$

Proof. Let $\varepsilon > 0$ and $x \in \mathbb{R}^{d_\zeta}$. First, assume that $0 \notin \partial\mathcal{Z}^{\mathrm{ad}}_x$. Due to the Slater condition, there exists a $\zeta^\star \in \mathrm{int}\left(\mathcal{Z}^{\mathrm{ad}}_x\right)$. Define the functions $f^-_\phi : \mathbb{R}^n \to \mathbb{R}^n$ and $f^+_\phi : \mathbb{R}^n \to \mathbb{R}^n$ as

$$f_\phi^- : z \mapsto (z - \zeta^\star)(1 - \phi) + \zeta^\star \quad \text{and} \quad f_\phi^+ : z \mapsto (z - \zeta^\star)(1 + \phi) + \zeta^\star.$$

Moreover, let $\mathcal{Z}^-(\phi, x) := f_\phi^-\left(\mathcal{Z}_x^{\mathrm{ad}}\right), \mathcal{Z}^+(\phi, x) := f_\phi^+\left(\mathcal{Z}_x^{\mathrm{ad}}\right)$ and let $\mathcal{K}^-(\phi, x)$ and $\mathcal{K}^+(\phi, x)$ be the conical hulls of the sets $\mathcal{Z}^-(\phi, x)$ and $\mathcal{Z}^+(\phi, x)$. Set $\mathcal{K}^\pm(\phi, x) := \mathcal{K}^+(\phi, x) \setminus \mathcal{K}^-(\phi, x)$. There exists a $\phi(\varepsilon) > 0$ such that

$$\mathbb{S}^{d_\zeta - 1} \cap \mathcal{K}^\pm(\phi(\varepsilon), x) \subseteq \mathcal{V}_\varepsilon(x).$$

There exists a $\delta(\varepsilon, x) > 0$ such that the inclusion $\partial\mathcal{Z}_y^{\mathrm{ad}} \subseteq \mathcal{Z}^+(\phi, x) \setminus \mathcal{Z}^-(\phi, x)$ holds true for all $y \in \mathcal{B}_{\delta(\varepsilon,x)}(x)$. This implies $\partial\mathcal{K}^*(y) \subseteq \mathcal{K}^\pm(\phi(\varepsilon), x)$ for all $y \in \mathcal{B}_{\delta(\varepsilon,x)}(x)$. In total, we obtain

$$\mathcal{V}(y) = \mathbb{S}^{d_\zeta - 1} \cap \partial\mathcal{K}^*(y) \subseteq \mathbb{S}^{d_\zeta - 1} \cap \mathcal{K}^\pm(\phi(\varepsilon), x) \subseteq \mathcal{V}_\varepsilon(x)$$

for all $y \in \mathcal{B}_{\delta(\varepsilon,x)}(x)$, i.e., we can simply choose $\mathcal{M}(\varepsilon, x) = \mathcal{V}_\varepsilon(x)$.

In the case that $0 \in \partial\mathcal{Z}_x^{\mathrm{ad}}$, we choose

$$\mathcal{M}(\varepsilon, x) := \left\{\zeta \in \mathbb{R}^{d_\zeta} \,:\, \zeta \in \mathcal{V}_{\varepsilon/2}(x) \text{ or } -\zeta \in \mathcal{V}_{\varepsilon/2}(x)\right\}$$

and consider $\delta(\frac{\varepsilon}{2}, x)$ instead. Then, the same steps as above yield the claim. □

Remark 11.1 In the proof of Lemma 11.5, the distinction whether or not $0 \in \partial\mathcal{Z}_x^{\mathrm{ad}}$ has a simple geometric reason: If 0 is a corner of $\mathcal{Z}_x^{\mathrm{ad}}$, the set of tangential directions rapidly changes, even for minor perturbations of x. To see this, assume that $x = 1$ and

$$\mathcal{Z}_x^{\mathrm{ad}} = \{\zeta \in \mathbb{R}^2 \,:\, \|\zeta - (1, x)^T\|_\infty \leq 1\}.$$

Then, the associated tangent directions are given by $\mathcal{V}(1) = \{(1, 0)^T, (0, 1)^T\}$. However, for any $\varepsilon > 0$, we have $\mathcal{V}(1 - \varepsilon) = \{(0, 1)^T, (0, -1)^T\}$. In general, if 0 is a corner of $\mathcal{Z}_x^{\mathrm{ad}}$ and $v \in \mathcal{V}(x)$ a tangent direction, translating $\mathcal{Z}_x^{\mathrm{ad}}$ in direction $-v$ will immediately result in $-v \in \mathcal{V}(\tilde{x})$, even if $-v \notin \mathcal{V}(x)$.

Note that the same steps as in the proof of Lemma 11.5 yield an analogous result for directions passing through an edge of $\mathcal{Z}_x^{\mathrm{ad}}$. Thus, we see that, under Assumptions 11.1 and 11.3, we indeed satisfy Assumption 11.2 and are able to apply Proposition 11.1 to our numerical examples.

11.5 Applications to Capacity Maximization

In this section we want to solve the problem of capacity maximization in the setting of stationary gas flow for a small example instance, where the random demand is given by a (multivariate) Gaussian distribution. The problem formulation has already been given in Chap. 10, "From Probabilistic to Probust Constraints: Optimization under Uncertainty". We recall from Sect. 10.2.2.1 that the capacity problem in the stationary case can be reformulated as a classical probabilistic program (10.14) that

is of the form (P). The random constraints are given in (10.13). They turn out to be quadratic in both the control and the random variable. This structure allows for an easy computation of the partial derivatives and the radius function ρ needed when applying the SRD method. For each control u and spherical radial v the computation of the radius $\rho(u, v)$ (see Sect. 10.3.1.1 of Chap. 10, "From Probabilistic to Probust Constraints: Optimization under Uncertainty") just requires solving ordinary quadratic equations. For more details we refer to [12], where in addition to the algorithmic aspects also a theoretical justification for the existence of gradients of the probability function is given.

For our numerical study, we consider the capacity problem example of medium size represented in [12, Sect. 6]. Although it is not clear whether the requirements for the convergence of the CSG method hold for the capacity maximization problem, we apply the CSG method to it. Concretely, we consider the case of equal pressure bounds, where the number of inequalities to calculate the constraint function can be significantly decreased, and the case of general pressure bounds. We choose the probability level $p = 0.9$ and the penalty parameter $\lambda = 10^7$. Furthermore, we choose the all-ones vector for the linear costs and start the CSG method with the zero-vector. In total, we perform 8000 iterations with the CSG method, but since the weight calculations become very time-consuming for this number of iterations, we restrict the maximal number of old sample points used for the gradient approximation to 4000 and discard the samples that are farthest away from the actual point based on the nearest neighbor computation for the weights. Furthermore, we use an adaptive step size rule, where we start each iteration with a constant step size $\tau_0 = 5$ and increase or decrease it if the gradient steps get very small or very large. Furthermore, after the first 5000 iterations, we additionally decrease this adaptively chosen step size by the factor $1/(n - 5000)^{0.9}$ in iteration n. To evaluate the probabilities with respect to the original problem we perform a QMC-approximation with 100000 sample points. Furthermore, we perform 500 random runs for both test cases to overcome the issue of randomness in the CSG method.

First, we study again the convergence of the CSG method by looking at the objective function values over the iterations. Comparing the original objective function and the penalized version, the behavior is very similar, but due to the huge penalty parameter there is more variation for the penalized version and the values are typically larger, but the differences are small, and so, we only show the median and some quantile values for the original objective function in Fig. 11.6. Since the behavior is also very similar for the case of equal and general pressure bounds we restrict to a visualization of the general case.

We see that the medians and quantiles converge. The maximal deviations are given by 0.16 for both problem formulations. Therefore, the CSG method indeed converges, providing numerical evidence that our theoretical requirements are satisfied. Furthermore, the penalty formulation works well since the maximal returned violation by the CSG method is for both settings given by 0.01.

For the feasibility with respect to the original chance constraint we consider the QMC-approximations. We note that in the median the estimated probability always equals the desired value 0.9, but single runs can be slightly infeasible and the probabilities range from 0.88 to 0.91. Nevertheless, we can conclude that the combination of CSG and SRD is able to solve this difficult class of problems. Furthermore, the running times for both

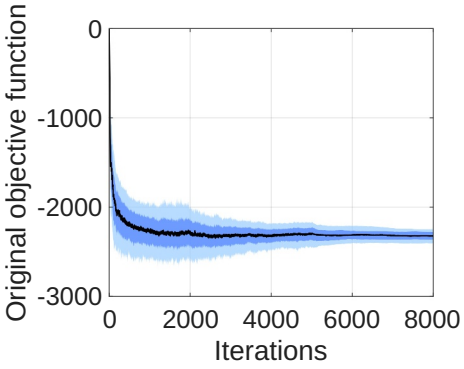


Fig. 11.6: Objective function values over iterations for the median (black line), shaded areas for quantiles $P_{0.25,0.75}$ (dark) and $P_{0.1,0.9}$ (light) for general pressure bounds

settings lie in the range of 240 to 270 seconds. We see no essential difference between the two settings since the number of total function evaluations is quite small, namely 8000, whereas Monte-Carlo based methods that require multiple function evaluations in every gradient iteration need significantly more time for the setting with general pressure bounds. Therefore, the CSG method should be preferred if the function or gradient evaluations are time-consuming and the stochastic dimension is small enough. Solving the example problem with SRD and by the built-in SQP solver of Matlab for the computation times in both settings we obtain approximately 40 and 120 seconds, respectively. Even if the SQP method in combination with SRD works faster in this example, we notice an increase of computation time of factor 3 in the general setting that involves substantial more random constraints. The CSG method turns out to be more self-contained if the effort of computing the probability function increases, which emphasizes the potential of this method.

11.6 Conclusion and Outlook

In this chapter, a new method for the solution of chance-constrained problems based on a combination of the SRD technique with the CSG method was presented. The convergence behavior of the CSG-SRD method was investigated using a class of academic test problems. Although standard assumptions required for the CSG convergence theory to hold were violated, our numerical studies demonstrated the correct behavior of the CSG method applied to the SRD formulation of the chance-constrained problem. This motivated us to establish a generalized convergence theory of the CSG method under weaker assumptions. It was also demonstrated that these weaker assumptions hold for a relevant class of problems covering the analytic test problems used in our numerical experiments. Beyond this, the CSG method using SRD has been applied to capacity maximization problems for gas networks. While for this problem it is open, if our new

convergence framework applies, again convincing numerical results could be obtained. A comparison to classical Monte-Carlo based approaches shows that our method needs far fewer function evaluations, and is therefore especially useful if function evaluations are time-consuming. As an extension of the presented capacity maximization problems with chance constraints relying on the algebraic gas model, our proposed method should be very efficient when moving to models including ODEs or PDEs as explained in Chap. 2, "A Catalog of Gas Network Models: PDEs, Coupling Conditions, and Numerical Schemes" of this book.

Acknowledgements This work was supported by the German Research Foundation (DFG) within Subprojects B04, B06, and B10 in the Sonderforschungsbereich/Transregio 154 "Mathematical Modelling, Simulation and Optimization using the Example of Gas Networks" (Project ID 239904186).

References

1. S. Ahmed and A. Shapiro. Solving chance-constrained stochastic programs via sampling and integer programming. In *State-of-the-art decision-making tools in the information-intensive age*, pages 261–269. Informs, 2008. doi:10.1287/educ.1080.0048.
2. A. Ben-Tal and A. Nemirovski. Robust convex optimization. *Mathematics of operations research*, 23(4):769–805, 1998. doi:10.1287/moor.23.4.769.
3. A. Ben-Tal and A. Nemirovski. Robust solutions of linear programming problems contaminated with uncertain data. *Mathematical programming*, 88:411–424, 2000. doi:10.1007/PL00011380.
4. D. Bernhard, F. Liers, M. Stingl, and A. Uihlein. A gradient-based method for joint chance-constrained optimization with continuous distributions. *Optimization Methods and Software*, 41(1):38–81, 2026. doi:10.1080/10556788.2025.2581585.
5. F. Besau. *Binary operations and floating bodies in spherical convexity*. PhD thesis, TU Wien, 2014. doi:10.34726/HSS.2014.27501.
6. L. Bottou, F. E. Curtis, and J. Nocedal. Optimization methods for large-scale machine learning. *SIAM Review*, 60(2):223–311, 2018. doi:10.1137/16M1080173.
7. G. Calafiore and M. C. Campi. Uncertain convex programs: randomized solutions and confidence levels. *Mathematical Programming*, 102:25–46, 2005. doi:10.1007/s10107-003-0499-y.
8. A. Charnes, W. W. Cooper, and G. H. Symonds. Cost horizons and certainty equivalents: An approach to stochastic programming of heating oil. *Management science*, 4(3):235–263, 1958. doi:10.1287/mnsc.4.3.235.
9. K.-T. Fang, S. Kotz, and K. W. Ng. *Symmetric Multivariate and Related Distributions*. Chapman and Hall/CRC, 2018. doi:10.1201/9781351077040.
10. C. Geiersbach, R. Henrion, and P. Pérez-Aros. Numerical solution of an optimal control problem with probabilistic and almost sure state constraints. *Journal of Optimization Theory and Applications*, 204(1), 2024. doi:10.1007/s10957-024-02578-0.
11. M. Grieshammer, L. Pflug, M. Stingl, and A. Uihlein. The continuous stochastic gradient method: part i–convergence theory. *Computational Optimization and Applications*, 87(3):935–976, 2023. doi:10.1007/s10589-023-00542-8.
12. H. Heitsch. On probabilistic capacity maximization in a stationary gas network. *Optimization*, 69(3):575–604, 2019. doi:10.1080/02331934.2019.1625353.
13. R. Henrion, G. Stadler, and F. Wechsung. Optimal control under uncertainty with joint chance state constraints: Almost-everywhere bounds, variance reduction, and application to (bi)linear elliptic PDEs. *SIAM/ASA Journal on Uncertainty Quantification*, 13(3):1028–1053, 2025. doi:10.1137/24m171557x.
14. L. J. Hong, Y. Yang, and L. Zhang. Sequential convex approximations to joint chance constrained programs: A Monte Carlo approach. *Operations Research*, 59(3):617–630, 2011. doi:10.1287/opre.1100.0910.

15. J. Luedtke and S. Ahmed. A sample approximation approach for optimization with probabilistic constraints. *SIAM Journal on Optimization*, 19(2):674–699, 2008. doi:10.1137/070702928.
16. A. Nemirovski and A. Shapiro. Scenario approximations of chance constraints. *Probabilistic and randomized methods for design under uncertainty*, pages 3–47, 2006. doi:10.1007/1-84628-095-8_1.
17. A. Nemirovski and A. Shapiro. Convex approximations of chance constrained programs. *SIAM Journal on Optimization*, 17(4):969–996, 2007. doi:10.1137/050622328.
18. B. K. Pagnoncelli, S. Ahmed, and A. Shapiro. Sample average approximation method for chance constrained programming: Theory and applications. *Journal of optimization theory and applications*, 142(2):399–416, 2009. doi:10.1007/s10957-009-9523-6.
19. L. Pflug, N. Bernhardt, M. Grieshammer, and M. Stingl. CSG: A new stochastic gradient method for the efficient solution of structural optimization problems with infinitely many states. *Structural and Multidisciplinary Optimization*, 61(6):2595–2611, 2020. doi:10.1007/s00158-020-02571-x.
20. A. Prékopa. *Stochastic Programming*. Mathematics and Its Applications. Springer Netherlands, 1995. doi:10.1007/978-94-017-3087-7.
21. Y. H. Ren, Y. Xiong, Y. H. Yan, and J. Gu. A smooth approximation approach for optimization with probabilistic constraints based on sigmoid function. *Journal of Inequalities and Applications*, 2022(1), 2022. doi:10.1186/s13660-022-02774-4.
22. H. Robbins and S. Monro. A stochastic approximation method. *Annals of Mathematical Statistics*, 22:400–407, 1951. doi:10.1214/aoms/1177729586.
23. R. T. Rockafellar and S. Uryasev. Optimization of conditional value-at-risk. *The Journal of Risk*, 2(3):21–41, 2000. doi:10.21314/jor.2000.038.
24. F. Shan, X. T. Xiao, and L. W. Zhang. Convergence analysis on a smoothing approach to joint chance constrained programs. *Optimization*, 65(12):2171–2193, 2016. doi:10.1080/02331934.2016.1233551.
25. F. Shan, L. Zhang, and X. Xiao. A smoothing function approach to joint chance-constrained programs. *Journal of Optimization Theory and Applications*, 163(1):181–199, 2014. doi:10.1007/s10957-013-0513-3.
26. W. S. van Ackooij and W. L. de Oliveira. *Methods of Nonsmooth Optimization in Stochastic Programming: From Conceptual Algorithms to Real-World Applications*. Springer Nature Switzerland, 2025. doi:10.1007/978-3-031-84837-7.
27. M. Wang, E. X. Fang, and H. Liu. Stochastic compositional gradient descent: Algorithms for minimizing compositions of expected-value functions. *Mathematical Programming*, 161(1–2):419–449, 2016. doi:10.1007/s10107-016-1017-3.
28. Y. Yuan, Z. Li, and B. Huang. Robust optimization approximation for joint chance constrained optimization problem. *Journal of Global Optimization*, 67:805–827, 2017. doi:10.1007/s10898-016-0438-0.

Open Access This chapter is licensed under the terms of the Creative Commons Attribution-NonCommercial-NoDerivatives 4.0 International License (http://creativecommons.org/licenses/by-nc-nd/4.0/), which permits any noncommercial use, sharing, distribution and reproduction in any medium or format, as long as you give appropriate credit to the original author(s) and the source, provide a link to the Creative Commons license and indicate if you modified the licensed material. You do not have permission under this license to share adapted material derived from this chapter or parts of it.

The images or other third party material in this chapter are included in the chapter's Creative Commons license, unless indicated otherwise in a credit line to the material. If material is not included in the chapter's Creative Commons license and your intended use is not permitted by statutory regulation or exceeds the permitted use, you will need to obtain permission directly from the copyright holder.





Chapter 12
Incremental–Decremental Optimization for the Transition to Hydrogen

Yann Disser[0000−0002−2085−0454],
Max Klimm[0000−0002−9061−2267],
Annette Lutz[0009−0008−7699−7018], and
Lea Strubberg[0009−0009−8505−3614]

Abstract Incremental–decremental optimization is a mathematical framework to capture the gradual transformation or renewal of infrastructures. Elements are transformed one at a time while minimizing the operational costs or maximizing the utility of the transformed and untransformed parts. We present an algorithm for finding an order in which to transform the elements such that the cost or utility is close to the optimum value in each step. Additionally, two examples are given for applying the framework to the transition from natural gas to hydrogen networks. Known bounds for incremental–decremental maximization are surveyed.

12.1 Transition from Gas to Hydrogen Networks

To achieve carbon-neutrality, a major transition from natural gas to hydrogen infrastructure is planned in Europe [11]. In Germany, the approved Hydrogen Core Network totals 9,040 km of which 56 % are converted from existing gas pipelines [4]. In this chapter, we give a mathematical framework, called incremental–decremental optimization, that addresses the question in which order the infrastructure should be repurposed.

We first discuss incremental–decremental *minimization*. In the incremental–decremental minimization problem, we are given two objective functions $g\colon 2^E \to \mathbb{R}_{\geq 0}$ and $h\colon 2^E \to \mathbb{R}_{\geq 0}$ defined on a finite set E of n elements, where g and h model the operating cost of the natural gas and hydrogen network on a subset of the network elements,

Yann Disser
Department of Mathematics, TU Darmstadt, Germany, e-mail: disser@mathematik.tu-darmstadt.de

Max Klimm
Institute of Mathematics, TU Berlin, Germany, e-mail: klimm@math.tu-berlin.de

Annette Lutz
Department of Mathematics, TU Darmstadt, Germany, e-mail: lutz@mathematik.tu-darmstadt.de

Lea Strubberg
Institute of Mathematics, TU Berlin, Germany, e-mail: strubberg@math.tu-berlin.de

© The Author(s) 2027

A. Martin et al. (eds.), *Mathematical Modelling, Simulation and Optimization using the Example of Gas Networks*, International Series of Numerical Mathematics 174,
https://doi.org/10.1007/978-3-032-34969-9_12

respectively. Then, $f\colon 2^E \to \mathbb{R}_{\geq 0}$ defined as $f(S) := h(S) + g(E \setminus S)$ gives the overall operating cost after repurposing a subset S and $S_k^* = \arg\min_{S\subseteq E}\{f(S) : |S| = k\}$ is the optimum solution minimizing the operating cost after repurposing k elements. The goal is to find the best order $(e_1, \ldots, e_n)$ in which to renew the elements such that in each step the cost of the partial solution $S_k := \{e_1, \ldots, e_k\}$ is as close as possible to the optimum value. That is, we want to minimize the competitive ratio

$$\rho := \max_{k\in\{1,\ldots,n\}} \min\{r \in \mathbb{R}_{\geq 0} : f(S_k) \leq r f(S_k^*)\}. \tag{12.1}$$

An order $(e_1, \ldots, e_n)$ is called a solution of the incremental–decremental problem. It is called ρ-competitive if its competitive ratio does not exceed ρ. An algorithm that obtains a succinct representation of the functions g and h on the set E as input, and returns a solution, is called ρ-competitive if all its computed solutions are ρ-competitive.

12.1.1 Chaper Outline

The remainder of this chapter is organized as follows. In Sect. 12.2, we introduce a double-greedy algorithm for incremental-decremental minimization. Initially, the algorithm has no element earmarked for early or late transition. In each step, the algorithm selects an element that provides the minimal increase in cost for either the new cost structure h or the old cost structure g. If the cost increase was minimal for h, it adds the element to the front of the sequence, and if the cost increase was minimal for g, the element is added to the back of the sequence.

In Sect. 12.3, we illustrate its performance on a transition challenge in a subnetwork of the German gas network. More specifically, the task is to convert possible exit nodes in the network (that correspond to energy consumers) from being gas consumers to being hydrogen consumers while minimizing a certain objective related to the operation of the networks in intermediate time steps.

In Sect. 12.4, we consider incremental–decremental *maximization* that has been introduced in [7] and is the maximization counterpart of the incremental–decremental minimization problems. Here, the functions g and h represent the utility of the gas or hydrogen network on a subset of elements, where f is defined as the overall value after repurposing a set of elements. Then, the optimum solution maximizing the utility is $S_k^* = \arg\max_{S\subseteq E}\{f(S) : |S| = k\}$ and the goal is to find an order $(e_1, \ldots, e_n)$ maximizing the value of the partial solutions S_k. Again, we want to minimize the competitive ratio, which for maximization is defined as follows

$$\rho := \max_{k\in\{1,\ldots,n\}} \min\{r \in \mathbb{R}_{\geq 0} : r f(S_k) \geq f(S_k^*)\}. \tag{12.2}$$

We show that the double-greedy algorithm achieves a competitive ratio of $1 + \frac{\mathrm{e}}{\mathrm{e}-1}$ when both g and h are submodular. Further known bounds on the competitive ratio for incremental–decremental maximization are mentioned in Sect. 12.4.1.

12.1.2 Related Work

Incremental optimization problems, where solutions must be near-optimal at every intermediate cardinality, were introduced by Hassin and Rubinstein [16]. They asked for matchings with the property that for each k, the total weight of the k heaviest edges in the matching provides a good approximation for the best matching of k edges. Matuschke et al. [19] showed that for this problem, the achievable approximation factor can be decreased by considering randomization. Goemans and Unda [13] considered incremental variants of classical combinatorial optimization problems. They, however, aimed to approximate the *average* performance of a solution where the average is taken over all intermediate solutions, and provided approximation guarantees for a large class of combinatorial optimization problems. Hartline and Sharp [15] considered an incremental flow problem where the capacities increase over time. Bernstein et al. [1] derived general bounds for incremental maximization and highlighted structural barriers that distinguish incremental objectives from their static counterparts. More recently, Disser et al. [8–10] provided further and improved results in these directions.

Lin et al. [18] studied incremental *minimization* problems and developed a general approximation framework motivated by hierarchical clustering and facility location. In particular, they showed that greedy-style algorithms provide bounded competitive ratios.

The incremental–decremental setting considered in this chapter generalizes these models by allowing simultaneous growth and shrinkage of two coupled systems. In particular, while classical incremental optimization corresponds to the special case where one objective function is identically zero, the incremental–decremental framework captures trade-offs between legacy and emerging infrastructures at every intermediate step. Incremental–decremental maximization was formally introduced and analyzed by Disser et al. [7], who established upper and lower bounds on the achievable competitive ratios under various structural assumptions, including submodularity, bounded curvature, and gross substitutability. The present chapter builds directly on that work, both algorithmically and analytically, and complements it by illustrating its relevance in a concrete infrastructure transition context.

The algorithmic design in this chapter is inspired by the seminal double-greedy algorithm of Buchbinder et al. [3] for unconstrained non-monotone submodular maximization, later refined and analyzed by Feige et al. [12]. Double-greedy methods maintain two complementary partial solutions that grow towards each other, enabling constant-factor approximations in settings where classical greedy algorithms fail. However, the problem studied here differs fundamentally from unconstrained submodular maximization. The presence of cardinality constraints at every intermediate step, combined with the interaction of two objective functions (representing gas and hydrogen networks), prevents a direct transfer of existing analyses. As a result, the competitive guarantees for incremental–decremental maximization require new arguments, as developed by Disser et al. [7], and no such guarantees are currently known for minimization.

12.2 Double-Greedy Algorithm

The double-greedy algorithm that we propose for incremental-decremental minimization proceeds in steps. In each step, it chooses an element with the lowest marginal increase for g or h and adds the element at the beginning or at the end of the ordering, respectively. The marginal increase measures how much the value increases when an element is added to the given solution. We introduce the notation $f(e \mid S) := f(\{e\} \cup S) - f(S)$ for the marginal increase in $f\colon 2^E \to \mathbb{R}_{\geq 0}$ of an element $e \in E$ with respect to $S \subseteq E$.

More precisely, initially, both the considered prefix and the considered suffix of the solution are empty. In each step, we compute for each remaining element its marginal increase in g relative to the current suffix, as well as its increase in h relative to the current prefix. Among all the remaining elements, we then choose the element with the smallest marginal increase in either g or h. It is then appended to the end of the current prefix if the minimum is attained for h, or to the start of the current suffix if the minimum is attained for g. For an illustration, see Fig. 12.1, and for the formal definition, we refer to the double-greedy algorithm for minimization above.

Algorithm 1 Double-greedy algorithm for minimization

input: $g, h\colon 2^E \to \mathbb{R}_{\geq 0}$ monotone
output: Ordering $(e_1, \ldots, e_n)$ of the elements in E
  $G_0 \leftarrow \emptyset$; $H_0 \leftarrow \emptyset$
  for $i \leftarrow 1, \ldots, n$:
    $e_i^* \leftarrow \arg\min\{\min\{g(e \mid G_{i-1}), h(e \mid H_{i-1})\} : e \in E \setminus (G_{i-1} \cup H_{i-1})\}$
    if $g(e_i^* \mid G_{i-1}) \leq h(e_i^* \mid H_{i-1})$:
      $G_i \leftarrow G_{i-1} \cup \{e_i^*\}$
      $H_i \leftarrow H_{i-1}$
      $e_{n-|G_i|+1} \leftarrow e_i^*$
    else
      $H_i \leftarrow H_{i-1} \cup \{e_i^*\}$
      $G_i \leftarrow G_{i-1}$
      $e_{|H_i|} \leftarrow e_i^*$

  return $(e_1, \ldots, e_n)$

In the next section, we explain the model for minimizing operational costs and illustrate the performance of the double-greedy algorithm on an example subinstance of the German gas network.

For incremental–decremental maximization, we modify the double-greedy algorithm to choose in each step an element with the highest marginal increase for g or h, see double-greedy algorithm for maximization. For this setting, the double-greedy algorithm is introduced and analyzed in [7]. Upper bounds on the competitive ratio are derived for the cases where the objective functions are submodular, gross substitute, or have a bounded generic submodularity ratio. In the first and last cases, if the functions also have bounded curvature, improved bounds are shown. We give an overview of

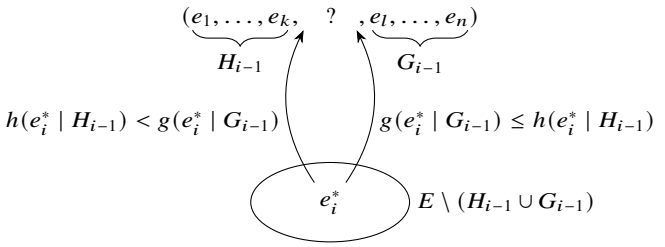


Fig. 12.1: In step i the double-greedy algorithm chooses the element e_i^* minimizing $\min\{g(e \mid G_{i-1}), h(e \mid H_{i-1})\}$ among the remaining elements $e \in E \setminus (G_{i-1} \cup H_{i-1})$ adding it to H_{i-1} or G_{i-1} depending on which marginal increase, $g(e_i^* \mid G_{i-1})$ or $h(e_i^* \mid H_{i-1})$, is smaller.

the upper bounds on the competitive ratio for incremental-decremental maximization achieved by the double-greedy algorithm in Sect. 12.4.

Algorithm 2 Double-greedy algorithm for maximization

input: $g, h\colon 2^E \to \mathbb{R}_{\geq 0}$ monotone
output: ordering $(e_1, \ldots, e_n)$ of the elements in E
  $G_0 \leftarrow \emptyset$; $H_0 \leftarrow \emptyset$
  for $i \leftarrow 1, \ldots, n$:
    $e_i^* \leftarrow \arg\max\{\max\{g(e \mid G_{i-1}), h(e \mid H_{i-1})\} : e \in E \setminus (G_{i-1} \cup H_{i-1})\}$
    if $h(e_i^* \mid H_{i-1}) \leq g(e_i^* \mid G_{i-1})$:
      $G_i \leftarrow G_{i-1} \cup \{e_i^*\}$
      $H_i \leftarrow H_{i-1}$
      $e_{n-|G_i|+1} \leftarrow e_i^*$
    else
      $H_i \leftarrow H_{i-1} \cup \{e_i^*\}$
      $G_i \leftarrow G_{i-1}$
      $e_{|H_i|} \leftarrow e_i^*$

  return $(e_1, \ldots, e_n)$

12.3 Incremental–Decremental Minimization of Operating Costs

In this section, we illustrate the algorithm for a concrete application. More precisely, we investigate the performance of the double-greedy algorithm for incremental-decremental minimization of the operating costs of a gas network that transitions from operation with natural gas to hydrogen on an example instance. In the beginning, we are given a natural gas network, with exactly one entry and several exit nodes, that is to be decommissioned over time while simultaneously building up a new hydrogen network.

In each time step, we choose one exit node to cut off from the natural gas supply and connect it to the hydrogen network instead.

Formally, we are given a tree network $G = (V, A)$ with a unique entry node $s \in V$, where natural gas and hydrogen are provided, and several exit nodes $E \subseteq V$. We assume all arcs are directed away from the entry node. All exit nodes $v \in E$ have an energy demand which can be fulfilled by a certain amount of natural gas d_v^g or hydrogen d_v^h. At the beginning, all exit nodes are provided with natural gas. In each step, we renew one of the exit nodes to be operated with hydrogen instead of natural gas. Our goal is to find an order to renew the exit nodes so that the operating cost of the network is minimized in all steps.

In practice, the pressure needs to stay within certain bounds, which is achieved by inserting compressors into the network when the loss is too large. This motivates us to model the operating cost via the maximum potential loss in the network. For each arc $a \in A$, the flow x_a is induced by potentials π_v corresponding to the squared pressure in its endpoints. In particular, in gas networks, we have

$$\pi_u - \pi_v = \beta_a |x_a| x_a \tag{12.3}$$

for every arc $a = (u, v)$ where β_a is the resistance of arc a, see (7.1) and (7.2) in Chap. 7, "Potential-Based Flows – An Overview". The resistances of the arcs also depend on the type of gas. When a subset of the exit nodes $S \subseteq E$ is renewed, we obtain the following balance vector for the hydrogen network

$$b_v^h(S) := \begin{cases} d_v^h & \text{for all renewed exit nodes } v \in S, \\ 0 & \text{for all remaining exit nodes } v \in E \setminus S, \\ 0 & \text{for all non-terminals } v \in V \setminus (E \cup \{s\}) \text{ and} \\ -\sum_{w \in S} d_w^h & \text{for the entry node} s = v. \end{cases}$$

Likewise, the balance vector for a subset $S \subseteq E$ of renewed exit nodes in the gas network is given by

$$b_v^g(S') := \begin{cases} 0 & \text{for all renewed exit nodes } v \in S, \\ d_v^g & \text{for all remaining exit nodes } v \in E \setminus S, \\ 0 & \text{for all non-terminals } v \in V \setminus (E \cup \{s\}) \text{ and} \\ -\sum_{w \in S} d_w^g & \text{for the entry node } s = v. \end{cases}$$

Since G is a tree, we obtain unique flows $x^h(S)$ and $x^g(S)$ in the hydrogen and the natural gas network fulfilling the balances at all vertices, i.e.,

$$b_v^h(S) = \sum_{a \in \delta^+(v)} x_a^h(S) - \sum_{a \in \delta^-(v)} x_a^h(S) \quad \text{and} \quad b_v^g(S) = \sum_{a \in \delta^+(v)} x_a^g(S) - \sum_{a \in \delta^-(v)} x_a^g(S),$$

where $\delta^+(v) := \{(v, w) \mid (v, w) \in A\}$ denotes the set of edges leaving v and $\delta^-(v) := \{(u, v) \mid (u, v) \in A\}$ denotes the set of edges entering v. The flow obtained by these balances also induces potentials $\pi^g(S)$ and $\pi^h(S)$, that are unique up to shifting all

entries by a constant, fulfilling (12.3) with resistances depending on the gas type, see Theorem 7.1 in Chap. 7, "Potential-Based Flows – An Overview".

We normalize both the potential differences in the gas and hydrogen network by dividing by the corresponding maximal potential difference (that is obtained when all exit nodes are operated with natural gas or hydrogen, respectively). Thus, the cost for providing a subset S of the exit nodes with natural gas or hydrogen is

$$g(S) := \frac{\pi_s^g(S) - \min_{v\in V} \pi_v^g(S)}{\pi_s^g(E) - \min_{v\in V} \pi_v^g(E)} \quad \text{or} \quad h(S) := \frac{\pi_s^h(S) - \min_{v\in V} \pi_v^h(S)}{\pi_s^h(E) - \min_{v\in V} \pi_v^h(E)}, \tag{12.4}$$

respectively.

In the following, we investigate the competitive ratio of the double-greedy algorithm on a subinstance of the German natural gas network. For this purpose, we use the combined natural gas–hydrogen instance described in Chap. 21, "Gas2Hydro – A Combined Natural Gas–Hydrogen Instance". For better illustration, we consider a subinstance, depicted in Fig. 12.2, of the `natural_gas.net` file. For this subinstance, we introduce one artificial entry node with the label s = GK marked in green. The exit nodes are E = {BB, BG, DD, GZ, LF, MB, MN, NR, OP, ZH}, where the labeled graph is shown in Fig. 12.3.

For the demand scenario, we set an equal demand of $d_v^g = 10{,}000 \frac{\mathrm{m}^3}{\mathrm{h}}$ at each exit node $v \in E$ for the natural gas case. This corresponds to a demand of $d_v^h = 28{,}602 \frac{\mathrm{m}^3}{\mathrm{h}}$ volumetric flow of hydrogen, where the factor of

$$2.8602 \approx \frac{36.4543670654\ \mathrm{MJ/m^3}}{12.745\ \mathrm{MJ/m^3}}$$

stems from the ratio of the calorific values of natural gas and hydrogen as stated in Chap. 21, "Gas2Hydro – A Combined Natural Gas–Hydrogen Instance". The resistances β_a^g and β_a^h are computed according to model ISO4 introduced in Chap. 2, "A Catalog of Gas Network Models: PDEs, Coupling Conditions, and Numerical Schemes"

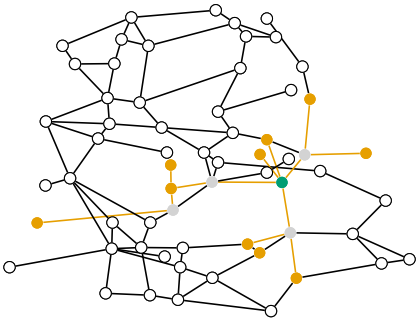
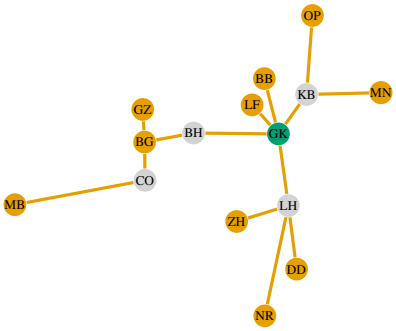
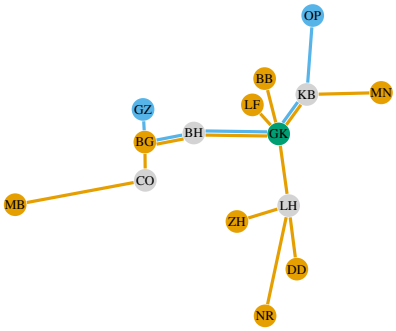


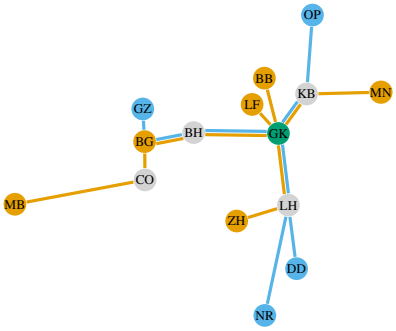
Fig. 12.2: Tree subinstance (orange and gray vertices and orange edges) within the remaining gas network in eastern Germany (hollow vertices); entry node marked in green.



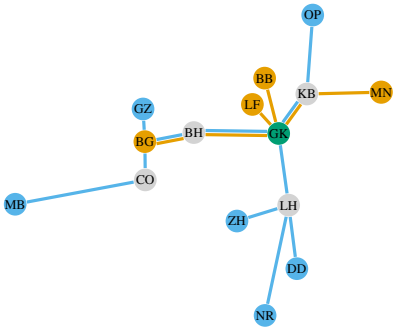
(a) Step 0



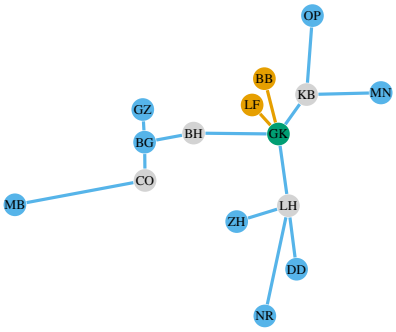
(b) Step 2



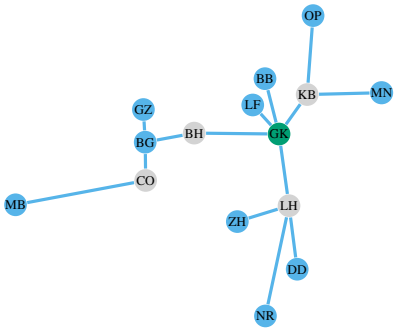
(c) Step 4



(d) Step 6



(e) Step 8



(f) Step 10

Fig. 12.3: Transition of the network from gas to hydrogen

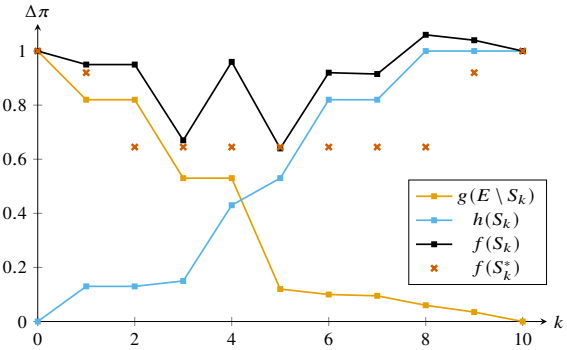


Fig. 12.4: Normalized potential difference $\Delta\pi$ as defined in (12.4) in the incremental–decremental solution computed by the double-greedy algorithm where $g(E \setminus S_k)$ shows the values for the natural gas network, $h(S_k)$ the values for the hydrogen network, $f(S_k)$ their sum, and $f(S_k^*)$ a corresponding optimal solution for each value of k.

using Nikuradze's formula for the pipe friction coefficient and the AGA model for the mean compressibility factor with physical quantities given in Chap. 21, "Gas2Hydro – A Combined Natural Gas–Hydrogen Instance" for every arc $a \in A$.

The double-greedy algorithm computes the solution

$$(\mathrm{GZ}, \mathrm{OP}, \mathrm{DD}, \mathrm{NR}, \mathrm{MB}, \mathrm{ZH}, \mathrm{MN}, \mathrm{BG}, \mathrm{BB}, \mathrm{LF})$$

that is 1.6466-competitive on this instance.

The transition of the graph from natural gas to hydrogen according to this solution is depicted in Fig. 12.3, where the natural gas network is shown in orange and the hydrogen network in blue. At each step of the transition, one exit node is disconnected from the natural gas network and connected to the hydrogen network. The parallel orange and blue arcs indicate connections that must exist in both the natural gas and hydrogen networks during that transition step.

The objective values of the double-greedy solution at each transition step are shown in Fig. 12.4. The figure illustrates how the values are composed of the functions $g(E \setminus \cdot)$ and h and compares the double-greedy solution to the optimum solution S_k^* at each step k. Further it is shown that the competitive ratio is attained at step $k = 8$.

In conclusion, we see that even though there are no known *theoretical* guarantees for incremental–decremental minimization, applying the double-greedy algorithm to compute an ordering for the transition of energy customers from natural gas to hydrogen yields a solution with moderate performance.

12.4 Incremental–Decremental Maximization

In this section, we consider the incremental maximization of flow values that can be realized in the network. Let $G = (V, A)$ be a graph with a unique entry node $s \in V$ and a set $E \subseteq V$ of exit nodes. For each exit node $v \in E$, there is an upper bound $d_v \geq 0$ on the amount of flow that the node can take. We here consider a slightly different flow model where the flow is not governed by flow potentials. Instead, for each arc a, there is a capacity $u_a \geq 0$, and we require for the flow x_a on arc a that $x_a \leq u_a$. We here slightly overload terminology, assuming that also the values u_a, $a \in A$, and d_v, $v \in E$ are part of the graph. For a subset $S \subseteq E$ of exit nodes, let us denote by

$$\mathcal{F}_G(S) = \left\{ x \in \mathbb{R}^A_{\geq 0} \;\middle|\; \begin{array}{ll} x_a \leq u_a & \text{for all } a \in A, \\ \sum_{a \in \delta^-(v)} x_a - \sum_{a \in \delta^+(v)} \leq d_v & \text{for all } v \in S, \text{ and} \\ \sum_{a \in \delta^-(v)} x_a - \sum_{a \in \delta^+(v)} x_a = 0 & \text{for all } v \in V \setminus (S \cup \{s\}) \end{array} \right\}$$

the set of flows that uses only $S \subseteq E$ as exit nodes. The function $\nu_G : 2^E \to \mathbb{R}$ defined as

$$\nu_G(S) = \max\{\textstyle\sum_{v \in S} \sum_{a \in \delta^-(v)} x_a - \sum_{a \in \delta^+(v)} x_a \mid x \in \mathcal{F}_G(S)\}$$

is called the *characteristic function* and measures how much flow can be sent in the network to the exit nodes in S. It is a well-known result from flow theory that the function ν_G is *submodular*, i.e., it satisfies the diminishing returns property

$$\nu_G(e \mid S_1) \geq v_G(e \mid S_2) \text{ for } S_1 \subseteq S_2, e \in E \setminus S_2. \tag{12.5}$$

Lemma 12.1 (Meggido [20]) *The characteristic function of a flow network is submodular.*

In the incremental–decremental setting, we assume that there are two networks $G = (V_G, A_G)$ and $H = (V_H, A_H)$ modelling the natural gas network and the hydrogen network, respectively. We further assume that there is a common set of exit nodes $E \subseteq V_G$ and $E \subseteq V_H$. Initially, the sinks, which correspond to consumers of energy, are only able to receive natural gas. Each exit $e \in E$ can be updated to receive hydrogen instead of natural gas. Our task is to find an update order so that eventually all sinks have been updated, and, in each step, the total energy that can be sent in both natural gas and hydrogen networks is a good approximation to the total energy that can be sent given this number of update steps. This yields an incremental–decremental maximization problem where the function h is defined as ν_H and g is defined as ν_G. In light of Lemma 12.1, both of these functions are submodular.

For general incremental–decremental maximization problems with submodular functions g and h, we show the following result.

Theorem 12.1 (Disser et al. [7]) *For normalized, monotone and submodular functions $h, g: 2^E \to \mathbb{R}_{\geq 0}$ the double-greedy algorithm is $(1 + \frac{e}{e-1})$-competitive for incremental-decremental maximization.*

Proof. For ease of exposition, we assume that there exist no ties when the algorithm compares elements by their marginal increase in either g or h with respect to any subset of E. In practice, this can be achieved by perturbing the values of the elements. Recall that $f\colon 2^E \to \mathbb{R}_{\geq 0}, S \mapsto f(S) = h(S) + g(E \setminus S)$, that S_k^* is the optimum solution for f of size k, i.e., $f(S_k^*) = \max_{S \subseteq E, |S|=k} f(S)$, and that $S_k = \{e_1, \ldots, e_k\}$ contains the first k elements of the order computed by the algorithm. Further recall that after iteration i of the algorithm, H_i denotes the elements contained in the current prefix and G_i denotes the elements contained in the current suffix of the output order.

First, we prove that the values $f(H_i)$ are non-decreasing for $0 \leq i \leq n$.

Claim 12.1 We have that

$$g(E) = f(H_0) \leq f(H_1) \leq \ldots \leq f(H_n). \tag{12.6}$$

Proof of Claim 12.1. The first equation follows immediately from the definition of $H_0 = \emptyset$ and of f. For the inequalities, we show $f(H_{i-1}) \leq f(H_i)$ for every $i = 1, \ldots, n$. Since the algorithm does not update the set H_i in every iteration, we focus on the case where $e_i \in H_i \setminus H_{i-1}$. By the submodularity of g and because $G_{i-1} \subseteq E \setminus H_i$ we know that $g(e_i \mid E \setminus H_i) \leq g(e_i \mid G_{i-1})$. Since the algorithm adds the element e_i to the prefix H_{i-1} and not to the suffix G_{i-1}, we conclude further that $g(e_i \mid G_{i-1}) \leq h(e_i \mid H_{i-1})$. Together with the definition of the marginal value, we obtain,

$$g(E \setminus H_{i-1}) - g(E \setminus H_i) = g(e_i \mid E \setminus H_i) \leq h(e_i \mid H_{i-1}) = h(H_i) - h(H_{i-1}),$$

which is equivalent to $f(H_{i-1}) \leq f(H_i)$. ◁

To prove that the double-greedy algorithm is $(1 + \frac{\mathrm{e}}{\mathrm{e}-1})$-competitive, we need to show that

$$f(S_k^*) \leq \left(1 + \frac{\mathrm{e}}{\mathrm{e}-1}\right) f(S_k) \qquad \text{for all } k = 1, \ldots, n.$$

We claim that it suffices to show

$$f(S_k^*) \leq \left(1 + \frac{\mathrm{e}}{\mathrm{e}-1}\right) f(H_k) \qquad \text{for all } k = 1, \ldots, |H_n|. \tag{12.7}$$

To see the claim, note that (12.7) implies the results for all $k \in \{1, \ldots, |H_n|\}$ since $f(H_k) \leq f(S_k)$ by Claim 12.1. If, on the other hand, we have $k > |H_n|$, we exchange the roles of g and h. As we assumed that there are no ties in the decisions of the algorithm, the algorithm will compute the reverse solution in that case, and we have $k \leq |H_n|$, so that it again suffices to show (12.7).

Next, we show that $f(H_k)$ approximates $h(S_k^*)$ by a factor of $\frac{\mathrm{e}}{\mathrm{e}-1}$.

Claim 12.2 We have that

$$f(H_k) \geq \frac{\mathrm{e}-1}{\mathrm{e}} h(S_k^*) \qquad \text{for all } k = 1, \ldots, |H_n|. \tag{12.8}$$

Before we prove Claim 12.2, we will first show that it implies the result. To see this, note that, by the definition of f, by (12.8) and by the fact that $f(H_k) \geq g(E) \geq g(E \setminus S_k^*)$,

due to (12.6), and monotonicity of g, we have

$$\begin{aligned} f(S_k^*) &= h(S_k^*) + g(E \setminus S_k^*) \\ &\leq \frac{\mathrm{e}}{\mathrm{e}-1} f(H_k) + g(E \setminus S_k^*) \\ &\leq \frac{\mathrm{e}}{\mathrm{e}-1} f(H_k) + f(H_k). \end{aligned}$$

Thus, we have proven (12.7), which finishes the proof of the theorem.

It remains to prove Claim 12.2.

Proof of Claim 12.2. Denote by $\varphi_i := \max\{h(e_i^* \mid H_{i-1}), g(e_i^* \mid G_{i-1})\}$ the maximum marginal increase in either h or g achievable by adding element e_i^* either to the prefix H_{i-1} or to the suffix G_{i-1} after iteration i of the algorithm. By monotonicity of g, by the definition of the marginal increase, and by the definition of the algorithm, we have

$$\begin{aligned} f(H_k) &\geq h(H_k) + g(G_k) \\ &= \sum_{i:e_i^* \in H_k} h(e_i^* \mid H_{i-1}) + \sum_{i:e_i^* \in G_k} g(e_i^* \mid G_{i-1}) \\ &\geq \sum_{i=1}^{k} \varphi_i. \end{aligned} \tag{12.9}$$

Denote by $F_i := H_i \cup G_i$ the set of elements that are added to the output order after iteration i of the algorithm. Then, we have for $0 \leq i \leq k-1$ that

$$\begin{aligned} h(S_k^*) &\leq h(F_i) + h(S_k^* \setminus F_i \mid F_i) \\ &\leq \sum_{i'=1}^{i} h(e_{i'}^* \mid F_{i'-1}) + h(S_k^* \setminus F_i \mid F_i) \\ &\leq \sum_{i'=1}^{i} h(e_{i'}^* \mid H_{i'-1}) + h(S_k^* \setminus F_i \mid F_i), \end{aligned}$$

where for the last inequality, we used the submodularity of h. Using the definition of the values φ_i yields

$$h(S_k^*) \leq \sum_{i'=1}^{i} \varphi_{i'} + h(S_k^* \setminus F_i \mid F_i).$$

Let now $\{s_1, \ldots, s_m\} = S_k^* \setminus F_i$. Using the definition of the marginal increase the submodularity of h together with the fact that $H_i \subseteq F_i$, and the definition of φ_{i+1}, we obtain

$$h(S_k^*) \leq \sum_{i'=1}^{i} \varphi_{i'} + \sum_{j=1}^{m} h(s_j \mid \{s_1 \ldots, s_{j-1}\} \cup F_i)$$

$$\leq \sum_{i'=1}^{i} \varphi_{i'} + \sum_{s \in S_k^* \setminus F_i}^{m} h(s \mid H_i)$$
$$\leq \sum_{i'=1}^{i} \varphi_{i'} + |S_k^* \setminus F_i| \, \varphi_{i+1}$$
$$\leq \sum_{i'=1}^{i} \varphi_{i'} + k\varphi_{i+1}.$$

Rearranging the terms, leads to

$$h(S_k^*) \leq k \sum_{i'=1}^{i+1} \varphi_{i'} - (k-1) \sum_{i'=1}^{i} \varphi_{i'}.$$

Adding $(k-1)h(S_k^*) - k \sum_{i'=1}^{i+1} \varphi_{i'}$ and dividing by k yields

$$h(S_k^*) - \sum_{i'=1}^{i+1} \varphi_{i'} \leq \frac{k-1}{k} \left(h(S_k^*) - \sum_{i'=1}^{i} \varphi_{i'} \right) \qquad \text{for all } 0 \leq i \leq k-1.$$

Applying this inequality iteratively, we obtain

$$h(S_k^*) - \sum_{i'=1}^{k} \varphi_{i'} \leq \left(\frac{k-1}{k} \right)^k h(S_k^*).$$

Rearranging yields

$$\sum_{i'=1}^{k} \varphi_{i'} \geq \left(1 - \left(\frac{k-1}{k} \right)^k \right) h(S_k^*). \tag{12.10}$$

Finally, we conclude using inequalities (12.9) and (12.10) that

$$f(H_k) \geq \sum_{i=1}^{k} \varphi_i \geq \left(1 - \left(\frac{k-1}{k} \right)^k \right) h(S_k^*) \geq \left(1 - \frac{1}{e} \right)^k h(S_k^*).$$

◁

Thus, Theorem 12.1 is proven. □

12.4.1 Further Results for Incremental–Decremental Maximization

In this section, we briefly review further results for incremental–decremental maximization obtained by Disser et al. [7]. First, they provide a more fine-grained analysis of the competitive ratio of the double-greedy algorithm that depends on two parameters. The first such parameter is the *generic submodularity ratio* γ that has been introduced by Gong et al. [14] and builds upon the closely related concept of the submodularity

ratio introduced by Das and Kempe [6]. The generic submodularity ratio γ is defined as

$$\gamma := \min\left\{ \frac{f(e \mid A)}{f(e \mid A \cup B)} : A, B \in 2^E, e \in E \text{ with } f(e \mid A \cup B) > 0 \right\}.$$

Intuitively, the generic submodularity ratio interpolates between general monotone functions with $\gamma = 0$ and submodular functions with $\gamma = 1$. To see this, note that for a submodular function, we have $f(e \mid A) \geq f(e \mid A \cup B)$ for all $A, B \in 2^E$ and $e \in E$, so that the minimum is attained for $B = \emptyset$ and the generic submodularity ratio is $\gamma = 1$.

The second such parameter is the curvature c. It has been introduced for monotone submodular functions by Conforti and Cornuéjols [5] and generalized to general monotone functions by Bian et al. [2]. In the latter case, it is defined as

$$c := 1 - \min\left\{ \frac{f(e \mid A \cup B)}{f(e \mid A)} : A, B \in 2^E, e \in E \setminus B \text{ with } f(e \mid A) > 0 \right\}.$$

Disser et al. [7] showed that the double-greedy algorithm has a competitive ratio of at most $\frac{1}{\gamma}(1 + c\frac{e^c}{e^c - 1})$ when g and h are functions with generic submodularity ratio γ and curvature c.

Second, Disser et al. [7] provided an improved bound on the competitive ratio of the double-greedy algorithm for the case that g and h are *gross substitute* functions, which are a subclass of submodular functions introduced by Kelso and Crawford [17]. Formally, a function $f\colon 2^E \to \mathbb{R}$ is *gross substitute* if for all modular price functions $p, p'\colon 2^E \to \mathbb{R}$ with $p \leq p'$ and all subsets $S \in \arg\max_{S \subseteq E}\{f(S) - p(S)\}$ there is a subset $S' \in \arg\max_{S \subseteq E}\{f(S) - p'(S)\}$ with $S \cap \{e \mid p(\{e\}) = p'(\{e\})\} \subseteq S'$.

Disser et al. [7] showed that the double-greedy algorithm is 2-competitive for incremental–decremental maximization when both g and h are gross substitute functions. They further discussed lower bounds on the competitive ratio of any algorithm for incremental–decremental maximization for different classes of functions.

Acknowledgements This work was supported by the German Research Foundation (DFG) within Subprojects A07 and A09 in the Sonderforschungsbereich/Transregio 154 "Mathematical Modelling, Simulation and Optimization using the Example of Gas Networks" (Project ID 239904186).

References

1. A. Bernstein, Y. Disser, M. Groß, and S. Himburg. General bounds for incremental maximization. *Mathematical Programming*, 191(2):953–979, 2022. doi:10.1007/s10107-020-01576-0.
2. A. A. Bian, J. M. Buhmann, A. Krause, and S. Tschiatschek. Guarantees for greedy maximization of non-submodular functions with applications. In *Proceedings of the 34th International Conference on Machine Learning (ICML)*, pages 498–507, 2017.
3. N. Buchbinder, M. Feldman, J. Naor, and R. Schwartz. A tight linear time (1/2)-approximation for unconstrained submodular maximization. *SIAM Journal on Computing*, 44(5):1384–1402, 2015. doi:10.1137/130929205.
4. Bundesnetzagentur. Bundesnetzagentur approves hydrogen core network, Oct. 2024. Accessed 2025-08-29. URL: https://www.bundesnetzagentur.de/EN/Areas/Energy/HydrogenCoreNetwork/start.html.

5. M. Conforti and G. Cornuéjols. Submodular set functions, matroids and the greedy algorithm: Tight worst-case bounds and some generalizations of the Rado-Edmonds theorem. *Discrete Applied Mathematics*, 7:251–274, 1984. doi:10.1016/0166-218X(84)90003-9.
6. A. Das and D. Kempe. Approximate submodularity and its applications: Subset selection, sparse approximation and dictionary selection. *Journal of Machine Learning Research*, 19(3):1–34, 2018.
7. Y. Disser, M. Klimm, A. Lutz, and L. Stubberg. Incremental–decremental maximization. In *Proceedings of the 23th Workshop on Approximation and Online Algorithms (WAOA)*, pages 97–110, 2025. doi:10.1007/978-3-032-06706-7_7.
8. Y. Disser, M. Klimm, K. Schewior, and D. Weckbecker. Incremental maximization via continuization. In *Proceedings of the 50th International Colloquium on Automata, Languages and Programming (ICALP)*, pages 47:1–17, 2023. doi:10.4230/LIPIcs.ICALP.2023.47.
9. Y. Disser and D. Weckbecker. Unified greedy approximability beyond submodular maximization. *SIAM Journal on Discrete Mathematics*, 38(1):348–379, 2024. doi:10.1137/22M1526952.
10. Y. Disser and D. Weckbecker. Incremental maximization for a broad class of objectives. In *Proceedings of the 33rd Annual European Symposium on Algorithms (ESA)*, pages 92:1–13, 2025. doi:10.4230/LIPIcs.ESA.2025.92.
11. European Parliament and Council of the European Union. Directive (EU) 2024/1788 of the European Parliament and of the Council of 13 June 2024 on common rules for the internal markets for renewable gas, natural gas and hydrogen. Official Journal of the European Union, L 1788, July 2024. Accessed 2025-08-29. URL: https://eur-lex.europa.eu/legal-content/EN/TXT/PDF/?uri=OJ:L_202401788.
12. U. Feige, V. S. Mirrokni, and J. Vondrak. Maximizing non-monotone submodular functions. *SIAM J. Comput.*, 40(4):1133–1153, 2011. doi:10.1137/090779346.
13. M. X. Goemans and F. Unda. Approximating incremental combinatorial optimization problems. In *Proceedings of the 20th/21st International Workshop on Approximation, Randomization, and Combinatorial Optimization. Algorithms and Techniques. (APPROX/RANDOM)*, volume 81, pages 6:1–6:14, 2017. doi:10.4230/LIPIcs.APPROX-RANDOM.2017.6.
14. S. Gong, Q. Nong, T. Sun, Q. Fang, D. Du, and X. Shao. Maximize a monotone function with a generic submodularity ratio. *Theoretical Computer Science*, 853:16–24, 2021. doi:10.1016/j.tcs.2020.05.018.
15. J. Hartline and A. Sharp. Incremental flow. *Networks*, 50(1):77–85, 2007. doi:10.1002/NET.20168.
16. R. Hassin and S. Rubinstein. Robust matchings. *SIAM Journal on Discrete Mathematics*, 15(4):530–537, 2002. doi:10.1137/S0895480198332156.
17. A. S. Kelso Jr and V. P. Crawford. Job matching, coalition formation, and gross substitutes. *Econometrica: Journal of the Econometric Society*, pages 1483–1504, 1982. doi:10.2307/1913392.
18. G. Lin, C. Nagarajan, R. Rajaraman, and D. P. Williamson. A general approach for incremental approximation and hierarchical clustering. *SIAM Journal on Computing*, 39(8):3633–3669, 2010. doi:10.1137/070698257.
19. J. Matuschke, M. Skutella, and J. A. Soto. Robust randomized matchings. *Mathematics of Operations Research*, 43(2):675–692, 2018. doi:10.1287/MOOR.2017.0878.
20. N. Megiddo. Optimal flows in networks with multiple sources and sinks. *Mathematical Programming*, 7(1):97–107, 1974. doi:10.1007/BF01585506.

Open Access This chapter is licensed under the terms of the Creative Commons Attribution-NonCommercial-NoDerivatives 4.0 International License (http://creativecommons.org/licenses/by-nc-nd/4.0/), which permits any noncommercial use, sharing, distribution and reproduction in any medium or format, as long as you give appropriate credit to the original author(s) and the source, provide a link to the Creative Commons license and indicate if you modified the licensed material. You do not have permission under this license to share adapted material derived from this chapter or parts of it.

The images or other third party material in this chapter are included in the chapter's Creative Commons license, unless indicated otherwise in a credit line to the material. If material is not included in the chapter's Creative Commons license and your intended use is not permitted by statutory regulation or exceeds the permitted use, you will need to obtain permission directly from the copyright holder.



Part IV
PDE-based Optimization and Control for Gas Network Applications

Chapter 13
Introduction to PDE-based Optimization and Control for Gas Network Applications

Falk M. Hante[0000−0001−9762−2903] and
Stefan Ulbrich[0000−0003−4036−2607]

Abstract This chapter provides an overview of the subsequent chapters focusing on contributions to the optimization and control of gas networks through physically detailed PDE-models as constraints.

The optimization of systems governed by partial differential equations (PDEs) represents one of the most challenging areas in applied mathematics. The transition from model-based numerical simulations to model-based design and optimal control is crucial for example in industrial or economic applications, as it enables the systematic improvement of system performance and efficiency. In gas network optimization, this transition is particularly valuable due to the economic and operational significance of these infrastructure systems.

Gas networks, which transport natural gas or hydrogen through pipeline systems, are governed by complex physical laws described by hyperbolic PDEs. The optimization of these networks involves determining control strategies (such as valve settings, compressor operations, or injection/extraction rates) that optimize certain objectives (such as minimizing operational costs or maximizing transport efficiency) while respecting physical constraints and operational requirements. This optimization problem is inherently challenging due to the PDE constraints, the presence of both continuous and discrete controls, the coupling conditions at network junctions, and the potential for state constraints.

A particular focus is on developing indirect solution approaches that rely on regularity properties of the underlying control-to-state map, gradient representations using adjoint equations, and appropriate treatment of both integer and state constraints. Standard methods from PDE-constrained optimization cannot be applied directly due to several factors: the heterogeneous domain of functions on graphs, the hyperbolic character of the

Falk M. Hante
Department of Mathematics, HU Berlin, Germany, e-mail: falk.hante@hu-berlin.de

Stefan Ulbrich
Department of Mathematics, TU Darmstadt, Germany, e-mail: ulbrich@mathematik.tu-darmstadt.de

© The Author(s) 2027

A. Martin et al. (eds.), *Mathematical Modelling, Simulation and Optimization using the Example of Gas Networks*, International Series of Numerical Mathematics 174,
https://doi.org/10.1007/978-3-032-34969-9_13

governing equations, the nonlinearities involved, and the complex coupling conditions at network junctions. Key challenges include

- existence and regularity of solutions to nonlinear Euler equations, including appropriate adjoint calculus;
- structural analysis such as steady-state characterizations, stabilization, controllability, and turnpike properties;
- characterizations of optimality with appropriate control- and state-constraint handling;
- decomposition techniques to keep larger systems or longer time horizons tractable;
- handling of non-smooth and combinatorial aspects in the control and the system's dynamics.

This collection of chapters advances our understanding and capabilities in gas network optimization through novel theoretical insights, methodological developments, and practical applications.

Theoretical foundations are established through the analysis of optimal control for discontinuous solutions of hyperbolic systems, examining the differentiability properties of entropy solutions for the Generalized Riemann Problem with respect to the initial state. Chap. 14, "Optimal Control of Discontinuous Solutions of Hyperbolic Systems of Balance Laws" provides crucial foundations for understanding how optimal controls influence shock positions and solution behavior in hyperbolic systems, which is fundamental to gas flow dynamics.

Attention then shifts to control methodologies, beginning with the extension of Sequential Action Control (SAC) to hybrid PDE systems in Chap. 15, "Sequential Action Control for Hybrid Dynamical Models of Gas Networks". This approach synthesizes control strategies that incorporate switches between different operational modes, addressing the practical reality of gas networks with discrete components such as valves and compressors. The development of a closed-form SAC control based on tailored adjoint calculus represents a significant step toward real-time operational capabilities.

Complementing these control methodologies, Chap. 16, "The Turnpike Property and the Optimal Control of Gas Networks", continues with structural properties of optimal solutions through the lens of the turnpike phenomenon. This analysis reveals how optimal controls and states in gas networks converge to static solutions for most of the operational horizon, with dynamic behavior concentrated at initial and terminal phases. This property has significant implications for operational planning, justifying the use of quasi-static approaches even when transient phases occur, and bridges theoretical optimal control with practical engineering considerations.

The computational challenges inherent in large-scale gas network optimization are addressed through domain decomposition techniques. The methods presented in Chap. 17, "Domain Decomposition for Gas Network Control", enable efficient and scalable simulation and optimization by decomposing complex network problems into more manageable subproblems. This includes also addressing combinatorial aspects of switching components. The exploration of randomized decomposition approaches further expands the toolkit for handling the computational complexity of transient gas network operations.

From a modeling perspective, Chap. 18, "A PDE-Constrained Generalized Nash Equilibrium Approach for Modeling Gas Transport with Strategic Suppliers", introduces game-theoretic approaches through generalized Nash equilibrium problems that capture strategic interactions among competing firms. This framework explicitly incorporates the dynamics of commodity transport into market models, allowing for the analysis of how linepacking strategies—using the network as temporary storage—affect market outcomes and which participants benefit from such practices.

In Chap. 19, "p-Wasserstein Distances on Networks and 3D to 1D Convergence", the mathematical foundations are further deepened through the study of transport distances on metric graphs representing gas networks. By examining the convergence of three-dimensional network domains to one-dimensional metric graphs and establishing the properties of p-Wasserstein distances in this context, this work provides rigorous mathematical tools for analyzing transport phenomena and optimization problems on network structures.

Together, these chapters form a comprehensive exploration of gas network optimization primarily from an optimal control theoretic perspective. They demonstrate the interdisciplinary nature of the field and highlight the connections between different aspects of gas network optimization, collectively advancing both theoretical understanding and practical solutions in this important application domain.

Acknowledgements This work was supported by the German Research Foundation (DFG) within Subprojects A02, A03, A05, B02, B07, B08, B09, C03, C05, C06, and C07 in the Sonderforschungsbereich/Transregio 154 "Mathematical Modelling, Simulation and Optimization using the Example of Gas Networks" (Project ID 239904186).

Open Access This chapter is licensed under the terms of the Creative Commons Attribution-NonCommercial-NoDerivatives 4.0 International License (http://creativecommons.org/licenses/by-nc-nd/4.0/), which permits any noncommercial use, sharing, distribution and reproduction in any medium or format, as long as you give appropriate credit to the original author(s) and the source, provide a link to the Creative Commons license and indicate if you modified the licensed material. You do not have permission under this license to share adapted material derived from this chapter or parts of it.

The images or other third party material in this chapter are included in the chapter's Creative Commons license, unless indicated otherwise in a credit line to the material. If material is not included in the chapter's Creative Commons license and your intended use is not permitted by statutory regulation or exceeds the permitted use, you will need to obtain permission directly from the copyright holder.





Chapter 14
Optimal Control of Discontinuous Solutions of Hyperbolic Systems of Balance Laws

Jannik Breitkopf[0009−0004−3640−7555] and
Stefan Ulbrich[0000−0003−4036−2607]

Abstract In this chapter, we analyze the optimal control of entropy solutions of the Generalized Riemann Problem (GRP) for strictly hyperbolic systems of conservation laws, where the control is the initial state. The GRP has a piecewise C^1-initial state with exactly one discontinuity. We assume that this discontinuity only generates shock curves but no rarefaction waves. Moreover, we assume that the time horizon $T > 0$ is sufficiently small such that no shocks interact or are newly generated. The control variable consists of the C^1-parts of the initial state and the position of the discontinuity. Since the shock positions depend on the control, we use a reference space, obtained by a transformation of the spatial variable, which keeps the shock positions a priori fixed. We then present stability and differentiability properties of the solution operator of the GRP, both in physical coordinates and in the reference space w.r.t. variations of the control. In particular, we obtain the differentiability of the shock positions and the smooth parts of the solution between the shock curves in the C^0-topology w.r.t. the control. This implies the differentiability of tracking-type objective functionals. Finally, we analyze the adjoint problem and characterize the correct reversible solution to obtain an adjoint gradient representation of a linear objective functional.

14.1 Introduction

The dynamics of a gas are described by the Euler equations (TA1) or possible extensions to the mixture of two different gases (2.40). The underlying PDEs belong to the class of hyperbolic systems of conservation or balance laws

$$y_t + f(y)_x = g(\cdot, y) \qquad \text{on } \mathcal{D}, \tag{14.1}$$

Jannik Breitkopf
Department of Mathematics, TU Darmstadt, Germany, e-mail: breitkopf@mathematik.tu-darmstadt.de

Stefan Ulbrich
Department of Mathematics, TU Darmstadt, Germany, e-mail: ulbrich@mathematik.tu-darmstadt.de

© The Author(s) 2027

A. Martin et al. (eds.), *Mathematical Modelling, Simulation and Optimization using the Example of Gas Networks*, International Series of Numerical Mathematics 174,
https://doi.org/10.1007/978-3-032-34969-9_14

on a suitable domain $\mathcal{D} \subset [0,T] \times \mathbb{R}$ such that $\mathcal{D} \cap (\{0\} \times \mathbb{R}) = \{0\} \times [-\ell, \ell]$ for some $\ell > 0$. In (14.1), $y : \mathcal{D} \to \mathbb{R}^n$ is the *state*, $f \in C^{2,1}(\mathbb{R}^n; \mathbb{R}^n)$ the *flux function*, and $g \in C^{1,1}(\mathcal{D} \times \mathbb{R}^n; \mathbb{R}^n)$ the *source term*. The system (14.1) is complemented by the initial condition

$$y(0, \cdot) = u_0. \tag{14.2}$$

A crucial feature of (14.1) is that solutions generally become discontinuous after a finite time, even if the data is arbitrarily smooth [20]. This is due to the formation of *shock curves*. Moreover, weak solutions are generally not unique. By additionally imposing an entropy condition, the physically relevant solution is characterized (Definition 14.1). Therefore, it is a natural choice to allow discontinuous initial states u_0 for (14.1).

The *Generalized Riemann Problem* (GRP) has a piecewise smooth initial state with exactly one discontinuity. Precisely, we assume for some fixed $\ell > 0$ and $\varepsilon \in (0, \ell)$ that

$$u_0(x) = \begin{cases} u_l(x) \text{ if } x \in [-\ell, x_0), \\ u_r(x) \text{ if } x \in (x_0, \ell], \end{cases} \tag{14.3}$$

where $x_0 \in (-\varepsilon, \varepsilon)$ is the location of the discontinuity, and $(u_l, u_r) \in \mathcal{V}_{\text{ad}}$ are the smooth left and right parts of u_0 for a suitable and later to be specified open subset $\mathcal{V}_{\text{ad}} \subset \mathcal{V} = C^1([-\ell, \varepsilon]; \mathbb{R}^n) \times C^1([-\varepsilon, \ell]; \mathbb{R}^n)$. This defines the set of admissible controls

$$u = (u_l, u_r, x_0) \in \mathcal{U}_{\text{ad}} := \mathcal{V}_{\text{ad}} \times (-\varepsilon, \varepsilon).$$

This chapter presents a sensitivity and adjoint calculus which is used to analyze optimal control problems of the form

$$\min_{u \in \mathcal{U}_{\text{ad}}} J(u) = \int_a^b \Phi\left(y(T,x), y_d(x)\right) \mathrm{d}x \quad \text{subject to } y \text{ solves (14.1), (14.2)} \tag{14.4}$$

with $\Phi \in C^{1,1}(\mathbb{R}^n \times \mathbb{R}^n)$ and a desired state $y_d \in BV([a,b]; \mathbb{R}^n)$, where $[a,b]$ is suitably chosen such that $\{T\} \times [a,b] \subset \mathcal{D}$.

We recall existence and regularity results for entropy solutions of the GRP. Then, we present differentiability properties of the solution w.r.t. the initial state u_0. This will also imply the differentiability of the objective functional of (14.4). Finally, we derive the adjoint problem and characterize the correct reversible solution which then yields an adjoint gradient representation.

14.1.1 Assumptions and Notation

We assume problem (14.1) to be strictly hyperbolic, i.e., the Jacobian matrix $A(y) = f'(y)$ has n real and distinct eigenvalues $\lambda_1(y) < \ldots < \lambda_n(y)$ for all $y \in \Omega$ in some open convex set $\Omega \subset \mathbb{R}^n$. Furthermore, we assume that there exist $\lambda_{\max} > 0$ and $\eta_{\min} > 0$ such that $|\lambda_i(y)| \leq \lambda_{\max}$ and $|\lambda_i(y) - \lambda_j(y)| \geq \eta_{\min}$ for all $y \in \Omega$ and $i \neq j \in \{1, \ldots, n\}$.

With $r_i(y), l_i(y) \in \mathbb{R}^n$, we denote the right and left eigenvectors of $A(y)$, i.e.,

$$A(y)r_i(y) = \lambda_i(y)r_i(y), \quad l_i(y)^\top A(y) = \lambda_i(y)l_i(y)^\top, \qquad |r_i(y)| \equiv 1,$$

and all $l_i(y)$ normalized such that for all $y \in \Omega$ it holds that $l_i(y)^\top r_j(y) = 0$ for $i \neq j$ and $l_i(y)^\top r_i(y) = 1$. We assume all characteristic fields $i \in \{1, \dots, n\}$ to be either *genuinely nonlinear*, i.e., $\nabla\lambda_i(y)^\top r_i(y) \neq 0$ for all $y \in \Omega$, or *linearly degenerate*, i.e., $\nabla\lambda_i(y)^\top r_i(y) = 0$. These are standard assumptions in the literature, see, e.g., [8, 14], and are also satisfied by the Euler equations, see Sect. 2.2.

We assume that the underlying domain is of the form

$$\mathcal{D} = \{(t, x) \in [0, T] \times \mathbb{R} \mid -\ell + t\lambda_{\max} \leq x \leq \ell - t\lambda_{\max}\}.$$

Note a solution on $\mathcal{D}$ is fully determined by the initial state on $[-\ell, \ell]$.

We use the notation $[n] := \{1, \dots, n\}$ and $[n]_0 := \{0, \dots, n\}$.

14.1.2 Related Literature

For scalar conservation laws, differentiability properties of entropy solutions w.r.t. the initial state are investigated, e.g., in [4, 9]. General variations of the smooth parts and of the positions of the discontinuities in the initial state are considered in [21] and extended to initial–boundary value problems in [16, 19]. Convergent numerical schemes of the adjoint problem are discussed in [17, 18].

Existence theories for entropy solutions of systems of conservation laws with discontinuous initial data have been established in the class of *BV* functions [8] and for piecewise smooth solutions [15]. A variational calculus for piecewise Lipschitz continuous solutions w.r.t. directional variations of the initial data is given in [10] and corresponding optimality conditions are derived in [11]. Another approach by horizontal shifts of initial controls is proposed in [2]. A formal sensitivity and adjoint computation for systems with piecewise smooth solutions and exactly one shock curve can be found in [1]. The optimal boundary control of classical solutions of networked quasilinear hyperbolic systems on a graph for small time horizons is discussed in [5].

14.2 Existence and Regularity Properties of Entropy Solutions

In this section, we recall existence and regularity properties of entropy solutions of the GRP, provided that suitable smallness assumptions are satisfied.

Weak solutions of (14.1) are generally not unique. To characterize the physically relevant one, an *entropy condition* is imposed. We use the *Lax Entropy Condition* [14]. The structure of *BV* functions is discussed, for instance, in [13, Sect. 1.7].

Definition 14.1 A function $y \in BV(\mathcal{D}; \mathbb{R}^n)$ is an *entropy solution* of (14.1) if

(i) y is a weak solution, i.e., $\operatorname{ess\,lim}_{t \searrow 0} \|y(t, \cdot) - u_0\|_{L^1(\mathbb{R}; \mathbb{R}^n)} = 0$ and

$$\int_{\mathcal{D}} y^\top \phi_t + f(y)^\top \phi_x + g(\cdot, y)^\top \phi = 0 \quad \forall \phi \in C_c^\infty(\mathcal{D}; \mathbb{R}^n) \text{ with } \phi|_{\partial\mathcal{D}} = 0.$$

(ii) Let $\mathcal{J} \subset \mathcal{D}$ be the set of approximate jump discontinuities of y. Then for almost all $(t,x) \in \mathcal{J}$ w.r.t. the one dimensional Hausdorff measure, one can associate a normal vector $\widehat{n} = (-s, 1)^\top \in \mathbb{R}^2$ and one-sided limits $y^\pm$. The Lax entropy condition requires that for some $j \in [n]$ it holds

$$\lambda_j(y^-) \geq s \geq \lambda_j(y^+), \quad \lambda_k(y^\pm) > s > \lambda_i(y^\pm) \quad \forall i < j < k. \tag{14.5}$$

The constant $s \in \mathbb{R}$ from (14.5) coincides with the speed of the shock curve almost everywhere. A weak solution of (14.1) satisfies the Rankine–Hugoniot jump condition.

Lemma 14.1 *Let $y \in BV(\mathcal{D}; \mathbb{R}^n)$ be a weak solution of* (14.1) *and assume that the graph $t \mapsto (t, \xi(t))$ of the Lipschitz curve $\xi \in C^{0,1}([t_0, t_1])$ is, up to a set of measure zero w.r.t. the one dimensional Hausdorff measure, contained in the set of approximate jump discontinuities $\mathcal{J}$ of y. Then for almost all $t \in [t_0, t_1]$ with the one-sided limits $y^\pm(t) = y(t, \xi(t)\pm)$ the Rankine–Hugoniot jump condition holds*

$$\dot{\xi}(t) \left(y^+(t) - y^-(t)\right) = f\left(y^+(t)\right) - f\left(y^-(t)\right). \tag{14.6}$$

Proof. A proof can be found in [8, Theorem 4.2]. □

Remark 14.1 The property (14.6) gives insights into the jump $y^+(t) - y^-(t)$. Let

$$A(y_1, y_2) = \int_0^1 A\left(s y_1 + (1-s) y_2\right) \mathrm{d}s \tag{14.7}$$

denote the averaged Jacobian matrix of f. If $|y_1 - y_2|$ is small, $A(y_1, y_2)$ has real and distinct eigenvalues $\lambda_i(y_1, y_2)$ with right and left eigenvectors $r_i(y_1, y_2)$ and $l_i(y_1, y_2)$. The condition (14.6) shows that for some $i \in [n]$ it must hold that $\dot{\xi} = \lambda_i(y^+, y^-)$ and $y^+ - y^-$ is a right eigenvector of $A(y^+, y^-)$ belonging to the i-th eigenvalue.

The simplest case of a discontinuous initial state is the *Riemann Problem*

$$y_t + f(y)_x = 0 \quad \text{on } [0,T] \times \mathbb{R}, \qquad y(0, \cdot) = u_0 = \begin{cases} u_L \text{ if } x < 0, \\ u_R \text{ if } x > 0, \end{cases} \tag{14.8}$$

for constants $u_L \neq u_R \in \Omega$. If $|u_L - u_R|$ is sufficiently small, there exists a unique entropy solution $\widehat{y}$ of (14.8). A proof can be found in [8, Theorem 5.3].

Assumption 14.1 The jump $|u_L - u_R|$ is small and for suitably small $M_0, M_1 > 0$ and

$$\mathcal{V}_{\text{ad}} = \left\{(u_l, u_r) \in \mathcal{V} \mid \|u_l - u_L\|_{C^0}, \|u_r - u_R\|_{C^0} < M_0,\ \|u_l'\|_{C^0}, \|u_r'\|_{C^0} < M_1\right\}, \tag{14.9}$$

all Riemann Problems with piecewise constant initial states

$$(v_L, v_R) \in \left\{ (u_l(x), u_r(x)) \in \mathbb{R}^n \times \mathbb{R}^n \mid (u_l, u_r) \in \mathcal{V}_{\text{ad}},\ -\varepsilon \leq x \leq \varepsilon \right\}$$

have a unique entropy solution only consisting of shock curves but no rarefaction waves.

The time horizon $T > 0$ is bounded by $T \leq T_{\max}$ where $T_{\max} > 0$ satisfies

$$\varepsilon + \lambda_{\max} T_{\max} < \ell - \lambda_{\max} T_{\max}, \tag{14.10}$$

which ensures that all shock curves generated at $(0, x_0)$ for all $-\varepsilon \leq x_0 \leq \varepsilon$ are contained in $\mathcal{D}$ for all times $t \in [0, T]$.

The existence of a piecewise classical entropy solution of the GRP is shown in [15].

Theorem 14.1 *Let Assumption 14.1 hold. Then there is a time $T > 0$ such that the GRP has for all initial states u_0 as in* (14.3) *with $(u_l, u_r, x_0) \in \mathcal{U}_{\text{ad}} = \mathcal{V}_{\text{ad}} \times (-\varepsilon, \varepsilon)$ a piecewise C^1 entropy solution $y \in BV(\mathcal{D}; \mathbb{R}^n)$. The smooth parts of y are separated by curves $\xi_k \in C^2([0, T])$ for $k \in [n]$ with $\xi_k(0) = x_0$ such that the entropy condition* (14.5) *is satisfied along ξ_k. Moreover, there is a uniform C^1-bound of the smooth parts of the solutions for all $(u_l, u_r, x_0) \in \mathcal{U}_{\text{ad}}$.*

14.3 Stability and Differentiability Properties

We analyze stability and differentiability properties of the solution operator

$$\mathcal{S} : u \in \mathcal{U}_{\text{ad}} \mapsto y \in BV(\mathcal{D}; \mathbb{R}^n) \quad \text{s.t. } y \text{ is unique entropy solution of the GRP}$$

and the objective functional (14.4). Since the shock curves $\xi_k = \xi_k(u)$ for $k \in [n]$ depend on the control $u \in \mathcal{U}_{\text{ad}}$, we first construct a reference space which is obtained by a transformation of the space variable. This will fix the position of the shock curves.

14.3.1 Solution Operator in the Reference Space

The reference domain is motivated by the structure of an entropy solution of the Riemann Problem. Since by Assumption 14.1 the Riemann Problem with the initial state (u_L, u_R) only contains shock curves and no rarefaction waves, the entropy solution of (14.8) is of the form

$$\widehat{y}(t, x) = \begin{cases} \widehat{y}_0 = u_L & \text{if } x/t < s_1, \\ \widehat{y}_i & \text{if } s_i < x/t < s_{i+1}, \ \forall i \in [n-1], \\ \widehat{y}_n = u_R & \text{if } x/t > s_n, \end{cases}$$

with constant states $\widehat{y}_1, \ldots, \widehat{y}_{n-1} \in \mathbb{R}^n$ and shock speeds $s_1 < \ldots < s_n$. For details, we refer to [8, Theorem 5.3].

We denote by $s_1 < \ldots < s_n$ the shock speeds of the solution of the Riemann Problem with initial state (u_L, u_R). With this, we define the sectors

$$\bar{D}_i = \{(t, \bar{x}) \in [0, T] \times \mathbb{R} \mid s_i t \leq \bar{x} \leq s_{i+1} t\}, \quad i \in [n-1]. \tag{14.11}$$

For the sectors left of the 1-shock and right of the n-shock curves, we use the reference speeds $s_l = \lambda_{\max}$ and $s_r = -\lambda_{\max}$ to define

$$\begin{aligned} \bar{D}_0 &= \{(t,\bar{x}) \in [0,T]\times\mathbb{R} \mid -\ell + s_l t \le \bar{x} \le s_1 t\}, \\ \bar{D}_n &= \{(t,\bar{x}) \in [0,T]\times\mathbb{R} \mid s_n t \le \bar{x} \le \ell + s_r t\}. \end{aligned} \tag{14.12}$$

Moreover, we define $\bar{D} = \cup_{i=0}^{n} \bar{D}_i$ and

$$PC^k(\bar{D}) = \times_{i=0}^{n} C^k(\bar{D}_i), \quad k \in \{0,1\}$$

and identify $\bar{y} \in PC^k(\bar{D})$ by $\bar{y} = (\bar{y}^j)_{j\in[n]_0}$ with $\bar{y}^j \in C^k(\bar{D}_j)$. The space $PC^k(\bar{D})$ is endowed with the canonical norm $\|\bar{y}\|_{PC^k(\bar{D})} = \max_j \|\bar{y}^j\|_{C^k(\bar{D}_j)}$.

Now, fix $y = \mathcal{S}(u)$ for some $u \in \mathcal{U}_{\mathrm{ad}}$. The shock curves $\xi_j = \xi_j(u) \in C^2([0,T])$ for $j \in [n]$ separate the domain $\mathcal{D}$ into the control-dependent sectors

$$\begin{aligned} D_0^{(u)} &= \{(t,x) \mid 0 \le t \le T,\ -\ell + t\lambda_{\max} \le x \le \xi_1(u)(t)\}, \\ D_j^{(u)} &= \{(t,x) \mid 0 \le t \le T,\ \xi_j(u)(t) \le x \le \xi_{j+1}(u)(t)\} \quad \forall j \in [n-1], \\ D_n^{(u)} &= \{(t,x) \mid 0 \le t \le T,\ \xi_n(u)(t) \le x \le \ell - t\lambda_{\max}\}. \end{aligned}$$

On $D_j^{(u)}$ for all $j \in [n-1]$, define the transformation of the space variable by

$$\bar{x}^{(u),j}(t,x) := \frac{x - \xi_j(u)(t)}{\xi_{j+1}(u)(t) - \xi_j(u)(t)} s_{j+1} t + \frac{\xi_{j+1}(u)(t) - x}{\xi_{j+1}(u)(t) - \xi_j(u)(t)} s_j t \tag{14.13}$$

for all $(t,x) \in D_j^{(u)}$. This establishes a one-to-one correspondence of the control-dependent domains $D_j^{(u)}$ with the reference domains $\bar{D}_j$ from (14.11), (14.12). With $(t,\bar{x}) \in \bar{D}_j$ we associate the position $(t,x) \in D_j^{(u)}$ in physical coordinates by using the inverse function of (14.13) which is given by

$$x = x^{(u),j}(t,\bar{x}) := \frac{\bar{x} - s_j t}{(s_{j+1} - s_j)t} \xi_{j+1}(u)(t) + \frac{s_{j+1} t - \bar{x}}{(s_{j+1} - s_j)t} \xi_j(u)(t). \tag{14.14}$$

We proceed analogously on $D_0^{(u)}$ and $D_n^{(u)}$.

Note that $T > 0$ and the constants M_0, M_1 in (14.9) have to be sufficiently small to ensure the well-definedness of the transformation of the space variable for all $u \in \mathcal{U}_{\mathrm{ad}}$. For details and specific bounds we refer to [6].

The previous transformation of the space variables allows to define the transformation of the state $y = \mathcal{S}(u)$ in the reference space. For this, let $j \in [n]_0$ be arbitrary and define a function $\bar{y}^j : \bar{D}_j \to \mathbb{R}^n$ by setting

$$\bar{y}^j(t,\bar{x}) := y(t, x^{(u),j}(t,\bar{x})) \qquad \text{for all } (t,\bar{x}) \in \mathrm{int}(\bar{D}_j). \tag{14.15}$$

Due to Theorem 14.1, the construction (14.15) can be continuously extended to a function $\bar{y}^j \in C^1(\bar{D}_j;\mathbb{R}^n)$. Repeating this for all $j \in [n]_0$ defines the state $\bar{y} \in PC^1(\bar{D})$

in the reference space associated to the solution $y = \mathcal{S}(u)$ of the GRP in physical coordinates. We denote the *solution operator in the reference space* by

$$\bar{\mathcal{S}} : u = (u_l, u_r, x_0) \in \mathcal{U}_{\text{ad}} \mapsto \bar{y} \in PC^1(\bar{D}) \qquad \text{such that } \bar{y} \text{ satisfies (14.15)},$$

where $\mathcal{U}_{\text{ad}}$ is equipped with the induced norm $\|\cdot\|_{\mathcal{U}}$ of

$$\mathcal{U} = C^1([-\ell, \varepsilon]; \mathbb{R}^n) \times C^1([-\varepsilon, \ell]; \mathbb{R}^n) \times \mathbb{R}.$$

Moreover, there exists a constant $C > 0$ depending on $\mathcal{U}_{\text{ad}}$ such that it holds

$$\|\bar{\mathcal{S}}(u)\|_{PC^1(\bar{D})} \leq C \quad \forall u \in \mathcal{U}_{\text{ad}}. \tag{14.16}$$

We now state continuity and differentiability properties of the solution operator in the reference space $\bar{\mathcal{S}}$. The proofs can be found in [6].

Theorem 14.2 *There is $L_{\bar{\mathcal{S}}} > 0$ such that for all $u = (u_l, u_r, x_0)$, $\tilde{u} = (\tilde{u}_l, \tilde{u}_r, \tilde{x_0}) \in \mathcal{U}_{\text{ad}}$ it holds that*

$$\|\bar{\mathcal{S}}(\tilde{u}) - \bar{\mathcal{S}}(u)\|_{PC^0(\bar{D})} \leq L_{\bar{\mathcal{S}}}(\|\tilde{u}_l - u_l\|_{C^0([-\ell,\varepsilon])} + \|\tilde{u}_r - u_r\|_{C^0([-\varepsilon,\ell])} + |\tilde{x_0} - x_0|).$$

Theorem 14.3 *The solution operator $\bar{\mathcal{S}} : \mathcal{U}_{\text{ad}} \to PC^1(\bar{D})$ is continuous.*

Theorem 14.4 *The operator $\bar{\mathcal{S}}$ is continuously Fréchet differentiable as a map*

$$\bar{\mathcal{S}} : \mathcal{U}_{\text{ad}} \to (PC^1(\bar{D}), \|\cdot\|_{PC^0(\bar{D})}).$$

Remark 14.2 The solution operator $\bar{\mathcal{S}}$ is only differentiable in the topology of $PC^0(\bar{D})$. Remainder terms are in general not small in $PC^1(\bar{D})$.

14.3.2 Solution Operator in Physical Coordinates

In this section, we exploit the stability and differentiability properties of the solution operator $\bar{\mathcal{S}}$ in the reference space from the previous section to deduce corresponding properties of the solution operator

$$\mathcal{S} : u \in \mathcal{U}_{\text{ad}} \mapsto y \in L^\infty(\mathcal{D}; \mathbb{R}^n) \quad \text{subject to } y \text{ solves (14.1)}$$

in physical coordinates. The detailed proofs can be found in [6].

Corollary 14.1 *For all $j \in [n]$, the j-shock curve $\xi_j(u) \in C^2([0,T])$ is continuously Fréchet differentiable as a map*

$$u \in \mathcal{U}_{\text{ad}} \mapsto \xi_j(u) \in C^1([0,T]).$$

For $t \in (0,T]$, let $\mathcal{I}_t = [-\ell + \lambda_{\max} t, \ell - \lambda_{\max} t]$ and denote the solution operator of (14.1) at time t by

$$\mathcal{S}_t : u \in \mathcal{U}_{\text{ad}} \mapsto \mathcal{S}(u)(t,\cdot) \in BV(\mathcal{I}_t;\mathbb{R}^n).$$

In regions between the shock curves, $\mathcal{S}_t$ satisfies the same stability and differentiability properties as in Theorems 14.2, 14.3, and 14.4 in the reference space.

Theorem 14.5 *Let $u \in \mathcal{U}_{\text{ad}}$ and $t \in (0,T]$ be arbitrary. Then*

$$\delta y = \delta\bar{y}(t,\bar{x}^{(u)}(t,\cdot)) + \bar{y}_{\bar{x}}(t,\bar{x}^{(u)}(t,\cdot))(d_u\bar{x}^{(u)}\cdot\delta u)(t,\cdot) \tag{14.17}$$

with $\bar{y} = \bar{\mathcal{S}}(u)$ and $\delta\bar{y} = d_u\bar{\mathcal{S}}(u)\cdot\delta u$ for $\delta u \in \mathcal{U}$ defines a bounded linear operator

$$\delta u \in \mathcal{U} \mapsto T(u)\cdot\delta u := \delta y \in L^\infty(\mathcal{I}_t). \tag{14.18}$$

Let $\mathcal{K} = [\alpha,\beta] \subset \mathcal{I}_t$ and $\mathcal{U}' \subset \mathcal{U}$ be an open set with $u \in \mathcal{U}' \subset \mathcal{U}_{\text{ad}}$. Assume that there exists no $j \in [n]$ with $\xi_j(u')(t) \in \mathcal{K}$ for any $u' \in \mathcal{U}'$. Then the map

$$u' \in \mathcal{U}' \mapsto Y(u') := \mathcal{S}_t(u')|_{\mathcal{K}} \in (C^1(\mathcal{K}), \|\cdot\|_{C^m(\mathcal{K})})$$

is continuously Fréchet differentiable for $m = 0$ and continuous for $m = 1$. Moreover, $\delta Y = d_uY(u)\cdot\delta u \in C^0(\mathcal{K})$ is given by

$$\delta Y(x) = \delta y(x) \quad \forall x \in \mathcal{K}.$$

For all u, $\tilde{u} = u + \delta u \in \mathcal{U}_{\text{ad}}$ with $x_j = \xi_j(u)(t)$ and $\tilde{x}_j = \xi_j(\tilde{u})(t)$, it holds on the set

$$C(u,\tilde{u}) := \mathcal{I}_t \setminus (\cup_{j=1}^n I(x_j,\tilde{x}_j))$$

with $I(x_j,\tilde{x}_j) := [\min(x_j,\tilde{x}_j),\max(x_j,\tilde{x}_j)] \subset \mathcal{I}_t$ and $y = \mathcal{S}(u)$, $\widehat{y} = \mathcal{S}(\tilde{u})$ that

$$\|\widehat{y} - y - \delta y\|_{C^0(C(u,\tilde{u}))} = o(\|\delta u\|_{\mathcal{U}}) \quad \text{for } \|\delta u\|_{\mathcal{U}} \to 0. \tag{14.19}$$

With this, it can be shown that the solution operator $\mathcal{S}$ is shift-differentiable in the sense of [21], which yields a first order approximation w.r.t. $\|\cdot\|_{L^1}$.

Lemma 14.2 *Fix $t \in (0,T]$ and $u = (u_l,u_r,x_0) \in \mathcal{U}_{\text{ad}}$. We define an operator*

$$T_s(u) : \mathcal{U} \to L^r(\mathcal{I}_t)\times\mathbb{R}^n \tag{14.20}$$

for any $r \in [1,\infty]$, which is defined for all $\delta u \in \mathcal{U}$ by $T_s(u)\cdot\delta u = (\delta y,\delta x)$, where $\delta y = T(u)\cdot\delta u$ with $T(u)$ from (14.18)*, and $\delta x_j = (d_u\xi_j(u)\cdot\delta u)(t)$ for all $j \in [n]$. Then,* (14.20) *defines a bounded linear operator $T_s(u) \in \mathcal{L}(\mathcal{U};L^r(\mathcal{I}_t)\times\mathbb{R}^n)$ for all $r \in [1,\infty]$. With the shock positions $x_j = \xi_j(u)(t)$ for all $j \in [n]$ and*

$$\mathbf{S}^x_{\mathcal{S}_t(u)} := \delta y + \sum_{j=1}^n \big(\mathcal{S}_t(u)(x_j-) - \mathcal{S}_t(u)(x_j+)\big)\operatorname{sgn}(\delta x_j)\mathbf{1}_{I(x_j,x_j+\delta x_j)} \in L^1(\mathcal{I}_t)$$

and $I(\alpha,\beta) = [\min(\alpha,\beta),\max(\alpha,\beta)]$ for $\alpha,\beta \in \mathbb{R}$, it holds that

$$\|\mathcal{S}_t(u+\delta u) - \mathcal{S}_t(u) - \mathbf{S}^x_{\mathcal{S}_t(u)}\|_{L^1(\mathcal{I}_t)} = o(\|\delta u\|_{\mathcal{U}}) \quad \text{for } \mathcal{U} \ni \delta u \to 0. \tag{14.21}$$

The previous result also implies the following L^1-stability.

Corollary 14.2 *For all $t \in (0,T]$, the solution operator $\mathcal{S}_t$ is Lipschitz continuous as a map $\mathcal{S}_t : \mathcal{U}_{\mathrm{ad}} \to L^1(\mathcal{I}_t)$.*

The next result shows that the dependence of the shock curves on the control prevents the solution of the GRP from being differentiable w.r.t. the control in the L^1-topology. We canonically identify $C^0(K;\mathbb{R}^n)^* \cong (\mathcal{M}(K))^n$ on any compact set $K \subset \mathbb{R}$ with the space $\mathcal{M}(K)$ of Radon measures and denote by $\mathcal{M}(K)^n - w^*$ the induced weak*-topology.

Theorem 14.6 *For all $t \in (0,T]$, the solution operator $\mathcal{S}_t$ is Fréchet differentiable as a map*

$$\mathcal{S}_t : \mathcal{U}_{\mathrm{ad}} \to \mathcal{M}(\mathcal{I}_t)^n - w^*.$$

Let $u \in \mathcal{U}_{\mathrm{ad}}$, $y = \mathcal{S}_t(u)$, and $x_j = \xi_j(u)(t)$. Then, $\delta\mu = d_u\mathcal{S}_t(u)\cdot\delta u$ is given by

$$\delta\mu = \delta y + \sum_{j=1}^{n} \left((d_u\xi_j(u)\cdot\delta u)(t)\right)\left(y(x_j-) - y(x_j+)\right)\delta(\cdot - x_j) \in \mathcal{M}(\mathbb{R})^n \tag{14.22}$$

with δy as in (14.17)*, and $\delta(\cdot)$ denoting a Dirac measure centered at* 0*.*

14.3.2.1 Objective Functional

The previous differentiability properties of the control-to-state map imply the differentiability of the objective functional (14.4).

Theorem 14.7 *Fix $t \in (0,T]$ and $\mathcal{I} := [a,b] \subset \mathcal{I}_t$. Let $\Phi \in C^{1,1}(\mathbb{R}^n \times \mathbb{R}^n)$ and $y_d \in BV(\mathcal{I};\mathbb{R}^n)$ be a desired state. Moreover, let $\bar{u} \in \mathcal{U}_{\mathrm{ad}}$ and $\bar{x}_j = \xi_j(\bar{u})(t)$ for all $j \in [n]$. Define*

$$u \in \mathcal{U}_{\mathrm{ad}} \mapsto J(u) := \int_a^b \Phi\left(\mathcal{S}_t(u)(x), y_d(x)\right)\mathrm{d}x. \tag{14.23}$$

(i) If y_d is approximately continuous in all $\bar{x}_j$, J is Fréchet differentiable at $\bar{u}$.
(ii) If an $\bar{x}_j$ is an approximate discontinuity of y_d, J is directionally differentiable at $\bar{u}$.
(iii) If y_d is continuous in a neighborhood of all $\bar{x}_j$, J is continuously Fréchet differentiable at $\bar{u}$.

14.4 The Adjoint Problem

In this section we give an introduction to the adjoint problem of (14.23) given by

$$p_t + A(y)^\top p_x = -g_y(\cdot,y)^\top p \quad \text{on } \mathcal{D}, \qquad p(T,\cdot) = p^T \text{ on } [a,b], \tag{14.24}$$

where $y = \mathcal{S}(u)$ for some fixed $u \in \mathcal{U}_{\mathrm{ad}}$. The correct terminal state p^T is specified later. Moreover, we assume in this section that

$$[a, b] = [-\ell + \lambda_{\max} T, \ell - \lambda_{\max} T].$$

For the sake of presentation and to reduce technical details, we use the following simplifications in this section. The results of this section, however, can still be shown even without these assumptions, see [7] for details.

(i) The position of the discontinuity x_0 in (14.3) is not varied and fixed at $x_0 = 0$. Therefore, the set of admissible controls in this section is a suitable bounded open subset
$$\mathcal{U}_{\text{ad}} \subset \mathcal{U} = C^1([-\ell, 0]; \mathbb{R}^n) \times C^1([0, \ell]; \mathbb{R}^n)$$
and $T > 0$ is sufficiently small such that all solutions of (14.1) belonging to controls $u = (u_l, u_r) \in \mathcal{U}_{\text{ad}}$ have precisely the structure of Theorem 14.1, i.e., they only contain shock curves, and no shock curves interact or are newly generated at times $t \in (0, T]$.
(ii) We only consider conservation laws, i.e., $g \equiv 0$.
(iii) The objective functional has for some $\varphi \in C^{0,1}([a, b]; \mathbb{R}^n)$ with $\varphi(a) = \varphi(b) = 0$ the linear structure
$$J(u) = \int_a^b \varphi(x)^\top y(T, x) \mathrm{d}x \quad \text{subject to } y \text{ solves (14.1), (14.2).} \tag{14.25}$$

The goal of this section is to derive the adjoint gradient representation

$$d_u J(u) \cdot \delta u = (p(0, \cdot), \delta u)_{L^2([-\ell, \ell]; \mathbb{R}^n)} \tag{14.26}$$

for (14.25), where we canonically identify $\delta u = (\delta u_l, \delta u_r) \in \mathcal{U}$ as a function

$$\delta u \in L^\infty([-\ell, \ell]; \mathbb{R}^n), \quad \delta u(x) = \begin{cases} \delta u_l(x) & \text{if } x \in [-\ell, 0), \\ \delta u_r(x) & \text{if } x \in (0, \ell]. \end{cases}$$

The analytical difficulty of the adjoint problem stems from the discontinuous coefficient $A(y)^\top = f'(y)^\top$ which is a consequence of the occurring shock curves. This makes solutions non-unique as discussed, e.g., in [12] for scalar linear transport equations with discontinuous coefficients. The non-uniqueness results from the fact that one can prescribe arbitrary values for the adjoint state p along shock curves of the state y. An example can be found in [3, Example 4.1.1].

14.4.1 Unique Existence of a Reversible Solution

We state interior boundary conditions which are prescribed along shock curves of y and show that this implies the unique existence of a solution of (14.24).

For this, let $\xi_j = \xi_j(u)$ be the j-shock curve for arbitrary $j \in [n]$ and denote by $y^\pm(t) = y(t, \xi_j(t)\pm)$ the left- and right-sided limits of y along ξ_j. With the averaged Jacobian matrix from (14.7), let $r_j\,(y^+(t), y^-(t))$ denote the right eigenvector of $A\,(y^+(t), y^-(t))$ belonging to the eigenvalue $\dot{\xi}_j(t) = \lambda_j\,(y^+(t), y^-(t))$, cf. Remark 14.1. Then the correct

adjoint state needs to satisfy with φ from (14.25) the *interior boundary conditions*

$$\begin{aligned} r_j(y^+(s), y^-(s))^\top \frac{\mathrm{d}}{\mathrm{d}s} p(s, \xi_j(s)) &= 0 \qquad \text{for a.a. } s \in [0,T], \\ r_j(y^+(T), y^-(T))^\top p(T, \xi_j(T)) &= r_j(y^+(T), y^-(T))^\top \varphi(\xi_j(T)). \end{aligned} \tag{14.27}$$

To fully determine the adjoint state on $\mathcal{D}$, it is not sufficient to prescribe terminal data only on $\{T\} \times [a,b]$. Additionally, zero boundary data has to be prescribed on

$$\partial \mathcal{D}_0 = \{(t, \pm(\ell - t\lambda_{\max})) \,|\, t \in (0,T]\}\,. \tag{14.28}$$

Theorem 14.8 *For all $\varphi \in C^{0,1}([a,b];\mathbb{R}^n)$ with $\varphi(a) = \varphi(b) = 0$ there exists a unique function $p \in C^{0,1}(\mathcal{D};\mathbb{R}^n)$ with $p(T,\cdot) = \varphi$ on $[a,b]$ and $p = 0$ on $\partial\mathcal{D}_0$ which satisfies* (14.24) *pointwise a.e. on $\mathcal{D}$ and* (14.27) *for all $j \in [n]$.*

Proof. The proof works by the standard method of characteristic curves w.r.t. the piecewise smooth coefficient $A(y)^\top$. □

Using the terminology of [3], we refer to the solution from Theorem 14.8 as the *reversible solution* of the adjoint problem.

14.4.2 Adjoint Gradient Representation

In this section, we prove that the reversible solution constructed in the previous section actually yields the gradient representation (14.26).

Theorem 14.9 *Let $u \in \mathcal{U}_{\mathrm{ad}}$ be arbitrary and $p \in C^{0,1}(\mathcal{D};\mathbb{R}^n)$ the reversible solution of* (14.24)*. Then the adjoint gradient representation* (14.26) *holds.*

Proof. Let $\tilde{u} = u + \delta u \in \mathcal{U}_{\mathrm{ad}}$ be arbitrary and denote $y = \mathcal{S}(u)$, $\tilde{y} = \mathcal{S}(\tilde{u})$. Since $y, \tilde{y}$ are weak solutions of (14.1), it follows that $\Delta y := \tilde{y} - y \in L^\infty(\mathcal{D};\mathbb{R}^n)$ is a weak solution of

$$\Delta y_t + \left(A(y,\tilde{y})\Delta y\right)_x = 0 \quad \text{on } \mathcal{D}, \qquad \Delta y(0,\cdot) = \delta u \tag{14.29}$$

with the averaged coefficient $A(y,\tilde{y})$ from (14.7). Using p as a test function on (14.29) and noting that p vanishes on $\partial\mathcal{D}_0$ from (14.28) yields after integration by parts

$$J(\tilde{u}) - J(u) = \left(p(0,\cdot), \delta u\right)_{L^2([-\ell,\ell];\mathbb{R}^n)} + \int_{\mathcal{D}} \Delta y^\top \left(p_t + A(y,\tilde{y})^\top p_x\right). \tag{14.30}$$

Let $(\delta u^\nu)_{\nu\in\mathbb{N}} \subset \mathcal{U}$ with $\lim_{\nu\to\infty} \|\delta u^\nu\|_{\mathcal{U}} = 0$ and $u^\nu = u + \delta u^\nu \in \mathcal{U}_{\mathrm{ad}}$ for all $\nu \in \mathbb{N}$ be arbitrary. By Corollary 14.1, we can choose a sequence $(\varepsilon_\nu)_{\nu\in\mathbb{N}} \subset [0,\infty)$ with

$$\varepsilon_\nu = O(\|\delta u^\nu\|_{\mathcal{U}})$$

such that it holds

$$\max_{i\in[n]} |\xi_i(u)(t) - \xi_i(u+\delta u^\nu)(t)| \le \varepsilon_\nu t \quad \forall \nu \in \mathbb{N},\ \forall t \in [0,T]. \tag{14.31}$$

The goal is now to apply Theorem 14.6 on Δy in (14.30). However, since $p_t + A(y,\tilde{y})^\top p_x$ is discontinuous, this argument needs some care.

To do so, we introduce a sequence $p^\nu \in C^{0,1}(\mathcal{D};\mathbb{R}^n)$ constructed by

$$p^\nu(t,x) = \begin{cases} p(t,\xi_k(t)) & \text{if } |x-\xi_k(t)| \le \varepsilon_\nu t \qquad \text{for some } k \in [n], \\ p(t,x_k^\nu(t,x)) & \text{if } x \in (\xi_k(t)+\varepsilon_\nu t, \xi_{k+1}(t)-\varepsilon_\nu t) \text{ for some } k \in [n-1], \\ p(t,x_0^\nu(t,x)) & \text{if } x < \xi_1(t), \\ p(t,x_n^\nu(t,x)) & \text{if } x > \xi_n(t), \end{cases}$$

with the abbreviations for $k \in [n-1]$

$$\begin{aligned} x_k^\nu(t,x) &= \frac{x-(\xi_k(t)+\varepsilon_\nu t)}{\xi_{k+1}(t)-\xi_k(t)-2\varepsilon_\nu t}\xi_{k+1}(t) + \frac{\xi_{k+1}(t)-\varepsilon_\nu t - x}{\xi_{k+1}(t)-\xi_k(t)-2\varepsilon_\nu t}\xi_k(t), \\ x_0^\nu(t,x) &= \frac{x-(-\ell+\lambda_{\max}t)}{\xi_1(t)-\varepsilon_\nu t-(-\ell+\lambda_{\max}t)}\xi_1(t) + \frac{\xi_1(t)-\varepsilon_\nu t - x}{\xi_1(t)-\varepsilon_\nu t-(-\ell+\lambda_{\max}t)}(-\ell+\lambda_{\max}t), \end{aligned} \tag{14.32}$$

and $x_n^\nu(t,x)$ analogous to $x_0^\nu(t,x)$. It is no restriction to assume that

$$\begin{aligned} \xi_{k+1}(t) - \xi_k(t) &\ge 3\varepsilon_\nu t \quad \forall t \in [0,T],\ \forall k \in [n], \\ \xi_1(t) - (-\ell+\lambda_{\max}t) &\ge 2\varepsilon_\nu t \quad \forall t \in [0,T], \\ \ell - \lambda_{\max}t - \xi_n(t) &\ge 2\varepsilon_\nu t \quad \forall t \in [0,T], \end{aligned} \tag{14.33}$$

holds for all $\nu \in \mathbb{N}$ since $\varepsilon_\nu \searrow 0$ for $\nu \to \infty$ and assumption (14.10). With this, the transformations (14.32) and p^ν are well-defined for all $\nu \in \mathbb{N}$. Moreover, it holds for all $x \in (\xi_k(t)+\varepsilon_\nu t, \xi_{k+1}(t)-\varepsilon_\nu t)$ that

$$|x_k^\nu(t,x) - x| \le \left| \frac{\varepsilon_\nu t(2x - \xi_{k+1}(t) - \xi_k(t))}{\xi_{k+1}(t)-\xi_k(t)-2\varepsilon_\nu t} \right| \to 0$$

for $\nu \to \infty$ uniformly w.r.t. (t,x). This is analogous for the cases $x < \xi_1(t)$ and $x > \xi_n(t)$. With this, it follows from the Lipschitz continuity of p that

$$\lim_{\nu\to\infty} \|p^\nu - p\|_{C^0(\mathcal{D})} = 0. \tag{14.34}$$

Moreover, it follows from (14.32) and (14.33) that $p^\nu \in C^{0,1}(\mathcal{D};\mathbb{R}^n)$ and $\|p^\nu\|_{C^{0,1}(\mathcal{D};\mathbb{R}^n)}$ can be bounded independently of $\nu \in \mathbb{N}$ and only depending on $\|p\|_{C^{0,1}(\mathcal{D};\mathbb{R}^n)}$.

Now consider an arbitrary characteristic field $k \in [n]$ and a time $t \in (0,T]$. By construction, p^ν is independent of x on the neighborhood

$$I_k^\nu(t) := (\xi_k(t) - \varepsilon_\nu t, \xi_k(t) + \varepsilon_\nu t) \tag{14.35}$$

of the k-shock position $\xi_k(t)$ and thus $p_x^\nu(t,x) = 0$. Since $p^\nu(t,x) = p(t,\xi_k(t))$, it follows from the interior boundary condition (14.27) that

$$r_k(y^+(t), y^-(t))^\top p_t^\nu(t,x) = 0 \tag{14.36}$$

for a.a. $t \in [0,T]$ and all $x \in I_k^\nu(t)$.

Taking $p^\nu - p \in C^{0,1}(\mathcal{D};\mathbb{R}^n)$ as a test function on (14.29) yields, after integration by parts and using that $p = p^\nu = 0$ on $\partial\mathcal{D}_0$ from (14.28), that

$$\begin{aligned}&\int_{\mathcal{D}} \Delta y^\top \left((p^\nu - p)_t + A(y,\tilde{y})^\top (p^\nu - p)_x\right)\\ &= \int_a^b (\Delta y^\top (p^\nu - p))(T,x)\mathrm{d}x - \int_{-\ell}^{\ell} (\Delta y^\top (p^\nu - p))(0,x)\mathrm{d}x.\end{aligned} \tag{14.37}$$

Using (14.34) and Corollary 14.2 yields with (14.37) that

$$\int_{\mathcal{D}} \Delta y^\top \left((p^\nu - p)_t + A(y,\tilde{y})^\top (p^\nu - p)_x\right) = o(\|\delta u^\nu\|_{\mathcal{U}}) \quad \text{for } \nu \to \infty.$$

This shows with (14.30) that to obtain the gradient representation (14.26), it suffices to prove

$$\int_{\mathcal{D}} \Delta y^\top \left(p_t^\nu + A(y,\tilde{y})^\top p_x^\nu\right) = o(\|\delta u^\nu\|_{\mathcal{U}}) \quad \text{for } \nu \to \infty. \tag{14.38}$$

We first analyze the limit process around shock curves of y in Case 1. After that, we analyze the region with positive distance to the shock curves where both y and $\tilde{y}$ are C^1. The shock center at $(0,0)$ is analyzed separately in Case 3.

Case 14.1 For arbitrary $k \in [n]$, we use the abbreviation $y^\pm(t) = y(t, \xi_k(t)\pm)$ and the basis

$$r_i(t) = r_i\left(y^+(t), y^-(t)\right), \quad l_i(t) = l_i\left(y^+(t), y^-(t)\right) \quad \forall i \in [n].$$

We decompose (14.38) on the neighborhood $I_1^k(t)$ of $\xi_k(t)$ from (14.35) as

$$\begin{aligned}\left(p_t^\nu + A(y,\tilde{y})^\top p_x^\nu\right)^\top \Delta y &= \sum_{i=1}^n r_i(t)^\top (p_t^\nu + A(y,\tilde{y})^\top p_x^\nu) l_i(t)^\top \Delta y\\ &= \sum_{i\neq k} r_i(t)^\top p_t^\nu l_i(t)^\top \Delta y\end{aligned} \tag{14.39}$$

for a.a. $t \in (0,T]$, where in the last step it was used that p_x^ν is zero on $I_k^1(t)$ and the interior boundary constraint (14.36) implies that the k-th summand in (14.39) is zero for a.a. $t \in (0,T]$. Now, fix $t \in (0,T]$ and let

$$\delta\mu^\nu = d_u \mathcal{S}_t(u) \cdot \delta u^\nu \in \mathcal{M}(\mathbb{R})^n$$

as given in (14.22). The singular part of $\delta\mu^\nu$ on $I_k^1(t)$ is orthogonal to all $l_i(t)$ for $i \neq k$ since $y^+(t) - y^-(t) = c\, r_k(t)$ for some $c \in \mathbb{R}$ by Remark 14.1. This shows with the operator $T(u)$ from (14.18) and $\delta y^\nu = T(u) \cdot \delta u^\nu$ as in (14.17) that even

$$l_i(t)^\top \delta\mu^\nu = l_i(t)^\top \delta y^\nu \in L^\infty(I_\nu^1(t)) \quad \forall i \neq k.$$

Applying Theorem 14.6 on $I_1^\nu(t)$ implies for all $i \neq k$

$$\int_{I_1^\nu(t)} r_i(t)^\top p_t^\nu l_i(t)^\top (\Delta y - \delta y^\nu) = o(\|\delta u^\nu\|_{\mathcal{U}}). \tag{14.40}$$

Moreover, using that $T(u) \in \mathcal{L}(\mathcal{U}; L^\infty(\mathcal{I}_t))$ by Theorem 14.5, this shows

$$\begin{aligned} \|r_i(t)^\top p_t^\nu l_i(t)^\top \delta y^\nu\|_{L^1(I_\nu^k(t))} &\le \|p^\nu\|_{C^{0,1}(\mathcal{D})} |l_i(t)| \|\delta y^\nu\|_{L^1(I_\nu^k(t))} \\ &\le 2\varepsilon_\nu \|p^\nu\|_{C^{0,1}(\mathcal{D})} |l_i(t)| \|\delta y^\nu\|_{L^\infty(I_\nu^k(t))} \\ &= O(\varepsilon_\nu^2), \end{aligned} \tag{14.41}$$

since $\operatorname{meas}(I_\nu^k(t)) = 2\varepsilon_\nu$ by (14.35). Using the uniform boundedness of $\|p^\nu\|_{C^{0,1}(\mathcal{D})}$ w.r.t. $\nu \in \mathbb{N}$, we obtain after inserting (14.41) into (14.40) and then (14.40) into (14.39) that

$$\int_{I_k^\nu(t)} \left| \left(p_t^\nu + A(y, \tilde{y})^\top p_x^\nu\right)^\top \Delta y \right| \mathrm{d}x = o(\|\delta u^\nu\|_{\mathcal{U}}) \quad \forall k \in [n], \text{ for a.a. } t \in [0, T].$$

Case 14.2 Consider the region between the shock curves where both y and $\tilde{y}$ are smooth. For all $\nu \in \mathbb{N}$ and $k \in [n-1]$ let

$$D_k^\nu = \{(t, x) \in [\varepsilon_\nu, T] \times \mathbb{R} \mid \xi_k(t) + \varepsilon_\nu t \le x \le \xi_{k+1}(t) - \varepsilon_\nu t\}$$

be a space-time domain between the shock curves of y. By construction, D_k^ν does not contain any shock curve of $\tilde{y}$ by (14.31). Therefore, it follows for $\Delta y = \tilde{y} - y \in C^1(D_k^\nu; \mathbb{R}^n)$ by Theorem 14.5 with a constant $C > 0$ independent of ν that

$$\|\Delta y(t, \cdot)\|_{C^0\left(D_k^\nu; \mathbb{R}^n\right)} \le C \|\delta u^\nu\|_{\mathcal{U}}. \tag{14.42}$$

We now show for all $k \in [n-1]$ that

$$\int_{D_k^\nu} \left(p_t^\nu + A(y, \tilde{y})^\top p_x^\nu\right)^\top \Delta y = o(\|\delta u^\nu\|_{\mathcal{U}}) \quad \text{for } \nu \to \infty. \tag{14.43}$$

To do so, we first rewrite (14.43) as

$$\begin{aligned} \int_{D_k^\nu} \left(p_t^\nu + A(y, \tilde{y})^\top p_x^\nu\right)^\top \Delta y = &\int_{D_k^\nu} \left((p^\nu - p)_t + A(y, \tilde{y})^\top (p^\nu - p)_x\right)^\top \Delta y \\ &+ \int_{D_k^\nu} \left(p_t + A(y, \tilde{y})^\top p_x\right)^\top \Delta y. \end{aligned} \tag{14.44}$$

Integration by parts of the first summand and using that (14.29) holds on D_k^ν in the classical sense yields

$$\int_{D_k^\nu} \left((p^\nu - p)_t + A(y, \tilde{y})^\top (p^\nu - p)_x\right)^\top \Delta y = \int_{\partial D_k^\nu} (p^\nu - p)^\top (n_t I + n_x A(y, \tilde{y})) \Delta y \, \mathrm{d}\sigma_k^\nu,$$

where σ_k^ν denotes the surface measure on ∂D_k^ν and $(n_t, n_x)^\top$ the unit normal vector. From (14.34) and (14.42) we obtain

$$\|(p^\nu - p)\|_{C^0(\partial D_k^\nu;\mathbb{R}^n)}\|\Delta y\|_{C^0(\partial D_k^\nu;\mathbb{R}^n)} = o(\|\delta u^\nu\|_{\mathcal{U}}).$$

Since the length $\sigma_k^\nu(\partial D_k^\nu)$ can be bounded independently of $\nu \in \mathbb{N}$, this yields

$$\left| \int_{D_k^\nu} \left((p^\nu - p)_t + A(y,\tilde{y})^\top (p^\nu - p)_x\right)^\top \Delta y \right| = o(\|\delta u^\nu\|_{\mathcal{U}}) \quad \text{for } \nu \to \infty. \tag{14.45}$$

To bound the second summand in (14.44), first observe that since p is a weak solution of the adjoint equation on D_k^ν and $\Delta y \in C^1(D_k^\nu;\mathbb{R}^n)$, it holds that

$$\int_{D_k^\nu} \left(p_t + A(y)^\top p_x\right)^\top \Delta y = 0.$$

Since $f \in C^{2,1}(\mathbb{R}^n;\mathbb{R}^n)$ by assumption, there exists a Lipschitz constant $L_A > 0$ of the averaged Jacobian matrix (14.7) w.r.t. both arguments. Using this and (14.42) implies

$$\|A(y) - A(y,\tilde{y})\|_{C^0(D_k^\nu;\mathbb{R}^n)} \leq L_A C \|\delta u^\nu\|_{\mathcal{U}}.$$

With this, we obtain

$$\int_{D_k^\nu} \left(p_t + A(y,\tilde{y})^\top p_x\right)^\top \Delta y = \int_{D_k^\nu} \left((A(y,\tilde{y}) - A(y))^\top p_x\right)^\top \Delta y = O(\|\delta u^\nu\|_{\mathcal{U}}^2), \tag{14.46}$$

since $p \in C^{0,1}(\mathcal{D})$ by Theorem 14.8 and $\operatorname{meas}(D_k^\nu)$ can be bounded independently of $\nu \in \mathbb{N}$. Combining (14.45) and (14.46) proves (14.43).

The previous argument works analogously on the regions

$$D_0^\nu(t) = \{(t,x) \mid -\ell + \lambda_{\max} t \leq x \leq \xi_1(t) - \varepsilon_\nu t\},$$
$$D_n^\nu(t) = \{(t,x) \mid \xi_n(t) + \varepsilon_\nu t \leq x \leq \ell - \lambda_{\max} t\}$$

left of the 1-shock curve and right of the n-shock curve.

Case 14.3 Finally, consider the region around the shock center $(0,0)$. For this, let

$$C^\nu = [0,\varepsilon_\nu] \times [-2\lambda_{\max}\varepsilon_\nu, 2\lambda_{\max}\varepsilon_\nu] \subset \mathcal{D} \quad \forall \nu \in \mathbb{N}.$$

Note that all shock curves of y and $\tilde{y}$ are contained in C^ν for all times $t \in [0,\varepsilon_\nu]$. Furthermore, it holds that

$$\operatorname{meas}(C^\nu) = 4\lambda_{\max}\varepsilon_\nu^2. \tag{14.47}$$

By (14.16), there is an a-priori bound for $y,\ \tilde{y} \in L^\infty(\mathcal{D})$ and thus also for $\Delta y \in L^\infty(\mathcal{D})$. This implies with (14.47) that

$$\int_{C^\nu} \left(p_t^\nu + A(y,\tilde{y})^\top p_x^\nu\right)^\top \Delta y = O(\|\delta u^\nu\|_{\mathcal{U}}^2) \quad \text{for } \nu \to \infty \tag{14.48}$$

by additionally using that $\|p^\nu\|_{C^{0,1}(\mathcal{D};\mathbb{R}^n)}$ can be bounded independently of $\nu \in \mathbb{N}$.

By construction of the Cases 1–3, we have that

$$\mathcal{D} \subset \left(\cup_{k=0}^{n} D_k^\nu\right) \cup C^\nu \cup \left\{(t,x) \in [\varepsilon_\nu, T] \times \mathbb{R} \mid x \in I_k^\nu(t) \text{ for some } k \in [n]\right\}$$

for all $\nu \in \mathbb{N}$. Combining the previous estimates yields

$$\int_{\mathcal{D}} \left(p_t^\nu + A(y,\tilde{y})^\top p_x^\nu\right)^\top \Delta y = o(\|\delta u^\nu\|_{\mathcal{U}}) \quad \text{for } \nu \to \infty.$$

□

Remark 14.3 Another approach to prove Theorem 14.9 is to prove suitable stability properties of solutions of the averaged adjoint equation

$$\tilde{p}_t + A(y,\tilde{y})^\top \tilde{p}_x = 0 \quad \text{on } \mathcal{D}, \qquad \tilde{p}(T,\cdot) = \varphi \text{ on } [a,b] \tag{14.49}$$

with $y = \mathcal{S}(u)$ and $\tilde{y} = \mathcal{S}(\tilde{u})$ for the limit $\tilde{u} \to u$ in $\mathcal{U}$.

If, for instance, one could prove the existence of a solution $\tilde{p} \in C^{0,1}(\mathcal{D};\mathbb{R}^n)$ of (14.49) with $\|\tilde{p} - p\|_{L^1(\mathcal{D};\mathbb{R}^n)} \to 0$ for $\tilde{u} \to u$ in $\mathcal{U}$ with the reversible solution $p \in C^{0,1}(\mathcal{D};\mathbb{R}^n)$ from Theorem 14.8, then taking $\tilde{p}$ instead of p as the test function on (14.29), Theorem 14.9 immediately follows from (14.30).

This technique is used in the scalar case in [22]. However, this relies on [3] which proves the stability of reversible solutions of scalar linear transport equations

$$p_t + a p_x = 0 \quad \text{on } [0,T] \times \mathbb{R}$$

with discontinuous coefficients $a \in L^\infty([0,T]\times\mathbb{R})$ w.r.t. perturbations of the coefficient a in $L^\infty([0,T]\times\mathbb{R}) - \mathrm{w}^*$ provided that a one-sided Lipschitz condition holds, i.e., there is $\alpha \in L^1(0,T)$ such that $a_x(t,\cdot) \le \alpha$ holds in the distributional sense for a.a. $t \in [0,T]$.

The results from [3] are not directly applicable to the system (14.49).

14.5 Conclusion

We presented various stability and differentiability properties of the solution operator of the Generalized Riemann Problem both in physical coordinates and in a reference space which keeps the positions of shock curves fixed by using a suitable transformation of the space variable. By combining these results, also the differentiability of a large class of tracking-type functionals followed.

Finally, we derived an adjoint gradient representation for a class of linear objective functionals.

Acknowledgements This work was supported by the German Research Foundation (DFG) within Subproject A02 in the Sonderforschungsbereich/Transregio 154 "Mathematical Modelling, Simulation and Optimization using the Example of Gas Networks" (Project ID 239904186).

References

1. C. Bardos and O. Pironneau. Data assimilation for conservation laws. *Methods and Applications of Analysis*, 12:103–134, 06 2005. doi:10.4310/MAA.2005.v12.n2.a3.
2. S. Bianchini. On the shift differentiability of the flow generated by a hyperbolic system of conservation laws. *Discrete and Continuous Dynamical Systems*, 6(2):329–350, 2000. doi:10.3934/dcds.2000.6.329.
3. F. Bouchut and F. James. One-dimensional transport equations with discontinuous coefficients. *Nonlinear Analysis: Theory, Methods & Applications*, 32(7):891–933, 1998. doi:10.1016/S0362-546X(97)00536-1.
4. F. Bouchut and F. James. Differentiability with respect to initial data for a scalar conservation law. In *Hyperbolic Problems: Theory, Numerics, Applications*, pages 113–118, Basel, 1999. Birkhäuser Basel. doi:10.1007/978-3-0348-8720-5_13.
5. J. Breitkopf, M. Gugat, and S. Ulbrich. Existence and optimal boundary control of classical solutions to networks of quasilinear hyperbolic systems of balance laws, 2025. Preprint. URL: https://opus4.kobv.de/opus4-trr154/610.
6. J. Breitkopf and S. Ulbrich. A variational calculus for optimal control of the generalized riemann problem for hyperbolic systems of conservation laws, 2025. Preprint. arXiv:2509.22076.
7. J. Breitkopf and S. Ulbrich. An adjoint calculus for optimal control of entropy solutions of the generalized riemann problem for hyperbolic systems of conservation laws with shocks, 2026. Preprint. URL: https://opus4.kobv.de/opus4-trr154/643.
8. A. Bressan. *Hyperbolic Systems of Conservation Laws: The One Dimensional Cauchy Problem*, volume 20 of *Oxford Lecture Series in Mathematics and its Applications*. Oxford University Press, New York, reprint edition, 2005.
9. A. Bressan and G. Guerra. Shift-differentiability of the flow generated by a conservation law. *Discrete and Continuous Dynamical Systems*, 3(1):35–58, 1997. doi:10.3934/dcds.1997.3.35.
10. A. Bressan and A. Marson. A variational calculus for discontinuous solutions of systems of conservation laws. *Communications in Partial Differential Equations*, 20(9-10):1491–1552, 1995. doi:10.1080/03605309508821142.
11. A. Bressan and W. Shen. Optimality conditions for solutions to hyperbolic balance laws. *Control Methods in PDE-Dynamical Systems Contemp. Math*, 426:129–152, 2007. doi:10.1090/conm/426.
12. E. D. Conway. Generalized solutions of linear differential equations with discontinuous coefficients and the uniqueness question for multidimensional quasilinear conservation laws. *Journal of Mathematical Analysis and Applications*, 18(2):238–251, 1967. doi:10.1016/0022-247X(67)90054-6.
13. C. M. Dafermos. *Hyperbolic Conservation Laws in Continuum Physics*. Grundlehren der mathematischen Wissenschaften, A Series of Comprehensive Studies in Mathematics. Springer, Berlin, Heidelberg, 4th ed. 2016 edition, 2016. doi:10.1007/978-3-662-49451-6.
14. P. D. Lax. Hyperbolic systems of conservation laws II. *Communications on Pure and Applied Mathematics*, 10(4):537–566, 1957. doi:10.1002/cpa.3160100406.
15. T. Li and W.-C. Yu. *Boundary Value Problems for Quasilinear Hyperbolic Systems*, volume V of *Duke University Mathematics Series*. Duke University Press, Durham, 1985.
16. S. Pfaff and S. Ulbrich. Optimal boundary control of nonlinear hyperbolic conservation laws with switched boundary data. *SIAM Journal on Control and Optimization*, 53(3):1250–1277, 2015. doi:10.1137/140995799.
17. P. Schäfer Aguilar, J. M. Schmitt, S. Ulbrich, and M. Moos. On the numerical discretization of optimal control problems for conservation laws. *Control and Cybernetics*, 48(2):345–376, 2019.
18. P. Schäfer Aguilar and S. Ulbrich. Convergence of numerical adjoint schemes arising from optimal boundary control problems of hyperbolic conservation laws. *SIAM Journal on Control and Optimization*, 64(1):335–362, 2026. doi:10.1137/23M1560975.
19. J. M. Schmitt and S. Ulbrich. Optimal boundary control of hyperbolic balance laws with state constraints. *SIAM Journal on Control and Optimization*, 59(2):1341–1369, 2021. doi:10.1137/19M129797X.

20. J. Smoller. *Shock Waves and Reaction-Diffusion Equations*, volume 258 of *Grundlehren der mathematischen Wissenschaften*. Springer New York, NY, 2 edition, 1994. doi:10.1007/978-1-4612-0873-0.
21. S. Ulbrich. A sensitivity and adjoint calculus for discontinuous solutions of hyperbolic conservation laws with source terms. *SIAM Journal on Control and Optimization*, 41(3):740–797, 2002. doi:10.1137/S0363012900370764.
22. S. Ulbrich. Adjoint-based derivative computations for the optimal control of discontinuous solutions of hyperbolic conservation laws. *Systems & Control Letters*, 48(3):313–328, 2003. doi:10.1016/S0167-6911(02)00275-X.

Open Access This chapter is licensed under the terms of the Creative Commons Attribution-NonCommercial-NoDerivatives 4.0 International License (http://creativecommons.org/licenses/by-nc-nd/4.0/), which permits any noncommercial use, sharing, distribution and reproduction in any medium or format, as long as you give appropriate credit to the original author(s) and the source, provide a link to the Creative Commons license and indicate if you modified the licensed material. You do not have permission under this license to share adapted material derived from this chapter or parts of it.

The images or other third party material in this chapter are included in the chapter's Creative Commons license, unless indicated otherwise in a credit line to the material. If material is not included in the chapter's Creative Commons license and your intended use is not permitted by statutory regulation or exceeds the permitted use, you will need to obtain permission directly from the copyright holder.





Chapter 15
Sequential Action Control for Hybrid Dynamical Models of Gas Networks

Yan Brodskyi[0000−0002−0550−2320],
Falk M. Hante[0000−0001−9762−2903], and
Antonia Topalović[0009−0001−4545−196X]

Abstract We generalize the framework of sequential action control (SAC) to hybrid systems of partial differential equations (PDEs). SAC is a feedback scheme based on a moving horizon optimization framework designed for advanced real-time capabilities. Applied to hybrid systems the scheme synthesizes a control strategy towards a target, including switches between different modes of operation occurring on certain conditions or events. For the hybrid system, we consider a dynamical system switching at discrete time points between abstract semilinear control systems in a Hilbert space. We show that this setting covers gas network dynamics with discrete components such as valves, check-valves and compressor switching. Based on an adjoint calculus tailored to such a hybrid setting, we derive a closed form for the SAC control. We present stability certificates for SAC-feedback based on linear-quadratic optimal control problems and provide numerical examples demonstrating its stabilizing abilities, including a study about pressure stabilization on a gas network.

15.1 Motivation

Optimization-based feedback control in gas network applications is challenging due to the nonlinear dynamics, large-scale character, and the discrete nature of key components. Valves, for example, perform critical functions including flow and pressure regulation, directional control, and safety operations such as emergency shutdowns. They operate in a binary manner (open or closed), which can lead to abrupt changes in flow and pressure, making continuous optimization in a transient setting very difficult.

Yan Brodskyi
Department of Mathematics, HU Berlin, Germany, e-mail: yan.brodskyi@hu-berlin.de

Falk M. Hante
Department of Mathematics, HU Berlin, Germany, e-mail: falk.hante@hu-berlin.de

Antonia Topalović
Department of Mathematics, HU Berlin, Germany, e-mail: antonia.topalovic@hu-berlin.de

© The Author(s) 2027

A. Martin et al. (eds.), *Mathematical Modelling, Simulation and Optimization using the Example of Gas Networks*, International Series of Numerical Mathematics 174,
https://doi.org/10.1007/978-3-032-34969-9_15

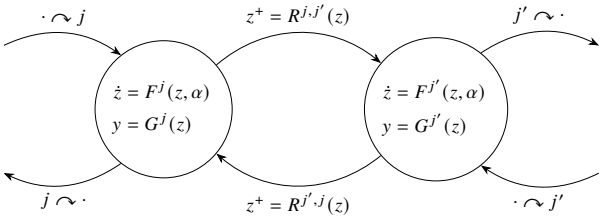


Fig. 15.1: Illustration of a hybrid dynamical system showing the transition structure between modes j and j' with corresponding output mappings. In each mode the system is governed by another dynamics, encoded in the right-hand side F^j, respectively. At a switching point in time τ, the reset map $R^{j,j'}$ describes the effect of the mode transition by $z^+(\tau) = R^{j,j'}(z^-(\tau))$, which might lead to discontinuities in the state trajectory z.

Addressing these challenges requires advanced modeling techniques that can accommodate both continuous aspects, such as the underlying dynamics, as well as discrete variables. Beyond modeling considerations, the numerical and algorithmic treatment of hybrid systems also demands sophisticated methods.

Generally, control systems that exhibit this mixed discrete-continuous structure are called hybrid (switching) systems and can (informally) be described by

$$\dot{z}(t) = F^j(z(t), \alpha(t)), \quad z = R^{j,j'}(z^-), \quad y = G^j(z), \tag{15.1}$$

where z describes the state of the system and $\{F^j\}_j$ is a family of right-hand sides each corresponding to a *mode* of the system. Here, z^- refers to the the left limit, defined as $z^-(t_0) = \lim_{t \uparrow x_0} z(t)$, analogously z^+ refers to the right limit. Furthermore, α is a continuous control variable, y an observable, and G^j a mode-dependent output-map. When a transition between a mode j and j' occurs, the *reset map* $R^{j,j'}$ describes how the state is updated after the transition; cf. Fig. 15.1. These resets might cause discontinuity of the state trajectory in time.

Optimal control problems governed by hybrid systems are both analytically and numerically challenging. In particular, due to the discontinuities in the state trajectory they provide little regularity and require appropriate tools to handle the additional discrete control variables.

A straightforward approach is to fully discretize the dynamics and thus to transform the optimal control problem into a mixed-integer nonlinear program (MINLP). Note that this can lead to potentially large systems, especially if the constraints originate from finite difference (FD) or finite element methods (FEM) for PDEs. Nonlinearities such as the friction term in gas dynamics expositioned, e.g., in Chap. 2.3, make these problems extremely difficult to solve. In [15] and specifically for gas network applications, a hierarchical approach is proposed to overcome these difficulties by a tailored linearization of the pressure drop along pipes, resulting in a predictive control scheme based on typically still very large mixed-integer linear programs (MILPs). Nevertheless, solving optimal control problems for nonlinear hybrid systems without resorting to approximations of the dynamics remains challenging.

For hybrid systems with mode dynamics governed by ordinary differential equations (ODEs), advanced strategies are available. For a broad overview of many significant approaches, see, e.g., [30]. A key direction concerns the reparameterization of the overall dynamics using switching times and discrete mode sequences. Optimization tasks can then be performed based on adjoint calculus for switching times and mode insertion sensitivities [4]. Motivated by gas network applications, these techniques have been extended to abstract evolution equations, including semilinear parabolic and hyperbolic PDEs [23, 25]. Another key direction that also extends to PDE-dynamics concerns relaxation techniques in combination with combinatorial integer approximation [9, 11, 12]. Studies specifically considering problems on gas networks include [10].

In the context of optimization-based feedback, classical methods like model predictive control (MPC) have been significantly extended to handle hybrid dynamical systems by incorporating techniques like MILP [19], multi-parametric programming [21], and piecewise affine systems [17], in order to achieve robust and efficient control. MPC relies on solving the underlying optimization problem repetitively. This can be computationally very costly, especially for problems governed by hybrid systems. The authors of [2] developed another feedback scheme based on a moving horizon problem called *sequential action control* (SAC). This method aims to find a control that drives the sensitivity (w.r.t. a nominal control) to a desired decrease, therefore causing improvement in the cost functional w.r.t. said nominal control. For control-affine problems, the SAC control action can be given in a closed form derived from adjoint calculus, and its computation requires solving the forward and adjoint equation only once.

This method also extends to continuous PDE systems with bilinear control structure and provides stability guarantees for SAC based on linear quadratic problems.

In this work, we consider an extension of SAC for hybrid systems with modes governed by semilinear PDEs building on [3]. We present the known stability guarantees for the case of linear quadratic PDE optimization problems. Furthermore, we show how a hybrid gas dynamics can be modeled as to fit into this framework. We complement our theoretical findings with numerical examples, including verification results for an unstable heat equation, an ODE problem where only discrete control decisions are available and a gas network problem with a mode switch occurring due to a compressor failure.

15.2 SAC Principle for Hybrid Semilinear Systems

In this section, we present an extension of the SAC principle to the setting of hybrid semilinear evolution systems in a Hilbert space. This framework is motivated by complex systems, for instance, gas networks, where continuous physical flows are governed by discrete operational changes like valve switches or compressor activations. The primary goal is to derive a closed-form expression for a control insertion inside a given mode of a hybrid trajectory. This insertion is designed to improve a cost functional involving both running and switching costs. We assume a fixed sequence of modes and fixed switching times. The present work extends and integrates the approaches developed in [3] and [23].

15.2.1 Problem Setup

Let H and U be real (separable) Hilbert spaces with inner products $\langle\cdot,\cdot\rangle_H$ and $\langle\cdot,\cdot\rangle_U$, and its topological dual spaces H^* and U^*, respectively. Further, let $\mathfrak{L}(U,H)$ denote the space of bounded linear operators from U to H. Consider a hybrid system defined by a finite index set of modes Q and a switching sequence $\{j_n\}_{n=0}^N \subseteq Q$ with corresponding switching times $0 = \tau_0 < \tau_1 < \cdots < \tau_N < \tau_{N+1} = T$. For each mode j_n we consider dynamics of the form

$$\dot{y}(t) = A^{j_n} y(t) + G^{j_n}(t, y(t)) + f^{j_n}(t, y(t))\, u^{j_n}(t), \quad t \in (\tau_n, \tau_{n+1}), \tag{15.2}$$

with reset maps

$$y(\tau_n) = g^{j_{n-1}, j_n}\left(y^-(\tau_n)\right), \quad n = 1, \ldots, N, \tag{15.3}$$

and initial condition

$$y(\tau_0) = y_0 \in H. \tag{15.4}$$

The associated cost functional, consisting of a running cost and switching penalties, is given as

$$J(u) = \int_0^T l(y(s))ds + \sum_{n=1}^{N} l^{j_{n-1}, j_n}\left(y^-(\tau_n)\right). \tag{15.5}$$

We impose the following assumptions.

- For each mode j_n, the operator A^{j_n} is densely defined on $D(A) \subset H$ and generates a strongly continuous semigroup on H.
- For each mode j_n, $G^{j_n}\colon [0,\infty) \times H \to H$ is a continuously Fréchet-differentiable function.
- For each mode j_n, $f^{j_n} \in C^1([0,\infty) \times H, \mathfrak{L}(U,H))$, and f^{j_n} is linearly bounded or defined on sufficiently small time interval (τ_n, τ_{n+1}).
- The cost functionals $l\colon H \to \mathbb{R}$ and $l^{j_{n-1}, j_n}\colon H \to \mathbb{R}$ are continuously differentiable in the sense of Fréchet and uniformly bounded.
- We have $y_0 \in D(A^{j_0})$ and the map $g^{j_{n-1}, j_n} : H \to H$ is continuously Fréchet-differentiable for all $n = 1, \ldots, N$, and satisfies the inclusion $g^{j_{n-1}, j_n}\left(D\left(A^{j_{n-1}}\right)\right) \subseteq D\left(A^{j_n}\right)$.

Using a definition from [23] a map $y\colon [\tau_0, \tau_{N+1}] \to H$ is called a mild solution to (15.2), if, for all $n \in \{0, \ldots, N\}$, there are functions $y^n\colon [\tau_n, \tau_{n+1}] \to H$ satisfying the following conditions:

(i) The function y^n is the only element of $C([\tau_n, \tau_{n+1}]; H)$ satisfying the variation of constants formula

$$y^n(t) = e^{(t-\tau_n)A^{j_n}} y_0^n + \int_{\tau_n}^{t} e^{(t-s)A^{j_n}} \left(G^{j_n}(t, y^n(s)) + f^{j_n}(s, y^n(s))\, u^{j_n}(s)\right) \mathrm{d}s \qquad \forall\, t \in [\tau_n, \tau_{n+1}],$$

where

$$y_0^n = \begin{cases} y_0, & \text{if } n = 0, \\ g^{j_{n-1},j_n}\left(y^{n-1}(\tau_n)\right), & \text{if } n \in \{1,\dots,N\}. \end{cases}$$

(ii) If $\tau_n < \tau_{n+1}$ for some $n \in \{0,\dots,N\}$, then $y|_{[\tau_n,\tau_{n+1})} \equiv y^n$.

We define $y^-(\tau_n) := y^{n-1}(\tau_n)$ for all $n \in \{1,\dots,N\}$.

The adjoint state $p(t)$ is defined piecewise over the intervals (τ_n, τ_{n+1}), satisfying

$$\dot{p}(t) = -\left(A^{j_n}\right)^* p(t) - \left(G_y^{j_n}(t,y(t)) + \left(f^{j_n}(t,y(t))u^{j_n}(t)\right)_y\right)^* p(t) - (l)_y\left(y(t)\right), \quad (15.6)$$

with terminal condition $p(T) = 0$ and with jump condition at each τ_n given by

$$p(\tau_n^-) = \left(g^{j_{n-1},j_n}\left(y^-(\tau_n)\right)_y\right)^* p\left(\tau_n^+\right) + \left(l^{j_{n-1},j_n}\right)_y\left(y^-\left(\tau_n\right)\right). \quad (15.7)$$

For sufficiently small $\tau_n > 0$, both the forward and adjoint problem admit a unique mild solution on $[\tau_n, \tau_{n+1}]$, respectively for each $n = 1,\dots,N$, [20, Theorem 6.1.4].

15.2.2 The SAC Principle

Let $u_1^{j_n}$ be a given nominal control, defined within the mode j on (τ_n, τ_{n+1}). We define a so-called needle variation $u_{\lambda,\tau,v}^{j_n}$ by applying a perturbation only within a small interval centered at $\tau \in (\tau_n, \tau_{n+1})$, for fixed n as

$$u_{\lambda,\tau,v}^{j_n}(t) = \begin{cases} v, & t \in [\tau - \frac{\lambda}{2}, \tau + \frac{\lambda}{2}], \\ u_1^{j_n}(t), & \text{otherwise}, \end{cases} \quad (15.8)$$

with $u^{j_k}(t) = u_1^{j_k}(t)$ for all $k \neq n$. We define the directional sensitivity of the cost (mode insertion gradient) as

$$\frac{\mathrm{d}J}{\mathrm{d}\lambda^+}(\tau, v) := \lim_{\lambda \downarrow 0} \frac{J\left(u_{\lambda,\tau,v}^{j_n}\right) - J\left(u_1\right)}{\lambda}. \quad (15.9)$$

This derivative exists due to [23, Theorem 10] and is given by

$$\frac{\mathrm{d}J}{\mathrm{d}\lambda^+}(\tau, v) = \left\langle p(\tau), f^{j_n}(\tau, y(\tau))\left(v - u_1^{j_n}(\tau)\right)\right\rangle_{H^*,H}, \quad (15.10)$$

pointwise in time for each $\tau \in (\tau_n, \tau_{n+1})$ corresponding to mode j_n, where $p(t)$ is the hybrid adjoint state.

The principle of SAC relies on choosing the control values $u_{\mathrm{opt}}^{j_n}(\tau)$ for a fixed mode j_n as

$$u_{\mathrm{opt}}^{j_n}(\tau) := \arg\min_{u \in U} l_2^{j_n}(u;\tau) := \frac{1}{2}\left[\frac{\mathrm{d}J}{\mathrm{d}\lambda^+}(\tau, u) - \alpha_d\right]^2 + \frac{1}{2}\langle u, Ru\rangle_U, \quad (15.11)$$

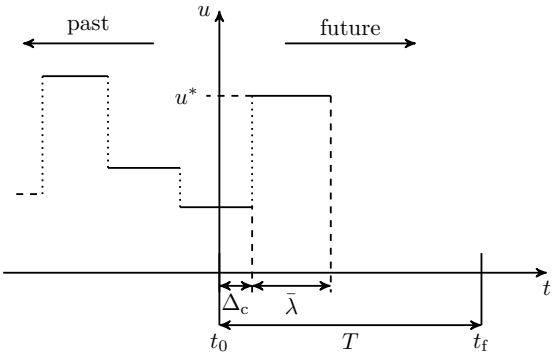


Fig. 15.2: A schematic illustration of the SAC principle [2]. The parameter Δ_c denotes the computational delay, while $[t_0, t_f]$ represents the prediction horizon. The value u^* is the sensitivity-based control found by the SAC procedure.

for some application time $\tau \in (\tau_n, \tau_{n+1})$, where $\alpha_d < 0$ is a desired rate of cost decrease and $R\colon U \to U$ is a bounded, self-adjoint, coercive operator, for which the estimate $\langle u, Ru\rangle \geq \gamma \|u\|_U$ holds for some $\gamma > 0$ and all $u \in U$. The fundamental principle of the SAC algorithm is illustrated schematically in Fig. 15.2. In general, the SAC procedure for hybrid systems is as follows:

(i) *Nominal Prediction:* Simulate the hybrid system forward with control u_1 to obtain $y(t)$ on all modes. Then solve the adjoint $p(t)$ backward using the hybrid adjoint equations with jump conditions.
(ii) *Compute Sensitivities:* For each mode j_n and time $\tau \in (\tau_n, \tau_{n+1})$, compute $\frac{\mathrm{d}J}{\mathrm{d}\lambda^+}(\tau, v)$ using $p(\tau)$ and $f^{j_n}(\tau, y(\tau))$.
(iii) *Optimize Control Insertion:* Compute $u^{j_n}_{\mathrm{opt}}(\tau)$ according to the SAC principle (15.11).
(iv) *Apply Control:* Choose insertion time τ and duration $\bar{\lambda} > 0$. Apply the control $u^{j_n}_{\bar{\lambda},\tau,u^{j_n}_{\mathrm{opt}}(\tau)}$ on $[\tau - \frac{\bar{\lambda}}{2}, \tau + \frac{\bar{\lambda}}{2}] \subset (\tau_n, \tau_{n+1})$.
(v) *Repeat:* Update $t_0 \mapsto t_0 + t_s$ and repeat steps at the next sampling time.

This approach guarantees a decrease in the predicted cost at each step due to the contribution of the optimal control insertion to both the running cost and the switching cost sensitivity, under the assumptions on differentiability and regularity of the dynamics and cost terms. Furthermore, the problem (15.11) admits an explicit solution. In our set-up, Theorem 2.1 in [3] can be reformulated as follows.

Theorem 15.1 *Let y be a mild solution of the state equation* (15.2) *with u being the given reference control* $u_1 \in C([0,T];U)$. *Furthermore, let p be the corresponding mild solution of the adjoint problem* (15.6) *and* $P^{j_n} \in C([\tau_n, \tau_{n+1}]; U^*)$, *defined by*

$$P^{j_n}(t)\colon w \mapsto \left\langle p(t), f^{j_n}(t, y(t))w \right\rangle_{H^*,\,H}, \quad n \in \{0, \ldots, N\}, \quad t \in (\tau_n, \tau_{n+1}), \quad (15.12)$$

If $R: U \to U$ is a bounded, self-adjoint and coercive operator, then the operators $P^{j_n}(t)^* P^{j_n}(t) + R^*$ each have a bounded inverse and the optimal solution $u_{\mathrm{opt}}^{j_n}(\tau)$ of the problem (15.11) *is given by*

$$u_{\mathrm{opt}}^{j_n}(\tau) = \left(P^{j_n}(\tau)^* P^{j_n}(\tau) + R^*\right)^{-1} \left(P^{j_n}(\tau)^* P^{j_n}(\tau) u_1^{j_n}(\tau) + P^{j_n}(\tau)^* \alpha_d\right) \tag{15.13}$$

for all $\tau \in (\tau_n, \tau_{n+1}), \quad n \in \{0, \ldots, N\}$.

Proof. Under the above assumptions and using the mode insertion gradient given in (15.10), the classical optimality conditions can be applied to obtain the explicit control. The remaining parts of the proof follow similar steps as to those in [3]. □

Moreover, for each fixed mode, the subproblem of determining the action duration $\bar{\lambda}$ at any time $t \in (\tau_n, \tau_{n+1})$, which ensures a decrease in the cost J given by (15.5), can be addressed by following a procedure analogous to that presented in [3].

The significance of Theorem 15.1 lies in providing an explicit, closed-form expression for the control update. In the control of high-dimensional systems, traditional optimization often requires solving expensive iterative subproblems at every step. Our result allows the SAC algorithm to remain computationally efficient and responsive.

Note that the SAC control action does not compute the full optimal control. Rather, it computes a modification of the nominal control by applying needle variations that locally decrease the cost. In fact, SAC synthesis does not even require the existence of a (unique) solution to the underlying optimal control problem. However, for the special case of a linear-quadratic base problem, there is a close connection between the closed-loop SAC control and Riccati feedback, which can also be used to derive stability guarantees for SAC schemes, as the following section will show.

15.3 Stabilization

To derive stabilization results, we begin by restricting the general framework of the preceding section to the linear setting where $f^{j_n}(t, y(t)) = B$, $A^{j_n} = A$, $G^{j_n} \equiv 0$, $\forall j = 0, \ldots, N$, with B denoting a bounded control operator mapping from the control space U into the state space H. In this situation, the dynamics reduces to the controlled linear evolution equation

$$\dot{y}(t) = Ay(t) + Bu(t),\ u(t) \in U, \quad t \in (0, T), \quad y(0) = y_0. \tag{15.14}$$

The corresponding adjoint system (15.6) takes the form

$$\dot{p}(t) = -A^* p(t) - (l_1)_y(y(t)), \qquad p(T) = m_y(y(T)). \tag{15.15}$$

Applying Theorem 15.1, we obtain an explicit expression for the optimal control associated with (15.11), namely

$$u_{\mathrm{opt}}(\tau) = \left(P(\tau)^* P(\tau) + R^*\right)^{-1} \left[P^\star(\tau) P(\tau) u_1(\tau) + P^\star(\tau) \alpha_d\right] \tag{15.16}$$

for every $\tau \in [0,T]$. Here the operator $P \in C([0,T];U^*)$ is defined via

$$P(t){:}w \mapsto \langle B^* p(t), w\rangle_{U^*,\,U}, \quad t \in [0,T]. \tag{15.17}$$

and $P^\star$ denotes its adjoint operator. We now focus on the particularly relevant case of quadratic stage costs. In this regime, the feedback representation admits a linearized form which, to first order, characterizes the closed-loop dynamics generated by continuous application of SAC-based controls. More precisely, the stage optimization problem is iteratively shifted from the initial horizon $[0,T]$ to the moving horizon $[t,t+T]$, $t>0$, yielding the cost functional

$$\tilde{J}_1(u) = \frac{1}{2}\int_t^{t+T} \|Q(y(\tau)-y_d)\|_H^2 \,\mathrm{d}\tau + \frac{1}{2}\langle P_T(y(t+T)-y_d), y(t+T)-y_d\rangle_H \tag{15.18}$$

subject to the dynamics (15.14), where $y_d = 0$, $u_1 = 0$, Q is a bounded linear operator on H, and P_T is positive and self-adjoint on H. Throughout, we identify $H^* \simeq H$ and $U^* \simeq U$. The analysis in [3] establishes that the SAC-induced nonlinear feedback is Fréchet differentiable, so that the closed-loop system admits a first-order linearization of the form

$$\begin{aligned} \dot{y} &= \left(A + \alpha_d B(R^*)^{-1}B^*\overline{F}\right) y(t), \quad t \geq 0, \\ y(0) &= y_0, \end{aligned} \tag{15.19}$$

where $F(\tau) : H \to H$ is the positive self-adjoint solution of the differential Lyapunov equation

$$\begin{aligned} \dot{F}(\tau) &= -A^*F(\tau) - F(\tau)A - Q^*Q, \quad \tau \in (0,T) \text{ a.e.} \\ F(T) &= P_T. \end{aligned} \tag{15.20}$$

With the operators A, B, Q, P_T, and R fixed, the stability properties of the closed-loop dynamics in (15.19) can be investigated. The operator $A + DG(0)$, which generates a strongly continuous semigroup $T(t)$, plays a central role. If it satisfies the decay estimate $\lim_{t\to\infty} t^{-1}\log\|T(t)\| < 0$, then the equilibrium $y_d = 0$ is exponentially asymptotically stable; see [16, Corollary 2.2]. In the case of parabolic evolution equations, the asymptotic stability of the linearization guarantees the asymptotic stability of the corresponding nonlinear dynamics in the state space; see [14, Theorem 5.1.1]. For broader families of evolution equations, stability can be investigated using linearization techniques, which are then complemented by suitable generalizations of the Hartman–Grobman theorem; see, for instance, [13, 18, 22].

15.3.1 Unstable Heat Equation

The following example was presented and investigated in [3]. To demonstrate stabilization via the SAC framework, we consider the one-dimensional reaction–diffusion equation

$$\begin{aligned} y_t(t,x) &= y_{xx}(t,x) + \mu\, y(t,x) + \sqrt{\beta}\,\chi_{(a,b)}(x)\,u(t,x), \quad (t,x) \in [0,\infty)\times(0,L), \\ y(t,0) &= y(t,L) = 0, \quad y(0,x) = y_0(x), \end{aligned} \tag{15.21}$$

with equilibrium target $y_d \equiv 0$ and quadratic stage cost

$$\widetilde{J}_1(u) \;=\; \frac{1}{2}\int_0^T\!\!\int_0^L (\bar{q}\,(y(t,x) - y_d(x)))^2\,\mathrm{d}x\,\mathrm{d}t, \tag{15.22}$$

where $\beta, \bar{q} > 0$, $\chi_{(a,b)}$ is the characteristic function of the control region $(a,b) \subset (0,L)$, and $\mu > (\pi/L)^2$ so that the uncontrolled heat equation ($u \equiv 0$) is exponentially unstable. See also [1] for related MPC stabilization.

Let $H = L^2(0,L)$, $U = L^2(0,L)$, $(a,b) = (0,L)$ (full domain), and define

$$Ay = \mu y + y_{xx}, \quad y \in D(A) = H_0^1(0,L) \cap H^2(0,L), \qquad Bu = \sqrt{\beta}\,u, \tag{15.23}$$

Then (15.21) can be written as

$$\dot{y}(t) = Ay(t) + Bu(t), \quad t \in (0,T), \quad y(0) = y_0. \tag{15.24}$$

With $Qy = \bar{q}\,y$, $P_T = 0$, and R being the identity on H, the cost (15.22) is of the form (15.18). The SAC closed-loop law (15.19) becomes

$$y_t = A\,y + \alpha_d\,\beta\,\overline{F}_q\,y, \quad y|_{x=0,L} = 0, \quad y(0) = y_0, \tag{15.25}$$

where $\overline{F}_q$ is the mild Riccati operator

$$\overline{F}_q\,y = \int_0^T e^{\sigma A^\star} Q^\star Q\, e^{\sigma A}\,y\;\mathrm{d}\sigma = \bar{q}^2 \int_0^T (e^{\sigma A})^2 y\;\mathrm{d}\sigma, \tag{15.26}$$

using the self-adjointness of A.

The solutions of (15.25) can be expressed via modal expansion in terms of the Dirichlet eigenfunctions $\{\phi_k\}_{k\geq 1}$ of $-\Delta$ on $(0,L)$ with eigenvalues $\lambda_k > 0$. Writing $y_0 = \sum_{k=1}^\infty \chi_k \phi_k$ with coefficients $\chi_k = \langle y_0, \phi_k\rangle_{L^2(0,L)}$, one obtains

$$y(t,x) = \sum_{k=1}^{\infty} \alpha_k(t)\,\phi_k(x), \qquad \alpha_k(0) = \chi_k, \tag{15.27}$$

where each mode evolves according to

$$\alpha_k(t) = \chi_k \exp\!\Big((\mu+\lambda_k)t - \frac{\alpha_d\beta\bar{q}^2}{2(\mu+\lambda_k)}\,t + \frac{\alpha_d\beta\bar{q}^2}{2(\mu+\lambda_k)}\,e^{2T(\mu+\lambda_k)}t\Big), \tag{15.28}$$

see [3, Lemma 3.2]. Furthermore, it follows that for any $T, \bar{q}, \beta > 0$ there exists a threshold $\bar{\alpha}_d < 0$ such that whenever $\alpha_d \leq \bar{\alpha}_d$, the closed-loop system (15.25) is asymptotically stable at $y_d = 0$, see [3, Theorem 3.2]. These results establish that SAC provides local uniform asymptotic stability in $H_0^1(0,L)$, guaranteeing the system returns to the desired state provided the initial disturbance is sufficiently small.

15.3.2 Numerical Results

We now turn to numerical experiments for (15.21), where we compare the performance of SAC applied on the full and partial domains, and examine its robustness with respect to parameter perturbations as well as in comparison with LQR. For the spatial discretization, we employ a Galerkin approximation using piecewise linear finite elements for the state and adjoint variables, while the control is discretized using piecewise constant functions on an equidistant grid with mesh size $h = 0.01$ (further details on discretization can be found in [3]). The resulting system of ODEs is integrated with the implicit Euler method using a sampling interval $t_s = 0.1$, while the computation time is set to $t_{\text{calc}} = 0$ and the control horizon to $\bar{\lambda} = t_s$ (cf. [2]). For the numerical simulations, we consider the specific case of (15.21), given by

$$\begin{aligned} y_t(t,x) &= y_{xx}(t,x) + 1.35\,\pi^2\, y(t,x) + \sqrt{1.6}\,\chi_{(a,b)}(x)\,u(t,x), \quad (t,x) \in [0,\infty) \times (0,1), \\ y(t,0) &= y(t,1) = 0, \quad y(0,x) = \frac{1}{5}\sin(\pi x), \end{aligned} \tag{15.29}$$

with quadratic stage cost being

$$\widetilde{J}_1 = \frac{1}{2}\int_0^T\int_0^1 (10\,y(t,x))^2\,\mathrm{d}x\,\mathrm{d}t. \tag{15.30}$$

The specific interval (a, b) and T will be stated for each numerical example separately.

Figure 15.3 illustrates SAC performance for full-domain control on $(a, b) = (0, 1)$. For $T = 1$ and $\gamma = -0.5$, the state and control are shown in panels (a)–(b). Larger negative values of γ accelerate decay but introduce overshoot due to fixed time steps, see panel (c), while increasing the horizon T reduces the asymptotic L^2-error, with exponential decay until sampling limitations are reached, see panel (d). For subdomain control, with actuation restricted to $\Omega_c = (0.5, 0.9)$ and perturbed instability $\mu = 1.2\pi^2$ (including up to 10 % random noise per step), Fig. 15.4 demonstrates that SAC achieves exponential stabilization and outperforms LQR in terms of robustness and error reduction, see panel (c). In particular, SAC reaches the target accuracy significantly earlier than LQR (0.33 s vs. 20.03 s CPU time), while for full-domain control, LQR eventually yields smaller ultimate error but SAC achieves practically useful performance much faster.

15.3.3 SAC for Systems with Discrete Control Decisions

Now, let us consider the special case of control systems, where only discrete controls are enforced. This can be modeled by

$$\dot{y}(t) + Ay(t) = f(y(t))v(t) \quad t \in (0,T) \tag{15.31}$$

with $v \in L^2(0,T;U)$, where v only takes values in a finite nonempty subset $\mathcal{V} \subset U$.

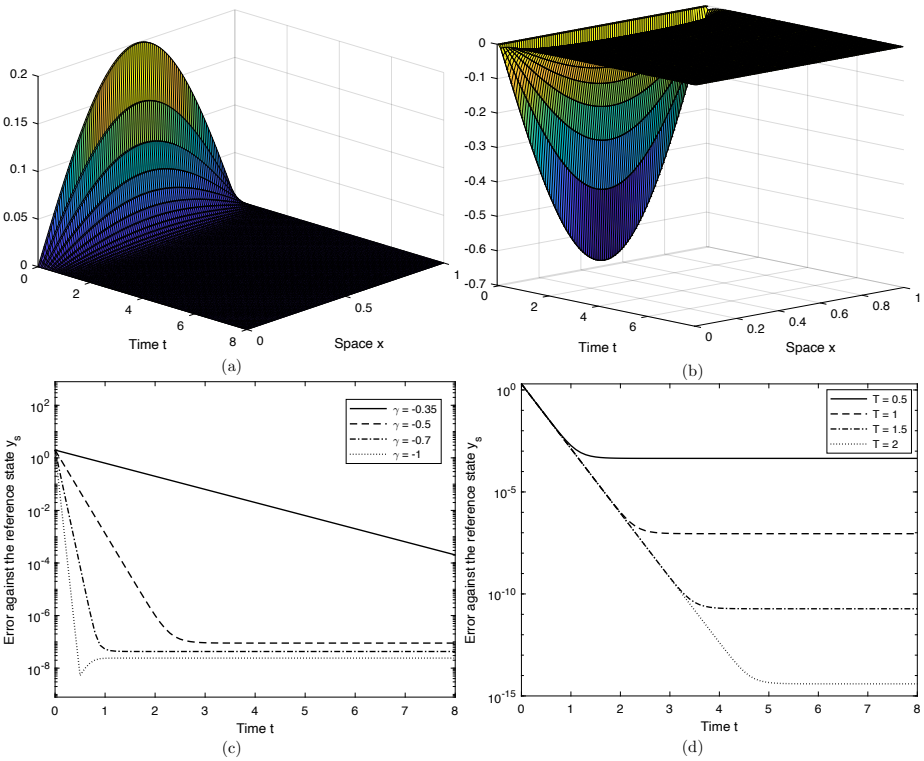


Fig. 15.3: Full-domain SAC: (a) state and (b) control for $T = 1, \gamma = -0.5$; (c) L^2-error vs. γ ($T = 1$); (d) L^2-error vs. T ($\gamma = -0.5$) [3].

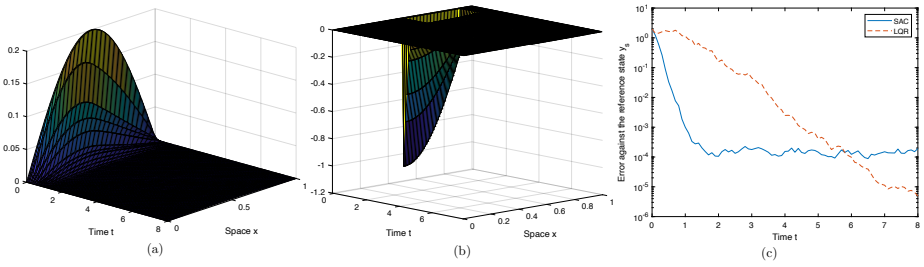


Fig. 15.4: Subdomain control on $(0.5, 0.9)$ with $\mu = 1.2\pi^2$ and 10 % disturbance: (a) state ($T = 1, \gamma = -1$), (b) control, (c) L^2-error: SAC vs. LQR [3].

For a given reference control $u_1 \in U$, the magnitude of the SAC-action is computed pointwise in time via

$$
\begin{aligned}
u_{\text{opt}}(\tau) &:= \arg\min_{v \in \mathcal{V}} l_2(v;\tau) := \frac{1}{2}\left[\frac{dJ}{d\lambda^+}(\tau, v) - \alpha_d\right]^2 + \frac{1}{2}\langle v, Rv\rangle_U \\
&:= \frac{1}{2}\left[\langle p(\tau), f(\tau, y(\tau))(v - u_1(\tau))\rangle_{H^*,H} - \alpha_d\right]^2 + \frac{1}{2}\langle v, Rv\rangle_U,
\end{aligned}
\tag{15.32}
$$

which reduces to a discrete optimization problem with quadratic cost since p, y are fully determined by the reference control u_1.

Example Inverted Pendulum

Consider an inverted coupled pendulum, also known as a cartpole. Its motion can be described by a ODE system $\dot{y} = f(y, u)$ with state $y = (\theta, \dot{\theta}, x, \dot{x})$, where $x \in \mathbb{R}$ denotes the position of the rod and $\theta \in [-\pi, \pi)$ denotes the angle between the vertical (a line orthogonal to the ground) and the pendulums' rod. The dynamics is given by the right-hand side

$$
f(y, u) = \begin{bmatrix} \dot{\theta} \\ \frac{g}{h}\sin\theta + \frac{u}{h}\cos(\theta) \\ \dot{x} \\ u \end{bmatrix}
\tag{15.33}
$$

where h is the length of the rod, g the gravitational constant, and the control enters via the acceleration of the cart. The unstable stationary points of this problem are given by

$$
y^* = (0, 0, x_p, 0), \quad u^* = 0
\tag{15.34}
$$

for any $x_p \in \mathbb{R}$. We restrict our set of admissible control values to $\mathcal{V} = \{-1, 1\}$. When computing the SAC-action in reference to $u_1 = u^*$ and a given cost functional J, we see that due to the symmetry of $\mathcal{V}$, equation (15.32) reduces to

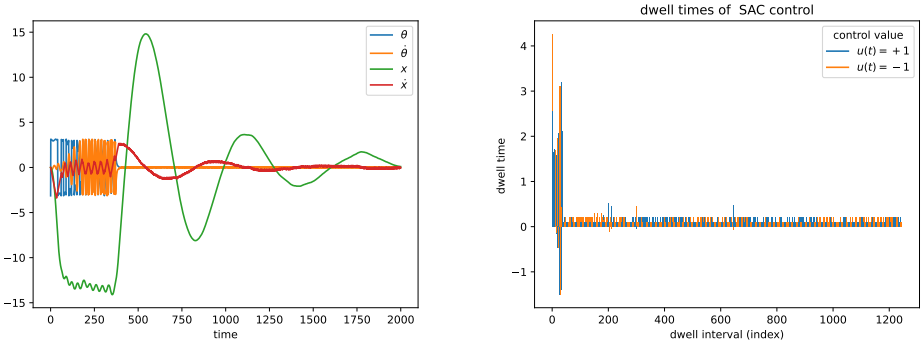
$$
\begin{aligned}
u_{\text{opt}}(\tau) &= \arg\min_{v \in \{-1,1\}} \frac{1}{2}\left[p(\tau)^T f(\tau, y(\tau))v - \alpha_d\right]^2 \\
&= \begin{cases} -1 & \text{if } p(\tau)^T f(\tau, y(\tau)) \geq 0, \\ 1 & \text{if } p(\tau)^T f(\tau, y(\tau)) < 0. \end{cases}
\end{aligned}
\tag{15.35}
$$

Note that this holds independently of the choice of $\alpha_d < 0$.

Figure 15.5 shows numerical results obtained by controlling the inverted pendulum via discrete SAC-actions. Here, we used $u_1 = u^* = 0$ as a reference control and a quadratic tracking-type cost functional

$$
J(u, y) = \int_0^T y(t)^T Q y(t)\, \mathrm{d}t + y(T)^T P y(T),
\tag{15.36}
$$

where Q, P are positive definite matrices. Figure 15.5 shows that the discrete SAC scheme succeeds in performing a so-called "swing-up", which refers to the task of controlling the system from its stable stationary point $y_1 = (\pi, 0, 0, 0)$ (the rod is hanging



(a) (b)

Fig. 15.5: Closed-loop trajectories (a) of the inverted pendulum (15.33) controlled via discrete SAC control with control values $v(t) \in \{-1, 1\}$ only and the corresponding dwell times (b). The weights for the quadratic cost are given by $Q = P = [[5, 0, 2, 0], [0, 5, 0, 2], [2, 0, 1, 0], [0, 2, 0, 1]]$. The magnitude of the SAC-action is computed via (15.35), the duration of the SAC action is fixed at $t_s = 0.1$, duration and time of action is determined via [2, Algorithm 1]. We see bang-bang behaviour of the control, which accumulates around the stable point, since the stabilizing control $u = 0$ is not admissible.

down) to an unstable stationary point (the rod is standing upright), here $y_2 = (0, 0, 0, 0)$, asymptotically.

This demonstrates that SAC synthesis is compatible not only with switching between modes but also with the incorporation of discrete control decisions.

15.4 Gas-Network Example

In this section, we demonstrate that SAC is applicable to gas network optimization problems. To this end, we introduce modeling aspects and provide an abstract problem formulation based on semigroup theory following [10]. In particular, the modelling involves discrete control elements in the form of valves. As we will show, although valve control appears on the boundary of the pipes, mathematically they can be modeled as distributed control decisions by utilizing the concept of short pipes. This aspect of the modelling makes the gas network dynamics compatible with the SAC framework.

15.4.1 Networks with Pipes, Valves, and Compressors

We describe our network topology as a finite connected metric graph $G(\mathcal{V}, \mathcal{E})$, which follows the notation laid out in Chap. 2.5.1. Additionally, each edge $e \in \mathcal{E}$ is represented by an interval $[0, L_e]$ with $L_e > 0$. We exclude self-loops, i.e., for every $(v_1, v_2) = e \in \mathcal{E}$, we have $v_1 \neq v_2$.

Our model includes typical network components, such as pipes, compressors, valves, entries, exits, and junctions. We split our edges into pipes and valves, which we will represent as short pipes, e.g., $\mathcal{E} = \mathcal{E}_p \cup \mathcal{E}_v$. Similarly, the set of vertices can be divided into inner nodes $\mathcal{V}_0$ and boundary nodes $\mathcal{V}_b$, which represent exits and entries. Furthermore, compressors are modeled as inner nodes, $\mathcal{V}_c \subset \mathcal{V}_0$.

For each transport pipe $e \in \mathcal{E}_p$, we consider the motion of a compressible non-viscous gas, whose dynamics is modeled by the isothermal semilinear Euler equations (ISO2). For better readability, we denote $(\rho^e, q^e) = (\rho, q)|_{[0,L_e]}$ for every edge e, ρ refers to the density of the gas, and q to the mass flux. We assume a constant speed of sound on the whole network, resulting in the state equation $p^e = c^2 \rho^e$ for all $e \in \mathcal{E}$ and $c = \sqrt{R_s T Z(T)}$, where $T > 0$ is the constant temperature on the network, R_s the specific gas constant, and $Z(T)$ the constant compressibility factor.

In order to simplify technical considerations, we assume that the density (and hence the pressure) and the flow remain within bounds $\rho \in [\underline{\rho}, \bar{\rho}]$ and $q \in [\underline{q}, \bar{q}]$ with $\underline{\rho} > 0$. Such bounds are typically required in pipeline operations and may also be considered explicitly in the optimization [6, 29].

We set

$$z^e = \begin{pmatrix} \rho^e \\ q^e \end{pmatrix}, \quad A^e = -\begin{bmatrix} 0 & 1 \\ c^2 & 0 \end{bmatrix}, \quad f^e(z) = \left(0, -\theta^e \frac{\min\{q^e|q^e|, \bar{q}\}}{\max\{\rho^e, \underline{\rho}\}}\right)^\top \tag{15.37}$$

for each $e \in \mathcal{E}_p$, where $\bar{\rho} > 0$ and $\bar{q} > 0$ are suitable truncation parameters to simplify theoretical considerations. With this, we can summarize the pipe model as

$$\partial_t z^e = A \partial_x z^e + f^e(z^e), \quad e \in \mathcal{E}_p. \tag{15.38}$$

In order to exploit the metric structure of the graph in our notation, we introduce $x(e, v) = \delta_{n^e(v),1}$ where δ denotes the Kronecker delta and $n^e(v)$ encodes the adjacency between vertices and edges as defined in equation (2.18).

At each node $v \in \mathcal{V}$, the coupling conditions on the network can be (generally) expressed as

$$\alpha^{e_k}_{x(e_k,v)} \rho^{e_k}(t, L_k x(e_k, v)) = \alpha^{e_l}_{x(e_l,v)} \rho^{e_l}(t, L_l x(e_l, v)), \quad \forall\, e_k, e_l \in \mathcal{E}(v),\ t \in [0, T]. \tag{15.39}$$

for the density variables, where $\alpha \in (0, \infty)^{2|\mathcal{E}|}$, as well as the flux balance given by

$$\sum_{e \in \mathcal{E}(v)} n^e(v) q^e(t, x(e, v) L_k) = q^v(t), \qquad t \in [0, T]. \tag{15.40}$$

Junctions can be modeled as nodes v such that $q^v \equiv 0$ and $\alpha^e_{x(e,v)} = 1$ for all $e \in \mathcal{E}(v)$. Entries and exists can be modeled as nodes v such that $\alpha^e_{n^e(v)} = 1$ for all $e \in \mathcal{E}(v)$, but $q^v \not\equiv 0$. We refer to v as an entry node if $q^v < 0$, or an exit node if $q^v > 0$. Compressors can be modeled as nodes v with $q^v \equiv 0$ and $\mathcal{E}_{\text{in}}(v) = \mathcal{E}_{\text{out}}(v) = 1$, where $\alpha_1^{e_{\text{out}}} = 1, \alpha_0^{e_{\text{in}}} = \bar{\alpha}$, where $e_{\text{in}}, e_{\text{out}}$ refer to the according ingoing and outgoing edge. The parameter $\bar{\alpha} > 1$ can be derived from the compressor specific enthalpy change described by equation (2.118).

Finally as mentioned above, valves can be modeled as short pipes. For each $e \in \mathcal{E}_v$, we may assume $0 < L^e \ll 1$. For simplicity, we may also assume that $(h^e)' = 0$, for all $e \in \mathcal{E}_v$, i.e., valves are horizontal network elements. For some $\varepsilon > 0$, we consider the valve action

$$f^e(\rho, q, w^e) = \begin{cases} f^e(\rho, q), & \text{if } w^e = 1 \text{ (valve open)} \\ \frac{1}{\varepsilon} f^e(\rho, q), & \text{if } w^e = 0 \text{ (valve closed).} \end{cases} \tag{15.41}$$

The valve action (15.41) can also be expressed as

$$f^e(\rho, q, w^e) = w^e f^e(\rho, q) + (1 - w^e)\frac{1}{\varepsilon} f^e(\rho, q), \quad w^e \in \{0, 1\}. \tag{15.42}$$

This valve model is meaningful only for ε sufficiently small, e.g., choosing $\varepsilon = \left(\min_j \theta^e\right)^2 \frac{\bar{q}}{\bar{\rho}}$. Although too small ε can cause very stiff problems numerically, this valve model is still valuable theoretically, as it allows for modelling valves as distributed controls. Alternatively, valves can be modeled as controlled junctions using $\alpha \in \{0, 1\}$.

As the objective for optimization, we consider integrals over some Fréchet-differentiable running cost $\ell\colon L^2(\mathcal{G}) \to \mathbb{R}$. With regard to stabilization tasks, a common choice is a tracking-type functional

$$\sum_{e \in \mathcal{E}} \int_0^T \int_0^{L_j} \gamma_1^e (\rho^e(t,x) - \rho_d^e(t,x))^2 + \gamma_2^e \left(q^e(t,x) - q_d^e(t,x)\right)^2 \, \mathrm{d}x \, \mathrm{d}t, \tag{15.43}$$

ρ_d^e and q_d^e are some desired states, and $\gamma_1^e, \gamma_2^e \geq 0$ are given constants, $e \in \mathcal{E}$.

15.4.2 Abstract Problem Formulation

We will set up an abstract formulation of the gas network system in terms of a semigroup and discuss its well-posedness. This will make the hybrid sequential action control scheme discussed in Sect. 15.2, applicable to the dynamics on the gas network.

For this, we consider a scenario where both discrete and continuous control decisions occur. Specifically, we control the switching of the valves and the gas flux on the supply nodes. We set $|\mathcal{E}_p| = n$, $|\mathcal{E}_v| = n_v$, $|\mathcal{V}| = m$ where $\mathcal{V}_s \subset \mathcal{V}$ contains the supply nodes of the network with $|\mathcal{V}_m| = m_s$.

As the state and control space, we introduce

$$Y = \left[\bigotimes_{j=1}^{n} L^2([0, L_j], \mathcal{R}^2)\right] \otimes L^2([0,\infty), \mathcal{R}^m), \quad U = L^2([0,\infty), \mathcal{R}^{m_s}), \quad \mathcal{V} = \{0,1\}^{n_v}, \tag{15.44}$$

with a corresponding state vector and control vectors

$$\begin{aligned} y &= \left((z^1)^\top, \dots, (z^n)^\top, q^{v_1}, \dots, q^{v_m}\right)^\top \in Y, \\ u = \left(u^1, \dots u^{m_s}\right) \in U, \quad v &= \left(w^1, \dots, w^{n_v}\right) \in \{0,1\}^{n_v} \in \mathcal{V}. \end{aligned} \tag{15.45}$$

We denote the initial state by $y_0 := \left((z_0^1)^\top, \dots, (z_0^n)^\top, q_0^{v_1}, \dots, q_0^{v_m}\right)^\top$. Further, we introduce the operators

$$A = \begin{bmatrix} A^1 & & \\ & \ddots & \\ & & A^n \end{bmatrix} \frac{\partial}{\partial x}, \qquad B = \mathrm{i}_m \frac{\partial}{\partial x}, \tag{15.46}$$

where i_m denotes the identity matrix and the nonlinear mappings $f: Y \times U \times \mathcal{V} \to Y$ defined by

$$\begin{aligned} &f(y,u,v) \\ &= \left(f^1(y^1, w^1), \dots, f^{n_v}(y^{n_v}, w^{n_v}), f^{n_v+1}(y^{n_v+1}), \dots, f^n(y^n), u^1, \dots, u^{m_s}, 0, \dots, 0\right)^\top. \end{aligned} \tag{15.47}$$

Remark 15.1 Instead of modeling the fluxes at the nodes of the network q^v, $v \in \mathcal{V}$, in terms of the boundary conditions associated with the pipe components $z^1, \dots z^n$ and the operator A, we represent them by separate components of the abstract dynamics y. In particular, they each obey the transport equation

$$\partial_t q^v(t,x) + \partial_x q^v(t,x) = \mathbf{1}_{\mathcal{V}_s}(v) u^v \quad \text{on } (0,\infty) \times (0,\infty), \tag{15.48}$$

where the position $x = 0$ represents the actual flux at the node v in the network. This allows us to choose the "simple" set Y as a superset of the domain of our semigroup generator and thus avoids the technical difficulties of incorporating the time-dependent coupling condition and boundary control into the underlying Hilbert space.

Moreover, we define the block diagonal operator $\mathrm{diag}(A, B)$ on the domain

$$D\left(\begin{bmatrix} A & 0 \\ 0 & B \end{bmatrix}\right) = \Big\{ y = (z^1, \ldots, z^n, q^{v_1}, \ldots, q^{v_m})^\top \in Y \,\Big|\, y \text{ is absolutely continuous,}$$
$$\alpha^k_{x(e_k,v)} z^k_1(t, L_k x(e_k, v)) = \alpha^l_{x(e_l,v)} z^l_1(t, L_l x(e_l, v))$$
$$\forall\, v \in V,\ e_k, e_l \in \mathcal{E}(v),$$
$$\sum_{e_j \in \mathcal{E}_{\text{in}}(v)} z^j_2(L_j) - \sum_{e_j \in \mathcal{E}_{\text{out}}(v)} z^j_2(0) = q^v(0) \quad \forall\, v \in V \Big\}. \tag{15.49}$$

Regarding well-posedness of the operator, we refer to the following result from [24].

Theorem 15.2 *The operator*

$$\left(D\left(\begin{bmatrix} A & 0 \\ 0 & B \end{bmatrix}\right), \begin{bmatrix} A & 0 \\ 0 & B \end{bmatrix} \right) \tag{15.50}$$

is the infinitesimal generator of a strongly continuous semigroup on Y.

The function f given in (15.47) is bounded and globally Lipschitz-continuous in y and u for each fixed $v \in \{0,1\}^{n_v}$, but not Fréchet-differentiable. To meet the regularity requirements of the SAC scheme presented in Sect. 15.2, we furthermore replace the friction term on each edge f^e by a smooth approximation, see, e.g., [8, 28]. We note that the function $f(y,u,v)$ as defined in (15.47) can be split into $f(y(t),u(t),v(t)) = g(y(t)) + \tilde{f}(y(t))(u(t),v(t)))$ where $g(y)$ entails the nonlinear friction terms on the pipes and $\tilde{f}$ has a bilinear structure with

$$g(y) = \left(\frac{1}{\varepsilon} f^1(y^1), \ldots, \frac{1}{\varepsilon} f^{n_v}(y^{n_v}), f^{n_v+1}(y^{n_v+1}), \ldots, f^{n+n_\nu}(y^{n+n_\nu}), 0, \ldots, 0 \right)^\top$$
$$\tilde{f}(y,u,v) =$$
$$\left(\left(1 - \frac{1}{\varepsilon}\right) f^1(y^1) w^1, \ldots, \left(1 - \frac{1}{\varepsilon}\right) f^{n_v}(y^{n_v}) w^{n_v}, 0, \ldots, 0, u^1, \ldots, u^m, 0, \ldots, 0 \right)^\top \tag{15.51}$$

This allows us to express the gas network dynamics with valve switching control as an abstract mixed-integer control problem

$$\dot{y}(t) = \begin{bmatrix} A & 0 \\ 0 & B \end{bmatrix} y(t) + \tilde{f}(y(t), u(t), v(t)) + g(y(t)), \quad t \in [0,T], \tag{15.52}$$

with the initial condition $y(t_0) = y_0$ with $t_0 = 0$.

This abstract representation of the gas network dynamics fits the theoretical requirements of Sect. 15.2 and thus allows for SAC-control synthesis for gas networks. Note, that on/off control decisions on the valves are mathematically interpreted as distributed controls.

15.4.3 Numerical Example

We illustrate the performance of the SAC strategy, implemented within the MPC framework, on the Gaslib-11 benchmark network [26, 27]. The network in our setup consists of: 8 pipelines (P01–P08), 3 gas entry nodes (`entry01`–`entry03`), 3 exit nodes (`exit01`–`exit03`), 2 compressor stations (`CS01`, `CS02`), 1 controllable valve (`V01`). An illustration of the network can be found in Fig. 15.6.

All nodes are subject to operational pressure limits

$$p_{\min} = 40 \text{ bar}, \quad p_{\max} = 60 \text{ bar}. \tag{15.53}$$

The control objective is to maintain pressures safely within these bounds, ideally close to a nominal target state, which can be formulated as maximizing the distance from the bounds or, equivalently, minimizing the deviation from the desired pressure profile. The physical dynamics of isothermal gas transport in pipelines with active compressor units are described by the ISO3 model (ISO3). It is consistent with the model hierarchy simplification of the ISO2 model (ISO2): while ISO2 retains the full momentum dynamics, including inertial terms, ISO3 neglects these inertial effects, resulting in a simpler and more tractable formulation.

The simulations are based on a conforming mixed finite element discretization in space and implicit Euler time integration for both the forward and adjoint equations, following [5]. The SAC-MPC controller operates in a receding-horizon fashion: at each control step, it computes an updated control profile based on the current network state, applies only the first segment of this profile, and then re-optimizes after receiving new measurements. This structure allows the controller to adapt to evolving conditions in real time. Two baseline operational configurations are considered:

(i) Single-compressor operation – only `CS01` is available, initially switched off.
(ii) Dual-compressor operation – both `CS01` and `CS02` are available, initially switched off.

To assess robustness and responsiveness, we introduce two critical events during operation:

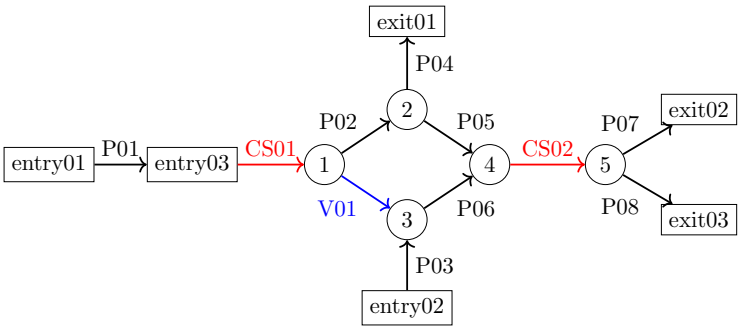


Fig. 15.6: GasLib-11 network

- extreme increase in gas demand at selected exit nodes (critical event 1),
- sudden failure of compressor station `CS02` (critical event 2).

Without intervention, these events can cause the solution to become infeasible, with exit flows failing to meet demand or pressures exceeding bounds. In contrast, the SAC controller responds by adjusting the operational settings of the remaining compressor, restoring feasibility, and guiding the system back toward its nominal operating state. In Figures 15.7 and 15.8, we present the simulation results for these scenarios, quantifying recovery times and demonstrating the controller's ability to stabilize the system in realistic and challenging conditions. Furthermore, in Fig. 15.8 we compare the controller found by SAC with a Gauss–Newton controller. The SAC maintains pressures within the prescribed limits throughout the critical event, highlighting its robustness advantage.

15.5 Conclusion and Future Work

We have presented an extension of SAC to hybrid PDE systems governed by semilinear control dynamics. In contrast to other moving-horizon feedback methods, in particular

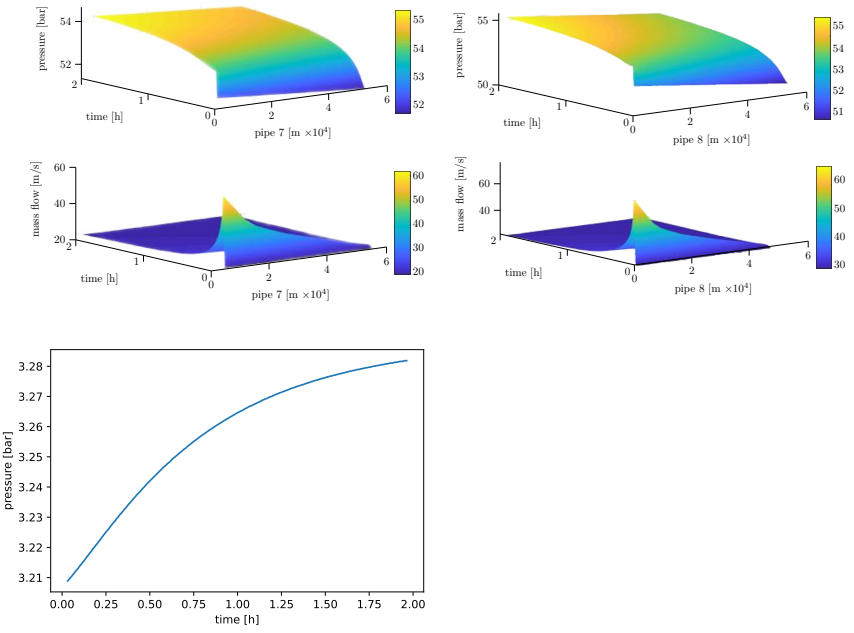


Fig. 15.7: Critical event 1. Pressure and mass flow distribution along pipes 7 and 8, and the corresponding control action in `CS01`.

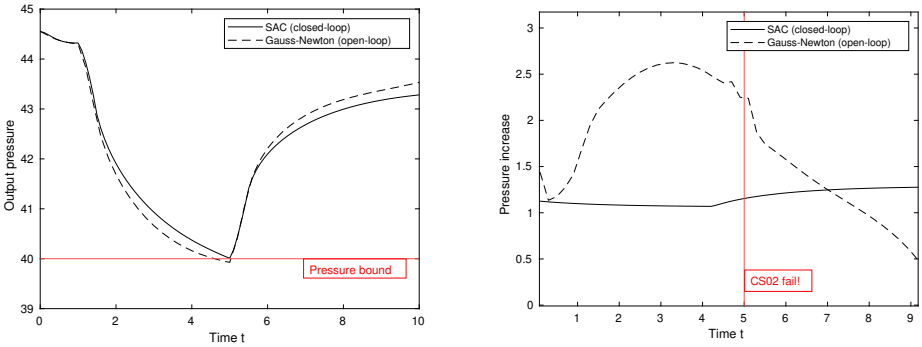


Fig. 15.8: Critical event 2. Output pressure at `exit01` and corresponding config:ctrol inputs (for SAC and Gauss–Newton control).

MPC, the computation of SAC control can be carried out without solving the numerically costly underlying hybrid optimal control problem. However, as a consequence, the stability and sub-optimality guarantees provided by MPC, which computes a full optimal solution, are not directly available. Nevertheless, our theoretical results provide a stability analysis for the linear-quadratic case. Together with the numerical examples, this illustrates not only the stabilizing capabilities of SAC but also its potential for real-time application due to its comparatively low computational cost.

A natural direction for future work would be the extension of SAC to (hybrid) optimal control problems with boundary control, including the derivation of a closed form for u_{opt} and the corresponding stability analysis. This can potentially be based on the abstract reformulation of boundary control problems discussed in [7]. Further aspects for future work on SAC include handling uncertainties, integrating state observers, enforcing state constraints, and extensions to different gas-related problems where real-time feedback and hybrid PDE dynamics play a crucial role.

Acknowledgements We would like to thank Robin Simon and Nora Philippi for their assistance with the numerical implementations used in this study.

This work was supported by the German Research Foundation (DFG) within Subproject A03 in the Sonderforschungsbereich/Transregio 154 “Mathematical Modelling, Simulation and Optimization using the Example of Gas Networks” (Project ID 239904186). This work was also supported by the German Research Foundation (DFG) in “The Berlin Mathematics Research Center MATH+” (EXC-2046/1, EXC-2046/2, Project ID: 390685689).

References

1. N. Altmüller and L. Grüne. Distributed and boundary model predictive control for the heat equation. *GAMM-Mitt.*, 35(2):131–145, 2012. doi:10.1002/gamm.201210010.
2. A. R. Ansari and T. D. Murphey. Sequential action control: Closed-form optimal control for nonlinear and nonsmooth systems. *IEEE Transactions on Robotics*, 32(5):1196–1214, 2016.

doi:10.1109/TRO.2016.2596768.
3. Y. Brodskyi, F. M. Hante, and A. Seidel. Stabilization of partial differential equations by sequential action control. *IMA Journal of Mathematical Control and Information*, 39(4):1008–1033, Dec 2022. doi:10.1093/imamci/dnac021.
4. M. Egerstedt, Y. Wardi, and H. Axelsson. Transition-time optimization for switched-mode dynamical systems. *IEEE Trans. Automat. Control*, 51(1):110–115, 2006. doi:10.1109/TAC.2005.861711.
5. H. Egger, J. Giesselmann, T. Kunkel, and N. Philippi. An asymptotic-preserving discretization scheme for gas transport in pipe networks. *IMA Journal of Numerical Analysis*, 43(4):2137–2168, Aug 2022. doi:10.1093/imanum/drac032.
6. H. Egger, T. Kugler, and W. Wollner. Numerical optimal control of instationary gas transport with control and state constraints. TRR 154 Preprint 214, 2017.
7. Z. Emirsjlow and S. Townley. From PDEs with boundary control to the abstract state equation with an unbounded input operator: A tutorial. *European Journal of Control*, 6(1):27–49, 2000. doi:10.1016/S0947-3580(00)70908-3.
8. L. Ghilardi, S. Naik, E. Martelli, F. Casella, and L. T. Biegler. Nonlinear dynamic optimization for gas pipelines operation. In F. Manenti and G. V. Reklaitis, ed., *34th European Symposium on Computer Aided Process Engineering / 15th International Symposium on Process Systems Engineering*, volume 53 of *Computer Aided Chemical Engineering*, pages 1657–1662. Elsevier, 2024. doi:10.1016/B978-0-443-28824-1.50277-5.
9. F. M. Hante. Relaxation methods for hyperbolic PDE mixed-integer optimal control problems. *Optimal Control Appl. Methods*, 38(6):1103–1110, 2017. doi:10.1002/oca.2315.
10. F. M. Hante. Mixed-integer optimal control for PDEs: relaxation via differential inclusions and applications to gas network optimization. In *Mathematical Modelling, Optimization, Analytic and Numerical Solutions*, Ind. Appl. Math., pages 157–171. Springer, Singapore, 2020. doi:10.1007/978-981-15-0928-5_7.
11. F. M. Hante. Relaxation methods for optimal switching control of PDE-dynamical systems. In *Numerical Control: Part B*, volume 24 of *Handb. Numer. Anal.*, pages 61–76. North-Holland, Amsterdam, 2023. doi:10.1016/bs.hna.2022.10.004.
12. F. M. Hante and S. Sager. Relaxation methods for mixed-integer optimal control of partial differential equations. *Comput. Optim. Appl.*, 55(1):197–225, 2013. doi:10.1007/s10589-012-9518-3.
13. M.-L. Hein and J. Prüss. The Hartman-Grobman theorem for semilinear hyperbolic evolution equations. *J. Differential Equations*, 261(8):4709–4727, 2016. doi:10.1016/j.jde.2016.07.015.
14. D. Henry. *Geometric theory of semilinear parabolic equations*, volume Vol.194 of Lecture Notes in Mathematics. Springer-Verlag, Berlin-New York, 1981. doi:10.1007/BFb0089647.
15. K. Hoppmann-Baum, F. Hennings, R. Lenz, U. Gotzes, N. Heinecke, K. Spreckelsen, and T. Koch. Optimal operation of transient gas transport networks. *Optim. Eng.*, 22(2):735–781, 2021. doi:10.1007/s11081-020-09584-x.
16. N. Kato. A principle of linearized stability for nonlinear evolution equations. *Trans. Amer. Math. Soc.*, 347(8):2851–2868, 1995. doi:10.2307/2154758.
17. M. Lazar, W. Heemels, S. Weiland, and A. Bemporad. Stabilizing model predictive control of hybrid systems. *IEEE Transactions on Automatic Control*, 51(11):1813–1818, 2006. doi:10.1109/TAC.2006.883059.
18. K. Lu. A Hartman-Grobman theorem for scalar reaction-diffusion equations. *J. Differential Equations*, 93(2):364–394, 1991. doi:10.1016/0022-0396(91)90017-4.
19. M. Morari and J. H. Lee. Model predictive control: Past, present and future. *Computers & Chemical Engineering*, 23(4-5):667–682, 1999. doi:10.1016/S0098-1354(98)00301-9.
20. A. Pazy. *Semigroups of Linear Operators and Applications to Partial Differential Equations*. Applied Mathematical Sciences Series. Springer-Verlag, New York, 1983. doi:10.1007/978-1-4612-5561-1.
21. E. N. Pistikopoulos, N. A. Diangelakis, and R. Oberdieck. *Multi-Parametric Optimization and Control*. Wiley Series in Operations Research and Management Science. John Wiley & Sons, Inc., Hoboken, NJ, 2021. doi:10.1002/9781119265245.
22. H. M. Rodrigues and J. G. Ruas-Filho. The Hartman–Grobman theorem for reversible systems on Banach spaces. *J. Nonlinear Sci.*, 7(3):271–280, 1997. doi:10.1007/s003329900031.

23. F. Rüffler and F. M. Hante. Optimal switching for hybrid semilinear evolutions. *Nonlinear Anal. Hybrid Syst.*, 22:215–227, 2016. doi:10.1016/j.nahs.2016.05.001.
24. F. Rüffler, V. Mehrmann, and F. M. Hante. Optimal model switching for gas flow in pipe networks. *Netw. Heterog. Media*, 13(4):641–661, 2018. doi:10.3934/nhm.2018029.
25. F. Rüffler. *Control and Optimization for Switched Systems of Evolution Equations*. PhD thesis, Friedrich-Alexander-Universität Erlangen-Nürnberg, Germany, 2019.
26. M. Schmidt, D. Aßmann, R. Burlacu, J. Humpola, I. Joormann, N. Kanelakis, T. Koch, D. Oucherif, M. E. Pfetsch, L. Schewe, R. Schwarz, and M. Sirvent. GasLib – A Library of Gas Network Instances. *Data*, 2(4):40, 2017. doi:10.3390/data2040040.
27. M. Schmidt, D. Aßmann, R. Burlacu, J. Humpola, I. Joormann, N. Kanelakis, T. Koch, D. Oucherif, M. E. Pfetsch, L. Schewe, R. Schwarz, and M. Sirvent. GasLib – A library of gas network instances. Technical report, Nov. 2017.
28. M. Schmidt, M. C. Steinbach, and B. M. Willert. High detail stationary optimization models for gas networks: validation and results. *Optimization and Engineering*, 17(2):437–472, 2016. doi:10.1007/s11081-015-9300-3.
29. J. M. Schmitt and S. Ulbrich. Optimal boundary control of hyperbolic balance laws with state constraints. *SIAM Journal on Control and Optimization*, 59(2):1341–1369, 2021. doi:10.1137/19M129797X.
30. F. Zhu and P. J. Antsaklis. Optimal control of hybrid switched systems: A brief survey. *Discrete Event Dyn. Syst.*, 25(3):345–364, 2015. doi:10.1007/s10626-014-0187-5.

Open Access This chapter is licensed under the terms of the Creative Commons Attribution-NonCommercial-NoDerivatives 4.0 International License (http://creativecommons.org/licenses/by-nc-nd/4.0/), which permits any noncommercial use, sharing, distribution and reproduction in any medium or format, as long as you give appropriate credit to the original author(s) and the source, provide a link to the Creative Commons license and indicate if you modified the licensed material. You do not have permission under this license to share adapted material derived from this chapter or parts of it.

The images or other third party material in this chapter are included in the chapter's Creative Commons license, unless indicated otherwise in a credit line to the material. If material is not included in the chapter's Creative Commons license and your intended use is not permitted by statutory regulation or exceeds the permitted use, you will need to obtain permission directly from the copyright holder.



Chapter 16
The Turnpike Property and the Optimal Control of Gas Networks

Martin Gugat[0000−0002−5281−110X] and
Michael Schuster[0000−0002−4689−3663]

Abstract This chapter investigates the turnpike property in dynamic optimal control problems arising in gas pipeline networks. For sufficiently long time horizons, optimal states and controls typically remain close to a steady-state solution for most of the time interval, with deviations occurring mainly near the initial and terminal phases. The theoretical background of the turnpike phenomenon is discussed and illustrated through two examples: an optimal control problem governed by a neural ordinary differential equation and an optimal compressor control problem for a gas network modeled by the isothermal Euler equations.

16.1 Theoretical Background on Turnpike Phenomena

In the operation of gas pipeline networks, the state of the gas in the pipes changes with time, due to changing supply and demand, and changing control actions at the control nodes. An important aspect is the uncertainty of future supply and demand in the system, that has to be taken into account for operational planning. Moreover, there are state constraints, for example the range of admissible pressures is bounded.

Thus, it is natural to state the optimal control problems for gas networks in a dynamic setting (see [14, 20]), where the system evolves according to a dynamical system, which depends on the control actions subject to the boundary conditions. The boundary data are uncertain, but in a simplified setting the expected values can be taken as fixed values. As usual, in the statement of the optimal control problem the initial data for the system are assumed to be known. In order to obtain an approximation of the initial state, an observer system can be used, see for example [7]. Dynamic optimal control problems of

Martin Gugat
Department of Mathematics, FAU Erlangen-Nürnberg, Germany, e-mail: martin.gugat@fau.de

Michael Schuster
Department of Data Science, FAU Erlangen-Nürnberg, Germany, e-mail: michi.schuster@fau.de

© The Author(s) 2027

A. Martin et al. (eds.), *Mathematical Modelling, Simulation and Optimization using the Example of Gas Networks*, International Series of Numerical Mathematics 174,
https://doi.org/10.1007/978-3-032-34969-9_16

this type can also be used in the context of model predictive control (MPC) or receding horizon control (RHC), see, e.g., [19].

The objective functional of the optimal control problem typically contains a control cost and a tracking term of integral type, where the integrand is the distance of the system state to a given desired state. A natural control cost in this context is the compressor cost that stems from thermodynamical considerations. The amount of energy input to the gas by a compressor is given by the product of the flow rate through the compressor and a function of the ratio between output pressure and input pressure, see, e.g., [22], (1). Also terminal costs that penalize any deviation of the final pipeline state from a desired terminal state are useful to avoid undesired terminal states.

For optimal control problems of the type described above, numerical computations often yield optimal controls and optimal states that have a so–called *turnpike structure* in the following sense: For sufficiently large time horizons $T > 0$, after a dynamic initial phase on a subinterval of the form $[0, t_0] \subset [0, T]$ the optimal control and the optimal state are very close to a static state on the long subinterval $[t_0, T - t_0]$. Only close to the final time, on the final subinterval $[T - t_0, T]$, again a dynamic phase can be observed sometimes.

Under certain conditions, the static 'attractor' of the optimal state–control pair (which we can also call the 'turnpike') can be characterized as the optimal solution for the static optimal control problems that corresponds to the dynamic optimal control problem. This static problem can be obtained from the dynamic problem by canceling the initial condition and the terminal costs in the objective function, and setting the time-derivatives in the differential equation to zero. In general, it is much easier to solve the static optimal control problem than the dynamic problem. The turnpike property provides a justification for planning processes that are based on static models, since it implies that for large time horizons, most of the time the optimal state, control and adjoint state for the dynamic problem will be close to the optimal solutions of the static problem.

Often the difference between the dynamic optimal control and the static optimal control decays exponentially fast both from the beginning of the time interval towards its interior and also from the end of the time interval towards its interior. This situation is called the *exponential turnpike property* (see, e.g., [16]). In [15], it is shown that under certain assumptions, with the time horizon converging towards infinity, there exist limit trajectories both for the initial phase of the control activity and for the terminal phase at the end of the time interval. Also for the optimal state there exist initial limit trajectories and terminal limit trajectories. The result is shown for linear systems and thus, not applicable to the non-linear models. However, on account of simulation results, we expect that similar results hold for the non-linear models.

The turnpike structure has been studied for a long time in economics, see for example the early references [21, 24]. Meanwhile, the turnpike phenomenon is also a well-established structural property in the field of optimal control, in particular due to its relation with model predictive control in a stabilization loop. For recent surveys see, e.g., [3, 28]. Problems in a general abstract setting are studied in [30]. In the turnpike analysis, the *(strict) dissipativity property* plays a prominent role. It has been introduced by Jan Willems, see [29]. A survey on its influence is presented in [4]. The dissipativity property requires the existence of a function $w(t)$ that is called the *supply rate* (depending on the control and the state at the time t), and a *storage function* S depending on the state.

As stated in [29], the storage function is 'a generalization of the concept of stored energy or entropy' (and therefore, bounded from below) and 'the storage function associated with a dissipative dynamical system satisfies an a priori inequality', namely for all time intervals (t_0, t_1) the dissipation inequality

$$S(x_1) \leq S(x_0) + \int_{t_0}^{t_1} w(t)\, dt,$$

where for $j \in \{0, 1\}$ the state at time t_j is denoted by x_j. In the context of optimal control problems, the supply rate can be considered as the integrand in the objective functional. It has been shown in [5] that strict dissipativity implies turnpike behavior for time-varying discrete time optimal control problems.

Strict dissipativity also plays an important role in the analysis of port-Hamiltonian systems, see [25], where the supply rate $w(t)$ has the form of a scalar product of the observed state and the control.

In contrast to systems with distributed control or systems that are governed by ordinary differential equations, there are only few contributions for systems with boundary control that are governed by hyperbolic partial differential equations. For a paper on the optimal Neumann control for the 1D wave equation and the corresponding exponential turnpike property, see [17]. A turnpike phenomenon for the optimal boundary control with a linear 2×2 system is studied in [8], where it is shown that the system has the *integral turnpike property*: This means that for the optimal values on the time intervals $[0, T]$, that are given by the objective functional J_T evaluated at an optimal control u_T we have

$$\sup_{T>0} J_T(u_T) < \infty. \tag{16.1}$$

Here the objective functional J_T has a similar structure as in (16.4) below. The integral turnpike property (16.1) implies in turn that for all $\varepsilon > 0$ there exists a number $\tilde{C}_\varepsilon > 0$ such that for all $T > 0$ we have

$$\mu\{t \in [0, T] : \|u_T(t) - u_\sigma\| > \varepsilon\} \leq \tilde{C}_\varepsilon. \tag{16.2}$$

Here u_σ denotes the optimal static control (i.e., the 'turnpike') and μ denotes the Lebesgue measure. Property (16.2) is called the *measure turnpike property*.

The results in [8] cover the case of a linearization of (ISO2), defined in (ISO2), that is linearized around a stationary state. Note that for the corresponding problem with the semi-linear system (ISO2), in general the uniqueness of the optimal control is lost, see [1]. An integral turnpike result for the optimal boundary control of gas pipeline flow governed by the isothermal Euler equations (ISO1) is presented in [9]. An integral turnpike result for optimal boundary control problems with the transport equation under uncertainty is shown in [23].

The turnpike phenomenon is an important justification for operational planning processes that are based on the optimization of static states. The reason is that if the turnpike property holds, for sufficiently large time horizons T the normalized difference between the optimal values of the static problem J_{stat} and the dynamic problems $J_T(u_T)$ becomes arbitrarily small in the sense that

$$\lim_{T\to\infty} \frac{1}{T} J_T(u_T) - J_{stat} = 0, \tag{16.3}$$

for details see [11], Theorem 3. Therefore, it makes sense to solve planning problems with static states, even if in the real operation transient phases occur on a regular basis. Property (16.3) can also be a justification for the quasi-static approach, see [10, 18] and for network designs that are based on static scenarios, see for example the study of optimal compressor location in [12, 26]. In order to control the transient situation, a feedback control can be used that steers the system to the computed static optimal control. Equation (16.3) implies that for sufficiently large time horizons T, this approach only leads to a small loss of optimality in the sense of a small increase in the objective functional. The turnpike property is also visible in the numerical simulations in [13], where a model of the European gas market is studied.

16.2 An Example with a Neural ODE

The following simple example illustrates the turnpike phenomenon. While the flow in gas pipelines can be modeled accurately by dynamics that are governed by partial differential equations (see the example in Sect. 16.3 below), we start with a simpler example that is governed by an ordinary differential equation (ODE). A general ODE has the form $y'(t) = f(t, y(t))$ and is thus determined by the continuous function f on the right-hand side. The universal approximation theorem (see [2]) implies that such a function can be approximated uniformly by neural network approximators on any bounded set. This motivates the consideration of neural ODEs, where the function f is given by a neural network of the form

$$f(t, y) = \sum_{i=1}^{p} \tanh\left(a_i^\top y + \alpha_i t + \beta_i\right) w_i(t)$$

with real numbers α_i, β_i, vectors a_i and vector-valued functions $w_i(t)$ ($i \in \{1, \cdots, p\}$) of the same dimension as the state y. These parameters can be considered as controls of the system. In order to simplify the setting, we only consider the functions $u(t) = (w_i(t))_{i=1}^p$ as controls.

Let an initial state $y_0 \in \mathbb{R}^d$ and a desired state $y_d \in \mathbb{R}^d$ be given. Let a terminal time $T > 0$ and a parameter $\gamma > 0$ be given. Consider the following optimal control problem with a neural ODE:

$$\mathbf{P}_T \left\{ \begin{array}{l} \min\limits_{u\in L^2(0,T)} \frac{1}{2} \int_0^T \sum\limits_{i=1}^{p} \|w_i(t)\|^2 \, dt + \frac{\gamma}{2} \int_0^T \|y(t) - y_d\|^2 \, dt \\ y(0) = y_0, \\ y'(t) = \sum_{i=1}^{p} \tanh\left(a_i^\top (y(t) - y_d) + \alpha_i t + \beta_i\right) w_i(t). \end{array} \right. \tag{16.4}$$

Here $\|\cdot\|$ denotes the Euclidean norm in $\mathbb{R}^d$. The corresponding static problem is

$$\min_{w_j \in \mathbb{R}^d,\, j \in \{1,\cdots,p\}} \sum_{i=1}^{p} \|w_i\|^2 + \frac{\gamma}{2} \|y - y_d\|^2$$

subject to the constraint $0 = \sum_{i=1}^{p} \tanh\left(a_i^\top (y - y_d) + \alpha_i t + \beta_i\right) w_i$.

Hence the static optimal control is $w_i^{stat} = 0$ $(i \in \{1, \ldots, p\})$ and the corresponding optimal static state is equal to y_d. For a real number r we use the notation

$$B_r(y_d) = \left\{ y \in \mathbb{R}^d : \|y - y_d\|^2 \leq r^2 \right\}.$$

Assume that there exists a radius $r > 0$ such that we have $y_0 \in B_r(y_d)$ and

$$m_0 = \inf_{y \in B_r(y_d),\, t \geq 0} \sum_{i=1}^{p} \tanh\left(a_i^\top (y - y_d) + \alpha_i t + \beta_i\right) > 0. \tag{16.5}$$

Then the following result holds: There exists a number $\bar{C} > 0$ that is independent of T such that for all $T > 0$ the optimal state and the optimal control for $\mathbf{P}_T$ have the *integral turnpike property* in the sense that we have

$$\int_0^T \|y(t) - y_d\|^2 + \sum_{i=1}^{p} \|w_i(t)\|^2 \, dt \leq \bar{C}. \tag{16.6}$$

This implies that for all $\varepsilon > 0$ we also have an upper bound $\tilde{C}_\varepsilon$ that is independent of T for the Lebesgue-measure μ of the set where the optimal integrand is greater than ε:

$$\mu\left\{ t \in [0, T] : \|y(t) - y_d\|^2 + \sum_{i=1}^{p} \|w_i(t)\|^2 > \varepsilon \right\} \leq \tilde{C}_\varepsilon$$

for all $T > 0$. Hence, the *measure-turnpike property* holds.

Now we show that (16.6) holds. Let us consider the control function that for $i \in \{1, \ldots, p\}$ is defined by the feedback law

$$w_i(t) = -\sqrt{\gamma}\,(y(t) - y_d). \tag{16.7}$$

Then for the Lyapunov function $L(t) = \frac{1}{2}\|y(t) - y_d\|^2$ we have

$$L'(t) = (y(t) - y_d)^\top y'(t) = -2\sqrt{\gamma} \sum_{i=1}^{p} \tanh\left(a_i^\top (y(t) - y_d) + \alpha_i t + \beta_i\right) L(t).$$

Due to (16.5), this yields the inequality

$$L'(t) \leq -2\sqrt{\gamma}\, m_0\, L(t),$$

and with Gronwall's Lemma this implies

$$L(t) \leq \exp\left(-2\sqrt{\gamma}\, m_0\, t\right) L(0).$$

Hence $\|y - y_d\|^2$ decays exponentially fast with the rate $2\sqrt{\gamma}\, m_0$. By the definition (16.7) of the w_i, this implies in turn that $\sum_{i=1}^{p} \|w_i\|^2$ decays exponentially fast with the same rate.

Since the control (16.7) is feasible for the optimal control problem $\mathbf{P}_T$, this implies (16.6), where the upper bound $\bar{C}$ is given by the value of the objective functional for the control $(w_i)_i$ defined in (16.7) and the generated state extended to the infinite time horizon $(0, \infty)$, to be precise by

$$\bar{C} = \int_0^\infty ||y(t) - y_d||^2 + \sum_{i=1}^{p} \|w_i(t)\|^2 \, dt.$$

Note that if $y_0 \neq y_d$, for the feedback control (16.7) for all t we have $w_i(t) \neq 0$, while the optimal control is switched off at the time T, that is at the end of the time horizon. For a more general analysis of the turnpike property for systems that are governed by neural ODEs see [6].

16.3 An Example with a Gas Network (Gaslib11)

In this section we consider an optimal compressor control problem for gas transport on the GasLib-11 (gaslib.zib.de) network, which consists of 11 nodes (3 inflows, 5 inner nodes, 3 outflows), 8 edges and 2 compressor controls, as visualized in Fig. 16.1. This example shows that optimal control problems with exponential damping on the boundary data (the gas outflow) satisfy a turnpike structure even if the state is not penalized in the objective function.

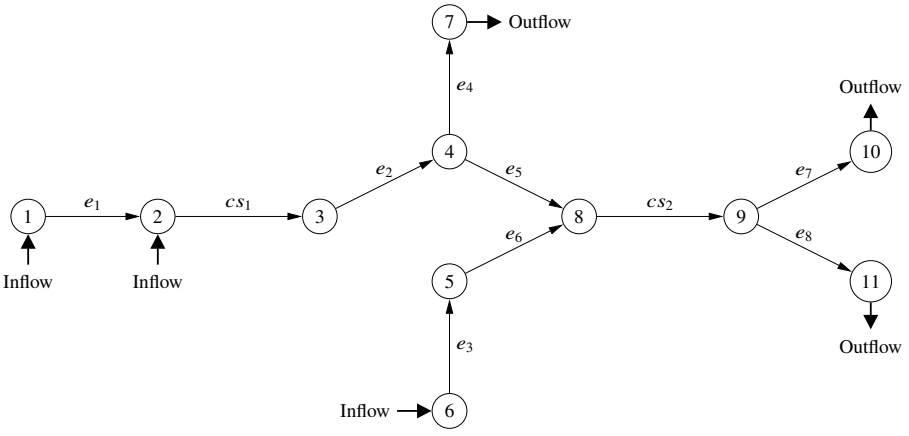


Fig. 16.1: A scheme of the GasLib-11 with closed valve

The gas flow on the edges $e_1 - e_8$ is defined by the isothermal Euler equations (introduced in Chap. 2.3)

$$\begin{aligned}
&\frac{\partial}{\partial t}p^e(t,x) + \frac{c^2}{A^e}\frac{\partial}{\partial x}q_m^e(t,x) \;=\; 0,\\
&\frac{\partial}{\partial t}q_m^e(t,x) + \frac{\partial}{\partial x}\left(A^e p^e(t,x) + \frac{c^2}{A^e}\frac{(q_m^e(t,x))^2}{p^e(t,x)}\right) \;=\; -\frac{\lambda^e}{2D^e}\frac{c^2}{A^e}\frac{q_m^e(t,x)|q_m^e(t,x)|}{p^e(t,x)},
\end{aligned} \tag{16.8}$$

where p^e is the pressure in Pa, q_m^e is the massflow in kg/s, q^e is the mass flux in kg/(m^{2}s), c is the speed of sound in the gas, A^e is the pipe cross section and λ^e is the pipe friction coefficient for edge e, respectively. For the boundary data we consider constant gas pressure at the inflow nodes, i.e., we consider

$$p_1(t) = 55 \text{ bar}, \qquad p_2(t) = 52 \text{ bar}, \qquad p_6(t) = 53 \text{ bar}. \tag{16.9}$$

Further let perturbed gas outflows at the nodes v_7, v_{10} and v_{11} in $kg/(m^2 s)$ be given, that decay exponentially fast

$$\begin{aligned}
b_7(t) &= 50 * \sin\left(\left(\frac{t}{24\cdot 60\cdot 60} - \frac{3}{2}\pi\right)\cdot 4\pi\right)\cdot \exp\left(-\frac{10\,t}{36\cdot 60\cdot 60}\right) + 125,\\
b_{10}(t) &= 70 * \sin\left(\frac{t}{24\cdot 60\cdot 60}\cdot 2\pi\right)\cdot \exp\left(-\frac{10\,t}{36\cdot 60\cdot 60}\right) + 115,\\
b_{11}(t) &= 60 * \sin\left(\left(\frac{t}{24\cdot 60\cdot 60} + \frac{1}{2}\pi\right)\cdot 2\pi\right)\cdot \exp\left(-\frac{10\,t}{36\cdot 60\cdot 60}\right) + 130.
\end{aligned} \tag{16.10}$$

These outflows are illustrated in Fig. 16.2 without damping and in Fig. 16.3 with damping.

At the network junctions v_k ($k \in \{3, 4, 5, 8, 9\}$), as coupling conditions, we consider conservation of mass and continuity in pressure (see Sect. 2.5.2). For the compressor stations we consider the multiplicative model (see Sect. 2.9)

$$\frac{p_{\text{out}}^{cs_i}(t)}{p_{\text{in}}^{cs_i}(t)} = u_i(t) \geq 1 \qquad i = 1, 2, \tag{16.11}$$

where $p_{\text{in}}^{cs_i}$ and $p_{\text{out}}^{cs_i}$ are the ingoing and outgoing pressure at the compressor stations, respectively. The initial condition corresponds to the steady states associated with the boundary data at $t = 0$ and compressor controls $u_1 = u_2 = 1$. Finally, let pressure

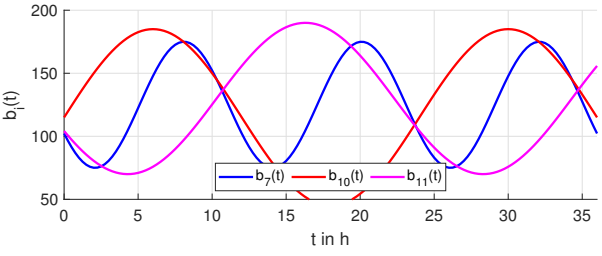


Fig. 16.2: Boundary data for the outflow nodes without damping

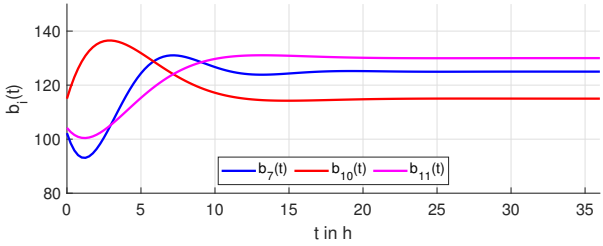


Fig. 16.3: Boundary data for the outflow nodes with damping

bounds

$$p_{\min} = 40 \text{ bar}, \qquad p_{\max} = 70 \text{ bar}, \tag{16.12}$$

be given at all nodes.

We consider the optimal compressor control problem

$$\begin{aligned} \min_{u(t)\in L^2(0,T)^2} \quad & \|u(t)\|^2_{L^2(0,T)}, \\ \text{s.t.} \quad & \text{isothermal Euler equations (16.8) on every edge,} \\ & \text{boundary conditions (16.9), (16.10) at nodes } v_1, v_2, v_6, v_7, v_{10}, v_{11}, \\ & \text{coupling conditions at nodes } v_3, v_4, v_5, v_8, v_9, \\ & \text{compressor model (16.11) on } cs_1, cs_2, \\ & \text{initial conditions at every edge,} \\ & \text{pressure bounds (16.12) at every node.} \end{aligned} \tag{16.13}$$

The optimal controls of (16.13) are shown in Fig. 16.4 for the boundary data without damping (cf. Fig. 16.2), and in Fig. 16.5 for the boundary data with exponential damping (cf. Fig. 16.3). A turnpike structure is clearly observable for the optimal control with exponential damping. While turnpike structures for optimal boundary control problems with hyperbolic PDEs such as (16.13) usually require an additional tracking term for the states in the objective function (see, e.g.,, [8, 23, 27]), the exponential damping of the boundary data suffices to ensure a turnpike structure.

The corresponding optimal pressures at the outflow nodes v_7, v_{10} and v_{11} are shown in Fig. 16.6 and Fig. 16.7. The optimal controls maintain pressures above the lower bound by compensating the pressure loss along the pipes caused by pipe friction. The exponential damping in the boundary data has a pronounced stabilizing effect on the system dynamics. As the perturbation of the boundary outflows decay over time, the optimal controls approach steady-state values more rapidly, leading to pressure profiles that remain close to their stationary counterparts over most of the time horizon. This behavior exemplifies the turnpike phenomenon, where both the control and the state spend the majority of the optimization horizon near the steady-state solution, deviating only near the initial and terminal phases.

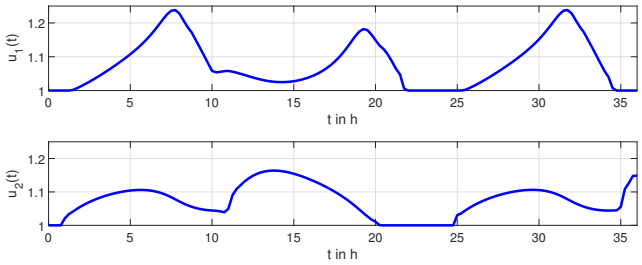


Fig. 16.4: Optimal compressor controls of (16.13) with the boundary data shown in Fig. 16.2

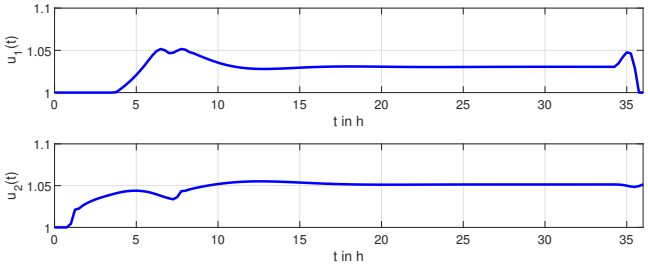


Fig. 16.5: Optimal compressor controls of (16.13) with the boundary data shown in Fig. 16.3

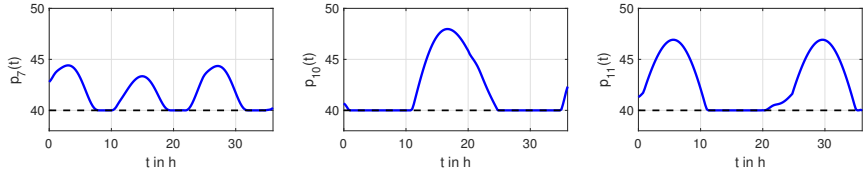


Fig. 16.6: Optimal pressures at the outflow nodes v_7, v_{10},v_{11} for the optimal controls shown in Fig. 16.4

In contrast, without damping, the persistent oscillations in the boundary data induce sustained temporal variations in the pressures, preventing convergence toward a quasi-stationary regime. The damping thus effectively suppresses transient fluctuations and promotes the emergence of a distinct turnpike structure in both the control and the pressure variables.

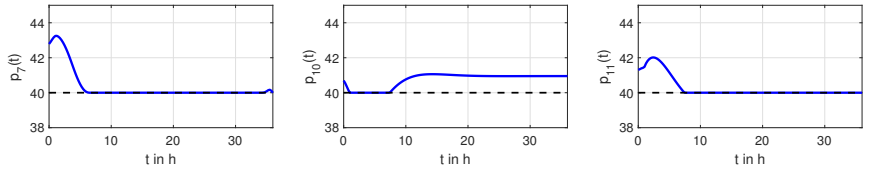


Fig. 16.7: Optimal pressures at the outflow nodes v_7, v_{10},v_{11} for the optimal controls shown in Fig. 16.5

Conclusion

This chapter studied turnpike behavior in the dynamic optimal control of gas networks, combining theoretical analysis with illustrative numerical examples. The neural ODE example admitted an analytical treatment via the Lyapunov method, while the GasLib-11 example highlighted the practical relevance of exponential boundary damping as a mechanism that suffices to generate a turnpike structure. A key finding is that exponential damping of boundary data alone can induce a turnpike structure, even in the absence of a state-tracking term in the objective functional. This relaxes a condition typically assumed in the hyperbolic PDE setting. The results reinforce the theoretical justification for static and quasi-static planning models in gas network operation, and suggest that turnpike-aware control design can reduce the computational burden without substantial loss of optimality.

Open questions include the extension of exponential turnpike results to quasi-linear hyperbolic systems and the characterization of turnpike behavior under stochastic supply and demand uncertainty. These properties are particularly relevant in model predictive control contexts, where exploiting the turnpike structure can substantially reduce the effective optimization horizon.

Acknowledgements This work was supported by the German Research Foundation (DFG) within Subprojects C03 and C05 in the Sonderforschungsbereich/Transregio 154 “Mathematical Modelling, Simulation and Optimization using the Example of Gas Networks” (Project ID 239904186).

References

1. C. Christof and D. Hafemeyer. On the nonuniqueness and instability of solutions of tracking-type optimal control problems. *Mathematical Control and Related Fields*, 12(2):421–431, 2022. doi:10.3934/mcrf.2021028.
2. G. Cybenko. Approximation by superpositions of a sigmoidal function. *Mathematics of Control, Signals and Systems*, 2(4):303–314, 1989. doi:10.1007/BF02551274.
3. T. Faulwasser and L. Grüne. Turnpike properties in optimal control: An overview of discrete-time and continuous-time results. In E. Trélat and E. Zuazua, ed., *Numerical Control: Part A*, volume 23 of *Handbook of Numerical Analysis*, chapter 11, pages 367–400. Elsevier, 2022. doi:10.1016/bs.hna.2021.12.011.

4. T. Faulwasser and C. M. Kellett. Dissipativity in infinite-horizon optimal control: Willems' 1971 paper revisited. *IFAC-PapersOnLine*, 55(30):49–54, 2022. doi:10.1016/j.ifacol.2022.11.027.
5. L. Grüne, S. Pirkelmann, and M. Stieler. Strict dissipativity implies turnpike behavior for time-varying discrete time optimal control problems. In *Control Systems and Mathematical Methods in Economics: Essays in Honor of Vladimir M. Veliov*, pages 195–218. Springer, 2018. doi:10.1007/978-3-319-75169-6_10.
6. M. Gugat. Optimal control of neural differential equations: The turnpike property. Available at SSRN. doi:10.2139/ssrn.5503851.
7. M. Gugat and J. Giesselmann. An observer for pipeline flow with hydrogen blending in gas networks: Exponential synchronization. *SIAM Journal on Control and Optimization*, 62(4):2273–2296, 2024. doi:10.1137/23M1563840.
8. M. Gugat and F. M. Hante. On the turnpike phenomenon for optimal boundary control problems with hyperbolic systems. *SIAM Journal on Control and Optimization*, 57(1):264–289, 2019. doi:10.1137/17M1134470.
9. M. Gugat and M. Herty. A turnpike result for optimal boundary control of gas pipeline flow. In *25th International Symposium on Mathematical Theory of Networks and Systems (MTNS 2022)*, pages 12–16, 2022. doi:10.15495/EPub_UBT_00006809.
10. M. Gugat, R. Krug, and A. Martin. Transient gas pipeline flow: Analytical examples, numerical simulation and a comparison to the quasi-static approach. *Optimization and Engineering*, 24(1):425–446, 2023. doi:10.1007/s11081-021-09690-4.
11. M. Gugat and M. Lazar. Turnpike properties for partially uncontrollable systems. *Automatica*, 149:110844, 2023. doi:10.1016/j.automatica.2022.110844.
12. M. Gugat, M. Schuster, and J. Sokołowski. The location problem for compressor stations in pipeline networks. *Mathematics and Mechanics of Complex Systems*, 12(4):507–546, 2024. doi:10.2140/memocs.2024.12.507.
13. M. Gugat, M. Schuster, and S. Steffensen. A dynamic multilevel model of the European gas market. *Communications in Optimization Theory*, 11:1–26, 2023. doi:10.23952/cot.2023.11.
14. M. Gugat and J. Sokolowski. On problems of dynamic optimal nodal control for gas networks. *Pure and Applied Functional Analysis*, 5:1699–1715, 2022. URL: http://yokohamapublishers.jp/online2/oppafa/vol7/p1699.html.
15. M. Gugat and J. Sokolowski. An aspect of the turnpike property. Long time horizon behavior. *Serdica Mathematical Journal*, 49:127–154, 2023. doi:10.55630/serdica.2023.49.127-154.
16. M. Gugat, J. Sokolowski, and M. Qian. Network Design and Control: Shape and Topology Optimization for the Turnpike Property for the Wave Equation. *Journal of Geometric Analysis*, 34, 2024. doi:10.1007/s12220-024-01712-8.
17. M. Gugat, E. Trélat, and E. Zuazua. Optimal Neumann control for the 1D wave equation: Finite horizon, infinite horizon, boundary tracking terms and the turnpike property. *Systems & Control Letters*, 90:61–70, 2016. doi:10.1016/j.sysconle.2016.02.001.
18. H. Heitsch, R. Henrion, and C. Tischendorf. Probabilistic maximization of time-dependent capacities in a gas network. *Optimization and Engineering*, 26(1):365–400, 2025. doi:10.1007/s11081-024-09908-1.
19. K. Kunisch and L. Pfeiffer. The effect of the terminal penalty in receding horizon control for a class of stabilization problems. *ESAIM: Control, Optimisation and Calculus of Variations*, 26:58, 2020. doi:10.1051/cocv/2019037.
20. K. Liu, L. T. Biegler, B. Zhang, and Q. Chen. Dynamic optimization of natural gas pipeline networks with demand and composition uncertainty. *Chemical Engineering Science*, 215:115449, 2020. doi:10.1016/j.ces.2019.115449.
21. L. W. McKenzie. Turnpike theorems for a generalized leontief model. *Econometrica: Journal of the Econometric Society*, pages 165–180, 1963. doi:10.2307/1910955.
22. A. J. Osiadacz and M. Kwestarz. Nonlinear steady-state optimization of large-scale gas transmission networks. *Energies*, 14(10):2832, 2021. doi:10.3390/en14102832.
23. N. Sakamoto and M. Schuster. A turnpike result for boundary control problems governed by the transport equation under uncertainty. *Mathematics of Control, Signals, and Systems*, 2025. doi:10.1007/s00498-025-00422-y.
24. P. A. Samuelson. A catenary turnpike theorem involving consumption and the golden rule. *The American Economic Review*, 55(3):486–496, 1965. URL: https://www.jstor.org/stable/1814560.

25. A. Sarkar, V. K. Singh, M. Schaller, and K. Worthmann. Energy-optimal control of discrete-time port-hamiltonian systems. *IEEE Control Systems Letters*, 2025. doi:10.1109/LCSYS.2025.35793910.
26. M. Schuster. On the optimal location of multiple compressor stations in pipeline networks under uncertainty. In *2025 29th International Conference on Methods and Models in Automation and Robotics (MMAR)*, pages 148–153. IEEE, 2025. doi:10.1109/MMAR65820.2025.11151027.
27. M. Schuster and J. Sokolowski. The topological derivative method for optimum shape design and control of gas networks. *Journal of Applied and Numerical Optimization*, 7(3):309–332, 2025. doi:10.23952/jano.7.2025.3.03.
28. E. Trélat and E. Zuazua. Turnpike in optimal control and beyond: A survey, 2025. arXiv:2503.20342, doi:10.48550/arXiv.2503.20342.
29. J. C. Willems. Dissipative dynamical systems part i: General theory. *Archive for Rational Mechanics and Analysis*, 45(5):321–351, 1972. doi:10.1007/BF00276493.
30. A. J. Zaslavski. *Turnpike Phenomenon in Metric Spaces*. Springer, 2023.

Open Access This chapter is licensed under the terms of the Creative Commons Attribution-NonCommercial-NoDerivatives 4.0 International License (http://creativecommons.org/licenses/by-nc-nd/4.0/), which permits any noncommercial use, sharing, distribution and reproduction in any medium or format, as long as you give appropriate credit to the original author(s) and the source, provide a link to the Creative Commons license and indicate if you modified the licensed material. You do not have permission under this license to share adapted material derived from this chapter or parts of it.

The images or other third party material in this chapter are included in the chapter's Creative Commons license, unless indicated otherwise in a credit line to the material. If material is not included in the chapter's Creative Commons license and your intended use is not permitted by statutory regulation or exceeds the permitted use, you will need to obtain permission directly from the copyright holder.



Chapter 17
Domain Decomposition for Gas Network Control

Falk M. Hante[0000−0001−9762−2903],
Martin Hernandez[0009−0003−4799−6853],
Günter Leugering[0000−0002−1086−991X],
Martin Schmidt[0000−0001−6208−5677], and
Enrique Zuazua[0000−0002−1377−0958]

Abstract We present domain decomposition techniques for efficient and scalable simulation and optimization of partial differential equations on network domains. Motivated by transient gas network applications, the state-of-the-art of space-and-time decompositions for systems derived from Euler's equations are presented. Moreover, combinatorial aspects of switching valves are addressed in a decomposition framework for mixed-integer and ODE-constrained problems and a convergence analysis is presented. Motivated by stochastic approximation, we also propose and explore randomized decomposition approaches. Some of these advanced solution strategies can be combined and regarded as variants of certain penalty alternating direction methods. We present the potential applications of these techniques by summarizing numerical results from the literature for transient GasLib instances modeling a realistic gas transport network.

17.1 Introduction

Partial differential equations posed on networked domains (metric graphs) arise in a variety of applications and have been extensively studied with contributions to diffusion and transport [7, 24, 51, 59, 67], singular perturbation regimes [11, 22], and control of

Falk M. Hante
Department of Mathematics, HU Berlin, Germany, e-mail: falk.hante@hu-berlin.de

Martin Hernandez
Department of Statistics and Data Science, University of California, Los Angeles, USA,
e-mail: martinh@g.ucla.edu

Günter Leugering
Department of Mathematics, FAU Erlangen-Nürnberg, Germany, e-mail: guenter.leugering@fau.de

Martin Schmidt
Department of Mathematics, Trier University, Germany, e-mail: martin.schmidt@uni-trier.de

Enrique Zuazua
Department of Mathematics, FAU Erlangen-Nürnberg, Germany, e-mail: enrique.zuazua@fau.de

© The Author(s) 2027

A. Martin et al. (eds.), *Mathematical Modelling, Simulation and Optimization using the Example of Gas Networks*, International Series of Numerical Mathematics 174,
https://doi.org/10.1007/978-3-032-34969-9_17

parabolic and hyperbolic systems [1, 12, 21]. A central motivating example throughout this chapter is transient gas transport in pipeline networks.

As the size and topological complexity of the network increase, solving these systems becomes computationally demanding, particularly in time-dependent and control problems [73]. This is especially the case for gas networks, where long horizons and operational tasks (e.g., estimation, scheduling, and feedback control) require repeated large-scale solves. To address this challenge, domain decomposition methods have been developed and widely applied [57]. Classic formulations include overlapping (Schwarz-type) and non-overlapping (Schur-complement) variants; see [57, Chap. III] and [75].

These techniques divide the global domain into smaller subdomains on which the problem is solved locally. In a typical setting, one proceeds iteratively: at each step, the PDE is solved over an individual subdomain for the entire time interval, using boundary data from neighboring subdomains computed in the previous iteration. This procedure defines a sequence of approximate solutions that, under technical conditions, converges in a suitable norm to a solution on the entire domain. While effective, this approach requires repeated resolution of full time-dependent problems on each subdomain, making the method computationally slow, especially when the number of subdomains or the time-horizon is large. In the gas network setting, a subdomain corresponds to a subnetwork of pipes and the interface data correspond to junction conditions, so global synchronization is a major cost driver. This naturally raises the question of whether it is possible to design methods that avoid solving the PDE in each subdomain over the full time interval, while still preserving approximation guarantees.

Classic space and time domain decomposition methods (STDDM) aim at efficient solvers for large-scale simulation, particularly in the context of optimal control problems for PDEs on networked domains. There are numerous textbooks available, cf. Quarteroni and Valli [75] for an early contribution, Dolean et al. [19] for a more recent textbook. The biannual proceedings of the "Domain Decomposition Conference"[1] can be seen as a regular update of the state of the art. See also [57] and [62] for an overview. We also refer to [61], where the two-link transmission problem has been discussed. As for time-domain decomposition, we refer to [27–29, 41, 57, 65, 86]. See further [19] and in particular Gander [30].

Another possible path to overcome the computational burden for solving a PDE in network settings is to relax the notion of convergence and to work in an average sense. This is precisely the philosophy behind the *Random Batch Method* (RBM). Originally introduced in the context of interacting particle systems, the RBM constructs a stochastic approximation of the dynamics by considering, over short time intervals, only the interactions within a randomly selected batch of particles, instead of computing all pairwise interactions. The method switches to a new random batch at each temporal window. In [46], it is shown that the RBM converges in expectation to the original interacting particle system as the time intervals decrease, i.e., as the batch switching increases. As expected, restricting to partial interaction information can yield a substantial reduction in both computational cost and memory usage.

In this chapter, we present advanced domain decomposition techniques designed for the efficient and scalable simulation as well as optimization of partial differential

[1] See https://www.ddm.org.

equations on network domains. The work is motivated by the complexities of transient gas network applications, where the need for robust and scalable solutions is paramount. We present state-of-the-art space-and-time decomposition methods tailored for semi-linear hyperbolic and nonlinear parabolic systems derived from Euler's equations. A significant contribution of our research is the integration of combinatorial aspects, such as switching valves, within a decomposition framework. We report on the available convergence analysis in the context of mixed-integer controls. Inspired by stochastic approximation techniques, we also propose and explore randomized decomposition methods.

Some of these innovative strategies can be combined and, in their primal reformulation, be viewed as variants of certain penalty alternating direction methods, offering flexible and powerful tools for solving complex network problems. To validate the potential of these techniques, we review extensive computational experiments on realistic and transient GasLib instances. Our findings underscore the practical applicability and effectiveness of the proposed methods in real-world scenarios. Throughout this article, we provide a comprehensive overview of our methodologies, their theoretical foundations, and their practical implications. This includes detailed discussions on the decomposition frameworks, convergence analyses, and the integration of combinatorial and stochastic elements. Our results not only advance the current state of the art but also pave the way for future research in the simulation and optimization of large-scale network systems.

The remainder of this chapter is organized as follows. Space-time domain decomposition methods are discussed in Sect. 17.2, while the ODE-constrained case including mixed-integer aspects is reviewed in Sect. 17.3. Randomized domain decomposition methods are the subject of Sect. 17.4. Then, a consensus-based penalty alternating direction method for the fully discretized case in presented in Sect. 17.5 before we close the chapter in Sect. 17.6 with some concluding remarks.

17.2 Space-Time Domain Decomposition Methods

In this section, we present abstract formulations of optimal control problems on gas networks and their possible decompositions both in space and time based on optimality conditions. We concentrate on two models from the catalog in Chap. 2, "A Catalog of Gas Network Models: PDEs, Coupling Conditions, and Numerical Schemes" of this book, namely (ISO2) and (ISO3), derived from the classic Euler system. In Sect. 17.2.1, the concept of metric graphs together with standard notation is introduced. We refer to (2.130) and (2.131) for the corresponding network problems. In Sect. 17.2.3, we discuss optimal control problems for (2.130) and their space-time decomposition based on optimality conditions. In Sect. 17.2.4 we discuss optimal control problems for (2.131) and their space-time decomposition. While these results are, in themselves, novel theoretical contributions, they may also be viewed as a starting point for the computational approaches presented in the upcoming sections. For earlier works motivated by gas transport network applications, we refer to [53, 54, 63]

17.2.1 Network Modeling

Let $G = (V, E)$ denote the graph of the gas network with vertices (nodes) $V = \{n_1, n_2, \ldots, n_{|V|}\} = \{n_j : j \in \mathcal{J}\}$ and directed edges (arcs) $E = \{e_1, e_2, \ldots, e_{|E|}\} = \{e_i : i \in \mathcal{I}\}$. For each directed edge e_i, $i \in I$, and each node n_j, $j \in \mathcal{J}$, we define the edge-node incidence coefficients

$$d_{ij} = \begin{cases} -1, & \text{if the the edge } e_i \text{ starts at node } n_j, \\ +1, & \text{if the edge } e_i \text{ ends at node } n_j, \\ 0, & \text{else.} \end{cases}$$

We introduce the edge degree $d_j := |\mathcal{I}_j|$ as the number of edges incident at node j. We introduce the set $\mathcal{J}^M$ for all nodes with node degree of at least 2 and the sets $\mathcal{J}^S_{D/N}$ represents simple Dirichlet or Neumann nodes.

17.2.1.1 The Semilinear Model (ISO2) on a Network

As presented in Chap. 2, "A Catalog of Gas Network Models: PDEs, Coupling Conditions, and Numerical Schemes", the semilinear pipe model (ISO2) yields the following dynamics on the graph G:

$$\begin{aligned}
&\frac{\partial}{\partial t}\rho_i + \frac{\partial}{\partial x}q_i = 0, && i \in \mathcal{I},\ x \in (0, \ell_i),\ t \in (0, T,) \\
&\frac{\partial}{\partial t}q_i + c^2\frac{\partial}{\partial x}\rho_i = -\frac{\lambda}{2D_i\rho_i}q_i|q_i|, && i \in \mathcal{I},\ x \in (0, \ell_i),\ t \in (0, T), \\
&\rho(n_j, t) = \rho(n_j, t), && \forall i, k \in \mathcal{I}_j,\ j \in \mathcal{J}^M,\ t \in (0, T), \\
&\sum_{i \in \mathcal{I}_j} d_{ij}q(n_j, t)) = 0, && j \in \mathcal{J}^M,\ t \in (0, T), \\
&\rho(n_j, t) = g_i(t), && i \in \mathcal{I}_j, j \in \mathcal{J}^S_D,\ t \in (0, T), \\
&q(n_j, t) = h_i(t), && i \in \mathcal{I}_j, j \in \mathcal{J}^S_N,\ t \in (0, T), \\
&\rho_i(x, 0) = \rho_{i,0}(x),\ q_i(x, 0) = q_{i0}(x), && x \in (0, \ell_i).
\end{aligned} \tag{17.1}$$

The system consists of a continuity equation and a momentum equation for gas densities ρ_i and gas mass flow q_i with parameters λ, D_i and c denoting a friction coefficient, pipe diameter, and the speed of sound in natural gas. Further modeling details and extensions including non-zero pipe slopes, compressor models, valves, etc. will be introduced in Sect. 17.5. For our purposes here, we regard $g_i(t), h_i(t)$, $i = 1, \ldots, m$, as controls and reformulate (17.1) as a system of semi-linear hyperbolic balance laws.

To this end, we introduce characteristics or Riemann invariants. We define $F_i(\rho_i, q_i) := -(\lambda)(2D_i\rho_i)q_i|q_i|$. Introduce the Riemann invariants $w_i^+ := q_i + c_i\rho_i, w_i^- := q_i - c_i\rho_i$, which propagate at speeds $+c_i$ and $-c_i$. In vector form,

$$y_i := \begin{pmatrix} w_i^+ \\ w_i^- \end{pmatrix}, \quad \Lambda_i := \begin{bmatrix} c_i & 0 \\ 0 & -c_i \end{bmatrix}.$$

Then, (17.1) with $\tilde{F}_i$ as F_i rewritten in (w_i^+, w_i^-) and stacking all edges, $y := \mathrm{col}(y_1, \ldots, y_{|E|}) \in \mathbb{R}^{2|E|}, \Lambda := \mathrm{blkdiag}(\Lambda_1, \ldots, \Lambda_{|E|})$, we obtain the global interior PDE

$$\partial_t y + \Lambda\, \partial_x y = \tilde{F}(y) \quad \text{in } (0,T) \times (0, L_1) \times \cdots \times (0, \ell_{|E|})$$

with initial data $y_i(0,x) = y_{i,0}(x)$. For each edge, we collect the four endpoint invariants

$$\mathbf{y}_i^{\mathrm{end}} := \begin{pmatrix} w_i^+(0) \\ w_i^-(0) \\ w_i^+(\ell_i) \\ w_i^-(\ell_i) \end{pmatrix} \in \mathbb{R}^4, \quad \mathbf{y}^{\mathrm{end}} := \mathrm{col}\left(\mathbf{y}_1^{\mathrm{end}}, \ldots, \mathbf{y}_{|E|}^{\mathrm{end}}\right) \in \mathbb{R}^{4|E|}.$$

At each node n_j, define the vectors of *incoming* and *outgoing* characteristics at the node location are given by

$$\boldsymbol{\beta}_j := \mathrm{col}\left(\beta_{ij}\right)_{i \in \mathcal{I}_j}, \quad \boldsymbol{\alpha}_j := \mathrm{col}\left(\alpha_{ij}\right)_{i \in \mathcal{I}_j}$$

with

$$\beta_{ij} := \begin{cases} w_i^-(0^+), & \text{if } d_{ij} = -1, \\ w_i^+(\ell_i^-), & \text{if } d_{ij} = +1, \end{cases} \quad \text{and} \quad \alpha_{ij} := \begin{cases} w_i^+(0^+), & \text{if } d_{ij} = -1, \\ w_i^-(\ell_i^-), & \text{if } d_{ij} = +1. \end{cases}$$

There exist fixed *selector matrices* $B_j, A_j \in \mathbb{R}^{d_j \times 4|E|}$ such that

$$\boldsymbol{\beta}_j = B_j\, \mathbf{y}^{\mathrm{end}}, \quad \boldsymbol{\alpha}_j = A_j\, \mathbf{y}^{\mathrm{end}}.$$

We proceed with an explicit construction of the matrices. Let $E_i^{(0)} \in \mathbb{R}^{2 \times 4|E|}$ pick the ith edge's $(\cdot, 0)$ entries, i.e.,

$$E_i^{(0)} := \Bigg[0 \cdots 0 \underbrace{\qquad I_2 \qquad}_{\mathrm{col\ ind} = 4(i-1)+1:4(i-1)+2} 0 \cdots 0 \Bigg],$$

$$E_i^{(\ell)} := \Bigg[0 \cdots 0 \underbrace{\qquad I_2 \qquad}_{\mathrm{col_{ind}} = 4(i-1)+3:4(i-1)+4} 0 \cdots 0 \Bigg],$$

and let $S^+ := [1\ 0]$ as well as $S^- := [0\ 1]$. Then the rth row of B_j (corresponding to edge $i_r \in \mathcal{I}_j$) is

$$\left(B_j\right)_{r,\cdot} = \begin{cases} S^- E_{i_r}^{(0)}, & \text{if } d_{i_r j} = -1, \\ S^+ E_{i_r}^{(\ell)}, & \text{if } d_{i_r j} = +1, \end{cases} \quad \text{and} \quad \left(A_j\right)_{r,\cdot} = \begin{cases} S^+ E_{i_r}^{(0)}, & \text{if } d_{i_r j} = -1, \\ S^- E_{i_r}^{(\ell)}, & \text{if } d_{i_r j} = +1. \end{cases}$$

Stacking all nodes, we get

$$\boldsymbol{\beta} := \operatorname{col}(\boldsymbol{\beta}_j)_{j\in\mathcal{J}} =: B\,\mathbf{y}^{\mathrm{end}}, \quad \boldsymbol{\alpha} := \operatorname{col}(\boldsymbol{\alpha}_j)_{j\in\mathcal{J}} =: A\,\mathbf{y}^{\mathrm{end}}, \tag{17.2}$$

with $B := \operatorname{blkdiag}(B_j)$ and $A := \operatorname{blkdiag}(A_j)$.

For an interior node n_j with equal characteristic impedances (or after impedance-weighting), the *scattering law*

$$\boldsymbol{\alpha}_j = S_j\,\boldsymbol{\beta}_j + \mathbf{s}_j(t), \quad S_j = I_{d_j} - \frac{2}{d_j}\mathbf{1}\mathbf{1}^{\top}, \quad S_j^2 = I_{d_j}, \tag{17.3}$$

enforces continuity of ρ and the Kirchhoff flux sum at n_j. For heterogeneous impedances $Z_{ij} > 0$, we have

$$S_j = I_{d_j} - 2\,\frac{Z_j^{-1}\mathbf{1}\,\mathbf{1}^{\top}}{\mathbf{1}^{\top}Z_j^{-1}\mathbf{1}}, \quad Z_j := \operatorname{diag}(Z_{ij})_{i\in\mathcal{I}_j}.$$

Prescribed boundary ports are absorbed in the affine term $\mathbf{s}_j(t)$ (Dirichlet/Neumann data).

Stacking (17.3) over all nodes and using (17.2) gives the *global block relation*

$$A\,\mathbf{y}^{\mathrm{end}}(t) = S\,B\,\mathbf{y}^{\mathrm{end}}(t) \;+\; \mathbf{s}(t), \quad S := \operatorname{blkdiag}(S_j)_{j\in\mathcal{J}}, \quad \mathbf{s} := \operatorname{col}(\mathbf{s}_j)_{j\in\mathcal{J}}. \tag{17.4}$$

Equivalently, $C\,\mathbf{y}^{\mathrm{end}}(t) = \mathbf{s}(t)$, $C := A - SB$. As for the boundary conditions, we define the global *incoming/outgoing* stacks in "left/right" order:

$$\mathbf{y}^{\mathrm{in}} := \begin{pmatrix} y^{+}(L) \\ y^{-}(0) \end{pmatrix}, \quad \mathbf{y}^{\mathrm{out}} := \begin{pmatrix} y^{+}(0) \\ y^{-}(L) \end{pmatrix}.$$

There exist permutation/selection matrices $P_{\mathrm{in}}, P_{\mathrm{out}} \in \mathbb{R}^{m\times 4|E|}$ (with $m = \sum_j d_j$) such that

$$\begin{aligned} \boldsymbol{\beta} = B\,\mathbf{y}^{\mathrm{end}} = P_{\mathrm{in}}\,\mathbf{y}^{\mathrm{end}} \;&\Longrightarrow\; \mathbf{y}^{\mathrm{in}} = \Pi_{\mathrm{in}}\,\boldsymbol{\beta}, \\ \boldsymbol{\alpha} = A\,\mathbf{y}^{\mathrm{end}} = P_{\mathrm{out}}\,\mathbf{y}^{\mathrm{end}} \;&\Longrightarrow\; \mathbf{y}^{\mathrm{out}} = \Pi_{\mathrm{out}}\,\boldsymbol{\alpha}, \end{aligned}$$

with $\Pi_{\mathrm{in}}, \Pi_{\mathrm{out}}$ simply reordering the node-incident entries into the stacked $y^{\pm}(\cdot)$ blocks. Since $P_{\mathrm{in}}, P_{\mathrm{out}}, \Pi_{\mathrm{in}}, \Pi_{\mathrm{out}}$ are (block) permutations, they are invertible with inverses equal to their transposes. Using (17.4),

$$\boldsymbol{\alpha} = S\,\boldsymbol{\beta} + \mathbf{s} \;\Longrightarrow\; \mathbf{y}^{\mathrm{out}} = \underbrace{\Pi_{\mathrm{out}}\,S\,\Pi_{\mathrm{in}}^{-1}}_{=:\,\mathsf{K}}\;\mathbf{y}^{\mathrm{in}} \;+\; \underbrace{\Pi_{\mathrm{out}}\,\mathbf{s}}_{=:\,\mathbf{k}(t)}.$$

Hence, in compact left/right form, we have

$$\begin{bmatrix} y^{+}(0) \\ y^{-}(L) \end{bmatrix} = \mathsf{K}\begin{bmatrix} y^{+}(L) \\ y^{-}(0) \end{bmatrix} \;+\; \mathbf{k}(t), \quad \mathsf{K} := \Pi_{\mathrm{out}}\,S\,\Pi_{\mathrm{in}}^{-1}.$$

This is equivalent to (17.4).

Remark 17.1 If boundary controls $u(t)$ act on a subset of ports (e.g., Neumann/Robin actuation), they appear (i) either by making $\mathbf{k}(t)$ affine in $u(t)$, or (ii) as source injections through a distributed term $B_d u(t)$. In the compact interior form we may write

$$\begin{aligned} &\partial_t y + \Lambda\, \partial_x y = \tilde{F}(y) \;+\; B_d\, u(t), && (x,t) \in (0,L)\times(0,T),\\ &\begin{bmatrix} y^+(0) \\ y^-(L) \end{bmatrix} = \mathsf{K} \begin{bmatrix} y^+(L) \\ y^-(0) \end{bmatrix} + \mathsf{K}_u\, u(t) + \mathbf{k}_0(t), && t \in (0,T), \\ &y(x,0) = y^0(x), && x \in (0,L). \end{aligned} \tag{17.5}$$

17.2.1.2 The Parabolic Case (ISO3) on a Network: The p-Parabolic Problem on the Network

Besides the semi-linear model (ISO2) for gas flow in a single pipe as used in (17.1) above, we here resort to a friction dominated gas flow model proposed by Bamberger [3]. For slowly varying flow regimes, $y = p^2$ denoting the squared pressure $p = c^2\rho$ and for zero slope of the pipes the Euler equations can be reduced to (cf. the (ISO3) model in Chap. 2, "A Catalog of Gas Network Models: PDEs, Coupling Conditions, and Numerical Schemes" and [64])

$$\partial_t \frac{y}{\sqrt{|y|}} - c\sqrt{\frac{D}{\lambda}}\partial_x \frac{\partial_x y}{\sqrt{|\partial_x y|}} = 0. \tag{17.6}$$

We introduce the monotone function $\beta(s) := s/(\sqrt{|s|})$. Then, (17.6) reads

$$\partial_t \beta(y) - \gamma \partial_x \beta(\partial_x y) = 0.$$

It is also possible to write this down in the p-Laplace format:

$$\partial_t \left(|y|^{p-2} y \right) - \gamma \partial_x \left(|\partial_x y|^{p-2} \partial_x y \right) = 0, \tag{17.7}$$

where $p = 3/2$. Equation (17.7) has come to be known as doubly nonlinear parabolic equation of p-Laplace type. See, e.g., [76] for an early contribution also in higher dimensions, [79] for a more recent functional analytic treatment. Notice that $p < 2$ and that the system is, therefore, singular for $\frac{\partial}{\partial x} y(x) = 0$. For $p > 2$ such equations exhibit instead degeneration. Equations similar to (17.6) have been considered in the literature, see, e.g., [3]. We note that the doubly nonlinear parabolic problem associated with the friction-dominated flow on a network has been considered in the thesis [85] and [70].

Similarly as for the pipe model (ISO2), we now describe the gas dynamics using the doubly nonlinear p-parabolic problem (17.7) on a network.

$$
\begin{aligned}
&\partial_t \beta(y_i(x,t)) - \partial_x\left(\beta(\partial_x y_i(x,t))\right) = u_i, && i \in \mathcal{I},\ x \in (0,\ell_i),\ t \in (0,T),\\
&y_i(n_j,t) = y_k(n_j,t), && \forall i,k \in \mathcal{I}_j,\ j \in \mathcal{J}^M,\ t \in (0,T),\\
&\sum_{i\in\mathcal{I}_j} d_{ij}\beta(\partial_x y_i(n_j,t)) = 0, && j \in \mathcal{J}^M,\ t \in (0,T),\\
&y_i(n_j,t) = g_i(t), && i \in \mathcal{I}_j,\ j \in \mathcal{J}_D^S,\ t \in (0,T),\\
&d_{ij}\beta(\partial_x y_i(n_j,t)) = u_j(t), && i \in \mathcal{I}_j,\ j \in \mathcal{J}_N^S,\ t \in (0,T),\\
&p_i(x,0) = p_{i,0}(x),\ q_i(x,0) = q_{i0}(x), && x \in (0,\ell_i),
\end{aligned}
\tag{17.8}
$$

where the functions $u_i, g_i,\ i \in \mathcal{I}, u_j, j \in \mathcal{I}_j,\ j \in \mathcal{J}^S$ serve as distributed and boundary controls, respectively.

We now embark on space-time domain decomposition of the network equations.

17.2.2 Space-Time Domain Decomposition

We partition the metric graph G into edge–disjoint subgraphs $G = \bigcup_{p=1}^{P} G^{(p)}$ and time into windows $0 = T_0 < T_1 < \cdots < T_M = T$. Define

$$
\begin{aligned}
\Omega_m^{(p)} &:= (T_{m-1}, T_m) \times \bigcup_{e\in G^{(p)}} (0,\ell_e),\\
\Sigma^{(p)} &:= \{(t,n_j) : t \in (T_{m-1},T_m),\ n_j \in \text{ports of } G^{(p)}\}.
\end{aligned}
$$

Our goal is to decompose the full space–time problem on G into local subproblems on $\Omega_m^{(p)}$, communicating iteratively across *time caps* $\{T_m\}$ and *spatial ports* $\{n_j\}$. The method may be viewed as *NeTI* (Network Tearing and Interconnection), a space–time analogue of the FETI paradigm.

For clarity we focus on the hyperbolic balance law

$$
\partial_t y^{(p,m)} + \Lambda^{(p)}\partial_x y^{(p,m)} = \tilde{F}^{(p)}(y^{(p,m)}),
$$

where $\Lambda^{(p)}(x)$ is diagonal with entries equal to the signed characteristic speeds along edges of $G^{(p)}$.

At any node n_j incident to $G^{(p)}$, decompose $y = (y^+, y^-)$ into outgoing and incoming components. Collect the outgoing and incoming traces belonging to $G^{(p)}$ into

$$
\boldsymbol{\alpha}_j^{(p,m)}(t) \in \mathbb{R}^{d_{j,p}^+}, \quad \boldsymbol{\beta}_j^{(p,m)}(t) \in \mathbb{R}^{d_{j,p}^-},
$$

and similarly for other subgraphs touching n_j. Denote by $\mathcal{N}_j$ the set of all subgraphs attached to n_j, and form the global stacked vectors

$$
\boldsymbol{\alpha}_j(t) := \bigoplus_{q\in\mathcal{N}_j} \boldsymbol{\alpha}_j^{(q,\cdot)}(t), \quad \boldsymbol{\beta}_j(t) := \bigoplus_{q\in\mathcal{N}_j} \boldsymbol{\beta}_j^{(q,\cdot)}(t).
$$

The *node scattering* is the symmetric involution

$$\boldsymbol{\alpha}_j(t) = S_j\,\boldsymbol{\beta}_j(t) + \boldsymbol{s}_j(t).$$

Each local subproblem uses only the restriction of $\boldsymbol{\alpha}_j$ to its own components.

17.2.3 Optimal Control Problems

Control of systems of hyperbolic balance laws is a well established field; see, e.g., [4] for a recent account of the literature. Here, we concentrate on the space-time-domain decomposition of optimal control problems. Again, to fix ideas, we begin with problems based on (17.5). Another restriction here is that we deal exclusively with boundary control problems and, in fact, with final value problems. The machinery to be developed is easily extended then to running costs and distributed controls which, in turn, are mathematically much more simple than boundary controls.

17.2.3.1 Hyperbolic Balance Laws: Final-Time Boundary Control and KKT System

Let $T > 0$. The global state is $y = (y_i)_{i\in E}$, $y_i = (w_i^+, w_i^-)^T$. Given targets $z_i^d = (\rho_i^d, q_i^d)$ at $t = T$, and control weight $\kappa > 0$, define

$$J(y,g) = \frac{1}{2}\sum_{i\in E}\int_0^{\ell_i}\Big(|\rho_i(T,x)-\rho_i^d(x)|^2+|q_i(T,x)-q_i^d(x)|^2\Big)\,\mathrm{d}x + \frac{\kappa}{2}\int_0^T \|u(t)\|^2\,\mathrm{d}t.$$

The *global optimal control problem* is

$$\min_{(y,g)} \quad J(y,g) \quad \text{s.t.} \quad \partial_t y_i + \Lambda_i \partial_x y_i = \tilde{f}_i(y_i) \ \text{ on } (0,T)\times(0,\ell_i)$$

with the following graph couplings: (i) scattering $\boldsymbol{\alpha} = \boldsymbol{S}\boldsymbol{\beta}$ at interior nodes, (ii) outer ports given by the boundary controls u (Dirichlet/Neumann/Robin), and initial data. Let $p_i = (p_{w^+}, p_{w^-})^\top$ be the adjoint in characteristic coordinates. Let $z_i = M^{(p)} y_i$ and $p_z = (M^{(p)})^\top p_i$, where $M^{(p)}$ translates the the original variables into the characteristic variables. The first-order optimality conditions are given by

$$\partial_t y_i + \Lambda_i \partial_x y_i = \tilde{f}_i(y_i), \tag{17.9a}$$

$$\partial_t p_i + \Lambda_i \partial_x p_i + \big(\partial_y \tilde{f}_i(y_i)\big)^\top p_i = 0, \quad p_i(T,\cdot) = (M_i^{(p)})^\top (z_i(T) - z_i^d), \tag{17.9b}$$

$$\boldsymbol{\alpha}(t) = \boldsymbol{S}\,\boldsymbol{\beta}(t), \quad \boldsymbol{\beta}_p(t) = \boldsymbol{S}^\top \boldsymbol{\alpha}_p(t), \tag{17.9c}$$

$$u(t) = \kappa^{-1} c_i^{-1} p_{w^-}(L_i, t). \tag{17.9d}$$

Equation (17.9c) for the adjoint is the correct transposed law (it follows from the boundary bilinear form and $(\boldsymbol{\alpha} = \boldsymbol{S}\boldsymbol{\beta})$); for equal impedances, $(\boldsymbol{S}^\top = \boldsymbol{S})$. A generic Robin law at a port, $d\,q + \sigma\,\rho = h(t)$, rewritten in (w^+, w^-) is: $(d\,c_i + \sigma)\,w^+ + (-d\,c_i + \sigma)\,w^- = h$. At the *left* end $x = 0$ the unknown is the incoming $w^-(0,t)$, so with outward $d = -d_{ij}$

and at the *right* end $x = \ell_i$ the unknown is $w^+(\ell_i, t)$, with outward $d = +d_{ik}$. So

$$w_i^-(0,t) = \frac{h_{ij}(t) - (\sigma - d_{ij}c_i)\, w_i^+(0,t)}{\sigma + d_{ij}c_i},$$
$$w_i^+(\ell_i,t) = \frac{h_{ik}(t) - (\sigma - d_{ik}c_i)\, w_i^-(\ell_i,t)}{\sigma + d_{ik}c_i}.$$

A positive impedance condition $\sigma + d\, c_i > 0$ yields well-posed port updates.

17.2.3.2 Space-Time Decomposition

Choose time cuts $0 = T_0 < \cdots < T_M = T$, $I_m = (T_{m-1}, T_m)$, and a partition of G into edge-disjoint subgraphs $G = \bigcup_{p=1}^{P} G^{(p)}$ meeting at interface nodes. On $\Omega_m^{(p)} := I_m \times \bigcup_{e_i \in G^{(p)}} (0, \ell_i)$ we impose local problems coupled by:

- *Time caps: value* coupling in *rotated* variables $\boldsymbol{\gamma} := y + \beta p$, $\boldsymbol{\delta} := y - \beta p$ at $t = T_{m-1}^+, T_m^-$. The corresponding time-domain iteration is exactly the one discussed in [53].
- *Spatial interfaces:* node scattering between subgraphs. If node n_j is shared by subgraphs indexed by $\mathcal{N}_j \subset \{1, \ldots, P\}$, we use the multi-port form

$$\boldsymbol{\alpha}_j^{(p)} = \sum_{q \in \mathcal{N}_j} \boldsymbol{S}_{j,pq}\, \boldsymbol{\beta}_j^{(q)} + \boldsymbol{s}_j(t), \quad \boldsymbol{\beta}_{p,j}^{(p)} = \sum_{q \in \mathcal{N}_j} \boldsymbol{S}_{j,pq}^{\top}\, \boldsymbol{\alpha}_{p,j}^{(q)}, \tag{17.10}$$

with $\boldsymbol{S}_j$ symmetric for equal impedances. We can also mix the forward and backward modes (rotated variables): $\boldsymbol{\gamma} = \boldsymbol{\alpha}_u + \tau \boldsymbol{\beta}_p$, $\boldsymbol{\delta} = \boldsymbol{\beta}_p - \tau \boldsymbol{\alpha}_u$. Then with

$$M(\tau) = \begin{bmatrix} I & \tau I \\ -\tau I & I \end{bmatrix}$$

and $R(\tau) = M(\tau)^{-1} \mathrm{diag}(S_u, S_p) M(\tau)$, we have, for a single multiple joint

$$\begin{pmatrix} \boldsymbol{\alpha}_u \\ \boldsymbol{\beta}_p \end{pmatrix} = R(\tau) \begin{pmatrix} \boldsymbol{\beta}_u \\ \boldsymbol{\alpha}_p \end{pmatrix}.$$

Boundaries controls act at simple joints, only. Thus, they do not enter the interface conditions. The identity can be read into a block identity over the entire graph using the notation in (17.10). In essence, spatial domain decomposition then amounts to apply a possibly under-relaxed Jacobi iteration for the corresponding block matrix equations. We omit the details and refer instead to [57] for similar spatial decomposition methods.

The *decomposed KKT* on $\Omega_m^{(p)}$ is exactly (17.9a)–(17.9d) restricted to edges of $G^{(p)}$, with the above cap and node couplings.

17.2.3.3 Virtual Control Formulations and Equivalence

We now introduce *state-only* local minimization problems whose first-order conditions reproduce the decomposed KKT couplings. The adjoint arises as the Lagrange multiplier; it is not imposed as a constraint.

17.2.3.4 Time-Cap Virtual Controls (TDD)

On $I_m \times G$ introduce virtual cap anchors $g_{m,m-1}$ at T_{m-1}. Define

$$\begin{aligned} \min_{y_m,\, s_m,\, g_{m,m-1}} \quad & J(y_m, s_m) + \frac{1}{2\mu} \int_G \left(\|y_m(T_m) - \phi_{m,m+1}\|^2 + \|g_{m-,m-1}\|^2 \right) \mathrm{d}x \\ \text{s.t.} \quad & \partial_t y_m + \Lambda \partial_x y_m = \tilde{f}(y_m), \\ & y(T_{m-1}) = \phi_{m,m-1} + g_{m,m-1}, \\ & \boldsymbol{\alpha}_m = S\boldsymbol{\beta}_m + \boldsymbol{s}_m. \end{aligned}$$

By standard variational arguments, for given $\phi^k_{m,m-1}, \phi^k_{m,m+1}$, we obtain

$$\begin{aligned} y_m^{k+1}(T_{m-1}) - \beta p_m^{k+1}(T_{m-1}) &= \phi^k_{m,m-1} \\ y_m^{k+1}(T_m) + \beta p_m^{k+1}(T_m) &= \phi^k_{m,m+1} \\ \phi^k_{m,m-1} &= y^k_{m-1}(T_{m-1}) - \beta p^k_{m-1}(T_{m-1}) \\ \phi^k_{m,m+1} &= y^k_{m+1}(T_m) + \beta p^k_{m+1}(T_m), \end{aligned}$$

which is precisely the time domain decomposition above.

Remark 17.2 We remark that the concept of virtual controls can be extended to the spatial decomposition (see [57]) and space-time domain decompositions [60].

Example 17.1 We consider a 3-star graph with controls at the leaves ($x = 1$) and standard final tracking cost. We refrain from a detailed description of the parameters and their role. We use particular initial conditions such that the information is traveling along characteristics. The initial condition is places in edge 1 only. The top figure in Fig. 17.1 shows the evolution of the state, the second the backward evolution of the adjoint corresponding to a final value cost indicated in Fig. 17.2 on the right. The left image in Fig. 17.2 shows the iteration history. We use 3 time slabs and apply the STDDM discussed above. The example should be seen as a proof of concept for the STDDM.

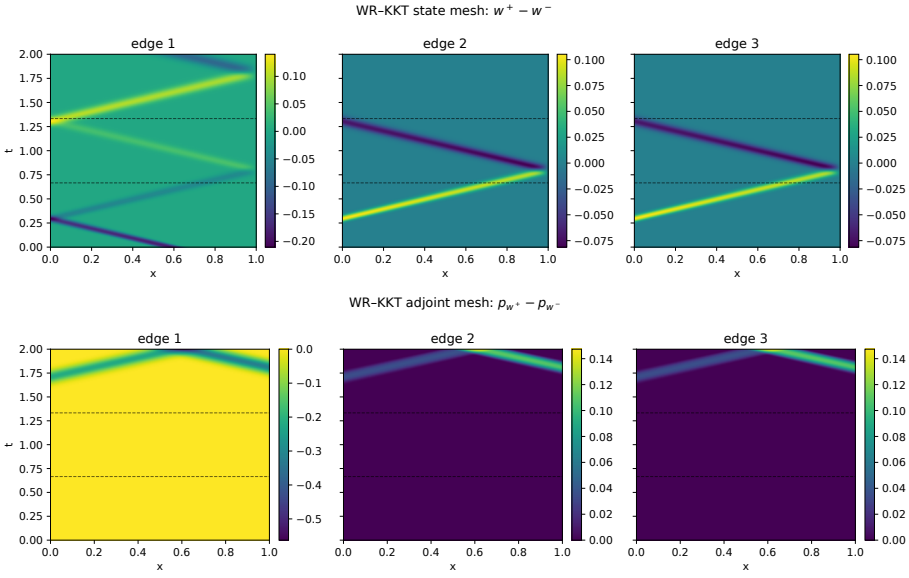


Fig. 17.1: OC of hyperbolic systems: meshes of states and adjoints

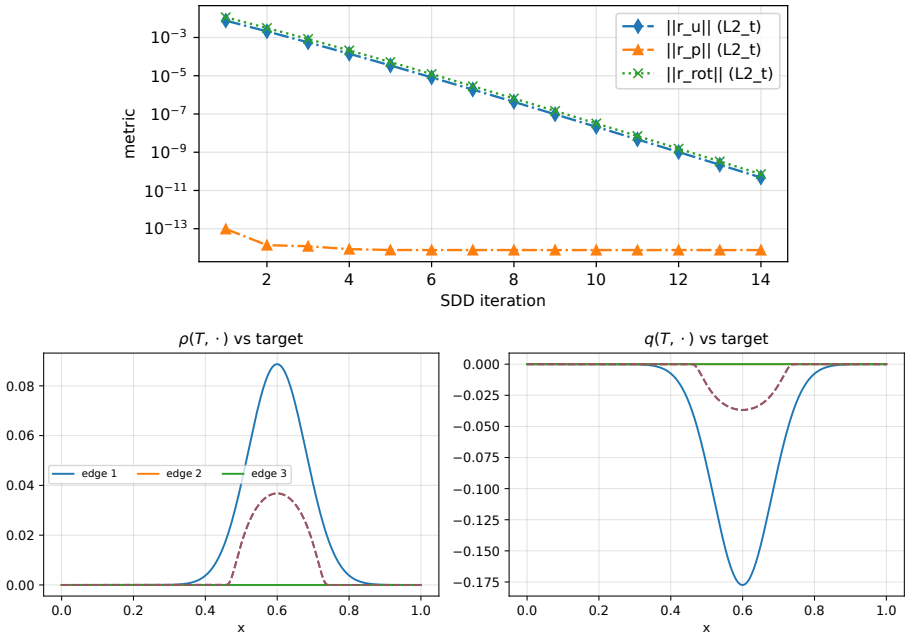


Fig. 17.2: OC of hyperbolic systems: error history and final values

17.2.4 Doubly-Nonlinear p-Parabolic Optimal Control on Graphs and STDD

Let $G = (\mathcal{V}, \mathcal{E})$ be a metric graph; each edge $e_i \in \mathcal{E}$ is identified with $(0, \ell_i)$. On e_i the controlled doubly-nonlinear p-parabolic state is

$$\partial_t \phi(y_i) \; - \; \partial_x \left(a_i(x) \, |\partial_x y_i|^{p_x - 2} \partial_x y_i \right) \; = \; f_i(x,t) + (B_i u)(x,t), \quad (x,t) \in (0,\ell_i) \times (0,T),$$

with $\phi(s) = |s|^{p_t - 2} s$, where $p_t > 1$, $p_x > 1$, and $a_i(x) \geq a_0 > 0$. At interior nodes n_j with incident set $\mathcal{I}_j$, we impose continuity and Kirchhoff laws

$$y_i(n_j, t) =: \lambda_j(t), \quad i \in \mathcal{I}_j, \quad \sum_{i \in \mathcal{I}_j} s_{ij} a_i |y_{i,x}|^{p_x - 2} \partial_x y_i(n_j, t) = 0,$$

where $s_{ij} \in \{\pm 1\}$ are outward signs. At leaf nodes we prescribe controls, e.g., Neumann $-a_i |y_{i,x}|^{p_x - 2} y_{i,x} = u_i(t)$ (Dirichlet/Robin variants are analogous). We track a desired state y_d and penalize u:

$$\min_{y,u} \; \mathcal{J}(y,u) \; = \; \frac{\omega}{2} \sum_i \int_0^T \int_0^{\ell_i} (y_i - y_{d,i})^2 \, \mathrm{d}x \, \mathrm{d}t \; + \; \frac{\kappa}{2} \sum_i \int_0^T |u_i|^2 \, \mathrm{d}t.$$

17.2.4.1 KKT System

Let p_i be the adjoint. The Lagrangian and its variations with respect to the corresponding test functions yield the first-order conditions:

$$\begin{aligned} \partial_t \phi(y_i) - \partial_x \left(a_i |y_{i,x}|^{p_x - 2} y_{i,x} \right) &= f_i + (B_i u), \\ -\partial_t \left(\phi'(y_i) \, p_i \right) - \partial_x \left((p_x - 1) \, a_i |y_{i,x}|^{p_x - 2} p_{i,x} \right) &= \omega \, (y_i - y_{d,i}) \end{aligned}$$

with $\phi'(y) = (p_t - 1)|y|^{p_t - 2}$. At interior nodes one has continuity $y_i(n_j, t) = \lambda_j(t)$, $p_i(n_j, t) = \pi_j(t)$, and Kirchhoff balances

$$\sum_{i \in \mathcal{I}_j} s_{ij} a_i |y_{i,x}|^{p_x - 2} y_{i,x}(n_j, t) = 0, \quad \sum_{i \in \mathcal{I}_j} s_{ij} (p_x - 1) a_i |y_{i,x}|^{p_x - 2} p_{i,x}(n_j, t) = 0.$$

For Neumann control at leaves $-a_i |y_{i,x}|^{p_x - 2} y_{i,x} = u_i$ the optimality is $\kappa u_i + p_i = 0$, hence $u_i = -(1/\kappa) p_i$. For the time caps we $p_i(\cdot, T) = 0$ and $\phi(y_i(\cdot, 0))$ is fixed by y_0.

17.2.4.2 Space-Time Robin-Robin Decomposition

We partition now the time horizon as $0 = T_0 < \cdots < T_M = T$ and split the graph into edge-disjoint subgraphs $G = \bigcup_{p=1}^{P} G^{(p)}$ meeting at interface nodes. On a space-time

subdomain $\Omega_m^{(p)} = (T_{m-1}, T_m) \times \cup_{e_i \in G^{(p)}}(0, \ell_i)$ we impose per-interface-edge Robin ports for the state

$$-d_{ij}\, a_i |y_{i,x}|^{p_x - 2} y_{i,x}(n_j, t) + \sigma\, y_i(n_j, t) = h_{ij}(t)$$

with d_{ij} the outward sign w.r.t. $G^{(p)}$ and the adjoint Robin

$$-d_{ij}\,(p_x - 1) a_i |y_{i,x}|^{p_x - 2} p_{i,x}(n_j, t) + \sigma\, p_i(n_j, t) = \widehat{h}_{ij}(t).$$

Across the touching subgraphs at n_j one applies a relaxation using the (block) scattering matrix $\mathbf{S}_j$:

$$\mathbf{h}_j^{(p),k+1} = (1 - \omega)\, \mathbf{h}_j^{(p),k} + \omega\, \mathbf{S}_j \left(2\sigma\, \mathbf{y}_j^{(\mathrm{nb}),k} - \mathbf{h}_j^{(\mathrm{nb}),k} \right)$$

with an analogous law for $\widehat{\mathbf{h}}_j$. At time caps we use the energetically natural pairings

$$\mathcal{B}_\beta^-(y, p) := \phi(y) - \beta p, \quad \mathcal{B}_\beta^+(y, p) := \phi(y) + \beta p, \quad \beta > 0,$$

with cap data $m_{m-1}^{(p)}(x)$ and $m_m^{(p)}(x)$ coupled the standard reflections between neighboring slabs.

Remark 17.3 We remark that is also possible to show that the algorithm is equivalent to a virtual optimal control problem on the individual edges analogous to the case of the hyperbolic system. We refrain from describing the details. Moreover, we can use a rotated variable variant in which we couple state and adjoint variables; see [61, 62].

17.3 Mixed-Integer Control

In this section we discuss the application of domain-decomposition techniques such as presented in Sect. 17.2 in the context of mixed-integer programming approaches. To this end, we mainly review the results in [39].

We will focus on time-domain decomposition and consider an optimal control problem on a fixed time horizon $[t_0, t_\mathrm{f}]$ of the form

$$\begin{aligned}
\min \quad & \varphi_0(x(t_0)) + \varphi_\mathrm{f}(x(t_\mathrm{f})) && \text{(17.11a)}\\
\text{s.t.} \quad & \dot{x} = f(x, u) \quad \text{a. e. in } (t_0, t_\mathrm{f}), && \text{(17.11b)}\\
& \chi(x(t_0)) = 0, && \text{(17.11c)}\\
& \psi(x(t_\mathrm{f})) = 0, && \text{(17.11d)}\\
& u(t) \in U \quad \text{a. e. in } [t_0, t_\mathrm{f}], && \text{(17.11e)}
\end{aligned}$$

where $x\colon [t_0, t_\mathrm{f}] \to \mathbb{R}^n$ is a state function, $u\colon [t_0, t_\mathrm{f}] \to \mathbb{R}^m$ is a control function and U is a non-empty and otherwise arbitrary set. In particular, U may be used to restrict certain components of $u(t)$ to integer-values modeling on/off characteristics of valves, and the ODE in (17.11) and the imposed boundary conditions may represent a spatially discretized dynamic of ISO2 or ISO3 on networks, cf. (17.1) and (17.8), while the

objective is, w.l.o.g., reduced to a Mayer-form, see, e.g. [39]. Related problems are considered in [5, 17, 34–38, 48, 58, 66, 72, 77, 80].

If χ and ψ satisfy regularity conditions and if (x, u) is optimal in the sense of Pontryagin, there exist a function λ and multipliers α, β such that

$$\begin{aligned}
\dot{x} &= f(x,u) \quad \text{a. e. in } (t_0, t_f),\\
\chi(x(t_0)) &= 0,\\
\psi(x(t_f)) &= 0,\\
u(t) &\in U \quad \text{a. e. in } [t_0, t_f],\\
\dot{\lambda} &= -\lambda^\top f_x(x,u) \quad \text{a. e. in } (t_0, t_f),\\
\lambda(t_0) &= \varphi_0'(x(t_0)) + \beta_1^\top \chi_x(x(t_0)),\\
\lambda(t_f) &= -\varphi_f'(x(t_f)) - \beta_2^\top \psi_x(x(t_f)),\\
\max_{u\in U} H(\lambda(t), x(t), u) &= H(\lambda(t), x(t), u(t)) \quad \text{a. e. in } (t_0, t_f),
\end{aligned} \tag{17.12}$$

holds, where $H(\lambda, x, u) = \lambda^\top f(x, u)$ denotes the Hamiltonian of the problem [2, 18, 71]. The optimality conditions (17.12) can be written piecewise in variables $x_0, \lambda_0, \ldots, x_K, \lambda_K$ with transmission conditions at intermediate times t_k

$$x_k(t_{k+1}) = x_{k+1}(t_{k+1}), \qquad k = 0, \ldots, K-1, \tag{17.13a}$$

$$\lambda_k(t_k) = \lambda_{k-1}(t_k), \qquad k = 1, \ldots, K. \tag{17.13b}$$

We now consider an iteration index ℓ and iterates x_k^ℓ, λ_k^ℓ, and u_k^ℓ for the unknowns x_k, λ_k, and u_k to decouple the transmission conditions (17.13) as

$$\begin{aligned}
x_k^\ell(t_{k+1}) + \gamma\lambda_k^\ell(t_{k+1}) &= \phi_{k,k+1}^{\ell-1}, \quad k = 0, \ldots, K-1,\\
x_k^\ell(t_k) - \gamma\lambda_k^\ell(t_k) &= \phi_{k,k-1}^{\ell-1}, \quad k = 1, \ldots, K.
\end{aligned}$$

The right-hand-sides $\phi_{k,k+1}^{\ell-1}, \phi_{k,k-1}^{\ell-1}$ are chosen as right/left neighboring data from the previous iteration

$$\begin{aligned}
\phi_{k,k+1}^{\ell-1} &= (1-\varepsilon)\left(x_{k+1}^{\ell-1}(t_{k+1}) + \gamma\lambda_{k+1}^{\ell-1}(t_{k+1})\right)\\
&\quad + \varepsilon\left(x_k^{\ell-1}(t_{k+1}) + \gamma\lambda_k^{\ell-1}(t_{k+1})\right), \quad k = 0, \ldots, K-1,\\
\phi_{k,k-1}^{\ell-1} &= (1-\varepsilon)\left(x_{k-1}^{\ell-1}(t_k) - \gamma\lambda_{k-1}^{\ell-1}(t_k)\right)\\
&\quad + \varepsilon\left(x_k^{\ell-1}(t_k) - \gamma\lambda_k^{\ell-1}(t_k)\right), \quad k = 1, \ldots, K.
\end{aligned}$$

Here, $\gamma > 0$ is arbitrary, but fixed, and $\varepsilon \in (0, 1)$ is a damping parameter.

Note that, if $x_k^\ell \to x_k$ and $\lambda_k^\ell \to \lambda_k$ for all $k = 0, \ldots, K$ and $\ell \to \infty$, we obtain the transmission conditions (17.13) for the limit. Moreover, all sub-conditions have primal interpretations.

For the first time sub-interval, i.e., $k = 0$, the problem reads

$$\begin{aligned}\min_{x_0,u_0} \quad & \varphi_0(x_0(t_0)) + \frac{1}{2\gamma}\|x_0(t_1) - \phi_{0,1}^{\ell-1}\|^2 \\ \text{s.t.} \quad & \dot{x}_0 = f(x_0,u_0) \quad \text{a. e. in } (t_0,t_1), \\ & \chi_j(x_0(t_0)) = 0, \\ & u_0(t) \in U \quad \text{a. e. in } [t_0,t_1].\end{aligned}$$

For the inner time sub-intervals k, we get

$$\begin{aligned}\min_{x_k,u_k,h_k} \quad & \frac{1}{2\gamma}\|h_k\|^2 + \frac{1}{2\gamma}\|x_k(t_{k+1}) - \phi_{k,k+1}^{\ell-1}\|^2 \\ \text{s.t.} \quad & \dot{x}_k = f(x_k,u_k) \quad \text{a. e. in } (t_k,t_{k+1}), \\ & x_k(t_k) = \phi_{k,k-1}^{\ell-1} + h_k, \\ & h_k \in \mathbb{R}^n, \\ & u_k(t) \in U \quad \text{a. e. in } [t_k,t_{k+1}],\end{aligned}$$

where h_k is a new (virtual) control variable. For the last time sub-interval, i.e., $k = K$, we obtain

$$\begin{aligned}\min_{x_K,u_K,h_K} \quad & \frac{1}{2\gamma}\|h_K\|^2 + \varphi_{\mathrm{f}}(x_K(t_{\mathrm{f}})) \\ \text{s.t.} \quad & \dot{x}_K = f(x_K,u_K) \quad \text{a. e. in } (t_K,t_{K+1}), \\ & x_K(t_K) = \phi_{K,K-1}^{\ell-1} + h_K, \\ & \psi_j(x_K(t_{\mathrm{f}})) = 0, \\ & h_K \in \mathbb{R}^n, \\ & u_K(t) \in U \quad \text{a. e. in } [t_K,t_{K+1}].\end{aligned}$$

We note that these virtual problems almost have the same control and state dimension, but live on smaller domains. Moreover, all $K+1$ primal problems can be solved in parallel, e.g., using direct transcription.

For the case of linear dynamics and quadratic in state objectives

$$\min \quad \frac{1}{2}x(t_0)^\top Q_0 x(t_0) + q_0^\top x(t_0) + \frac{1}{2}x(t_{\mathrm{f}})^\top Q_{\mathrm{f}} x(t_{\mathrm{f}}) + q_{\mathrm{f}}^\top x(t_{\mathrm{f}}) + \int_{t_0}^{t_{\mathrm{f}}} L(u)\,\mathrm{d}t \tag{17.14a}$$

$$\text{s.t.} \quad \dot{x} = Ax + Bu + c \quad \text{a. e. in } (t_0,t_{\mathrm{f}}), \tag{17.14b}$$

$$R_0 x(t_0) = c_0, \tag{17.14c}$$

$$R_{\mathrm{f}} x(t_{\mathrm{f}}) = c_{\mathrm{f}}, \tag{17.14d}$$

$$u(t) \in U \quad \text{a. e. in } [t_0,t_{\mathrm{f}}] \tag{17.14e}$$

with $Q_0, Q_{\mathrm{f}} \in \mathbb{R}^{n\times n}$ positive semi-definite, convergence can be analyzed by fixed-point methods. To this end, consider the errors

$$\tilde{x}_k^\ell := x_k^\ell - x_k, \quad \tilde{u}_k^\ell := u_k^\ell - u_k, \quad \tilde{\lambda}_k^\ell := \lambda_k^\ell - \lambda_k$$

and set $\tilde{U} := U - U = \{u - v : u, v \in U\}$. With

$$X^\ell := \left(\left(\tilde{\phi}^{\ell-1}_{k,k+1} \right)_{k=0}^{K-1}, \left(\tilde{\phi}^{\ell-1}_{k,k-1} \right)_{k=1}^{K} \right), \quad TX^\ell := \left(\left(\tilde{\phi}^{\ell}_{k,k+1} \right)_{k=0}^{K-1}, \left(\tilde{\phi}^{\ell}_{k,k-1} \right)_{k=1}^{K} \right),$$

the methods acts as

$$T_\varepsilon := (1 - \varepsilon)T + \varepsilon I.$$

Moreover, X is a fixed point of T and T_ε if and only if the transmission conditions for the errors hold

$$\begin{aligned} \tilde{x}_k(t_{k+1}) &= \tilde{x}_{k+1}(t_{k+1}), && k = 0, \dots, K-1, \\ \tilde{\lambda}_k(t_k) &= \tilde{\lambda}_{k-1}(t_k), && k = 1, \dots, K. \end{aligned}$$

We note that T and T_ε are nonlinear, but one can actually show that T is non-expansive, i.e.,

$$\|TX_1 - TX_2\| \leq \|X_1 - X_2\|.$$

An application of Schäfer's Theorem [81] then gives the following result proved in [39].

Theorem 17.1 *If the proposed domain decomposition method is applied to the linear-quadratic problem* (17.14)*, the iterates* $(x_k^\ell, \lambda_k^\ell)$ *for* $k = 0, \dots, K$ *converge in the sense*

$$\begin{aligned} x_k^\ell(t_{k+1}) - x_{k+1}^\ell(t_{k+1}) &\to 0, \\ \lambda_k^\ell(t_{k+1}) - \lambda_{k+1}^\ell(t_{k+1}) &\to 0 \end{aligned}$$

for all $k = 0, \dots, K-1$ *as* $\ell \to \infty$.

In [39], we demonstrate on numerical examples that this procedure can provide computational advantages compared to solving the direct discretization of the original problem on the entire time horizon. We also discuss the choice of additional parameters of the proposed algorithm. Typical convergence rates are shown in Fig. 17.3.

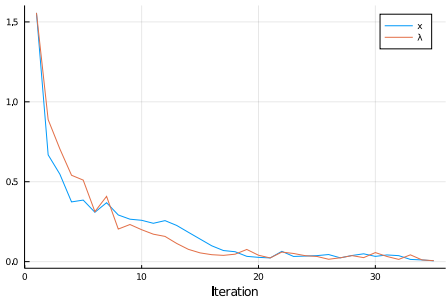


Fig. 17.3: Convergence in error for a linear quadratic test problem from [39] with a splitting into 4 subdomains and solutions computed by ANTIGONE over the iterates k.

Our computational experiments show that this advantage also pays off for the case of nonlinear problems if the procedure converges. For other than the linear-quadratic case however, a convergence theory or convergence enhancing mechanisms are still to be investigated. An application to a GasLib instance related to these findings is presented in Sect. 17.5.

17.4 Randomized Domain Decomposition

We introduce the Random Batch Method (RBM) for PDEs on graphs as a randomized domain decomposition: over short time windows, we evolve the dynamics only on a randomly selected domain, while the complement is temporarily frozen. In gas networks, this means advancing the state on a randomly chosen set of pipes during short intervals. The payoff is reduced memory and runtime while retaining convergence guarantees.

Two complementary formulations are developed. The *discretize+randomize* approach (Sect. 17.4.1) applies RBM to the linear PDE after spatial semi-discretization, i.e., to the resulting ODE system. By contrast, the *continuous* approach (Sect. 17.4.2) introduces randomization directly at the PDE level for parabolic problems on graphs.

17.4.1 RBM for Discretized PDEs

In this section we introduce the RBM for discretized PDEs. We first analyze the RBM in the setting of finite-dimensional systems. Consider the linear control system

$$\begin{aligned} \dot{x}(t) + Ax(t) = Bu(t), \quad t \in (0,T), \\ x(0) = x_0, \end{aligned} \tag{17.15}$$

where $x : [0,T] \to \mathbb{R}^d$ denotes the state, $u \in L^2(0,T;\mathbb{R}^q)$ the control input, $B \in \mathbb{R}^{d\times q}$ the control matrix, and $A \in \mathbb{R}^{d\times d}$ the system matrix.

Our aim is to approximate these dynamics by means of a randomized time-splitting method. To this end, we first decompose the system matrix A as a finite sum

$$A = \sum_{m=1}^{M} A_m, \tag{17.16}$$

where each $A_m \in \mathbb{R}^{d\times d}$. This decomposition is not unique, and different choices of $\{A_m\}_{m=1}^M$ are possible. Next, introduce N nonempty subsets (called *batches*) such that

$$\mathcal{B}_1, \dots, \mathcal{B}_N \subset \{1, \dots, M\}, \quad \bigcup_{j=1}^{N} \mathcal{B}_j = \{1, \dots, M\}. \tag{17.17}$$

We partition the time interval $[0,T]$ into K subintervals $I_k := [(k-1)h, kh)$ of fixed length h, for $k \in \{1,\dots,K\}$. At each interval, a batch will be chosen at random. To formalize this, let $\{\omega_k\}_{k=1}^K$ be i.i.d. random variables taking values in $\{1,\dots,N\}$ with probabilities

$$\mathbb{P}(\omega_k = j) = p_j > 0, \quad \sum_{j=1}^{N} p_j = 1. \tag{17.18}$$

For each $t \in (0,T)$, let $k_t := \min\{k \in \{1,\dots,K\} : t < kh\}$ and $\mathcal{B}(t) := \mathcal{B}_{\omega_{k_t}}$. We then define the random matrix

$$A_{\mathrm{rb}}(t) := \sum_{i \in \mathcal{B}(t)} \frac{A_i}{\pi_i}, \quad \pi_i := \sum_{\{j : i \in \mathcal{B}_j\}} p_j. \tag{17.19}$$

The weights π_i serve as normalization constants ensuring that $A_{\mathrm{rb}}(t)$ is an *unbiased estimator* of A, namely $\mathbb{E}[A_{\mathrm{rb}}(t)] = A$ for all $t \in [0,T]$. Since $\mathcal{B}(t)$ is piecewise constant in time, $A_{\mathrm{rb}}(t)$ inherits this structure. We assume $\pi_i > 0$ for every $i \in \{1,\dots,M\}$.

The RBM dynamics is then defined by

$$\begin{cases} \dot{x}_r(t) + A_{\mathrm{rb}}(t)x_r(t) = Bu(t), & t \in [0,T], \\ x_r(0) = x_0. \end{cases} \tag{17.20}$$

In practice, $A_{\mathrm{rb}}(t)$ is typically much sparser than the full matrix A. Consequently, solving (17.20) is computationally cheaper and requires less memory than solving the original dynamics (17.15). In fact, the per-step cost scales with the average batch size rather than the full dimension, so that RBM achieves reduction in the problem size, at the expense of introducing stochastic error.

Regarding the relation between (17.20) and (17.15), it was shown in [88] that the mean-square error between the RBM solution $x_r(t)$ and the exact solution $x(t)$ vanishes as $h \to 0$. To make this precise, define the variance of the random matrix A_{rb} by

$$\mathrm{Var}[A_{\mathrm{rb}}] := \sum_{j=1}^{N} \left\| A - \sum_{m \in \mathcal{B}_j} \frac{A_m}{\pi_m} \right\|^2 p_j, \tag{17.21}$$

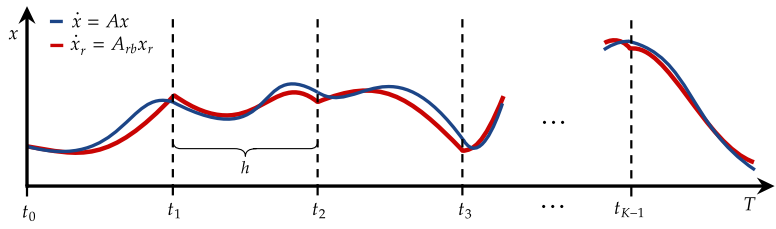


Fig. 17.4: Representation of the RBM. In blue, the real dynamics; in red, the RBM. At each subinterval, a random batch is selected, and the dynamics switches.

where $\|\cdot\|$ denotes the spectral norm (ℓ^2-norm). This quantity measures the randomization error induced by the batch design. Then, we have the following result.

Theorem 17.2 ([88]) *Let x and x_r denote the solutions of* (17.15) *and* (17.20)*, respectively. Then, for every $t \in (0,T)$, one has*

$$\mathbb{E}[\|x(t) - x_r(t)\|^2] \;\le\; C(A,u,T,x_0)\, Var[A_{\mathrm{rb}}]\, h, \tag{17.22}$$

where $C(A,u,T,x_0) > 0$ is a constant depending on A, u, T, and x_0, but independent of h.

Remark 17.4 The proof of Theorem 17.2 is based on standard energy estimates, together with the boundedness of $\|A\|$ in finite dimension. Moreover, by Jensen's inequality and estimate (17.22), we deduce

$$\|x(t) - \mathbb{E}[x_r(t)]\|^2 \le\; C(A,u,T,x_0)\,\mathrm{Var}[A_{\mathrm{rb}}]\, h, \quad t \in (0,T).$$

In particular, the expected trajectory $\mathbb{E}[x_r(t)]$ converges to the exact solution $x(t)$ as $h \to 0$.

17.4.1.1 Discretized PDEs

In high-friction, slowly varying regimes, the isothermal Euler equations on a single pipe—after neglecting inertia in the momentum equation—reduce to a nonlinear parabolic model (17.7); linearizing about a steady state then yields a heat-type evolution for the pressure. With this interpretation in mind, we instantiate the framework on the one–dimensional heat equation, viewed as the linear high-friction approximation of the isothermal Euler model on a pipe. Consider

$$\begin{aligned} \partial_t y - \partial_{xx} y &= f, \quad (x,t) \in (0,L)\times(0,T),\\ y(0,t) = y(L,t) &= 0, \quad t \in (0,T),\\ y(x,0) &= y^0(x), \quad x \in (0,L). \end{aligned} \tag{17.23}$$

Here $y^0 \in L^2(0,L)$ is the initial condition and $f \in L^2(0,T;H^{-1}(0,L))$ a source term. According to [25, Sect. 7.1.2], problem (17.23) admits a unique solution

$$y \in C([0,T];L^2(0,L)) \cap L^2(0,T;H_0^1(0,L)).$$

A finite element semi-discretization of (17.23) is obtained as follows. Let $\{x_j\}_{j=0}^{n+1}$ be a uniform partition of $(0,L)$ with mesh-size $\delta > 0$, let $\{\phi_j\}_{j=1}^{n}$ denote the P_1 basis functions, and define $V_n := \mathrm{span}\{\phi_j\}_{j=1}^{n}$. The semi-discrete formulation is: find $y_n \in C^1(0,T;V_n)$ such that

$$\begin{aligned} (\partial_t y_n(\cdot,t),\phi_j)_{L^2(0,L)} + (\partial_x y_n(\cdot,t),\partial_x\phi_j)_{L^2(0,L)} &= (f(\cdot,t),\phi_j)_{L^2(0,L)},\\ (y_n(\cdot,0),\phi_j)_{L^2(0,L)} &= (y^0(\cdot),\phi_j)_{L^2(0,L)}, \end{aligned} \tag{17.24}$$

for every $t \in (0,T)$ and all $j \in \{1,\dots,n\}$. Writing $y_n(\cdot,t) = \sum_{j=1}^n y_j(t)\phi_j(\cdot)$, the coefficient vector $\mathbf{y}_n(t) = (y_1(t),\dots,y_n(t))$ satisfies

$$\begin{aligned} E_n\,\partial_t \mathbf{y}_n + R_n\,\mathbf{y}_n &= \mathbf{f}_n, \quad t \in (0,T), \\ E_n\,\mathbf{y}_n(0) &= \mathbf{y}_n^0, \end{aligned} \tag{17.25}$$

where $E_n, R_n \in \mathbb{R}^{n\times n}$ are the mass and stiffness matrices, respectively.

Since (17.25) is a finite-dimensional system, we may apply RBM. In this setting, the stiffness matrix R_n plays the role of A. Decompose $R_n = \sum_{m=1}^M R_{n,m}$ as in (17.16), and define

$$R_{rb}(\omega,t) = \sum_{i\in\mathcal{B}(t)} \frac{R_{n,i}}{\pi_i}, \quad t \in (0,T),$$

with π_i as in (17.19). The corresponding RBM dynamics reads

$$\begin{aligned} E_n\,\partial_t \mathbf{y}_r(\omega,t) + R_{rb}(\omega,t)\,\mathbf{y}_r(\omega,t) &= \mathbf{f}_n, \quad t \in (0,T), \\ E_n\,\mathbf{y}_r(0) &= \mathbf{y}_n^0. \end{aligned} \tag{17.26}$$

Only the stiffness matrix is randomized; the mass matrix remains deterministic. We define the finite element function associated with $\mathbf{y}_r(\omega,t)$ by

$$y_r(x,t,\omega) := \sum_{j=1}^n (\mathbf{y}_r)_j(\omega,t)\,\phi_j(x), \tag{17.27}$$

where $(\mathbf{y}_r)_j$ denotes the j-th component of $\mathbf{y}_r(\omega,t)$.

Theorem 17.3 ([43]) *Let y_r be given by* (17.27)*, and let y be the solution of* (17.23) *with $y^0 \in H_0^1(0,L)$ and $f \in L^2(0,T;L^2(0,L))$. If $\delta < \sqrt{6T}$, then for every $t \in (0,T)$,*

$$\mathbb{E}\Big[\|y_r(t) - y(t)\|^2_{L^2(0,L)}\Big] \;\le\; C\Big(\delta^4 + \frac{h}{\delta^7}C(M)\Big), \tag{17.28}$$

where $C > 0$ and $C(M) > 0$ are independent of δ, h, and $C(M)$ depends only on the chosen decomposition.

Remark 17.5

- The proof of Theorem 17.3 combines Theorem 17.2—applied to (17.26) versus (17.25)—with standard finite element error bounds for (17.24) versus (17.23) (see [74, Prop. 11.2.1]), and then uses the triangle inequality. Accordingly, the FEM discretization contributes the term of order $O(\delta^4)$, while the RBM approximation contributes the term of order $O(h/\delta^7)$ in (17.28). Thus, convergence is ensured whenever $\delta \to 0$ and $h \to 0$ in such a way that $h/\delta^7 \to 0$.
- The factor $C(M)$ is essentially the variance $\mathrm{Var}[R_{\mathrm{rb}}]$, determined entirely by the chosen decomposition of R_n. Hence, the batch and decomposition design directly governs the trade-off between accuracy and efficiency. On the one hand, a decomposition that maximizes sparsity (leading to faster linear solves and reduced memory)

may increase the variance, thereby forcing very small h and offsetting the computational gains. On the other hand, a decomposition that reduces variance (and hence decreases $C(M)$) often produces denser batches, which makes each linear system more expensive to solve. Balancing these two effects is a central open problem in the design of RBM decompositions.

17.4.1.2 Further Extensions

The analysis in Theorem 17.3 extends to finite difference methods (FDM). However, obtaining an L^2-in-space error estimate between the FD approximation and the exact solution requires smoother data; see, for instance, [44, Theorem 16.5], where the estimate depends on $\|\partial_x^4 y\|_{L^2(0,T;C(0,L))}$.

In addition, [43] applies the discretize+RBM strategy to the linear–quadratic regulator (LQR) for the heat equation: the PDE is discretized via FEM, and a randomized optimal control is introduced to approximate the discrete optimal control problem. By combining the convergence of the FEM discretization for LQR (see [52]) with the RBM convergence for linear systems (see [88]), one derives an overall convergence estimate for the randomized optimal control.

17.4.1.3 Applications to PDEs on Graphs

Motivated by gas pipeline networks, we model the infrastructure as a metric graph whose edges (pipes) are coupled at junctions (vertices). Thus, we consider $\mathcal{G} := (\mathcal{E}, \mathcal{V})$ to be a metric graph, where $\mathcal{V}$ denotes the vertices and $\mathcal{E}$ the edges, each $e \in \mathcal{E}$ being identified with $(0, L)$ with $L = 1$. On each edge $e \in \mathcal{E}$, consider

$$\begin{aligned}
\partial_t y^e - \partial_{xx} y^e &= f^e, \quad (x,t) \in (0,L) \times (0,T), \\
y^{e'}(v,t) &= y^{e''}(v,t), \quad (v,t) \in \mathcal{V}_0 \times (0,T),\ e', e'' \in \mathcal{E}(v), \\
\sum_{e \in \mathcal{E}(v)} \partial_x y^e(v,t)\, n_e(v) &= 0, \quad (v,t) \in \mathcal{V}_0 \times (0,T), \\
y^e(v,t) &= 0, \quad (v,t) \in \mathcal{V}_b \times (0,T),\ e \in \mathcal{E}(v), \\
y^e(x,0) &= y_e^0(x), \quad x \in (0,L),
\end{aligned} \tag{17.29}$$

where y_e^0 is the initial condition and f^e the source term on e. Here $\mathcal{E}(v)$ denotes the set of edges incident to v, and $n_e(v)$ is the incidence indicator of e at v. Let $f = \{f^e\}_e$ and $y^0 = \{y_e^0\}_e$. We assume $f \in L^2(0,T; L^2(\mathcal{E}))$ and $y^0 \in H_0^1(\mathcal{E})$ (see [67, Chap. 3] or [42, Appendix A] for Sobolev spaces on graphs). According to [22], there exists a unique solution $y \in C(0,T; L^2(\mathcal{E})) \cap L^2(0,T; H_0^1(\mathcal{E}))$ of (17.29). In what follows, to describe the RBM applied to (17.29), we consider the graph $\mathcal{G}$ illustrated in Fig. 17.5.

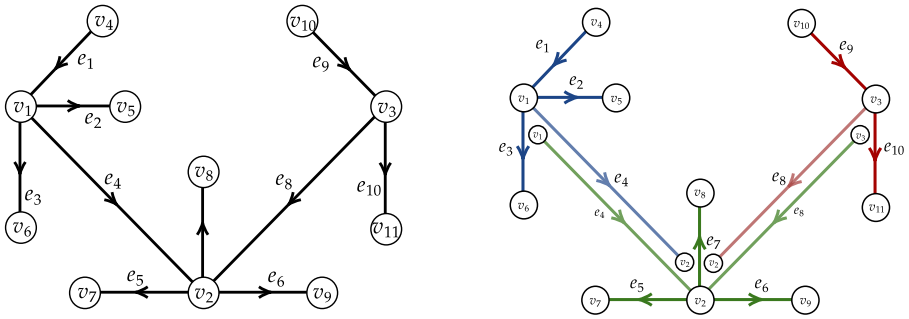


Fig. 17.5: Illustration of the graph $\mathcal{G}$ and its decomposition. (a) The graph $\mathcal{G}$ has edges $\mathcal{E} = \{e_i\}_{i=1}^{10}$ and vertices $\mathcal{V} = \mathcal{V}_0 \cup \mathcal{V}_b$, where $\mathcal{V}_0 = \{v_i\}_{i=1}^{3}$ are interior vertices and $\mathcal{V}_b = \{v_i\}_{i=4}^{11}$ are boundary vertices. (b) Overlapping decomposition. The subgraphs with edges $\{e_1, \dots, e_4\}$, $\{e_4, \dots, e_8\}$, and $\{e_8, e_9, e_{10}\}$ are associated with batches $\mathcal{B}_1$, $\mathcal{B}_2$, and $\mathcal{B}_3$, respectively.

17.4.1.4 Finite Element Method on Graphs

Let $V_n^{\mathcal{E}}$ be the P_1 finite element space on the graph, spanned by $\{\phi_j\}_{j=1}^{n}$ (see [43, Sect. 4]). The semi-discrete variational formulation of (17.29) reads: find $y_n \in C^1(0,T;V_n^{\mathcal{E}})$ such that

$$(\partial_t y_n(\cdot,t), \phi_j(\cdot))_{L^2(\mathcal{E})} + (\partial_x y_n(\cdot,t), \partial_x \phi_j(\cdot))_{L^2(\mathcal{E})} = (f(\cdot,t), \phi_j(\cdot))_{L^2(\mathcal{E})},$$
$$(y_n(\cdot,0), \phi_j(\cdot))_{L^2(\mathcal{E})} = (y^0(\cdot), \phi_j(\cdot))_{L^2(\mathcal{E})},$$

for every $j \in \{1,\dots,n\}$ and $t \in (0,T)$. As in (17.24)–(17.25), the coefficient vector $\mathbf{Y}_n(t)$ solves

$$\boldsymbol{E}_n\, \partial_t \mathbf{Y}_n + \boldsymbol{R}_n\, \mathbf{Y}_n = \mathbf{F}_n, \quad t \in (0,T),$$
$$\boldsymbol{E}_n\, \mathbf{Y}_n(0) = \mathbf{Y}_n^0,$$

where $\boldsymbol{E}_n$ and $\boldsymbol{R}_n$ are the mass and stiffness matrices on the graph, and $\mathbf{F}_n$ is the load vector. As in (17.26), one introduces a random system by randomizing only the stiffness matrix. The estimate in Theorem 17.3 then applies to the heat equation on $\mathcal{G}$.

The matrices $\boldsymbol{E}_n$ and $\boldsymbol{R}_n$ are block-structured: each edge contributes a block, and the interior-vertex coupling contributes additional nonzero rows/columns. Hence, $\boldsymbol{R}_n$ encodes both dynamics and topology. A natural decomposition of $\boldsymbol{R}_n$ is therefore guided by the graph structure. Fig. 17.6 (a) shows the structure of the matrix $\boldsymbol{R}_n$ in which each block is associated with one subgraph shown in Fig. 17.5.

Table 17.1: Comparison between the discretize+RBM approach and the full graph implicit Euler method. The error for the full graph method and discretize+RBM scheme is computed as $\sup_t \|y - y_n\|^2_{L^2}$ and $\sup_t \mathbb{E}[\|y - y_r\|^2_{L^2}]$, respectively.

Metric	Discretize+RBM	Full Graph (IE)
Time (s)	2.72	6.78
Memory (MB)	187.88	418.52
Error	9.3951×10^{-3}	9.6152×10^{-3}

17.4.1.5 Numerical Examples

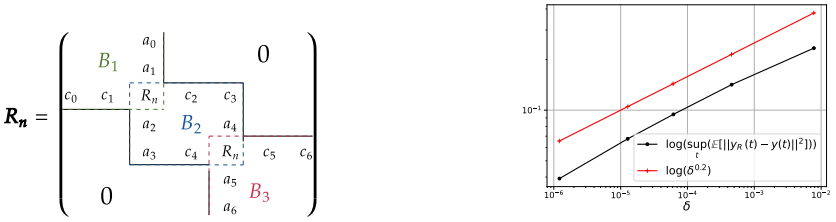
We consider a decomposition of $\boldsymbol{R}_n$ based on an overlapping decomposition. For the numerical test we adopt the manufactured-solution setting of [43]: on each edge e_i, $i \in \{1, \dots, 10\}$, we prescribe

$$y_{e_i}(x,t) = p_{e_i}\, x(1-x)\, e^{-t}, \quad y^0_{e_i}(x) = p_{e_i}\, x(1-x), \quad f_{e_i}(x,t) = p_{e_i}\,(2 - x + x^2)\, e^{-t},$$

with weights $(p_{e_1}, \dots, p_{e_{10}}) = (1, -1, -1, 1, -1, -1, -1, 2, -1, -1)$. Spatial discretization uses P_1 finite elements with 300 elements per edge; we set $T = L = 1$ and employ implicit Euler in time with 201 time steps. The expectation is approximated by the average of 30 i.i.d. RBM realizations.

Table 17.1 compares the accuracy, (average) memory usage, and computational time of the discretize+RBM approach versus the full graph solver. We observe that the expected RBM solution closely approximates the exact solution, while requiring about half the memory and achieving roughly a twofold speedup.

To corroborate the theoretical rate of convergence in Theorem 17.3, we follow Remark 17.5 and choose $h = \delta^{7+\varepsilon}$ with $\varepsilon > 0$. The corresponding convergence is illustrated in Fig. 17.6.



(a) (b)

Fig. 17.6: (a) Illustration of the stiffness matrix $\boldsymbol{R}_n$ associated with the heat equation on the graph. c_i's and a_i's denote row and column vectors, while R_n denotes 1-d stiffness matrix. (b) Convergence of the RBM solution in expectation as $\delta \to 0$ with $h = \delta^{7+\varepsilon}$

17.4.2 Continuous RBM for Parabolic PDEs on Graphs

In the previous section we observed that RBM for PDEs on graphs can be interpreted as a random domain decomposition. At the same time, the convergence bound in Theorem 17.3 shows a limitation of the discretize+randomize strategy: the error contains a term of order $O(h/\delta^7)$, so that the RBM step h must decrease much faster than the mesh size δ.

This motivates the development of a formulation whose accuracy depends only on h, independently of the discretization parameter. In the next section we therefore introduce a continuous RBM for parabolic PDEs, where the randomization acts directly at the PDE level, without passing through a prior discretization.

Let $\mathcal{G} = (\mathcal{E}, \mathcal{V})$ be a metric graph and $T > 0$. On each edge $e \in \mathcal{E}$, consider the parabolic equation

$$\begin{aligned} \partial_t y_e - \partial_x(a_e \partial_x y_e) + b_e \partial_x y_e + p_e y_e &= f_e, && (x,t) \in e \times (0,T), \\ y_{e'}(v,t) &= y_{e''}(v,t), && v \in \mathcal{V}_0,\ \forall e', e'' \in \mathcal{E}(v), \\ y_e(v,t) &= g_v(t), && v \in \mathcal{V}_b,\ e \in \mathcal{E}(v), \\ \sum_{e \in \mathcal{E}(v)} \partial_x y_e(v,t) n_e(v) &= 0, && v \in \mathcal{V}_0, \\ y_e(x,0) &= y_e^0(x), && x \in e, \end{aligned} \tag{17.30}$$

for every $t \in (0,T)$. Here y^0 is the initial condition, f the source term, g the boundary data, and (a,b,p) the coefficients (diffusion, convection, potential). System (17.30) generalizes the heat equation (17.29) previously analyzed on the graph. Regarding the well-posedness of (17.30), the following maximal regularity result holds.

Theorem 17.4 ([42]) *Let $(a,b,p) \in W^{1,\infty}(\mathcal{E}) \times L^\infty(\mathcal{E}) \times L^\infty(\mathcal{E})$ satisfy*

$$a_e > a_0 > 0, \quad \textit{for every } e \in \mathcal{E}, \quad \textit{and} \quad \sum_{e \in \mathcal{E}(v)} b_e(v) n_e(v) = 0, \quad \textit{for every } v \in \mathcal{V}_0.$$

Assume that $f \in L^2(0,T; L^2(\mathcal{E}))$, $y^0 \in H^1(\mathcal{E})$ and $g \in H^1(0,T; l^2(\mathcal{V}_b))$ satisfy the compatibility condition $y_e^0(v) = g_v(0)$ for each $v \in \mathcal{V}_b$. Then, there exists a unique solution $y \in C([0,T]; H^1(\mathcal{E})) \cap L^2(0,T; H^2(\mathcal{E})) \cap H^1(0,T; L^2(\mathcal{E}))$ of (17.30).

17.4.2.1 Random Domain Decomposition

Let us consider a decomposition of $\mathcal{G}$ via a family of subgraphs $\{\mathcal{G}_s^m\}_{m=1}^M := \{(\mathcal{E}_s^m, \mathcal{V}_s^m)\}_{m=1}^M$ that is pairwise edge-disjoint and covers $\mathcal{G}$. Denote by $\mathcal{V}_{s,0}^m$ and $\mathcal{V}_{s,b}^m$ the interior and boundary vertices of each $\mathcal{V}_s^m$, respectively. Denote by $\mathcal{E}_s^m(v)$ the set of edges in $\mathcal{E}_s^m$ that are adjacent to v. For every $v \in \mathcal{V}_{s,0}^i$, we assume that $\mathcal{E}_s^i(v) = \mathcal{E}(v)$, that is, interior vertices in the subgraphs keep all adjacent edges. Fig. 17.7 illustrates a decomposition of a diamond-shaped graph satisfying these assumptions.

Now, let us consider the batches $\mathcal{B}_1, \dots, \mathcal{B}_N$ introduced in (17.17). Then, for every $j \in \{1, \dots, N\}$ the batches determine the sets

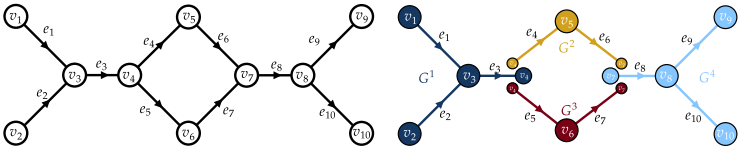


Fig. 17.7: Feasible decomposition. The graph is decomposed into $M = 4$ edge-disjoint subgraphs, such that $\mathcal{E}_s^m(v) = \mathcal{E}(v)$ for every $m \in \{1, \dots, 4\}$.

$$\mathcal{E}^j := \bigcup_{m \in \mathcal{B}_j} \mathcal{E}_s^m, \quad \mathcal{V}^j := \bigcup_{m \in \mathcal{B}_j} \mathcal{V}_s^m, \quad \mathcal{V}_0^j := \{v \in \mathcal{V}^j : \mathcal{E}^j(v) = \mathcal{E}(v)\}, \tag{17.31}$$

and $\mathcal{V}_b^j := \mathcal{V}^j \setminus \mathcal{V}_0^j$, where $\mathcal{E}^j(v)$ is the subset of edges in $\mathcal{E}^j$ that are adjacent to v. Hence, $\mathcal{V}_0^j$ collects the vertices whose incident edges are all in $\mathcal{E}^j$, while $\mathcal{V}_b^j$ contains the remaining (interface) vertices.

Assumption 17.1 For every $v \in \mathcal{V}_0$ there exists a batch $\mathcal{B}_\star$ such that $v \in \mathcal{V}_0^\star$, where $\mathcal{V}_0^\star$ is defined as in (17.31).

This structural assumption ensures that the Kirchhoff flux condition is enforced in expectation across the whole graph. In particular, every interior vertex has a positive chance of being activated as an interior vertex of some batch, which is crucial for the consistency of the randomized scheme.

For every $i \in \{1, \dots, M\}$ and $\psi : \mathcal{G} \to \mathbb{R}$ let

$$\chi_\psi^{i,j}(x) := \psi(x)\, \mathbf{1}_{S_j^i}(x), \quad S_j^i := \mathcal{G}_s^i \setminus (\mathcal{V}_b^j \cap \mathcal{V}_0),$$

where $\mathbf{1}_{S_j^i}$ denotes the indicator function on S_j^i. By definition, $\chi_\psi^{i,j}$ is a function with support on $\mathcal{G}_s^{i,j}$ such that $\sum_i \chi_\psi^{i,j} = \psi$ on every edge $e \in \mathcal{E}$. That is, $\chi_\psi^{i,j}$ is a localization of the function on a given subgraph.

Now consider the time subintervals $\{I_k\}_{k=1}^K$, the i.i.d. random variables $\{\omega_k\}_{k=1}^K$, and their probabilities $p_1, \dots, p_N$ as introduced in (17.18). For $t \in (0, T)$, consider

$$\zeta_\psi(x,t) := \sum_{i \in \mathcal{B}(t)} \frac{\chi_\psi^{i,\omega_{k_t}}(x)}{\pi_i},$$

where π is as in (17.19). Since $\mathcal{B}(t)$ is constant on each I_k, $\zeta_\psi(\cdot, t)$ is a piecewise constant function in time and—by construction—an *unbiased* estimator of ψ for every $t \in (0, T)$. Moreover, observe that

$$\operatorname{supp} \zeta_\psi(\cdot, t) \subset \mathcal{G}^{\mathcal{B}(t)} := \bigcup_{i \in \mathcal{B}(t)} \mathcal{G}^i, \quad \text{with} \quad \mathcal{G}^i := (\mathcal{E}^i, \mathcal{V}^i).$$

Figures 17.7 and 17.8 illustrate the function ζ_ψ in a particular example for a batch satisfying Assumption 17.1.

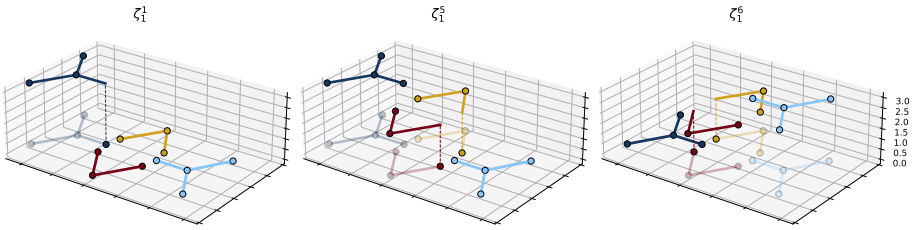


Fig. 17.8: Illustration of ζ_ψ with $\psi \equiv 1$. We denote by ζ_ψ^j when the batch j is chosen. Here the batches $\mathcal{B}_1 = \{1\}$, $\mathcal{B}_2 = \{2\}$, $\mathcal{B}_3 = \{3\}$, $\mathcal{B}_4 = \{4\}$, $\mathcal{B}_5 = \{1,2,3\}$, and $\mathcal{B}_6 = \{2,3,4\}$, satisfy Assumption 17.1. For $\mathcal{B}_5$ we have $\mathcal{V}_0^1 = \{v_4\}$, and $\zeta_1^5 = \chi_1^{1,5}/\pi_1 + \chi_1^{2,5}/\pi_2 + \chi_1^{3,5}/\pi_3$.

17.4.2.2 Continuous RBM System

The continuous RBM system reads as

$$\begin{aligned}
\partial_t z_e - \partial_x(\zeta_a \partial_x z_e) + \zeta_b \partial_x z_e + \zeta_p z_e &= \zeta_1 f_e, && (x,t) \in e \times (0,T),\\
z_{e_1}(v,t) &= z_{e_2}(v,t), && v \in \mathcal{V}_0,\ e_1, e_2 \in \mathcal{E}(v),\\
\zeta_1(v,t)(z_e(v,t) - g_v(t)) &= 0, && v \in \mathcal{V}_b,\ e \in \mathcal{E}(v),\\
\sum_{e \in \mathcal{E}(v)} \zeta_1(v,t)\partial_x z_e(v,t) n_e(v) &= 0, && v \in \mathcal{V}_0,\\
z_e(x,0) &= y_e^0(x), && x \in e,
\end{aligned} \tag{17.32}$$

for every $e \in \mathcal{E}$. Note that the vertex–continuity condition in (17.32) is enforced on the entire graph, whereas the boundary and flux terms are switched on or off by the function ζ_1. Hence, (17.32) encodes two dynamics within a single formulation: the PDE dynamics on the active subgraph $\mathcal{G}^{\mathcal{B}(t)}$ and, on its complement, a system of first-order ODEs that freezes the solution over the interval I_{k_t}.

Theorem 17.5 ([42]) *Assume that the initial and boundary data satisfy the regularity conditions of Theorem 17.4. Then there exists a unique solution z of* (17.32) *belonging to the class $H^1(0,T;L^2(\mathcal{E})) \cap C([0,T];H^1(\mathcal{E}))$.*

The proof of Theorem 17.5 hinges on two facts: (i) by Theorem 17.4, on each interval I_k, the system restricted to the active subgraph admits a unique solution whose terminal value lies in H^1 on that subgraph, and (ii) the vertex–continuity condition in (17.32) propagates this H^1 regularity to the full graph. Starting with $z_0 \in H^1(\mathcal{E})$, we therefore obtain $z(t_1) \in H^1(\mathcal{E})$ after the first step, and the argument can be re-applied on I_2. Induction over $k \in \{1,\dots,K\}$ yields global well-posedness.

Let us introduce $\Lambda : (0,T) \to \mathbb{R}_+$, defined by

$$\Lambda(t) := \mathbb{E}\left[\|\partial_x((a-\zeta_a)\partial_x y)\|^2_{L^2(\mathcal{E})}\right] + \mathbb{E}\left[\|(b-\zeta_b)\partial_x y\|^2_{L^2(\mathcal{E})}\right] + \mathbb{E}\left[\|(p-\zeta_p)y\|^2_{L^2(\mathcal{E})}\right] + \mathbb{E}\left[\|(\zeta_1-1)f\|^2_{L^2(\mathcal{E})}\right],$$

where y is the solution of (17.30), and f and (a, b, p) are the respective source term and coefficients. The quantity Λ is the continuous analogue of the RBM variance (17.21), and depends on the subgraphs, batches, and probabilities considered.

Theorem 17.6 ([42]) *Assume Assumption 17.1 and the regularity assumptions from Theorem 17.4. Let y be the solution of* (17.30) *and z the solution of* (17.32)*. Then, $\Lambda \in L^1(0,T)$ is uniformly bounded with respect to h, and*

$$\sup_{t\in[0,T]} \mathbb{E}[\|z(t)-y(t)\|^2_{L^2(\mathcal{E})}] \le C\|\Lambda\|^{1/2}_{L^1(0,T)}h,$$

where $C > 0$ depends on the problem data but is independent of $h > 0$.

Remark 17.6 The proof of Theorem 17.6 relies on energy estimates and two key facts: (i) ζ is an unbiased estimator; and (ii) $z \in H^1(0,T;L^2(\mathcal{E}))$ and $y \in L^2(0,T;H^2_{\mathrm{pw}}(\mathcal{E}))$, where $H^2_{\mathrm{pw}}(\mathcal{E})$ denotes edgewise H^2 regularity on the graph (see [42]). The argument is concluded by applying Grönwall's lemma and verifying that all constants are uniform in h. The regularity results 17.4 and 17.5 are crucial for establishing Theorem 17.6.

On the other hand, the constant $C > 0$ in the convergence estimate deteriorates as $\pi_* := \min_i \pi_i \to 0$, which highlights the importance of a balanced batch distribution. Finally, in contrast to Theorem 17.3, Theorem 17.6 provides an estimate independent of δ.

17.4.2.3 Numerical Examples

In addition to the theoretical analysis, we present numerical experiments.

On each edge e, we consider the coefficients: $a_e(x) = x(x-1)+\frac{1}{2}$, $b_e(x) = \frac{1}{2}\sin(\pi x)$, $p_e(x) = \sin(\pi x)$, and following the manufactured-solution method, we consider the exact solution as $y_e(x,t) = w_e(x)\,v(t)$ with $v(t) = \sin(2\pi t)$ and $w_e(x) = \alpha_e x^4 + \beta_e x^3 + x^2 + x + 1$ (see [42, Table 1] for (α_e, β_e)). Then f_e, g_v, and y_e^0 are defined consistently from the PDE. The FEM space uses a P_1 basis with *100 basis functions per edge* plus one basis per vertex (10 vertices), hence $n = 1010$; we set $T = 1$ and $\Delta t = 0.002$. The RBM expectation is approximated with 20 i.i.d. realizations.

Table 17.2 shows the average execution time and the memory usage for both the RBM and the full graph solver. We consider two time discretizations: Implicit Euler (IE, first-order) and Crank–Nicolson (CN, second-order). For the full graph solver and the RBM, the errors are measured by

$$\sup_{t\in[0,T]} \|y-y_n\|^2_{L^2(\mathcal{E})} \quad \text{and} \quad \sup_{t\in[0,T]} \mathbb{E}[\|y-z_n\|^2_{L^2(\mathcal{E})}],$$

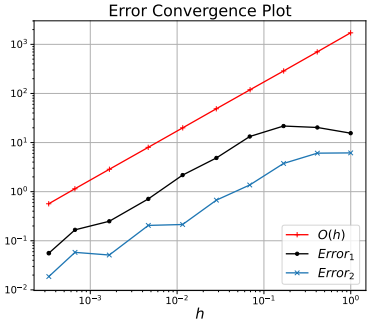
respectively. Here, y_n and z_n denote the FEM approximation of (17.30) and (17.32), while y is the exact solution. As shown in Table 17.2, the CN discretization does not

Table 17.2: Performance comparison: Full graph vs. RBM with varying h

Metric	Full Graph		RBM					
			h = 0.002		h = 0.004		h = 0.006	
	IE	CN	IE	CN	IE	CN	IE	CN
Time (s)	47.9800	64.3542	20.7443	37.1141	21.6726	33.9533	23.8093	29.4326
Memory (MB)	112.52	120.00	103.14	104.30	105.48	103.56	103.49	101.75
Error	3.764e-1	7.327e-2	3.773e-1	3.731e-1	6.120e-1	6.245e-1	9.846e-1	9.808e-1

reduce the error with respect to the IE, confirming that the RBM is first-order and suggests that the convergence rate in Theorem 17.6 is sharp. This also highlights a key feature of the continuous RBM: It approximates the solution independently of the time discretization, and thus it can be coupled with any standard first-order time integrator without affecting its order of accuracy.

As expected, smaller values of h yield RBM errors closer to those of the full solver, while retaining computational savings in time and memory. Moreover, the log–log plot in Fig. 17.9 demonstrates the theoretical rate of convergence $O(h)$.



(a)

h	Error_1	Error_2
3.333×10^{-4}	5.530×10^{-2}	1.744×10^{-2}
6.667×10^{-4}	1.675×10^{-1}	6.139×10^{-2}
1.667×10^{-3}	2.502×10^{-1}	4.924×10^{-2}
4.667×10^{-3}	7.118×10^{-1}	2.125×10^{-1}
1.167×10^{-2}	2.150×10^{0}	2.074×10^{-1}
2.833×10^{-2}	4.826×10^{0}	6.793×10^{-1}
6.933×10^{-2}	1.310×10^{1}	1.358×10^{0}
1.687×10^{-1}	2.147×10^{1}	3.818×10^{0}
4.107×10^{-1}	2.016×10^{1}	6.128×10^{0}
1.000×10^{0}	1.538×10^{1}	6.128×10^{0}

(b)

Fig. 17.9: (a) Log–log plot of the errors versus the RBM step size h. The black curve with dots represents $\text{Error}_1 := \sup_t \mathbb{E}[\|y - z_n\|^2_{L^2(\mathcal{E})}]$, the blue curve with crosses represents $\text{Error}_2 = \sup_t \|y - \mathbb{E}[z_n]\|^2_{L^2(\mathcal{E})}$, and the red line with plus markers indicates the expected $O(h)$ convergence. (b) lists the corresponding error values for different h.

17.4.3 Related Work and Comments

17.4.3.1 Related Work

Random Batch Methods (RBM) were introduced for large interacting particle systems and later adapted to finite-dimensional dynamics, including linear–quadratic and model predictive control, as well as kinetic models such as mean-field, Landau, and Fokker–Planck; see, e.g., [13, 45–47, 50, 68, 87, 88]. In the PDE context, much of the literature proceeds via prior discretization—randomized domain decomposition for nonlinear PDEs, stochastic evolution equations, and gradient flows are representative examples [8, 14, 23]. The discretize+randomize scheme discussed in Sect. 17.4.1 fits naturally within this family [43]. By contrast, the continuous formulation [42], discussed in Sect. 17.4.2, introduces randomization directly at the PDE level in a parabolic setting. Readers interested in broader perspectives on graphs and gas networks may also consult the references cited in the introduction.

17.4.3.2 Comments

We presented the Random Batch Method (RBM) as a randomized domain–decomposition paradigm for PDEs on graphs. In the *discretize+randomize* formulation (Sect. 17.4.1), RBM is applied after spatial semi-discretization to the resulting finite-dimensional dynamics, with the convergence estimate Theorem 17.3; this setting also covers optimal control (see [43]). In the *continuous* formulation (Sect. 17.4.2), randomization acts directly at the PDE level; Theorem 17.5 ensures well-posedness and Theorem 17.6 yields a mesh-independent first-order error bound governed by the RBM step h. In both cases, evolving only active subnetworks over short windows reduces memory footprint and wall-time while retaining convergence.

Discretize+randomize vs. continuous RBM: The *discretize+randomize* formulation is broadly applicable to linear PDEs (parabolic, hyperbolic, or mixed), integrates naturally with LQR optimal control, and leverages graph structure. However, its error bound features a mesh-dependent term ($O(h/\delta^7)$ in Theorem 17.3), which forces $h \ll \delta^7$ and can render simulations that strictly meet the theoretical guarantees impractical. By contrast, the *continuous RBM* acts at the PDE level and delivers a mesh-independent approximation for parabolic problems, with error controlled by h (Theorem 17.6). Its current analysis is confined to parabolic operators with specific vertex conditions; extending it to other systems will require new analysis.

Let us finally discuss some open problems and directions.

Optimal decompositions: As noted in Remark 17.5, batch design must balance sparsity (cheaper local solves, lower memory) against variance (randomization error). Spectral cuts (Fiedler vectors), clustering, and optimization-based designs, are natural candidates for constructing batch decompositions on the graph; see [43, Sect. 5].

Beyond the heat equation: Extend the continuous RBM to hyperbolic and mixed systems, or cast it within a semi-group framework. Since the heat equation is a

linear approximation of the isothermal Euler model in high-friction regimes (see Sect. 17.4.1.1), it is natural to extend both RBM approaches—discrete and continuous—to nonlinear gas-transport models, such as those introduced in [20], and to provide error estimates between the proposed model solution and the exact solution.

Optimal control: Extend the continuous RBM to LQR and MPC on graphs, establishing convergence guarantees and *a priori* error bounds. In parallel, extend both the discretize+RBM and continuous RBM approaches to general optimal control beyond quadratic costs and linear dynamics. For applications to gas and fluid transport on networks-central to TRR154-RBM-based optimal control is essential for reducing computational cost. A formulation consistent with standard gas-network models can follow the framework in [40].

17.5 A Consensus-Based Penalty Alternating Direction Method for Graph-Decompositions of Gas Networks

We now consider dynamic and discretized gas transport optimization problems, which lead to large-scale and nonconvex mixed-integer nonlinear optimization problems (MINLPs). Usually, the resulting instances are too challenging to be solved by today's general-purpose MINLP solvers. In this section, we briefly sketch a graph decomposition approach developed in [55] to obtain multiple optimization problems on sub-graphs, which can even be solved in parallel. Instead of employing a fixed-point iteration as used in the previous Sections 17.2 and 17.3 to achieve feasibility at the interfaces of the blocks, we here use a tailored consensus-based penalty alternating direction method.

17.5.1 Modeling

We consider a fixed and finite time horizon $[0, T]$ and the network is again modeled as a directed and weakly connected graph G. We continue referring to nodes V consisting of entries V_+, exits V_-, and inner nodes V_0, i.e.,

$$V = V_+ \cup V_- \cup V_0,$$

while, in the following, we refer to edges as arcs consist of pipes, short pipes, valves, compressor stations, and control valves, i.e.,

$$A = A_{\mathrm{p}} \cup A_{\mathrm{sp}} \cup A_{\mathrm{v}} \cup A_{\mathrm{cs}} \cup A_{\mathrm{cv}}.$$

We now model the separate gas network components and state possible objective functions.

17.5.1.1 Pipes

The one-dimensional semi-linear Euler equations (see, e.g., [40]) that we use to model the gas flow in a pipe $a \in A_{\mathrm{p}}$ are given by

$$\partial_t p_a + \frac{c^2}{A_a}\partial_x q_a = 0, \qquad (t,x) \in (0,T)\times(0,L), \quad (17.33a)$$

$$\partial_t q_a + A_a \partial_x p_a = -\frac{\lambda_a c^2}{2D_a A_a}\frac{q_a|q_a|}{p_a} - \frac{gA_a h_a'}{c^2}p_a, \quad (t,x) \in (0,T)\times(0,L). \quad (17.33b)$$

They detail and extend the ISO2 model as used in (17.1) above, now in variables pressure p_a and mass flow q_a. Here and in what follows, A, D, L, and h' describe the cross-sectional area, the diameter, the length, and the slope of the pipe. Furthermore, g is the gravitational acceleration. In what follows, the notation $p_{a,v}(t)$ stands for the pressure in the pipe a at time t directly at the interface to node v.

There is a multitude of ways to model the friction coefficient λ_a; see, e.g., [26, 84]. For the modeling in this paper, we use the flow-independent law of Nikuradse, i.e.,

$$\lambda_a = \left(2\log_{10}\left(\frac{D_a}{k_a}\right) + 1.138\right)^{-2},$$

where the parameter k_a describes the roughness of the pipe's inner wall.

Finally, we assume that the mass flow inside of every pipe and every other element of the network is uniformly (over time) bounded from below and above, i.e.,

$$q_a(t,x) \in \left[q_a^-, q_a^+\right] \qquad (17.34)$$

holds on $(0,T)\times(0,L)$. The same holds true for pressures, i.e.,

$$p_a(t,x) \in \left[p_a^-, p_a^+\right] \qquad (17.35)$$

holds on $(0,T)\times(0,L)$.

17.5.1.2 Short Pipes

Short pipes $a = (v,w) \in A_{\mathrm{sp}}$ are artificial modeling tools to directly connect two nodes so that there is no pressure loss, i.e.,

$$p_{a,v}(t) = p_{a,w}(t), \quad t \in [0,T], \qquad (17.36)$$

and there is only one mass flow variable $q_a(t) = q_{a,v}(t) = q_{a,w}(t)$ for every point in time $t \in T$.

17.5.1.3 Valves

At each point in time $t \in [0,T]$, a valve $a = (v,w) \in A_{\mathrm{v}}$ is either open or closed. If it is open, it is modeled as a short pipe. If the valve is closed, gas flow is blocked and the pressures at both incident nodes are decoupled. Thus we have $p_{a,v}(t) = p_{a,w}(t)$ if the valve a is open and $q_a(t) = 0$, if the valve a is closed. This can be modeled by using a binary variable $o_a(t) \in \{0,1\}$ that indicates if the valve is open ($o_a(t) = 1$) or closed ($o_a(t) = 0$). The mixed-integer model for valves then reads

$$p_{a,v}(t) \geq p_{a,w}(t) - (p_a^+ - p_a^-)(1 - o_a(t)), \tag{17.37a}$$
$$p_{a,v}(t) \leq p_{a,w}(t) + (p_a^+ - p_a^-)(1 - o_a(t)), \tag{17.37b}$$
$$q_a(t) \geq q_a^- o_a(t), \tag{17.37c}$$
$$q_a(t) \leq q_a^+ o_a(t) \tag{17.37d}$$

for all $a \in A_{\mathrm{v}}$ and all $t \in [0,T]$.

17.5.1.4 Compressor Stations and Control Valves

Similar to valves, compressor stations $a \in A_{\mathrm{cs}}$ can be open or closed. If they are open, they can be either active or in bypass mode. Active compressor stations can increase the pressure by a controlled and positive amount $\Delta p_a \in [\Delta p_a^-, \Delta p_a^+]$ with $0 < \Delta p_a^- \leq \Delta p_a^+$. Finally, compressor stations in bypass mode behave like short pipes. The flow direction of a compressor station $a \in A_{\mathrm{cs}}$ is fixed, i.e., $q_a^- = 0$, and we assume that all compressor stations are always open for the ease of presentation. Hence, we have

$$\begin{aligned} p_{a,v}(t) + \Delta p_a(t) &= p_{a,w}(t), && \text{if the compressor station } a \text{ is active,} \\ p_{a,v}(t) &= p_{a,w}(t), && \text{if the compressor station } a \text{ is in bypass mode.} \end{aligned}$$

To obtain a mixed-integer linear model for this, we introduce a binary variable $b_a(t) \in \{0,1\}$. This variable indicates if the compressor station is active ($b_a(t) = 1$) or in bypass mode ($b_a(t) = 0$). The mixed-integer compressor station model then reads

$$\Delta p_a(t) \geq \Delta p_a^- b_a(t), \tag{17.38a}$$
$$\Delta p_a(t) \leq \Delta p_a^+ b_a(t), \tag{17.38b}$$
$$p_{a,v}(t) + \Delta p_a(t) = p_{a,w}(t). \tag{17.38c}$$

Note that there are much more realistic nonlinear compressor station models in the literature; see, e.g., [69, 78].

We model control valves $a = (v,w) \in A_{\mathrm{cv}}$ similar to compressor stations, but instead of increasing the pressure they can decrease it. This can be modeled by using the compressor station model (17.38) with $\Delta p \in [\Delta p^-, 0]$. Note that by choosing the upper bound as 0, the bypass case is always included in the active case.

17.5.1.5 Nodes

The model for nodes $v \in V$ has to capture pressure continuity

$$p_v(t) = p_{a,v}(t) \quad \text{for all } a \in \delta(v) \quad \text{for all } t \in [0,T], \tag{17.39}$$

i.e., the node pressure $p_v(t)$ is equal to the adjacent arc pressures $p_{a,v}(t)$ at the interface to the respective node v. Here, we use $\delta(v) = \delta^{\text{in}}(v) \cup \delta^{\text{out}}(v)$, where $\delta^{\text{in}}(v)$ and $\delta^{\text{out}}(v)$ are the sets of in- and outgoing arcs of node v. Moreover, the pressure at all nodes are bounded from below and above via

$$p_v(t) \in \left[p_v^-, p_v^+\right] \quad \text{for all } t \in [0,T]. \tag{17.40}$$

Furthermore, at nodes, we have to model mass balance via

$$q_v(t) + \sum_{a \in \delta^{\text{in}}(v)} q_{a,v}(t) - \sum_{a \in \delta^{\text{out}}(v)} q_{a,v}(t) = 0 \tag{17.41}$$

for $v \in V$ and $t \in [0,T]$, where $q_v(t)$ is the mass flow that is supplied or withdrawn from the network at node v. It holds

$$q_v(t) \begin{cases} \geq 0 & \text{for entries } v \in V_+, \\ \leq 0 & \text{for exits } v \in V_-, \\ = 0 & \text{for inner nodes } v \in V_0 \end{cases}$$

and the mass flow at nodes is also bounded from below and above, i.e.,

$$q_v(t) \in \left[q_v^-, q_v^+\right] \quad \text{for all } v \in V, t \in [0,T]. \tag{17.42}$$

17.5.1.6 Objective Function

A classic objective function in gas transport optimization is to minimize the operational costs of the compressor stations, i.e., one wants to minimize

$$f_{\text{c}} = \sum_{a \in A_{\text{cs}}} \int_0^T \Delta p_a(t)\, \mathrm{d}t. \tag{17.43}$$

Another possibility is the tracking-type objective function on entries V_+ and exits V_-,

$$f_{\text{t}} = \sum_{v \in V_+ \cup V_-} \eta \left(p_v(T) - \widehat{p}_v\right)^2 + \theta \left(q_v(T) - \widehat{q}_v\right)^2, \tag{17.44}$$

for given factors η, θ and target pressures $\widehat{p}$ and mass flows $\widehat{q}$.

17.5.1.7 Problem Statement

Combining all the parts presented before, we arrive at the optimization problem

$$\begin{aligned} \min \quad & (17.43) \text{ or } (17.44) \\ \text{s.t.} \quad & \text{Euler equations: } (17.33), \\ & \text{short pipe model: } (17.36), \\ & \text{valve model: } (17.37), \\ & \text{compressor station and control valve model: } (17.38), \\ & \text{pressure continuity equations: } (17.39), \\ & \text{mass balance equation: } (17.41), \\ & \text{variable bounds: } (17.34), (17.35), (17.40), (17.42). \end{aligned} \tag{17.45}$$

The variables of this problem are the following. We have pressure $p_a(\cdot, \cdot)$ and mass flow variables $q_a(\cdot, \cdot)$ for all pipes $a \in A_\mathrm{p}$. Moreover, the model includes variables $p_{a,u}$, $p_{a,v}$, and q_a for short pipes, valves, compressor stations, and control valves, i.e., for $a = (u, v) \in A_\mathrm{sp} \cup A_\mathrm{v} \cup A_\mathrm{cs} \cup A_\mathrm{cv}$. Finally, we have variables o_a for valves $a \in A_\mathrm{v}$, Δp_a for compressor stations $a \in A_\mathrm{cs}$ and control valves $a \in A_\mathrm{cv}$ as well as pressure variables p_u for all nodes $u \in V$. Finally, we have variables b_a for compressor stations and control valves $a \in A_\mathrm{cs} \cup A_\mathrm{cv}$.

17.5.1.8 Discretization

Model (17.45) is a time-dependent mixed-integer optimization problem that is further constrained by partial differential equations. In this paper, we follow the first-discretize-then-optimize approach. To this end, we have to discretize the Euler equations (17.33) in space and time. For both dimensions, we apply the implicit Euler method. For time, we use the grid given by the points t_κ, $\kappa = 0, \ldots, N_t$, with $t_0 = 0$, $t_{N_t} = T$, and $t_\kappa < t_{\kappa+1}$. We assume that all variables at time point $t_0 = 0$ are fixed as they constitute the initial state of the system. For the spatial discretization, we use the grid given by the points $x_{a,\nu}$, $\nu = 0, \ldots, N_x^a$, with $x_{a,0} = 0$, $x_{a,N_x^a} = L_a$, and $x_{a,\nu} < x_{a,\nu+1}$. Note that the spatial grid depends on the specific pipe $a \in A_\mathrm{p}$. For the ease of presentation, we consider an equidistant discretization in time and space with a fixed time step

$$\Delta t = T/N_t = t_{\kappa+1} - t_\kappa \quad \text{for all } \kappa = 0, \ldots, N_t - 1$$

and spatial step

$$\Delta x_a = L_a/N_x^a = x_{a,\nu+1} - x_{a,\nu} \quad \text{for all } \nu = 0, \ldots, N_x^a - 1,\ a \in A_\mathrm{p}.$$

Using this notation, we get the fully discretized set of Euler equations

$$\frac{p_a(t_{\kappa+1}, x_{a,\nu+1}) - p_a(t_\kappa, x_{a,\nu+1})}{\Delta t} + \frac{c^2}{A_a} \frac{q_a(t_{\kappa+1}, x_{a,\nu+1}) - q_a(t_{\kappa+1}, x_{a,\nu})}{\Delta x_a} = 0,$$

$$\frac{q_a(t_{\kappa+1}, x_{a,\nu+1}) - q_a(t_\kappa, x_{a,\nu+1})}{\Delta t} + A_a \frac{p_a(t_{\kappa+1}, x_{a,\nu+1}) - p_a(t_{\kappa+1}, x_{a,\nu})}{\Delta x_a} + \frac{\lambda_a c^2}{2 D_a A_a} \frac{q_a |q_a|}{p_a}(t_{\kappa+1}, x_{a,\nu+1}) + \frac{g A_a h_a'}{c^2} p_a(t_{\kappa+1}, x_{a,\nu+1}) = 0$$

for all $a \in A_\mathrm{p}$, $\kappa = 0, \dots, N_t$, and $\nu = 0, \dots, N_x^a$. We now replace (17.33) in Model (17.45) with these discretized equations and further discretize the remaining algebraic constraints by simply writing them for all time points t_κ with $\kappa = 1, \dots, N_t$. Moreover, we discretize the objective function (17.43) via the right Riemannian sum

$$f_\mathrm{c} = \sum_{a \in A_\mathrm{cs}} \sum_{\kappa=1}^{N_t} \Delta t \Delta p_a(t_\kappa).$$

Note that $\Delta p_a(t_0)$ is given and thus not part of the sum in the objective function. The tracking-type objective function (17.44) stays unchanged because it only depends on the time point $t_{N_t} = T$. In this way, we obtain a large-scale but finite-dimensional and structured mixed-integer nonlinear optimization problem. Here, the nonlinearities are all contained in the model of the pipes, namely in the discretized momentum equation.

17.5.2 Classic Penalty Alternating Direction Methods

For the moment, let us consider the optimization problem

$$\begin{aligned} \min_{x,y} \quad & f(x,y) \\ \text{s.t.} \quad & g(x,y) = 0, \\ & x \in X,\ y \in Y \end{aligned}$$

with $X \subseteq \mathbb{R}^{n_x}$ as well as $Y \subseteq \mathbb{R}^{n_y}$ being non-empty and compact sets and $f : \mathbb{R}^{n_x+n_y} \to \mathbb{R}$ as well as $g : \mathbb{R}^{n_x+n_y} \to \mathbb{R}^m$ are continuous functions. Classic PADMs try to compute so-called partial minima of this problem, which are points (x^*, y^*) that satisfy

$$\begin{aligned} f(x^*, y^*) &\le f(x, y^*) \quad \text{for all } x \in X \text{ with } g(x, y^*) = 0, \\ f(x^*, y^*) &\le f(x^*, y) \quad \text{for all } y \in Y \text{ with } g(x^*, y) = 0. \end{aligned}$$

For what follows, we introduce the penalized objective function

$$\phi(x, y; \mu) = f(x, y) + \sum_{j=1}^{m} \mu_j g_j(x, y)^2 \tag{17.46}$$

with penalty parameters $\mu \in \mathbb{R}^m_{>0}$ and the penalty problem

$$\min_{x,y} \quad \phi(x, y; \mu) \quad \text{s.t.} \quad x \in X,\ y \in Y. \tag{17.47}$$

Note that we have a separate penalty parameter for every constraint. With this, we can state the PADM, which is formally given in Algorithm 1.

For a thorough discussion of the convergence properties of this method we refer the interested reader to [32]. Several applications of this method to different applied fields can be found in [15, 31, 33, 49, 82].

17.5.3 A Consensus-Based Penalty Alternating Direction Method

The graph decomposition described in the next section leads to problems of the general form

$$\min_{x^1,\dots,x^\ell,z} \quad \sum_{i=1}^{\ell} f_i(x^i) \tag{17.48a}$$

$$\text{s.t.} \quad (x^i, z) \in X_i \quad \text{for } i = 1, \dots, \ell, \tag{17.48b}$$

$$z \in Z \tag{17.48c}$$

with $X_i \subseteq \mathbb{R}^{n_i} \times \mathbb{R}^{n_z}$, $f_i : \mathbb{R}^{n_i} \to \mathbb{R}$ for $i = 1, \dots, \ell$, and a convex set $Z \subseteq \mathbb{R}^{n_z}$. The problem consists of ℓ constraint blocks X_i that are connected via the so-called linking variables $z \in Z$. Informally speaking, we call such problems "quasi-separable" if the dimension of the coupling variables in (17.48c) is not too large.

We reformulate problem (17.48) by introducing a copy z^i of z for each block, which yields the equivalent problem

$$\min_{x^1,\dots,x^\ell,z^1,\dots,z^\ell,z} \quad \sum_{i=1}^{\ell} f_i(x^i) \tag{17.49a}$$

$$\text{s.t.} \quad (x^i, z^i) \in X_i \quad \text{for } i = 1, \dots, \ell, \tag{17.49b}$$

$$z \in Z, \tag{17.49c}$$

$$z^i = z \quad \text{for } i = 1, \dots, \ell, \tag{17.49d}$$

$$z^i \in Z \quad \text{for } i = 1, \dots, \ell. \tag{17.49e}$$

Algorithm 1 Penalty Alternating Direction Method

Require: $x^{0,0} \in X$, $y^{0,0} \in Y$, and penalty parameters $\mu^0 \in \mathbb{R}^m_{>0}$.

for $k = 0, 1, 2, \dots$ **do**
  Set $l = 0$.
  while $(x^{k,l}, y^{k,l})$ is not a partial minimum of (17.47) **do**
    Compute $x^{k,l+1} \in \arg\min_x \{\phi(x, y^{k,l}; \mu^k) : x \in X\}$.
    Compute $y^{k,l+1} \in \arg\min_y \{\phi(x^{k,l+1}, y; \mu^k) : y \in Y\}$.
    Set $l \leftarrow l + 1$.
  end while
  Choose new penalty parameters $\mu^{k+1} \geq \mu^k$.
  Set $(x^{k+1,0}, y^{k+1,0}) \leftarrow (x^{k,l}, y^{k,l})$.
end for

To this setup, we can now apply the penalty alternating direction method given in Algorithm 1 with $x = (x^1, z^1, \ldots, x^\ell, z^\ell)$, $y = z$, $X = (X_1 \cap (\mathbb{R}^{n_1} \times Z)) \times \cdots \times (X_\ell \cap (\mathbb{R}^{n_\ell} \times Z))$, and $Y = Z$. Moreover, the constraints g are identified with the equality constraints (17.49d). The optimization problem in Step 4 of Algorithm 1 is then given by

$$\begin{aligned} \min_{x^1,\ldots,x^\ell,z^1,\ldots,z^\ell} \quad & \sum_{i=1}^{\ell} \left(f_i(x^i) + \sum_{j=1}^{n_z} \mu_j^i \left(z_j^i - (z_j)^{k,l} \right)^2 \right) \\ \text{s.t.} \quad & (x^i, z^i) \in X_i \quad \text{for } i = 1, \ldots, \ell, \\ & z^i \in Z \quad \text{for } i = 1, \ldots, \ell. \end{aligned}$$

This problem is completely separable. Therefore, we can instead solve

$$\begin{aligned} \min_{x^i,z^i} \quad & f_i(x^i) + \sum_{j=1}^{n_z} \mu_j^i \left(z_j^i - (z_j)^{k,l} \right)^2 \\ \text{s.t.} \quad & (x^i, z^i) \in X_i, \\ & z^i \in Z \end{aligned}$$

for all blocks $i = 1, \ldots, \ell$, which can be done in parallel. The optimization problem in Step 5 of Algorithm 1 reads

$$\min_{z \in Z} \quad \sum_{i=1}^{\ell} \sum_{j=1}^{n_z} \mu_j^i \left(\left(z_j^i \right)_k^{l+1} - z_j \right)^2.$$

The solution for this so-called consensus problem is the weighted arithmetic mean

$$z_j = \frac{1}{\sum_{i=1}^{\ell} \mu_j^i} \sum_{i=1}^{\ell} \mu_j^i \left(z_j^i \right)_k^{l+1}$$

for all $j = 1, \ldots, n_z$, since Z is convex and $\left(z^i \right)_k^{l+1} \in Z$ for all $i = 1, \ldots, \ell$ because of (17.49e); see, e.g., [6].

17.5.4 Decomposition of Gas Networks

To efficiently apply the PADM to the discretized version of Problem (17.45), we need to identify a quasi-separable structure as in (17.48). To this end, we can utilize the fact that we model the problem on a graph. As each variable can be associated with a certain location in this graph it follows that decomposing the graph yields corresponding blocks (indexed with i) of variables with respective constraint sets X_i. If the network is decomposed in a way that the resulting sub-networks are only coupled in a sparse way, then the number of linking variables z stays small and we have the desired quasi-separable structure.

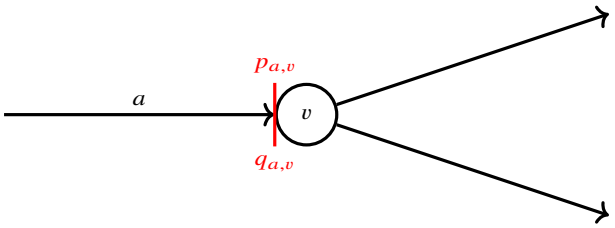


Fig. 17.10: The vertical red line represents a possible decomposition at node v that minimizes the number of linking variables.

The question is still open on how to decompose the graph. One might assume that it is a good idea to decompose a network at selected nodes of the network. This, however, significantly increases the number of linking variables if the degree of the respective nodes is large since the pressures and mass flows of all adjacent arcs are connected across the node by the pressure continuity equation (17.39) and the mass balance equation (17.41). This undesired aspect can be avoided by splitting the network at points that lie on arcs instead of nodes. To still assign each arc to exactly one sub-network, we decide to only split an arc at the interface to its start or end node. Figure 17.10 depicts a possible decomposition at the interface to a node of degree three. The only linking variables in this situation are $p_{a,v}$ and $q_{a,v}$ for all time points t_κ.

More precisely, we decompose the graph (V, A) into blocks (V_i, A_i) for $i = 1, \dots, \ell$ with

$$V = \bigcup_{i=1}^{\ell} V_i, \quad A = \bigcup_{i=1}^{\ell} A_i$$

and

$$\begin{aligned} V_i \cap V_j &= \emptyset \quad \text{for } i, j = 1, \dots, \ell,\ i \neq j, \\ A_i \cap A_j &= \emptyset \quad \text{for } i, j = 1, \dots, \ell,\ i \neq j. \end{aligned}$$

Thus, each node $v \in V$ and each arc $a \in A$ belongs to exactly one block (V_i, A_i). Note that a block (V_i, A_i) itself is not a graph, as $a = (v, w) \in A_i$ does not imply $v \in V_i$ and $w \in V_i$. Vice versa, it can happen that $a \notin A_i$ for some arc $a \in \delta^{\text{in}}(v) \cup \delta^{\text{out}}(v)$ with $v \in V_i$. These cases appear exactly at the interfaces of the blocks. We define the interfaces of a single block $i \in \{1, \dots, \ell\}$ as

$$I_i := \{(v, a) \in V_i \times A \colon a \in \delta(v) \text{ and } a \notin A_i\} \cup \{(v, a) \in V \times A_i \colon a \in \delta(v) \text{ and } v \notin V_i\}\,.$$

The set of all interfaces is then given by

$$I := \bigcup_{i=1}^{\ell} I_i.$$

We now use this graph decomposition for gas networks. The constraint system of Problem (17.45) can then be written as

Euler equations: (17.33) for $A_{\mathrm{p}} \cap A_i$,
short pipe model: (17.36) for $A_{\mathrm{sp}} \cap A_i$,
valve model: (17.37) for $A_{\mathrm{v}} \cap A_i$,
compressor station and control valve model: (17.38) for $(A_{\mathrm{cs}} \cup A_{\mathrm{cv}}) \cap A_i$,
pressure continuity equations: (17.39) for V_i,
mass balance equation: (17.41) for V_i,
variable bounds: (17.34), (17.35), (17.40), (17.42) for (V_i, A_i).

Moreover, the objectives (17.43) and (17.44) can be rewritten as

$$f_{\mathrm{c}} = \sum_{i=1}^{\ell} \sum_{a \in A_{\mathrm{cs}} \cap A_i} \int_0^T \Delta p_a(t)\, \mathrm{d}t$$

and

$$f_{\mathrm{t}} = \sum_{i=1}^{\ell} \sum_{v \in (V_+ \cup V_-) \cap V_i} \eta \left(p_v(T) - \widehat{p}_v\right)^2 + \theta \left(q_v(T) - \widehat{q}_v\right)^2 .$$

The linking constraints between the blocks are finally given by

$$\begin{aligned} p^i_{a,v} &= p_{a,v} \quad \text{for } (v,a) \in I_i,\ i = 1, \ldots, \ell, \\ q^i_{a,v} &= q_{a,v} \quad \text{for } (v,a) \in I_i,\ i = 1, \ldots, \ell. \end{aligned}$$

Finally note that there are multiple strategies to decompose a gas network. If more sub-networks are created, the number of linking variables increases, which potentially makes it harder to find a point that is feasible at all the sub-networks' interfaces. This can lead to a higher number of iterations required by Algorithm 1 and, therefore, longer computation times. However, multiple smaller problems may be easier to solve than a few larger ones. This trade-off needs to be considered when choosing the number of sub-networks.

17.5.5 Numerical Results

In this section, we apply a PADM for quasi-separable problems to the transient gas network optimization problems. To this end, we implemented the method in Python 3.8. We use GAMS 36.2.0 [9] to model the optimization problems, which we then solve using the solver CPLEX 20.1.0.1 [16] for LPs and MIPs and the solver KNITRO 12.4.0 [10] for NLPs and MINLPs. We also tested other MINLP solvers but KNITRO delivered the best results. However, KNITRO is a not a global solver but only solves nonconvex (MI)NLPs to local optimality. Since the different decompositions tested in the following lead to different models, the used solver might end up in different local minimizers. In our opinion, the choice of KNITRO, even if it is a local solver, is legitimate since we are mainly interested in running times and since the overall objective values of KNITRO are rather good.

All computations were done on nodes of the HPC cluster Woody at FAU Erlangen-Nürnberg with Xeon E3-1240 v6 CPUs on 4 cores, 3.7 GHz, and 32 GB RAM. For the discretization, we choose a time step size of $\Delta t = 3600\,\mathrm{s} = 1\,\mathrm{h}$ and a spatial step size of $\Delta x = 5000\,\mathrm{m}$. For each problem, we set a time limit of 1000 s.

All details about further implementation details such as the chosen tolerances, the initialization and update of penalty parameters, etc., can be found in [55]. Moreover, all code and data used for the presented numerical results are publicly available [56].

17.5.5.1 Transient Gas Network Data

The gas network instance GasLib-134 used for the numerical experiments is taken from the GasLib [83]. It contains the network data as well as 1234 different stationary scenarios and each of these scenarios represents a day between the 1st of November 2011 and the 17th of February 2016. This information is used to create transient scenarios on a time horizon of $T = 24\,\mathrm{h}$. First, we fix the mass flow q_v of each exit node $v \in V_-$ and the pressure p_v for each entry node $v \in V_+$. For the mass flow at an exit node at $t = 0$ we use the value given in the stationary scenario. Then, we apply a vertically shifted sine curve with period T and an amplitude of 0.1 to this initial value to receive the mass-flow curve for the complete time horizon:

$$q_v(t) = \left(1 + 0.1 \sin\left(t\frac{2\pi}{T}\right)\right) q_v(0), \quad v \in V_-,\ t \in [0,T].$$

The pressure at the entry nodes stays constant over the time horizon. We first solve all 1234 stationary scenarios by using the discretized version of Problem (17.45) with only one time point $t = 0 = T$. To this end, we use the stationary Euler equations

$$\partial_x q_a = 0, \quad \partial_x p_a = -\frac{\lambda_a c^2}{2D_a A_a^2}\frac{q_a|q_a|}{p_a} - \frac{g h_a'}{c^2} p_a,$$

where all time derivatives vanished, a simplified compressor station model without integer variables (see [55] again), and the objective function (17.43), which now reads

$$f_c = \sum_{a \in A_{cs}} \Delta p_a.$$

Then, we fix the entry pressures to the corresponding values of the obtained stationary solution. Since for two of the stationary problems, the solver reported infeasibility, this results in 1232 transient scenarios for the GasLib-134 network.

For the initial conditions of each scenario we used the solution of the corresponding stationary model. The same holds for the terminal condition that are needed for the tracking-type objective function (17.44). This stationary solution is also used to initialize all variables including the linking variables.

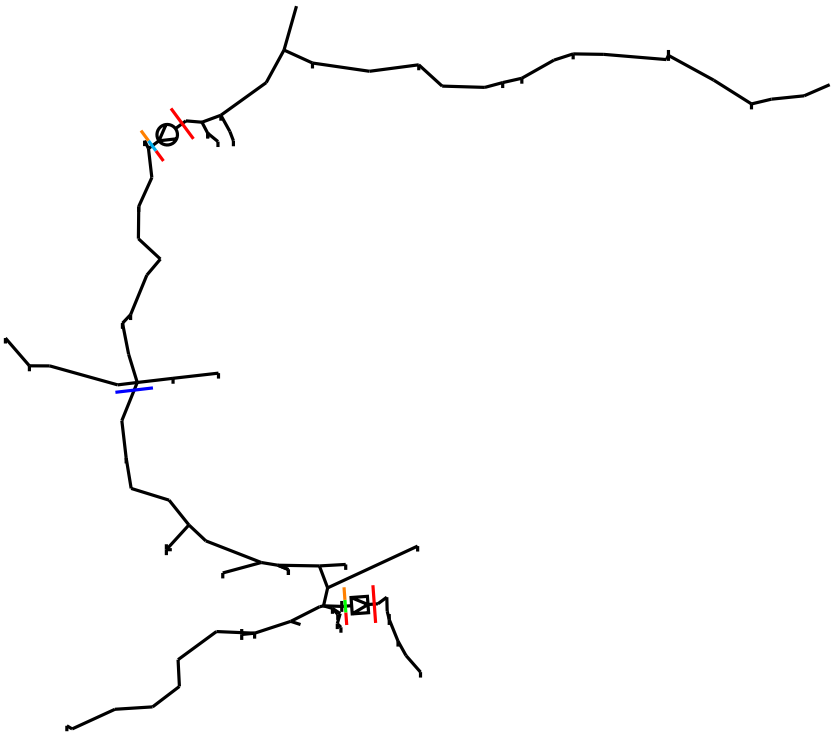


Fig. 17.11: Different decompositions of the GasLib-134 network: Active (red), Halves (blue), CS Arm (cyan), CV Arm (green), Both Arms (orange)

17.5.6 Discussion of the Results for the GasLib-134 Network

Preliminary tests on smaller test networks showed that applying the consensus-based PADM to transient gas network problems can yield a significant benefit w.r.t. the solution times as well as the objective value. However, the results can vary strongly and are dependent on a number of factors including the objective function, the network's structure, and, in particular, the chosen decomposition. Therefore, we test different graph decompositions for solving the real-world gas network GasLib-134. GasLib-134 models the gas network of Greece and consists of 134 nodes including 3 entries and 45 exits, 86 pipes, 45 short pipes, 1 compressor station, and 1 control valve. The total pipe length is 1447.02 km. The network is a tree with the compressor station in the north and the control valve in the south east.

Figure 17.11 shows GasLib-134 and the different decompositions we use. The details can be found in [55]. All block details of the proposed decompositions are shown in Table 17.3. This includes the number of nodes, entries, exits, pipes, short pipes, compressor stations, and control valves as well as the model type of each block.

Table 17.3: Decompositions of GasLib-134

Block Nr.	#nodes	#entries	#exits	#pipes	#sp	#cs	#cv	Type
			No decomp.					
1	134	3	45	86	45	1	1	MINLP
			Active					
1	42	2	13	28	13	0	0	NLP
2	81	1	28	52	28	0	0	NLP
3	11	0	4	6	4	0	0	NLP
4	0	0	0	0	0	1	0	MIP
5	0	0	0	0	0	0	1	MIP
			Halves					
1	65	1	23	41	23	0	1	MINLP
2	69	2	22	45	22	1	0	MINLP
			CV Arm					
1	11	0	4	6	4	0	1	MINLP
2	123	3	41	80	41	1	0	MINLP
			CS Arm					
1	42	2	13	28	13	1	0	MINLP
2	92	1	32	58	32	0	1	MINLP
			Both Arms					
1	42	2	13	28	13	1	0	MINLP
2	11	0	4	6	4	0	1	MINLP
3	81	1	28	52	28	0	0	NLP

Figure 17.12 shows the percentage of instances that can be solved in which amount of time for each type of tested decomposition and objective function. The decompositions “Active”, “Halves”, “CV Arm”, and “Both Arms” outperform “No decomp.” for most of the scenarios. For both objective models, “CV Arm” and “Both Arms” perform especially well while the overall worst results are produced by “CS Arm” and “No decomp.”. Moreover, for the tracking-type objective, also “Halves” can lead to some benefit for some scenarios.

Hence, the results show that decomposition approaches may lead to significant computational benefits. However, the impact strongly depends on the specific instance and the specific decomposition used. The question on how to compute a good decomposition for an arbitrarily given network is still open research question.

17.6 Conclusion

We presented advanced domain decomposition techniques for the efficient and scalable simulation and optimization of partial differential equations on network domains with a particular focus on transient gas network applications. We sketched novel space-and-time decomposition methods for semilinear hyperbolic and nonlinear parabolic

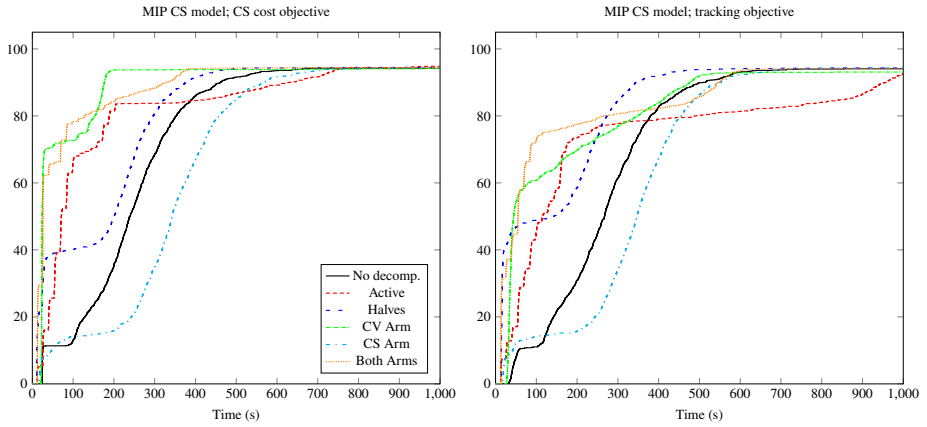


Fig. 17.12: Percentage of solved instances of GasLib-134 in the time limit of 1000 s for different decompositions as well as compressor station cost (17.43) and tracking-type (17.44) objective functions.

systems derived from Euler's equations. We also addressed combinatorial aspects of switching valves for the case of ODE-constrained problems. The convergence analysis in this context is yet limited to linear-quadratic problems though. The exploration of randomized decomposition methods has opened new avenues for stochastic approximation techniques. Through reviewed computational experiments on transient scenarios for a realistic gas transport network, the practical applicability and effectiveness of domain decomposition approaches is illustrated. Overall, our findings not only advance the current state of the art but also provide a solid foundation for future research in the simulation and optimization of large-scale network systems, offering flexible and powerful tools for solving complex network problems.

Acknowledgements This work was supported by the German Research Foundation (DFG) within Subprojects A03, A05, B08, and C07 in the Sonderforschungsbereich/Transregio 154 "Mathematical Modelling, Simulation and Optimization using the Example of Gas Networks" (Project ID 239904186).

References

1. J. Apraiz and J. A. Bárcena-Petisco. Observability and control of parabolic equations on networks with loops. *J. Evol. Equ.*, 23(2):Paper No. 37,33, 2023. doi:10.1007/s00028-023-00882-2.
2. A. Arutyunov and D. Karamzin. A survey on regularity conditions for state-constrained optimal control problems and the non-degenerate maximum principle. *Journal of Optimization Theory and Applications*, 184(3):697–723, 2020. doi:10.1007/s10957-019-01623-7.
3. A. Bamberger. Étude d'une équation doublement non linéaire. *J. Functional Analysis*, 24(2):148–155, 1977. doi:10.1016/0022-1236(77)90051-9.
4. G. Bastin and J.-M. Coron. *Stability and Boundary Stabilization of 1-D Hyperbolic Systems*, volume 88 of *Progress in Nonlinear Differential Equations and their Applications*. Birkhäuser/Springer, 2016. Subseries in Control. doi:10.1007/978-3-319-32062-5.

5. H. Bock and R. Longman. Optimal control of velocity profiles for minimization of energy consumption in the new york subway system. In *Proceedings of the Second IFAC Workshop on Control Applications of Nonlinear Programming and Optimization, International Federation of Automatic Control*, pages 34–43, 1980.
6. S. Boyd, N. Parikh, E. Chu, B. Peleato, and J. Eckstein. Distributed optimization and statistical learning via the alternating direction method of multipliers. *Foundations and Trends® in Machine Learning*, 3(1):1–122, 2011. doi:10.1561/2200000016.
7. J. Brouwer, I. Gasser, and M. Herty. Gas pipeline models revisited: Model hierarchies, non-isothermal models, and simulations of networks. *Multiscale Model. Simul.*, 9(2):601–623, 2011. doi:10.1137/100813580.
8. E. Buckwar, A. Djurdjevac, and M. Eisenmann. A domain decomposition method for stochastic evolution equations. *SIAM J. Numer. Anal.*, 62(6):2611–2639, 2024. doi:10.1137/24M1629845.
9. M. R. Bussieck and A. Meeraus. General algebraic modeling system (GAMS). In *Modeling Languages in Mathematical Optimization*, pages 137–157. Springer, 2004. doi:10.1007/978-1-4613-0215-5_8.
10. R. H. Byrd, J. Nocedal, and R. A. Waltz. KNITRO: An integrated package for nonlinear optimization. In *Large Scale Nonlinear Optimization*, pages 35–59. Springer Verlag, 2006. doi:10.1007/0-387-30065-1_4.
11. J. A. Bárcena-Petisco, M. Cavalcante, G. M. Coclite, N. De Nitti, and E. Zuazua. Control of hyperbolic and parabolic equations on networks and singular limits. *Mathematical Control and Related Fields*, 15(1):348–389, 2025. URL: http://hdl.handle.net/10810/73759.
12. P. Cannarsa, A. Duca, and C. Urbani. Exact controllability to eigensolutions of the bilinear heat equation on compact networks. *Discrete Contin. Dyn. Syst. Ser. S*, 15(6):1377–1401, 2022. doi:10.3934/dcdss.2022011.
13. J. A. Carrillo, S. Jin, and Y. Tang. Random batch particle methods for the homogeneous Landau equation. *Commun. Comput. Phys.*, 31(4):997–1019, 2022. doi:10.4208/cicp.oa-2021-0200.
14. A. D. Corella and M. Hernández. Mini-batch descent in semiflows. *ESAIM Control Optim. Calc. Var.*, 31:Paper No. 28,31, 2025. doi:10.1051/cocv/2025018.
15. C. M. Costa, D. Kreber, and M. Schmidt. An alternating method for cardinality-constrained optimization: A computational study for the best subset selection and sparse portfolio problem. *INFORMS Journal on Computing*, 34(6):2968–2988, 2022. doi:10.1287/ijoc.2022.1211.
16. CPLEX, IBM ILOG. *V12. 1: User's Manual for CPLEX*, 2009.
17. A. De Marchi. On the mixed-integer linear-quadratic optimal control with switching cost. *IEEE Control Systems Letters*, 3(4):990–995, 2019. doi:10.1109/LCSYS.2019.2920425.
18. A. V. Dmitruk and A. M. Kaganovich. The hybrid maximum principle is a consequence of Pontryagin maximum principle. *Systems & Control Letters*, 57(11):964–970, 2008. doi:10.1016/j.sysconle.2008.05.006.
19. V. Dolean, P. Jolivet, and F. Nataf. *An Introduction to Domain Decomposition Methods*. Society for Industrial and Applied Mathematics (SIAM), Philadelphia, PA, 2015. Algorithms, theory, and parallel implementation. doi:10.1137/1.9781611974065.
20. P. Domschke, B. Hiller, J. Lang, V. Mehrmann, R. Morandin, and C. Tischendorf. Gas network modeling: An overview, 2021. URL: https://opus4.kobv.de/opus4-trr154/411.
21. R. Dáger and E. Zuazua. *Wave Propagation, Observation and Control in 1-d Flexible Multi-Structures*, volume 50. Springer Science & Business Media, 2006.
22. H. Egger and N. Philippi. On the transport limit of singularly perturbed convection-diffusion problems on networks. *Math. Methods Appl. Sci.*, 44(6):5005–5020, 2021. doi:10.1002/mma.7084.
23. M. Eisenmann and T. Stillfjord. A randomized operator splitting scheme inspired by stochastic optimization methods. *Numerische Mathematik*, 2024. doi:10.1007/s00211-024-01396-w.
24. K.-J. Engel and M. Kramar Fijavž. Waves and diffusion on metric graphs with general vertex conditions. *Evol. Equ. Control Theory*, 8(3):633–661, 2019. doi:10.3934/eect.2019030.
25. L. C. Evans. *Partial Differential Equations*, volume 19 of *Graduate Studies in Mathematics*. American Mathematical Society, Providence, RI, second edition, 2010. doi:10.1090/gsm/019.
26. A. Fügenschuh, B. Geißler, R. Gollmer, A. Morsi, M. E. Pfetsch, J. Rövekamp, M. Schmidt, K. Spreckelsen, and M. C. Steinbach. Physical and technical fundamentals of gas networks.

In T. Koch, B. Hiller, M. E. Pfetsch, and L. Schewe, ed., *Evaluating Gas Network Capacities*, SIAM-MOS series on Optimization, chapter 2, pages 17–43. SIAM, 2015. doi:10.1137/1.9781611973693.ch2.

27. M. J. Gander. Analysis of the parareal algorithm applied to hyperbolic problems using characteristics. *Boletin de la Sociedad Espanola de Matemática Aplicada*, 42:21–35, 2008.
28. M. J. Gander and F. Kwok. Schwarz methods for the time-parallel solution of parabolic control problems. In *Domain Decomposition Methods in Science and Engineering XXII*, volume 104 of *Lecture Notes in Computational Science and Engineering*, pages 207–216. Springer, Cham, 2016.
29. M. J. Gander and S. Vandewalle. Analysis of the parareal time-parallel time-integration method. *SIAM Journal on Scientific Computing*, 29(2):556–578, 2007. doi:10.1137/05064607X.
30. M. J. Gander, S.-L. Wu, and T. Zhou. Time parallelization for hyperbolic and parabolic problems. *Acta Numerica*, 34:385–489, July 2025. doi:10.1017/s0962492924000072.
31. B. Geißler, A. Morsi, L. Schewe, and M. Schmidt. Solving power-constrained gas transportation problems using an MIP-based alternating direction method. *Computers & Chemical Engineering*, 82:303–317, 2015. doi:10.1016/j.compchemeng.2015.07.005.
32. B. Geißler, A. Morsi, L. Schewe, and M. Schmidt. Penalty alternating direction methods for mixed-integer optimization: A new view on feasibility pumps. *SIAM Journal on Optimization*, 27(3):1611–1636, 2017. doi:10.1137/16M1069687.
33. B. Geißler, A. Morsi, L. Schewe, and M. Schmidt. Solving highly detailed gas transport MINLPs: Block separability and penalty alternating direction methods. *INFORMS Journal on Computing*, 30(2):309–323, 2018. doi:10.1287/ijoc.2017.0780.
34. M. Gerdts. A variable time transformation method for mixed-integer optimal control problems. *Optimal Control Applications & Methods*, 27(3):169–182, 2006. doi:10.1002/oca.778.
35. S. Göttlich, F. M. Hante, A. Potschka, and L. Schewe. Penalty alternating direction methods for mixed-integer optimal control with combinatorial constraints. *Math. Program.*, 188(2, Ser. B):599–619, 2021. doi:10.1007/s10107-021-01656-9.
36. M. Gugat, G. Leugering, A. Martin, M. Schmidt, M. Sirvent, and D. Wintergerst. MIP-based instantaneous control of mixed-integer PDE-constrained gas transport problems. *Computational Optimization and Applications*, 70(1):267–294, 2018. doi:10.1007/s10589-017-9970-1.
37. M. Gugat, G. Leugering, A. Martin, M. Schmidt, M. Sirvent, and D. Wintergerst. Towards simulation based mixed-integer optimization with differential equations. *Networks*, 72(1):60–83, 2018. doi:10.1002/net.21812.
38. F. M. Hante. Relaxation methods for optimal switching control of PDE-dynamical systems. In E. Trélat and E. Zuazua, ed., *Numerical Control: Part B*, volume 24 of *Handbook of Numerical Analysis*, chapter 3, pages 61–76. Elsevier, 2023. doi:10.1016/bs.hna.2022.10.004.
39. F. M. Hante, R. Krug, and M. Schmidt. Time-domain decomposition for mixed-integer optimal control problems. *Appl. Math. Optim.*, 87(3):Paper No. 36,36, 2023. doi:10.1007/s00245-022-09949-x.
40. F. M. Hante, G. Leugering, A. Martin, L. Schewe, and M. Schmidt. Challenges in optimal control problems for gas and fluid flow in networks of pipes and canals: From modeling to industrial applications. In P. Manchanda, R. Lozi, and A. H. Siddiqi, ed., *Industrial Mathematics and Complex Systems: Emerging Mathematical Models, Methods and Algorithms*, pages 77–122. Springer Singapore, 2017. doi:10.1007/978-981-10-3758-0_5.
41. M. Heinkenschloss. A time-domain decomposition iterative method for the solution of distributed linear quadratic optimal control problems. *Journal of Computational and Applied Mathematics*, 173(1):169–198, 2005. doi:10.1016/j.cam.2004.03.005.
42. M. Hernández. Random domain decomposition for parabolic PDEs on graphs, 2025. arXiv:2508.21557.
43. M. Hernández and E. Zuazua. Random batch methods for discretized PDEs on graphs, 2025. arXiv:2506.11809.
44. A. Iserles. *A First Course in the Numerical Analysis of Differential Equations*. Cambridge Texts in Applied Mathematics. Cambridge University Press, second edition, 2009. doi:10.1017/CBO9780511995569.
45. S. Jin and L. Li. On the mean field limit of the random batch method for interacting particle systems. *Sci. China Math.*, 65(1):169–202, 2022. doi:10.1007/s11425-020-1810-6.

46. S. Jin, L. Li, and J.-G. Liu. Random batch methods (RBM) for interacting particle systems. *J. Comput. Phys.*, 400:108877,30, 2020. doi:10.1016/j.jcp.2019.108877.
47. S. Jin, L. Li, and J.-G. Liu. Convergence of the random batch method for interacting particles with disparate species and weights. *SIAM J. Numer. Anal.*, 59(2):746–768, 2021. doi:10.1137/20M1327641.
48. C. Kirches, F. Lenders, and P. Manns. Approximation properties and tight bounds for constrained mixed-integer optimal control. *SIAM Journal on Control and Optimization*, 58(3):1371–1402, 2020. doi:10.1137/18M1182917.
49. T. Kleinert and M. Schmidt. Computing feasible points of bilevel problems with a penalty alternating direction method. *INFORMS Journal on Computing*, 33(1):198–215, 2021. doi:10.1287/ijoc.2019.0945.
50. D. Ko and E. Zuazua. Model predictive control with random batch methods for a guiding problem. *Math. Models Methods Appl. Sci.*, 31(8):1569–1592, 2021. doi:10.1142/S0218202521500329.
51. M. Kramar Fijavž, D. Mugnolo, and E. Sikolya. Variational and semigroup methods for waves and diffusion in networks. *Appl. Math. Optim.*, 55(2):219–240, 2007. doi:10.1007/s00245-006-0887-9.
52. M. Kroller and K. Kunisch. Convergence rates for the feedback operators arising in the linear quadratic regulator problem governed by parabolic equations. *SIAM J. Numer. Anal.*, 28(5):1350–1385, 1991. doi:10.1137/0728071.
53. R. Krug, G. Leugering, A. Martin, M. Schmidt, and D. Weninger. Time-domain decomposition for optimal control problems governed by semilinear hyperbolic systems. *SIAM Journal on Control and Optimization*, 59(6):4339–4372, 2021. doi:10.1137/20M138329X.
54. R. Krug, G. Leugering, A. Martin, M. Schmidt, and D. Weninger. Time-domain decomposition for optimal control problems governed by semilinear hyperbolic systems with mixed two-point boundary conditions. *Control and Cybernetics*, 50(4):427–455, 2021. doi:10.2478/candc-2021-0026.
55. R. Krug, G. Leugering, A. Martin, M. Schmidt, and D. Weninger. A consensus-based alternating direction method for mixed-integer and PDE-constrained gas transport problems. *INFORMS Journal on Computing*, 2023. doi:10.1287/ijoc.2022.0319.
56. R. Krug and D. Weninger. gas-network-opti-padm. URL: https://github.com/RichardKrug/gas-network-opti-padm.
57. J. E. Lagnese and G. Leugering. *Domain Decomposition Methods in Optimal Control of Partial Differential Equations*, volume 148 of *International Series of Numerical Mathematics*. Birkhäuser Verlag, Basel, 2004. doi:10.1007/978-3-0348-7885-2.
58. H. W. J. Lee, K. L. Teo, V. Rehbock, and L. S. Jennings. Control parametrization enhancing technique for optimal discrete-valued control problems. *Automatica. A Journal of IFAC, the International Federation of Automatic Control*, 35(8):1401–1407, 1999. doi:10.1016/S0005-1098(99)00050-3.
59. G. Leugering. *Partial Differential Equations on Metric Graphs: A Survey of Results on Optimization, Control, and Stabilizability Problems with Special Focus on Shape and Topological Sensitivity Problems*, pages 77–115. Springer Singapore, 2020. doi:10.1007/978-981-15-0928-5_4.
60. G. Leugering. Space-time-domain decompositions for optimal control problems goverend by linear hyperbolic systems. *Journal of Optimization, Differential Equations and their Applications (JODEA)*, 29(2):24–47, 2021. doi:10.15421/142107.
61. G. Leugering. Nonoverlapping domain decomposition for instantaneous optimal control of friction dominated flow in a gas-network. In *Proceedings of the INDAM Conference 2020*. INDAM, 2022. doi:10.1007/978-981-96-6182-4_9.
62. G. Leugering. Nonoverlapping domain decomposition and virtual controls for optimal control problems of p-type on metric graphs. In E. Trélat and E. Zuazua, ed., *Numerical Control: Part B*, volume 24 of *Handbook of Numerical Analysis*, chapter 7, pages 217–260. Elsevier, 2023. doi:10.1016/bs.hna.2022.11.002.
63. G. Leugering, A. Martin, M. Schmidt, and M. Sirvent. Nonoverlapping domain decomposition for optimal control problems governed by semilinear models for gas flow in networks. *Control and Cybernetics*, 46(3):191–225, 2017.

64. G. Leugering and G. Mophou. Instantaneous optimal control of friction dominated flow in a gas-network. In V. Schulz and D. Seck, ed., *Shape Optimization, Homogenization and Optimal Control: DFG-AIMS workshop held at the AIMS Center Senegal, March 13–16, 2017*, pages 75–88. Springer International Publishing, 2018. doi:10.1007/978-3-319-90469-6_5.
65. J.-L. Lions, Y. Maday, and G. Turinici. Résolution d'EDP par un schéma en temps "pararéel". *Comptes Rendus de l'Académie des Sciences – Series I – Mathematics*, 332(7):661–668, 2001. doi:10.1016/S0764-4442(00)01793-6.
66. Z. Liu, S. Li, and K. Zhao. Extended multi-interval Legendre–Gauss–Radau pseudospectral method for mixed-integer optimal control problem in engineering. *International Journal of Systems Science. Principles and Applications of Systems and Integration*, 52(5):928–951, 2021. doi:10.1080/00207721.2020.1849862.
67. D. Mugnolo. *Semigroup Methods for Evolution Equations on Networks*. Understanding Complex Systems. Springer, Cham, 2014. doi:10.1007/978-3-319-04621-1.
68. L. Pareschi and M. Zanella. Reduced variance random batch methods for nonlocal PDEs. *Acta Appl. Math.*, 191:Paper No. 4,23, 2024. doi:10.1007/s10440-024-00656-z.
69. M. E. Pfetsch, A. Fügenschuh, B. Geißler, N. Geißler, R. Gollmer, B. Hiller, J. Humpola, T. Koch, T. Lehmann, A. Martin, A. Morsi, J. Rövekamp, L. Schewe, M. Schmidt, R. Schultz, R. Schwarz, J. Schweiger, C. Stangl, M. C. Steinbach, S. Vigerske, and B. M. Willert. Validation of nominations in gas network optimization: models, methods, and solutions. *Optimization Methods and Software*, 30(1):15–53, 2015. doi:10.1080/10556788.2014.888426.
70. N. Philippi. *Asymptotic Analysis and Numerical Approximation of some Partial Differential Equations on Networks*. PhD thesis, TU Darmstadt, 2023.
71. L. S. Pontryagin, V. G. Boltyanskii, R. V. Gamkrelidze, and E. F. Mishchenko. *The Mathematical Theory of Optimal Processes*. Translated from the Russian by K. N. Trirogoff; edited by L. W. Neustadt. Interscience Publishers John Wiley & Sons, Inc. New York-London, 1962. doi:10.1002/zamm.19630431023.
72. D. Preda and J. Noailles. Mixed integer programming for a special logic constrained optimal control problem. *Mathematical Programming. A Publication of the Mathematical Programming Society*, 103(2, Ser. B):309–333, 2005. doi:10.1007/s10107-005-0584-5.
73. Y. Qiu, S. Grundel, M. Stoll, and P. Benner. Efficient numerical methods for gas network modeling and simulation. *Netw. Heterog. Media*, 15(4):653–679, 2020. doi:10.3934/nhm.2020018.
74. A. Quarteroni and A. Valli. *Numerical Approximation of Partial Differential Equations*, volume 23 of *Springer Series in Computational Mathematics*. Springer-Verlag, Berlin, 1994. doi:10.1007/978-3-540-85268-1.
75. A. Quarteroni and A. Valli. *Domain Decomposition Methods for Partial Differential Equations*. Numerical Mathematics and Scientific Computation. The Clarendon Press, Oxford University Press, 1999. doi:10.1007/978-3-540-85268-1.
76. P. A. Raviart. Sur la résolution de certaines équations paraboliques non linéaires. *J. Functional Analysis*, 5:299–328, 1970. doi:10.1016/0022-1236(70)90031-5.
77. M. Ringkamp, S. Ober-Blöbaum, and S. Leyendecker. On the time transformation of mixed integer optimal control problems using a consistent fixed integer control function. *Mathematical Programming*, 161(1-2):551–581, 2017. doi:10.1007/s10107-016-1023-5.
78. D. Rose, M. Schmidt, M. C. Steinbach, and B. M. Willert. Computational optimization of gas compressor stations: MINLP models versus continuous reformulations. *Mathematical Methods of Operations Research*, 83(3):409–444, 2016. doi:10.1007/s00186-016-0533-5.
79. T. Roubíček. *Nonlinear Partial Differential Equations with Applications*, volume 153 of *International Series of Numerical Mathematics*. Birkhäuser/Springer Basel AG, Basel, second edition, 2013. doi:10.1007/978-3-0348-0513-1.
80. S. Sager, H. G. Bock, and M. Diehl. The integer approximation error in mixed-integer optimal control. *Mathematical Programming*, 133(1–2):1–23, 2012. doi:10.1007/s10107-010-0405-3.
81. H. Schaefer. Über die Methode sukzessiver Approximationen. *Jahresbericht der Deutschen Mathematiker-Vereinigung*, 59:131–140, 1957.
82. L. Schewe, M. Schmidt, and D. Weninger. A decomposition heuristic for mixed-integer supply chain problem. *Operations Research Letters*, 48(3):225–232, 2020. doi:10.1016/j.orl.2020.02.006.

83. M. Schmidt, D. Aßmann, R. Burlacu, J. Humpola, I. Joormann, N. Kanelakis, T. Koch, D. Oucherif, M. E. Pfetsch, L. Schewe, R. Schwarz, and M. Sirvent. GasLib – A library of gas network instances. *Data*, 2(4), 2017. doi:10.3390/data2040040.
84. M. Schmidt, M. C. Steinbach, and B. M. Willert. High detail stationary optimization models for gas networks. *Optimization and Engineering*, 16(1):131–164, 2015. doi:10.1007/s11081-014-9246-x.
85. L. Schöbel-Kröhn. *Analysis and Numerical Approximation of Nonlinear Evolution Euqations on Network Structures*. PhD thesis, Technical University of Darmstadt, 2020.
86. S. Ulbrich. Generalized SQP methods with "parareal" time-domain decomposition for time-dependent PDE-constrained optimization. In *Real-time PDE-constrained optimization*, volume 3 of *Computational Science & Engineering*, pages 145–168. SIAM, 2007.
87. D. W. M. Veldman, A. Borkowski, and E. Zuazua. Stability and convergence of a randomized model predictive control strategy. *IEEE Transactions on Automatic Control*, pages 1–8, 2024. doi:10.1109/TAC.2024.3375253.
88. D. W. M. Veldman and E. Zuazua. A framework for randomized time-splitting in linear-quadratic optimal control. *Numer. Math.*, 151(2):495–549, 2022. doi:10.1007/s00211-022-01290-3.

Open Access This chapter is licensed under the terms of the Creative Commons Attribution-NonCommercial-NoDerivatives 4.0 International License (http://creativecommons.org/licenses/by-nc-nd/4.0/), which permits any noncommercial use, sharing, distribution and reproduction in any medium or format, as long as you give appropriate credit to the original author(s) and the source, provide a link to the Creative Commons license and indicate if you modified the licensed material. You do not have permission under this license to share adapted material derived from this chapter or parts of it.

The images or other third party material in this chapter are included in the chapter's Creative Commons license, unless indicated otherwise in a credit line to the material. If material is not included in the chapter's Creative Commons license and your intended use is not permitted by statutory regulation or exceeds the permitted use, you will need to obtain permission directly from the copyright holder.



Chapter 18
A PDE-Constrained Generalized Nash Equilibrium Approach for Modeling Gas Transport with Strategic Suppliers

Veronika Grimm[0000−0002−9025−9731],
Michael Hintermüller[0000−0001−9471−2479],
Olivier Huber[0000−0002−4447−8650],
Lars Schewe[0000−0002−3778−262X],
Martin Schmidt[0000−0001−6208−5677], and
Gregor Zöttl[0000−0002−2729−1173]

Abstract We investigate a class of generalized Nash equilibrium problems (GNEPs) in which the objectives of the individuals are interdependent and the shared constraint consists of a system of partial differential equations. This setup is motivated by the modeling of strategic interactions of competing firms, which explicitly take into account the dynamics of transporting a commodity such as natural gas or hydrogen. We establish the existence of a variational equilibrium of the GNEP. In the case of symmetric firms, we identify an equivalent optimization problem. We use this model to numerically explore the impact of linepacking, that is the use of the network as a temporary storage device. In particular, we study the firms' decisions under various linepacking abilities and analyze which market participants benefit from it.

Veronika Grimm
Energy Systems & Market Design, University of Technology Nuremberg (UTN), Germany,
e-mail: veronika.grimm@utn.de

Michael Hintermüller
Weierstrass Institute for Applied Analysis and Stochastics, Berlin, Germany,
e-mail: michael.hintermueller@wias-berlin.de

Olivier Huber
Wisconsin Institute for Discovery, University of Wisconsin-Madison, USA, e-mail: ohuber2@wisc.edu

Lars Schewe
School of Mathematics and Maxwell Institute for Mathematical Sciences, The University of Edinburgh, UK, e-mail: lars.schewe@ed.ac.uk

Martin Schmidt
Department of Mathematics, Trier University, Germany, e-mail: martin.schmidt@uni-trier.de

Gregor Zöttl
Industrial Organization and Energy Markets, FAU Erlangen–Nürnberg, Germany, e-mail: gregor.zoettl@fau.de

© The Author(s) 2027

A. Martin et al. (eds.), *Mathematical Modelling, Simulation and Optimization using the Example of Gas Networks*, International Series of Numerical Mathematics 174,
https://doi.org/10.1007/978-3-032-34969-9_18

18.1 Introduction

The framework of equilibrium problems considerably contributes to the understanding of a wide array of real-world problems, ranging from management and microeconomics applications to a variety of design problems in engineering. Specifically, non-cooperative game theory has turned out to be a useful tool in analyzing the actions of agents (also denoted by players) on markets. In such a context, one seeks solutions in which each player's individual objective is maximized subject to individual (also denoted private) constraints, and no player has an incentive to take decisions deviating from a *Nash equilibrium* [30]. For classic Nash equilibrium problems (NEPs), the coupling between individuals occurs in the objective functionals only, whereas the feasible sets of player's decisions are independent. If the latter are also interdependent, one faces a so-called generalized Nash equilibrium problem (GNEP).

In this work, we investigate a particular GNEP in which the dynamics of transporting a given good are described by a system of partial differential equations (PDEs), which constitutes a shared constraint that is taken into account by all players. This is highly relevant, e.g., in the case of liberalized energy markets, where conversion and trading of energy carriers is organized by competing private companies that seek to maximize their profits in a non-cooperative fashion. Within a short time horizon, as in an intraday market, it is important to consider a high-fidelity model of the dynamics when transporting goods with slow transients such as natural gas or hydrogen. Moreover, in our setup, the objective functionals are interdependent, so that the actions of a player's rivals directly affect the value of that player's objective. This is thus closely related to classic oligopolistic situations of strategically interacting firms in a market context; see, e.g., [10] for a seminal article in this area. The focus here is on the solution concept called *variational equilibrium* (VE) for which the multipliers associated with the shared constraints have a clear economic interpretation.

In view of the aforementioned application regarding liberalized gas markets, in this work we first provide conditions for the existence of a solution to the governing system of PDEs with enough regularity to ensure the existence of multipliers to the shared constraints. Second, we show the existence of a VE that solves the underlying jointly convex GNEP. For symmetric setups, we identify a reformulation of the original equilibrium problem as a single optimization problem, which allows us to derive a solution algorithm for finding such a VE. Finally, we apply our algorithm to a suitable test instance, which is motivated by the trading and transporting of natural gas. Our numerical results highlight crucial dynamical aspects in the context of natural gas such as the impact and value of *linepacking*. The latter refers to the action of changing the amount of gas stored in the pipe, the so-called linepack. When such a linepacking occurs, the pipe acts as a temporary storage device. This allows to take advantage of price variations or to overcome fluctuations in supply and demand.

Our work contributes to several strands of the literature. Indeed, equilibrium problems that are subject to network constraints have received considerable attention. In the context of energy markets, these settings have been studied mainly for the analysis of electricity and gas markets. There, we find many contributions that consider strategic interactions of firms in the presence of shared and static, i.e., stationary, network

constraints; see, e.g., [7, 33, 37, 39] as well as, more recently, [22]. Due to its physical properties, a steady-state approximation of electricity transmission is well accepted for many market applications. Owing to slower speeds of propagation, a stationary approach cannot capture, however, all aspects of the dynamic evolution of gas transported in a single pipe or in an entire network.

Another strand of literature explicitly considers strategic interaction of firms in a dynamic context—but in the absence of shared network constraints. In several contributions, firms experience adjustment costs when changing their output; see [6, 24, 40]. Other contributions have analyzed situations in which strategic firms exploit a private resource stock [28] or accumulate private productive capacities over time [27]. Similar to our approach, in these contributions, the interactive nature of the situation analyzed also arises due to firms' profits being influenced by all rivals' actions. However, there are no shared constraints that restrict the choices of the firms.

Several works on dynamic oligopoly models do consider shared constraints; [3, 4] study differential games in which firms jointly exploit a common renewable production asset. More recent articles further elaborate on this; see, e.g., [8, 9, 42], who consider different types of strategic behavior among firms. Note that for all these problems, the shared constraint can be represented by a single state variable governed by an ordinary differential equation (ODE). For a proper modeling of the physics underlying the transportation aspect of our setup, we have to consider a spatially distributed state variable governed by a system of PDEs.

Several recent works analyze GNEPs involving shared constraints governed by PDEs [13, 16, 19, 20, 25]. While the structural assumptions vary among these contributions, the results and methods are mostly applied to instances in which objective functionals are of tracking type and the shared constraint is a scalar PDE. In our setup, we consider objectives that model market interaction of strategic firms. In addition, the shared constraint comprises a system of PDEs, which allows to appropriately capture the physical phenomena under consideration.

The remainder of this paper is structured as follows. After this introduction, we present the stylized GNEP model coupling trading and transport phenomena in Sect. 18.2. Section 18.3 provides general well-posedness results for the system of PDEs under investigation. In Sect. 18.4, we establish the existence of a VE for the jointly convex GNEP under consideration. A reformulation of the GNEP is given that allows for a computational approach to determine a VE. We illustrate the important role of linepacking in Sect. 18.5 and finally conclude in Sect. 18.6.

Notations For a given Banach space X, its dual is given by X^*. If $A: X \to Y$ is a linear and continuous mapping between Banach spaces, its adjoint is denoted by $A^*: Y^* \to X^*$. The continuous and dense embedding of a Banach space X into Y is represented by $X \hookrightarrow Y$. With Ω being an open interval of $\mathbb{R}$, for any integer p (and even for $p = +\infty$), the function space $L^p(\Omega)$ is the standard Lebesgue space. For any real s, $H^s(\Omega)$ is the $L^2(\Omega)$-based Sobolev space of order s. Let $f: \mathbb{R} \to X$ and $T > 0$. If $t \mapsto \|f(t)\|_X$ lies in $L^p(0,T)$ and is Bochner measurable, then $f \in L^p(0,T;X)$. The space $C([0,T];X)$ consists of all X-valued continuous functions on $[0,T]$ equipped with the norm of uniform convergence. For more background on these spaces, see, e.g., [1]. As we have only one spatial dimension, denoted by x, the Laplacian operator Δ has

the same action as taking second partial derivatives $\partial^2/\partial x^2$. When applied to a vector-valued function, its action is to take second partial derivatives of each component. As a shorthand notation, for any function f depending on x and t, f_t, f_x, and f_{xx} denote the first-order derivative with respect to t, x, and the second-order derivative with respect to x, respectively. For a given set S, its closure is denoted by $\bar{S}$, its interior by $\operatorname{int} S$, and its indicator function by δ_S. Given a convex set S, its normal cone is denoted by $N_S(\cdot)\colon X \rightrightarrows X^*$, where "$\rightrightarrows$" indicates that it is a set-valued map. The subdifferential of a convex function $g\colon X \to \mathbb{R} \cup \{+\infty\}$ is represented by $\partial g\colon X \rightrightarrows X^*$.

18.2 A GNEP Model for Gas Transport with Strategic Suppliers

We investigate a stylized market situation where a commodity, e.g., natural gas or hydrogen, which is supplied by several competing firms has to be transported through a single pipe e. The pipe's diameter $D^e > 0$ is typically much smaller than its length $L^e > 0$. Hence, a one-dimensional model for the flow of gas is appropriate. Let $A^e := (D^e)^2\pi/4$ be the constant cross-sectional area of the pipe. We consider the case of an isothermal flow, i.e., the temperature $T_{\text{emp}} > 0$ of gas is constant. We denote the density by ρ^e, the pressure by p^e, and the speed of sound by $c_{\text{s}} = \sqrt{R_{\text{s}} T_{\text{emp}}}$ for a given specific gas constant R_{s}. The state equation is given by the ideal gas law $p^e = c_{\text{s}}^2 \rho^e$, and the velocity of gas is assumed to be small with respect to c_{s}. Given the operational conditions in a pipeline system, the evolution of the gas can be modeled by the system

$$\begin{aligned} &p_t^e - \varepsilon p_{xx}^e + \frac{c_{\text{s}}^2}{A^e} q_x^e = 0, \\ &q_t^e - \varepsilon q_{xx}^e + A^e p_x^e = -\sigma^e A^e \frac{\check{q}^e}{\check{p}^e} \left(q^e - \frac{\check{q}^e}{2\check{p}^e} p^e \right) - \frac{A^e g \sin \varphi^e}{c_{\text{s}}^2} p^e, \end{aligned} \tag{18.1}$$

where $\varepsilon > 0$, $\sigma^e := 16 c_{\text{s}}^2 \lambda^e / (\pi^2 (D^e)^5)$, $\lambda^e \geq 0$ is the friction coefficient, g is the gravitational acceleration, and φ^e is the constant angle of the pipe with the horizontal plane. The pair $(\check{p}, \check{q})$, with $\check{p} > 0$ and $\check{q} > 0$, is a reference state. System (18.1) comes from the linearization and viscosity regularization of the hyperbolic system known as "ISO2" in Chap. 2, "A Catalog of Gas Network Models: PDEs, Coupling Conditions, and Numerical Schemes", which presents different models for gas flow in pipelines depending on the operational conditions. The boundary conditions for (18.1) are of Dirichlet type. Among other gases, flows of natural gas and hydrogen can be modeled by (18.1).

Alternatively to the single-pipe scenario, a small pipeline network whose graph is a directed tree, could be considered. In such a setting, at a node at which multiple pipes meet, two relations have to hold: (i) The pressures at the common endpoints of these pipes are identical and (ii) the inflows and outflows of gas are balanced. In our subsequent exposition we will, however, stick to the single-pipe setting for convenience as this allows us to emphasize the GNEP aspect. We consider supply decisions of strategic firms which ship and sell the commodity through a pipe. The two nodes are

labeled in and out, respectively. For the ease of notation, subsequently we drop all superscripts related to the pipe's identifier. Further, we assume that M strategic firms (producers) may inject gas at the in node and sell it at the out node. Concerning the equilibrium setting, we consider the case of Cournot competition, i.e., suppliers choose quantities supplied and sold, then market prices at the output node result in equilibrium. More specifically: With the goal of maximizing their respective profit over a finite time period $[0, T]$, $T > 0$, each firm strategically decides on the injected mass flow q_i^{in} at pressure p_i^{in} and the withdrawn mass flow q_i^{out} at pressure p_i^{out}. Our setup thus considers an open loop situation in which strategic players simultaneously choose their optimal strategies which then determines all transported and consumed quantities for all $t \in [0, T]$.

Note that we use the terms "firm", "agent", or "player" as synonyms. We denote by $u_i := (p_i^{\text{in}}, q_i^{\text{in}}, p_i^{\text{out}}, q_i^{\text{out}})$ the decisions of firm i, and let $u := (u_1, \ldots, u_M)$ be the entire decision vector. With respect to notation, we use the classic game-theoretic convention that for any i, $u = (u_i, u_{-i})$, where u_{-i} collects the decisions of all the other firms except i. Mathematically, it is supposed that each u_i belongs to $U \subseteq L^2(0, T)^4$. In the pipe, the state variable is $y := (p, q)$: $(0, L)\times(0, T) \to \mathbb{R}^2$. The aforementioned Dirichlet boundary conditions are given by $y(0, \cdot) = u_\Gamma^0$ and $y(L, \cdot) = u_\Gamma^L$, where the nodal state values $u_\Gamma^0 := (p^{\text{in}}, q^{\text{in}})$ and $u_\Gamma^L := (p^{\text{out}}, q^{\text{out}})$ are related to the firms' actions by

$$u_\Gamma^0 = \left(\sum_{i=1}^{M} \frac{p_i^{\text{in}}}{M}, \sum_{i=1}^{M} q_i^{\text{in}} \right), \quad u_\Gamma^L = \left(\sum_{i=1}^{M} \frac{p_i^{\text{out}}}{M}, \sum_{i=1}^{M} q_i^{\text{out}} \right). \tag{18.2}$$

The relations on the mass flows fit the above stated conditions at a junction. For the pressures, this is also the case if all firms choose the same pressures, and we focus on this case. Furthermore, we consider lower and upper bound constraints on the pressures and mass flows. For given bounds $\underline{y} := (\underline{p}, \underline{q})$ and $\bar{y} := (\bar{p}, \bar{q})$, these state constraints are represented by

$$y \in K := \{ y \in C([0, T]; C([0, L])^2) \mid \underline{y} \le y(x, t) \le \bar{y} \; \forall (x, t) \in [0, L] \times [0, T] \}, \tag{18.3}$$

where the space $C([0, T]; C([0, L])^2)$ is chosen to ensure the existence of the associated Lagrange multipliers for a primal-dual stationarity characterization of optimal solutions or equilibria. Since firms are fully aware of both the system (18.1) and the bound constraints (18.3), they all take into account the same, and thus shared, network constraints. Let S be the so-called control-to-state operator, which gives the solution (state) y of the PDE system for a given (control) u. Then, the inclusion $y = S(u) \in K$ represents the shared constraint of the underlying GNEP.

Now, at any time $t \in [0, T]$, there is a given demand of gas at the consumption node out. The price of gas is given by an inverse demand function $P(t, q^{\text{out}}(t))$, where $q^{\text{out}}(t)$ is the total amount of gas at the exit node. On the other hand, each firm chooses to inject the amount $q_i^{\text{in}}(t)$ at a cost of $c_i(t)\, q_i^{\text{in}}(t)$. For our subsequent investigation, we make the following assumptions on the data.

Assumption. (i) *We have $P(t, q^{\text{out}}(t)) := \beta(t) - \alpha(t)\, q^{\text{out}}(t)$, and both α and β are measurable functions in t.*

(ii) *There exist finite numbers* $\alpha_{\min}$ *and* $\alpha_{\max}$ *such that* $0 < \alpha_{\min} \leq \alpha(t) \leq \alpha_{\max}$ *holds for almost all* $t \in (0,T)$.

(iii) *For any firm* $i \in \{1,\dots,M\}$*, there exists a constant* $\bar{c}_i > 0$ *such that* $|c_i(t)| \leq \bar{c}_i$ *for almost all* $t \in (0,T)$ *and* c_i *is measurable.*

For any $i \in \{1,\dots,M\}$, the maximization problem for firm $i \in \{1,\dots,M\}$ reads

$$\max_{u_i \in U} \quad \int_0^T \left(P\left(t, \sum_{k=1}^{M} q_k^{\text{out}}(t)\right) q_i^{\text{out}}(t) - c_i(t)\, q_i^{\text{in}}(t) \right) \mathrm{d}t - \mathcal{R}_i(u_i) \tag{18.4a}$$

$$\text{s.t.} \quad 0 \leq q_i^{\text{in}}(t) \leq \bar{q}_i^{\text{in}} \quad \text{for almost all } t \in (0,T), \tag{18.4b}$$

$$\int_0^T \left(q_i^{\text{out}}(t) - q_i^{\text{in}}(t) \right) \mathrm{d}t \leq 0, \tag{18.4c}$$

$$S(u_i, u_{-i}) \in K, \tag{18.4d}$$

where $\bar{q}_i^{\text{in}}$ is a given production-specific capacity bound. The convex function $\mathcal{R}_i$ in the objective function (18.4a) is there to influence, specifically regularize, the state at the end of the time period (i.e., at $t = T$) in the pipe. Indeed, the initial state $y_0 := (p_0, q_0)$ is likely to be rather regular (in space), but without any additional consideration the final state is only required to satisfy the constraint (18.4d). Constraint (18.4c) ensures that over the entire time period each firm has injected at least as much gas as it has withdrawn. This is important since at the beginning of the time period, the pipe does contain some gas as we require the initial state y_0 to fulfill the given upper and lower bounds. Hence, the constraint (18.4c) ensures that there is no free gas for any of the firms. In problem (18.4), the constraints (18.4b) and (18.4c) are private, whereas (18.4d) is shared among producers. The collection of these M-many optimization problems gives rise to a GNEP, which is studied in more detail in Sect. 18.4.

As a benchmark for the GNEP solution, we consider the corresponding *welfare maximization problem*. In fact, the overall welfare is given by the total consumer surplus minus the total production cost:

$$\int_0^T \left(\int_0^{q^{\text{out}}(t) = \sum_{i=1}^{M} q_i^{\text{out}}(t)} P(t,\tau)\, \mathrm{d}\tau - \sum_{i=1}^{M} c_i(t) q_i^{\text{in}}(t) \right) \mathrm{d}t.$$

After replacing the innermost integral by its expression and noting that we only need to consider the total amount of gas withdrawn, the associated welfare maximization problem reads

$$\begin{aligned} \max_{\mathbf{u} \in \mathbf{U}} \quad & \int_0^T \left(\beta(t) q^{\text{out}}(t) - \frac{1}{2}\alpha(t) q^{\text{out}}(t) q^{\text{out}}(t) - \sum_{i=1}^{M} c_i(t) q_i^{\text{in}}(t) \right) \mathrm{d}t - \mathcal{R}(\mathbf{u}) \\ \text{s.t.} \quad & 0 \leq q_i^{\text{in}}(t) \leq \bar{q}_i^{\text{in}} \quad \text{for almost all } t \in (0,T) \text{ and all } i \in \{1,\dots,M\}, \\ & \int_0^T \left(q^{\text{out}}(t) - \sum_{i=1}^{M} q_i^{\text{in}}(t) \right) \mathrm{d}t \leq 0, \\ & S(\mathbf{u}) \in K, \end{aligned} \tag{18.5}$$

where $\mathbf{u} := (p^{\text{in}}, p^{\text{out}}, (q_1^{\text{in}}, \dots, q_M^{\text{in}}), q^{\text{out}})$ and $\mathcal{R}$ sums up all $\mathcal{R}_i$, $i = 1, \dots, M$. Note that from any solution $u^\star$ of the GNEP with identical pressure variables, i.e., $(u_i^\star, u_{-i}^\star)$ is a solution to (18.4) for all $i \in \{1, \dots, M\}$ and $(p_i^{\text{in}}, p_i^{\text{out}}) = (p_j^{\text{in}}, p_j^{\text{out}})$ for all $i, j \in \{1, \dots, M\}$, a feasible point for the welfare maximization problem can be constructed. Therefore, from a solution of the GNEP, a lower bound on the optimal function value in (18.5) can be obtained.

18.3 Well-Posedness of the Gas Flow PDE System

Before analyzing our GNEP, we first address the well-posedness of the PDE system (18.1) over a pipe with a solution of sufficient regularity to ensure the existence of multipliers for the shared constraint.

The spatial domain of the pipe is $\Omega := (0, L)$, with $L > 0$, and we set $\Omega_T := \Omega \times (0, T)$ for a time horizon $T > 0$. The system of PDEs modeling the flow of gas is given by

$$p_t - \varepsilon p_{xx} + \frac{c_{\text{s}}^2}{A} q_x = 0 \qquad \text{in } \Omega_T, \tag{18.6a}$$

$$q_t - \varepsilon q_{xx} + A p_x = -\sigma A \frac{\check{q}}{\check{p}} \left(q - \frac{\check{q}}{2\check{p}} p \right) - \frac{A g \sin \varphi}{c_{\text{s}}^2} p \qquad \text{in } \Omega_T, \tag{18.6b}$$

$$p(0, \cdot) = p^{\text{in}}, \quad p(L, \cdot) = p^{\text{out}}, \quad q(0, \cdot) = q^{\text{in}}, \quad q(L, \cdot) = q^{\text{out}} \qquad \text{in } (0, T), \tag{18.6c}$$

$$p(\cdot, 0) = p_0, \quad q(\cdot, 0) = q_0 \qquad \text{in } \Omega, \tag{18.6d}$$

where (p_0, q_0) is the initial state and $(\check{p}, \check{q}) \in C([0, T]; C(\bar{\Omega})^2)$, with $\check{p}$ bounded away from zero, is a given reference state. For our analysis, we transform (18.6) into a system of PDEs with homogeneous Dirichlet boundary conditions. For this purpose, we require the boundary data $(p^{\text{in}}, p^{\text{out}}, q^{\text{in}}, q^{\text{out}})$ to be in the Sobolev space $H^1(0, T)^4$. Then, for the boundary data $u_\Gamma^p := (p^{\text{in}}, p^{\text{out}})$ and $u_\Gamma^q := (q^{\text{in}}, q^{\text{out}})$, we construct extensions u_Ω^p (resp. u_Ω^q) of u_Γ^p (resp. u_Γ^q) to the entire domain Ω. Specifically, for any $(x, t) \in \Omega_T$, we set $u_\Omega^p(x, t)$ and $u_\Omega^q(x, t)$ to be the linear interpolation of the values of u_Γ^p and u_Γ^q at both ends of the pipe. More precisely, we define the operator $\mathcal{E}: H^1(0, T)^2 \to H^1(0, T; H^s(\Omega))$, with s being an arbitrary positive integer, as

$$\mathcal{E}(v_1, v_2)(t)(x) := \frac{L - x}{L} v_1(t) + \frac{x}{L} v_2(t). \tag{18.7}$$

This yields $u_\Omega^p := \mathcal{E}(u_\Gamma^p)$ as well as $u_\Omega^q := \mathcal{E}(u_\Gamma^q)$. From the expression in (18.7), $(u_\Omega^p)_x$ and $(u_\Omega^q)_x$ are constant with respect to x. Hence, these extensions indeed belong to $H^1(0, T; H^s(\Omega))$. We then consider the shifted state variables $\tilde{p} := p - u_\Omega^p$ and $\tilde{q} := q - u_\Omega^q$, which are solutions to the system

$$\tilde{p}_t - \varepsilon \tilde{p}_{xx} + \frac{c_s^2}{A}\tilde{q}_x = -(u_\Omega^p)_t - \frac{c_s^2}{A}(u_\Omega^q)_x \qquad \text{in } \Omega_T, \quad (18.8a)$$

$$\tilde{q}_t - \varepsilon \tilde{q}_{xx} + A\tilde{p}_x + \sigma A \frac{\check{q}}{\check{p}}\tilde{q} + \left[\frac{Ag\sin\varphi}{c_s^2} - \sigma A \frac{\check{q}^2}{2\check{p}^2}\right]\tilde{p}$$
$$= -(u_\Omega^q)_t - A(u_\Omega^p)_x + \sigma A \frac{\check{q}}{\check{p}} u_\Omega^q + \left[\frac{Ag\sin\varphi}{c_s^2} - \sigma A \frac{\check{q}^2}{2\check{p}^2}\right] u_\Omega^p \qquad \text{in } \Omega_T, \quad (18.8b)$$

$$\tilde{p}(0,\cdot) = \tilde{p}(L,\cdot) = 0, \quad \tilde{q}(0,\cdot) = \tilde{q}(L,\cdot) = 0 \qquad \text{in } (0,T), \quad (18.8c)$$

$$\tilde{p}(\cdot,0) = \tilde{p}_0 := p_0 - u_\Omega^p(\cdot,0), \quad \tilde{q}(\cdot,0) = \tilde{q}_0 := q_0 - u_\Omega^q(\cdot,0) \qquad \text{in } \Omega. \quad (18.8d)$$

Remember that the feasible set of each firm includes the constraint $y \in K$ with K given in (18.3), and that for analytical but also numerical reasons one wishes to characterize a solution of (18.4) by Lagrange multipliers. This leads us to seek solutions of (18.6) with higher regularity than the classic parabolic one; cf. (18.10) below for the latter. In this vein, our subsequent approach provides us, under appropriate assumptions, with a unique solution of (18.6) in the space

$$Y := \{y \in L^2(0,T;H^2(\Omega)^2) \cap L^\infty(0,T;H^1(\Omega)^2) \text{ and } y_t \in L^2(0,T;L^2(\Omega)^2)\}.$$

Then, by the Aubin–Lions Lemma (see Lemma 18.5 in Appendix A), we have the (even compact) embedding of Y into $C([0,T];C(\bar{\Omega})^2)$. The latter space is instrumental in proving the existence of an interior point for the constraint $y \in K$. As a consequence, Slater's constraint qualification (CQ) is satisfied, which yields the existence of a (bounded) Lagrange multiplier for this constraint.

For the proof of higher regularity we proceed as follows. First, the existence and uniqueness of a solution with classic parabolic regularity is obtained via classic results on abstract parabolic problems. Then, for the additional regularity, we do not wish to follow the usual path of showing temporal regularity and then spatial regularity as terms involving the time derivative of the control are already present in (18.8a) and (18.8b). Rather, we only show additional spatial regularity, first for $(\tilde{p},\tilde{q})$ and then for $(\tilde{p}_t,\tilde{q}_t)$. Indeed, under appropriate regularity of the shifted initial state and the right-hand side, the solution $(\tilde{p},\tilde{q})$ satisfies

$$(\tilde{p},\tilde{q}) \in L^2(0,T;H^2(\Omega)^2) \cap L^\infty(0,T;H_0^1(\Omega)^2),$$
$$(\tilde{p}_t,\tilde{q}_t) \in L^2(0,T;L^2(\Omega)^2),$$

which leads to $(p,q) \in Y$.

Let $\mathcal{V} := H_0^1(\Omega)^2$ and $\mathcal{H} := L^2(\Omega)^2$. We denote any element v of $\mathcal{V}$, resp. $\mathcal{H}$, by (v_p, v_q), where both v_p and v_q belong to $H_0^1(\Omega)$, resp. $L^2(\Omega)$. This specific notation is inspired by the variable names for gas pressure and flow. It is well-known that $H_0^1(\Omega)$ is dense in $L^2(\Omega)$ and that the embedding of $H_0^1(\Omega)$ into $L^2(\Omega)$ is compact. Therefore, we have the Gelfand triple

$$\mathcal{V} \hookrightarrow \mathcal{H} \hookrightarrow \mathcal{V}^*.$$

Let $(\cdot,\cdot)_{\mathcal{H}}$ denote the inner product of $\mathcal{H}$ and let $\|\cdot\|_{\mathcal{H}}$ be the corresponding norm. For any v, w in $\mathcal{H}$, we have $(v,w)_{\mathcal{H}} = \left(v_p, w_p\right)_{L^2(\Omega)} + \left(v_q, w_q\right)_{L^2(\Omega)}$ and $\|v\|^2_{\mathcal{H}} = \|v_p\|^2_{L^2(\Omega)} + \|v_q\|^2_{L^2(\Omega)}$. The norm of $\mathcal{V}$ is denoted by $\|\cdot\|_{\mathcal{V}}$. In the following, we consider a system of parabolic PDEs with the lower-order terms having generic coefficients. This allows us to streamline the presentation and also invoke these results for an associated adjoint system in future works. Let the bilinear form $a_\tau\colon [0,T]\times\mathcal{V}\times\mathcal{V}\to\mathbb{R}$ be defined as

$$\begin{aligned} a_\tau(t,v,w) := &-\varepsilon\,(\nabla v, \nabla w)_{\mathcal{H}} + \theta_p\left(\nabla v_q, w_p\right)_{L^2(\Omega)} + \theta_q\left(\nabla v_p, w_q\right)_{L^2(\Omega)} \\ &+ \sum_{i,j\in\{p,q\}} \left(\gamma_{ij}(t) v_i, w_j\right)_{L^2(\Omega)} + \tau\,(v,w)_{\mathcal{H}}, \end{aligned} \tag{18.9}$$

where $\varepsilon > 0$, both θ_p and θ_q are non-zero constants, and each γ_{ij} belongs to $C([0,T]; C(\bar{\Omega}))$ with magnitude bounded by $\bar{\gamma}_{ij}$. The parameter τ is fixed later. By applying the Cauchy–Schwarz inequality to each term in (18.9), we see that the bilinear form a_τ is bounded, i.e., there exists $C_{a_\tau} > 0$ such that $|a_\tau(t,v,w)| \le C_{a_\tau}\|v\|_{\mathcal{V}}\|w\|_{\mathcal{V}}$ for all $v, w \in \mathcal{V}$ and $t \in [0,T]$. Let $\mathcal{L}_\tau(t)$ be an operator in $\mathcal{H}$ with action

$$\mathcal{L}_\tau(t)v := -\begin{pmatrix}\varepsilon & 0\\ 0 & \varepsilon\end{pmatrix}\Delta v + \begin{pmatrix}0 & \theta_p\\ \theta_q & 0\end{pmatrix}\nabla v + \begin{pmatrix}\gamma_{pp}(t)+\tau & \gamma_{pq}(t)\\ \gamma_{qp}(t) & \gamma_{qq}(t)+\tau\end{pmatrix} v,$$

and domain $D(\mathcal{L}_\tau(t)) \equiv (H^2(\Omega)\cap H_0^1(\Omega))^2$. Recall that $v \in D(\mathcal{L}_\tau(t))$ is equivalent to

$$v \in \mathcal{V}, \quad \mathcal{L}_\tau(t)v \in \mathcal{H}, \quad \text{and} \quad (\mathcal{L}_\tau(t)v, w)_{\mathcal{H}} = a_\tau(t,v,w) \quad \text{for all } w \in \mathcal{V}.$$

We are going to investigate a problem of the following form: Find $v \in L^2(0,T;\mathcal{V})$ with $v_t \in L^2(0,T;\mathcal{V}^*)$ such that given $v_0 \in \mathcal{H}$ and $\ell \in L^2(0,T;\mathcal{V}^*)$, it satisfies $v(0) = v_0$ and for all $w \in \mathcal{V}$, we have

$$\frac{\mathrm{d}}{\mathrm{d}t}(v(\cdot), w)_{\mathcal{H}} + a_0(\cdot, v(\cdot), w) = (\ell(\cdot), w)_{\mathcal{H}}$$

in the sense of $\mathcal{D}^*(0,T)$, the space of distribution on $(0,T)$. This is referred to as Problem (P). As it is usual in the parabolic case, rather than requiring the coercivity of the bilinear form a_0, it is sufficient to check that a_0 satisfies a weaker condition, namely Gårding's inequality (also known as weak coercivity).

Lemma 18.1 (Gårding's inequality for a_0) *Consider the bilinear form defined in* (18.9)*. Then, there exists two constants $\bar{\tau}$, ζ, with $\zeta > 0$, such that for all $v \in \mathcal{V}$ and $t \in [0,T]$, we have*

$$a_0(t,v,v) + \bar{\tau}\|v\|^2_{\mathcal{H}} \ge \zeta\|v\|^2_{\mathcal{V}}.$$

Proof. Take $t \in [0,T]$. We use classic inequalities to get the following bound on the second term in the right-hand side of (18.9):

$$\left(\nabla v_q, v_p\right)_{L^2(\Omega)} \ge -\|\nabla v_q\|_{L^2(\Omega)}\|v_p\|_{L^2(\Omega)} \ge -\kappa_2\|\nabla v_q\|^2_{L^2(\Omega)} - \frac{1}{4\kappa_2}\|v_p\|^2_{L^2(\Omega)}$$

for any $\kappa_2 > 0$. Similarly, for the third term of (18.9) we have

$$\left(\nabla v_p, v_q\right)_{L^2(\Omega)} \geq -\kappa_3 \|\nabla v_p\|^2_{L^2(\Omega)} - \frac{1}{4\kappa_3}\|v_q\|^2_{L^2(\Omega)},$$

with $\kappa_3 > 0$. Finally, each term in the sum (fourth term of (18.9)) is bounded from below by

$$\begin{aligned}
&\left(\gamma_{pp}(t)v_p, v_p\right)_{L^2(\Omega)} \geq -\bar{\gamma}_{pp}\|v_p\|^2_{L^2(\Omega)}, \ \left(\gamma_{qq}(t)v_q, v_q\right)_{L^2(\Omega)} \geq -\bar{\gamma}_{qq}\|v_q\|^2_{L^2(\Omega)},\\
&\left(\gamma_{pq}(t)v_p, v_q\right)_{L^2(\Omega)} \geq -\kappa_{pq}\bar{\gamma}_{pq}\|v_p\|^2_{L^2(\Omega)} - \frac{\bar{\gamma}_{pq}}{4\kappa_{pq}}\|v_q\|^2_{L^2(\Omega)},\\
&\left(\gamma_{qp}(t)v_q, v_p\right)_{L^2(\Omega)} \geq -\kappa_{qp}\bar{\gamma}_{pq}\|v_q\|^2_{L^2(\Omega)} - \frac{\bar{\gamma}_{pq}}{4\kappa_{qp}}\|v_p\|^2_{L^2(\Omega)},
\end{aligned}$$

where $\kappa_{pq} > 0$ and $\kappa_{qp} > 0$ involve $\bar{\gamma}_{pq}$ and $\bar{\gamma}_{pq}$. Now, we set $\kappa_2 := \frac{\varepsilon}{2|\theta_p|}$ and $\kappa_3 := \frac{\varepsilon}{2|\theta_q|}$ and let $\bar{\tau}_p := \bar{\gamma}_{pp} + \bar{\gamma}_{pq}\kappa_{pq} + \bar{\gamma}_{qp}(4\kappa_{qp})^{-1}$ as well as $\bar{\tau}_q := \bar{\gamma}_{qq} + \bar{\gamma}_{qp}\kappa_{qp} + \bar{\gamma}_{pq}(4\kappa_{pq})^{-1}$. Then, we get

$$\begin{aligned}
a_0(t, v, v) &\geq \frac{\varepsilon}{2}\|\nabla v\|^2_{\mathcal{H}} - \left(\frac{|\theta_p|}{2\varepsilon} + \bar{\tau}_p\right)\|v_p\|^2_{L^2(\Omega)} - \left(\frac{|\theta_q|}{2\varepsilon} + \bar{\tau}_q\right)\|v_q\|^2_{L^2(\Omega)}\\
&\geq \frac{\varepsilon}{2}\|v\|^2_{\mathcal{V}} - \left(\frac{\theta_p^2}{2\varepsilon} + \bar{\tau}_p + \frac{\varepsilon}{2}\right)\|v_p\|^2_{L^2(\Omega)} - \left(\frac{\theta_q^2}{2\varepsilon} + \bar{\tau}_q + \frac{\varepsilon}{2}\right)\|v_q\|^2_{L^2(\Omega)}.
\end{aligned}$$

With $\bar{\tau}$ being the maximum of the coefficients in front of $\|v_p\|^2_{L^2(\Omega)}$ and $\|v_q\|^2_{L^2(\Omega)}$, we obtain

$$a_0(t, v, v) \geq \frac{\varepsilon}{2}\|v\|^2_{\mathcal{V}} - \bar{\tau}\|v\|^2_{\mathcal{H}},$$

which completes the proof. □

Since the time horizon T is finite, we continue our investigation with the coercive bilinear form $a := a_{\bar{\tau}}$. Indeed, if z is the solution of

$$\begin{aligned}
\frac{\mathrm{d}}{\mathrm{d}t}(z, w)_{\mathcal{H}} + a(t, z, w) &= \left(e^{\bar{\tau}t}\ell, w\right)_{\mathcal{H}} \quad \text{for all } w \in \mathcal{V},\\
z(0) &= v_0
\end{aligned}$$

in the sense of $\mathcal{D}^*(0, T)$, then $v = z\, e^{\bar{\tau}t}$ is a solution of Problem (P). For more details, see [11, Remark 2, p. 512], [31, p. 383] or [35, Appendix A]. In the following, we set $\mathcal{L} := \mathcal{L}_{\bar{\tau}}$ and we continue to use ℓ to denote the constant terms of the system of PDEs.

Proposition 18.1 *Suppose that $v_0 \in \mathcal{H}$ and $\ell \in L^2(0, T; V^*)$. Then, there exists a unique solution v to Problem (P) with*

$$v \in L^2(0, T; \mathcal{V}) \quad \text{and} \quad v_t \in L^2(0, T; \mathcal{V}^*). \tag{18.10}$$

Moreover, there exists $C > 0$ such that the following estimate holds for all $t \in (0, T]$:

$$\|v(t)\|^2_{\mathcal{H}} + \|v\|^2_{L^2(0,t;\mathcal{V})} \leq C(\|v_0\|^2_{\mathcal{H}} + \|\ell\|^2_{L^2(0,t;\mathcal{V}^*)}). \tag{18.11}$$

Proof. The existence result is classic; see Theorem 1 and 2 in [11] (on Pages 512–513), Theorem 1.37 in [21], or Theorem 11.3 in [31]. The estimate is provided in [11, Page 515] and [21, Theorem 1.35]. □

For the additional regularity, we follow the procedure outlined in [11, Remark 2, Page 532] for our system. Let us first check that over the domain Ω, the operator $\mathcal{L}$ satisfies the Ladyzhenskaya–Sobolevski inequality.

Lemma 18.2 (Ladyzhenskaya–Sobolevski-type inequality) *There exists $c_1, c_2 > 0$ such that for any fixed $t \in [0,T]$, we have*

$$(\mathcal{L}(t)v, -\Delta v)_{\mathcal{H}} \geq c_1 \|v\|^2_{H^2(\Omega)^2} - c_2 \|v\|^2_{\mathcal{H}} \quad \textit{for all } v \in D(\mathcal{L}(t)).$$

Proof. We proceed as in [29, Proof of Theorem 1.1]. Let $v \in D(\mathcal{L}(t)) \equiv (H^2(\Omega) \cap H_0^1(\Omega))^2$ and consider the splitting $v =: (v_p, v_q)$. First, thanks to Lemma 18.7, we get that the second-order terms in $\mathcal{L}$ satisfy

$$\varepsilon \left(\Delta v_p, \Delta v_p\right)_{L^2(\Omega)} + \varepsilon \left(\Delta v_q, \Delta v_q\right)_{L^2(\Omega)} \geq \frac{\varepsilon}{2} \|v\|^2_{H^2(\Omega)^2} - \varepsilon(C'' + 1)\|v\|^2_{\mathcal{H}} \tag{18.12}$$

for some constant $C'' > 0$. Then, moving on to the first-order terms in $\mathcal{L}$, we have

$$\begin{aligned} \left(\nabla v_q, \Delta v_p\right)_{L^2(\Omega)} &\geq -\|\nabla v_q\|_{L^2(\Omega)} \|\Delta v_p\|_{L^2(\Omega)} \\ &\geq -\kappa_1 \|v_q\|_{H^2(\Omega)} \|\Delta v_p\|_{L^2(\Omega)} - C_{\kappa_1} \|v_q\|_{L^2(\Omega)} \|\Delta v_p\|_{L^2(\Omega)} \\ &\geq -\frac{\kappa_1}{2} \|v_q\|^2_{H^2(\Omega)} - C_{\kappa_1} C_{\kappa_1'} \|v_q\|^2_{L^2(\Omega)} - (\kappa_1' + \frac{\kappa_1}{2}) \|v_p\|^2_{H^2(\Omega)}, \end{aligned} \tag{18.13}$$

where we used the relation (18.41) in Lemma 18.6 given in Appendix A and Cauchy's inequality. Similarly, we have

$$\left(\nabla v_p, \Delta v_q\right)_{L^2(\Omega)} \geq -\frac{\kappa_2}{2} \|v_p\|^2_{H^2(\Omega)} - C_{\kappa_2} C_{\kappa_2'} \|v_p\|^2_{L^2(\Omega)} - (\kappa_2' + \frac{\kappa_2}{2}) \|v_q\|^2_{H^2(\Omega)}. \tag{18.14}$$

Finally, with $\tau_{pp} = \tau_{qq} = \bar{\tau}$ and $\tau_{pq} = \tau_{qp} = 0$, for i, j being p or q we have

$$\left((\tau_{ij} + \gamma_{ij}(t))v_i, \Delta v_j\right)_{L^2(\Omega)} \geq (\tau_{ij} + \bar{\gamma}_{ij}) \left(-\kappa_{i,j} \|v_j\|^2_{H^2(\Omega)} - C_{\kappa_{i,j}} \|v_i\|^2_{L^2(\Omega)}\right) \tag{18.15}$$

for all $t \in [0,T]$. Summarizing, we derived lower bounds for $(\mathcal{L}(t)v, \Delta v)_{\mathcal{H}}$ in terms of $\|v_p\|^2_{H^2(\Omega)}$, $\|v_q\|^2_{H^2(\Omega)}$, $\|v_p\|^2_{L^2(\Omega)}$, and $\|v_q\|^2_{L^2(\Omega)}$ for all $t \in [0,T]$. Furthermore, the magnitude of the terms $\|v_p\|^2_{H^2(\Omega)}$ and $\|v_q\|^2_{H^2(\Omega)}$ in (18.13)–(18.15) can be controlled by choosing $\kappa_1, \kappa_1', \kappa_2, \kappa_2'$, and $\kappa_{i,j}$. Hence, for any values of $\theta_p, \theta_q, \bar{\tau}$, and $\bar{\gamma}_{ij}$, one can select these quantities such that the contribution of $\|v_p\|^2_{H^2(\Omega)}$ (resp. $\|v_q\|^2_{H^2(\Omega)}$) in (18.13)–(18.15) is larger than $-\frac{\varepsilon}{4}\|v_p\|^2_{H^2(\Omega)}$ (resp. $-\frac{\varepsilon}{4}\|v_q\|^2_{H^2(\Omega)}$). Finally, using (18.12), we obtain

$$(\mathcal{L}(t)v, -\Delta v)_{\mathcal{H}} \geq \frac{\varepsilon}{4} \|v\|^2_{H^2(\Omega)^2} - C_{\text{total}} \|v\|^2_{\mathcal{H}},$$

with a suitably chosen $C_{\text{total}} > 0$. □

Now, we are ready to state the desired regularity result.

Proposition 18.2 *Suppose that $v_0 \in \mathcal{V}$ and $\ell \in L^2(0,T;\mathcal{H})$. Then, the solution v to Problem (P) satisfies*

$$v \in L^\infty(0,T;\mathcal{V}) \cap L^2(0,T;H^2(\Omega)^2)$$

with the estimate

$$\|v\|_{L^\infty(0,T;\mathcal{V})} + \|v\|_{L^2(0,T;H^2(\Omega)^2)} \leq C(\|v_0\|_{\mathcal{V}} + \|\ell\|_{L^2(0,T;\mathcal{H})})$$

for some $C > 0$.

Proof. We follow [11, Remark 2, Page 532]. To this end, we consider the following approximation

$$\mathcal{V}_m := \operatorname{span}\{\mathcal{W}_j\}_{j=1}^m$$

of $\mathcal{V}$, where $\mathcal{W}_j = (e_j, e_j)$ is defined by the (normalized) eigenfunctions e_j of the Laplacian in the Dirichlet problem

$$-\Delta e_j = \nu_j e_j \quad \text{in } \Omega$$

and $e_j(0) = e_j(L) = 0$. These functions form an orthonormal basis of $L^2(\Omega)$ and belong to $H_0^1(\Omega) \cap C^\infty(\Omega)$; see [5, Theorem 9.31]. Note that the sequence $\{e_j/\sqrt{\nu_j + 1}\}_{j=1}^\infty$ forms an orthonormal basis of $H_0^1(\Omega)$. For the initial state of the finite-dimensional problem over $\mathcal{V}_m$, we choose $v^{(m)}(0) \in \mathcal{V}_m$ such that $v^{(m)}(0)$ converges to v_0 as $m \to \infty$ in $\mathcal{V}$. With $v^{(m)} = \sum_{j=1}^m \zeta_j \mathcal{W}_j$ being the solution to the Galerkin approximation of order m to Problem (P), for almost all $t \in (0,T)$, we have

$$\left(\frac{\mathrm{d}}{\mathrm{d}t} v^{(m)}(t), w\right)_{\mathcal{H}} + a(t, v^{(m)}(t), w) = (\ell(t), w)_{\mathcal{H}} \tag{18.16}$$

for all $w \in \mathcal{V}_m \subset \mathcal{H}$. For almost all t in $(0,T)$, we take $w = \nu_j \zeta_j(t) \mathcal{W}_j$ in (18.16) and sum all the equalities. This yields

$$\left(\frac{\mathrm{d}}{\mathrm{d}t} v^{(m)}(t), -\Delta v^{(m)}(t)\right)_{\mathcal{H}} + \left(\mathcal{L}(t) v^{(m)}(t), -\Delta v^{(m)}(t)\right)_{\mathcal{H}} = \left(\ell(t), -\Delta v^{(m)}(t)\right)_{\mathcal{H}}.$$

After integrating by part the first term and exchanging the partial derivatives, we have

$$\left(\frac{\mathrm{d}}{\mathrm{d}t} \nabla v^{(m)}(t), \nabla v^{(m)}(t)\right)_{\mathcal{H}} + \left(\mathcal{L}(t) v^{(m)}(t), -\Delta v^{(m)}(t)\right)_{\mathcal{H}} = \left(\ell(t), -\Delta v^{(m)}(t)\right)_{\mathcal{H}}.$$

Then, we integrate w.r.t. t and get

$$\begin{aligned} &\frac{1}{2}\|\nabla v^{(m)}(t)\|_{\mathcal{H}}^2 + \int_0^t \left(\mathcal{L}(t) v^{(m)}(s), -\Delta v^{(m)}(s)\right)_{\mathcal{H}} \mathrm{d}s \\ &= \int_0^t \left(\ell(s), -\Delta v^{(m)}(s)\right)_{\mathcal{H}} \mathrm{d}s + \frac{1}{2}\|\nabla v^{(m)}(0)\|_{\mathcal{H}}^2. \end{aligned}$$

Using Lemma 18.2, there exists strictly positive constants c_1 and c_2 such that

$$\begin{aligned}&\frac{1}{2}\|\nabla v^{(m)}(t)\|^2_{\mathcal{H}}+c_1\int_0^t\|v^{(m)}(s)\|^2_{H^2(\Omega)^2}\mathrm{d}s\\ &\leq\frac{1}{2}\|\nabla v^{(m)}(0)\|^2_{\mathcal{H}}+\int_0^t\|\ell(s)\|_{\mathcal{H}}\|\Delta v^{(m)}(s)\|_{\mathcal{H}}\mathrm{d}s+c_2\int_0^t\|v^{(m)}(s)\|^2_{\mathcal{H}}\mathrm{d}s,\end{aligned}\tag{18.17}$$

where we used that $\ell\in L^2(0,T;\mathcal{H})$. Now, there exists $C_{\frac{c_1}{2}}>0$ such that

$$\int_0^t\|\ell(s)\|_{\mathcal{H}}\|\Delta v^{(m)}(s)\|_{\mathcal{H}}\,\mathrm{d}s\leq C_{\frac{c_1}{2}}\int_0^t\|\ell(s)\|^2_{\mathcal{H}}\mathrm{d}s+\frac{c_1}{2}\int_0^t\|v^{(m)}(s)\|^2_{H^2(\Omega)^2}\,\mathrm{d}s.$$

Using the estimate in (18.11), we know that there exists a positive constant C_{c_2} such that

$$c_2\int_0^t\|v^{(m)}(s)\|^2_{\mathcal{H}}\mathrm{d}s\leq C_{c_2}\left[\int_0^t\|\ell(s)\|^2_{\mathcal{V}^*}\mathrm{d}s\right]+\frac{1}{2}\|v^{(m)}(0)\|^2_{\mathcal{H}}-\frac{1}{2}\|v^{(m)}(t)\|^2_{\mathcal{H}}$$

holds. To get an upper bound independent of m, we use the last two relations in (18.17) and the boundedness of the sequence $v^{(m)}(0)\in\mathcal{V}_m$ as it converges to v_0 as $m\to\infty$ in $\mathcal{V}$. Thus, we get

$$\frac{1}{2}\|v^{(m)}(t)\|^2_{\mathcal{V}}+\frac{c_1}{2}\int_0^t\|v^{(m)}(s)\|^2_{H^2(\Omega)^2}\,\mathrm{d}s\leq\ C_0\|v_0\|^2_{\mathcal{V}}+C_{\mathrm{rhs}}\int_0^t\|\ell(s)\|^2_{\mathcal{H}}\mathrm{d}s.\tag{18.18}$$

Hence, $v^{(m)}\in L^\infty(0,T;\mathcal{V})\cap L^2(0,T;H^2(\Omega)^2)$. Then, using classic arguments, at the limit $m\to\infty$, the solution v also fulfills (18.18). The estimate is then obtained based on this inequality. □

Let us now turn our attention to the characterization of the control-to-state mapping. We start with the following relation between ℓ and the boundary values.

Lemma 18.3 *Let $u_\Gamma\in H^1(0,T)^4$ and ℓ be the right-hand side of the equations* (18.8a)–(18.8b). *Then, there exists $C>0$ such that*

$$\|\ell\|_{L^2(0,T;\mathcal{H})}\leq C\|u_\Gamma\|_{H^1(0,T)^4}.$$

Proof. In this proof, C is a positive constant that may take different values depending on the context. We show that the inequality $\|\ell\|^2_{L^2(0,T;\mathcal{H})}\leq C\|u_\Gamma\|^2_{H^1(0,T)^4}$ holds. First, note that for any $(x,t)\in\Omega_T$, we have

$$(u^p_\Omega)_t(x,t)=\frac{L-x}{L}(p^{\mathrm{in}})_t(t)+\frac{x}{L}(p^{\mathrm{out}})_t(t),\quad(u^p_\Omega)_x(x,t)=\frac{p^{\mathrm{out}}(t)-p^{\mathrm{in}}(t)}{L},$$

and similar relations hold for $(u^q_\Omega)_t$ and $(u^q_\Omega)_x$. With $\ell=:(\ell^p,\ell^q)$, for all $s\in(0,T)$, we have

$$\|\ell^p(\cdot,s)\|^2_{L^2(\Omega)}\leq C\left(\|(u^p_\Omega)_t(\cdot,s)\|^2_{L^2(\Omega)}+\|(u^q_\Omega)_x(\cdot,s)\|^2_{L^2(\Omega)}\right).$$

Using the expressions above for $(u_\Omega^p)_t$ and $(u_\Omega^p)_x$, we obtain

$$\|\ell^p(\cdot,s)\|^2_{L^2(\Omega)} \leq C\left((p^{\mathrm{in}}(s))^2 + ((p^{\mathrm{out}})_t(s))^2 + (q^{\mathrm{in}}(s))^2 + (q^{\mathrm{out}}(s))^2\right).$$

Now for ℓ^q, using similar arguments, we have

$$\begin{aligned}
&\|\ell^q(\cdot,s)\|^2_{L^2(\Omega)}\\
&\leq C\left(\|(u_\Omega^q)_t(\cdot,s)\|^2_{L^2(\Omega)} + \|(u_\Omega^p)_x(\cdot,s)\|^2_{L^2(\Omega)} + \|u_\Omega^q(\cdot,s)\|^2_{L^2(\Omega)} + \|u_\Omega^p(\cdot,s)\|^2_{L^2(\Omega)}\right)\\
&\leq C\Big((q^{\mathrm{in}}(s))^2 + ((q^{\mathrm{out}})_t(s))^2 + (p^{\mathrm{in}}(s))^2 + ((p^{\mathrm{out}})_t(s))^2\\
&\qquad + (p^{\mathrm{in}}(s))^2 + (p^{\mathrm{out}}(s))^2 + (q^{\mathrm{in}}(s))^2 + (q^{\mathrm{out}}(s))^2\Big).
\end{aligned}$$

Hence, it follows that

$$\begin{aligned}
&\|\ell\|^2_{L^2(0,T;\mathcal{H})}\\
&= \|\ell^p\|^2_{L^2(0,T;L^2(\Omega))} + \|\ell^q\|^2_{L^2(0,T;L^2(\Omega))}\\
&\leq C\Big[\|p^{\mathrm{in}}\|^2_{L^2(0,T)} + \|p^{\mathrm{out}}\|^2_{L^2(0,T)} + \|q^{\mathrm{in}}\|^2_{L^2(0,T)} + \|q^{\mathrm{out}}\|^2_{L^2(0,T)}\\
&\qquad + \|(p^{\mathrm{in}})_t\|^2_{L^2(0,T)} + \|(p^{\mathrm{out}})_t\|^2_{L^2(0,T)} + \|(q^{\mathrm{in}})_t\|^2_{L^2(0,T)} + \|(q^{\mathrm{out}})_t\|^2_{L^2(0,T)}\Big].
\end{aligned}$$

This concludes the proof. □

Finally, the desired regularity result for the solution of the system can be obtained. As the shifted initial state has to be in $H_0^1(\Omega)^2$, there are compatibility conditions between the initial state and the value of the controls at $t = 0$. To capture these, we define

$$\begin{aligned}
Z := \{(y_0, u_\Gamma) \in H^1(\Omega)^2 \times H^1(0,T)^4 \mid\ & p_0(0) = p^{\mathrm{in}}(0),\ p_0(L) = p^{\mathrm{out}}(0),\\
& q_0(0) = q^{\mathrm{in}}(0),\ q_0(L) = q^{\mathrm{out}}(0)\}.
\end{aligned}$$

Lemma 18.4 *Given $y_0 \in H^1(\Omega)^2$, assume that the boundary control u_Γ satisfies $(y_0, u_\Gamma) \in Z$. Then, the unique solution $y = (p, q)$ of (18.6) has regularity*

$$y \in L^\infty(0,T; H^1(\Omega)^2) \cap L^2(0,T; H^2(\Omega)^2) \quad \text{and} \quad y_t \in L^2(0,T;\mathcal{H}),$$

and there is a linear and continuous mapping $S_{\mathrm{PDE}}\colon Z \to Y$ such that $y = S_{\mathrm{PDE}}(y_0, u_\Gamma)$.

Proof. The hypothesis allows us to invoke Lemma 18.3 and Proposition 18.2. Given data $(y_0, u_\Gamma) \in Z$, let v be the unique solution of Problem (P) with initial state $v_0 = y_0 - (\mathcal{E}(u_\Gamma^p), \mathcal{E}(u_\Gamma^q))^\top(\cdot, 0)$. From Proposition 18.2, we have

$$v \in L^\infty(0,T; H_0^1(\Omega)^2) \cap L^2(0,T; H^2(\Omega)^2) \ \subset\ L^2(0,T; (H^2(\Omega) \cap H_0^1(\Omega))^2), \quad (18.19)$$

and then $v \in D(\mathcal{L}(t))$ for all $t \in [0,T]$. Moreover, Problem (P) is equivalent to $v_t = \ell - \mathcal{L}v$ in $L^2(0,T;\mathcal{V}^*)$ plus initial and boundary conditions; see [11, Remark 2, p. 512]. As

$\ell - \mathcal{L}v \in L^2(0,T;\mathcal{H}) \subset L^2(0,T;\mathcal{V}^*)$, we have $v_t \in L^2(0,T;\mathcal{H})$. Furthermore, with v satisfying (18.19), the estimate

$$\begin{aligned}\|v_t\|_{L^2(0,T;\mathcal{H})} &\leq \|\ell\|_{L^2(0,T;\mathcal{H})} + \|\mathcal{L}v\|_{L^2(0,T;\mathcal{H})} \\ &\leq \|\ell\|_{L^2(0,T;\mathcal{H})} + C_{\mathcal{L}}\|v\|_{L^2(0,T;H^2(\Omega)^2)}\end{aligned}$$

holds due to the boundedness of $\mathcal{L}$. In combination with the estimates from Proposition 18.2 and Lemma 18.3, we get

$$\|v\|_{L^\infty(0,T;\mathcal{V})} + \|v_t\|_{L^2(0,T;\mathcal{H})} + \|v\|_{L^2(0,T;H^2(\Omega)^2)} \leq C(\|v_0\|_{\mathcal{V}} + \|u_\Gamma\|_{H^1(0,T)^4}).$$

From v, the unique solution y of (18.6) is given by

$$y = v + \begin{pmatrix} \mathcal{E}(u_\Gamma^p) \\ \mathcal{E}(u_\Gamma^q) \end{pmatrix}.$$

Recall that $\mathcal{E}\colon H^1(0,T)^2 \to H^1(0,L;H^2(\Omega))$ is linear and bounded. Therefore, we get the boundedness of S_{PDE}. □

Before moving on to the analysis of the GNEP, let us define the control-to-state mapping S. The compatibility condition $(y_0, u_\Gamma) \in Z$ restricts the solution operator to be well-defined on a subset of $H^1(0,T)^4$. More precisely, with $u_\Gamma^{y_0} := (p_0(0), p_0(L), q_0(0), q_0(L))$, the set of boundary controls compatible with y_0 is $U_{y_0} := \{u_\Gamma \in H^1(0,T)^4 \mid u_\Gamma(0) = u_\Gamma^{y_0}\}$. With $\widehat{u}^{y_0} \in U_{y_0}$ the constant function $\widehat{u}^{y_0} \equiv u_\Gamma^{y_0}$, the relation between any boundary control $u_\Gamma \in U_{y_0}$ and the state can be written as

$$y = S_{\mathrm{PDE}}(y_0, u_\Gamma) = S_{\mathrm{PDE}}(y_0, \widehat{u}^{y_0}) + S_{\mathrm{PDE}}(0, u_\Gamma - \widehat{u}^{y_0}),$$

where

$$u_\Gamma - \widehat{u}^{y_0} \in \widehat{U} := \{\widehat{u} \in H^1(0,T)^4 \mid \widehat{u}(0) = 0\} \tag{18.20}$$

is the Banach space (with the norm of $H^1(0,T)^4$) of controls compatible with the initial state being 0. With $\widehat{S}_0\colon \widehat{U} \to Y$ given by $\widehat{u} \mapsto S_{\mathrm{PDE}}(0, \widehat{u})$, the control-to-state operator $S\colon U_{y_0} \to Y$ is given by

$$S(u_\Gamma) := S_{\mathrm{PDE}}(y_0, \widehat{u}^{y_0}) + \widehat{S}_0(u_\Gamma - \widehat{u}^{y_0}) = y. \tag{18.21}$$

18.4 Analysis of the Jointly Convex GNEP

Given the well-posedness of the PDE governing the gas flow, we now study the underlying GNEP. The space of pressures (resp. mass flows) at the pipe's endpoints is $P := H^1(0,T)^2$ (resp. $Q := H^1(0,T)^2$). Each firm's decision variable $u_i =: (p_i, q_i)$, where p_i and q_i are the pressure and mass flow variables, is an element of $U := P \times Q$, and we define $\mathcal{U} := U^M$ as we consider M-many firms. The set of initial states compatible with the constraint $y \in K$ is given by:

$$Y_0^{\mathrm{ad}} := \{y_0 \in H^1(\Omega)^2 \mid \underline{y} \le y_0(x) \le \bar{y} \text{ for all } x \in [0, L]\},$$

where $\underline{y}, \bar{y} \in \mathbb{R}$ with $\underline{y} \le \bar{y}$ are fixed. The mapping in (18.2) between the players' decisions and the boundary values is $\mathcal{L}\colon \mathcal{U} \to U$ with

$$\mathcal{L} := (\mathcal{L}^p, \mathcal{L}^q) \quad \text{with} \quad \mathcal{L}^p(u) := \frac{1}{M}\sum_{i=1}^{M} p_i \quad \text{and} \quad \mathcal{L}^q(u) := \sum_{i=1}^{M} q_i.$$

While this does not impose the continuity of the pressure, we shall see that this particular choice of $\mathcal{L}^p$ allows us to show existence of solutions to the game such that the continuity of pressure holds.

In our analysis below we invoke the following notation. As previously discussed, the control-to-state operator S is only well-defined on a subset of $\mathcal{U}$ that lacks the vector space structure. To facilitate the handling of the compatibility conditions, we perform a change of variables. Given $y_0 = (p_0, q_0)$, consider the constant functions $\widehat{p}^0(t) := (p_0(0), p_0(L))$ and $\widehat{q}^0(t) := (q_0(0)/M, q_0(L)/M)$ for all $t \in [0, T]$. With $\widehat{u}_i^{y_0} := (\widehat{p}^0, \widehat{q}^0)$, the shifted decisions for player i are given by $\widehat{u}_i = u_i - \widehat{u}_i^{y_0}$, and these quantities are collected in $\widehat{u}$ and $\widehat{u}^{y_0}$. With $\widehat{P} := \{\widehat{p} \in P \mid \widehat{p}(0) = 0\}$ and $\widehat{Q} := \{\widehat{q} \in Q \mid \widehat{q}(0) = 0\}$, the assumptions stated in (18.25a) and (18.25b) below allow us to define the feasible sets for the pressures and mass flows as $\widehat{P}^{\mathrm{ad}} := \{\widehat{p} \in \widehat{P} \mid \widehat{p} + \widehat{p}^0 \in P^{\mathrm{ad}}\}$ and $\widehat{Q}_i^{\mathrm{ad}} := \{\widehat{q} \in \widehat{Q} \mid \widehat{q} + \widehat{q}^0 \in Q_i^{\mathrm{ad}}\}$. In the light of the definition of $\widehat{U}$ in (18.20), we note that $\widehat{U} = \widehat{P} \times \widehat{Q}$. Also, as closed subspaces of $H^1(0,T)^2$, equipped with the norm of $H^1(0,T)^2$, both $\widehat{P}$ and $\widehat{Q}$ are Banach spaces. Furthermore, from the inclusions $H_0^1(0,T)^2 \subset \widehat{P} \subset L^2(0,T)^2$ and $\widehat{P}^* \subset H^{-1}(0,T)^2$, we infer that $\widehat{P}$ is dense in $L^2(0,T)^2$. Coupled with the continuous injection of $H^1(0,T)$ in $L^2(0,T)$, we deduce that we have the Gelfand triples $\widehat{P} \hookrightarrow L^2(0,T)^2 \hookrightarrow \widehat{P}^*$ and $\widehat{Q} \hookrightarrow L^2(0,T)^2 \hookrightarrow \widehat{Q}^*$. The space $\mathcal{Z} := (\widehat{U}^*)^M$ is isomorphic to $\widehat{\mathcal{U}}^*$, denoted by $\mathcal{Z} \simeq \widehat{\mathcal{U}}^*$. We can thus identify any element of $\mathcal{Z}$ with a unique element of $\widehat{\mathcal{U}}^*$ and vice-versa. The duality pairing between $\widehat{\mathcal{U}}$ and $\mathcal{Z}$ is given by $\langle z, u\rangle_{\mathcal{Z},\widehat{\mathcal{U}}} = \sum_{i=1}^{M} \langle z_i, u_i\rangle_{\widehat{U}^*,\widehat{U}}$. Then, the feasible set for $\widehat{u}_i$ is a subset of the Banach space $\widehat{U}$. The affine mapping $\widehat{S}\colon \widehat{\mathcal{U}} \to Y$, from the players' actions to the state, is given by

$$y = \widehat{S}(\widehat{u}) = S_{\mathrm{PDE}}(y_0, \widehat{u}^{y_0}) + \widehat{S}_0(\mathcal{L}(\widehat{u})).$$

With $\mathcal{L}_i\colon \widehat{P} \times \widehat{Q} \to \widehat{P} \times \widehat{Q}$ given by $\mathcal{L}_i(\widehat{u}_i) := (\widehat{p}_i, \widehat{q}_i/M)$ for all $i \in \{1, \dots, M\}$, we define $\widehat{S}_i(\widehat{u}_i) := \widehat{S}_0(\mathcal{L}_i(\widehat{u}_i))$. Then, for a given $\widehat{u}_{-i}$, the mapping from each player's control $\widehat{u}_i$ to the state y reads

$$\widehat{S}(\widehat{u}_i, \widehat{u}_{-i}) = \widehat{S}_i(\widehat{u}_i) + S_{\mathrm{PDE}}(y_0, \widehat{u}^{y_0}) + \widehat{S}_0(\mathcal{L}(0, \widehat{u}_{-i})).$$

Note that $\widehat{S}_i\colon \widehat{U} \to Y$ is well defined and linear. The feasible set for each agent is given by the set-valued map $\widehat{C}_i\colon \widehat{U}^{M-1} \rightrightarrows \widehat{U}$ defined as

$$\widehat{C}_i(\widehat{u}_{-i}) := \{\widehat{u}_i \in \widehat{U}_i^{\mathrm{ad}} \mid \widehat{S}(\widehat{u}_i, \widehat{u}_{-i}) \in K\}, \tag{18.22}$$

where $\widehat{U}_i^{\mathrm{ad}} := \widehat{P}^{\mathrm{ad}} \times \widehat{Q}_i^{\mathrm{ad}}$. As both $\widehat{U}_i^{\mathrm{ad}}$ and K are non-empty, closed, and convex, the fact that $\widehat{S}$ is affine ensures that the images of $\widehat{C}_i(\widehat{u}_{-i})$ are closed and convex (if non-empty). The part of the objective functional that intertwines the players' decision variables is the revenue functional

$$r_i(q_i^{\mathrm{out}}, q_{-i}^{\mathrm{out}}) := \int_0^T \left(\alpha(t) \sum_{k=1}^{M} q_k^{\mathrm{out}}(t) - \beta(t) \right) q_i^{\mathrm{out}}(t) \mathrm{d}t.$$

With $\widehat{u}_i =: (\widehat{p}_i^{\mathrm{in}}, \widehat{p}_i^{\mathrm{out}}, \widehat{q}_i^{\mathrm{in}}, \widehat{q}_i^{\mathrm{out}})$, in the shifted variables, we get

$$\begin{aligned}\widehat{r}_i(\widehat{q}_i^{\mathrm{out}}, \widehat{q}_{-i}^{\mathrm{out}}) &:= r_i(\widehat{q}_i^{\mathrm{out}} + q_0(L)/M, \widehat{q}_{-i}^{\mathrm{out}} + q_0(L)/M) \\ &= \int_0^T \left[\alpha(t) \sum_{k=1}^{M} \widehat{q}_k^{\mathrm{out}}(t) - (\beta(t) - \alpha(t) q_0(L)) \right] \left[\widehat{q}_i^{\mathrm{out}}(t) + q_0(L)/M \right] \mathrm{d}t.\end{aligned}$$

Note that for all $\widehat{q}_{-i}^{\mathrm{out}} \in L^2(0,T)^{M-1}$, the mapping $\widehat{q}_i^{\mathrm{out}} \mapsto \widehat{r}_i(\widehat{q}_i^{\mathrm{out}}, \widehat{q}_{-i}^{\mathrm{out}})$ is convex and continuously Fréchet differentiable. The expression of the gradient w.r.t. the first variable reads

$$\nabla_{\widehat{q}_i^{\mathrm{out}}} \widehat{r}_i(\widehat{q}_i^{\mathrm{out}}, \widehat{q}_{-i}^{\mathrm{out}}) = \alpha \sum_{k=1}^{M} \widehat{q}_k^{\mathrm{out}} + \alpha\, \widehat{q}_i^{\mathrm{out}} - (\beta - \widehat{\alpha} q_0(L))$$

with $\widehat{\alpha} := \alpha(1+M)/M$. Let $e \in \widehat{U}^*$, $d_1 \colon \widehat{U} \times \widehat{U}^{M-1} \to \widehat{U}^*$, and $d_2 \colon \widehat{U} \to \widehat{U}^*$ such that for any $w_i = (w_i^{p0}, w_i^{pL}, w_i^{q0}, w_i^{qL}) \in \widehat{U}$ the following holds:

$$\langle d_1(\widehat{u}_i, \widehat{u}_{-i}), w_i \rangle_{\widehat{U}^*, \widehat{U}} = \left(\alpha \sum_{k=1}^{M} \widehat{q}_k^{\mathrm{out}}, w_i^{qL} \right)_{L^2(0,T)}, \tag{18.23a}$$

$$\langle d_2(\widehat{u}_i), w_i \rangle_{\widehat{U}^*, \widehat{U}} = \left(\alpha\, \widehat{q}_i^{\mathrm{out}}, w_i^{qL} \right)_{L^2(0,T)}, \tag{18.23b}$$

$$\langle e, w_i \rangle_{\widehat{U}^*, \widehat{U}} = \left(\beta - \widehat{\alpha} q_0(L), w_i^{qL} \right)_{L^2(0,T)}. \tag{18.23c}$$

We are now ready to state our main result.

Theorem 18.1 *Given an initial state $(p_0, q_0) \in Y_0^{\mathrm{ad}}$, consider the following jointly convex GNEP with M players, where the optimization problem associated with player $i \in \{1, \ldots, M\}$ is given by*

$$\begin{aligned} \min_{u_i \in U} \quad & f_i(u_i, u_{-i}) := \int_0^T \left(\alpha(t) \sum_{k=1}^{M} q_k^{\mathrm{out}}(t) - \beta(t) \right) q_i^{\mathrm{out}}(t) \mathrm{d}t + g_i(u_i) \\ s.t. \quad & u_i \in P^{\mathrm{ad}} \times Q_i^{\mathrm{ad}}, \quad S(u_i, u_{-i}) \in K, \end{aligned} \tag{18.24}$$

where $g_i(u_i)$ is any function defined as $g_i(u_i) = g^p(p_i) + g_i^q(q_i)$ with both g^p and g_i^q being lower semicontinuous and proper convex functions. Assume that the subdifferentials ∂g^p and ∂g_i, for each player, have full domain and that the sets K, $P^{\mathrm{ad}} \subset P$ as

well as $Q_i^{\mathrm{ad}} \subset Q$ are closed and convex. In addition, P^{ad} and Q_i^{ad} satisfy the property that

$$p \in P^{\mathrm{ad}} \implies p^{\mathrm{in}}(0) = p_0(0) \text{ and } p^{\mathrm{out}}(0) = p_0(L), \tag{18.25a}$$

$$q \in Q_i^{\mathrm{ad}} \implies Mq_i^{\mathrm{in}}(0) = q_0(0) \text{ and } Mq_i^{\mathrm{out}}(0) = q_0(L). \tag{18.25b}$$

Furthermore, suppose that there exists $\bar{u} \in \prod_{i=1}^{M}(P^{\mathrm{ad}} \times Q_i^{\mathrm{ad}})$ such that Slater's constraint qualification (CQ)

$$S(\bar{u}) \in \operatorname{int} K \tag{18.26}$$

holds. Finally, assume that the subdifferential of the sum $Mg^p(p) + \sum_{i=1}^{M} g_i^q(q_i)$, when restricted to $P^{\mathrm{ad}} \times \prod_{i=1}^{M} Q_i^{\mathrm{ad}}$, is coercive. Then, there exists a variational equilibrium to the GNEP with all pressures p_i, $i \in \{1, \dots, M\}$, being identical.

Proof. We proceed in three steps: First, we show that there exists a solution to the GNEP for which the first-order conditions for the players' optimization problems exhibit the same multiplier for the shared constraint $S(u) \in K$. Second, we formulate a reduced generalized equation with only one boundary pressure variable and show that its solution set is non-empty. Lastly, from any solution of the latter problem, we construct a solution to an operator equation associated with the first part and therefore to the jointly convex GNEP. Note that this investigation is performed in the shifted variable spaces introduced before the theorem statement, as it facilitates the handling of the compatibility conditions.

Step 1. We focus on the first-order optimality condition for the minimization problem associated with player i. For this purpose, take any fixed $\widehat{u}_{-i}$ such that $\widehat{C}_i(\widehat{u}_{-i}) \neq \emptyset$ holds. Since for any $\widehat{u}_{-i}$, the partial map $f_i(\cdot, \widehat{u}_{-i})$ is lower semicontinuous and convex, for $\bar{u}_i$ to be optimal, it is necessary and sufficient that the inclusion

$$0 \in \partial(f_i(\cdot, \widehat{u}_{-i}) + \delta_{\widehat{C}_i(\widehat{u}_{-i})})(\bar{u}_i) \tag{18.27}$$

holds, where $\delta_{\widehat{C}_i(\widehat{u}_{-i})}$ is the indicator function of the set $\widehat{C}_i(\widehat{u}_{-i})$. Let $\widehat{g}^p(\widehat{p}_i) := g^p(\widehat{p}_i + \widehat{p}^0)$ and $\widehat{g}_i^q(\widehat{q}_i) := g_i^q(\widehat{q}_i + \widehat{q}^0)$. As $\widehat{r}_i$ is C^1 and $\partial\widehat{g}_i$ has full domain, by applying the sum rule for convex subdifferentials we obtain

$$\partial(f_i(\cdot, \widehat{u}_{-i}) + \delta_{\widehat{C}_i(\widehat{u}_{-i})})(\widehat{u}_i) = d_1(\widehat{u}_i, \widehat{u}_{-i}) + d_2(\widehat{u}_i) - e + \partial\widehat{g}_i(\widehat{u}_i) + \partial(\delta_{\widehat{C}_i(\widehat{u}_{-i})})(\widehat{u}_i),$$

where d_1, d_2, and e were defined in (18.23a)–(18.23c). Using the chain rule for convex subdifferentials we get that for any $\widehat{u}_i \in \widehat{U}_i^{\mathrm{ad}}$ with $\widehat{S}(\widehat{u}_i, \widehat{u}_{-i}) \in K$, the inclusion

$$\partial\delta_{\widehat{C}_i(\widehat{u}_{-i})}(\widehat{u}_i) \supseteq N_{\widehat{U}_i^{\mathrm{ad}}}(\widehat{u}_i) + \partial(\delta_K(\widehat{S}(\widehat{u}_i, \widehat{u}_{-i}))) \tag{18.28}$$

holds. Hence, any solution to the generalized equation

$$0 \in d_1(\widehat{u}_i, \widehat{u}_{-i}) + d_2(\widehat{u}_i) - e + \partial\widehat{g}_i(\widehat{u}_i) + N_{\widehat{U}_i^{\mathrm{ad}}}(\widehat{u}_i) + \partial(\delta_K(\widehat{S}(\widehat{u}_i, \widehat{u}_{-i}))) \tag{18.29}$$

satisfies (18.27) and therefore is optimal for player i. Recall from (18.21) that $\widehat{u}_i \mapsto \widehat{S}(\widehat{u}_i, \widehat{u}_{-i})$ is an affine mapping. Invoking again the chain rule for convex subdifferentials, we have

$$\partial(\delta_K(\widehat{S}(\widehat{u}_i, \widehat{u}_{-i}))) \supseteq \widehat{S}_i^* N_K(\widehat{S}(\widehat{u}_i, \widehat{u}_{-i})). \tag{18.30}$$

With $\mu_i \in N_K(\widehat{S}(\widehat{u}_i, \widehat{u}_{-i}))$, from (18.29) we get the generalized equation

$$e \in d_1(\widehat{u}_i, \widehat{u}_{-i}) + d_2(\widehat{u}_i) + \partial \widehat{g}_i(\widehat{u}_i) + N_{\widehat{U}_i^{\mathrm{ad}}}(\widehat{u}_i) + \widehat{S}_i^* \mu_i.$$

Any $\widehat{u} \in \widehat{\mathcal{U}}$ that satisfies the above inclusion for all $i \in \{1, \dots, M\}$ is a solution of the GNEP. Note that if an appropriate constraint qualification, like Slater's CQ, were to hold for $\widehat{C}_i(\widehat{u}_{-i})$ as given in (18.22), then both (18.28) and (18.30) would hold with equality. Since the state variable $y = \widehat{S}(\widehat{u}_i, \widehat{u}_{-i})$ is the same for all players, we can restrict all μ_i to be equal. This leads us to the following operator equations:

$$e \in d_1(\widehat{u}_i, \widehat{u}_{-i}) + d_2(\widehat{u}_i) + \partial \widehat{g}_i(\widehat{u}_i) + N_{\widehat{U}_i^{\mathrm{ad}}}(\widehat{u}_i) + \widehat{S}_i^* \mu, \quad i \in \{1, \dots, M\}, \tag{18.31a}$$

$$\mu \in N_K(\widehat{S}(\widehat{u})). \tag{18.31b}$$

Any $\widehat{u} \in \widehat{\mathcal{U}}$ that satisfies the above relations is a variational equilibrium of the GNEP. To conclude the first step and streamline the remainder of the proof, let us provide an equivalent system of inclusions that characterize a solution to the jointly convex GNEP. Let $\tilde{d}_1 \colon \widehat{Q} \times \widehat{Q}^{M-1} \to \widehat{Q}^*$ and $\tilde{d}_2 \colon \widehat{Q} \to \widehat{Q}^*$ be such that

$$\begin{aligned}
\left\langle \tilde{d}_1(\widehat{q}_i, q_{-i}), w_i \right\rangle_{\widehat{Q}^*, \widehat{Q}} &= \left(\alpha \sum_{k=1}^{M} \widehat{q}_k^{\mathrm{out}}, w_i^{\mathrm{out}} \right)_{L^2(0,T)}, \\
\left\langle \tilde{d}_2(\widehat{q}_i), w_i \right\rangle_{\widehat{Q}^*, \widehat{Q}} &= \left(\alpha\, \widehat{q}_i^{\mathrm{out}}, w_i^{\mathrm{out}} \right)_{L^2(0,T)}, \\
\langle \tilde{e}, w_i \rangle_{\widehat{Q}^*, \widehat{Q}} &= \left(\beta - \widehat{\alpha} q_0(L), w_i^{\mathrm{out}} \right)_{L^2(0,T)},
\end{aligned}$$

for any $w_i = (w_i^{\mathrm{in}}, w_i^{\mathrm{out}}) \in \widehat{Q}$. Remembering that $\mathcal{Z} \simeq \widehat{\mathcal{U}}^*$, we conclude that the solution set of the system (18.31a)–(18.31b) coincides with the one of

$$0 \in \partial \widehat{g}^p(\widehat{p}_i) + N_{\widehat{P}^{\mathrm{ad}}}(\widehat{p}_i) + M^{-1} \eta^p, \qquad i \in \{1, \dots, M\}, \tag{18.32a}$$

$$\tilde{e} \in \tilde{d}_1(\widehat{q}_i, \widehat{q}_{-i}) + \tilde{d}_2(\widehat{q}_i) + \partial \widehat{g}_i^q(\widehat{q}_i) + N_{\widehat{Q}_i^{\mathrm{ad}}}(\widehat{q}_i) + \eta^q, \qquad i \in \{1, \dots, M\}, \tag{18.32b}$$

$$\mu \in N_K(\widehat{S}(\widehat{u})), \tag{18.32c}$$

$$\begin{pmatrix} \eta^p \\ \eta^q \end{pmatrix} = \widehat{S}_0^* \mu. \tag{18.32d}$$

Step 2. We are interested in the existence of a solution for which the endpoint pressure is the same for all players. For this purpose, we consider the operator equation in the

space $\tilde{\mathcal{U}} := \widehat{P} \times \widehat{Q}^M$. Let $\tilde{\mathcal{L}}\colon \widehat{P} \times \widehat{Q}^M \to \widehat{P} \times \widehat{Q}$ be given by $\tilde{\mathcal{L}}(\tilde{p}, \widehat{q}) = (\tilde{p}, \sum_{i=1}^M \widehat{q}_i)$. The relation between the state variable y and the controls $(\tilde{p}, \widehat{q}) \in \tilde{\mathcal{U}}$ is now given by $\tilde{S}(\tilde{p}, \widehat{q}) := S_{\mathrm{PDE}}(y_0, \widehat{u}^{y_0}) + \widehat{S}_0(\tilde{\mathcal{L}}(\tilde{p}, \widehat{q}))$. The constraint set is $\tilde{C} := \{(\tilde{p}, \widehat{q}) \in \widehat{P}^{\mathrm{ad}} \times \widehat{Q}^{\mathrm{ad}} \mid \tilde{S}(\tilde{p}, \widehat{q}) \in K\}$ with $\widehat{Q}^{\mathrm{ad}} := \prod_{i=1}^M \widehat{Q}_i^{\mathrm{ad}}$. Thanks to the convexity of $\widehat{P}^{\mathrm{ad}}$, Condition (18.26) ensures the non-emptiness of $\tilde{C}$. With $\tilde{\mathcal{Z}} := \widehat{P}^* \times (\widehat{Q}^*)^M$, we associate the operators $\tilde{\mathcal{A}}\colon \tilde{\mathcal{U}} \to \tilde{\mathcal{Z}}$ and $\tilde{\mathcal{B}}\colon \tilde{\mathcal{U}} \rightrightarrows \tilde{\mathcal{Z}}$ with

$$\tilde{\mathcal{A}}(\tilde{p}, \widehat{q}) = \begin{pmatrix} 0 \\ \tilde{d}_1(\widehat{q}_1, \widehat{q}_{-1}) + \tilde{d}_2(\widehat{q}_1) \\ \vdots \\ \tilde{d}_1(\widehat{q}_M, \widehat{q}_{-M}) + \tilde{d}_2(\widehat{q}_M) \end{pmatrix} \quad \text{and} \quad \tilde{\mathcal{B}}(\tilde{p}, \widehat{q}) = \begin{pmatrix} \partial M \widehat{g}^p(\tilde{p}) \\ \partial \widehat{g}_1^q(\widehat{q}_1) \\ \vdots \\ \partial \widehat{g}_M^q(\widehat{q}_M) \end{pmatrix}. \tag{18.33}$$

Our goal is to show existence of a solution to the generalized equation

$$\tilde{\mathbf{e}} \in \tilde{\mathcal{A}}'(\tilde{p}, \widehat{q}) + \tilde{\mathcal{B}}'(\tilde{p}, \widehat{q}) + N_{\tilde{C}}(\tilde{p}, \widehat{q}), \tag{18.34}$$

where $\tilde{\mathbf{e}} := (0, \tilde{e}, \dots, \tilde{e})$ and $\tilde{\mathcal{A}}'$ as well as $\tilde{\mathcal{B}}'$ are defined by identifying the sets $\tilde{\mathcal{A}}(\tilde{p}, \widehat{q})$ and $\tilde{\mathcal{B}}(\tilde{p}, \widehat{q})$ with the corresponding subsets of $\tilde{\mathcal{U}}^*$. Conversely, the operator $\tilde{C}\colon \tilde{\mathcal{U}} \rightrightarrows \tilde{\mathcal{Z}}$ is defined by setting $\tilde{C}(\tilde{p}, \widehat{q})$ to the corresponding subset of $N_{\tilde{C}}(\tilde{p}, \widehat{q})$. We show that the sum $\tilde{\mathcal{A}} + \tilde{\mathcal{B}} + \tilde{C}$ is maximally monotone and start by establishing that $\tilde{\mathcal{A}}$ is monotone and demicontinuous. The latter property is true whenever for any sequence $\{v_n\} \subset \bar{D}\tilde{\mathcal{A}}$ converging strongly to v in $\tilde{\mathcal{U}}$, we have that $\tilde{\mathcal{A}}(v_n)$ converges weakly to $\tilde{\mathcal{A}}(v)$ in $\tilde{\mathcal{Z}}$; see [2, Definition 1.137]. With $z^p \in \widehat{P}$, $z_i^q \in \widehat{Q}$, $z_i^q =: (z_i^{\mathrm{in}}, z_i^{\mathrm{out}})$, and z^q collecting all the z_i^q, we have

$$\begin{aligned} \left\langle \tilde{\mathcal{A}}(\tilde{p}, \widehat{q}), (z^p, z^q) \right\rangle_{\tilde{\mathcal{Z}}, \tilde{\mathcal{U}}} &= \sum_{i=1}^M \left[\left(\alpha \sum_{k=1}^M \widehat{q}_k^{\mathrm{out}}, z_i^{\mathrm{out}} \right)_{L^2(0,T)} + \left(\alpha \widehat{q}_i^{\mathrm{out}}, z_i^{\mathrm{out}} \right)_{L^2(0,T)} \right] \\ &= \left(\sum_{k=1}^M \widehat{q}_k^{\mathrm{out}}, \sum_{i=1}^M \alpha z_i^{\mathrm{out}} \right)_{L^2(0,T)} + \sum_{i=1}^M \left(\widehat{q}_i^{\mathrm{out}}, \alpha z_i^{\mathrm{out}} \right)_{L^2(0,T)}. \end{aligned}$$

As $\alpha \in L^\infty(0,T)$, we have $\alpha z_i^{\mathrm{out}} \in L^2(0,T)$. Then, for any sequence $\{(\tilde{p}_n, \widehat{q}_n)\} \subset \bar{D}\tilde{\mathcal{A}}$ strongly converging to $(\tilde{p}, \widehat{q})$, we have weak convergence of all the terms in the sum above and $\tilde{\mathcal{A}}(\tilde{p}_n, \widehat{q}_n)$ converges weakly to $\tilde{\mathcal{A}}(\tilde{p}, \widehat{q})$. For the monotonicity, as $\widehat{q} \mapsto \tilde{d}_1(\widehat{q}_i, \widehat{q}_{-i})$ is linear, the operator $\tilde{\mathcal{A}}$ is a linear. Taking $z^p = \tilde{p}$ and $z^q = \widehat{q}$ in the previous relation yields

$$\begin{aligned} \left\langle \tilde{\mathcal{A}}(\tilde{p}, \widehat{q}), (\tilde{p}, \widehat{q}) \right\rangle_{\tilde{\mathcal{Z}}, \tilde{\mathcal{U}}} &= \sum_{i=1}^M \left[\left(\alpha \sum_{k=1}^M \widehat{q}_k^{\mathrm{out}}, \widehat{q}_i^{\mathrm{out}} \right)_{L^2(0,T)} + \left(\alpha \widehat{q}_i^{\mathrm{out}}, \widehat{q}_i^{\mathrm{out}} \right)_{L^2(0,T)} \right] \\ &= \left(\alpha \sum_{k=1}^M \widehat{q}_k^{\mathrm{out}}, \sum_{i=1}^M \widehat{q}_i^{\mathrm{out}} \right)_{L^2(0,T)} + \sum_{i=1}^M \left(\alpha \widehat{q}_i^{\mathrm{out}}, \widehat{q}_i^{\mathrm{out}} \right)_{L^2(0,T)}. \end{aligned}$$

Since $\alpha(t) \geq \alpha_{\min} > 0$ for almost all $t \in (0,T)$, we infer that

$$\left\langle \tilde{\mathcal{A}}(\tilde{p},\widehat{q}),(\tilde{p},\widehat{q})\right\rangle_{\tilde{\mathcal{Z}},\tilde{\mathcal{U}}} \geq \alpha_{\min}\|\sum_{i=1}^{M}\widehat{q}_i^{\,\mathrm{out}}\|^2_{L^2(0,T)}+\alpha_{\min}\sum_{i=1}^{M}\|\widehat{q}_i^{\,\mathrm{out}}\|^2_{L^2(0,T)}.$$

As $\tilde{\mathcal{A}}$ has full domain, is monotone and demicontinuous, it is maximally monotone; see [2, Corollary 1.142]. The maximal monotonicity of the sum $\tilde{\mathcal{A}}+\tilde{\mathcal{B}}+\tilde{C}$ follows from the fact that both $\tilde{\mathcal{A}}$ and $\tilde{\mathcal{B}}$ have full domain.

For the existence of a solution to (18.34), we rely on the coercivity of the maximally monotone sum $\tilde{\mathcal{A}}+\tilde{\mathcal{B}}+\tilde{C}$; see [2, Definition 1.138]. By the assumption on the subdifferential of $Mg^p(p)+\sum_{i=1}^{M} g_i^q(q_i)$, namely $\tilde{\mathcal{B}}$, we have the coercivity of the sum $\tilde{\mathcal{B}}+\tilde{C}$. As $\tilde{\mathcal{A}}$ has full domain and is maximally monotone, the sum $\tilde{\mathcal{A}}+\tilde{\mathcal{B}}+\tilde{C}$ is coercive. Now under the isomorphism between $\tilde{\mathcal{Z}}$ and $\tilde{\mathcal{U}}^*$, the operator $\tilde{\mathcal{A}}'+\tilde{\mathcal{B}}'+N_{\tilde{C}}$ is also coercive and maximally monotone. It is well-known that a coercive and maximally monotone operator from a reflexive Banach space to its dual is surjective; see, e.g., [2, Theorem 1.143]. Therefore, there is a solution of the operator equation

$$\mathbf{e}\in(\tilde{\mathcal{A}}'+\tilde{\mathcal{B}}'+N_{\tilde{C}})(u). \tag{18.35}$$

Step 3. Finally, we construct from any solution $(p^\star,q^\star)$ of this generalized equation a solution $u^\star$ of the system (18.31a)–(18.31b) and, thus, of the GNEP. First, since (18.26) holds at $\bar{u}=(\bar{p},\bar{q})$, we infer that with $p':=(\frac{1}{M}\sum_{i=1}^{M}\bar{p}_i)-\widehat{p}^0$ and $q'\in\widehat{Q}^M$ defined as $q_i':=\bar{q}_i-\widehat{q}^0$, the inclusion

$$\tilde{S}(p',q')\in\operatorname{int}K$$

holds and $(p',q')\in\tilde{C}$. Invoking the chain rule for convex subdifferentials, we get that for any $(\tilde{p},\widehat{q})\in\tilde{C}$, we have

$$N_{\tilde{C}}(\tilde{p},\widehat{q})=N_{\widehat{P}^{\mathrm{ad}}\times\widehat{Q}^{\mathrm{ad}}}(\tilde{p},\widehat{q})+\tilde{\mathcal{L}}^*\widehat{S}_0^*N_K(\tilde{S}(\tilde{p},\widehat{q})).$$

Let $\mu^\star\in N_K(\tilde{S}(p^\star,q^\star))$ be such that the inclusion (18.35) holds. With $\eta^\star:=\widehat{S}_0^*\mu^\star$, we get $(\eta^p)^\star\in\widehat{P}^*$ and $(\eta^q)^\star\in\widehat{Q}^*$ from $\eta^\star$. Then, from (18.35) we obtain that

$$0\in\partial M\widehat{g}^p(p^\star)+N_{\widehat{P}^{\mathrm{ad}}}(p^\star)+(\eta^p)^\star$$

holds. Since $\partial M\widehat{g}^p(p^\star)=M\partial\widehat{g}^p(p^\star)$, the following inclusion is satisfied:

$$0\in\partial\widehat{g}^p(p^\star)+N_{\widehat{P}^{\mathrm{ad}}}(p^\star)+M^{-1}(\eta^p)^\star. \tag{18.36}$$

We define $u^\star\in\widehat{U}^{\mathrm{ad}}$ by setting $u_i^\star:=(p^\star,q_i^\star)$ and since $\tilde{S}(p^\star,q^\star)=S(u^\star)$ by construction, we have $\mu^\star\in N_K(S(u^\star))$. Using the definition of the operators in (18.33) and of $\tilde{\mathcal{L}}$, for all $i\in\{1,\dots,M\}$ we get

$$0\in\tilde{d}_1(q_i^\star,q_{-i}^\star)+\tilde{d}_2(q_i^\star)+\partial\widehat{g}_i^q(q_i^\star)+N_{\widehat{Q}_i^{\mathrm{ad}}}(q_i^\star)+(\eta^q)^\star. \tag{18.37}$$

Since $\mu^\star\in N_K(S(u^\star))$, $\eta^\star=\widehat{S}_0^*\mu^\star$, and (18.36)–(18.37) hold for all $u_i^\star$, we infer that $u^\star$ satisfies (18.32). □

Corollary 18.1 *Given an initial state $(p_0, q_0) \in Y_0^{\mathrm{ad}}$, consider the GNEP formed by the collection of problems of the form* (18.4)*. Suppose that for each firm i, the functional $\mathcal{R}_i(p_i, q_i) = \mathcal{R}_i^q(q_i) + \mathcal{R}^p(p_i)$ with both $\mathcal{R}_i^q : Q \to \mathbb{R}$ and $\mathcal{R}^p : P \to \mathbb{R}$ being lower semicontinuous, proper and convex with subdifferentials having full domain. We set*

$$Q_i^{\mathrm{ad}} = \{(q^{\mathrm{in}}, q^{\mathrm{out}}) \in Q \mid q_0(0) = Mq^{\mathrm{in}}(0),\ q_0(L) = Mq^{\mathrm{out}}(0),\ \int_0^T q^{\mathrm{out}}(t) - q^{\mathrm{in}}(t)\,\mathrm{d}t \le 0,\ 0 \le q^{\mathrm{in}} \le \bar{q}_i^{\mathrm{in}},\ 0 \le q^{\mathrm{out}} \le \bar{q}\ \textit{a.e. in}\ (0,T)\}$$

and

$$P^{\mathrm{ad}} = \{(p^{\mathrm{in}}, p^{\mathrm{out}}) \in P \mid \underline{p} \le p^{\mathrm{in}}, p^{\mathrm{out}} \le \bar{p},\ p_0(0) = p^{\mathrm{in}}(0)\ \textit{and}\ p_0(L) = p^{\mathrm{out}}(0)\}.$$

Assume that there exists $\bar{u} \in \prod_{i=1}^M (P^{\mathrm{ad}} \times Q_i^{\mathrm{ad}})$ such that $S(\bar{u}) \in \operatorname{int} K$ holds. Suppose that the subdifferential of the sum $M\mathcal{R}^p(p) + \sum_{i=1}^M \mathcal{R}_i^q(q_i)$, when restricted to $P^{\mathrm{ad}} \times \prod_{i=1}^M Q_i^{\mathrm{ad}}$, is coercive. Then, there exists a variational equilibrium to the GNEP with all pressures p_i being identical.

Proof. To fit into the format of (18.24), we let

$$g_i(u_i) = \int_0^T c_i(t)\, q_i^{\mathrm{in}}(t)\,\mathrm{d}t + \mathcal{R}_i(u_i)$$

and note that all the hypotheses are satisfied. □

Remark 18.1 The existence of feasible controls satisfying (18.26) is automatically given whenever the initial state y_0 is a stationary solution satisfying the bound constraints and there exists feasible controls to satisfy the injection requirements given in (18.25b). The coercivity condition is satisfied whenever the feasible set of each agent is bounded. Otherwise, like in our test instance, this condition is satisfied whenever each feasible set is bounded in the L^2 sense and each $\mathcal{R}$ is the square of the L^2 norm of the weak time derivative; see (18.43) below.

Remark 18.2 For the existence of a variational equilibrium, the mild Slater condition (18.26), involving all players' decisions, needs to hold. If one seeks a stronger characterization of the solution set of the GNEP, so that any variational equilibrium is a solution of System (18.31a)–(18.31b), then we need both (18.28) and (18.30) to hold with equality. For this, a sufficient condition is that for all i, and any feasible $\widehat{u}_{-i}$, there exists $\widehat{u}_i \in \widehat{U}_i^{\mathrm{ad}}$ such that

$$\widehat{S}(\widehat{u}_i, \widehat{u}_{-i}) \in \operatorname{int} K,$$

which is much more stringent.

Furthermore, if the producers have the same feasible sets and cost functionals, then a solution to the GNEP can be constructed from the solution to an optimization problem. We refer to this case as the *symmetric case*. Note that this is a simplified but not a trivial

setting since this symmetric case does not necessarily lead to symmetric equilibria; see, e.g., [32].

Proposition 18.3 *Consider the GNEP of Theorem 18.1 with a given initial state y_0 and assume that the players' problems are identical. Suppose that all the assumptions of Theorem 18.1 hold, except for the boundedness of the P^{ad} and Q^{ad}. Let $Q^{\mathrm{ad}}_{\mathrm{opt}} := MQ^{\mathrm{ad}}$ and suppose that there exists $\bar{u} \in P^{\mathrm{ad}} \times Q^{\mathrm{ad}}_{\mathrm{opt}}$ such that $S(\bar{u}) \in \operatorname{int} K$ holds. Then, a variational equilibrium of the GNEP can be constructed from any solution of the optimization problem*

$$\begin{aligned} \min_{u \in U} \quad & \int_0^T \left(\frac{M+1}{2M} \alpha(t) q^{\mathrm{out}}(t) - \beta(t) \right) q^{\mathrm{out}}(t) \, \mathrm{d}t + g(u) \\ \text{s.t.} \quad & u \in P^{\mathrm{ad}} \times Q^{\mathrm{ad}}_{\mathrm{opt}}, \quad S(u) \in K, \end{aligned} \tag{18.38}$$

where $g(p,q) = Mg^p(p) + Mg^q_i(M^{-1}q)$.

Proof. We use the same functional analytic setting as in the proof of Theorem 18.1 and we also perform the change of variables $\widehat{p} := p - \widehat{p}^0$ and $\widehat{q} := q - \widehat{q}^0$ with $\widehat{p}^0(t) := (p_0(0), p_0(L))$ and $\widehat{q}^0(t) := (q_0(0), q_0(L))$ for all $t \in [0,T]$. We also use the same functional analytic setting as in the previous proof. The space $\widehat{Q}^{\mathrm{ad}}_{\mathrm{opt}}$ is defined as $\{\widehat{q} \in \widehat{Q} \mid \widehat{q} + \widehat{q}^0 \in Q^{\mathrm{ad}}_{\mathrm{opt}}\}$. We show that any $(\widehat{p}, \widehat{q})$ satisfying the first-order optimality condition of this problem can be used to construct an element $\widehat{u} \in \widehat{P} \times \widehat{Q}$ satisfying the first-order optimality condition (18.34). From basic results of convex analysis, we have $\partial_{\widehat{q}} \widehat{g}(\widehat{p}, \widehat{q}) = \partial g^q_i(M^{-1}(\widehat{q} + \widehat{q}^0))$. Recall that $\widehat{\alpha} = (1 + M^{-1})\,\alpha$. The revenue part $\widehat{r}_{\mathrm{opt}} \colon L^2(0,T) \to \mathbb{R}$ of the objective functional with the shifted variables reads

$$\widehat{r}_{\mathrm{opt}}(\widehat{q}^{\mathrm{out}}) = \int_0^T \left[\frac{1}{2} \widehat{\alpha}(t) \widehat{q}^{\mathrm{out}}(t) - \beta(t) + \frac{1}{2} \widehat{\alpha}(t) q_0(L) \right] \left[\widehat{q}^{\mathrm{out}}(t) + q_0(L) \right] \, \mathrm{d}t.$$

It is Fréchet differentiable and its gradient is given by

$$\nabla \widehat{r}_{\mathrm{opt}}(\widehat{q}^{\mathrm{out}}) = \widehat{\alpha} \widehat{q}^{\mathrm{out}} + \widehat{\alpha} q_0(L) - \beta.$$

With the assumptions on the cost function and the fact that Slater's CQ holds, any solution of the optimization problem satisfies

$$\begin{aligned} 0 &= M \partial g^p(p^\star) + \zeta_p + \eta^p, \\ \tilde{e} &= \begin{pmatrix} 0 \\ \alpha\,(1 + M^{-1})(q^{\mathrm{out}})^\star \end{pmatrix} + \partial g^q_i(M^{-1}(q^\star + \widehat{q}^0)) + \zeta_q + \eta^q, \end{aligned}$$

where $\zeta_p \in N_{\widehat{P}^{\mathrm{ad}}}(p^\star)$, $\zeta_q \in N_{\widehat{Q}^{\mathrm{ad}}_{\mathrm{opt}}}(q^\star)$, $\mu \in N_K(\widehat{S}(u^\star))$, (η^p, η^q) are obtained from $\widehat{S}^*_0 \mu$ and $\tilde{e}$ satisfies $\langle \tilde{e}, w_i \rangle_{\widehat{Q}^*, \widehat{Q}} = \left(\beta - \widehat{\alpha} q_0(L), w_i^{\mathrm{out}}\right)_{L^2(0,T)}$ for any $w_i = (w_i^{\mathrm{in}}, w_i^{\mathrm{out}}) \in \widehat{Q}$. Note that $\tilde{\zeta}_p := M^{-1} \zeta_p$ also belongs to $N_{\widehat{P}^{\mathrm{ad}}}(p^\star)$. Now let $\widehat{q}_i = M^{-1} q^\star$ and $\widehat{\mathbf{q}}$ collects all $\widehat{q}_i$. Then, after some algebraic manipulations, we get that the following holds:

$$0 = \partial g^p(p^\star) + \tilde{\zeta}_p + M^{-1}\eta^p,$$
$$\tilde{e} = \begin{pmatrix} 0 \\ \alpha \sum_k \widehat{q}_k^{\text{out}} + \alpha \widehat{q}_i^{\text{out}} \end{pmatrix} + \partial g_i^q(\widehat{q}_i + M^{-1}\widehat{q}^0) + \zeta_q + \eta^q.$$

Note that $g_i^q(\widehat{q}_i + M^{-1}q_0(L)) = \widehat{g}_i^q(\widehat{q}_i)$ holds by the definition of the latter function. Since $\widehat{S}(u^\star) = \tilde{S}(p^\star, \widehat{\mathbf{q}})$, we have $\mu \in N_K(\tilde{S}(p^\star, \widehat{\mathbf{q}}))$. Then, one can see that for all i, the generalized equation (18.32) holds with $u_i = (p^\star, \widehat{q}_i)$. Therefore, the strategy profile $u = (u_1, \ldots, u_M)$ is a variational equilibrium of the GNEP. □

Existence of a solution of the optimization problem (18.38) is easily obtained using classical arguments. The feasible set is a non-empty, convex, and closed subset of a reflexive Banach space. In addition to the hypotheses of Proposition 18.3, assume that

$$\lim_{\|u\| \to +\infty} g(u) + \delta_{P^{\text{ad}} \times Q_{\text{opt}}^{\text{ad}}}(u) = +\infty.$$

This ensures that the level sets of the objective functional are bounded over the feasible set. The objective functional is also proper lower semicontinuous and convex with full domain. Then, there exists a minimizer; see, e.g., [2, Theorem 2.11].

18.5 Test Cases: The Influence of Linepacking on Market Outcomes

The dynamics of transport in networks, as formalized in our analysis, capture important intertemporal aspects that are highly relevant in real-world market interactions. One important example arises in gas markets, where transport dynamics enable the network itself to function as a temporal storage device—a phenomenon referred to as linepacking. The importance of linepacking in the operation of real-world gas transport is documented, for instance, in [26, Page 212]. It has been estimated that for, e.g., the Great Britain national gas transmission system, the average hourly linepack stores energy of about 3743 GWh, but that the available linepack flexibility varies widely over the year [38]. In that study, the available within-day flexibility of the transmission system ranged from 13 GWh to 427 GWh.

In what follows, based on a stylized numerical test example, we use our framework to illustrate how the ability of linepacking can influences market outcomes in gas markets. Specifically, we investigate how linepacking is used for storage by market participants and who benefits to which degree.

To this end, we consider M identical and strategically acting firms that trade natural gas, which is transported over a single pipe. The time horizon of 4 h is split into two periods of 2 h each. Purchase cost $c(t)$ and inverse demand $P(t, q(t)) = \beta(t) + \alpha(t)q(t)$ do not change within each period. With $i \in \{1, 2\}$, we use c_i, α_i, and β_i to denote their values, which are given by

$$c(t) = \begin{cases} 388.8, & t \in [0, 2\,\text{h}), \\ 432.0, & t \in [2\,\text{h}, 4\,\text{h}]. \end{cases}$$

$$\alpha(t) = \begin{cases} -16.6, & t \in [0, 2\,\mathrm{h}), \\ -20.7, & t \in [2\,\mathrm{h}, 4\,\mathrm{h}], \end{cases}$$

$$\beta(t) = \begin{cases} 1500.8, & t \in [0, 2\,\mathrm{h}), \\ 2000.3, & t \in [2\,\mathrm{h}, 4\,\mathrm{h}], \end{cases}$$

The purchase cost of gas is 10 % cheaper in the first period and the inverse demand function $P(t, q(t))$ reflects higher demand in the second period. This choice of parameters thus incentivizes producers to use the pipe as a temporal storage for the gas acquired in the first period for its use in the second one to reduce the overall costs. Taking piecewise constant data allows us, moreover, to easily formulate a "static" counterpart of the considered scenario. For this counterpart, we associate a mass flow q_i and boundary pressures $(p_i^{\mathrm{in}}, p_i^{\mathrm{out}})$ for each period. We consider the flow to be stationary and that each triple $(q_i, p_i^{\mathrm{in}}, p_i^{\mathrm{out}})$ satisfies the Weymouth equation as a stationary approximation of gas flow in a pipe. Our choice of parameters ensures that no congestion occurs for the stationary flow. In the stationary case, this implies that the bounds on pressure and mass flow do not influence the market outcomes. As we will see, however, these bounds play an important role in the instationary model.

The physical parameters of the instance, inspired by [34], are as follows: The pipe has length $L = 50\,\mathrm{km}$, a cross-sectional diameter $D = 0.5\,\mathrm{m}$, a slope angle $\varphi = 0$, and its wall has a roughness $k = 1 \times 10^{-4}\,\mathrm{m}$. The gas temperature is $T_{\mathrm{emp}} = 15\,^{\circ}\mathrm{C}$, its molar mass is and $m = 0.016\,043\,\mathrm{kg\,mol^{-1}}$. The latter two values are those for methane, which usually dominates the composition of natural gas. With $R = 8.3145\,\mathrm{J\,mol^{-1}\,K^{-1}}$ being the universal gas constant, the specific gas constant $R_{\mathrm{s}} := R/m$ has value $518.26\,\mathrm{J\,kg\,K^{-1}}$. The friction coefficient is modeled using the formula by Nikuradse, i.e., $\lambda = (2\log_{10}(\frac{D}{k}) + 1.138)^{-2}$; see Page 25 in [26] for a discussion of this model.

The initial state is assumed to be stationary and is given by $q_0 = 48.289\,\mathrm{kg\,s^{-1}}$ and the pressure at the entry node being 50 bar. Remember that the pressure and mass flow admit, in a pointwise sense, upper $(\bar{p}, \bar{q})$ and lower $(\underline{p}, \underline{q})$ bounds in the pipe. The values for the last three bounds are fixed to

$$\underline{p} = 40\,\mathrm{bar}, \quad \underline{q} = 10.9\,\mathrm{kg\,s^{-1}}, \quad \bar{q} = 163\,\mathrm{kg\,s^{-1}}.$$

The value of $\bar{p}$ directly influences the maximal linepack capability in our setup and, thus, we will vary it in our test cases. By using the ideal gas law $p = c_{\mathrm{s}}^2\rho$, the total amount of gas in the pipe linearly depends on the integral of the pressure profile over the pipe. Thus, pressure is the variable we monitor when studying linepack effects. In our setup, we vary $\bar{p}$ in the range of $[50.1, 70.0]$ bar.

With this calibration, we solve the model described in (18.4). More precisely, we are in the setting of Proposition 18.3. The specific discretization of the PDE system (18.1) is described in Appendix C. To keep the presentation focused on the actual results, we moved the detailed problem formulations for this test case to Appendix B. There, we also present the modeling environments and solvers used for the computations.

Let us first present the time evolution of the physical quantities in the case of 3 firms. We start with the evolution of the mass flows at the endpoints of the pipe as shown in Fig. 18.1. For most parts of the time horizon, the output q^{out} is constant but has rather

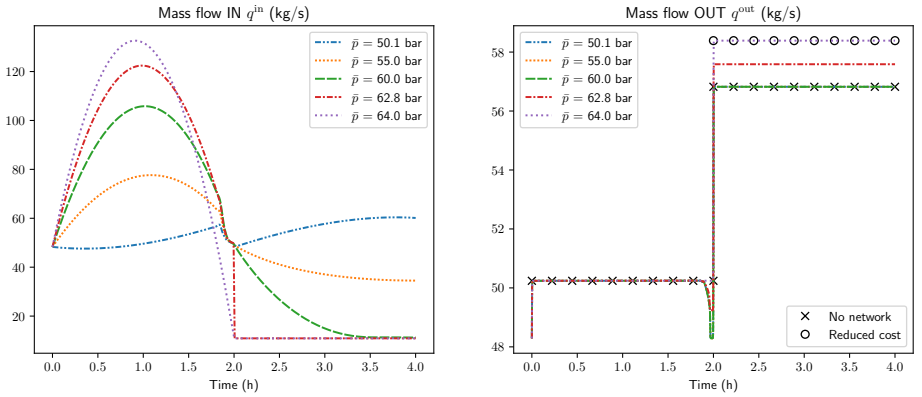


Fig. 18.1: Mass flow boundary controls q^{in} and q^{out} for different values of the upper pressure bound $\bar{p}$. On the right figure, the crosses indicate the optimal flow given by the static model. The circles indicate the optimal mass flow during the second period with the cost of gas being c_1 rather than c_2 also for the static model.

different values in each period. Each value is very close to the one obtained by the static model, which is indicated by the crosses in the figure. Two transitions are present: (i) at the beginning from the initial state to the desired output value and (ii) at the interface of the two time periods at $t = 2$ h. The latter has a drop in the outflow, which we will discuss later. The evolution of q^{in} is distinct for each value of $\bar{p}$. The general trend is that when $\bar{p}$ increases, more gas is injected during the first period and less during the second one. This leads to the situation that only the minimum amount $\underline{q}$ is injected during or towards the end of the second period. The exception to this behavior is for $\bar{p} = 50.1$ bar, where the ability to steer the system from one operational point to another one is difficult due to the small gap between the initial pressure and its upper bound.

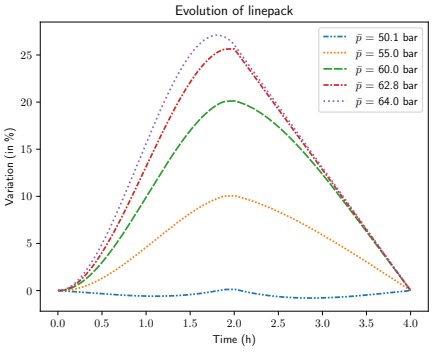


Fig. 18.2: Evolution of the linepack (total mass of gas in the pipe). The instance is the same as in Fig. 18.1.

In Fig. 18.2, the evolution of the linepack relative to its initial value is displayed. Except for $\bar{p} = 50.1$ bar, the curves are similar with an increase in the first period, leading to a maximum around the switching time of 2 h, which is finally followed by an almost linear decrease. A higher value of $\bar{p}$ leads to a higher linepack peak. Any value $\bar{p}$ greater than 64 bar yields the same result for this instance. As mentioned before, the linepack is related to the pressure profile in the pipe. Figure 18.3 displays the values

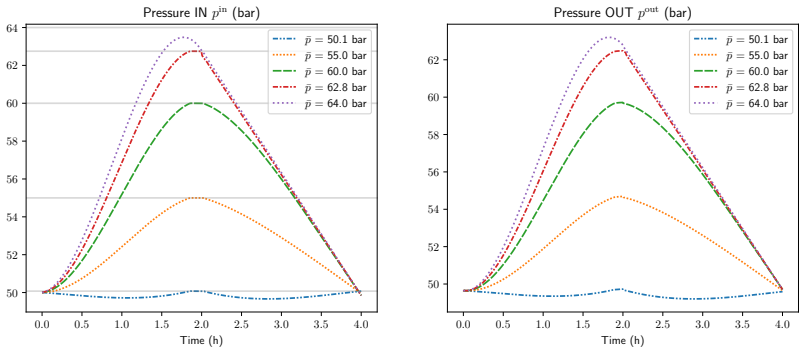


Fig. 18.3: Evolution of the pressure at the endpoints. The instance is the same as in Fig. 18.1.

of p^{in} and p^{out} over the time horizon. For a given $\bar{p}$, these pressures evolve similarly except for the period just before $t = 2$ h. Except for $\bar{p} = 64$ bar, p^{in} reaches a plateau close to its upper bound. Note that this is not the case for p^{out} or the linepack, which is due to the drop in q^{out} for this short time interval, leading to a higher linepack. This drop disappears when the upper pressure constraint is not active; see, e.g., the plot for $\bar{p} = 64$ bar.

We now move on to the economical interpretation of these results. First, note that the cost and demand structure indeed incentivizes linepacking. The case $\bar{p} = 50.1$ bar is an exception since the physical constraints appear to be too tight—remember that $p^{\text{in}}(0) = 50$ bar—so that linepacking is not observed to a significant degree. There, the transition between the different desired output values drives the decisions. With $\bar{p}$ large enough, the quantity of gas stored during the first period covers the amount sold during the second one with $q^{\text{in}}(t) = \underline{q}$ for $t \in [2\,\text{h}, 4\,\text{h}]$. If more gas can be stored, this leads to an increased value of q^{out}. This lasts until q^{out} reaches the solution of the static problem with purchase cost c_1 rather than c_2; see the results for $\bar{p} = 64$ bar. Then, a further increase in the linepack ability does not yield any change.

Next, we look at the price of gas at the output node as shown in Fig. 18.4. There, as a reference, we display the purchase cost $c(t)$ and static strategic prices given by $c(t) + \beta M^{-1} q^{\text{out}}(t)$. These would occur if firms choose standard strategic markups for a given $q^{\text{out}}(t)$. Again, the two transitions induce price variations. Furthermore, the discontinuity of P at $t = 2$ h leads to a jump in prices. For low and moderate linepack capability, i.e., $\bar{p} \in \{50.1, 55.0, 60.0\}$ bar, pricing apparently takes place based on the current purchase cost c. Firms, rather than consumers, benefit from savings due to

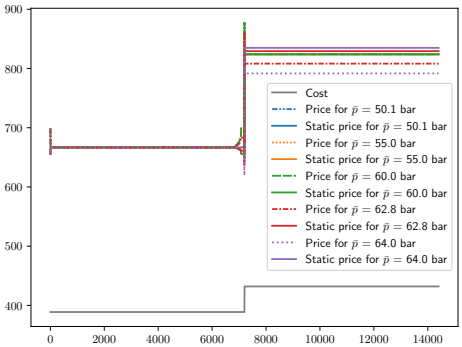


Fig. 18.4: Evolution of the "static" and actual price at the output node. The instance is the same as in Fig. 18.1.

linepacking. When the storage capacity is large, i.e., $\bar{p} \in \{62.8, 64.0\}$ bar, we observe a significant decrease of consumer prices. In these cases, the firms can purchase all the gas that they plan to sell minus the minimum amount induced by $\underline{q}$. The static price prediction, as the relevant marginal purchase cost, is not only determined by the purchase cost c_2 but also takes into account c_1. If the upper pressure bound is never active, then c_1 is the only relevant purchase cost for the entire time horizon. Market prices in hours 2 to 4 are then also based on c_1 only.

To further understand how the market participants benefit from additional linepack ability, we look at the evolution of the aggregated firms' profits, the consumer surplus, and the overall welfare over time if $\bar{p}$ varies in $[51, 70]$ bar. In addition to the case of 3 firms, we solved the same instance in the case of perfect competition. To better see the different occurring effects, we split the overall firms profit into three components:

$$\begin{aligned}
&\int_0^{4\,\mathrm{h}} \left(P(t, q^{\mathrm{out}}(t)) q^{\mathrm{out}}(t) - c(t) q^{\mathrm{in}}(t) \right) \mathrm{d}t \\
&= \int_0^{4\,\mathrm{h}} \left(q^{\mathrm{out}}(t) - q^{\mathrm{in}}(t) \right) c(t)\, \mathrm{d}t \\
&\quad + \int_0^{4\,\mathrm{h}} \left(\alpha M^{-1} q^{\mathrm{out}}(t) \right) q^{\mathrm{out}}(t)\, \mathrm{d}t \\
&\quad + \int_0^{4\,\mathrm{h}} \left(P(t, q^{\mathrm{out}}(t)) - \left(\alpha M^{-1} q^{\mathrm{out}}(t) + c(t) \right) \right) q^{\mathrm{out}}(t)\, \mathrm{d}t \\
&=: \boxed{\text{linepack savings}} + \boxed{\text{static strategic profits}} + \boxed{\text{network rent}}.
\end{aligned} \tag{18.39}$$

The first term captures the reduction in total purchase cost thanks to linepacking that allows them to separate purchase and selling time. Next, we have profits obtained by the exercise of static market power. Last, the network rent captures the impact of the network on market prices. These are defined as the earnings obtained from the difference between the observed market price and the static price. In Fig. 18.5, the welfare and its two components are displayed. We can observe that there are two

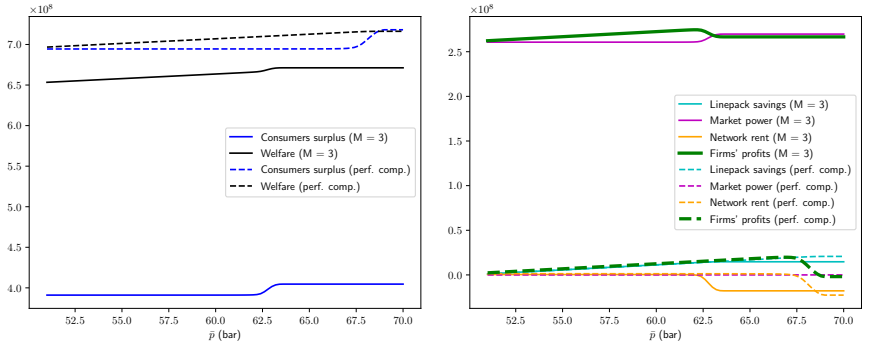


Fig. 18.5: Aggregated consumer surplus and welfare (left) and firms' profits partitioned in components (right) for the test instance in the case of 3 producers and under perfect competition.

different regimes with different solution structures: Low linepacking ability and high linepacking ability. As seen in Fig. 18.5 (left), if the linepacking ability is low, the consumer surplus remains constant, while the welfare increases with $\bar{p}$. This implies that firms' profits become larger, which is confirmed in Fig. 18.5 (right), where we see that the linepack savings are increasing. This structure of the solution stays the same for linepack abilities below a threshold of around $\bar{p} = 62$ bar for 3 firms and $\bar{p} = 67$ bar for the case of perfect competition. With $\bar{p}$ above these values, the structure of the solution changes. In those cases additional linepack capability increases the availability of cheaper gas. As discussed previously, the market price in the second period is then based on both c_1 and c_2. From this, the consumers benefit and their surplus increases, leading to higher welfare values. Finally, for very high linepack capability, purchase cost c_2 does no longer influence the market price at all, but it is exclusively determined based on the lower purchase cost c_1, inducing lower market prices in the second period. This beneficial effect of linepacking, inducing lower market prices is observed for a larger range of linepack capabilities in case of strategically acting firms rather than for the perfectly competitive case. This is due to the fact that strategically behaved firms in general tend to sell less gas and smaller linepack capabilities allow to fully cover all sales by period 1 purchases. As a consequence of the drop in market prices for large linepack capabilities we observe a drop of firms profits in those cases, which is caused by network rents becoming negative in those cases; see Fig. 18.5 (right). By looking at its definition in (18.39), it is clear that as soon as the market price drops during the second period, this quantity becomes negative. As firms are forced to purchase a minimum amount of gas for all points in time t ($q^{\text{in}}(t) \geq \underline{q}$) in the case of perfect competition, the firms' overall profit even becomes negative for large $\bar{p}$.

We have thus seen that our setup is suitable to analyze dynamic network transport in a market environment and thus contributes to the understanding of phenomena such as linepacking, which is highly important in the context of gas markets. We are able to analyze how the ability of linepacking can influence market outcomes in gas markets and which market participants benefit to which degree. Interestingly, for low linepacking

capabilities mainly firms can increase their profits due to an improved purchase cost structure. This reverts in case of high linepack capabilities where reduced market prices induce a significant increase of consumer surplus.

18.6 Conclusion

We investigated a stylized market situation in which strategic suppliers transport and sell a commodity (e.g., natural gas or hydrogen) to consumers. This has been modeled as a GNEP in which the evolution equations for the gas flow are shared constraints. We showed the well-posedness of this system of PDEs with a solution regular enough to ensure the existence of Lagrange multipliers. Then, we proved the existence of a variational equilibrium of the GNEP, which is consistent with the continuity of pressures at the nodes. When producers are identical, we identified an equivalent optimization problem in the sense that a variational equilibrium can be constructed from any solution to the latter. We illustrated the insights gained via such a PDE model compared to a static one. In particular, we highlighted how linepacking impacts the market outcomes and determined who benefits from additional linepacking ability. For this purpose, we considered a simple instance in which the time horizon is split into two periods and gas is cheaper during the first one. While the quantity of gas sold is most of the time close to the solution of the static problem, the inflow is rather different and changes with the linepacking ability. Indeed, the producers seek to reduce their overall cost by storing cheap gas as much as possible in the pipe. There, linepacking only benefits the producers and this lasts until it is possible to store enough gas to cover the sale of the second period while fulfilling the flow constraints. Then, the amount sold during that time interval increases until it reaches the value given by the solution of the static problem for the second period, but with the cost of the first one. This indicates a decoupling between injection and withdrawal of gas from the pipe and induces an increase of the consumer surplus as well as a decrease of the firms' profit, while the overall welfare is still increasing.

These results encourage further investigation of such models. On the one hand, other models for the evolution of the gas flow can be considered; see, e.g., [12]. In this case, the shared constraint consists of a semilinear system of hyperbolic PDEs. On the other hand, one can depart from the deterministic setting and investigate the market outcomes when uncertainties are present. These could originate either from the physical model, where, e.g., the friction coefficient is unknown, or from the economical data such as demand or supply.

A Fundamental Results

In this section, we review some fundamental results from convex optimization and the theory of PDEs. For our work, we need to prove that our problems have solutions of high regularity (see Sect. 18.3) to ensure the existence of multipliers of the state

constraints. For this, we need to review some results from PDE theory, starting with the Aubin–Lions lemma.

Lemma 18.5 (Aubin–Lions lemma; [36, Corollary 4]) *Let X_0, X, and X_1 be three Banach spaces with $X_0 \subseteq X \subseteq X_1$. Suppose that X_0 is compactly embedded in X and that X is continuously embedded in X_1. For $1 \leq p, q \leq +\infty$, let*

$$W := \{u \in L^p(0,T;X_0) \mid u_t \in L^q(0,T;X_1)\}.$$

(i) If $p < +\infty$, then the embedding of W into $L^p(0,T;X)$ is compact.
(ii) If $p = +\infty$ and $q > 1$, then the embedding of W into $C([0,T];X)$ is compact.

We use this lemma with $X_0 = H_0^1(\Omega)^2$, $X = C(\bar{\Omega})^2$, and $X_1 = H^{-1}(\Omega)^2$. The proof of additional regularity of the solution to the PDE system uses the Ladyzhenskaya–Sobolevski inequality for the Laplacian. For convenience, we provide a proof of this result and also state its main ingredient: the interpolation inequalities of Gagliardo–Nirenberg.

Lemma 18.6 (Interpolation inequalities of Gagliardo–Nirenberg; [5, p. 234]) *Let I be an open and bounded interval. Then, there exists a constant $C > 0$ such that for any $v \in H^2(I)$, we have*

$$\|\nabla v\|_{L^2(I)} \leq C\|v\|_{H^2(I)}^{1/2}\|v\|_{L^2(I)}^{1/2}, \tag{18.40}$$

and for a given $\kappa > 0$, there exists C_κ such that

$$\|\nabla v\|_{L^2(I)} \leq \|v\|_{H^1(I)} \leq \kappa\|v\|_{H^2(I)} + C_\kappa\|v\|_{L^2(I)}. \tag{18.41}$$

We can now state and prove the Ladyzhenskaya–Sobolevski inequality for the Laplacian.

Lemma 18.7 (Ladyzhenskaya–Sobolevski inequality for Δ) *Let I be an open and bounded interval. Then, there exists a constant $C > 0$ such that for all $v \in H^2(I)$, we have*

$$(\Delta v, \Delta v)_{L^2(I)} \geq \frac{1}{2}\|v\|_{H^2(I)}^2 - C\|v\|_{L^2(I)}^2.$$

Proof. From Inequality (18.40) in Lemma 18.6, we have

$$\|\nabla v\|_{L^2(I)}^2 \leq C'\|v\|_{H^2(I)}\|v\|_{L^2(I)}.$$

Using Cauchy's inequality, there exists $C'' > 0$ such that

$$\|\nabla v\|_{L^2(I)}^2 \leq \frac{1}{2}\|v\|_{H^2(I)}^2 + C''\|v\|_{L^2(I)}^2$$

holds and by further using the definition of the H^2-norm as well as by rearranging terms, we obtain

$$\|\Delta v\|^2_{L^2(I)} \geq \|\nabla v\|^2_{L^2(I)} + \|v\|^2_{L^2(I)} - 2(C'' + 1)\|v\|^2_{L^2(I)},$$
$$2\|\Delta v\|^2_{L^2(I)} \geq \|v\|^2_{H^2(I)} - 2(C'' + 1)\|v\|^2_{L^2(I)}.$$

Finally, we get

$$(\Delta v, \Delta v)_{L^2(I)} \geq \frac{1}{2}\|v\|^2_{H^2(I)} - (C'' + 1)\|v\|^2_{L^2(I)}. \qquad \square$$

B Optimization Models Used for the Test Instance

In Sect. 18.5, all producers are identical. In this case, we can solve the optimization problem given in Proposition 18.3. Remember that the price functional in the symmetric case is given by

$$\tilde{P}(t, q(t)) = \beta(t) - \frac{M+1}{2M}\alpha(t)\, q(t).$$

With $u = (q^{\text{in}}, q^{\text{out}}, p^{\text{in}}, p^{\text{out}})$, the optimization problem associated with the symmetric case reads

$$\max_{u \in H^1(0,T)^4} \int_0^T \left(\tilde{P}\big(t, q^{\text{out}}(t)\big)\, q^{\text{out}}(t) - c(t) q^{\text{in}}(t)\right) \mathrm{d}t - \mathcal{R}(p, q, u) \tag{18.42a}$$

$$\text{s.t.} \quad p_t - \varepsilon p_{xx} + \frac{c_s^2}{A} q_x = 0 \quad \text{in } (0, L) \times (0, T), \tag{18.42b}$$

$$q_t - \varepsilon q_{xx} + A p_x = -\frac{1}{2}\sigma A \left(\frac{2\check{q}}{\check{p}} q - \frac{\check{q}^2}{\check{p}^2} p\right) \quad \text{in } (0, L) \times (0, T), \tag{18.42c}$$

$$p(0, \cdot) = p^{\text{in}}, \quad p(L, \cdot) = p^{\text{out}} \quad \text{in } (0, T), \tag{18.42d}$$

$$q(0, \cdot) = q^{\text{in}}, \quad q(L, \cdot) = q^{\text{out}} \quad \text{in } (0, T), \tag{18.42e}$$

$$p(\cdot, 0) = p_0, \quad q(\cdot, 0) = q_0 \quad \text{in } (0, L), \tag{18.42f}$$

$$\underline{p} \leq p \leq \bar{p}, \quad \underline{q} \leq q \leq \bar{q} \quad \text{in } [0, L] \times [0, T], \tag{18.42g}$$

$$p_0(0) = p^{\text{in}}(0), p_0(L) = p^{\text{out}}(0), q_0(0) = q^{\text{in}}(0), q_0(L) = q^{\text{out}}(0), \tag{18.42h}$$

$$\int_0^T q^{\text{out}}(t) - q^{\text{in}}(t)\, \mathrm{d}t \leq 0. \tag{18.42i}$$

Thanks to the regularity of the solution to the system in (18.42b)–(18.42f), any feasible (boundary) controls also satisfy the same bounds as in (18.42g) pointwise in time. As in our instance the lower and upper bounds at the nodes are identical to the ones in the pipe, we do not add explicit bounds at the nodes. The compatibility conditions between the initial state and the decision variables are given in (18.42h). Remember that Inequality (18.42i) ensures that the market participants do not get gas for free out of the initial state. The regularization functional $\mathcal{R}$ has the structure

$$\mathcal{R}(p, q, u) = \gamma_1^p \|\nabla p^{\text{in}}\|^2_{L^2(0,T)^2} + \gamma_1^q \|\nabla q^{\text{in}}\|^2_{L^2(0,T)^2} + \eta_1 \|\nabla q(\cdot, T)\|^2_{L^2(\Omega)} \tag{18.43}$$

with non-negative coefficients. By the regularity of the solution, we have $q \in C([0,T];H^1(\Omega))$, which ensures that $\nabla q(\cdot,T) \in L^2(\Omega)$. The last term aims at avoiding unrealistic final states. For any sequence $u_n \in H^1(0,T)^4$ such that $\|\nabla u_n\|_{L^2(0,T)^4} \to +\infty$, we have $\lim \mathcal{R}(S(u_n),u_n) = +\infty$. As any feasible control of Problem (18.42) is bounded in $L^2(0,T)^4$, the level sets of the objective functional are bounded. The latter is also lower semicontinuous, proper, and its subdifferential has full domain. Furthermore, the feasible set is non-empty, closed, and convex. Thus, there exists a solution of Problem (18.42). In order to discretize System (18.42), we use a discretization scheme that is motivated by analogous schemes for the semilinear Euler equations; for details, see Appendix C. It better captures the problem structure than a generic discretization scheme for parabolic PDE.

Problem (18.42) is parametric in the linearization point $(\check{p},\check{q})$. Inspired by sequential programming approaches, we seek a tuple $(u^\star,p^\star,q^\star)$ such that $(u^\star,p^\star,q^\star) \in \mathrm{SOL}(p^\star,q^\star)$, where SOL is the solution mapping of Problem (18.42). Starting with $(\bar{p}^0,\bar{q}^0) = (p_0(0),q_0)$, a sequence of solutions $(\bar{u}^k,\bar{p}^k,\bar{q}^k) \in \mathrm{SOL}(\bar{p}^{k-1},\bar{q}^{k-1})$ is computed. Whenever the relative difference between $(\bar{p}^{k-1},\bar{q}^{k-1})$ and $(\bar{p}^k,\bar{q}^k)$ falls below a given threshold, the procedure stops and a solution is returned.

The corresponding stationary model is given as follows. The time interval $[0,T]$ is partitioned into J subintervals $[t_k,t_{k+1})$. The flow q is constant along the pipe and the pressure monotonically changes according to the Weymouth equation

$$p^2(x) = p^2(0) - \sigma q|q|x;$$

see Sect. 2.3.1.2 in [26] for a derivation of this relation. Hence, for each time subinterval, the state consists of the scalar flow q_k and the endpoint pressures p_k^{in} and p_k^{out}. With α_k, β_k, and c_k being the constant data of the inverse demand and cost functions on each subinterval $[t_k,t_{k+1})$, we obtain the problem

$$\begin{aligned}
\max_{q,p^{\mathrm{in}},p^{\mathrm{out}}} \quad & \sum_{k=1}^{J}(t_{k+1}-t_k)\left[(\beta_k - (M^{-1}+1)\alpha_k q_k)q_k - c_k q_k\right] & \\
\text{s.t.} \quad & (p_k^{\mathrm{out}})^2 = (p_k^{\mathrm{in}})^2 - \Lambda q_k^2, & 1 \le k \le J, \\
& \underline{p} \le p_k^{\mathrm{in}} \le \bar{p}, \quad \underline{p} \le p_k^{\mathrm{out}} \le \bar{p}, \quad \underline{q} \le q_k \le \bar{q}, & 1 \le k \le J,
\end{aligned} \tag{18.44}$$

with $\Lambda := \sigma L$. As q_k is constant on each time subintervals, Constraint (18.42i) is automatically satisfied.

We use two different computational setups for the PDE-constrained and the stationary problem. The discretized version of Problem (18.44) is a convex QP. The latter is solved using the barrier algorithm of Gurobi 9.5.0; see [17]. We use JuMP as the modeling environment; see [14]. The complete instance data as well as the code to perform the numerical computations and create the figures can be found at [23]. The nonconvex stationary problem (18.44) is solved by Ipopt 3.14.1 via the Pyomo modeling environment; see [41] and [18], respectively.

C Discretization Scheme

Coming back to Problem (18.42), as a first step towards solving such instances, we pursue a discretize-then-optimize approach. For the discretization of the system in (18.42b)–(18.42f), rather than using a generic scheme for parabolic PDEs, we retain a numerical scheme that can be related to the linearized version of the ISO2 system. Indeed, the relations in (18.42b)–(18.42c) are obtained from the semilinear Euler equations

$$\begin{aligned} p_t + \frac{c_s^2}{A} q_x &= 0, \\ q_t + A p_x &= -\frac{1}{2}\sigma A \frac{q|q|}{p} - gA \sin\varphi \frac{p}{c_s^2}, \end{aligned}$$

by linearizing the right-hand side and adding a viscosity term. Using the Riemann invariants $R_\pm := c_s A^{-1} q \pm p$, we obtain the diagonal system

$$\begin{aligned} (R_+)_t + c_s (R_+)_x &= F(R_+, R_-), \\ (R_-)_t - c_s (R_-)_x &= F(R_+, R_-), \end{aligned} \tag{18.45}$$

in which the coupling between R_+ and R_- is through the right-hand side

$$F(R_+, R_-) := -\frac{\lambda c_s}{4D}(R_+ + R_-)\frac{|R_+ + R_-|}{R_+ - R_-} - g \sin\varphi \frac{R_+ - R_-}{2c}.$$

This diagonal form is useful to investigate theoretical properties of the system as well as for developing numerical schemes; see [15]. For the relations in (18.42b)–(18.42c), the same change of variables results in

$$\begin{aligned} (R_+)_t - \varepsilon (R_+)_{xx} + c_s (R_+)_x &= F_{\text{aff}}(R_+, R_-), \\ (R_-)_t - \varepsilon (R_-)_{xx} - c_s (R_-)_x &= F_{\text{aff}}(R_+, R_-), \end{aligned} \tag{18.46}$$

where F_{aff} is the affine approximation of F around the operational points $\check{p} > 0$ and $\check{q} > 0$.

Let us first discretize the linearized version of the hyperbolic system (18.45), where F has been substituted by F_{aff}. Specifically, we integrate $R_\pm$ along the characteristic lines using a triangular grid as illustrated on Fig. 18.6. There, the solid line from node i to node k (resp. from j to k) represents the characteristic line for R_+ (resp. R_-). The characteristics passing through a given pair $(\bar{x}, \bar{t})$ are the images of the mappings $\xi_+(s, \bar{x}, \bar{t}) := (\bar{x} + c_s(s - \bar{t}), s)$ and $\xi_-(s, \bar{x}, \bar{t}) := (\bar{x} - c_s(s - \bar{t}), s)$, respectively. Along the characteristics, System (18.45) is compactly given by

$$\frac{\mathrm{d}}{\mathrm{d}s}(R_\pm \circ \xi_\pm) = (R_\pm)_t \circ \xi_\pm + c_s (R_\pm)_x \circ \xi_\pm = F(R_+, R_-) \circ \xi_\pm. \tag{18.47}$$

Let us denote by $R_\pm^i$, $R_\pm^j$, and $R_\pm^k$ the values of the Riemann invariants at the nodes i, j, and k. We have $\Delta x = x_l - x_{l-1} = x_{l+1} - x_l$, $\Delta t = t_{n+1} - t_n$, and $\Delta x = c_s \Delta t$ as well as $R_+^k = R_+(\xi_+(t_n + \Delta t, x_{l-1}, t_n))$ and $R_-^k = R_-(\xi_-(t_n + \Delta t, x_{l+1}, t_n))$. Integrating

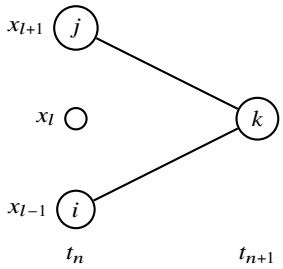


Fig. 18.6: Triangular grid used for integration

System (18.47) along the characteristics starting from node i (node j) for R_+ (R_-) and using the midpoint rule for approximating the right-hand side yields

$$R_+^k - R_+^i = \frac{\Delta t}{2}\,[F_{\text{aff}}(R_+^i, R_-^i) + F_{\text{aff}}(R_+^k, R_-^k)],$$
$$R_-^k - R_-^j = \frac{\Delta t}{2}\,[F_{\text{aff}}(R_+^j, R_-^j) + F_{\text{aff}}(R_+^k, R_-^k)].$$

Next, we relate this discretized system with one obtained by discretizing the viscosity regularized system. We proceed just with R_+ as the reasoning is similar with R_-. We discretize the left-hand side of the first relation in (18.46) using a finite difference scheme with $\Delta x = c_s \Delta t$ and $\varepsilon = c_s \Delta x$. Using a central difference formula for the second-order term, one obtains

$$\begin{aligned}
&\frac{R_+^k - R_+(x_l, t_n)}{\Delta t} - c_s \Delta x \frac{R_+^j + R_+^i - 2R_+(x_l, t_n)}{(\Delta x)^2} + c_s \frac{R_+^j - R_+(x_l, t_n)}{\Delta x} \\
&= \frac{R_+^k - R_+(x_l, t_n)}{\Delta t} - \frac{R_+^j + R_+^i - 2R_+(x_l, t_n)}{\Delta t} + \frac{R_+^j - R_+(x_l, t_n)}{\Delta t} \\
&= \frac{R_+^k - R_+^i}{\Delta t}.
\end{aligned}$$

With our choice of the right-hand side, the values of the Riemann invariants at (x_l, t_n) do not appear in any relation. This gives the grid its triangular shape.

Acknowledgements This work was supported by the German Research Foundation (DFG) within Subprojects A05, B02, B07, B08, and B09 in the Sonderforschungsbereich/Transregio 154 "Mathematical Modelling, Simulation and Optimization using the Example of Gas Networks" (Project ID 239904186).

This research has been performed as part of the Energie Campus Nürnberg and is supported by funding of the Bavarian State Government.

References

1. R. Adams and J. Fournier. *Sobolev Spaces*. Academic Press, 2 edition, 2003.
2. V. Barbu and T. Precupanu. *Convexity and Optimization in Banach Spaces*. Springer Monographs in Mathematics. Springer Netherlands, 4 edition, 2012. doi:10.1007/978-94-007-2247-7.
3. H. Benchekroun. Unilateral production restrictions in a dynamic duopoly. *Journal of Economic Theory*, 111(2):214–239, 2003. doi:10.1016/S0022-0531(03)00090-5.
4. H. Benchekroun. Comparative dynamics in a productive asset oligopoly. *Journal of Economic Theory*, 138(1):237–261, 2008. doi:10.1016/j.jet.2006.10.012.
5. H. Brezis. *Functional Analysis, Sobolev Spaces and Partial Differential Equations*. Springer New York, 2010. doi:10.1007/978-0-387-70914-7.
6. G. Caruana and L. Einav. Production targets. *The RAND Journal of Economics*, 39(4):990–1017, 2008. doi:10.1111/j.1756-2171.2008.00047.x.
7. X. Chen and Z. Wang. Differential variational inequality approach to dynamic games with shared constraints. *Mathematical Programming*, 146(1):379–408, 2014. doi:10.1007/s10107-013-0689-1.
8. L. Colombo and P. Labrecciosa. On the Markovian efficiency of Bertrand and Cournot equilibria. *Journal of Economic Theory*, 155:332–358, 2015. doi:10.1016/j.jet.2014.11.007.
9. L. Colombo and P. Labrecciosa. Stackelberg versus Cournot: A differential game approach. *Journal of Economic Dynamics and Control*, 101:239–261, 2019. doi:10.1016/j.jedc.2018.10.007.
10. A. Cournot. *Recherches sur les principes mathématiques de la théorie des richesses*. Hachette Paris, 1838.
11. R. Dautray and J.-L. Lions. *Mathematical Analysis and Numerical Methods for Science and Technology: Evolution Equations I*. Springer Berlin Heidelberg, 2000. doi:10.1007/978-3-642-58090-1.
12. P. Domschke, B. Hiller, J. Lang, V. Mehrmann, R. Morandin, and C. Tischendorf. Gas network modeling: An overview. Technical report, Technische Universität Darmstadt, 2021. URL: https://opus4.kobv.de/opus4-trr154/frontdoor/index/index/docId/411.
13. A. Dreves and J. Gwinner. Jointly convex generalized Nash equilibria and elliptic multiobjective optimal control. *Journal of Optimization Theory and Applications*, 168(3):1065–1086, 2016. doi:10.1007/s10957-015-0788-7.
14. I. Dunning, J. Huchette, and M. Lubin. JuMP: A modeling language for mathematical optimization. *SIAM Review*, 59(2):295–320, 2017. doi:10.1137/15M1020575.
15. M. Gugat, J. Habermann, M. Hintermüller, and O. Huber. Constrained exact boundary controllability of a semilinear model for pipeline gas flow. *European Journal of Applied Mathematics*, 34(3):532–553, 2023. doi:10.1017/S0956792522000389.
16. M. Gugat and S. Steffensen. Dynamic boundary control games with networks of strings. *ESAIM: Control, Optimisation and Calculus of Variations*, 24(4):1789–1813, 2018. doi:10.1051/cocv/2017082.
17. Gurobi Optimization, LLC. Gurobi Optimizer Reference Manual, 2021. URL: https://www.gurobi.com.
18. W. E. Hart, C. D. Laird, J.-P. Watson, D. L. Woodruff, G. A. Hackebeil, B. L. Nicholson, and J. D. Siirola. *Pyomo – Optimization Modeling in Python*, volume 67 of *Springer Optimization and Its Applications*. Springer, 2017. doi:10.1007/978-3-319-58821-6.
19. M. Hintermüller and T. Surowiec. A PDE-constrained generalized Nash equilibrium problem with pointwise control and state constraints. *Pacific Journal on Optimization*, 9(2):251–273, 2013.
20. M. Hintermüller, T. Surowiec, and A. Kämmler. Generalized Nash equilibrium problems in Banach spaces: Theory, Nikaido–Isoda-based path-following methods, and applications. *SIAM Journal on Optimization*, 25(3):1826–1856, 2015. doi:10.1137/14096829X.
21. M. Hinze, R. Pinnau, M. Ulbrich, and S. Ulbrich. *Optimization with PDE Constraints*, volume 23 of *Mathematical Modelling: Theory and Applications*. Springer Netherlands, 2009. doi:10.1007/978-1-4020-8839-1.

22. P. Holmberg and A. B. Philpott. On supply-function equilibria in radial transmission networks. *European Journal of Operational Research*, 271(3):985–1000, 2018. doi:10.1016/j.ejor.2018.05.070.
23. O. Huber. PDE-Cournot-code, 2023. URL: https://github.com/xhub/PDE-Cournot-code, doi:10.5281/zenodo.7702535.
24. B. Jun and X. Vives. Strategic incentives in dynamic duopoly. *Journal of Economic Theory*, 116(2):249–281, 2004. doi:10.1016/j.jet.2003.08.005.
25. C. Kanzow, V. Karl, D. Steck, and D. Wachsmuth. The multiplier-penalty method for generalized Nash equilibrium problems in Banach spaces. *SIAM Journal on Optimization*, 29(1):767–793, 2019. doi:10.1137/17M114114X.
26. T. Koch, B. Hiller, M. E. Pfetsch, and L. Schewe, ed. *Evaluating Gas Network Capacities*. Society for Industrial and Applied Mathematics, 2015. doi:10.1137/1.9781611973693.
27. L. Lambertini and A. Palestini. On the feedback solutions of differential oligopoly games with hyperbolic demand curve and capacity accumulation. *European Journal of Operational Research*, 236(1):272–281, 2014. doi:10.1016/j.ejor.2013.12.008.
28. A. Ledvina and R. Sircar. Dynamic Bertrand oligopoly. *Applied Mathematics & Optimization*, 63(1):11–44, 2011. doi:10.1007/s00245-010-9110-0.
29. P. L. Lions. Une inégalité pour les opérateurs elliptiques du second ordre. *Annali di Matematica Pura ed Applicata*, 127(1):1–11, 1981. doi:10.1007/bf01811715.
30. J. F. Nash. Equilibrium points in n-person games. *Proceedings of the National Academy of Sciences*, 36(1):48–49, 1950. doi:10.1073/pnas.36.1.48.
31. M. Renardy and R. C. Rogers. *An Introduction to Partial Differential Equations*, volume 13. Springer-Verlag, 2004. doi:10.1007/b97427.
32. S. S. Reynolds and B. J. Wilson. Bertrand–Edgeworth competition, demand uncertainty, and asymmetric outcomes. *Journal of Economic Theory*, 92(1):122–141, 2000. doi:10.1006/jeth.1999.2624.
33. D. A. Schiro, J.-S. Pang, and U. V. Shanbhag. On the solution of affine generalized Nash equilibrium problems with shared constraints by Lemke's method. *Mathematical Programming*, 142(1):1–46, 2013. doi:10.1007/s10107-012-0558-3.
34. M. Schmidt, D. Aßmann, R. Burlacu, J. Humpola, I. Joormann, N. Kanelakis, T. Koch, D. Oucherif, M. Pfetsch, L. Schewe, R. Schwarz, and M. Sirvent. GasLib – A library of gas network instances. *Data*, 2(4):40, 2017. doi:10.3390/data2040040.
35. C. Schwab and R. Stevenson. Space-time adaptive wavelet methods for parabolic evolution problems. *Mathematics of Computation*, 78(267):1293–1318, 2009. doi:10.1090/s0025-5718-08-02205-9.
36. J. Simon. Compact sets in the space $L^p(0, T; B)$. *Annali di Matematica Pura ed Applicata*, 146(1):65–96, 1986. doi:10.1007/bf01762360.
37. J.-Y. Wei and Y. Smeers. Spatial oligopolistic electricity models with Cournot generators and regulated transmission prices. *Operations Research*, 47(1):102–112, 1999. doi:10.1287/opre.47.1.102.
38. G. Wilson and P. Rowley. Flexibility in Great Britain's gas networks: analysis of linepack and linepack flexibility using hourly data. Briefing note, UK Energy Research Centre, 2019. URL: https://ukerc.ac.uk/publications/linepack/.
39. R. Wilson. Supply function equilibrium in a constrained transmission system. *Operations Research*, 56(2):369–382, 2008. doi:10.1287/opre.1070.0421.
40. F. Wirl. Dynamic demand and noncompetitive intertemporal output adjustments. *International Journal of Industrial Organization*, 28(3):220–229, 2010. doi:10.1016/j.ijindorg.2009.08.002.
41. A. Wächter and L. T. Biegler. On the implementation of an interior-point filter line-search algorithm for large-scale nonlinear programming. *Mathematical Programming*, 106(1):25—57, 4 2005. doi:10.1007/s10107-004-0559-y.
42. B. Xin and M. Sun. A differential oligopoly game for optimal production planning and water savings. *European Journal of Operational Research*, 269(1):206–217, 2018. doi:10.1016/j.ejor.2017.07.016.

Open Access This chapter is licensed under the terms of the Creative Commons Attribution-NonCommercial-NoDerivatives 4.0 International License (http://creativecommons.org/licenses/by-nc-nd/4.0/), which permits any noncommercial use, sharing, distribution and reproduction in any medium or format, as long as you give appropriate credit to the original author(s) and the source, provide a link to the Creative Commons license and indicate if you modified the licensed material. You do not have permission under this license to share adapted material derived from this chapter or parts of it.

The images or other third party material in this chapter are included in the chapter's Creative Commons license, unless indicated otherwise in a credit line to the material. If material is not included in the chapter's Creative Commons license and your intended use is not permitted by statutory regulation or exceeds the permitted use, you will need to obtain permission directly from the copyright holder.



Chapter 19
p-Wasserstein Distances on Networks and 3D to 1D Convergence

Martin Burger[0000−0003−2619−2912],
Ariane Fazeny[0009−0002−0008−3646],
Gilles Mordant[0000−0003−1821−5168], and
Jan-Frederik Pietschmann[0000−0003−0383−8696]

Abstract We study transport distances on metric graphs representing gas networks. Starting from the dynamic formulation of the Wasserstein distance, we review extensions to networks, with and without the possibility of storing mass on the vertices. Next, we examine the asymptotic behavior of the static Wasserstein distance on a three-dimensional network domain that converges to a metric graph. We show convergence of the distance with a proof that is based on the characterization of optimal transport plans as c-cyclically monotone sets. We conclude by illustrating our finding with several numerical examples.

19.1 Introduction

The theory of optimal transport, introduced by G. Monge in [25] and reformulated by L. V. Kantorovich in [18], is nowadays an ubiquitous tool in many areas of applied mathematics, statistics, and data science [2, 9, 13, 14, 19, 20, 29, 30, 32, 35]. The theory arose from the "logistic" problem of moving mass from a source configuration to a target configuration at overall minimal cost. Here, the ground cost encodes the difficulty

Martin Burger
Helmholtz Imaging, Deutsches Elektronen-Synchrotron DESY, Germany,
e-mail: martin.burger@desy.de
Department of Mathematics, Universität Hamburg, Germany, e-mail: martin.burger@uni-hamburg.de

Ariane Fazeny
Helmholtz Imaging, Deutsches Elektronen-Synchrotron DESY, Germany,
e-mail: ariane.fazeny@desy.de

Gilles Mordant
Applied and Computational Mathematics, Yale University, USA, e-mail: gilles.mordant@yale.edu

Jan-Frederik Pietschmann
Institute for Mathematics and Centre for Advanced Analytics and Predictive Sciences (CAAPS), Universität Augsburg, Germany, e-mail: jan-f.pietschmann@uni-a.de

© The Author(s) 2027

A. Martin et al. (eds.), *Mathematical Modelling, Simulation and Optimization using the Example of Gas Networks*, International Series of Numerical Mathematics 174,
https://doi.org/10.1007/978-3-032-34969-9_19

of transporting one unit of mass from a point x to a point y. As such, the overall optimal cost thus defines a metric (or more general distance functional) between probability distributions that leverages the ground metric, which makes it a versatile tool.

Additionally to the optimal transport plan, establishing how to reorganize the mass from the source to the target, it is sometimes possible to add a time component to the problem and track how the reorganization should evolve as time passes. The problem without the time component is often called the *static formulation*, while the other version of the problem is called the *dynamic formulation*, provided it exists.

This dynamic formulation further connects certain evolution equations to gradient flows in the space of probability measures endowed with the Wasserstein metric. This view, motivated by physical principles [16, 17, 23, 24, 28], has had a tremendous impact in the PDE community. In the Euclidean case, a gradient flow is given by a smooth curve $x : \mathbb{R}_{\geq 0} \to \Omega$, $x(t) = x_t$ for some space domain Ω, such that $\mathrm{d}x_t/\mathrm{d}t = -\nabla E(x_t)$ for $t \geq 0$, where $E : \Omega \to \mathbb{R}$ is some (typically convex) energy function. Then the gradient flow x_t minimizes E following the steepest descent. If we now want to evaluate an energy function at not only a point in space $x_t \in \Omega$, but rather for a probability distribution $\rho_t \in \mathcal{P}(\Omega)$ on the space domain Ω, then in order to have a well-defined gradient of E with respect to probability distributions we need a way of quantifying the distance between two probability measures.

One popular metric for quantifying the distance (in the sense of optimal transport cost) between two probability measures is the the *Wasserstein distance*. Given a domain $\Omega \subset \mathbb{R}^d$, $d \in \mathbb{N}$, and two probability measures $\mu,\ \nu \in \mathcal{P}(\Omega)$, the minimal total transport cost of going from μ to ν is given by

$$W_p(\mu, \nu) := \min_{\pi \in \Pi(\mu,\nu)} \left\{ \int_{\Omega\times\Omega} ||x - y||^p \, \mathrm{d}\pi(x, y) \right\}^{1/p}, \tag{WDS}$$

where $\Pi(\mu, \nu)$ denotes the set of all joint probability distributions π on $\Omega \times \Omega$, with the respective marginals μ and ν, meaning that $\mu(A) = \pi(A, \Omega)$ and $\nu(B) = \pi(\Omega, B)$ for all Borel measurable sets $A, B \subset \Omega$. In the definition above, the ground cost, generally denoted by c, is the p-th power of the Euclidean distance. Further, this formulation of the Wasserstein distance solely involves an infimum over so-called couplings π on $\Omega \times \Omega$ without any time component, thus it corresponds to the static formulation.

In the case of a non-convex domain Ω, the formulation (WDS) generally also allows mass transport outside of Ω, as the costs only consider the Euclidean distance. In order to restrict the feasible transport to the space domain Ω, one can alternatively also define the static formulation of the Wasserstein distance as

$$W_p(\mu, \nu) := \min_{\pi \in \Pi(\mu,\nu)} \left\{ \int_{\Omega\times\Omega} d_{\Omega,p}(x, y)^p \, \mathrm{d}\pi(x, y) \right\}^{1/p}, \tag{19.1}$$

where $d_{\Omega,p}$ is the shortest path distance on Ω given by

$$d_{\Omega,p}(x, y) = \inf_{\substack{\xi \in C^1([0,1]),\\ \xi(0)=x,\ \xi(1)=y}} \left\{ \int_0^1 \left\| \dot{\xi}(t) \right\|_p^p \, \mathrm{d}t \right\}^{1/p}. \tag{19.2}$$

Here, the infimum is taken over all (continuous) curves ξ in Ω which are connecting $x \in \Omega$ to $y \in \Omega$.

The optimization problem (WDS) is linear in the coupling π, which also needs to fulfill the marginal constraints. Hence, it is natural to express the constraints by relying on Lagrange multipliers. Doing so, one obtains an "inf-sup" problem where it turns out that the *inf* and the *sup* can be exchanged. This crucial fact gives rise to a dual formulation of the problem, which we recall later in Theorem 19.2.

A further important aspect is the notion of c-cyclical monotonicity of the set on which an optimal coupling $\pi^\star$ for the problem (WDS) is concentrated, see Definition 19.6. The c-cyclical monotonicity expresses the fact that the optimality of $\pi^\star$ would be contradicted by the possibility to re-route the mass of $\pi^\star$ to produce a coupling achieving a smaller overall cost. Such considerations thus induce strong geometric constraints on the support of $\pi^\star$, which will be leveraged in some of our following results.

In the seminal contribution of J.D. Benamou and Y. Brenier in 2000, [3], the minimization problem (WDS) was shown to have an equivalent dynamic formulation. The main idea is to consider curves of probability measures $(\rho_t)_{0\le t\le 1} \subset \mathcal{P}(\Omega)$ over an artificial time interval $[0, 1]$, which connect the two measures μ and ν, such that $\rho_0 = \mu$ and $\rho_1 = \nu$. As mass is preserved along this evolution from μ to ν, the curves $(\rho_t)_{0\le t\le 1}$ are characterized by solutions (in the sense of distributions) to the continuity equation, i.e.,

$$\begin{aligned} \partial_t \rho_t + \nabla \cdot (\rho_t v_t) &= 0, \\ \rho_0 = \mu, \quad \rho_1 &= \nu, \end{aligned} \tag{19.3}$$

for some (measure-valued) velocity field v_t. We denote the set of all such curves $(\rho_t)_{0\le t\le 1} \subset \mathcal{P}(\Omega)$ fulfilling (19.3) by $\mathsf{CE}(\mu, \nu)$. Then, selecting the curve with minimal kinetic energy from $\mathsf{CE}(\mu, \nu)$, thus corresponding to an optimal transport from μ to ν, one recovers the 2-Wassertein distance, i.e.,

$$W_2(\mu, \nu) = \inf_{(\rho_t, v_t) \in \mathsf{CE}(\mu,\nu)} \left\{ \int_0^1 \int_\Omega |v_t|^2 \, \mathrm{d}\rho_t \right\}^{1/2}. \tag{2-WDD}$$

The connection of the dynamic formulation of the Wasserstein distance to the problem of gas transport within a complicated network is done by extending (2-WDD) to metric graphs as the domain Ω, modeling a gas network. Roughly speaking, metric graphs are combinatorial graphs in which a one-dimensional interval is associated to each edge (see Sect. 19.2.1 for a rigorous definition). Then, the continuity equation (19.3) can be used on each of the edges to ensure mass conservation in the individual pipes. However, to enforce global mass conservation on the entire network, additional coupling conditions at the vertices, corresponding to pipe junctions, have to be introduced.

So far, two approaches have been considered in the literature: In [11], homogeneous Kirchhoff conditions were imposed. In this setting, the sum of mass entering the node is equal to the mass leaving it, which means that no mass is stored on the node and no additional gas is entering the network through the node. This also allows for a static formulation on the metric graph, analogous to (WDS), by choosing a metric graph as the domain Ω and replacing the Euclidean norm distance by the distance (GD) on the metric graph, defined in Sect. 19.2.1.

The second approach, introduced in [4], allows for storage of mass on a node, utilizing a more general version of Kirchhoff's law. Here, additional continuity equations on the vertices are imposed. It was then a striking observation, made in [12], and rigorously proven in [34], that the ISO3 model for gas flow, given as

$$\begin{aligned} \partial_t \rho^{\mathsf{e}} + \partial_x \left(\rho^{\mathsf{e}} v^{\mathsf{e}}\right) &= 0 \\ \partial_x p^{\mathsf{e}}\left(\rho^{\mathsf{e}}\right) &= -\frac{\lambda^{\mathsf{e}}}{2D^{\mathsf{e}}} \rho^{\mathsf{e}} v^{\mathsf{e}} \left|v^{\mathsf{e}}\right| - g\rho^{\mathsf{e}} \sin\left(\omega^{\mathsf{e}}\right) \end{aligned} \tag{ISO3}$$

can be interpreted as a 3-Wasserstein gradient flow for a certain energy functional E. Here, the superscript-e-notation corresponds to the restriction of the respective functions defined on the whole gas network to a single pipe e. The derivation of the ISO3 model is described in detail in (ISO3), alongside an entire hierarchy of models for the gas flow within one pipe, all derived from the Euler equations system for compressible, inviscid fluids. Note that, here the pipe inclination angle ω_e relative to the ground is used instead of the pipe hight function b_e. Both approaches for the coupling conditions at vertices, [11] and [4], are based on a dynamic formulation of the Wasserstein distance on a metric graph, where the second approach is closely related to the study of transport on coupled domains of different dimension (the 1-dimensional edges and the 0-dimensional vertices), such as [6, 7, 26].

While the setting of metric graphs is a convenient way to model gas networks, it has the inherent limitation that pipes are modeled as one-dimensional entities, only, utilizing an averaging argument over the pipe cross sections. This gives rise to the question whether this approach can be justified by a limiting procedure, starting from a fully three-dimensional model and, in turn, letting the diameter of the pipes go to zero. We study this question in Sect. 19.3 and are indeed able to prove the convergence of the Wasserstein metric in its static formulation (corresponding to the case without mass storage on vertices). This serves as a starting point for further investigations of the convergence of the (equivalent) dynamic formulation and, subsequently, also the convergence of Wasserstein gradient flows.

19.2 Dynamic Transport Distances on Metric Graphs

Our next aim is to give a brief review of dynamic transport distances on metric graphs and their connection to the ISO3 model, following the results of [11, 12, 15, 34].

19.2.1 Metric Graphs

Using the notation of [15], we start with an undirected connected graph, which is a (finite) node set V with edge set $\mathsf{E} \subset \mathsf{V} \times \mathsf{V}$, such that if $\mathsf{vw} \in \mathsf{E}$ then $\mathsf{wv} \notin \mathsf{E}$. We use $\mathsf{E}(\mathsf{v})$ to denote the set of all edges adjacent to node v. Based on this combinatorial graph (V, E), we construct a metric graph M by fixing an orientation for each edge $\mathsf{e} \in \mathsf{E}$

and then associating this oriented edge with a finite line segment $[0, \ell^{\mathsf{e}}] \subset \mathbb{R}$, for some edge length $\ell^{\mathsf{e}} > 0$.

To fix notations, given $\mathsf{e} = \mathsf{vw}$, we will call v *tail* and w *head* and give those the orientation

$$\mathsf{n} : \mathsf{V} \times \mathsf{E} \to \{-1, 0, 1\} \quad \text{with} \quad \mathsf{n}_{\mathsf{v}}^{\mathsf{e}} = \begin{cases} -1, & \text{if } \mathsf{v} \text{ is the tail node of } \mathsf{e}; \\ 0, & \text{if } \mathsf{v} \notin \mathsf{e}; \\ 1, & \text{if } \mathsf{v} \text{ is the head node of } \mathsf{e}. \end{cases} \tag{19.4}$$

Note that the orientation of edges is used to determine the flow direction later on, with a positive sign of the velocity if the flow goes from head to tail, and a negative sign otherwise.

We associate the edge length ℓ^{e} to each $\mathsf{e} \in \mathsf{E}$ via the function

$$\ell : \mathsf{E} \to (0, \infty), \qquad \text{giving rise to the set} \qquad \mathsf{L} = \bigsqcup_{\mathsf{e} \in \mathsf{E}} \left[0, \ell^{\mathsf{e}}\right]. \tag{19.5}$$

Here, and in the following, $\bigsqcup_{\mathsf{e} \in \mathsf{E}} [0, \ell^{\mathsf{e}}]$ denotes the disjoint union, also called coproduct, understood as the set of ordered pairs $\bigcup_{e \in \mathsf{E}} \{(e, [0, \ell^e])\}$. The *metric graph* is now the triplet $\mathsf{M} = (\mathsf{V}, \mathsf{E}, \mathsf{L})$, where in our application, V represents the set of pipe junctions and pipe endpoints, while E are the pipes of the gas network, which we assume to be finite and connected.

Definition 19.1 (1D distance on metric graph) For $x, y \in \mathsf{G}$, we define the local distance as

$$d_{\mathrm{loc}}(x, y) := \begin{cases} |x - y|, & \text{if } x, y \in [0, \ell^{\mathsf{e}}], \text{ for the same edge } \mathsf{e} \in \mathsf{E} \\ +\infty, & \text{otherwise} \end{cases},$$

and extend it to the whole metric graph G with edges E as

$$d(x, y) := \min_{\emptyset \subsetneq \{i_1, i_2, \ldots, i_n\} \subseteq \{1, 2, \ldots, k\}} \left\{ \sum_{i=i_1}^{i_n} d_{\mathrm{loc}}(x_i, y_i) \;\middle|\; \begin{array}{l} x_{i_1} = x, y_{i_n} = y, \\ \forall j \in \{1, 2, \ldots, n-1\} : \\ y_{i_j}, x_{i_{j+1}} \in \mathsf{V},\ y_{i_j} \sim x_{i_{j+1}} \end{array} \right\}. \tag{GD}$$

The metric graph distance corresponds to the shortest path from $x \in \mathsf{e}_{i_1}$ to $y \in \mathsf{e}_{i_n}$ along the edges $\mathsf{e}_{i_2}, \mathsf{e}_{i_3}, \ldots, \mathsf{e}_{i_{n-1}}$.

Note that with the results from [27], we immediately obtain that (G, d) is a geodesic space. Furthermore, the previously introduced Wasserstein distance is hence also well-defined in the metric graph setting, and by [11], we get that $(\mathcal{P}(\mathsf{G}), W_2)$ is a geodesic space as well. For general $p \geq 1$, in [22], it was shown that $\left(\mathcal{P}(\mathsf{G}), W_p\right)$ is a geodesic space.

19.2.2 Continuity Equations

To obtain a dynamic formulation of optimal transport, we first need to introduce a notion of the continuity equation, generalizing (19.3) to metric graphs. Note that instead of using a velocity vector field, we introduce the momentum (also known as mass flux) $J_t = \rho_t v_t$. This has the advantage of rendering the continuity equation linear in ρ_t and J_t, and resulting in a convex optimization problem in (2-WDD).

We will separately discuss the case of mass storage on nodes, and the case with classical Kirchhoff conditions. We will closely follow the definitions and notations of [15], but also see [4, 12] for properties of the Wasserstein metric with node mass storage and [11] for the version with classical Kirchhoff conditions.

19.2.2.1 Mass Storage on Nodes

To arrive at a continuity equation structure on M, we start with the definition of the continuity equation on the metric edges L, for which we specify a family of time-dependent (and in the case of j signed) measures $\rho : [0,1] \to \mathcal{M}_{\geq 0}(\mathsf{L})$, $\rho(t) =: \rho_t$ and fluxes $j : [0,1] \to \mathcal{M}(\mathsf{L})$, $j(t) =: j_t$. Here, we write the shortcut notation $\rho_t \in \mathcal{M}(\mathsf{L})$ for $\rho_t = \left\{\rho_t^{\mathsf{e}} \in \mathcal{M}([0,\ell^{\mathsf{e}}])\right\}_{\mathsf{e}\in\mathsf{E}}$, and $j_t \in \mathcal{M}(\mathsf{L})$ for $j_t = \{j^e \in \mathcal{M}([0,\ell^e])\}_{e\in\mathsf{E}}$ and we call the pair (ρ, j) a solution of the continuity equation if ut holds true that

$$\forall t \in (0,1),\, x \in \left(0,\ell^{\mathsf{e}}\right) : \quad \partial_t \rho_t^{\mathsf{e}}(x) + \partial_x j_t^{\mathsf{e}}(x) = 0, \qquad \text{for all edges } \mathsf{e} \in \mathsf{E}, \tag{19.6}$$

where for all $\mathsf{e} \in \mathsf{E}$ we have measures ρ^{e} and j^{e} from the dual space of the continuous functions defined on $[0,\ell^{\mathsf{e}}]$. Note that we do not impose any continuity or differentiability constraints at the nodes.

To obtain a mass preserving evolution, we complement the continuity equation with a local Kirchhoff condition, which receives the mass leaving from the metric edges due to the net-balance of the normal fluxes of $\{j^{\mathsf{e}}\}_{\mathsf{e}\in\mathsf{E}}$ evaluated in the head- and tail nodes of the edges, and which acts as a reservoir for each of the metric edges. Since, in general, $j_t \in \mathcal{M}(\mathsf{L})$ does not posses a normal flux, we introduce a new set of variables $\bar{j}_{\mathsf{v}}^{\mathsf{e}} : [0,1] \to \mathbb{R}$ for any $(\mathsf{v},\mathsf{e}) \in \mathsf{V}\times\mathsf{E}$, which are coupled in a weak sense by imposing the following integration by parts formula on the metric edges: For any $j_t^{\mathsf{e}} \in \mathcal{M}([0,\ell^{\mathsf{e}}])$ with smooth density $j_t^{\mathsf{e}}(x)\,\mathrm{d}x$, we impose the identity

$$\int_0^{\ell^{\mathsf{e}}} \varphi^{\mathsf{e}}(x)\partial_x j_t^{\mathsf{e}}(x)\,\mathrm{d}x = \sum_{\mathsf{v}\in\mathsf{V}(\mathsf{e})} \varphi^{\mathsf{e}}|_{\mathsf{v}}\, \bar{j}_{\mathsf{v},t}^{\mathsf{e}} - \int_0^{\ell^{\mathsf{e}}} \partial_x\varphi^{\mathsf{e}}\,\mathrm{d}j_t^{\mathsf{e}}. \tag{19.7}$$

Here, we write $\mathsf{V}(\mathsf{e})$ for the set of the head- and tail node of a given edge e and $\varphi : \mathsf{L} \to \mathbb{R}$ denotes a test function, which is continuous across all nodes and continuously differentiable within the respective edge.

The net-balance is stored in the node density γ_{v} for each node $\mathsf{v} \in \mathsf{V}$ and the *local Kirchhoff law* becomes

$$\forall \mathsf{v} \in \mathsf{V}: \qquad \partial_t \gamma_{\mathsf{v},t} = \sum_{\mathsf{e}\in\mathsf{E}(\mathsf{v})} \bar{j}^{\mathsf{e}}_{\mathsf{v},t} \qquad \text{for a.e. } t \in [0,1]. \tag{19.8}$$

We define the space of probability measures on M as tuples $\mu_t = (\gamma_t, \rho_t) \in \mathcal{P}(\mathsf{M}) \subseteq \mathcal{M}_{\geq 0}(\mathsf{V}) \times \mathcal{M}_{\geq 0}(\mathsf{L})$ such that $\gamma_t(\mathsf{V}) + \rho_t(\mathsf{L}) = 1$. We are now in a position to introduce our notion of the continuity equation on a metric graph with node mass storage.

Definition 19.2 (Continuity equation, [15]) A family of curves of probability measures $\mu = (\gamma, \rho) : [0,1] \to \mathcal{P}(\mathsf{M})$ with a flux pair $\mathrm{j} = (\bar{\jmath}, j) : [0,1] \to \mathcal{M}((\mathsf{V}\times\mathsf{E})\times\mathsf{L})$ satisfies the *continuity equation on the metric graph with node reservoirs* if (19.6) and (19.8) hold, and (μ, j) solves the abstract continuity equation

$$\partial_t \mu_t + \operatorname{div} \mathrm{j}_t = 0, \tag{19.9}$$

where for a.e. $t \in (0,1)$, the measures μ and j are form the dual space of the continuous functions defined on $\mathsf{V} \times \mathsf{L}$. For such a solution we then write $(\mu, \mathrm{j}) \in \mathsf{CE}_{\mathsf{V}}$. In terms of duality, for $\Phi = (\phi, \varphi) \in C^1(\mathsf{V} \times \mathsf{L})$ the abstract version of the continuity equation is defined by

$$\begin{aligned} &\frac{\mathrm{d}}{\mathrm{d}t}\left[\sum_{\mathsf{v}\in\mathsf{V}} \phi_{\mathsf{v}}\gamma_{\mathsf{v},t} + \sum_{\mathsf{e}\in\mathsf{E}} \int_0^{\ell^{\mathsf{e}}} \varphi^{\mathsf{e}}(x)\,\mathrm{d}\rho^{\mathsf{e}}_t\right] = \\ &\sum_{\mathsf{v}\in\mathsf{V}} \sum_{\mathsf{e}\in\mathsf{E}(\mathsf{v})} \left(\phi_{\mathsf{v}} - \varphi^{\mathsf{e}}|_{\mathsf{v}}\right) \bar{j}^{\mathsf{e}}_{\mathsf{v},t} + \sum_{\mathsf{e}\in\mathsf{E}} \int_0^{\ell^{\mathsf{e}}} \partial_x \varphi^{\mathsf{e}}\,\mathrm{d}j^{\mathsf{e}}_t \end{aligned} \tag{19.10}$$

for a.e. $t \in (0,1)$. Furthermore, we denote by $\mathsf{CE}_{\mathsf{V}}(\mu^0, \mu^1)$ the set of all weak solutions (μ, j) to (19.9), such that given initial- and final conditions $\mu_0 = \mu^0$ and $\mu_1 = \mu^1$ are fulfilled.

Among the solutions to (19.9) with bounded flux, we can find an absolutely continuous representative.

Lemma 19.1 (Well-posedness of CE, [15]) *Let* $(\mu, \mathrm{j}) \in \mathsf{CE}$ *with*

$$\int_0^1 \left[\sum_{\mathsf{v}\in\mathsf{V}} \sum_{\mathsf{e}\in\mathsf{E}(\mathsf{v})} \left|\bar{j}^{\mathsf{e}}_{\mathsf{v},t}\right| + \sum_{\mathsf{e}\in\mathsf{E}} \int_0^{\ell^{\mathsf{e}}} \mathrm{d}\left|j^{\mathsf{e}}_t\right|\right] \mathrm{d}t < \infty, \tag{19.11}$$

then there exists $(\tilde{\mu}, \tilde{\mathrm{j}}) \in \mathsf{CE}$ *such that* $(\tilde{\mu}_t)_{t\in[0,1]} \subset \mathcal{P}(\mathsf{M})$ *is an absolutely continuous curve equipped with the narrow topology of measures. This means that for all pairs* $\Phi = (\phi, \varphi) \in C(\mathsf{V} \times \mathsf{L})$ *the map*

$$t \mapsto \langle \varphi, \tilde{\mu}_t \rangle_{\mathsf{V}\times\mathsf{L}} := \sum_{\mathsf{v}\in\mathsf{V}} \phi_{\mathsf{v}} \tilde{\gamma}_{\mathsf{v},t} + \sum_{\mathsf{e}\in\mathsf{E}} \int_0^{\ell^{\mathsf{e}}} \varphi^{\mathsf{e}}\,\mathrm{d}\tilde{\rho}^{\mathsf{e}}_t$$

is absolutely continuous.

Proof. The proof is completely analogous to [1, Lemma 8.1.2] for the metric edge parts and [10, Lemma 3.1] for the edge-node-transition parts. □

19.2.2.2 Kirchhoff Case

In the case of classical Kirchhoff's law at the nodes, we make use of the continuity equation structure introduced in [11], which is set on the quotient space

$$\mathsf{G} := \mathsf{L}/\sim,$$

where the equivalence relation $\sim$ identifies the head and tail nodes of different intervals corresponding to the same node. This means that we consider a situation where the edges are glued together at the nodes to form one connected space domain.

The main difference compared to the previous section is the use of test functions that are continuous over the complete graph. Thus, the boundary terms which were present in (19.10) disappear in the weak formulation, encoding a Kirchhoff condition on the fluxes.

Definition 19.3 (Continuity equation (Kirchhoff) [11]) A family of curves $(\rho_t, J_t)_{t\in[0,1]}$ consisting of probability measures $\rho_t \in \mathcal{P}(\mathsf{G})$ and signed measures $J_t \in \mathcal{M}(\mathsf{L})$, such that for all Borel sets A the map $t \mapsto (\rho_t(A), J_t(A))$ is Borel measurable, is called a weak solution of *continuity equation on the metric graph with Kirchhoff condition* if for all test functions $\psi \in C^1(\mathsf{L}) \cap C(\mathsf{G})$ and a.e. $t \in (0,1)$ it holds

$$\frac{\mathrm{d}}{\mathrm{d}t}\int_{\mathsf{G}} \psi \,\mathrm{d}\rho_t = \int_{\mathsf{L}} \nabla_x \psi \cdot \mathrm{d}J_t, \tag{19.12}$$

where we assume

(1) $\forall \psi : t \mapsto \int_{\mathsf{G}} \psi \,\mathrm{d}\rho_t$ is absolutely continuous,
(2) $\int_{(0,1)} |J_t|(\mathsf{L})\,\mathrm{d}t < \infty$.

We denote by $\mathsf{CE}_K(\rho^0, \rho^1)$ the set of all weak solutions (ρ, J) to (19.12) such that $\rho_0 = \rho^0$ and $\rho_1 = \rho^1$.

Remark 19.1 The Kirchhoff condition is implicitly contained in the weak formulation (19.12). Indeed, if the flux would be sufficiently regular to allow for integration by parts, due to the continuity of the test function across nodes, we would obtain that

$$\sum_{e\in\mathsf{E}(v)} j_{\mathsf{v}}^{\mathsf{e}} = \sum_{\mathsf{e}\in\mathsf{E}(\mathsf{v})} j_t^{\mathsf{e}}(\mathsf{v})\mathsf{n}_{\mathsf{v}}^{\mathsf{e}} = 0 \qquad \text{for all } \mathsf{v} \in \mathsf{V}$$

must hold.

19.2.3 Action Functionals and Dynamic Distances

We are now able to define dynamic transport distances based on the minimization of action functionals over curves which satisfy the respective continuity equations.

19.2.3.1 Mass Storage on Nodes

In view of our application, mass storage on nodes may have different interpretations. It is for example possible to use mass storage on nodes to model gas inflow and outflow for the network. To this end, one differentiates between boundary nodes $\partial\mathsf{V}$, where gas may enter or exit the network (as supply or demand), and interior nodes $\mathring{\mathsf{V}}$. Then, the set of interior nodes is defined as

$$\mathring{\mathsf{V}} = \mathsf{V} \backslash \partial\mathsf{V},$$

which directly implies $\partial\mathsf{V} \cup \mathring{\mathsf{V}} = \mathsf{V}$ and $\partial\mathsf{V} \cap \mathring{\mathsf{V}} = \emptyset$ so that each node is either a boundary node or an interior node.

For the set of boundary nodes $\partial\mathsf{V}$, it is possible to differentiate further between source nodes $\partial^{+}\mathsf{V}$, which supply the network with gas, and sink nodes $\partial^{-}\mathsf{V}$, at which gas is taken out of the network to meet given demands.

The inflow and outflow of gas into and out from the network can then be modeled via time-dependent boundary conditions at $\partial\mathsf{V}$. For the sake of readability, however, we will limit our exposition to the case without boundary nodes and refer to [12] for details on those.

For given initial- and final mass distributions $\mu^0 := (\gamma^0, \rho^0)$ and $\mu^1 := (\gamma^1, \rho^1)$, we define the dynamical formulation of the Wasserstein distance as

$$W_{\mathsf{V},p}\left(\mu^0, \mu^1\right) = \min_{(\mu,j)\in \mathsf{CE}_{\mathsf{V}}(\mu^0,\mu^1)} \left\{ \int_0^1 \sum_{\mathsf{e}\in\mathsf{E}} \left(\int_0^{\ell^{\mathsf{e}}} h\left(j_t^{\mathsf{e}}, \rho_t^{\mathsf{e}}\right) \,\mathrm{d}\eta \right) + \sum_{\mathsf{v}\in\mathsf{V}} h\left(\sum_{\mathsf{e}\in\mathsf{E}(\mathsf{v})} \bar{j}_{\mathsf{v},t}^{\mathsf{e}}, \gamma_{\mathsf{v},t} \right) \mathrm{d}t \right\}^{1/p}, \tag{19.13}$$

where the *perspective function* $h : \mathbb{R}\times\mathbb{R} \longrightarrow \mathbb{R}_{\geq 0}$ is given as

$$(a,b) \mapsto h(a,b) = \begin{cases} \frac{|a|^p}{b^{p-1}}, & \text{if } b > 0, \\ 0, & \text{if } b = a = 0, \\ +\infty, & \text{if } b < 0 \ \vee \ b = 0,\ a \neq 0, \end{cases}$$

and it is responsible for penalizing negative densities and non-zero flux in the case of zero densities. Here, η denotes a reference measure and, abusing notation, we denote densities of j^{e} and ρ^{e} with respect to η still by the same symbols.

While (19.13) was introduced in [12], the gradient flows studied in [15] are understood with respect to a different version of the Wasserstein distance. Indeed, in (19.13), the contributions at the nodes depend on

$$\sum_{\mathsf{e}\in\mathsf{E}(\mathsf{v})} \bar{j}_{\mathsf{v},t}^{\mathsf{e}},$$

i.e., the net flux summing the contributions of all edges adjacent to the node v. In contrast to that, in [15], each contribution is considered separately which yields the metric

$$\overline{W}_{\mathsf{V},p}(\mu^0,\mu^1) = \min_{(\mu,j)\in \mathsf{CE}_{\mathsf{V}}(\mu^0,\mu^1)} \left\{ \int_0^1 \sum_{\mathsf{e}\in\mathsf{E}} \left(\int_0^{\ell^{\mathsf{e}}} h\left(j_t^{\mathsf{e}}, \rho_t^{\mathsf{e}}\right) \,\mathrm{d}\eta \right) + \sum_{\mathsf{v}\in\mathsf{V}} \sum_{\mathsf{e}\in\mathsf{E}(\mathsf{v})} h\left(\bar{j}_{\mathsf{v},t}^{\mathsf{e}}, \gamma_{\mathsf{v},t}\right) \,\mathrm{d}t \right\}^{1/p}. \tag{19.14}$$

19.2.3.2 Kirchhoff Case

In the classical Kirchhoff case, we are considering curves $(\rho, J) \in \mathsf{CE}_K\left(\rho^0, \rho^1\right)$ for given initial- and final densities $\rho^0, \rho^1 \in \mathcal{P}(\mathsf{G})$. The Wasserstein distance is then given by

$$W_{K,p}(\rho^0,\rho^1) = \min_{(\rho,\rho v)\in \mathsf{CE}_K\left(\rho^0,\rho^1\right)} \left\{ \int_0^1 \sum_{\mathsf{e}\in\mathsf{E}} \int_0^{\ell^{\mathsf{e}}} |v_t|^p \,\mathrm{d}\rho_t \,\mathrm{d}t \right\}^{1/p},$$

with $\mathsf{CE}_K\left(\rho^0,\rho^1\right)$ as in Definition 19.3. In order for the right hand side of $J_t = v_t\,\rho_t$ to be well-defined, we need a characterization of absolutely continuous curves in the p-Wasserstein space. This is given by a theorem proven in [34], which requires the following two definitions.

Definition 19.4 (Absolutely continuous curve [1]) A curve $\zeta : [0,1] \to \mathcal{P}(\mathsf{G})$ is called p-absolutely continuous in the p-Wasserstein space for $p \geq 1$, if there exists a function $m \in L^p(0,1)$ such that for all $0 < s \leq t < 1$ it holds true that

$$W_p(\zeta(s),\zeta(t)) \leq \int_s^t m(r)\,\mathrm{d}r. \tag{19.15}$$

Definition 19.5 (Metric derivative [1]) For every p-absolutely continuous curve (in the p-Wasserstein space) $\zeta : [0,1] \to \mathcal{P}(\mathsf{G})$, its metric derivative is defined as

$$\left|\dot{\zeta}\right|(t) := \lim_{s\to t} \frac{d(\zeta(s),\zeta(t))}{|s-t|}$$

for $t \in (0,1)$ and it exists for a.e. such t, where d is the shortest path distance on the metric graph, see (GD).

In [1], it is proven that the metric derivative of a p-absolutely continuous curve exists for a.e. $t \in (0,1)$ and that $\left|\dot{\zeta}\right| \in L^p(0,1)$. Furthermore, $\left|\dot{\zeta}\right|$ satisfies (19.15) chosen as m, and $\left|\dot{\zeta}\right|$ is minimal, meaning that for any other $m \in L^p(0,1)$ satisfying the equation, it holds true that $\left|\dot{\zeta}\right|(t) \leq m(t)$ for a.e. $t \in (0,1)$.

Theorem 19.1 (Absolutely continuous curves)

(i) If $\rho : [0,1] \to \mathcal{P}(\mathsf{G})$ is an absolutely continuous curve in $\left(\mathcal{P}(\mathsf{G}), W_p\right)$ then there exists, for a.e. $t \in (0,1)$, a vector field $v_t \in L^p(\rho_t)$ such that $\int_{\mathsf{G}} ||v_t||\,\mathrm{d}\rho_t \leq |\dot{\rho}|(t)$ and $(\rho,\rho v)$ is a weak solution to the continuity equation, as defined in 19.3.

(ii) If $(\rho,\rho v)$ is a weak solution to the continuity equation, as specified in 19.3 and

$$\int_{(0,1)} \int_{\mathsf{G}} ||v_t||\,\mathrm{d}\rho_t\,\mathrm{d}t < \infty,$$

then $\rho : [0,1] \to \mathcal{P}(\mathsf{G})$ *is an absolutely continuous curve in* $\big(\mathcal{P}(\mathsf{G}), W_p\big)$ *and for almost every* $t \in (0,1)$*, we obtain* $|\dot\rho(t)| \le \int_{\mathsf{G}} ||\mathsf{v}_t||\,\mathrm{d}\rho_t$.

This result was already proven for $p = 2$ in [11], and it was generalized to $p \ge 1$ in [34]. It is an important result, as Theorem 19.1 (i) shows that every W_p-absolutely continuous curve ρ_t can be realized as a physical mass flow with an L^p-finite velocity field v_t and mass conservation, so ρ_t encodes a feasible optimal transport of the gas through the network. Moreover, Theorem 19.1 (ii) shows the opposite direction, meaning that having a mass flow with finite p-energy, which also satisfies the continuity equation, then the corresponding mass trajectory ρ_t is an W_p-absolutely continuous curve, thus any weak solution of 19.12 with an integrable velocity v_t is a feasible optimal transport. Regarding the dynamic formulation of the p-Wasserstein distance, this theorem ensures that the mass flux J_t from a weak solution of the continuity equation can be decomposed into $J_t = \rho_t\, v_t$.

19.2.4 Gradient Flows on Metric Graphs

Since the introduction of Otto-Wasserstein gradient flow, [16, 17, 28], many equations were recognized as gradient flows in Wasserstein-type metrics. We briefly review some results for equations set on metric graphs.

19.2.4.1 Mass Storage on Nodes

So far, gradient flows in the setting of mass storage on nodes have not been studied in relation to gas networks. Instead, linear drift-diffusion equations were considered in [15]. To introduce the system, we fix a positive reference probability measure $(\omega, \pi) \in \mathcal{P}_+(\mathsf{M})$, where we assume π to have a density given by $\pi(\mathrm{dx}) = e^{-P(x)}\mathrm{dx}$ for some potential $P : \mathsf{L} \to \mathbb{R}$, such that $P^{\mathsf{e}} : [0, \ell^{\mathsf{e}}] \to \mathbb{R}$ is Lipschitz for all $\mathsf{e} \in \mathsf{E}$. With this, we consider for a.e. $t \in (0,1)$, the system

$$\partial_t \rho^{\mathsf{e}} = d^{\mathsf{e}} \partial_x \cdot \big(\partial_x \rho^{\mathsf{e}} + \rho^{\mathsf{e}} \partial_x P^{\mathsf{e}}\big), \qquad \text{on } [0, \ell^e] \text{ for every } \mathsf{e} \in \mathsf{E}, \tag{19.16a}$$

$$-d^{\mathsf{e}} \left(\partial_x \rho^{\mathsf{e}} + \rho^{\mathsf{e}} \partial_x P^{\mathsf{e}}\right)\Big|_{\mathsf{v}} \cdot \mathsf{n}^{\mathsf{e}}_{\mathsf{v}} = r(\mathsf{e},\mathsf{v})\ \rho^{\mathsf{e}}\big|_{\mathsf{v}} - r(\mathsf{v},\mathsf{e})\gamma_{\mathsf{v}}, \quad \text{for all } \mathsf{e} \in \mathsf{E},\ \mathsf{v} \in \mathsf{V}, \tag{19.16b}$$

$$\partial_t \gamma_{\mathsf{v}} = \sum_{\mathsf{e} \in \mathsf{E}(\mathsf{v})} \Big(r(\mathsf{e},\mathsf{v})\ \rho^{\mathsf{e}}\big|_{\mathsf{v}} - r(\mathsf{v},\mathsf{e})\gamma_{\mathsf{v}}\Big), \qquad \text{for all } \mathsf{v} \in \mathsf{V}\,. \tag{19.16c}$$

We set $\rho^{\mathsf{e}}|_{\mathsf{v}} = \rho^{\mathsf{e}}(0)$ if $\mathsf{e} = \mathsf{vw}$, and we set $\rho^{\mathsf{e}}|_{\mathsf{v}} = \rho^{\mathsf{e}}(\ell^{\mathsf{e}})$ if $\mathsf{e} = \mathsf{wv}$ for some $\mathsf{w} \in \mathsf{V}$. Moreover, we introduced the parameter $d^{\mathsf{e}} > 0$ as the diffusion constant on the metric edge e, $r(\mathsf{e},\mathsf{v})$ as the jump rate from the endpoint of the metric edge associated with

e to an adjacent node v, and $r(\mathsf{v},\mathsf{e})$ for the reverse jump rate from the node v to the adjacent edge e.

The main result of [15] is that system (19.16) admits a gradient flow formulation, provided that the jump rates satisfy the *detailed balance condition*, with respect to the reference measure $(\omega,\pi)\in\mathcal{P}_+(\mathsf{M})$, that is it holds

$$r(\mathsf{e},\mathsf{v})\sqrt{\frac{\pi^{\mathsf{e}}|_{\mathsf{v}}}{\omega_{\mathsf{v}}}} = r(\mathsf{v},\mathsf{e})\sqrt{\frac{\omega_{\mathsf{v}}}{\pi^{\mathsf{e}}|_{\mathsf{v}}}} =: \mathscr{K}_{\mathsf{v}}^{\mathsf{e}} \qquad \text{for all } \mathsf{e}\in\mathsf{E},\ \mathsf{v}\in\mathsf{V}\,. \tag{19.17}$$

The driving entropy functional is given by

$$\mathcal{E}(\mu) := \mathcal{E}_{\mathsf{L}}(\rho)+\mathcal{E}_{\mathsf{V}}(\gamma) := \sum_{\mathsf{e}\in\mathsf{E}}\mathcal{H}\left(\rho^{\mathsf{e}}\middle|\pi^{\mathsf{e}}\right)+\sum_{\mathsf{v}\in\mathsf{V}}\mathcal{H}\left(\gamma_{\mathsf{v}}|\omega_{\mathsf{v}}\right)\,, \tag{19.18}$$

where the relative entropy $\mathcal{H}$ is defined as

$$\mathcal{H}\left(\mu|\nu\right) := \begin{cases}\int\eta(\frac{\mathrm{d}\mu}{\mathrm{d}\nu})\,\mathrm{d}\nu, & \text{if } \mu\ll\nu\,,\\ +\infty, & \text{else,}\end{cases} \tag{19.19}$$

where $\eta(r) := r\log r - r + 1$ for $r\geq 0$. Here and in the following, we use the convention that $0\cdot\log 0 = 0$.

Remark 19.2 As the above system (19.16) is a combination of diffusion on the metric edges and a reaction-like mechanism for the mass exchange between edges and nodes, the gradient flow structure also consists of two parts. While the edge dynamics can be captured by quadratic action functionals as introduced above, the reaction part requires a non-linear cosh-type functional. Thus, even on a formal level, the combination of quadratic diffusion terms with non-linear reaction terms does not yield a metric structure, and instead a JKO approach as in (19.20), one uses an $\mathcal{R}^*$–$\mathcal{R}$ formulation, see also [21] for details.

19.2.4.2 Kirchhoff Case

In [12], it was shown that the (ISO3) model is a $W_{K,3}$-gradient flow with respect to the energy functional

$$\mathcal{E}(\rho) := \sum_{\mathsf{e}\in\mathsf{E}}\mathcal{E}^{\mathsf{e}}\left(\rho^{\mathsf{e}}\right) = \sum_{\mathsf{e}\in\mathsf{E}}\int_0^{\ell^{\mathsf{e}}} F^{\mathsf{e}}\left(\rho^{\mathsf{e}}\right)+\frac{2D^{\mathsf{e}}g}{\lambda^{\mathsf{e}}}\sin\left(\omega^{\mathsf{e}}\right)\rho^{\mathsf{e}}x + d^{\mathsf{e}}\rho^{\mathsf{e}}\,\mathrm{d}x.$$

Here, the entropy density F^{e} for each edge e is defined based on the pressure-entropy relation

$$F^{\mathsf{e}\prime\prime}\left(\rho^{\mathsf{e}}\right) = \frac{2D^{\mathsf{e}}}{\lambda^{\mathsf{e}}}\frac{p'(\rho^{\mathsf{e}})}{\rho^{\mathsf{e}}}$$

together with $F^{\mathsf{e}}(0) := 0$. Moreover, the integration constants d_e arise from the fact that even though the global mass within the network is conserved, the mass per edge can change between ρ_0 and ρ_1.

In order to derive p-Wasserstein gradient flows with the defined energy $\mathcal{E}$, the optimality conditions of the *minimizing movement scheme*

$$\rho_{(i+1)\tau} = \arg\min_{\rho\in\mathcal{P}(\mathsf{G})} \left\{ \frac{1}{p\,\tau^{p-1}} W_{K,p}^{p}(\rho, \rho_{i\tau}) + \mathcal{E}(\rho) \right\}, \tag{19.20}$$

starting at the initial network state $\rho_0 := \rho_0$, for step size $\tau > 0$ are analyzed. It is then proven that for $\tau \to 0$, an appropriate time interpolation of the minimizers converges to a solution of the respective p-Wasserstein gradient flow.

The minimizing movement scheme provides a variational time discretization of the gradient flow associated with the energy functional $\mathcal{E}$ in the p-Wasserstein space, where in each time step the new $\rho_{(i+1)\tau}$ is chosen such that on the one hand it is "close enough" to the previous network state $\rho_{i\tau}$ (minimizing the transport cost), and on the other hand such that the new network state is a low energy state (as we aim at minimizing the energy $\mathcal{E}$).

Taking $\tau \to 0$ in the optimality conditions, then the resulting equation system of the p-Wasserstein gradient flow is given by

$$\begin{aligned} &\partial_t \rho^{\mathsf{e}} + \partial_x j^{\mathsf{e}} = 0, \\ &j^{\mathsf{e}} \left| j^{\mathsf{e}} \right|^{p-2} = -\left(\rho^{\mathsf{e}}\right)^{p-1} \partial_x \left(\mathcal{E}'\left(\rho^{\mathsf{e}}\right) \right). \end{aligned}$$

Plugging in our specific choice for the energy functional $\mathcal{E}$ as well as $p = 3$ results in (ISO3), expressed by

$$\begin{aligned} &\partial_t \rho^{\mathsf{e}} + \partial_x j^{\mathsf{e}} = 0, \\ &j^{\mathsf{e}} \left| j^{\mathsf{e}} \right|^{p-2} = -\left(\rho^{\mathsf{e}}\right)^2 \left(\frac{2D^{\mathsf{e}}}{\lambda^{\mathsf{e}} \rho^{\mathsf{e}}} \partial_x p^{\mathsf{e}}\left(\rho^{\mathsf{e}}\right) + \frac{2D^{\mathsf{e}} g}{\lambda^{\mathsf{e}}} \sin\left(\omega^{\mathsf{e}}\right) \right). \end{aligned}$$

For the same Wasserstein distance, yet in the case $p = 2$, the authors of [11] rigorously proved that the drift–diffusion–aggregation equation

$$\partial_t \rho = \Delta \rho + \nabla \cdot \Big(\rho (\nabla V + \nabla W[\rho]) \Big)$$

with non-local interaction part

$$W[\mu](x) := \int_{\mathsf{G}} W(x, y)\, \mathrm{d}\mu(y)$$

is a gradient flow with respect to the metric $W_{K,2}$. In this case, the energy functional is given as a sum of the logarithmic entropy and the non-local part

$$\mathcal{W}(\rho) := \frac{1}{2} \int_{\mathsf{G}\times\mathsf{G}} W(x, y)\, \mathrm{d}\rho(x) \mathrm{d}\rho(y),$$

where $W : \mathsf{G} \times \mathsf{G} \to \mathbb{R}$ is symmetric and Lipschitz continuous.

19.3 Zero-Width Limit of Gas Networks

To prove our main results we need to introduce some concepts that can be found in most textbooks on the subject of optimal transport, such as [32,33]. The major concepts introduced below were already motivated in the introduction.

Definition 19.6 (Cyclical monotonicity) Let X,Y be arbitrary sets, and take a cost function $c : X \times Y \to (-\infty, +\infty]$. A subset $\Gamma \subset X \times Y$ is said to be c-cyclically monotone if, for any $N \in \mathbb{N}$, and any family $(x_1, y_1), \ldots, (x_N, y_N)$ of points in Γ, the inequality

$$\sum_{i=1}^{N} c(x_i, y_i) \leq \sum_{i=1}^{N} c(x_i, y_{i+1}).$$

holds, using the convention $y_{N+1} = y_1$. A transference plan or coupling is said to be c-cyclically monotone if it is concentrated on a c-cyclically monotone set.

Definition 19.7 (c-concavity) A function $\phi : Y \to \mathbb{R} \cup \{-\infty\}$ is called c-concave if it is not identically $-\infty$ and there exists $\psi : X \to \mathbb{R} \cup \{+\infty\}$, such that

$$\phi(y) = \inf_{x \in X} \Big\{ c(x, y) - \psi(x) \Big\}.$$

Theorem 19.2 (Kantorovich Duality) *Let X and Y be Polish spaces, let $\mu \in \mathcal{P}(X)$ and $\nu \in \mathcal{P}(Y)$, and let $c : X \times Y \to \mathbb{R}_+ \cup \{+\infty\}$ be lower semicontinuous. Then the following holds:*

(i) Kantorovich duality:

$$\mathrm{OT}(\mu, \nu, c) := \inf_{\pi \in \Pi(\mu,\nu)} \left\{ \int c \, \mathrm{d}\pi \right\} = \sup_{\substack{\phi \in L^1(\mu),\, \psi \in L^1(\nu), \\ \phi(x) + \psi(y) \leq c(x,y)}} \left\{ \int \phi \, \mathrm{d}\mu + \int \psi \, \mathrm{d}\nu \right\}. \quad (19.21)$$

(ii) If c is real-valued and the optimal cost $\mathrm{OT}(\mu, \nu, c)$ is finite, then there exists a π-measurable c-cyclically monotone set $\Gamma \subset X \times Y$ (closed if c is continuous) such that for any $\pi \in \Pi(\mu, \nu)$ the following statements are equivalent:

a. π is optimal;
b. π is c-cyclically monotone;
c. π is concentrated on Γ;
d. there exists a c-concave function ϕ such that the equation $\phi(x) + \phi^c(y) = c(x, y)$ holds π-almost surely.

For a proof we refer to Theorem 5.10 in [33].

19.3.1 3D Modeling of Gas Network

In the three-dimensional case, we assume that each pipe has diameter $D = 2\varepsilon > 0$ and thus it will be represented by a cylinder with length ℓ^ε and radius ε, instead of a segment.

Remark 19.3 (3D metric graph) While the sets V and E remain the same in the 3D setting, the set L changes to

$$\mathsf{L} = \bigsqcup_{e\in\mathsf{E}} B_\varepsilon \times [0, \ell^\varepsilon],$$

where $B_\varepsilon := \left\{x \in \mathbb{R}^2 \,\middle|\, ||x||_2 \le \varepsilon\right\}$ is the two-dimensional ε-disk around the origin. Depending on the angle between pipes, for two connected three-dimensional edges $e_1, e_2 \in \mathsf{E}$ the spaces $B_\varepsilon \times (0, \ell^{e_1})$ and $B_\varepsilon \times (0, \ell^{e_2})$ are in general not disjoint. Therefore, alternatively the edges e can also only be assigned the respective disjoint space

$$B_\varepsilon \times [0, \ell^e] \Big\backslash \Big(\bigcup_{\tilde{e}\in\mathsf{E}\setminus\{e\}} B_\varepsilon \times \left[0, \ell^{\tilde{e}}\right] \Big),$$

while the remaining "shared" space is assigned to the corresponding vertex, so for each $\mathsf{v} \in \mathsf{V}$ we would assign

$$\bigcup_{\substack{e_1,e_2\in\mathsf{E}:\, e_1\neq e_2,\\ \mathsf{v}\in e_1,\, \mathsf{v}\in e_2}} (B_\varepsilon \times [0, \ell^{e_1}]) \cap (B_\varepsilon \times [0, \ell^{e_2}]).$$

For our following results this distinction is of no importance, as we will always consider the union of all three-dimensional edges embedded in $\mathbb{R}^3$.

19.3.2 Main Results

Let $\overline{\mathcal{N}} := \mathcal{G} \subset \mathbb{R}$ be the one-dimensional metric graph, which encodes the general structure of the gas network. Furthermore, we encode the three-dimensional gas network with $\mathcal{N}_\varepsilon := \overline{\mathcal{N}} + \mathbb{B}_\varepsilon \subset \mathbb{R}^3$, where the sum means Minkowski addition of sets and $\mathbb{B}_\varepsilon := \left\{x \in \mathbb{R}^3 \,\middle|\, ||x||_2 \le \varepsilon\right\}$ is the closed ball of radius ε in $\mathbb{R}^3$. Then, $\mathcal{N}_0$ corresponds to the 1D metric graph embedded in $\mathbb{R}^3$, thus its intrinsic dimension is 1.

For a well-defined limit $\varepsilon \to 0$ of the densities, describing the distribution of gas in the network, we need probability measures $(\mu_\varepsilon)_\varepsilon, (\nu_\varepsilon)_\varepsilon \in \mathcal{P}\left(\mathbb{R}^3\right)$ with support $\mathcal{N}_\varepsilon$, which weakly converge to probability measures $\mu_0, \nu_0 \in \mathcal{P}(\mathcal{N}_0)$. These limits μ_0 and ν_0 correspond to lifted versions of probability measures $\overline{\mu}, \overline{\nu} \in \mathcal{P}(\overline{\mathcal{N}})$, where the mass is allocated only along the lines of $\overline{\mathcal{N}}$. This means that μ_0 and ν_0 can be written as

$$\mu_0 = \overline{\mu} \otimes \delta_{x_2,x_3=0} \in \mathcal{P}(\mathcal{N}_\varepsilon) \quad \text{and} \quad \nu_0 = \overline{\nu} \otimes \delta_{y_2,y_3=0} \in \mathcal{P}(\mathcal{N}_\varepsilon),$$

for the Dirac measure δ on $\mathbb{R}^3$, so for any $Z \subseteq \mathbb{R}^3$ it is defined as

$$\delta_{z_2,z_3=0}(Z) = \begin{cases} 1 & \text{if } \exists z \in Z : \ z_2 = z_3 = 0, \\ 0 & \text{otherwise.} \end{cases}$$

In the following, for the support of the probability measures we will use the short-hand notation $\operatorname{spt}(\mu_\varepsilon), \operatorname{spt}(\nu_\varepsilon) = \mathcal{N}_\varepsilon$.

19.3.3 Convergence on the Entire Network

We first define a penalty function $\iota_{\mathcal{N}_\varepsilon}$ on $\mathbb{R}^3$, that incorporates the geometry of the 3D gas network $\mathcal{N}_\varepsilon$, penalizing any transport outside of the network. For a compact set $U \subset \mathbb{R}^3$, let

$$\iota_U(x) := \begin{cases} 0, & \text{if } x \in U, \\ +\infty, & \text{else.} \end{cases}$$

It is a standard result from convex analysis that $\iota_U(x)$ is lower-semicontinuous when U is closed.

By $C(x, y)$ we denote the set of all piecewise continuously differentiable curves $\gamma : [0, 1] \to \mathbb{R}^3$, $t \mapsto \gamma_t$ with endpoints x, y, i.e., $\gamma \in C(x, y)$ implies that $\gamma_0 = x$, $\gamma_1 = y$ and $\dot\gamma_t := \mathrm{d}\gamma_t/\mathrm{d}t$ is well-defined for a.e. $t \in [0, 1]$.

Define the cost function $c_\varepsilon(x, y) : \mathbb{R}^3 \times \mathbb{R}^3 \to \mathbb{R} \cup \{+\infty\}$ as

$$c_\varepsilon(x, y) := \inf_{\gamma \in C(x,y)} \left\{ \int_0^1 \|\dot\gamma_t\|^2 + \iota_{\mathcal{N}_\varepsilon}(\gamma_t)\, \mathrm{d}t \right\}. \tag{19.22}$$

Importantly, remark that for two points x, y in the same pipe of the three-dimensional network, the infimum in (19.22) is attained and the optimal path γ_t is a straight line between x and y. The defined cost function is particularly attractive as it combines the aforementioned property, while ensuring that the cost function is well defined between any two points of the network and thus gives rise to a geodesic-type of distance.

The optimal transport problem on the 3D network is then given by

$$\mathrm{OT}(\mu_\varepsilon, \nu_\varepsilon, c_\varepsilon) = \inf_{\pi_\varepsilon \in \Pi(\mu_\varepsilon, \nu_\varepsilon)} \left\{ \int_{\mathbb{R}^3 \times \mathbb{R}^3} c_\varepsilon(x, y)\, \mathrm{d}\pi_\varepsilon(x, y) \right\}, \tag{OT}$$

as in (19.21).

19.3.3.1 Properties of the Cost

First, notice that defining cost functions based on action minimizing curves is a classical theme in optimal transport, see for instance [33, Chap. 7]. The problem of interest can be thought of as plain optimal transport, where the trajectories γ need to avoid exiting the pipes, a problem conceptually not far from optimal transport in the presence of obstacles. In this last setting for instance, [5] relies on a similar construction.

In a more computational context, [31] proposed to study a similar problem where $\iota_U(x)$ is replaced by a smooth function acting as a barrier. A smooth penalty function has indeed additional computational benefits, however it does not strictly enforce the condition of staying within the network, which could lead to γ "cutting the corner" at pipe intersections.

The introduced cost function relies on curves minimizing the *action*

$$\mathcal{A}(\gamma) := \int_0^1 \|\dot\gamma_t\|^2 + \iota_{\mathcal{N}_\varepsilon}(\gamma_t)\,\mathrm{d}t,$$

where the integrand is often called a *Lagrangian*. This framework is covered in detail in [33, Chap. 7]. It can be easily verified that $\|v\|^2 + \iota_{\mathcal{N}_\varepsilon}(x)$ is convex and superlinear in v.

Lemma 19.2 *For any $x \in \mathrm{int}(\mathcal{N}_\varepsilon)$, the interior of $\mathcal{N}_\varepsilon$, assume that there is a unique geodesic $\gamma_t^\star$, i.e., a unique minimizer in the definition of $c_\varepsilon(x, y)$, joining x to a given $y \in \mathcal{N}_\varepsilon$. Then the cost $c_\varepsilon(x, y)$ is C^1 in x and*

$$\nabla_x c_\varepsilon(x, y) = -2\dot\gamma_t^\star|_{t=0}.$$

Proof. Under the assumption of a unique optimizer $\gamma_t^\star$ in (19.22), we get

$$c_\varepsilon(x, y) = \int_0^1 \|\dot\gamma_t^\star\|^2\,\mathrm{d}t.$$

To obtain the derivative, first pick $x' \in \mathcal{N}_\varepsilon$ sufficiently close to x, such that there exists a unique geodesic connecting x and x' in $\mathcal{N}_\varepsilon$. We will establish the limit as $x' \to x$. Then, due to the continuous dependence of $\gamma_t^\star$ on x, we can "slightly modify" $\gamma_t^\star$ to become γ_t', which now connects x' and y, instead of x and y, and thus

$$c_\varepsilon(x', y) \le \int_0^1 \|\dot\gamma_t{}'\|^2\,\mathrm{d}t,$$

as the path γ_t' might not be optimal. The formula of first variation then gives

$$c_\varepsilon(x', y) \le \int_0^1 \left(\|\dot\gamma_t^\star\|^2 - 2\langle\dot\gamma_0^\star, x' - x\rangle\right)\mathrm{d}t + \mathrm{o}\left(\sup_{0\le t\le 1}\|\gamma_t^\star - \gamma_t'\|\right),$$

which quantifies the difference between the action of the optimal curve connecting x' and y, and the action of the slightly perturbed curve γ_t'.

A suitable choice of γ_t' ensures that $\sup_{0\le t\le 1}\|\gamma_t^\star - \gamma_t'\| = \|x' - x\|$. Therefore, we obtain by subtracting the equality $c_\varepsilon(x, y) = \int_0^1 \|\dot\gamma_t^\star\|^2\,\mathrm{d}t$ from the above inequality

$$c_\varepsilon(x', y) - c_\varepsilon(x, y) \le -2\langle\dot\gamma_0^\star, x' - x\rangle + \mathrm{o}\left(\|x' - x\|\right),$$

which establishes that $-2\dot\gamma_0^\star$ is an upper gradient of $c_\varepsilon(x, y)$.

By exchanging the roles of x and x', coupled with the continuity of the geodesics, a similar argument then yields a matching lower bound, and the claim follows. □

19.3.4 Existence of an Optimal Map

To prove the existence of a unique coupling $\pi_\varepsilon^\star$ in (OT), one possibility is to prove the existence of a unique map T such that each point $x \in \mathcal{N}_\varepsilon$ is sent to a unique $y = T(x) \in \mathcal{N}_\varepsilon$. Given our previous discussion on the cost function, the standard proofs for uniqueness of a coupling do not apply in this setting. Indeed, the latter proofs would usually try to extract such a map T from the dual formulation (19.21), i.e., from the relationship

$$\phi(x) + \phi^c(y) = c_\varepsilon(x, y) \quad \text{for } (x, y) \in \operatorname{spt}(\pi_\varepsilon^\star).$$

The idea of deriving $y = T(x)$ is to argue along the lines of the implicit function theorem. Assuming differentiability of ϕ, the above equality gives

$$\nabla\phi(x) = \nabla_x c_\varepsilon(x, y),$$

from which the transport plan could be obtained if the map $y \mapsto \nabla_x c_\varepsilon(x, y)$ was injective for every fixed $x \in \mathcal{N}_\varepsilon$. However, contrary to the case covered in [33, Remark 10.32], the minimizing curves $\gamma_t^\star$ are not uniquely determined by their starting point x and their initial velocity $\dot\gamma_t^\star|_{t=0}$, hence the set of y corresponding to a pair $\left(x, \dot\gamma_t^\star|_{t=0}\right)$ is generally not a singleton.

The issue of absence of injectivity also appears in the case of *branching geodesics*, which has attracted some attention, see for instance [8] and [11]. This means that for two geodesics $\gamma_t^\star$ and $\beta_t^\star$ with the same starting point x and initial velocities $\dot\gamma_t^\star|_{t=0} = \dot\beta_t^\star|_{t=0}$, there exists a point in time $t_0 \in (0, 1)$, such that

$$\forall t \in [0, t_0] : \gamma_t^\star = \beta_t^\star \quad \text{and} \quad \forall t \in (t_0, 1] : \gamma_t^\star \neq \beta_t^\star.$$

In the network setting this phenomenon arises as soon as there exists at least one junction (of at least three pipes), such as in the example graph below in Fig. 19.1.

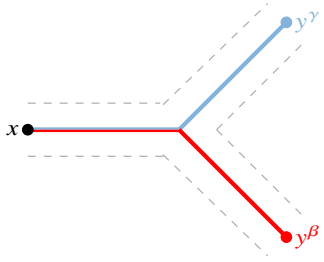


Fig. 19.1: Example for branching geodesics at junctions

19.3.4.1 Main Results

We start by establishing that the optimal transport cost (OT) converges for $\varepsilon \to 0$. To this end, let us first recall that a measure μ is called atomeless if for all μ-measurable sets $A \subset \mathbb{R}^3$ with $\mu(A) > 0$, there exists a μ-measurable set $B \subset A$ with $0 < \mu(B) < \mu(A)$.

Proposition 19.1 *Assume that the sequences (μ_ε) and (ν_ε) are sequences of absolutely continuous probability measures with respect to the Lebesgue measure, that further converge weakly to atomeless probability measures μ_0, ν_0 supported on $\mathcal{N}_0$. Then,*

$$\mathrm{OT}(\mu_\varepsilon, \nu_\varepsilon, c_\varepsilon) \to \mathrm{OT}(\mu_0, \nu_0, c_0), \quad \text{as } \varepsilon \to 0.$$

Proof. Denote by P the projection of a point from $\mathcal{N}_\varepsilon$ to the closest point in $\mathcal{N}_0$, with respect to the Euclidean distance, and in the case of the closest point in $\mathcal{N}_0$ not being unique (which can happen at the junction of pipes), pick an arbitrary point from the contenders in $\mathcal{N}_0$.

For Lebesgue-almost every pair $(x, y) \in \mathcal{N}_\varepsilon \times \mathcal{N}_\varepsilon$, it holds

$$c_\varepsilon(x, y) \le c_0(P(x), P(y)) + 2\varepsilon^2,$$

as this construction amounts to picking a non-optimal path between x and y. Recall that for any μ-nullset E, integrating a function f with $f(x) = +\infty$ for all $x \in E$ evaluates at 0, so $\int_E f(x)\,\mathrm{d}\mu(x) = 0$. Therefore, we do not need the previous inequality for x or $y \in \mathbb{R}^3 \setminus \mathcal{N}_\varepsilon$. This then yields

$$\begin{aligned}\int_{\mathbb{R}^3\times\mathbb{R}^3} c_\varepsilon(x, y)\,\mathrm{d}\pi_\varepsilon(x, y) &\le \int_{\mathbb{R}^3\times\mathbb{R}^3} c_0(P(x), P(y))\,\mathrm{d}\pi_\varepsilon(x, y) + 2\varepsilon^2 \\ &= \int_{\mathbb{R}^3\times\mathbb{R}^3} c_0\,\mathrm{d}(P, P)_\#\pi_\varepsilon + 2\varepsilon^2,\end{aligned}$$

where for any probability measure $\mu \in \mathcal{P}(X)$, the notation $F_\#\mu$ for a measurable function $F : X \to Y$ corresponds to the pushforward measure defined as $F_\#\mu \in \mathcal{P}(Y)$ with $F_\#\mu(B) := \mu\big(F^{-1}(B)\big)$ for measurable $B \subseteq Y$.

Now, for any coupling π_ε of the marginals $\mu_\varepsilon, \nu_\varepsilon$, the term $(P, P)_\#\pi_\varepsilon$ corresponds to a coupling between $P_\#\mu_\varepsilon \in \mathcal{P}(\mathcal{N}_0)$ and $P_\#\nu_\varepsilon \in \mathcal{P}(\mathcal{N}_0)$. Optimizing over π_ε is thus equivalent to optimizing over couplings of $P_\#\mu_\varepsilon$ and $P_\#\nu_\varepsilon$ and so, we obtain

$$\inf_{\pi_\varepsilon \in \Pi(\mu_\varepsilon, \nu_\varepsilon)} \left\{ \int_{\mathbb{R}^3\times\mathbb{R}^3} c_0\,\mathrm{d}(P, P)_\#\pi_\varepsilon \right\} = \inf_{\pi_\varepsilon^P \in \Pi(P_\#\mu_\varepsilon, P_\#\nu_\varepsilon)} \left\{ \int_{\mathbb{R}^3\times\mathbb{R}^3} c_0\,\mathrm{d}\pi_\varepsilon^P \right\}.$$

Further, $P_\#\mu_\varepsilon, P_\#\nu_\varepsilon$ converge weakly to $P_\#\mu_0 = \mu_0$ and $P_\#\nu_0 = \nu_0$, by the continuous mapping theorem. Note that the assumption on the absence of atoms of the limits μ_0, ν_0 is required here, because of the absence of continuity of the projection P at junctions, which are not charged as P is continuous μ_0- and ν_0-almost everywhere.

One can then invoke Theorem 1.51 in [32] (where we once again use the argument that $P_\#\mu_\varepsilon(\mathbb{R}^3 \setminus \mathcal{N}_0) = 0$ and $P_\#\nu_\varepsilon(\mathbb{R}^3 \setminus \mathcal{N}_0) = 0$ for all $\varepsilon > 0$, as well as $P_\#\mu_0(\mathbb{R}^3 \setminus \mathcal{N}_0) = 0$ and $P_\#\nu_0(\mathbb{R}^3 \setminus \mathcal{N}_0) = 0$ to circumvent the non-compactness of $\mathbb{R}^3$ and c_0 being non-

continuous) to conclude that

$$\inf_{\pi_\varepsilon^P \in \Pi(P_\#\mu_\varepsilon, P_\#\nu_\varepsilon)} \left\{ \int_{\mathbb{R}^3\times\mathbb{R}^3} c_0 \, \mathrm{d}\pi_\varepsilon^P \right\} \to \inf_{\pi_0 \in \Pi(\mu_0,\nu_0)} \left\{ \int_{\mathbb{R}^3\times\mathbb{R}^3} c_0 \, \mathrm{d}\pi_0 \right\} = \mathrm{OT}\,(\mu_0, \nu_0, c_0),$$

as $\varepsilon \to 0$, which yields

$$\mathrm{OT}\,(\mu_\varepsilon, \nu_\varepsilon, c_\varepsilon) \le \mathrm{OT}\,(\mu_0, \nu_0, c_0).$$

In the other direction, for Lebesgue-almost every pair $(x, y) \in \mathcal{N}_\varepsilon \times \mathcal{N}_\varepsilon$, we have

$$c_\varepsilon(x, y) \ge c_0(P(x), P(y)) - K\varepsilon^2,$$

where $K > 0$ is some constant depending on the network. This constant K is necessary as the network $\mathcal{N}_\varepsilon$ allows for shorter paths around a corner (at junctions) compared to the graph $\mathcal{N}_0$. Since the number of pipes and junctions is finite, the amount of path length that can be "saved" in $\mathcal{N}_\varepsilon$, compared to $\mathcal{N}_0$, can be bounded from above.

The length of the path obtained by projecting first two points $x, y \in \mathcal{N}_\varepsilon$ on $\mathcal{N}_0$, and then joining them by the shortest path on $\mathcal{N}_0$ must thus stay within a term $K\varepsilon^2$. The claim then follows from a similar argument as above. We have

$$\begin{aligned}\int_{\mathbb{R}^3\times\mathbb{R}^3} c_\varepsilon(x, y) \, \mathrm{d}\pi_\varepsilon(x, y) &\ge \int_{\mathbb{R}^3\times\mathbb{R}^3} c_0(P(x), P(y)) \, \mathrm{d}\pi_\varepsilon(x, y) - K\varepsilon^2 \\ &= \int_{\mathbb{R}^3\times\mathbb{R}^3} c_0 \, \mathrm{d}(P, P)_\#\pi_\varepsilon - K\varepsilon^2\end{aligned}$$

with the equality from before

$$\inf_{\pi_\varepsilon \in \Pi(\mu_\varepsilon,\nu_\varepsilon)} \left\{ \int_{\mathbb{R}^3\times\mathbb{R}^3} c_0 \, \mathrm{d}(P, P)_\#\pi_\varepsilon \right\} = \inf_{\pi_\varepsilon^P \in \Pi(P_\#\mu_\varepsilon, P_\#\nu_\varepsilon)} \left\{ \int_{\mathbb{R}^3\times\mathbb{R}^3} c_0 \, \mathrm{d}\pi_\varepsilon^P \right\},$$

where the convergence of the right-hand-side term for $\varepsilon \to 0$ gives us the desired inequality

$$\mathrm{OT}\,(\mu_\varepsilon, \nu_\varepsilon, c_\varepsilon) \ge \mathrm{OT}\,(\mu_0, \nu_0, c_0).$$

Therefore, for $\varepsilon \to 0$, based on the sandwich theorem, we can conclude

$$\mathrm{OT}(\mu_\varepsilon, \nu_\varepsilon, c_\varepsilon) \to \mathrm{OT}(\mu_0, \nu_0, c_0). \qquad \square$$

The question of establishing the convergence of π_ε as $\varepsilon \to 0$ is thus a stability issue with respect to both measures $\mu_\varepsilon, \nu_\varepsilon$ and cost c_ε. This question is addressed in Chap. 5 of [33], for instance. This being said, the results therein do not apply directly to our context because our cost function does not converge uniformly on $\mathcal{N}_\varepsilon$.

Our main theorem is the following.

Theorem 19.3 *Let $(\mu_\varepsilon)_\varepsilon, (\nu_\varepsilon)_\varepsilon$ be sequences of probability measures with support $\mathcal{N}_\varepsilon$, and consider the sequence of cost functions $(c_\varepsilon)_\varepsilon$ defined in* (19.22)*. Moreover, by $\pi_\varepsilon^\star$ we denote any optimizer of problem* (OT)*, which might not be uniquely determined. If $\pi_0^\star$, the solution of* (OT) *for $\varepsilon = 0$, is unique, then (all)*

$$\pi_\varepsilon^\star \to \pi_0^\star$$

weakly as $\varepsilon \to 0$. Otherwise, each convergent subsequence of $\pi_\varepsilon^\star$ converges to one of the optimizers $\pi_0{}^\star$ of (OT).

Proof. As μ_ε and ν_ε are weakly convergent sequences, by Prokhorov's theorem they constitute tight sets, so for all $\xi > 0$ there exist compact sets $K_\mu, K_\nu \subset \mathbb{R}^3$ such that

$$\sup_{0<\varepsilon<1} \left\{\mu_\varepsilon\left(\mathbb{R}^3 \backslash K_\mu\right)\right\}, \sup_{0<\varepsilon<1} \left\{\nu_\varepsilon\left(\mathbb{R}^3 \backslash K_\nu\right)\right\} < \xi.$$

Then, by Lemma 4.4 in [33], the couplings $\pi_\varepsilon \in \Pi(\mu_\varepsilon, \nu_\varepsilon)$ all lie in a tight set of $\mathbb{R}^3 \times \mathbb{R}^3$.

First, let us recall that optimizers $\pi_\varepsilon^\star$ of (OT) exist, i.e., the infimum is attained as the set of couplings is compact and $\pi \mapsto \int c \, \mathrm{d}\pi$ is a lower-bounded, linear functional. Due to the tightness of the couplings, applying Prokhorov's theorem to a sequence of optimizers $\pi_\varepsilon^\star$, we can extract a subsequence, still denoted $\pi_\varepsilon^\star$ for simplicity, which converges weakly to some $\pi_0^* \in \Pi(\mu_0, \nu_0)$. We aim at proving that this limiting coupling π_0^* is an optimizer of (OT) for $\varepsilon = 0$, by showing that it is c_0-cyclically monotone.

Note that in $\mathcal{N}_\varepsilon \times \mathcal{N}_\varepsilon$, c_ε is continuous and upper bounded, implying that $\mathrm{OT}(\mu_\varepsilon, \nu_\varepsilon, c_\varepsilon)$ is bounded as well. We can thus apply Theorem 19.2 and as $\pi_\varepsilon^\star$ is optimal, each $\pi_\varepsilon^\star$ is concentrated on a c_ε-cyclically monotone set. Moreover, for any $N \geq 1$ pick arbitrary points $(x_1, y_1), \ldots, (x_N, y_N)$ from the support of $\pi_\varepsilon^\star$ and denote this set of points by $\pi_\varepsilon^{\otimes N}$. Additionally, define the set $C_\varepsilon(N)$ as the set of all sets of N points $\{(\tilde{x}_1, \tilde{y}_1), \ldots, (\tilde{x}_N, \tilde{y}_N)\}$ from $\mathcal{N}_\varepsilon \times \mathcal{N}_\varepsilon$ such that

$$\sum_{i=1}^{N} c_\varepsilon(\tilde{x}_i, \tilde{y}_i) \leq \sum_{i=1}^{N} c_\varepsilon(\tilde{x}_i, \tilde{y}_{i+1}), \tag{19.23}$$

with the convention $\tilde{y}_{N+1} = \tilde{y}_1$.

By the c_ε-cyclical monotonicity of $\pi_\varepsilon^\star$, the set $\pi_\varepsilon^{\otimes N}$ is thus concentrated on $C_\varepsilon(N)$. Further, as the cost function c_ε is continuous on $\mathcal{N}_\varepsilon \times \mathcal{N}_\varepsilon$, the set of sets $C_\varepsilon(N)$ is closed. As a next step, we show that $\pi_\varepsilon^{\otimes N}$ is also concentrated on another set. Let $\delta > 0$ and N be given, define $C_\delta(N)$ as the set of all sets of N points $\{(\widehat{x}_1, \widehat{y}_1), \ldots, (\widehat{x}_N, \widehat{y}_N)\}$ from $\mathcal{N}_\varepsilon \times \mathcal{N}_\varepsilon$ such that

$$\sum_{i=1}^{N} c_0(\widehat{x}_i, \widehat{y}_i) \leq \sum_{i=1}^{N} c_0(\widehat{x}_i, \widehat{y}_{i+1}) + \delta, \tag{19.24}$$

which corresponds to a δ-approximate c_0-cyclical monotonicity. We now want to prove that, for ε small enough, the set $\pi_\varepsilon^{\otimes N}$ is concentrated on $C_\delta(N)$. We do so by distinguishing two cases: First, either at least one of the x_i's or the y_i's from $\pi_\varepsilon^{\otimes N}$ is not in $\mathcal{N}_0$, in which case both sides of the inequality (19.24) are $+\infty$ and the inequality holds trivially. Second, if $\pi_\varepsilon^{\otimes N} \subset \mathcal{N}_0 \times \mathcal{N}_0$ observe that for all $x, y \in \mathcal{N}_0$ we get

$$c_\varepsilon(x, y) \leq c_0(x, y),$$

which together with the c_ε-cyclical monotonicity of $\pi_\varepsilon^\star$, so (19.23), results in

$$\sum_{i=1}^{N} c_\varepsilon(x_i, y_i) \leq \sum_{i=1}^{N} c_\varepsilon(x_i, y_{i+1}) \leq \sum_{i=1}^{N} c_0(x_i, y_{i+1}).$$

Finally, $c_\varepsilon(x, y)$ converges uniformly to $c_0(x, y)$ for $x, y \in \mathcal{N}_0$, so there exists $\varepsilon > 0$ small enough such that for all $x, y \in \mathcal{N}_0$ we obtain

$$|c_\varepsilon(x, y) - c_0(x, y)| \leq \frac{\delta}{N}.$$

Therefore, (19.24) indeed also holds for all x_i, y_i's in $\mathcal{N}_0$, which consequently yields $\operatorname{spt}\left(\pi_\varepsilon^{\otimes N}\right) \subseteq C_\delta(N)$ for ε small enough. Since $C_\delta(N)$ is a closed set, the weak convergence of $\pi_\varepsilon^\star$ to π_0^* also implies $\operatorname{spt}\left(\pi_0^{\otimes N}\right) \subseteq C_\delta(N)$. To show that $C_\delta(N)$ is closed, a sublevel set argument for the function $f : \left(\mathbb{R}^3 \times \mathbb{R}^3\right)^N \to \mathbb{R} \cup \{+\infty\}$ with $((x_1, y_1), \ldots, (x_N, y_N)) \mapsto \sum_{i=1}^N c_0(x_i, y_i) - \sum_{i=1}^N c_0(x_i, y_{i+1})$ can be used for $C_\delta(N) = \{z \mid f(z) \leq \delta\}$.

As the inequality (19.24) holds for all $((x_1, y_1), \ldots, (x_N, y_N)) \in \operatorname{spt}\left(\pi_0^{\otimes N}\right)$ for all $\delta > 0$, in the limit $\delta \to 0$, we get

$$\sum_{i=1}^{N} c_0(x_i, y_i) \leq \sum_{i=1}^{N} c_0(x_i, y_{i+1})$$

for all $((x_1, y_1), \ldots, (x_N, y_N)) \in \operatorname{spt}\left(\pi_0^{\otimes N}\right)$. Therefore, π_0^* is c_0-cyclically monotone, which guarantees the optimality of π_0^* in (OT) for $\varepsilon = 0$ by Theorem 19.2.

Finally, in the case of a unique $\pi_0^\star$, we conclude the convergence of each subsequence $\pi_\varepsilon^\star$ to $\pi_0^\star$, so that the whole sequence converges to $\pi_0^\star$ by a classical subsequence argument. □

Remark 19.4 In the somewhat trivial case of a network consisting of a single pipe, all the presented results still apply. The unique difference is that then the initial velocity is sufficient to characterize a geodesic, and uniqueness of the transport plan holds for each $\varepsilon > 0$ under the assumption of the measures $\mu_\varepsilon, \nu_\varepsilon$ having a density with respect to the Lebesgue measure.

19.3.5 Towards a Dynamical Understanding

The issue underlying the absence of uniqueness of optimizers $\pi_\varepsilon^\star$ was pointed out above and relates to the fact that minimizing curves in the network change directions. Still, one intuits that minimal additional knowledge could suffice to still get a transport plan in "well-behaved" examples. To make a step in that direction and explain the open questions, let us consider the space-time lifting of the problem, i.e., we extend the measures μ_ε and ν_ε to $\mu_\varepsilon \otimes \delta_{t=0}$ and $\nu_\varepsilon \otimes \delta_{t=1}$ and utilize the cost function

$$\tilde{c}((x,s),(y,t)) = \inf\left\{\int_s^t \|\dot{\gamma}_u\|^2 + \iota_{\mathcal{N}_\varepsilon}(\gamma_u)\,\mathrm{d}u : \gamma(s) = x, \gamma(t) = y\right\},$$

for a piecewise absolutely continuous curve γ_u and $s, t \in [0,1]$.

From the characterization of the dual problem, if the following quantities were well-defined and the function

$$G_{(x,s)}(y,t) := (y,t) \mapsto \begin{pmatrix} \nabla_x \tilde{c}((x,s),(y,t)) \\ \partial_s \tilde{c}((x,s),(y,t)) \end{pmatrix}$$

was invertible, then the optimal transport map in the space-time domain is given by

$$T(x,t) = G^{-1}_{(x,s)} \begin{pmatrix} \nabla_x \psi(x,s) \\ \partial_s \psi(x,s) \end{pmatrix},$$

where $\psi(x,s)$ is an optimal dual potential.

19.3.6 Stability with Respect to the Gas Network Topology

An important question is to know how the optimal gas transport depends on the topology of the network, and in particular how the cost of transport would be affected in case of modifications of the network structure.

To better understand this, let us introduce the following setting. We consider two probability measures μ, ν that are supported on $\check{\mathcal{N}}_0 := \mathcal{N}_0 \setminus \mathcal{M}$, where $\mathcal{M}$ is a set of edges in the central portion of the graph, which are removed to get a new graph structure. Usually, one thinks of μ as a source and ν as a target, such that μ is flowing to ν through $\mathcal{M}$ (at least partially). As a next step we can add new edges as a substitute for $\mathcal{M}$, which we denote by $\widetilde{\mathcal{M}}$ to get the new graph $\widetilde{\mathcal{N}} := \mathcal{N}_0 \setminus \mathcal{M} \cup \widetilde{\mathcal{M}}$. Note that we require $\widetilde{\mathcal{N}}$ to be still connected to allow for a feasible transport. Then, we define the modified cost function

$$\tilde{c}(x,y) := \inf_{\gamma \in C(x,y)} \int_0^1 \|\dot{\gamma}_t\|^2 + \iota_{\widetilde{\mathcal{N}}}(\gamma_t)\,\mathrm{d}t,$$

as well as the modified optimal transport problem

$$\mathrm{OT}(\mu,\nu,\tilde{c}) := \inf_{\pi \in \Pi(\mu,\nu)} \int_{\check{\mathcal{N}}_0 \times \check{\mathcal{N}}_0} \tilde{c}\,\mathrm{d}\pi.$$

Recall that μ and ν are supported on $\check{\mathcal{N}}_0$ and thus π is supported on $\check{\mathcal{N}}_0 \times \check{\mathcal{N}}_0$, however the transport through the new section of the graph $\widetilde{\mathcal{M}}$ is accounted for in the cost function $\tilde{c}$ as the feasible shortest-path curves γ live on the space domain $\widetilde{\mathcal{N}}$.

We denote by $O^\star$ and $\widetilde{O}^\star$ the set of optimal couplings in both problems, i.e.,

$$O^\star := \left\{\pi \in \Pi(\mu,\nu) : \int_{\check{\mathcal{N}}_0 \times \check{\mathcal{N}}_0} c\,\mathrm{d}\pi = \inf_{\pi \in \Pi(\mu,\nu)} \int_{\check{\mathcal{N}}_0 \times \check{\mathcal{N}}_0} c\,\mathrm{d}\pi\right\},$$

$$\widetilde{O}^\star := \left\{ \tilde{\pi} \in \Pi(\mu,\nu) : \int_{\check{\mathcal{N}}_0 \times \check{\mathcal{N}}_0} \tilde{c}\, \mathrm{d}\tilde{\pi} = \inf_{\tilde{\pi} \in \Pi(\mu,\nu)} \int_{\check{\mathcal{N}}_0 \times \check{\mathcal{N}}_0} \tilde{c}\, \mathrm{d}\tilde{\pi} \right\}.$$

The following theorem relates the values of the optimal costs between the two situations, i.e., before and after modification of the gas network.

Theorem 19.4 *In the above setting, it holds true that*

$$\begin{aligned} |\operatorname{OT}(\mu,\nu,\tilde{c}) - \operatorname{OT}(\mu,\nu,c)| &\le \max\left\{ \inf_{\pi \in O^\star} \int_{\check{\mathcal{N}}_0 \times \check{\mathcal{N}}_0} |\tilde{c} - c| \mathrm{d}\pi,\ \inf_{\tilde{\pi} \in \widetilde{O}^\star} \int_{\check{\mathcal{N}}_0 \times \check{\mathcal{N}}_0} |\tilde{c} - c| \mathrm{d}\tilde{\pi} \right\} \\ &\le \|\tilde{c} - c\|_\infty. \end{aligned}$$

Remark 19.5 The middle bound expresses the natural intuition that one might have: The difference in cost between the two network topologies depends on the difference between the costs weighted by the mass transported between these points.

Remark 19.6 (Deleting one connection) If the change consists in removing a single pipe within the network, then for all $x, y \in \check{\mathcal{N}}_0$ it holds true that

$$c(x,y) \le \tilde{c}(x,y),$$

as each path that was going through this pipe now should be at least as long. Thus,

$$\operatorname{OT}(\mu,\nu,\tilde{c}) - \operatorname{OT}(\mu,\nu,c) \le \inf_{\pi \in O^\star} \int_{\check{\mathcal{N}}_0 \times \check{\mathcal{N}}_0} (\tilde{c} - c)\, \mathrm{d}\pi^\star.$$

Proof of Theorem 19.4. Plugging in the definitions of OT, we get the equality

$$\operatorname{OT}(\mu,\nu,\tilde{c}) - \operatorname{OT}(\mu,\nu,c) = \inf_{\pi \in \Pi(\mu,\nu)} \int_{\check{\mathcal{N}}_0 \times \check{\mathcal{N}}_0} \tilde{c}\, \mathrm{d}\pi - \inf_{\pi \in \Pi(\mu,\nu)} \int_{\check{\mathcal{N}}_0 \times \check{\mathcal{N}}_0} c\, \mathrm{d}\pi,$$

and then taking any $\pi^\star$ that is an optimal coupling for the problem involving the cost c, we obtain

$$\begin{aligned} \operatorname{OT}(\mu,\nu,\tilde{c}) - \operatorname{OT}(\mu,\nu,c) &\le \int_{\check{\mathcal{N}}_0 \times \check{\mathcal{N}}_0} \tilde{c}\, \mathrm{d}\pi^\star - \underbrace{\inf_{\pi \in \Pi(\mu,\nu)} \int_{\check{\mathcal{N}}_0 \times \check{\mathcal{N}}_0} c\, \mathrm{d}\pi}_{= \int_{\check{\mathcal{N}}_0 \times \check{\mathcal{N}}_0} c\, \mathrm{d}\pi^\star} \\ &= \int_{\check{\mathcal{N}}_0 \times \check{\mathcal{N}}_0} (\tilde{c} - c)\, \mathrm{d}\pi^\star \\ &\le \int_{\check{\mathcal{N}}_0 \times \check{\mathcal{N}}_0} |\tilde{c} - c|\, \mathrm{d}\pi^\star. \end{aligned}$$

So that, because of the arbitrariness of $\pi^\star \in O^\star$,

$$\operatorname{OT}(\mu,\nu,\tilde{c}) - \operatorname{OT}(\mu,\nu,c) \le \inf_{\pi \in O^\star} \int_{\check{\mathcal{N}}_0 \times \check{\mathcal{N}}_0} |\tilde{c} - c|\, \mathrm{d}\pi.$$

For the other direction, apply the same idea, picking a coupling $\tilde{\pi}^\star \in \widetilde{O}^\star$, to get

$$\mathrm{OT}(\mu,\nu,c)-\mathrm{OT}(\mu,\nu,\tilde{c})\leq \inf_{\tilde{\pi}\in\widetilde{O}^{\star}}\int_{\check{N}_0\times\check{N}_0}|\tilde{c}-c|\,\mathrm{d}\tilde{\pi}.$$

The first part of the claim follows. For the second part, note that $\|c-\tilde{c}\|_{\infty}\geq\int|c-\tilde{c}|\,\mathrm{d}\pi$, as $\int\mathrm{d}\pi=1$. □

19.4 Numerical Illustrations

In this final section, we exhibit (estimated) trajectories of a shortest path metric constrained to stay within the network. Based on a uniform grid in the network, we construct a graph linking each grid point (or pixel for the later representation) to its 8 surrounding nearest neighbors and itself with the following squared distance matrix

$$\begin{pmatrix}2&1&2\\1&0&1\\2&1&2\end{pmatrix}.$$

Then, given random points on the structure, we compute the cost matrix based on the shortest path between each pair of points (obtained using Dijkstra's algorithm) and solve a linear assignment problem.

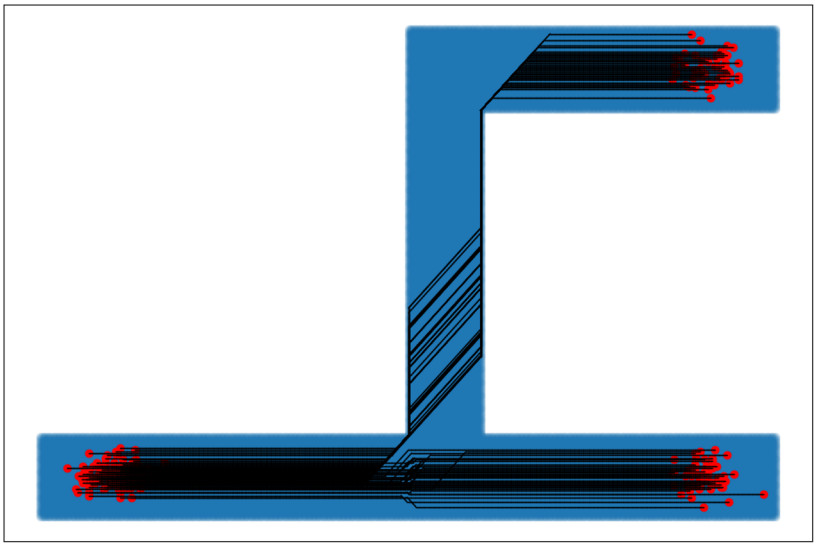


Fig. 19.2: Example of estimated trajectories based on a space-discretized version of the problem. The source measure is the set of points in the lower left corner, while the target measure are the two accumulations of points at the right hand side.

We finally represent the trajectories between the matched points in Fig. 19.2. We clearly see the fact that in this example geodesics branch and also collapse. This explains why the standard proofs of uniqueness of transport plans do not apply—recall Sect. 19.3.3.1—and why the construction in Sect. 19.3.5 would be required to derive a potential existence of a unique transport plan.

Acknowledgements This work was supported by the German Research Foundation (DFG) within Subproject C06 in the Sonderforschungsbereich/Transregio 154 "Mathematical Modelling, Simulation and Optimization using the Example of Gas Networks" (Project ID 239904186).

JFP thanks the DFG for support via the Research Unit "FOR 5387 POPULAR" (Project ID 461909888). AF and MB acknowledge support from DESY (Hamburg, Germany), a member of the Helmholtz Association HGF.

References

1. L. Ambrosio. Gradient flows in metric spaces and in the spaces of probability measures, and applications to fokker-planck equations with respect to log-concave measures. *Bollettino dell'Unione Matematica Italiana*, 1(1):223–240, 2008.
2. M. Arjovsky, S. Chintala, and L. Bottou. Wasserstein generative adversarial networks. In *International conference on machine learning*, pages 214–223. Pmlr, 2017. doi:10.5555/3305381.3305404.
3. J.-D. Benamou and Y. Brenier. A computational fluid mechanics solution to the monge-kantorovich mass transfer problem. *Numerische Mathematik*, 84(3):375–393, 2000. doi:10.1007/s002110050002.
4. M. Burger, I. Humpert, and J.-F. Pietschmann. Dynamic optimal transport on networks. *ESAIM: Control, Optimisation and Calculus of Variations*, 29:54, 2023. doi:10.48550/arXiv.2101.03415.
5. P. Cardaliaguet and C. Jimenez. Optimal transport with convex obstacle. *Journal of mathematical analysis and applications*, 381(1):43–63, 2011. doi:10.1016/j.jmaa.2011.04.007.
6. M. Carioni, J. Krautz, and J.-F. Pietschmann. Dynamic optimal transport with optimal preferential paths, 2025. arXiv:2504.03285.
7. M. Carioni, J. Krautz, and J.-F. Pietschmann. Dynamic optimal transport with optimal star-shaped graphs. *PAMM*, 26(1):e70076, 2026. doi:10.48550/arXiv.2506.15007.
8. F. Cavalletti. Optimal transport with branching distance costs and the obstacle problem. *SIAM Journal on Mathematical Analysis*, 44(1):454–482, 2012. doi:10.1137/100801433.
9. M. Cuturi. Sinkhorn distances: Lightspeed computation of optimal transport. *Advances in neural information processing systems*, 26, 2013. doi:10.48550/arXiv.1306.0895.
10. M. Erbar. Gradient flows of the entropy for jump processes. In *Annales de l'IHP Probabilités et statistiques*, volume 50, pages 920–945, 2014. doi:10.1214/12-AIHP537.
11. M. Erbar, D. Forkert, J. Maas, and D. Mugnolo. Gradient flow formulation of diffusion equations in the wasserstein space over a metric graph, 2021. arXiv:2105.05677.
12. A. Fazeny, M. Burger, and J.-F. Pietschmann. Optimal transport on gas networks. *European Journal of Applied Mathematics*, pages 1–33, 2025. doi:10.1017/S0956792525000051.
13. C. Frogner, C. Zhang, H. Mobahi, M. Araya, and T. Poggio. Learning with a wasserstein loss. *Advances in neural information processing systems*, 28, 2015. doi:10.48550/arXiv.1506.05439.
14. M. Hallin, G. Mordant, and J. Segers. Multivariate goodness-of-fit tests based on Wasserstein distance. *Electronic Journal of Statistics*, 15(1), 2021. doi:10.1214/21-EJS1816.
15. G. Heinze, J.-F. Pietschmann, and A. Schlichting. Gradient flows on metric graphs with reservoirs: Microscopic derivation and multiscale limits. *arXiv preprint arXiv:2412.16775*, 2024. doi:10.48550/arXiv.2412.16775.
16. R. Jordan, D. Kinderlehrer, and F. Otto. Free energy and the fokker-planck equation. *Physica D: Nonlinear Phenomena*, 107(2-4):265–271, 1997. doi:10.1016/S0167-2789(97)00093-6.

17. R. Jordan, D. Kinderlehrer, and F. Otto. The variational formulation of the Fokker–Planck equation. *SIAM journal on mathematical analysis*, 29(1):1–17, 1998. doi:10.1137/S0036141096303359.
18. L. V. Kantorovich. On the translocation of masses. *Journal of Mathematical Sciences*, 133(4), 2006. doi:10.1007/s10958-006-0049-2.
19. S. Kolouri, S. R. Park, M. Thorpe, D. Slepcev, and G. K. Rohde. Optimal mass transport: Signal processing and machine-learning applications. *IEEE signal processing magazine*, 34(4):43–59, 2017. doi:10.1109/MSP.2017.2695801.
20. H. Lavenant, S. Zhang, Y.-H. Kim, and G. Schiebinger. Towards a mathematical theory of trajectory inference, 2021. arXiv:2102.09204, doi:10.1214/23-AAP1969.
21. M. Liero, A. Mielke, M. A. Peletier, and D. Renger. On microscopic origins of generalized gradient structures, 2015. arXiv:1507.06322, doi:10.3934/dcdss.2017001.
22. S. Lisini. Characterization of absolutely continuous curves in wasserstein spaces. *Calculus of variations and partial differential equations*, 28(1):85–120, 2007. doi:10.1007/s00526-006-0032-2.
23. A. Mielke. An introduction to the analysis of gradients systems, 2023. arXiv:2306.05026.
24. A. Mielke, M. A. Peletier, and D. M. Renger. On the relation between gradient flows and the large-deviation principle, with applications to Markov chains and diffusion. *Potential Analysis*, 41(4):1293–1327, 2014. doi:10.1007/s11118-014-9418-5.
25. G. Monge. Mémoire sur la théorie des déblais et des remblais. *Mem. Math. Phys. Acad. Royale Sci.*, pages 666–704, 1781.
26. L. Monsaingeon. A new transportation distance with bulk/interface interactions and flux penalization. *Calculus of Variations and Partial Differential Equations*, 60(3):101, 2021. doi:10.1007/s00526-021-01946-2.
27. D. Mugnolo. What is actually a metric graph?, 2019. arXiv:1912.07549.
28. F. Otto. The geometry of dissipative evolution equations: The porous medium equation. *Communications in Partial Differential Equations*, 26, 2001. doi:10.1081/PDE-100002243.
29. V. M. Panaretos and Y. Zemel. Statistical aspects of Wasserstein distances. *Annual Review of Statistics and its Application*, 6(1):405–431, 2019. doi:10.1146/annurev-statistics-030718-104938.
30. G. Peyré and M. Cuturi. Computational optimal transport: With applications to data science. *Foundations and Trends in Machine Learning*, 11(5–6):355–607, 2019. doi:10.1561/2200000073.
31. A.-A. Pooladian, C. Domingo-Enrich, R. T. Chen, and B. Amos. Neural optimal transport with Lagrangian costs, 2024. arXiv:2406.00288.
32. F. Santambrogio. *Optimal Transport for Applied Mathematicians: Calculus of Variations, PDEs, and Modeling*, volume 87 of *Progress in Nonlinear Differential Equations and Their Applications*. Birkhäuser/Springer, Cham, 2015. doi:10.1007/978-3-319-20828-2.
33. C. Villani. *Optimal Transport: Old and New*, volume 338 of *Grundlehren der mathematischen Wissenschaften*. Springer, 2009. doi:10.1007/978-3-540-71050-9.
34. L. Weigand, A. Fazeny, and M. Burger. p-diffusion equations on graphs, 2026+. In preparation.
35. S. Zhang, G. Mordant, T. Matsumoto, and G. Schiebinger. Manifold learning with sparse regularised optimal transport, 2023. arXiv:2307.09816.

Open Access This chapter is licensed under the terms of the Creative Commons Attribution-NonCommercial-NoDerivatives 4.0 International License (http://creativecommons.org/licenses/by-nc-nd/4.0/), which permits any noncommercial use, sharing, distribution and reproduction in any medium or format, as long as you give appropriate credit to the original author(s) and the source, provide a link to the Creative Commons license and indicate if you modified the licensed material. You do not have permission under this license to share adapted material derived from this chapter or parts of it.

The images or other third party material in this chapter are included in the chapter's Creative Commons license, unless indicated otherwise in a credit line to the material. If material is not included in the chapter's Creative Commons license and your intended use is not permitted by statutory regulation or exceeds the permitted use, you will need to obtain permission directly from the copyright holder.



Part V
Practical Challenges and a Benchmark Instance for Gas–Hydrogen Networks

Chapter 20
Introduction to Practical Challenges and a Benchmark Instance for Gas–Hydrogen Networks

Frauke Liers[0000−0002−1671−0344] and
Alexander Martin[0000−0001−7602−3653]

Abstract This chapter belongs to the book *Mathematical Modelling, Simulation and Optimization using the Example of Gas Networks*. It summarizes key practical questions in gas networks as discussed subsequently. In addition, a new realistic instance is presented for the transition from natural gas to hydrogen networks.

Gas networks are prime examples of systems where many mathematically and practically relevant questions arise, requiring novel approaches in modeling, simulation, and optimization. These include computing solutions that enable efficient transitions between states, ensuring robustness against uncertainties, addressing market-related issues, and managing the transition from natural gas to hydrogen networks. In addition, hydrogen transport introduces specific challenges that must be addressed. Practical instances and scenarios are essential to evaluate and test new methodologies, as they require a realistic hydrogen network topology and accurate forecasts of demands and production. Such data also provide a common basis for benchmarking different approaches. The next chapters cover:

- Chap. 21, "Gas2Hydro – A Combined Natural Gas–Hydrogen Instance", introduces a new, realistic hydrogen network instance, providing a practical basis for testing and evaluating methods applicable to the transition from natural gas to hydrogen networks.
- Chap. 22, "Mathematical Questions Arising from Practical Challenges in Gas Networks", summarizes practical questions in gas network operations and shows how different mathematical approaches contribute to their solution.

All of the questions and problems addressed in this chapter have been selected and designed in such a way that no single mathematical discipline is sufficient to answer them.

Frauke Liers
Department of Data Science and Department of Mathematics, FAU Erlangen-Nürnberg, Germany,
e-mail: frauke.liers@fau.de

Alexander Martin
Analytics & Optimization, University of Technology Nuremberg (UTN), Germany,
e-mail: alexander.martin@utn.de

© The Author(s) 2027

A. Martin et al. (eds.), *Mathematical Modelling, Simulation and Optimization using the Example of Gas Networks*, International Series of Numerical Mathematics 174,
https://doi.org/10.1007/978-3-032-34969-9_20

It always takes a combination of different mathematical disciplines, be it mixed-integer optimization, control theory, or the analysis of certain partial differential equations, up to models and concepts from market design or the inclusion of uncertainties, to solve these challenging questions.

At the same time, the instances and results demonstrate that cooperation between disciplines is essential and that the disciplines themselves had to gain additional new insights in their fields in order to achieve realistic results.

Acknowledgements This work was supported by the German Research Foundation (DFG) within Subprojects A05, A07, A09, B02, B06, B07, B08, B10, and C03 in the Sonderforschungsbereich/Transregio 154 "Mathematical Modelling, Simulation and Optimization using the Example of Gas Networks" (Project ID 239904186).

Open Access This chapter is licensed under the terms of the Creative Commons Attribution-NonCommercial-NoDerivatives 4.0 International License (http://creativecommons.org/licenses/by-nc-nd/4.0/), which permits any noncommercial use, sharing, distribution and reproduction in any medium or format, as long as you give appropriate credit to the original author(s) and the source, provide a link to the Creative Commons license and indicate if you modified the licensed material. You do not have permission under this license to share adapted material derived from this chapter or parts of it.

The images or other third party material in this chapter are included in the chapter's Creative Commons license, unless indicated otherwise in a credit line to the material. If material is not included in the chapter's Creative Commons license and your intended use is not permitted by statutory regulation or exceeds the permitted use, you will need to obtain permission directly from the copyright holder.



Chapter 21
Gas2Hydro – A Combined Natural Gas–Hydrogen Instance

Daniela Bernhard[0009−0001−7839−202X],
Julian Born[0009−0005−4105−4659],
Yann Disser[0000−0002−2085−0454],
Caroline Geiersbach[0000−0002−6518−7756],
Johannes Hahn[0009−0005−3016−2996],
Anton Hoof[0009−0003−3436−9738], and
Lea Strubberg[0009−0009−8505−3614]

Abstract We introduce Gas2Hydro, a publicly available instance designed to model, optimize, and test the transition from natural gas to hydrogen networks. While natural gas and hydrogen share similar transport principles, their physical properties differ, and until now, no open dataset exists to study their combined operation. Based on the development plans of the German gas transmission operators (FNB Gas), we construct a realistic network that reflects both the current natural gas infrastructure and the planned hydrogen core network. The instance is implemented in a format compatible with the established GasLib library to ensure seamless integration with existing gas network optimization tools. In addition, we provide demand and supply scenarios derived from official planning frameworks and survey data. Although simplified in some aspects, Gas2Hydro represents the first openly accessible benchmark instance

Daniela Bernhard
Department of Data Science & Department of Mathematics, FAU Erlangen-Nürnberg, Germany, e-mail: daniela.db.bernhard@fau.de

Julian Born
Department of Mathematics, TU Darmstadt, Germany, e-mail: born@mathematik.tu-darmstadt.de

Yann Disser
Department of Mathematics, TU Darmstadt, Germany, e-mail: disser@mathematik.tu-darmstadt.de

Caroline Geiersbach
Department of Mathematics, University of Klagenfurt, Austria, e-mail: caroline.geiersbach@aau.at

Johannes Hahn
Analytics & Optimization, University of Technology Nuremberg (UTN), Germany, e-mail: johannes.hahn@utn.de

Anton Hoof
Department of Data Science & Department of Mathematics, FAU Erlangen-Nürnberg, Germany, e-mail: anton.hoof@fau.de

Lea Strubberg
Institute of Mathematics, TU Berlin, Germany, e-mail: strubberg@math.tu-berlin.de

© The Author(s) 2027

A. Martin et al. (eds.), *Mathematical Modelling, Simulation and Optimization using the Example of Gas Networks*, International Series of Numerical Mathematics 174,
https://doi.org/10.1007/978-3-032-34969-9_21

to support methodological research and planning studies for the transition towards a hydrogen economy.

Database: github.com/TRR154/Gas2Hydro

21.1 Introduction

In this chapter, we introduce a new gas network instance[1] that integrates the hydrogen core network designed by FNB Gas into the existing German natural gas infrastructure. This marks, to the best of our knowledge, the first reality-based and open-source instance that enables the evaluation and comparison of different approaches for the transition from natural gas to hydrogen with respect to network design and operation.

21.1.1 Motivation

The German climate target for 2030 is to reduce greenhouse gas emissions by at least 55 % compared to the year 1990 [3, p. 7]. As of now, the energy sector has the largest share of Germany's emissions [17, p. 69]. While natural gas releases CO_2 during combustion, hydrogen produced from renewable energies such as solar or wind energy does not. Consequently, one of the main strategies to reach the climate target is therefore to gradually reduce the usage of natural gas over the next decades and transition to energy supplied by hydrogen [5, p. 18]. Establishing an appropriate transport infrastructure is essential for ensuring a reliable energy supply throughout this transformation. Several projects are currently being funded by the EU and the German government that focus on how such a hydrogen network can be established [18]. In addition to new pipeline constructions, existing natural gas pipes can be repurposed [7, p. 7], and the extent to which natural gas can be mixed with hydrogen is also being investigated, see Chap. 3, "Gas Mixtures on Networks: Modeling, Simulation and Optimization".

The transition from natural gas to hydrogen should be executed cost-efficiently with respect to both the construction and repurposing costs for the pipelines, while at the same time guaranteeing a basic energy supply. During this transition period, two partially interacting but technically separate energy sectors will coexist. However, there might be an interaction between different agents involved in natural gas and hydrogen trading. The organization of gas networks is handled by transmission system operators (TSO). This management leads to equilibrium problems if two different TSOs act independently. This gives rise to several theoretical and practical questions:

(i) How can existing gas networks be downsized and/or rededicated to efficiently integrate hydrogen transport?

[1] Strictly speaking, we introduce three instances. However, since two of them are subinstances of the third, we found it more convenient to refer to them in the singular. In sections where we discuss the instances in detail, we occasionally use the plural form.

(ii) How can interactions between agents acting in both sectors be organized?

Addressing these two questions, various mathematical approaches are of interest as described in Chap. 22, "Mathematical Questions Arising from Practical Challenges in Gas Networks". To ensure that the resulting methods can be compared and validated in a consistent setting, we chose to develop a common network instance representing both hydrogen and natural gas systems.

We therefore propose a new network instance complementary to GasLib [14] – an open library of natural gas instances. Since, to the best of our knowledge, no combined instances are currently available, and to properly address the central research questions, we developed the model for our purposes. The resulting instance represents an excerpt of the long-distance transmission network in Germany and serves as a basis for investigating various questions related to the planning and organization of the energy transition.

21.1.2 Prior Work

The newly created instance realizes a future hydrogen network and has been developed in alignment with the GasLib framework. We specifically aimed to make the instance seamlessly usable, similar to existing GasLib instances.

21.1.2.1 GasLib

GasLib [14] is a library of natural gas instances. Its goal is to provide a set of publicly available gas network instances that can be used by researchers in the field of gas transport. The library instances are encoded in an XML (Extensible Markup Language) format. For our purpose to continue this work and augment it by adding the interesting aspect of hydrogen networks that work in parallel, we stick close to its encoding and structure.

21.1.2.2 FNB Gas Hydrogen Report

A hydrogen report submitted by a consortium of TSOs (FNB Gas) [8] shows how the transport infrastructure can be developed efficiently, quickly, and in a targeted manner by integrating hydrogen network planning into the proven gas network planning. Since this report has a statutory basis [2], is prepared jointly by all TSOs, and is published at regular intervals, it provides a reliable and enduring reference. This makes this report particularly interesting for our purpose to create an instance that combines the different gas types. At the same time, the topic remains highly dynamic: the estimated future demand and political framework conditions may change quickly. Future tasks will therefore include updating the instance and incorporating new information.

21.1.3 Challenges

In creating an instance that involves hydrogen as an energy source we face various challenges. These lie both in the novelty of the energy source and in the challenge of creating a combined instance, thus making it compatible and connectable with natural gas. The three main challenges we faced are:

(i) *Disjoint but interdependent networks:* Both energy sources behave similarly but we assume they cannot be mixed. Consequently, two separate yet interdependent network instances must be modeled. This constitutes a significant challenge: while the network topologies must remain disjoint due to the non-mixability, the corresponding demand developments are closely correlated, as both gases partially substitute each other.

(ii) *Limited market data:* The distribution of hydrogen is a *new* market economy, e.g., only few experience and information can be found about

- demand scenarios and future predictions, as well as
- compressor stations and other technical components.

(iii) *Computational complexity:* Depending on the modeling approach, the resulting instance can become large, which may significantly increase computational effort. For efficient computation, reduced or simplified instances are therefore preferable.

21.2 Description of GasLib Instances

We aim to build our combined instance in accordance with the existing library, maintaining the same structure, description, and encoding. This ensures that anyone familiar with GasLib can use the combined instance without significant effort. For a comprehensive and complete understanding of GasLib, we refer to [14] but provide an overview of the main structure of the library here. In this overview, we deliberately omit the description of files and features that were not used for our instance.

A GasLib network is described using different files. The full set for specifying a single stationary demand scenario (nomination) for a gas transport network requires at least two files: The *network topology* is specified in a `.net` file, and a *nomination or demand scenario* is specified by an `.scn` file. It is possible to have several `.scn` files per `.net` file.

21.2.1 The `.net` File

The network topology is a directed graph in which the nodes represent junctions of the arcs and is described in the `.net` file together with the technical parameters of the network elements. Each `node` is specified by its type and location coordinates. There are three node types: `source`, `sink` and `innode`. Source and sink nodes represent entry

Table 21.1: Parameter list of the different nodes and connection types used by Gas2Hydro

Types	Parameters
`Node` *types* each with location coordinates	
`source`	`height`, `pressureMin`, `pressureMax`, `flowMin`, `flowMax`, `gasTemperature`, `calorificValue`, `normDensity`, `molarMass`, `pseudocriticalPressure`, `pseudocriticalTemperature`
`sink`	`height`, `pressureMin`, `pressureMax`, `flowMin`, `flowMax`
`innode`	`height`, `pressureMin`, `pressureMax`
`Connection` *types* each with start and end node	
`pipe`	`flowMin`, `flowMax`, `length`, `diameter`, `roughness`, `heatTransferCoefficient`, `speedLimit`
`shortPipe`	`flowMin`, `flowMax`

and exit points of the network, respectively, whereas innodes represent junctions of two or more pipelines where no gas flow is injected or discharged. A `pipe` and a `short pipe` are connections between a start and an end node. Short pipes are connections with zero length. Table 21.1 lists the different elements and corresponding parameters.

21.2.2 The `.scn` File

The `.scn` files define demand and supply scenarios for the nodes specified in the corresponding `.net` file. Each `scenario` is identified by a unique `id`, allowing multiple scenarios to be distinguished within a single instance. Within a scenario, a `flow` value must be specified for every `node` defined in the associated `.net` file. A positive `flow` value denotes an injection into the network, whereas a negative value represents a withdrawal. Since a stationary gas flow model is considered, the total supplied flow must balance the total discharged flow. That is, the sum of all supplies at source nodes equals the sum of all withdrawals at sink nodes.

21.3 The Gas2Hydro Instance

The *Gas2Hydro-62* is a simplified model of the northeastern region of Germany and is based on both the hydrogen report [8] and the network development plan [9] of FNB Gas. Both documents schematically depict the transmission network for natural gas transportation [9, p. 43] and plans for a hydrogen core network [8, p. 18]. The instance models a passive network containing no active elements, like compressor stations or switches.

Besides the Gas2Hydro-62 instance, we also provided two smaller subinstances called *Gas2Hydro-12* and *Gas2Hydro-62-tree*. The instance Gas2Hydro-12 models

the supra-regional pipeline system around Berlin, whereas Gas2Hydro-62-tree forms a spanning tree of Gas2Hydro-62.

As a basis for the natural gas demand, we relied on the NEP database [10], which compiles the data reported by the TSOs. This ensures consistency with the official network development planning and provides a transparent foundation for our demand assumptions. For hydrogen, we consulted a case study by Egerer et al. [6] assessing the future hydrogen demand in various industry sectors in Germany. For the physical quantities of the nodes and pipes, we refer in part to the FNB Gas network development planning database [9]. As this does not list all the quantities required by the corresponding namespaces in the GasLib instances, we also draw on other publicly available sources which are further specified in Sect. 21.3.2.

In the following, we first describe in detail how the topology and scenario files were built with the data at hand, and later on give in Tables 21.5 and 21.6 an overview of the physical quantities that we used for modeling natural gas and hydrogen pipeline networks.

21.3.1 Realizing a Combined Natural Gas–Hydrogen Instance

The main issue with the compatibility with GasLib is that its framework supports the transportation of one type of gas only, emphasizing the necessity of addressing Challenge i. We tackled this problem by dividing each Gas2Hydro instance into two parts so that they basically consist of two parallel instances, one for hydrogen and one for natural gas, as further described in the following.

21.3.1.1 Topology

The Gas2Hydro instances consist of two `.net` files with the suffix `_natural_gas.net` and `_hydrogen.net`, since some physical specifications, such as density and calorific value, depend on the gas type.

Each of the two topology files contains an identical set of nodes. However, the type declaration might differ in general. This means that a given node may act as a source in one network file while serving as a sink in the other. Even within a single network, the role of a node can change over time (e.g., in the case of gas storage facilities). To address this, we chose to model both a source node and a sink node at every such potential location and connect them via a short pipe. This approach elegantly resolves all these inconsistencies by introducing only one additional short pipe per source node.

The natural gas file contains all pipes that can be used for the transportation of natural gas and potentially rededicated in the transition process over time. Whereas the hydrogen file contains old natural gas pipelines that are being converted, as well as new hydrogen pipelines that are to be newly built.

An illustration of the Gas2Hydro-62 instance can be found in Fig. 21.1. Table 21.2 shows the number of elements in each `.net` file.

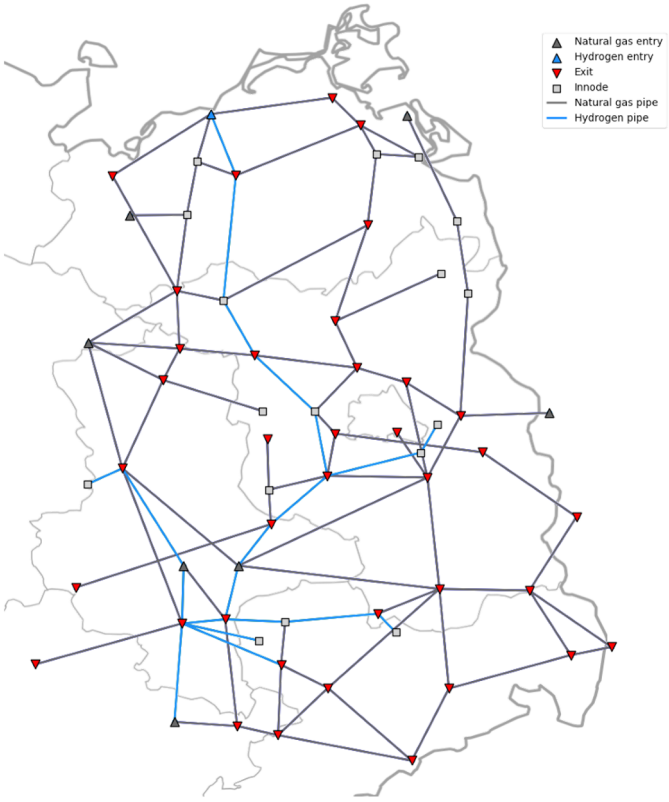


Fig. 21.1: Topology of the *Gas2Hydro-62* instance

Table 21.2: Number of nodes and pipes in each topology file of the Gas2Hydro-62 instance

	Natural gas	Hydrogen
Sources	7	1
Sinks	41	30
Innodes	21	32
Pipes	75	20
Short pipes	7	1

A Tree-Shaped Subinstance

For applications necessitating that the underlying graph of the instance contains no cycle, we provide a subinstance of Gas2Hydro-62 called *Gas2Hydro-62-Tree*. Note that the underlying graph of `G2H_62_hydrogen.net` is already a tree. It is therefore identical to the file `G2H_62_tree_hydrogen.net`. Whereas the underlying graph of the file `G2H_62_tree_natural_gas.net` is an actual spanning tree of the graph induced by

`G2H_62_natural_gas.net`. For an illustration, see Fig. 21.2, and Table 21.3 for the number of elements in the `.net` files of the tree-shaped subinstance.

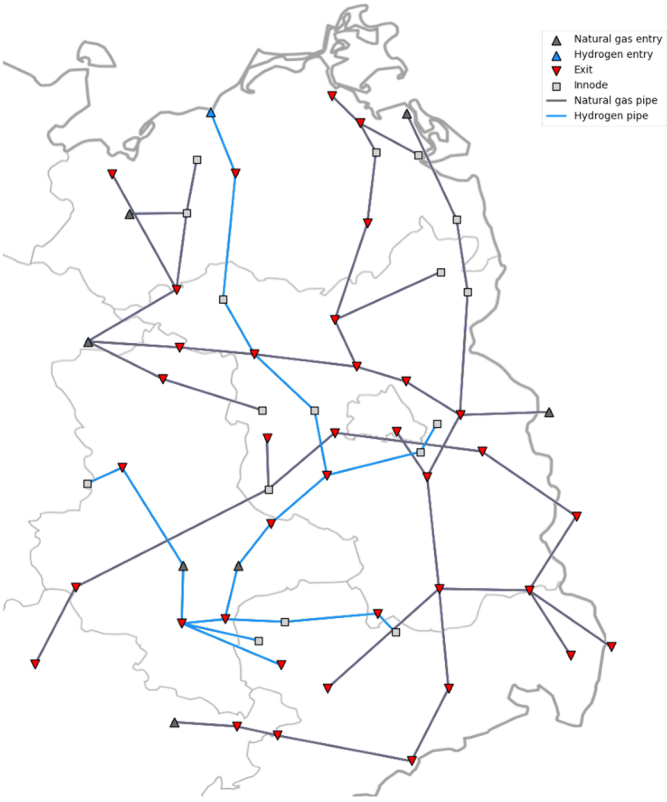


Fig. 21.2: Topology of the tree-shaped *Gas2Hydro-62-Tree* subinstance

Table 21.3: Number of nodes and pipes in each topology file of the tree-shaped *Gas2Hydro-62-Tree* subinstance. Here, we deliberately omitted the number of short pipes.

	Natural gas	Hydrogen
Sources	5	1
Sinks	34	30
Innodes	28	32
Pipes	43	19
Short pipes	5	1

A small-scale subinstance

As we point out in Challenge iii a smaller instance could be very useful. The subinstance *Gas2Hydro-12* includes only twelve nodes and can be used for more complex computations that might be too heavy on the whole network. It induces a subgraph right out of the center of the complete instance Gas2Hydro-62. See Fig. 21.3 for an illustration, and Table 21.4 for the number of elements in each `.net` file of the small-scale subinstance.

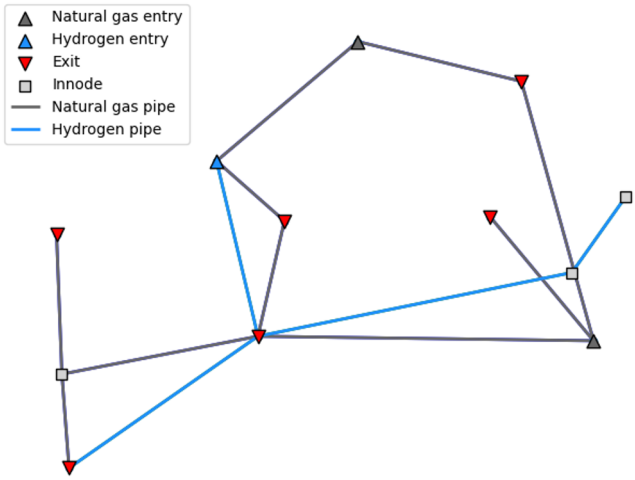


Fig. 21.3: Topology of the small-scale *Gas2Hydro-12* subinstance

Table 21.4: Number of nodes and pipes in each topology file of the small-scale *Gas2Hydro-12* subinstance. Here, we deliberately omitted the number of short pipes.

	Natural gas	Hydrogen
Sources	2	1
Sinks	6	4
Innodes	6	8
Pipes	10	4
Short pipes	2	1

21.3.1.2 Scenarios

In order to model the transition from natural gas to hydrogen, we show the demand trend for both gases over the next decades within the scenario files. For this purpose,

we created for each instance three natural gas scenarios for the years 2018, 2025, and 2030, as well as four hydrogen scenarios, two for the year 2030 and two for the year 2050. The two hydrogen scenarios for each year model a minimum and a maximum demand for the respective year.

For the Gas2Hydro-62 instance, we have three natural gas scenario files called

- `2018_NG_G2H_62.scn`,
- `2025_NG_G2H_62.scn`,
- `2030_NG_G2H_62.scn`,

as well as four hydrogen scenario files called

- `2030_Hmin_G2H_62.scn`,
- `2030_Hmax_G2H_62.scn`,
- `2050_Hmin_G2H_62.scn`,
- `2050_Hmax_G2H_62.scn`.

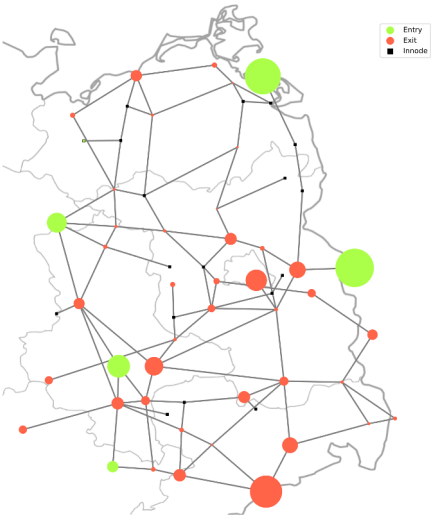
Figures 21.4 and 21.5 show the three natural gas scenarios and the two hydrogen scenarios for the year 2050, respectively. The size of the nodes is scaled according to the absolute demand (red) or supply (green) at that node.

It is important to note that the all three natural gas scenarios are feasible on the topology given by `G2H_62_natural_gas.net`. The two scenarios `2030_Hmin_G2H_62.scn` and `2030_Hmax_G2H_62.scn` are furthermore feasible on the topology given by `G2H_62_hydrogen.net`. The two hydrogen scenarios for the year 2050, however, are not feasible on the `G2H_62_hydrogen.net` topology. The reason for including these infeasible hydrogen scenarios is that we want the user of the Gas2Hydro instance to tackle the three questions stated in Sect. 21.1.1, see Sect. 21.4 for a concrete application.

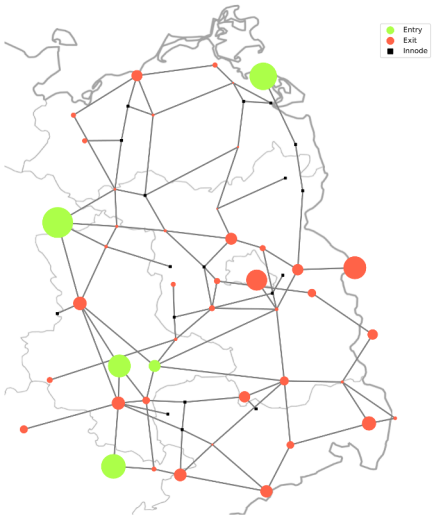
In the following, we describe the data on which we based the scenario files, first for natural gas and then for hydrogen, and further explain the integration of the data into the Gas2Hydro instances.

We extracted the data for the natural gas scenarios from the so-called *NEP-Gas data base* [10] provided and managed by the German association of the supraregional gas transmission companies, FNB Gas. The NEP-Gas database includes, besides network development plans that we used for the topology files, also scenario frameworks, which are both published every two years. A scenario framework forecasts the natural gas and hydrogen capacities for the next 10 to 15 years and is the basis for the associated network development plan. Capacity in connection with gas transmission defines the maximal possible amount of gas that can be inserted into or extracted from the network. According to the Energy Industry Act (EnWG) § 15b [2], the scenarios shall be based on reasonable assumptions about the development of the extraction or production of gas. FNB Gas is furthermore obliged to involve all affected network operators in Germany appropriately in the creation process of the scenario framework.

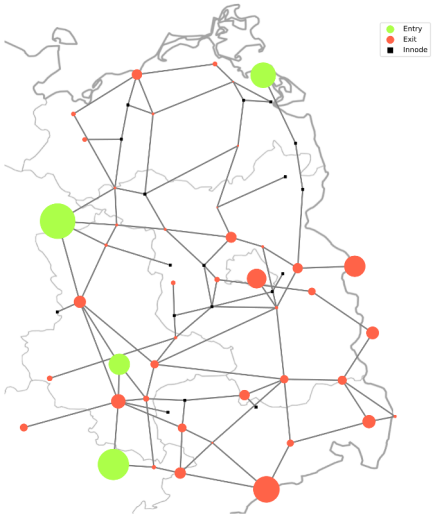
While natural gas as an energy source is primarily used in the energy sectors, industry, as well as residential and commercial heating, the German national hydrogen strategy states that the primary use of hydrogen shall be within the industry and transportation sectors [4][pp. 19–25]. Therefore, we make use of data reflecting the expected hydrogen consumption of several industry sectors, like steel, cement, paper, etc., for



(a) `2018_NG_G2H_62.scn`



(b) `2025_NG_G2H_62.scn`

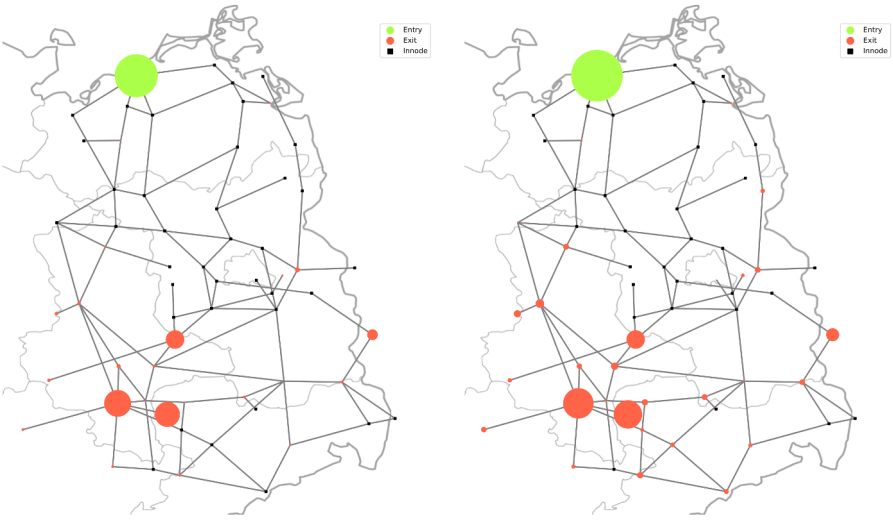


(c) `2030_NG_G2H_62.scn`

Fig. 21.4: Natural gas scenarios

the year 2050 [6]. The data provides information about the geographical coordinates of each surveyed company as well as its expected maximum and minimum hydrogen consumption.

In order to transfer the available demand data into the scenario files for our topology, several preprocessing steps were required. The main challenges resulted from the different data sources and from the fact that, unlike the reported natural gas data from



(a) `2050_Hmin_G2H_62.scn` (b) `2050_Hmax_G2H_62.scn`

Fig. 21.5: 2050 hydrogen scenarios

past years, the future natural gas and hydrogen demands are non-empirical and often only rough estimates.

For the natural gas part, the database covers the entire German transmission system, while our instance is restricted to the northeastern region. The dataset was therefore filtered according to the relevant operators active in this region. Regarding the assignment of entry and exit points, certain points in the dataset were matched to the closest node in the instance with respect to their geographical location. Since the database itself does not provide coordinates but only names of points, an additional manual mapping was necessary to ensure a consistent alignment between data and topology. Besides these main challenges, several smaller inconsistencies within the database were also resolved, which required individual adjustments. As the instance's topology describes a passive network without any active elements, like compressor stations, it cannot be expected that the demand extracted from the NEP database can be transported without violating physical safety constraints like pressure bounds. Therefore, the extracted demand was scaled by a factor of 0.3 to ensure feasibility with respect to the pressure constraints.

The hydrogen data for the year 2050 posed a somewhat different set of challenges. First, the consumption data was split by sector, which was not required in our case. The demand was therefore aggregated at each node across all sectors. Moreover, the data was provided at specific coordinate pairs, which were integrated into our topology by means of a nearest-neighbor mapping. Another challenge was that the dataset contained only consumption values and no injection data. To obtain a balanced system, a single injection point was therefore introduced at the port of Rostock, where hydrogen is assumed to enter the network. Since the data distinguishes between minimum and

maximum demand, two separate scenario files were created to represent both cases explicitly.

Lastly, while the hydrogen data was estimated for the year 2050, the network infrastructure of the Gas2Hydro instances reflects the network development plans for the year 2030 only. In order to provide the Gas2Hydro instances with a feasible hydrogen scenario, we extracted from the 2050 scenario only those exit nodes that are connected to the hydrogen network induced by the respective `hydrogen.net` file. This resulted in the two hydrogen scenarios for the year 2030.

21.3.2 Physical Quantities

Some of the physical quantities required by GasLib depend on the type of gas. Table 21.5 lists the required quantities for the namespace `source`, the corresponding values for each type of gas, and the references from which the values are obtained. An analogue for the namespace `pipe` can be found in Table 21.6.

Table 21.5: Physical quantities of the `source` nodes in each `.net` file

	Natural gas	Hydrogen	Reference
`calorificValue`	36.454 $\mathrm{MJ\,m^{-3}}$	12.745 $\mathrm{MJ\,m^{-3}}$	GasLib-11, [12, p. 16]
`flowMin`	-10^7 $\mathrm{m^3\,h^{-1}}$	-10^7 $\mathrm{m^3\,h^{-1}}$	GasLib-11
`flowMax`	10^7 $\mathrm{m^3\,h^{-1}}$	10^7 $\mathrm{m^3\,h^{-1}}$	GasLib-11
`gasTemperature`	10 °C	10 °C	GasLib-11
`height`	0 m	0 m	GasLib-11
`molarMass`	19 $\mathrm{kg\,kmol^{-1}}$	2.016 $\mathrm{kg\,kmol^{-1}}$	[16]
`normDensity`	0.785 $\mathrm{kg\,m^{-3}}$	0.083 75 $\mathrm{kg\,m^{-3}}$	GasLib-11, [11]
`pressureMin`	70 bar	40 bar	GasLib-11
`pressureMax`	70 bar	40 bar	GasLib-11
`pseudocriticalPressure`	45.929 bar	13 bar	GasLib-11, [15]
`pseudocriticalTemperature`	188.54 K	33.15 K	GasLib-11, [15]

Table 21.6: Physical quantities of a `pipe` in each `.net` file

	Natural gas	Hydrogen	Reference
`flowMin`	-10^7 $\mathrm{m^3\,h^{-1}}$	-10^7 $\mathrm{m^3\,h^{-1}}$	GasLib-11
`flowMax`	10^7 $\mathrm{m^3\,h^{-1}}$	10^7 $\mathrm{m^3\,h^{-1}}$	GasLib-11
`length`	in km	in km	[10] or estimate
`diameter`	in mm	in mm	[10] or estimate
`roughness`	0.1 mm	0.1 mm	GasLib-11
`pressureMax`	80 bar	80 bar	[10] or estimate

21.3.3 Validation

The instance was validated by confirming that all flows satisfy the quadratic pressure–flow relationship. Specifically, the Weymouth equation (ISO4-ALG) in Chap. 2, "A Catalog of Gas Network Models: PDEs, Coupling Conditions, and Numerical Schemes" hold throughout, and all computed pressures remain within their technical bounds. While the absence of active components naturally restricts the network's operational flexibility, the validation confirms that at least 30 % of realistic loads can be transported without violating physical constraints.

Figures 21.6 and 21.7 visualize these valid flows for the three natural gas scenarios and the two hydrogen scenarios for the year 2030, respectively. The magnitude of each flow is represented by the edge's thickness, and its direction is indicated by an arrow along the edge.

21.4 Application

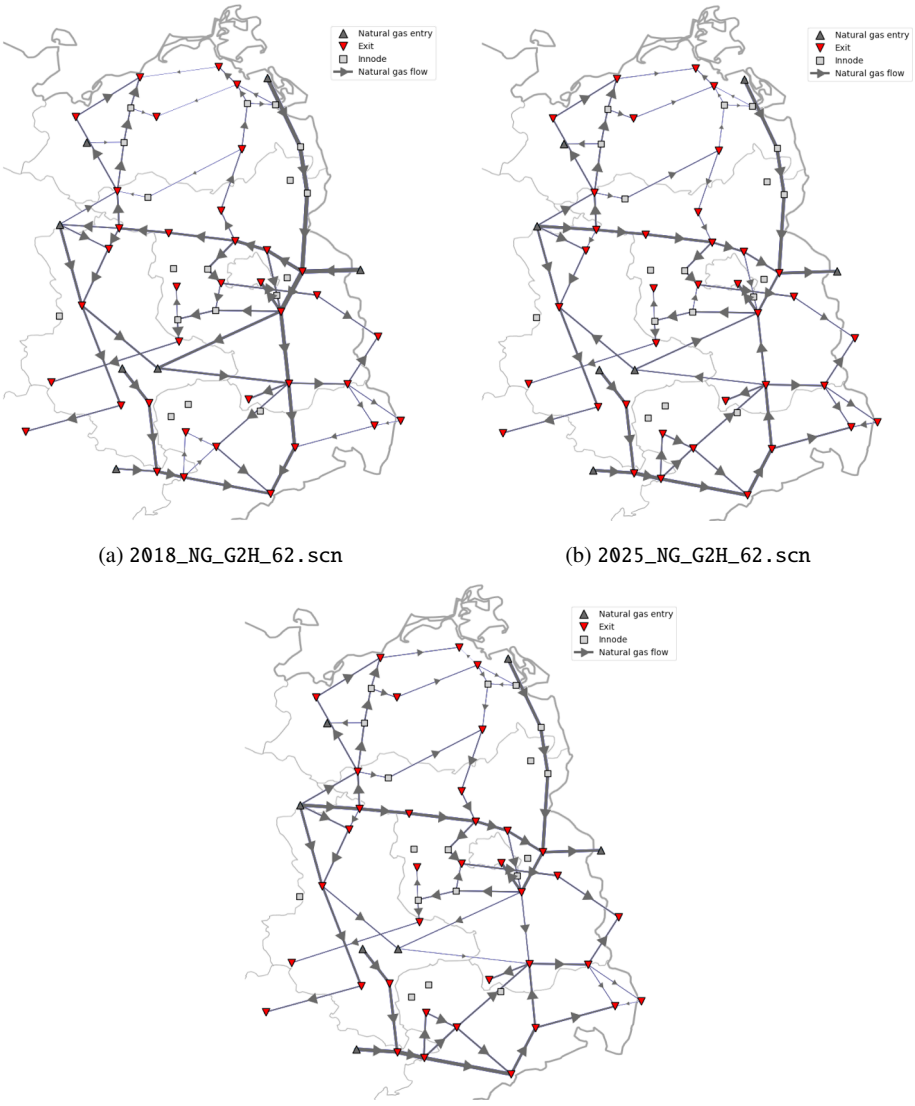
In the final section, we model the transition from natural gas to hydrogen using the combined instance Gas2Hydro. More specifically, we identify which of the existing natural gas pipelines should be incorporated into the hydrogen network in response to a future hydrogen demand scenario (Question i). We formalize this question as a topology optimization problem, also known as the network design problem. This problem is defined on a graph representing the existing natural gas infrastructure. Each edge represents a pipeline and has a given hydrogen repurposing cost. Furthermore, we are given a hydrogen demand and a pressure constraint at every node. The objective is to determine a cost-minimal subset of edges so that the hydrogen network that is induced by this subset is feasible, where feasibility means that there exists a hydrogen flow in the induced network satisfying the given demand scenario while respecting the pressure constraints. For a formal definition of the problem, we refer to Sect. 7.5 in Chap. 7, "Potential-Based Flows – An Overview".

We apply this optimization framework to the Gas2Hydro-62 instance shown in Fig. 21.1 for each of the two 2050 hydrogen scenarios illustrated in Fig. 21.5. The graph is induced by the two topology files `G2H_62_natural gas.net` and `G2H_62_hydrogen.net`. We extend the topology optimization problem so that the pipes in the `G2H_62_hydrogen.net` must be contained in the solution. The costs of repurposing a pipeline with diameter D are modeled according to [13] and given by

$$1.05 \cdot 278.24 \cdot e^{1.6 \cdot D} \quad \text{EUR/m}.$$

For the pressure constraints, we use the specification of the two parameters `pressureMin` and `pressureMax` as stated in Table 21.5. For the computations, we used the code from [1].

The solution for each of the two hydrogen scenarios is depicted in Fig. 21.8. In the lower right corner of both subfigures, we observe that the solutions choose a detour via an innode rather than repurposing a shorter but larger-diameter pipeline.

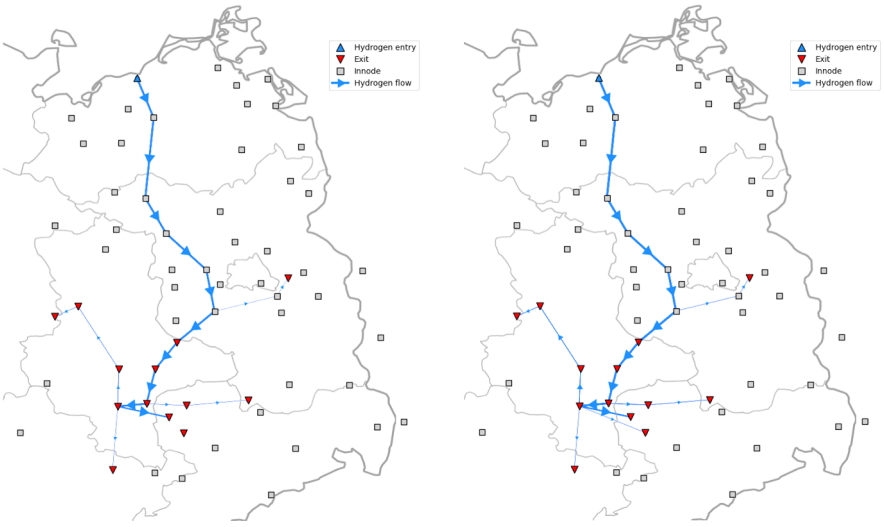


(a) `2018_NG_G2H_62.scn` (b) `2025_NG_G2H_62.scn`

(c) `2030_NG_G2H_62.scn`

Fig. 21.6: Valid flows for the natural gas scenarios

Furthermore, parallel connections need to be constructed as shown on the left side in both subfigures. The practical acceptability of such artifacts depends on the intended application. Connecting additional innodes via such detours or parallel pipelines could be advantageous for accommodating future demand growth. A limitation of this model



(a) `2030_Hmin_G2H_62.scn` (b) `2030_Hmax_G2H_62.scn`

Fig. 21.7: Valid flows for the hydrogen scenarios

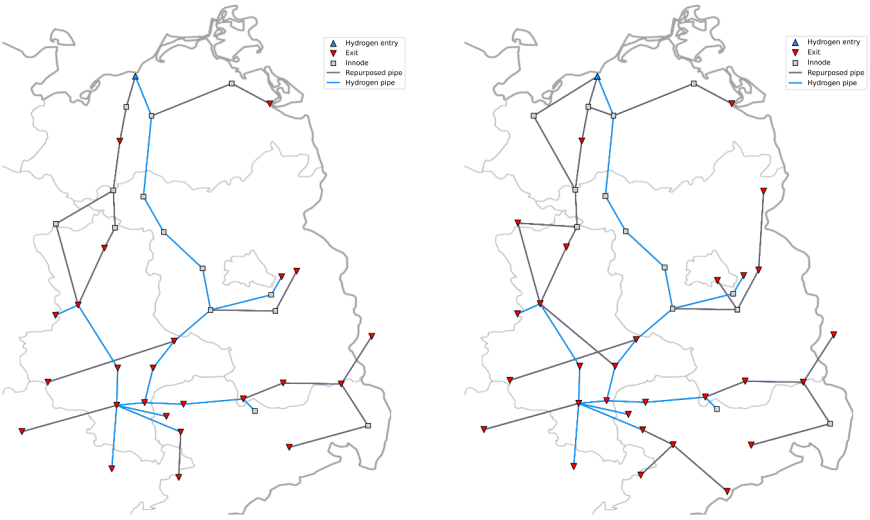
is that it only considers the repurposing of existing pipelines, neglecting the possibility of building new hydrogen pipelines with different diameter options.

While we acknowledge the limitations and simplifications of the current Gas2Hydro instance, we emphasize that it represents one of the first openly available instances for simulating the transition of natural gas networks to hydrogen. Its open-source nature allows users to adapt, extend, and refine it for specific use cases, such as including new pipeline options or more detailed physical constraints. We expect this instance to serve as a foundation for further methodological and practical developments in this field.

Acknowledgements This work was supported by the German Research Foundation (DFG) within Subprojects A07, A09, B02, B06, and B07 in the Sonderforschungsbereich/Transregio 154 "Mathematical Modelling, Simulation and Optimization using the Example of Gas Networks" (Project ID 239904186).

References

1. P. Börner, M. Klimm, A. Lutz, M. E. Pfetsch, M. Skutella, and L. Strubberg. Valid cuts for the design of potential-based flow networks. In N. Megow and A. Basu, ed., *Integer Programming and Combinatorial Optimization*, pages 142–156, Cham, 2025. Springer. doi:10.1007/978-3-031-93112-3_11.
2. Bundesministerium der Justiz und für Verbraucherschutz. Energiewirtschaftsgesetz (EnWG) § 15, 2005. Accessed: 2025-09-26. URL: https://www.gesetze-im-internet.de/enwg_2005/__15.html.



(a) Serving the `2050_Hmin_G2H_62.scn` scenario.

(b) Serving the `2050_Hmax_G2H_62.scn` scenario.

Fig. 21.8: Cost-minimal extensions of the hydrogen core network (blue) with repurposed pipelines (gray) from the natural gas network to serve a given hydrogen demand scenario

3. Bundesministerium für Umwelt, Naturschutz, Bau und Reaktorsicherheit. Klimaschutzplan 2050, 2016. Accessed: 2024-06-20. URL: https://www.bmwk.de/Redaktion/DE/Publikationen/Industrie/klimaschutzplan-2050.pdf.
4. Bundesministerium für Wirtschaft und Klimaschutz. Fortschreibung der Nationalen Wasserstoffstrategie, 2023. Accessed: 2025-09-03. URL: https://www.bundeswirtschaftsministerium.de/Redaktion/DE/Wasserstoff/Downloads/Fortschreibung.pdf?__blob=publicationFile&v=4.
5. Bundesministerium für Wirtschaft und Klimaschutz. Energiewende und Klimaschutz, 2024. Accessed: 2024-08-08. URL: https://www.bmwk.de/Redaktion/DE/Publikationen/Klimaschutz/klimaschutz-energiewende.pdf.
6. J. Egerer, N. Farhang-Damghani, V. Grimm, and P. Runge. The industry transformation from fossil fuels to hydrogen will reorganize value chains: Big picture and case studies for germany. *Applied Energy*, 358:122485, 03 2024. doi:10.1016/j.apenergy.2023.122485.
7. Federal Ministry for Economic Affairs and Energy. The national hydrogen strategy, 2020. Accessed: 2024-08-08. URL: https://www.bundeswirtschaftsministerium.de/Redaktion/EN/Publikationen/Energie/the-national-hydrogen-strategy.pdf.
8. FNB Gas. Wasserstoffbericht, 2022. Accessed: 2024-06-20. URL: https://fnb-gas.de/wp-content/uploads/2022/08/2022-09-01_FNB-Gas_Wasserstoffbericht.pdf.
9. FNB Gas. Netzentwicklungsplan Gas 2022–2032, 2024. Accessed: 2024-06-20. URL: https://fnb-gas.de/wp-content/uploads/2024/03/2024_03_20_NEP-2022_Gas_FINAL_DE.pdf.
10. FNB Gas. NEP Gas database, 2025. Accessed: 2025-09-26. URL: https://www.nep-gas-datenbank.de.
11. H2Tools. Basic hydrogen properties. Accessed: 2024-06-20. URL: https://h2tools.org/hyarc/hydrogen-data/basic-hydrogen-properties.
12. K. Hoppmann-Baum, F. Hennings, J. Zittel, U. Gotzes, E.-M. Spreckelsen, K. Spreckelsen, and T. Koch. From natural gas towards hydrogen – a feasibility study on current transport network infrastructure and its technical control. Technical Report 20-27, ZIB, Takustr. 7, 14195 Berlin, 2020.

13. M. Reuß, L. Welder, J. Thürauf, J. Linßen, T. Grube, L. Schewe, M. Schmidt, D. Stolten, and M. Robinius. Modeling hydrogen networks for future energy systems: A comparison of linear and nonlinear approaches. *Int. J. Hydrog. Energy*, 44(60):32136–32150, 2019. doi: 10.1016/j.ijhydene.2019.10.080.
14. M. Schmidt, D. Aßmann, R. Burlacu, J. Humpola, I. Joormann, N. Kanelakis, T. Koch, D. Oucherif, M. E. Pfetsch, L. Schewe, R. Schwarz, and M. Sirvent. GasLib – a library of gas network instances. *Data*, 2(4), 2017. doi:10.3390/data2040040.
15. The Engineering ToolBox. Critical temperatures and pressures for some common substances, 2003. Accessed: 2024-06-20. URL: https://www.engineeringtoolbox.com/gas-critical-temperature-pressure-d_161.html.
16. The Engineering ToolBox. Molecular weight of substances, 2009. Accessed: 2024-08-13. URL: https://www.engineeringtoolbox.com/molecular-weight-gas-vapor-d_1156.html.
17. Umweltbundesamt. Berichterstattung unter der Klimarahmenkonvention der Vereinten Nationen und dem Kyoto-Protokoll 2023, 2023. Accessed: 2024-08-08. URL: https://www.umweltbundesamt.de/sites/default/files/medien/11850/publikationen/28_2023_cc_berichterstattung_unter_der_klimarahmenkonvention.pdf.
18. J. Wettengel. EU greenlights €4.6 billion in German state support for hydrogen projects, 2024. Accessed: 2024-08-13. URL: https://www.cleanenergywire.org/news/eu-greenlights-eu46-billion-german-state-support-hydrogen-projects.

Open Access This chapter is licensed under the terms of the Creative Commons Attribution-NonCommercial-NoDerivatives 4.0 International License (http://creativecommons.org/licenses/by-nc-nd/4.0/), which permits any noncommercial use, sharing, distribution and reproduction in any medium or format, as long as you give appropriate credit to the original author(s) and the source, provide a link to the Creative Commons license and indicate if you modified the licensed material. You do not have permission under this license to share adapted material derived from this chapter or parts of it.

The images or other third party material in this chapter are included in the chapter's Creative Commons license, unless indicated otherwise in a credit line to the material. If material is not included in the chapter's Creative Commons license and your intended use is not permitted by statutory regulation or exceeds the permitted use, you will need to obtain permission directly from the copyright holder.



Chapter 22
Mathematical Questions Arising from Practical Challenges in Gas Networks

Julia Grübel[0009−0001−0808−9463],
Frauke Liers[0000−0002−1671−0344],
Alexander Martin[0000−0001−7602−3653],
Lars Schewe[0000−0002−3778−262X], and
Michael Schuster[0000−0002−4689−3663]

Abstract Motivated by concrete real-world challenges in gas network operation, this chapter highlights how applied mathematics contributes to the analysis, optimization, and control of large-scale energy infrastructures. Through selected case studies, we show that applicable solutions require the integration of diverse mathematical disciplines and that close interaction with practice drives both methodological innovation and interdisciplinary collaboration.

22.1 Introduction

Gas transmission networks pose a wide range of practical challenges that arise from the interaction of physical gas dynamics, operational constraints, and market-driven decision-making across multiple time scales. Addressing these challenges requires mathematical models and algorithms that are not only theoretically sound, but also capable of supporting real-world operational planning and control.

Julia Grübel
Analytics & Optimization, University of Technology Nuremberg (UTN), Germany,
e-mail: julia.gruebel@utn.de

Frauke Liers
Department of Data Science and Department of Mathematics, FAU Erlangen-Nürnberg, Germany,
e-mail: frauke.liers@fau.de

Alexander Martin
Analytics & Optimization, University of Technology Nuremberg (UTN), Germany,
e-mail: alexander.martin@utn.de

Lars Schewe
School of Mathematics, The University of Edinburgh, UK, e-mail: lars.schewe@ed.ac.uk

Michael Schuster
Department of Data Science, FAU Erlangen-Nürnberg, Germany, e-mail: michi.schuster@fau.de

© The Author(s) 2027

A. Martin et al. (eds.), *Mathematical Modelling, Simulation and Optimization using the Example of Gas Networks*, International Series of Numerical Mathematics 174,
https://doi.org/10.1007/978-3-032-34969-9_22

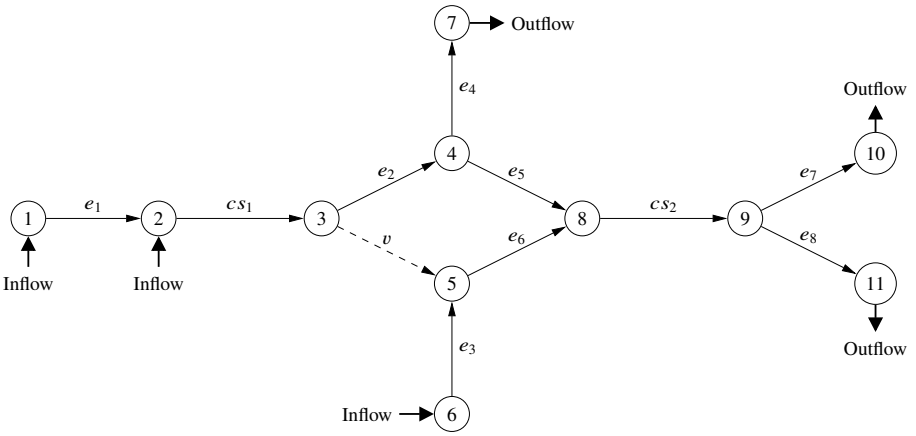


Fig. 22.1: The GasLib-11, a network instance with 11 nodes $\{1, \ldots, 11\}$, 8 edges $\{e_1, \ldots, e_8\}$, two compressor stations $\{cs_1, cs_2\}$, and one valve $\{v\}$ (Network data can be found on gaslib.zib.de.)

This chapter focuses on mathematical questions motivated directly by practical problems in the operation and control of gas networks. Using selected, representative scenarios, we illustrate how different mathematical approaches—ranging from nonlinear and mixed-integer optimization to control theory, analysis of partial differential equations, as well as stochastic and game-theoretic modeling—can be combined to analyze and solve complex operational tasks. The emphasis is not on a single unified approach, but on demonstrating how tailored methods interact within an integrated workflow.

The examples in this chapter cover short-term operational control, transient behavior, robustness with respect to uncertainty, and market-related decisions across different time horizons. Together, they show how stationary and dynamic models, optimization-based methods, fast heuristics, and high-fidelity simulations complement each other for practical applications. By grounding these developments in concrete network instances such as GasLib-11 (see Figures 22.1 and 22.6) and realistic operational questions, this chapter highlights both the necessity of interdisciplinary collaboration within applied mathematics and the new mathematical insights that emerge when novel theoretical developments are driven by practical requirements.

The remainder of this chapter is structured as follows. Section 22.2 focuses on practical challenges in the modeling and control of gas network operation. It demonstrates how an integrated workflow combining modeling, simulation, and optimization enables the analysis and validation of gas flows and supports short-term operational decision-making. Section 22.3 shifts the perspective to gas markets and real-time operation, illustrating how mathematical methods provide decision support for market design, strategic interaction among agents, and robust operational control under uncertainty. Finally, Sect. 22.4 addresses the long-term transformation of gas infrastructures toward hydrogen and hybrid networks, highlighting the mathematical challenges arising

in network restructuring, hybrid operation, and market organization during the energy transition.

22.2 Practical Challenges in Modeling and Control of Gas Networks

The operation of gas transmission networks poses a range of practical challenges arising from the interplay between physical dynamics, operational constraints, and decision-making over time. While stationary flow models form the basis of many planning and operational tools, real-world operation is rarely steady. Frequent short-term changes in supply and demand—triggered, for instance, by updated nominations, unplanned fluctuations in gas production, or injections originating from power-to-gas facilities—require the network to transition between different operating states. Such transitions typically unfold over time horizons of several hours and must respect strict pressure bounds as well as the operational constraints of active elements such as compressors and valves. Capturing and controlling these transient effects in a computationally tractable way is therefore a central challenge for reliable network operation. Mathematical models for such settings are compiled in Chap. 2, "A Catalog of Gas Network Models: PDEs, Coupling Conditions, and Numerical Schemes".

A particularly important aspect in this context is the inherent storage capability of gas networks, commonly referred to as *line pack*. By temporarily increasing or decreasing the amount of gas stored in the pipelines, operators can buffer short-term imbalances and shift energy across time without relying on external storage facilities. This flexibility is especially valuable in future energy systems with a high share of renewable generation and power-to-gas technologies [41, 45, 46]. At the same time, its effective exploitation poses substantial mathematical challenges: (i) control actions are governed by nonlinear transient gas dynamics, (ii) discrete operational decisions interact with continuous control variables, and (iii) feasible strategies must be computed within tight time constraints. These challenges have motivated the development of transient control and optimization approaches for gas networks including instantaneous control concepts, and form the starting point for the developments presented in this section.

22.2.1 From Stationary Models as a Reference Point to Physically-Detailed Transient Models

Although transient models are indispensable for capturing dynamic behavior, stationary gas flow models play a central role in both planning and operational practice. They provide a mathematically well-understood description of admissible operating states for fixed supplies and demands and serve as reference points for feasibility assessment, initialization, and evaluation of transient scenarios. The existence and uniqueness of such stationary operating points has been established for broad classes of gas network models and topologies, providing a rigorous foundation for their use in practice (see, e.g., Chap. 7, "Potential-Based Flows – An Overview" and [23, 25, 50, 51]). Building on

this theoretical basis, it has also been shown that globally optimal stationary solutions can be computed reliably for realistic network instances using nonlinear optimization techniques (see, e.g., Chap. 6, "Mixed-Integer Nonlinear Optimization in the Context of Gas Networks" and [27, 49]). As a result, stationary models form a reference layer that anchors transient simulations and optimization problems and enables the systematic study of transitions between different operating regimes.

From this perspective, stationary models provide a baseline description of admissible operating states and serve as reference points for operational planning. Capturing the temporal evolution of gas flows during transitions between such states, however, requires transient models governed by gas dynamics in pipelines and typically described by systems of partial differential equations. Depending on the required level of physical detail, this leads to a hierarchy of transient models that balance accuracy and computational efficiency (see Sect. 2.3 in Chap. 2, "A Catalog of Gas Network Models: PDEs, Coupling Conditions, and Numerical Schemes"). High-fidelity formulations based on the full Euler equations capture transient effects in detail but are computationally demanding, whereas simplified models enable faster simulation and optimization at the cost of physical realism. Since, in practical operational settings, it is often necessary to compute feasible control strategies for gas networks quickly, fast heuristic approaches based on instantaneous or receding-horizon control concepts have been proposed [24]. Although the resulting admissible control actions are not guaranteed to be globally optimal with respect to the underlying transient optimization problem, they provide valuable initial solutions and serve as fallbacks when computational resources or time are limited. The physical consistency of the computed control strategies can be ensured by validation using high-resolution simulation models. Transient simulations based on the full Euler equations, combined with adaptive discretization and model hierarchies, have been employed to assess feasibility and to quantify model errors for refined control strategies on realistic network instances [11, 12, 36]. Together, fast heuristic methods and high-resolution simulations for validation form a crucial complement to optimization-based approaches, enabling both timely decision-making and reliable validation of transient operating strategies.

22.2.2 From Coarse-Scale to Refined Operations: A Line Pack Example

Next, we present an example of a global optimization-based framework addressing the particularly important aspect of line pack. Afterward, we use this example to demonstrate the mutual benefits of coarse-scale and more detailed optimization approaches for such a practical application.

A systematic formulation and solution approach for short-term storage operation in gas networks was presented in [7]. The authors introduce a transient optimization problem that explicitly exploits line pack by controlling injections, withdrawals, and active network elements over a finite time horizon. Starting from a stationary operating state, the network is operated in an injection phase followed by a withdrawal phase, with the objective of maximizing the amount of usable energy stored in the network subject to pressure bounds, flow constraints, and operational limitations of compressors and valves.

To obtain globally optimal solutions, the transient gas dynamics are described by a simplified model derived from the isothermal Euler equations and discretized in time and space. This discretization leads to a mixed-integer nonlinear optimization problem that captures both nonlinear flow relations and discrete operational decisions. Using tailored solution techniques, globally optimal solutions can be computed for representative network instances, including the widely used GasLib-11 benchmark network [48] (see Fig. 22.1), providing a computationally tractable yet physically meaningful description of line pack usage. In particular, the mixed-integer nonlinear optimization problems arising from the discretized transient models are solved using adaptive MILP-based refinement strategies as described in [8], which enable the reliable computation of global solutions and form a foundation for subsequent refinement and validation steps.

Building on this coarse-scale solution concept [7], the globally optimal controls obtained from the simplified discretized transient model provide natural reference trajectories for optimal control frameworks based on more accurate gas flow descriptions. In these frameworks, the gas dynamics are described by more detailed transient models, and the objective is typically formulated as a tracking-type functional that penalizes deviations from the previously computed reference solution. Mathematical foundations for such a refinement step are developed in [43, 44], where adjoint-based gradient representations for transient gas flow models are derived, enabling the efficient use of gradient-based optimization methods. To ensure strict adherence to operational constraints such as pressure bounds, barrier and interior-point techniques can be employed, as investigated in [12]. Together, these approaches allow the systematic refinement of coarse-scale solutions toward physically consistent transient control strategies.

22.2.3 The Impact of Perturbations and Uncertainties on Operations

Beyond feasibility and optimality under nominal conditions, the practical applicability of transient operating strategies crucially depends on their robustness with respect to perturbations and modeling uncertainties. In particular, transient gas flows are sensitive to variations in supplies and demands, boundary conditions, and physical parameters such as friction coefficients. To quantify these effects, sensitivity analyses for discretized transient gas flow models have been developed, providing measures for the impact of parameter changes on the resulting network states and control trajectories [56]. Complementary to this, the influence of uncertainty on operating strategies has been investigated using optimization-based approaches that explicitly account for uncertain data, allowing the assessment of solution stability and performance degradation under perturbations (see, e.g., [1, 2] for stationary models and [54, 55] for transient models). These analyses contribute to a more comprehensive understanding of transient control strategies and help identify operating regimes in which line pack can be exploited reliably in practice.

22.2.4 Integration of Different Areas of Applied Mathematics to Obtain Validated Operations

We conclude this section by demonstrating on a realistic network instance how the interaction between the different mathematical disciplines leads to a thoroughly analyzed and validated transient gas flow. The considered instance combines a larger transmission network [13, 24] with a smaller distribution network [60]; see Fig. 22.2. The transmission network consists of 16 nodes, including two sources, three terminal nodes, and one flexible node that can act as either a source or a terminal node over time. It further includes 12 pipes, three compressors, one valve, and one control valve. The distribution network contains 10 nodes, including six terminal nodes, and 10 pipes. It is connected to the transmission network through a terminal node of the transmission network. The workflow across modeling, simulation, and optimization required to obtain a thoroughly analyzed and validated transient gas flow on this network over a three-hour time horizon is illustrated in Fig. 22.3.

First, using the software package [28], friction coefficients in the gas pipes are identified together with information about their distributions. Second, the results of [25] on the existence and uniqueness of stationary states of the isothermal Euler equations ensure the existence of stationary operating states for given boundary data. Third, using spherical radial decomposition, tighter pressure bounds at the terminal node connecting the transmission and distribution network are computed [18, 57, 60]. These tighter bounds guarantee that the lower pressure bounds at all nodes of the distribution network are satisfied with high probability, allowing the subsequent analysis to focus exclusively on the transmission network.

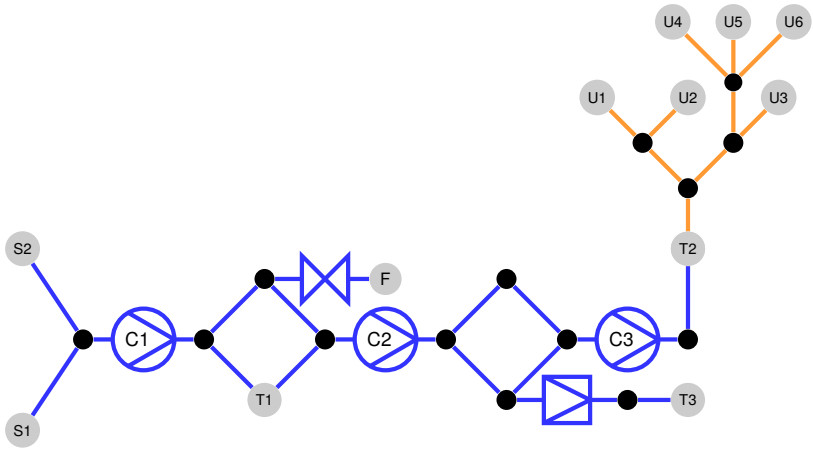


Fig. 22.2: An instance combined of a transmission (blue) and a distribution (orange) network with 26 nodes, 22 pipes, three compressor stations, one control valve, and one valve

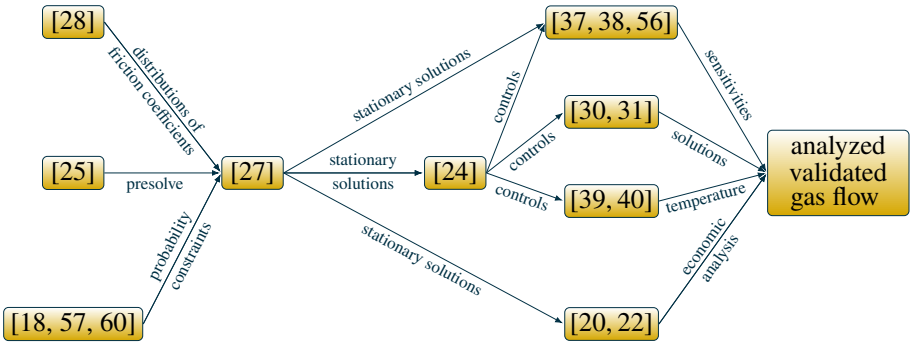


Fig. 22.3: The workflow to obtain a thoroughly analyzed and validated transient gas flow for the instance depicted in Fig. 22.2

Building on the identified friction coefficients, the existence of stationary operating states, and the tightened pressure bounds at the connection node of the transmission and distribution networks, initial and terminal stationary states are computed using the spatial branch-and-bound approach developed in [27]. The MIP-based instantaneous control algorithm from [24] then determines transient control strategies to steer the system from the initial to the terminal state over the given three-hour time horizon. These controls can subsequently be refined through simulation of a DAE system that preserves key properties of the underlying PDAE system [30, 31]. Moreover, the simulation approach [39, 40] allows for the consideration of temperature dependencies.

For resulting trajectories and a comparison of the three different simulations see Fig. 22.4. The upper three plots in Fig. 22.4 depict the boundary data as well as the compressor control over the considered time horizon. The upper-middle plot in particular highlights the pronounced demand at the terminal node T2, arising from the fact that the connected distribution network is supplied through this node. The lower three plots in Fig. 22.4 provide insights into the simulation results. The lower-left plot shows the pressure evolution for the three different simulation approaches at the terminal node T2, which is a key node due to linking the transmission and distribution networks. The lower-middle plot illustrates in more detail the corresponding pressure differences at this node between the coarser simulation [24] and one of the refined approaches. Lastly, the lower-right plot presents an exemplary temperature trajectory, here for the compressor station C1. In addition to the simulations, sensitivity analyses are carried out to estimate the effects of data uncertainty as well as modeling, discretization, and rounding errors in the numerical simulations [37, 38, 56]. Finally, the methods proposed in [20, 22] enable an assessment of whether the initial and terminal stationary states correspond to market equilibria under given demand and supply conditions.

Overall, the approaches discussed in this section illustrate how short-term operational challenges in gas networks can be addressed through an integrated workflow that combines modeling, optimization, and simulation. Stationary operating points provide a reliable reference layer, while transient models capture the dynamic behavior

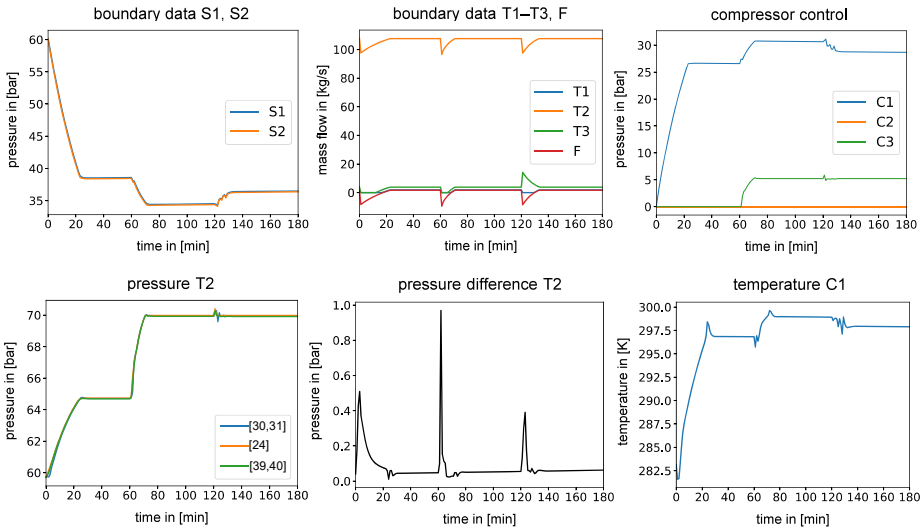


Fig. 22.4: Boundary data (above) and simulation results (below) for the instance depicted in Fig. 22.2 over a three-hour time horizon

required to exploit line pack as a flexible storage mechanism. Coarse-scale optimization enables the computation of globally meaningful control strategies, which can be systematically refined using optimal control techniques based on more accurate physical models. Fast heuristic methods support timely decision-making in operational settings, and high-fidelity simulations together with sensitivity and robustness analyses ensure physical feasibility and reliability under perturbations (see, e.g., [7,24,27,36,56]). This integrated multi-stage framework demonstrates how different areas of applied mathematics can be effectively combined to support operational planning in gas networks and provides a foundation for addressing similar challenges in future gas and hydrogen infrastructures.

22.3 Practical Challenges in Gas Markets and Real-Time Operation of Gas Networks

Practical challenges in gas markets and gas transport arise across all relevant time scales. In particular, real-time operational control is exceptionally demanding. Network operators must respond to renomination requests at very short notice and ideally determine control strategies that remain robust under such perturbations. At the same time, rare but critical events—such as the unexpected failure of compressors, valves, or even entire sub-networks—require effective countermeasures to preserve operational stability. Beyond the physical real-time control of gas flows, the preceding decisions made by the

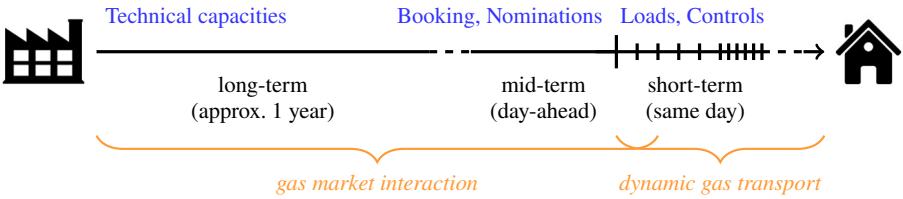


Fig. 22.5: Time scales in gas markets and gas transport

various agents participating in the market are equally important. Explicitly accounting for these decisions, as well as the interactions among market participants, significantly increases problem complexity and introduces additional practical challenges.

Figure 22.5 provides an overview of the various time scales relevant to gas markets and gas transport. In the following, we proceed along these time scales—from the coarsest to the finest level of detail—and use selected examples to illustrate how we addressed practical challenges of the types introduced above through the interplay of key applied mathematics disciplines, namely modeling, simulation, and optimization. All results are demonstrated using a common test instance, either GasLib-11 (see Fig. 22.1 and [48]) or a passive variant of GasLib-11 (see Fig. 22.6).

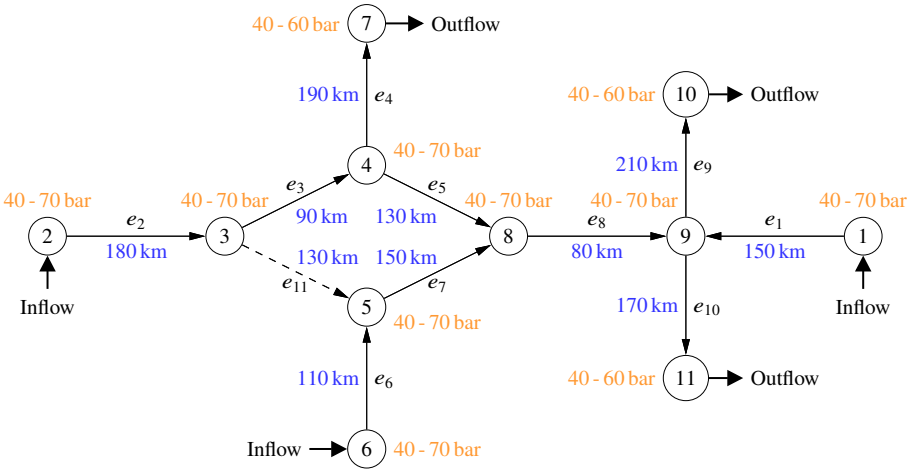


Fig. 22.6: The passive, tree (without e_{11}) or cyclic (with e_{11}) network variant of the GasLib-11, a network instance with 11 nodes and 10 or 11 edges, respectively (based on the instance considered in [29])

22.3.1 Long-Term Perspective: Network Topology and Technical Capacities

The long-term perspective focuses on decisions concerning network topology and technical capacities. By combining the strengths of *multilevel optimization* and *economic theory*, the cost of decoupling trade and transport in the European entry-exit system was quantified for the first time in [9]. The analysis relies on the deterministic four-level model introduced in Chap. 8, "Models for Gas Markets", assuming perfect competition and linear flows in general (possibly cyclic) networks. On the one hand, robustness requirements on technical capacities—namely, that a physically feasible transport must exist for all allocations within the specified capacity ranges—are very relevant and should be taken into account. On the other hand, a computational study on the passive tree variant of the GasLib-11 from Fig. 22.6 indicates that this requirement can lead to welfare losses exceeding 11.5 %, suggesting that the requirement of strict robustness may be restrictive in practice. However, even modest adjustments to market design or network configuration can substantially mitigate these losses. The second-best approach of [9], which determines technical capacities such that the resulting market allocation outcomes are feasible though not all gas allocations compatible with the nodal capacity bounds, already leads to a significant improvement. Similarly, the robust network topology concept of [32]—a graph-theoretic characterization of network structures that ensure monotonicity of maximal potentials under decreasing demands by excluding certain forbidden labeled minors—yields comparable benefits. When applied to the same test instance, both approaches reduce welfare losses to approximately 1 %.

A further source of complexity arises when uncertainty in nominations is taken into account. In real-world settings, there are exit players—such as large municipal utilities—who at the time of nomination do not yet know the exact demand they will have to serve. Nevertheless, these players must ensure that they can meet this uncertain load with a specified safety level in order to avoid penalties. By integrating multilevel and stochastic optimization techniques, the authors of [29] develop a cutting-plane algorithm for solving the four-level gas market model with chance constraints at the nominations level. Computational results on the passive cyclic variant of the GasLib-11 with relaxed pressure bounds (see Sect. 3.5 in [29]) indicate that moderate safety levels of up to 90 % lead to only modest welfare losses [29, Fig. 4]. Such safety levels therefore appear advisable—particularly since the proposed approach safeguards against substantially more load scenarios than simpler strategies based on nominating the mean or the 0.9-quantile.

22.3.2 Mid-Term Perspective: Capacity Booking and Subsequent Nominations

In the mid-term perspective, decisions concerning capacity booking and subsequent nominations become central. Strategic interaction among market participants plays an important role, as past experience in gas markets has repeatedly shown. Game-

theoretic frameworks that explicitly account for such strategic behavior, such as the model presented in [21], are therefore of considerable practical relevance. The algorithm developed in [21] makes it possible to quantify the welfare effects of strategic booking and nomination decisions. For instance, considering the economic data as in the computational studies previously addressed in this section and building on the technical capacities computed via the approach in [9], when firms act strategically rather than as price-takers under perfect competition, a welfare loss of 8.4 % arises during periods in which the network operates at its capacity limit, i.e., in the winter months from November to March. For an overview of further game-theoretic approaches addressing strategic aspects in the entry-exit market model see Sect. 8.5 in Chap. 8, "Models for Gas Markets".

The benefits of dynamic formulations over stationary ones are examined in [26] and Chap. 18, "A PDE-Constrained Generalized Nash Equilibrium Approach for Modeling Gas Transport with Strategic Suppliers", the latter with a particular emphasis on capturing line pack effects. One key finding of this chapter is that line pack can notably increase welfare when the gas purchase cost are lower during the first half of the time horizon.

22.3.3 Short-Term Perspective: Robust Operations Under Uncertainty

Finally, short-term operation concerns the physical transport of gas under fixed nominations. In practice, network operators often lack precise knowledge of important physical parameters, such as friction coefficients in the pipes. To avoid violating operational limits, they must therefore ensure robustness with respect to these uncertainties. This means that a feasible transport must exist for every admissible realization of the physical parameters. In the stationary setting, this leads to a nonlinear robust optimization problem. This can be tackled using the adaptive bundle method of [34], which iteratively refines approximate worst-case evaluations and subgradients and uses them within a nonconvex bundle framework to achieve convergence. Computational experiments on the passive tree variant of the GasLib-11 (cf. Fig. 22.6) reveal a pronounced sensitivity to uncertain physics with welfare losses of up to 26.3 %. Notably, these losses drop substantially when the network satisfies the robustness conditions of [32], highlighting the strong influence of network structure on operational resilience.

In operational practice, network operators aim to design control strategies that remain robust under perturbations such as short-notice renominations. To this end, in [55], a methodology has been developed to quantify the *probabilistic* robustness of given *control* decisions, that is, the probability that the pressure constraints remain satisfied under uncertain renominations over the time horizon. Based on a stochastic collocation approach, [35] characterize the impact of uncertain gas outflows, representing short-notice changes, on the resulting pressures in the network. Building on this, the kernel density estimator approach proposed in [52, 54] is used to compute the probability that the pressure bounds are satisfied. This probability serves as a quantitative robustness metric for the deterministic optimal control, measuring its stability with respect to uncertainty. The approach is illustrated for the GasLib-11 instance (see Fig. 22.1).

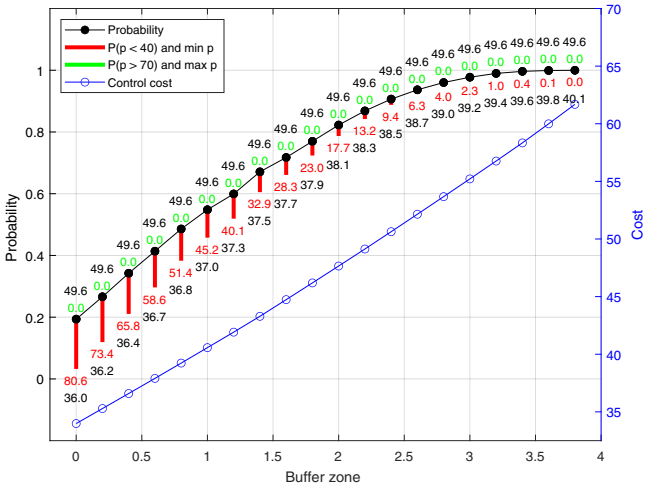


Fig. 22.7: Probabilistic robustness and control cost for different buffer zones Δp [55, Fig. 4 (a)]

Optimal control decisions are computed using the Penalty Alternating Direction Method from [17] for different buffer zones $\Delta p \geq 0$. A buffer zone of $\Delta p \geq 0$ implies that the pressures p are constrained to the tightened interval $p \in [p^{\min} + \Delta p; p^{\max} - \Delta p]$ in the open-loop control problem. Figure 22.7 shows the resulting probabilistic robustness as a function of the buffer size, together with the associated compressor cost. A buffer zone of 0.75 bar already yields a robustness level of 50 %, while full probabilistic robustness is achieved at $\Delta p = 3.5$ bar, at the expense of increased control cost.

The approach proposed in [54] further allows the computation of the tightest physical pressure bounds, namely the lowest feasible upper bound and the highest feasible lower bound, that achieve a prescribed probabilistic robustness level for given inlet pressures and controls. If these probabilistically required bounds violate the physical pressure limits, this indicates an increased risk of pipe or compressor failures under short-notice changes and thus points to the need for appropriate countermeasures. For the GasLib-11 instance with pressures of $(60, 58, 60)$ bar at the inflow nodes, the numerical results show that a probabilistic robustness level of 75 % can be achieved without exceeding the system's physical pressure bounds. This demonstrates that, for this operating point, the desired robustness level is attainable within the given technical limits. An extended convergence analysis for probabilistic constrained optimization problems, with particular emphasis on the kernel density estimator-based approximation discussed above, is provided in [53].

22.3.4 Real-Time Perspective: Adapting to System Changes

Finally, the challenge of adapting to system changes in real time is addressed by combining *simulation* and *optimization* techniques. The Sequential Action Control (SAC) framework developed in [5] updates the control at every time step while explicitly incorporating newly available data, such as measurements. This enables rapid reactions to critical events, for instance compressor failures, and allows the perturbed system to be stabilized efficiently toward the desired operating state. For the common test instance, simulations, discretizations, and adjoint equations from [12] serve as input for the SAC on the fixed prediction interval. The resulting stabilizing control successfully drives the GasLib-11 instance back to the desired state in real time, within 10 seconds after the failure of a compressor station, thereby demonstrating the practical relevance of SAC for maintaining operational stability.

In summary, our computational results on the considered test instances highlight the potential of the underlying methods to support decision-making in the design and modification of market rules and network topologies. Furthermore, the numerical experiments on the dynamic GasLib-11 instance demonstrate that the novel approaches have the potential to evolve into powerful tools for the reliable real-time operation of gas networks, enabling robust responses to uncertainty and critical events. Taken together, these findings illustrate how the integration of optimization, simulation, stochastic modeling, and game-theoretic analysis contributes to addressing practical challenges in gas markets and network transport across all relevant time scales.

22.4 Practical Challenges in the Transition of Natural Gas and Hydrogen Networks

The European Green Deal outlines a strategic pathway toward carbon neutrality and a resource-efficient economy. Within this transition, hydrogen is widely regarded as a key energy carrier [58], with its share in the European gas mix predicted to increase from approximately 2 % in 2018 to 13–14 % by 2050 [14]. At present, hydrogen production remains largely centralized and mostly carbon-intensive (so-called gray hydrogen), and is mainly used in refining, petrochemical, and fertilizer industries. As a consequence of its limited and sector-specific utilization, large-scale hydrogen trading markets have not yet emerged [15]. As Europe advances toward decarbonization, hydrogen production is expected to increasingly shift toward green, carbon-neutral sources. At the same time, hydrogen use in industry, transport, and heating is anticipated to expand significantly [58]. Meeting this growing demand will require the development of a dedicated hydrogen transmission infrastructure [14, 58], giving rise to complex design, planning, and operational challenges.

From a modeling perspective, the transport of pure natural gas or pure hydrogen in pipeline networks is commonly described by the isothermal Euler equations, a system of hyperbolic partial differential equations. In contrast, the transport of gas mixtures requires an extended modeling framework that accounts for additional physical effects,

in particular interactions and collisions between different particle species. Such effects influence both the macroscopic flow behavior and the thermodynamical properties of the mixture. A detailed analysis of these modeling challenges, with a particular emphasis on the pressure-density relation for gas mixtures, is provided in Sect. 3.2 in Chap. 3, "Gas Mixtures on Networks: Modeling, Simulation and Optimization". While these modeling aspects are essential for accurately describing mixed-gas transport, the focus of the present section lies on network restructuring, hybrid operation without mixing, and market-related questions arising from the coexistence of natural gas and hydrogen infrastructures.

We next summarize key mathematical questions that arise in the development and organization of hydrogen transmission networks, including their restructuring and hybrid operation alongside existing gas systems. In particular, the following questions are of central relevance:

(i) How can existing gas networks be downsized and/or repurposed to enable the efficient integration of hydrogen transport?
(ii) How can interactions among agents operating across both sectors be coordinated?

Addressing these questions requires the consideration of multiple interacting aspects, including network topology planning, operation and control of hybrid infrastructures, the treatment of uncertainties in supply and demand, and market-related mechanisms, all of which give rise to challenging mathematical problems. Further aspects consist of taking gas mixtures into account. Mathematical questions on gas mixtures in networks are addressed in Chap. 3, "Gas Mixtures on Networks: Modeling, Simulation and Optimization". For an instance that is explicitly designed to model, optimize, and test the transition from natural gas to hydrogen networks see Chap. 21, "Gas2Hydro – A Combined Natural Gas–Hydrogen Instance".

22.4.1 Reducing Gas Networks and Integration of Hydrogen

In the transition toward carbon neutrality and increasing hydrogen use, overall demand for natural gas is expected to decline. As a result, a significant share of the European gas transmission network is predicted to become redundant by the end of the decade, in particular due to the phase-out of low-calorific gas [14,58]. This development raises the critical question of how to efficiently plan and manage the decommissioning of natural gas pipelines. Beyond identifying which pipelines should be retired, the reduction process must be scheduled over time while ensuring safe and efficient operation of the remaining network, for example with respect to pressure constraints.

The transition toward hydrogen further increases both design and operational complexity. As demand for natural gas declines, network flows must be reconfigured to accommodate the growing integration of hydrogen and other alternative energy carriers. Managing this transition requires a systematic and uncertainty-aware approach to ensure reliable operation and sufficient network capacity throughout the transformation process. In the following, we summarize selected results obtained to date.

We begin by focusing on stationary models. Since future hydrogen and natural gas demand is inherently uncertain, it is essential to appropriately safeguard gas network operation against demand fluctuations. One modeling approach consists in guaranteeing feasibility of nomination validation in the network only with a prescribed high probability with respect to the probability distribution generating the demands. This requirement can be formulated using robust chance constraints. The resulting optimization problem naturally includes binary decisions, such as whether pipelines should be constructed or repurposed. Consequently, the model takes the form of a mixed-integer nonlinear optimization problem with robust chance constraints. This problem class can be addressed using a tailored branch-and-cut algorithm [4]. The main idea of this algorithm is based on relaxing the robust chance constraint and strengthening the lower bound problem with cover inequalities inspired from those from the knapsack problem in combinatorial optimization. Furthermore, upper bounds for the branch-and-cut procedure can be built with a scenario-based bundle method [3].

With respect to network extension and adaptation, incremental–decremental optimization addresses the gradual transformation or renewal of infrastructure systems. In Chap. 12, "Incremental-Decremental Optimization for the Transition to Hydrogen", this framework is used to study the order in which an existing natural gas network can be reconstructed to operate with hydrogen instead. The goal is to minimize operational cost at each stage of the reconstruction process. The chapter introduces a double-greedy approach to determine an ordering in which individual sinks are switched from natural gas to hydrogen operation. The performance of the proposed algorithm is demonstrated using a subnetwork of the eastern German gas transmission system. In addition, established theoretical results on incremental–decremental maximization, as presented in [10], are summarized.

Subsequently, we shift focus to dynamic models. In Chap. 19, "p-Wasserstein Distances on Networks and 3D to 1D Convergence", methods are developed that link optimal transport on realistic three-dimensional gas networks, characterized by small diameter-to-length ratios, to their asymptotic limits on one-dimensional graph representations. This connection enables the analysis of realistic operational scenarios within a reduced modeling framework. A central question in this context is whether existing and newly planned compressor stations allow a feasible dynamic control for given demand scenarios. This issue is investigated in [47], where least-squares collocation methods are employed to assess controllability. Moreover, the residuals of the collocation solutions provide valuable insight into the temporal and spatial locations at which pressure constraints are violated when no feasible dynamic control exists.

Comparisons of optimal transport solutions across different network topologies further form a basis for informed decommissioning decisions. To this end, transport metrics on gas networks are introduced that allow Kantorovich-type optimal transport problems to be formulated and solved as linear programs. Transport efficiency can be further enhanced by incorporating density constraints into the optimal transport model; corresponding dynamic formulations are developed in [6, 16].

22.4.2 Organizing the Interaction between Agents Participating in Both Sectors

A key open question concerns the regulatory organization of hydrogen transmission networks. In the natural gas sector, a transmission system operator (TSO) is responsible for managing network capacities according to the entry-exit system. For hydrogen networks, a similar organizational structure, potentially also governed by a TSO, is widely anticipated (cf. EU Directive 2024/1788). If the gas and hydrogen TSOs operate independently, however, their interaction gives rise to equilibrium problems across the coupled networks.

In [42], coupled dynamical systems are studied using *co-simulation* techniques. A particular application is the joint operation of coupled networks across different sectors. The studied framework, for instance, enables the coupling of simulations based on coarser models for natural gas networks over long distances with simulations employing refined models for hydrogen networks over shorter distances, provided that suitable interface conditions between the simulation tools are satisfied. Moreover, topological convergence criteria [42, Theorem 4.2.3] for the co-simulation are derived, accounting for the chosen modeling and space discretizations, the underlying network topology, and the design of the interfaces.

Typically, end consumers do not purchase gas directly on wholesale markets but are supplied via intermediaries, commonly referred to as retail companies, which charge retail tariffs. While fixed tariffs may be preferable when consumers exhibit high risk aversion, dynamic tariffs combined with congestion-based network pricing can enable more efficient consumption and switching decisions between the coupled energy carriers.

In [59], a comprehensive framework for modeling retail competition is developed. In this setting, multiple strategic retailers purchase gas or hydrogen on wholesale markets at fluctuating prices and offer retail contracts over a longer time horizon. End consumers choose among these contracts and subsequently decide on consumption quantities. The framework captures customer preferences that depend not only on price-related contract attributes such as fixed fees and volumetric prices, but also on retailer-specific non-price characteristics such as the retailer's regional origin or the product's environmental footprint.

After contract selection, customers determine consumption quantities over time, contingent on contracted prices. The resulting model constitutes a multi-leader-multi-follower game, with retailers acting as leaders and customers as followers. The methods developed in [59] enable the characterization of market equilibria and their derivation for both fixed-price tariffs and real-time pricing in the general case of asymmetric retailers. For the case of symmetric retailers [59, Assumption 6.1], i.e., all retailers face identical optimization problems, an analytical comparison of tariff schemes is provided in terms of retailer profits, consumer benefits, and total welfare. In the general asymmetric case, the model is calibrated using real-world data and evaluated on a test instance motivated by a market scenario in Germany.

From a mathematical perspective, the modeling yields nonsmooth optimization problems, due to the complementarity conditions employed to reformulate the lower-level

problem. To address this structure, specialized algorithms were developed that explicitly exploit nonsmoothness while accommodating moderate nonlinearities; see, for example, [19] and [33] for related applications. These new algorithms were successfully applied to solve the optimization problem arising in the general asymmetric case for the market setting motivated by the German energy sector described above [59]. Incorporating risk aversion introduces additional sources of nonsmoothness, which naturally integrate into the overall algorithmic framework. Initial numerical experiments for this extended setting have likewise yielded promising results.

The analysis demonstrates that real-time pricing increases customer benefits and overall welfare, with these effects strengthened under higher wholesale price volatility. Additionally, a surrogate reduced-order model was constructed to quantify the welfare gains from shifting from fixed-price tariffs to real-time pricing [59, Sect. 6].

22.5 Outlook

This chapter has used three examples to show how important and scientifically beneficial it is to address interesting and challenging questions from practice, in this specific case from the field of gas network planning and control, through mathematical research. First, in Sect. 22.2, we demonstrate how an integrated workflow combining modeling, simulation, and optimization can resolve short-term operational challenges in gas networks and lead to thoroughly analyzed and validated transient gas flows. Second, we highlight in Sect. 22.3 that the integration of these mathematical methods also provides valuable decision support for regulatory authorities and policy-makers in shaping market rules and network topologies, as well as for gas network operators in real-time operation to enable reliable responses to uncertainties and critical events. Finally, we emphasize in Sect. 22.4 how these disciplines can jointly contribute to addressing the societal challenge of climate change by supporting the transformation of gas infrastructures toward low-carbon energy carriers, in particular the transition from natural gas to future hydrogen networks.

The research approach described in this chapter allowed us to address several aspects that we consider essential. First of all, applied mathematics does not consist solely of looking at which mathematics is needed in practice and trying to implement it, but is inspired in particular by facing the challenges of reality, taking up the questions addressed and arising there, transferring them to mathematics, and developing mathematics within the field. This is precisely what has been achieved here in an exemplary manner. And not only has it been successful, but it has also become clear that this requires new mathematics. New mathematics not only in the individual disciplines that comprise this fascinating field of applied mathematics in gas network operation, but also at their interfaces and in their interaction with economic modeling and market design. All these practical challenges could and can only be addressed and solved through collaboration between different disciplines within mathematics.

Against this background, these examples can serve as models for further initiatives in applied mathematics, encouraging researchers to confront the demands of reality,

identify the resulting mathematical questions, and thereby develop and promote new mathematics both within and across disciplines.

However, a critical remark is warranted at this point. What has not yet happened is the transfer back into the application in the real world. We have seen and continue to see from these examples that mathematics can make significant contributions to addressing the challenges posed by gas networks, for example, and can also provide valuable solutions. However, putting these into practice in the real world requires even more. And this "more" is not to be found purely in mathematics. This means that we, as mathematicians, must take the step of engaging in direct exchange with users, even if we leave the field of mathematics, in order to not only develop our algorithms as prototypes, but also to implement them in professional software and integrate them into existing systems in industry. The final steps are very laborious, very time-consuming, and, as a rule, do not result in mathematical publications. That is why, in our view, this step is often missing. But we would like to take this opportunity to draw attention to whether mathematics might want to go down this path in the future. It would be for the good of our society.

Acknowledgements This work was supported by the German Research Foundation (DFG) within Subprojects A05, B06, B07, B08, B10, and C03 in the Sonderforschungsbereich/Transregio 154 "Mathematical Modelling, Simulation and Optimization using the Example of Gas Networks" (Project ID 239904186).

References

1. D. Aßmann, F. Liers, and M. Stingl. Decomposable robust two-stage optimization: An application to gas network operations under uncertainty. *Networks*, 74(1):40–61, 2019. doi:10.1002/net.21871.
2. D. Aßmann, F. Liers, M. Stingl, and J. C. Vera. Deciding robust feasibility and infeasibility using a set containment approach: An application to stationary passive gas network operations. *SIAM Journal on Optimization*, 28(3):2489–2517, 2018. doi:10.1137/17M112470X.
3. D. Bernhard, F. Liers, and M. Stingl. Robust chance-constrained optimization with discrete distributions. Preprint, TRR 154, 2024. URL: https://opus4.kobv.de/opus4-trr154/564.
4. D. Bernhard, F. Liers, and M. Stingl. Branch-and-cut for mixed-integer robust chance-constrained optimization with discrete distributions. Preprint, TRR 154, 2025. URL: https://opus4.kobv.de/opus4-trr154/609.
5. Y. Brodskyi, F. M. Hante, and A. Seidel. Stabilization of partial differential equations by sequential action control. *IMA Journal of Mathematical Control and Information*, 39(4):1008–1033, 2022. doi:10.1093/imamci/dnac021.
6. M. Burger, I. Humpert, and J.-F. Pietschmann. Dynamic optimal transport on networks. *ESAIM: Control, Optimisation and Calculus of Variations*, 29, 2023. Article 54. doi:10.1051/cocv/2023027.
7. R. Burlacu, H. Egger, M. Groß, A. Martin, M. E. Pfetsch, L. Schewe, M. Sirvent, and M. Skutella. Maximizing the storage capacity of gas networks: A global MINLP approach. *Optimization and Engineering*, 20:543–573, 2019. doi:10.1007/s11081-018-9414-5.
8. R. Burlacu, B. Geißler, and L. Schewe. Solving mixed-integer nonlinear programmes using adaptively refined mixed-integer linear programmes. *Optimization Methods and Software*, 35(1):37–64, 2020. doi:10.1080/10556788.2018.1556661.

9. T. Böttger, V. Grimm, T. Kleinert, and M. Schmidt. The cost of decoupling trade and transport in the European entry-exit gas market with linear physics modeling. *European Journal of Operational Research*, 297(3):1095–1111, 2022. doi:10.1016/j.ejor.2021.06.034.
10. Y. Disser, M. Klimm, A. Lutz, and L. Strubberg. Incremental–decremental maximization. In J. Matuschke and J. Verschae, ed., *Approximation and Online Algorithms. WAOA 2025*, volume 16077 of *Lecture Notes in Computer Science*, pages 97–110, Cham, 2026. Springer. doi:10.1007/978-3-032-06706-7_7.
11. P. Domschke, A. Dua, J. J. Stolwijk, J. Lang, and V. Mehrmann. Adaptive refinement strategies for the simulation of gas flow in networks using a model hierarchy. Preprint, TRR 154, 2017. URL: https://opus4.kobv.de/opus4-trr154/127.
12. H. Egger, T. Kugler, and W. Wollner. Numerical optimal control of instationary gas transport with control and state constraints. Preprint, TRR 154, 2017. URL: https://opus4.kobv.de/opus4-trr154/214.
13. K. Ehrhardt and M. C. Steinbach. Nonlinear optimization in gas networks. In H. G. Bock, H. X. Phu, E. Kostina, and R. Rannacher, ed., *Modeling, Simulation and Optimization of Complex Processes*, pages 139–148, Berlin, Heidelberg, 2005. Springer. doi:10.1007/3-540-27170-8_11.
14. European Commission. A hydrogen strategy for a climate-neutral Europe, 2020. COM/2020/301. URL: https://eur-lex.europa.eu/legal-content/EN/TXT/?uri=CELEX:52020DC0301.
15. European Commission, Directorate-General for Energy. Quarterly report on European gas markets, Volume 14 (issue 1, first quarter of 2021), 2021. URL: https://circabc.europa.eu/ui/group/3ef9355f-1ffe-4c82-ba19-f60a3ed2f652/library/0a6315f3-48fd-4763-b6bd-fad789f28ff1/details.
16. A. Fazeny, M. Burger, and J.-F. Pietschmann. Optimal transport on gas networks. *European Journal of Applied Mathematics*, 37(3):553–585, 2026. doi:10.1017/S0956792525000051.
17. B. Geißler, A. Morsi, L. Schewe, and M. Schmidt. Solving highly detailed gas transport MINLPs: Block separability and penalty alternating direction methods. *INFORMS Journal on Computing*, 30(2):309–323, 2018. doi:10.1287/ijoc.2017.0780.
18. C. Gotzes, H. Heitsch, R. Henrion, and R. Schultz. On the quantification of nomination feasibility in stationary gas networks with random load. *Mathematical Methods of Operations Research*, 84:427–457, 2016. doi:10.1007/s00186-016-0564-y.
19. G. Graser, T. Kreimeier, and A. Walther. Solving linear generalized Nash games using an active signature method. *Optimization Methods and Software*, pages 1–24, 2025. doi:10.1080/10556788.2025.2576221.
20. V. Grimm, J. Grübel, L. Schewe, M. Schmidt, and G. Zöttl. Nonconvex equilibrium models for gas market analysis: Failure of standard techniques and alternative modeling approaches. *European Journal of Operational Research*, 273(3):1097–1108, 2019. doi:10.1016/j.ejor.2018.09.016.
21. V. Grimm, D. Nowak, L. Schewe, M. Schmidt, A. Schwartz, and G. Zöttl. A tractable multi-leader multi-follower peak-load-pricing model with strategic interaction. *Mathematical Programming*, 195:605–647, 2022. doi:10.1007/s10107-021-01708-0.
22. J. Grübel, O. Huber, L. Hümbs, M. Klimm, M. Schmidt, and A. Schwartz. Nonconvex equilibrium models for energy markets: Exploiting price information to determine the existence of an equilibrium. *Optimization Methods and Software*, 38(1):153–183, 2023. doi:10.1080/10556788.2022.2117358.
23. M. Gugat, F. M. Hante, M. Hirsch-Dick, and G. Leugering. Stationary states in gas networks. *Networks and Heterogeneous Media*, 10(2):295–320, 2015. doi:10.3934/nhm.2015.10.295.
24. M. Gugat, G. Leugering, A. Martin, M. Schmidt, M. Sirvent, and D. Wintergerst. MIP-based instantaneous control of mixed-integer PDE-constrained gas transport problems. *Computational Optimization and Applications*, 70:267–294, 2018. doi:10.1007/s10589-017-9970-1.
25. M. Gugat, R. Schultz, and D. Wintergerst. Networks of pipelines for gas with nonconstant compressibility factor: Stationary states. *Computational and Applied Mathematics*, 37:1066–1097, 2018. doi:10.1007/s40314-016-0383-z.
26. M. Gugat, M. Schuster, and S. Steffensen. A dynamic multilevel model of the European gas market. *Communications in Optimization Theory*, 2023:1–26, 2023. Article 11.
27. O. Habeck, M. E. Pfetsch, and S. Ulbrich. Global optimization of mixed-integer ODE constrained network problems using the example of stationary gas transport. *SIAM Journal on Optimization*, 29(4):2949–2985, 2019. doi:10.1137/17M1152668.

28. S. Hajian, M. Hintermüller, and N. Strogies. UQ: An uncertainty quantification package for identifying friction coefficient in gas pipes. https://github.com/fg8/UQ, 2018. Release v0.1.
29. H. Heitsch, R. Henrion, T. Kleinert, and M. Schmidt. On convex lower-level black-box constraints in bilevel optimization with an application to gas market models with chance constraints. *Journal of Global Optimization*, 84:651–685, 2022. doi:10.1007/s10898-022-01161-z.
30. C. Huck and C. Tischendorf. Perturbation analysis of hyperbolic PDAEs describing flow networks. Preprint, TRR 154, 2017. URL: https://opus4.kobv.de/opus4-trr154/183.
31. C. Huck and C. Tischendorf. Topology motivated discretization of hyperbolic PDAEs describing flow networks. Preprint, TRR 154, 2017. URL: https://opus4.kobv.de/opus4-trr154/137.
32. M. Klimm, M. E. Pfetsch, R. Raber, and M. Skutella. On the robustness of potential-based flow networks. *Mathematical Programming*, 197:337–374, 2023. doi:10.1007/s10107-021-01760-w.
33. T. Kreimeier, M. Kuchlbauer, F. Liers, M. Stingl, and A. Walther. Towards the solution of robust gas network optimization problems using the constrained active signature method. In C. Büsing and A. M. C. A. Koster, ed., *Proceedings of the 10th International Network Optimization Conference (INOC)*, pages 45–50, Aachen, 2022. OpenProceedings.org.
34. M. Kuchlbauer, F. Liers, and M. Stingl. Adaptive bundle methods for nonlinear robust optimization. *INFORMS Journal on Computing*, 34(4):2106–2124, 2022. doi:10.1287/ijoc.2021.1122.
35. J. Lang, P. Domschke, and E. Strauch. Adaptive single- and multilevel stochastic collocation methods for uncertain gas transport in large-scale networks. In R. Sevilla, S. Perotto, and K. Morgan, ed., *Mesh Generation and Adaptation*, volume 30 of *SEMA SIMAI Springer Series*, pages 113–135. Springer, Cham, 2022. doi:10.1007/978-3-030-92540-6_6.
36. J. Lang and P. Mindt. Entropy-preserving coupling conditions for one-dimensional Euler systems at junctions. *Networks and Heterogeneous Media*, 13(1):177–190, 2018. doi:10.3934/nhm.2018008.
37. V. Mehrmann, M. Schmidt, and J. J. Stolwijk. Model and discretization error adaptivity within stationary gas transport optimization. *Vietnam Journal of Mathematics*, 46:779–801, 2018. doi:10.1007/s10013-018-0303-1.
38. V. Mehrmann and J. J. Stolwijk. Error analysis for the Euler equations in purely algebraic form. Preprint, TRR 154, 2015. URL: https://opus4.kobv.de/opus4-trr154/4.
39. P. Mindt. *Hierarchical Gas Model Coupling on Networks*. Dissertation, Technische Universität Darmstadt, 2018. doi:10.26083/tuprints-00008710.
40. P. Mindt, J. Lang, and P. Domschke. Entropy-preserving coupling of hierarchical gas models. *SIAM Journal on Mathematical Analysis*, 51(6):4754–4775, 2019. doi:10.1137/19M1240034.
41. G. Müller-Syring, M. Henel, W. Köppel, H. Mlaker, M. Sterner, and T. Höcher. Entwicklung von modularen Konzepten zur Erzeugung, Speicherung und Einspeisung von Wasserstoff und Methan ins Erdgasnetz, 2013. Forschungsbericht G1-07-10, DVGW Deutscher Verein des Gas- und Wasserfaches e.V. URL: https://www.dvgw.de/medien/dvgw/forschung/berichte/g1_07_10.pdf.
42. J. Pade. *Analysis and Waveform Relaxation for a Differential-Algebraic Electrical Circuit Model*. Dissertation, Humboldt-Universität zu Berlin, 2021. doi:10.18452/23044.
43. S. Pfaff and S. Ulbrich. Optimal boundary control of nonlinear hyperbolic conservation laws with switched boundary data. *SIAM Journal on Control and Optimization*, 53(3):1250–1277, 2015. doi:10.1137/140995799.
44. S. Pfaff and S. Ulbrich. Optimal control of scalar conservation laws by on/off-switching. *Optimization Methods and Software*, 32(4):904–939, 2017. doi:10.1080/10556788.2016.1236796.
45. P. Pinson, L. Mitridati, C. Ordoudis, and J. Østergaard. Towards fully renewable energy systems: Experience and trends in Denmark. *CSEE Journal of Power and Energy Systems*, 3(1):26–35, 2017. doi:10.17775/CSEEJPES.2017.0005.
46. E. Raheli, Y. Werner, and J. Kazempour. Flexibility of integrated power and gas systems: Gas flow modeling and solution choices matter. *IEEE Transactions on Power Systems*, 40(3):2130–2142, 2025. doi:10.1109/TPWRS.2024.3502541.
47. H. Sauter. *Least-Squares Collocation for DAEs and its Application in Optimal Control*. Dissertation, Humboldt-Universität zu Berlin, 2025. doi:10.18452/34451.
48. M. Schmidt, D. Aßmann, R. Burlacu, J. Humpola, I. Joormann, N. Kanelakis, T. Koch, D. Oucherif, M. E. Pfetsch, L. Schewe, R. Schwarz, and M. Sirvent. GasLib – A library of gas network instances. *Data*, 2(4), 2017. Article 40. doi:10.3390/data2040040.

49. M. Schmidt, M. Sirvent, and W. Wollner. A decomposition method for MINLPs with Lipschitz continuous nonlinearities. *Mathematical Programming*, 178:449–483, 2019. doi: 10.1007/s10107-018-1309-x.
50. M. Schmidt, M. C. Steinbach, and B. M. Willert. High detail stationary optimization models for gas networks. *Optimization and Engineering*, 16:131–164, 2015. doi:10.1007/s11081-014-9246-x.
51. M. Schmidt, M. C. Steinbach, and B. M. Willert. High detail stationary optimization models for gas networks: Validation and results. *Optimization and Engineering*, 17:437–472, 2016. doi:10.1007/s11081-015-9300-3.
52. M. Schuster. *Nodal Control and Probabilistic Constrained Optimization Using the Example of Gas Networks*. Dissertation, Friedrich-Alexander Universität Erlangen-Nürnberg, 2021. URL: https://opus4.kobv.de/opus4-trr154/410.
53. M. Schuster. On the convergence of optimization problems with kernel density estimated probabilistic constraints. *Applied Set-Valued Analysis and Optimization*, 7(2):209–221, 2025. doi:10.23952/asvao.7.2025.2.05.
54. M. Schuster, E. Strauch, M. Gugat, and J. Lang. Probabilistic constrained optimization on flow networks. *Optimization and Engineering*, 23:1–50, 2022. doi:10.1007/s11081-021-09619-x.
55. M. Schuster, E. Strauch, H. Wilka, J. Lang, and M. Gugat. Probabilistic robustness for compressor controls in transient pipeline networks. Preprint, TRR 154, 2025. URL: https://opus4.kobv.de/opus4-trr154/603.
56. J. J. Stolwijk and V. Mehrmann. Error analysis and model adaptivity for flows in gas networks. Preprint, TRR 154, 2017. URL: https://opus4.kobv.de/opus4-trr154/124.
57. W. van Ackooij and R. Henrion. (Sub-)gradient formulae for probability functions of random inequality systems under Gaussian distribution. *SIAM/ASA Journal on Uncertainty Quantification*, 5(1):63–87, 2017. doi:10.1137/16M1061308.
58. A. Wang, K. van der Leun, D. Peters, and M. Buseman. European hydrogen backbone: How a dedicated hydrogen infrastructure can be created, 2020. Enagás, Energinet, Fluxys Belgium, Gasunie, GRTgaz, NET4GAS, OGE, ONTRAS, Snam, Swedegas, Teréga. URL: https://ehb.eu/files/downloads/2020_European-Hydrogen-Backbone_Report.pdf.
59. A.-K. Wiertz, A. Walther, and G. Zöttl. Strategic retailers in the energy sector. Preprint, TRR 154, 2024. URL: https://opus4.kobv.de/opus4-trr154/561.
60. D. Wintergerst. Application of chance constrained optimization to gas networks. Preprint, TRR 154, 2017. URL: https://opus4.kobv.de/opus4-trr154/158.

Open Access This chapter is licensed under the terms of the Creative Commons Attribution-NonCommercial-NoDerivatives 4.0 International License (http://creativecommons.org/licenses/by-nc-nd/4.0/), which permits any noncommercial use, sharing, distribution and reproduction in any medium or format, as long as you give appropriate credit to the original author(s) and the source, provide a link to the Creative Commons license and indicate if you modified the licensed material. You do not have permission under this license to share adapted material derived from this chapter or parts of it.

The images or other third party material in this chapter are included in the chapter's Creative Commons license, unless indicated otherwise in a credit line to the material. If material is not included in the chapter's Creative Commons license and your intended use is not permitted by statutory regulation or exceeds the permitted use, you will need to obtain permission directly from the copyright holder.

